The integration of petrologic and isotopic data from the Boulder Conglomerate to determine the age of the Navan orebody, Ireland.

Volume I Text

by

Colin Victor Ford, B.Sc, M.Sc.

Thesis submitted for the degree of Doctor of Philosophy in the Faculty of Science, Department of Geology and Applied Geology, University of Glasgow.

August 1996.

ABSTRACT

The Boulder Conglomerate is the Lower Carboniferous sedimentary allochthon deposited in the second order half graben created by major listric normal faults in the Navan area. The base of the Boulder Conglomerate comprises erosive-based, highly immature rock avalanches which are interbedded with hemipelagic limestone. Sulphide mineralisation in the autochthon, the Pale Beds Ore, is truncated by the fault-generated unconformity and is reworked as clasts and matrix into the basal Boulder Conglomerate. Matrix-deficient breccia beds deposited on the unconformity possess mineralisation as cement to interclast porosity. This cement is contiguous with replacement and fracture-cementing mineralisation in limestone strata beneath the unconformity. Mineralisation associated within the interbeds to the Boulder Conglomerate occurs as early diagenetic concretions and as stratiform replacement. The $\delta^{34}S$ of these sulphides ranges from -21‰ to +1‰.

The rock avalanches are overlain by clast-bearing carbonate mud strata. The carbonate mud is replaced by pyrite and paragenetically later sphalerite and galena. The isotopic range of $\delta^{34}S$ for pyrite (-32‰ to -35‰) is distinct from that of the zinc and lead sulphides (-18‰ to +6‰).

The uppermost Boulder Conglomerate is characterised by slumped and brecciated mineralisation which is dominated by pyrite. The $\delta^{34}S$ values of the *in-situ* and reworked mineralisation range from -40‰ to -23‰.

The Thinly Bedded Unit overlies the Boulder Conglomerate and comprises interlayered shales and calcarenite and laterally impersistent, erosive-based, graded bioclastic and oolitic microbreccias. Mineralisation occurs as selective replacement to the microbreccia and as stratiform sphalerite and pyrite mud. The latter occur in-situ as laminae and as channelised debris flows. The reworked sulphide mud supports plant fragments which exhibit exceptional preservation by pyrite, sphalerite and galena. The $\delta^{34}S$ of the laminated and reworked sulphides ranges from -37‰ to -41‰.

The $\delta^{34}S$ signature of the sulphide minerals in the Boulder Conglomerate show that the bulk of the sulphur was produced by the bacteriogenic reduction of seawater sulphate ($\delta^{34}S$ of +19‰) in an open system. The isotopic data converges with petrology to show that the timing of mineralisation was synsedimentary relative to the deposition of the Boulder Conglomerate and the overlying Thinly Bedded Unit.

CONTENTS

DECLARATION

The material presented in this thesis is the result of research carried out between October 1992 and August 1996 in the Department of Geology and Applied Geology, University of Glasgow, under the supervision of Professor Mike Russell.

This thesis is based on my own independent research and any published or unpublished material used by me has been given full acknowledgement in the text.

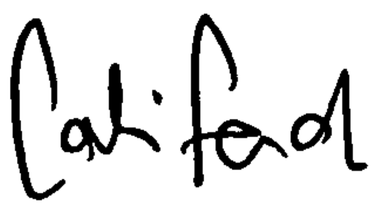

Colin Ford.

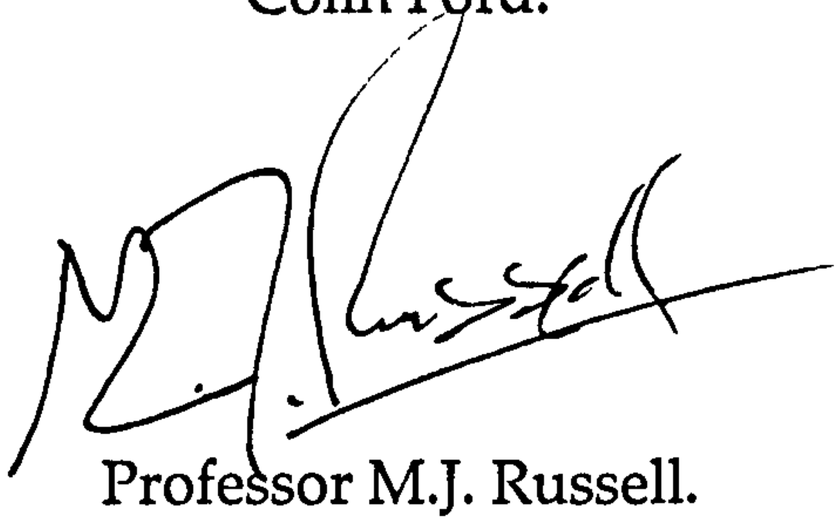

Professor M.J. Russell.

ACKNOWLEDGEMENTS

Glasgow:

I would like to thank Mike Russell for enlisting me into his school of thought. Specialist geological input was provided by the following members of the academic community: Colin Braithwaite (carbonate sedimentology and C.L. microscopy); Brian Bluck (massflow sedimentology); Adrian Boyce and Tony Fallick, of S.U.R.R.C. (sulphur isotopes); Neil Clarke, of the Hunterian Museum (palaeobotany). The following staff provided technical support without which the research could not have flourished: Douglas Maclean (expert photography and microscopy); Andrew Monoghan, Alan Jones and John Gilleece (rock preparation and thin sections); Dugald Turner and Murdo McLeod (XRD); Peter Ainsworth (SEM); Jim Kavanagh (computing); Roddy Morrison (equipment); Ian Gardiner, of the Civil Engineering Department (rock cutting); Mighty John Young (a gorilla with a heart of gold).

Aldo, Erchie, Bertie and William Welsh, amongst innumerable others, were responsible for a great deal of fun during my stay in Glasgow.

Ireland:

I would like to thank the Tara Mines geology department for their hospitality and help during the field work. I am indebted to Peter Powell for finding me employment as field technician prior to the research. John Ashton familiarised me with the geology and layout of the mine. Special thanks to Johnny Smith for the many occasions on which he took me underground.

Mike Philcox was a regular visitor to the mine. I am grateful for the interest he took in this research and for his help in familiarising me with the stratigraphy of Ireland and the Navan area.

Whilst out in Ireland, I was fortunate to have met Martin Forde and the people of Rathmoylan, Barney Guinan, Mickey Marmion, Pete Kane, Paul McParland, Martin Donelan, the Smiths of Kilcarn Court, Arthur Guinness and John Jameson.

Liverpool:

Fawzi Nagar. Stephen Norman. South African Paul (R.I.P.). Yusuf Ashour. Lee Kwende and family. Dennis. Barry. Paul. Tony Clarke. Tony Boediger (R.I.P.). Victor Immundi, Sr. (R.I.P.) and Jr.

CHAPTER ONE. INTRODUCTION

The Navan Orebody, located 1.5 km to the northwest of Navan in the Republic of Ireland, is Europe's largest zinc-lead mine. The deposit comprises 69.9 million tonnes of ore, grading 10.1 % zinc (as sphalerite) and 2.6 % lead (galena) [Ashton et al., 1986]. It is hosted by a faulted sequence of Dinantian (Lower Carboniferous) sedimentary rocks. Pyrite, barite, dolomite and calcite are intimately associated with the ore and represent the gangue minerals.

The mineralisation is divided stratigraphically and mineralogically into two parts: the autochthonous Pale Beds Ore (P.B.O.) and the allochthonous Conglomerate Group Ore (C.G.O.) [Table 1.; frontispiece to Volume II]. The P.B.O. comprises 97% of the total mineable reserves and is hosted by the mixed carbonate-siliciclastic Navan Group sequence. Mineralisation in the autochthon is developed to greatest intensity in association with limestone-rich strata of the Pale Beds: the P.B.O. occurs as five stratiform lenses. Non-stratiform mineralisation of the P.B.O. is represented by vertical coalesence of the lenses (producing up to 70m of vertically contiguous ore) and local vein-type ore. The Navan Group autochthon is variably dolomitised. Dolomite is spatially and temporally associated with the ore (Anderson, 1990; Rizzi, 1992) and possesses a northeast-southwest trending, plume-shaped geometry (Rizzi, 1992). Dolomitisation of the autochthon has been interpreted as syn-mineralisation and hydrothermal (Anderson, 1990; Rizzi, 1992).

Rizzi (1992) regarded the metallogenesis of the autochthon as controlled by the existence sedimentary heterogeneities within the Pale Beds and Micrite Unit which he believed to represent karren-type palaeo--emersion surfaces. He strongly contested the findings of Anderson

(1990), who interpreted the development and configuration of the P.B.O. as the product of hydrothermal corrosion. The metallogenic processes advocated by Anderson (1990) were most effective at lithologic and/or diagenetic heterogeneities: a stratiform morphology was thus imposed on the ore.

Although the metallogenesis of the Pale Beds was not the primary research issue of this thesis, the occurrence of reworked mineralisation in the allochthon demanded a knowledge of the petrography of the P.B.O. Diamond drillcore intersections of the P.B.O. were utilised in this respect. The study of the P.B.O. also furnished information significant to resolving the processes responsible for the metallogenesis of the autochthon.

The allochthonous sediments deposited over the submarine unconformity in the Navan area are collectively referred to as the Boulder Conglomerate. Mineralisation associated with the Boulder Conglomerate is termed the Conglomerate Group Ore (C.G.O.). It is characterised by high pyrite content and rare dolomite. The C.G.O. pyrite is characteristically developed as replacement to variably conglomeratic carbonate mud. The C.G.O. occurs as reworked ore, as cement to breccia beds and as in-situ replacement. The gross geometry of the C.G.O. in relation to the Boulder Conglomerate is stratiform. Cross-cutting mineralisation is present, however, on both the microscopic and macroscopic scales.

Previous research of the Navan Orebody was economically directed and involved the characterisation of the P.B.O. in terms of its lithostratigraphic timing. Three conclusions were produced: synsedimentary (Andrew and Ashton, 1985), syndiagenetic (Anderson, 1990) and epigenetic (Rizzi, 1992). The aim of this thesis is to relate the

evidence afforded by the C.G.O. to decide which of these conclusions is correct. The Boulder Conglomerate is selected as the sedimentary reference stratum to which the lithostratigraphic timing of the mineralisation is related. Hypotheses are constructed to characterise the timing of the mineralisation grounded in geologic and isotopic principles. The predictions are tested against observation and analysis.

Rizzi (1992) stated unequivocally that the Argillaceous Bioclastic Limestone Group, of which the Waulsortian Limestone is the stratigraphically highest facies, is unmineralised (undolomitised). This total absence of ore-related mineralisation was regarded as dubious owing to the common association of mineralisation with temporally and sedimentologically equivalent sediments throughout Ireland, for example, Silvermines (Andrew, 1986), Tynagh (Clifford et al., 1986), Ballinallack (Jones and Brand, 1986), and the more recently discovered Lisheen deposit (Redmond, 1995). Logging of the Waulsortian Limestone and underlying Argillaceous Bioclastic Limestone was intially undertaken to determine its depositional history in relation to the mid--Dinantian submarine extensional tectonism described by Philcox (1989). As the logging commenced and the sedimentary-tectonic relationships became apparent, Rizzi's (1992) palaeo-emersion surface hypothesis was refuted. Mineralisation is related to the sedimentology of the Argillaceous Bioclastic Limestone Group: implications for the metallogenic controls stated by Rizzi (1992) are reconsidered.

CHAPTER TWO. RESEARCH APPROACH AND METHODS

For seven months prior to starting the research, I was employed by Tara Mines Ltd. as a field technician. During this contract I gained experience of the Navan geology through the examination of diamond drillcore and mapping and sampling underground. The underground environment provides an exacting field laboratory for the geologist: the inherent dangers associated with subsurface excavations, coupled with the absence of natural light renders even the most simple geology equivocal (c.f. Andrew and Ashthon [1985] versus Rizzi [1992]). Underground exposure, however, is critical to understanding the three-dimensional configuration of the geology. Three large coresheds house over 1200 diamond drillholes through the orebody and its surrounds. Drillcore represents subvertical line source information of the regional geology. Interpretation of the geology in drillcore was influenced greatly by the appearance of the geology underground.

During the employment, the questions to be appraised by the research were formulated. These were:

1) What is the relationship of the C.G.O. to the P.B.O.?

2) Was the metallogenesis of the C.G.O. syngenetic or epigenetic?

3) What is the $\delta^{34}S$ isotopic signature of the C.G.O.? How does this relate to question 2) with regard to a reasonable sulphur source?

4) What is the depositional setting and mechanism of formation of the Boulder Conglomerate?

5) What is the sedimentology of the Argillaceous Bioclastic Limestone Group?

6) Why is the Waulsortian Limestone relatively unmineralised, in view of its frequent association with carbonate-hosted Zn-Pb mineralisation in Ireland?

On starting the research officially, I commenced a comprehensive literature review to gain familiarity with the geological disciplines involved. These were:

1) Geology of the Navan Orebody.

2) Geology and genesis of Irish, carbonate-hosted, Zn-Pb deposits.

3) Geology of Ireland.

4) Sedimentology of submarine megabreccias.

5) Mechanisms of formation and the petrography of autoclastic breccias.

6) Development of Waulsortian mud mounds.

7) Characteristics of submarine, sediment-hosted Zn-Pb deposits.

8) Characteristics of Mississippi Valley-type Zn-Pb deposits.

9) Precipitation of sedimentary pyrite.

With the geology familiarised, I embarked on numerous field trips to the mine. Two hundred and sixty three diamond drillholes were logged and samples were taken at the relevant intervals. Accessible underground exposures of the C.G.O. were mapped and sampled extensively. It was imperative to sample at the time of availability: headings into ore have a high premium and are rapidly worked out; dangerous exposures are masked with shotcrete and/or are considered inaccessible.

The samples were cut and polished, and the slabs photographed. It proved necessary to photograph the highly pyritic samples immediately after preparation owing to their rapid oxidation and decomposition: prolific growth of melanterite ($FeSO_4 \cdot 7H_2O$) occurs as a mould-like chemical weathering to pyrite treated with water and stored under

normal humidity - the samples expand and disintegrate. Relevant samples were selected for preparation as polished and unpolished thin sections. Their petrography was related to the underground mapping and/or drillcore and the geology interpreted. The mineralogy was defined petrographically, and verified by X.R.D. and S.E.M. analysis. Use of the C.L. microscope was an integral part of the research and proved instrumental in determining the paragenesis and modes of mineral growth. Complete understanding of the spatial and temporal distribution of the mineralisation was required for valid interpretation of the sulphur isotopes. The $\delta^{34}S$ values obtained were related to the metallogenesis.

The fieldwork was done iteratively: initial interpretations served to dictate the form of later fieldwork; the validity of early interpretations was constantly challenged as the database increased and apparent contradictions were resolved.

CHAPTER THREE. GEOLOGY OF IRELAND AND THE NAVAN AREA

3.1 GEOLOGIC HISTORY OF IRELAND

Late Ordovician, oblique east-west continental collision of the Laurentian and Avalonian plates resulted in the closure of the Iapetus Ocean: the Caledonian Orogeny was initiated (Pattrick and Polya, 1993; Figure. 1). The Solway-Navan-Silvermines Line is considered to be the locus of this collision (Soper, 1988; McKerrow and Soper, 1989), forming the Iapetus Suture. Final collision in the end-Silurian to mid-Devonian involved the underthrusting of East Avalonia beneath Laurentia and removal of the remaining seaways. Regional uplift and deformation accompanied the collision, culminating in the Middle Devonian (*c*.395 Ma) Acadian event. Complex open folding and low-grade metamorphism of the Lower Palaeozoic rocks on either side of the suture ensued. It was during this period that major left-lateral movements took place on the terrane boundaries and produced the NE-SW lineaments which characterise the Caledonide structural grain (Soper, 1988; Figure. 2).

Subduction-related perturbation of the geothermal gradient caused extensive calc-alkaline magmatism in the late Silurian to mid-Devonian: granitoid batholiths intruded into the Lower Palaeozoic rocks (Barker and Gayer, 1985; Zhou, 1985; Fig. 2). The sites of granitic intrusion were critical in dictating the post-orogeny topography and subsequent sedimentation patterns. The intrusive centres were resistant to erosion and formed large areas of positive, subaerial relief: the Longford Down Massif (contiguous with the Southern Uplands), the Leinster Massif, and the Galway-Mayo High (contiguous with the Scottish Highlands). The Irish Midlands were an area

of low relief, bounded to the west, north, east and southeast by these granitic palaeohighs (Cope et al., 1992).

The Late Devonian palaeolatitude was tropical and the climate semi--arid. Rivers drained radially inwards from the orogenic/granitic highs into the Irish Midlands. Red, fluviatile sandstones, equivalent to the Old Red Sandstone of England, were deposited in basins related to NE-SW subsidence (Cope et al., 1992; Pattrick and Polya, 1993).

Increase in relative sea level produced epicontinental marine conditions within the developing Dublin Basin. Post Old Red Sandstone sediments were transitionally succeeded by a clastic-dominated to marine-dominated succession of regionally-correlatable Courceyan sediments (Philcox, 1984; Figure. 3). The sediments lapped onto the eroded massifs as relative sea level continued to rise. Nolan (1989) reports no evidence for subaerial exposure within the Courceyan marine limestone sequence deposited in the Dublin Basin.

Reactivation of the Caledonide basement during the Chadian and into the Arundian caused rapid and catastrophic tectonic subsidence. Major vertical displacement of the limestone sequence produced a block and basin submarine relief. Restructuring of the Dublin Basin is manifested in the Mid-Dinantian stratigraphy as a diverse suite of locally deposited and therefore lithologically uncorrelatable sedimentary complexes: the depositional substrate is characteristically a tectonically-generated seafloor unconformity (Hitzman and Large, 1986). Syntectonic sediments in the Dublin Basin are represented by Waulsortian Limestone build-ups and mass flow complexes. Hiatuses developed in areas of sediment starvation,

characteristically the submarine highs. Anoxic, hemipelagic shales were deposited and achieve greatest thicknesses in the downthrown troughs.

Deposition of the Waulsortian Limestone and reworking of the horst blocks ceased as limestone turbidites debauched onto the seafloor, eventually infilling the Dublin Basin. This rhythmic limestone facies is Arundian in age and is referred to as the Calp; it is equivalent to the Upper Dark Limestone in the Navan area. Maximum recorded thickness of the Calp is 1500m (Andrew and Ashton, 1985).

The Variscan Orogeny (330 Ma) caused the compressive reactivation of Caledonide structures. Maximum compression in Ireland occurred in the south and was coincident with the Variscan tectonic front: the stratigraphy was folded and uplifted.

3.2 GENERAL GEOLOGY OF THE NAVAN AREA

The Navan orebody is located in an extensionally-faulted, mixed carbonate-siliciclastic Courceyan sequence (the Navan Group autochthon) and overlying Chadian-Lower Arundian sedimentary breccia (the Boulder Conglomerate) on the southern margin of the Longford Down Lower Palaeozoic Inlier (Fig. 4). The geology of the Navan area is shown in Figure. 5. The Longford Down Lower Palaeozoic palaeo-massif provided the basement upon which the Navan Group was unconformably deposited (Figure. 3).

Figure 6 shows a summary of the stratigraphy in the Navan area. Major (inter-Period) and minor (intra-Period) unconformities occur in the stratigraphy of the Navan area; all the unconformities exhibit angular stratigraphic relationships. The minor, i.e. intra-Carboniferous submarine

unconformities represent the boundary between autochthonous Navan Group rocks and post-Navan Group rocks, i.e. the Boulder Conglomerate and the Argillaceous Bioclastic Limestone Group. The minor unconformities formed in response to extensional submarine tectonism. The major unconformity separates the Upper Devonian and Lower Carboniferous sediments from the Lower Palaeozoic basement; the contact is sharp and represents the subaerially-eroded Caledonian Orogen.

Figure 7 shows an isometric view of serial, NE-SW strike sections across the Navan orebody. The regional dip of the autochthon is 20º to the southwest (Ashton et al, 1986). The Pale Beds Ore is located in the submarine horst structure defined by two suites of normal faults. The Liscarton and Castle Faults are major extensional faults which strike NE-SW and downthrow to the northwest. The opposing suite of normal faults to the southeast, the B and T Faults, have curvilinear traces and are listric in profile; the B and T Faults also strike NE-SW, but they downthrow to the southeast. The intervening horst structure is the site of multiple minor NE-SW trending normal faults; these are identified by displacement of distinct marker beds within the Navan Group stratigraphy. They are regarded as failed equivalents of the major normal faults which define the submarine horst (Andrew and Ashton, 1985).

The Argillaceous Bioclastic Limestone Group is located in the northwest graben and unconformably overlies a reduced succession of Shaley Pales; the contact is depositional. Removal of the Shaley Pales is attributed to extension-related sliding (Philcox, 1989). The sedimentology of the Argillaceous Bioclastic Limestone Group is discussed in Chapter Four.

The Boulder Conglomerate is a locally-derived mass flow complex. Clast composition comprises Navan Group, Argillaceous Bioclastic Limestone Group and rare Lower Palaeozoic lithologies. Although the distribution of the Boulder Congomerate is ubiquitous across the mine area, maximum thickness of the Boulder Conglomerate is developed in the half graben defined by the T Fault: the depositional site was fault-controlled (Figure. 8). Vertical displacement on the T Fault is at least 200 m and for this reason it is the largest of the extensional faults present in the Navan area. Displacement of the stratigraphy by the T Fault was primarily responsible for the local stratigraphic downcutting event into the footwall to the north. Deposition of the Boulder Conglomerate records periodic failure and reworking of Lower Palaeozoic and Navan Group lithologies from the submarine fault scarp, and the Argillaceous Bioclastic Limestone Group. The sedimentology of the Boulder Conglomerate is discussed in detail in Chapter Five. Mineralisation in the Boulder Conglomerate comprises the Conglomerate Group Ore.

The Boulder Conglomerate is conformably overlain by rhythmically inter-layered calcarenite and shale (the Thinly Bedded Unit). These are transitional into the Upper Dark Limestones: calcturbidites interbedded with shale. The Upper Dark Limestones lap onto the eroded horst block and Argillaceous Bioclastic Limestone Group.

Evidence for the effects of Variscan tectonism in the Navan area are represented by major reverse faults. The A-C-D Fault Complex strikes NE-SW and displaces the Lower Carboniferous stratigraphy in the palaeodepositional site of the Boulder Conglomerate; displacement is sinistral and estimated at 2 km (J. Ashton, pers. comm. 1992); the stratigraphy

within the fault zone dips steeply and is traversed by splay faults. The Randalstown Fault strikes NNE-SSW and is responsible for displacement of the Lower Carboniferous stratigraphy in the palaeodepositional site of the Argillaceous Bioclastic Limestone Group.

The compressional faulting of the Lower Carboniferous stratigraphy is interpreted as due to reactivation of the basement Caledonoid structure. This interpretation is supported by the intersection of the Navan area with the inferred Navan-Tipperary Linear (Figure. 2).

CHAPTER FOUR. SEDIMENTOLOGY OF THE ARGILLACEOUS BIOCLASTIC LIMESTONE GROUP

4.1 DEPOSITIONAL SETTING

The Argillaceous Bioclastic Limestone Group (A.B.L. Group) is located in the graben structure defined by a series of northeast-southwest striking normal faults that dip to northwest and which are exemplified by the Castle and Liscarton Faults (Figure 7). The contact of the A.B.L. Group with the underlying Navan Group is unconformable.

4.2 SEDIMENTARY DESCRIPTION OF THE ARGILLACEOUS BIOCLASTIC LIMESTONE GROUP

In ascending stratigraphic order, the A.B.L. Group in the Navan area is subdivided into three lithofacies: i) the Argillaceous Bioclastic Limestone, ii) the Reefoid Argillaceous Bioclastic Limestone, and iii) the Waulsortian Limestone. Photo. 1 shows a complete sequence of the A.B.L. Group in drillcore. Figure 9 shows a graphic log of the A.B.L. Group. Mineralisation associated with the A.B.L. Group is considered in Chapter 8 and is related to the sedimentology described here.

4.2.1 Argillaceous Bioclastic Limestone (A.B.L.)

The A.B.L. comprises crinoidal calcarenite interbedded with crinoidal argillite (Photo. 2). Bed thickness ranges from centimetre to decimetre. Bedding contacts range from gradational to sharp according to the ratio of argillite to calcarenite; the contacts are undulatory on the scale of BQ (36.5 mm diameter) drillcore. The crinoids commonly occur as articulated stem pieces and single ossicles in both the argillaceous and limestone beds (Photo. 3).

4.2.2 Reefoid Argillaceous Bioclastic Limestone (R.A.B.L.)

The R.A.B.L. is a sedimentologically varied lithofacies, comprising interbedded in-situ and reworked Argillaceous Bioclastic Limestone Group lithologies. The contact of the R.A.B.L. with the underlying A.B.L. is gradational.

In-situ R.A.B.L. is represented by crinoidal limestone interlayered with crinoidal argillite; limestone predominates and distinguishes this facies from the underlying A.B.L. The argillite interlayers range from millimetric seams (Photo. 4) to decimetre interbeds of crinoidal argillite and limestone (Photo. 5.). Breccia interbeds to the R.A.B.L. comprise reworked crinoidal limestone and crinoidal argillite (Photo. 6). The crinoidal limestone consistently occurs as angular clasts set in a matrix of limestone and/or argillite; the matrix crinoids are represented by single ossicles which exhibit variable degrees of fragmentation and/or abrasion.

4.2.3 Waulsortian Limestone (W.L)

The W.L. is the stratigraphically highest lithofacies of the A.B.L. Group and is gradational with the underlying R.A.B.L. The W.L. comprises massive, pale grey biomicrite and biosparite. Bioclasts are the predominant constituent of the limestone and are represented by crinoids, bryozoa and brachiopods.

The bioclasts are in various states of fragmentation. This appears to be related to the fragility of the organism: crinoids are present as single ossicles and occasional stem peices, whereas the more fragile bryozoa are degraded to branch fragments and zooecia.

The groundmass to the bioclasts is represented by either a carbonate mud matrix or sparite cement. The carbonate mud matrix is often pelletal and supports the bioclasts (Photo. 7). In the absence of a

matrix, the bioclasts are in contact and are cemented by sparite; this calcite cement commonly occurs as syntaxial overgrowths to the ubiquitous crinoidal ossicle component (Photo. 8).

The vertical extent of the W.L. is characterised by a breccia fabric. The breccia comprises clast-supported W.L.; non-limestone clasts are rare and are represented by mudstone pebbles (Photo. 9). The limestone clasts are angular and range in size from pebble to boulder. Matrix is rare, but is important as it permits discrimination of the clasts. Two types of matrix are present: i) argillite (Photo. 10), and ii) carbonate mud (Photos. 11 and 12). In drillcore, the appearance of the W.L. comprises obvious breccia intervals separated by monotonous sequences of massive biomicrite and biosparite.

Swarms of calcite-cemented micro-veins cut through the W.L. Photos. 8 and 12 show calcite veining cutting across syntaxially-cemented crinoidal limestone and W.L. breccia, respectively.

4.3 INTERPRETATION OF THE ARGILLACEOUS BIOCLASTIC LIMESTONE GROUP

The A.B.L. Group was locally deposited in the submarine graben structure created by the suite of northwest dipping normal faults. Evidence for removal of the Shaley Pales and subsequent unconformable deposition of the A.B.L. Group is provided by the significant reduction in the thickness of the former where overlain by the latter. The tectonic control on the depositional site of the A.B.L. Group is in accordance with the distribution of equivalent sediments throughout Ireland. The sporadic distribution of these Waulsortian build-ups in the Lower Carboniferous of the Navan area is regarded as the result of diachronous sedimentation during faulting of the seafloor into a block and basin

configuration: deposition in the south commenced lithostratigraphically earlier and migrated northwards as relative sea level increased; deposition of Waulsortian facies within pre-existing basins resulted in localised distribution and rapid thickness and facies changes (Lees, 1964; Sevastopulo, 1981).

The A.B.L. Group records a vertical transition in its sedimentology. Early deposition is represented by calcarenite interbedded with argillite: the Argillaceous Bioclastic Limestone. The common occurrence of bioclasts within both the limestone and argillite proves the continuous supply of skeletal grains. The articulated state of the bioclasts and their lack of fragmentation and abrasion indicates a local source and/or lack of energetic reworking.

The gradation into the Reefoid Argillaceous Bioclastic Limestone records bioclastic-dominated sedimentation and represents the transition into the Waulsortian Limestone: deposition of skeletal grains and carbonate mud exceeded argillite. Reworking of the Reefoid Argillaceous Bioclastic Limestone as monomict interbeds proves local derivation and selective early diagenetic cementation of the limestone. Reactivated extensional tectonism is invoked as the mechanism which generated the topographic head and caused the reworking.

Deposition of the Waulsortian Limestone records the prolific production of a marine, calcite-precipitating biosphere. Reworking of the limestone as a sedimentary breccia proves early, submarine cementation by calcite and pelletal carbonate mud during active extensional tectonism. The presence of contemporary carbonate mud as matrix to the breccia suggests that reworking was syndepositional. The processes of brecciation and transport downslope is proven by the generation of mudstone intraclasts and the different C.L. characteristics of the clast and matrix

limestone. The majority of the contemporaneous argillite was unlithified and was reworked as matrix. It is not possible to discriminate in drillcore whether the monotonous intervals of Waulsortian Limestone represent megaclasts or re-established in-situ deposition of this lithofacies.

The occurrence of swarms of calcite-cemented microfractures through both early diagenetic calcite and reworked Waulsortian Limestone proves that the depositional site of A.B.L. Group was subject to long-lived extensional tectonism and multiple calcite cementation events.

Evidence for a later phase of compressive tectonism is represented by the Randalstown Fault: a major reverse fault which displaces the Lower Carboniferous stratigraphy in the northwest of the mine area. The fault is interpreted as the result of basin inversion during the Variscan Orogeny and is consistent with the interpretion of Doyle and Bowden (1995) for the A.B.L. Group-equivalent sediments of the Galmoy area. It is hypothesised that the basin inversion was related to reactivation of the basement Caledonoid structure.

CHAPTER FIVE. SEDIMENTOLOGY OF THE BOULDER CONGLOMERATE AND THE THINLY BEDDED UNIT

Section A. SEDIMENTOLOGY OF THE BOULDER CONGLOMERATE

5A.1 Introduction

Underground exposure of the Boulder Conglomerate is incomplete; development is restricted to only those areas proven to be economically viable. Ore-rich Boulder Conglomerate is termed the Conglomerate Group Ore (C.G.O.). Headings into the C.G.O. were mapped and representative samples were taken. This chapter characterises the sedimentology of the Boulder Conglomerate. The petrographies of the clasts and matrix are used to determine: i) the diagenetic state of the autochthon at the time of reworking, ii) the provenance of the clasts, and iii) the sedimentology of contemporaneous sediments. Mineralisation in the C.G.O. is considered in detail in Chapters 9, 10 and 11 and is related to the sedimentology of the Boulder Conglomerate.

5A.2 The Boulder Conglomerate in underground exposure

5A.2.1 1315 CGO

Description of the submarine unconformity

Plan 1 shows the mapping of the unconformity from the exposure of the C.G.O. on 1315 Level. The stratigraphic level of the unconformity in the hanging wall of the T Fault is the Shaley Pales. The Pale Beds are located in the footwall of the T Fault. The Shaley Pales pinch out against the Pale Beds at the contact with the T Fault where the unconformity continues as the palaeo-fault scarp. The depositional site of the Boulder Conglomerate is the half graben defined by the T Fault (Figure 8).

A horizontal transect across the T Fault reveals a transition in the rheology of the footwall and hanging wall lithologies. The Pale Beds in the footwall, away from the fault zone, are undeformed. With increasing proximity to the fault zone, the Pale Beds are fractured: impersistent fractures delineate angular, in-situ clasts which show no rotation and possess no matrix (Photos. 13 and 14). The fault zone itself is 0.5 - 1.0 m wide and comprises a fault-parallel breccia in which granule to boulder-sized, angular clasts of oolitic limestone are set in subordinate matrix of comminuted clasts, quartz and feldspar sand and argillite (Photos. 13 and 15). The fault zone breccia is developed only in the Pale Beds and is contiguous both above and below the fault trace.

The Shaley Pales which are in contact with the T Fault possess a sheared, fault-parallel fabric. The Shaley Pales are inclined against the footwall Pale Beds and form an open syncline. The intensity of shearing within the Shaley Pales decreases perpendicularly away from the T Fault.

The dip of the T Fault, and correspondingly that of the fault scarp/unconformity is 50° to the SSE. The unconformity in the hanging wall is subhorizontal on the scale of the entire exposure, but is characterised by inflections and/or fractures of various magnitude. These are represented by:

i) concave depressions with smooth floors, up to 80 m in width and 6 m deep, e.g. CGO AC;

ii) high amplitude inflections with ragged margins, up to 4 m wide and 1.5 m deep, e.g. P1S (Photo. 16); the Shaley Pales beneath these inflections are fractured. The infill comprises polymict Boulder Conglomerate which is petrographically distinct from the Shaley Pales substrate (Photo. 17);

iii) step-like inflections, down to a depth 1.5 m (Photo. 18). The Shaley Pales beneath the unconformity comprises interbedded bioclastic

limestone, arenite and argillite. The former possesses a primary calcite cement which occurs as syntaxial overgrowths to the abundant crinoid ossicle component (Photo. 19) and bioporosity-occluding sparite (Photo. 20). Interstratal shearing within the hanging wall Shaley Pales is characteristically associated with the argillite (Photo. 21);

iv) fractures up to 2 m long and perpendicular to the unconformity (Photo. 22).

Interpretation

Submarine normal faulting ruptured the Navan Group autochthon. The Pale Beds were exposed as a steeply-dipping, submarine, fault plane scarp, corresponding to the unconformity located in the footwall of the T Fault. The lithified state of the Pale Beds is shown by their brittle deformation and the high angle of the fault scarp.

The Shaley Pales were downthrown and emplaced as the hanging wall of the T Fault. The Shaley Pales were sheared against the Pale Beds, forming a synclinal drag fold. The rheology of the Shaley Pales was plastic and indicates incomplete lithification at the time of faulting.

Shearing in the fault zone caused tectonic erosion: Pale Beds in the footwall were brecciated, plucked out and then sheared and rotated. Matrix was generated by degradation of the footwall and hanging wall lithologies in the fault zone. Evidence for tectonic brecciation by displacement on the T Fault is also seen in diamond drillcore: hole N1012 intersected a breccia zone which is 5 m in apparent thickness and comprises angular Pale Beds and Micrite Unit clasts (Photo. 23). The breccia zone coincides with a major stratigraphic omission which is recorded by the mine log as the T Fault.

The local relief on the unconformity in the footwall is interpreted as being the result of i) primary slide removal of the Shaley Pales and ii) subsequent erosion by the Boulder Conglomerate. Philcox (1989) relates the Shaley Pales sliding event to early extensional submarine tectonism which culminated in the fragmentation of the Navan Group autochthon by major normal faults. Gawthorpe and Clemmey (1985) documented the equivalent tectonic processes effecting the equivalent Lower Carboniferous stratigraphy in the Bowland Basin. Here, extensional tectonism also caused the synsedimentary, submarine mass movement of the Dinantian carbonate succession. The subsiding basin was the depositional site of large slide blocks. Gawthorpe and Clemmey (1985) relate the integrity of the slide blocks to the diagenetic state of the strata. In the Navan area, the slide blocks comprise coherent, subhorizontal slabs of the Shaley Pales stratigraphy (Philcox, 1989), indicating that the autochthon was in a state of advanced lithification at the time of mass movement. The contact of the slide blocks with the autochthon exhibits the omission or repetition of stratigraphy and is characteristic of extensionally delaminated terranes (Dahlstrom, 1970).

Gawthorpe and Clemmey (1985) define slide structures in terms of *local detachment surfaces* and *major slide planes*. Drillcore through the delaminated Shaley Pales in the Navan area intersected the equivalent tectonic surfaces. Local detachment surfaces are represented by zones of intrastratal deformation and polished shale beds across which there is no measurable stratigraphic omission. The strata within the deformation zones are characterised by boudinaged, interbedded calcsilt-shale which is sheared to high angles (Photo. 24). Major slide planes are identified by the presence of vertically extensive breccia zones across which the Shaley Pales succession is repeated. The breccia zone comprises angular, rotated

clasts of limestone and/or arenite in a shale matrix (Photo. 25). The clasts are derived from the hanging wall and footwall. The common occurrence of plastically-deformed shale within deformation zones of both the local detachment surfaces and major slide planes suggests that the development of slide planes was dependent upon the presence of unlithified argillite. The depositional site of the slide blocks in the Navan area proves that contemporaneous subsidence was at its maximum here. The source of the slide blocks was updip and to the north.

Continuation of the Navan mine area as the locus of regional subsidence is proved by the displacement of the autochthon by the suite of normal faults which are exemplified by the T Fault. The faulting was catastrophic and exposed the entire Navan Group in its footwall as a broad slump scar. The dynamics of this event are comparable to the middle Miocene collapse of the west Florida carbonate platform margin (Mullins et al., 1986). Here, catastrophic failure of the slope also created an irregularly embayed, concave slump scar. The faulting was responsible for the removal of up to 350 m of late Palaeogene and early Neogene strata and the generation of a sub-basin with a width of 30 km.

In the Navan area, catastrophic faulting ruptured the previously delaminated autochthon and the seafloor unconformity was downthrown to the south. The broad, concave-up inflections in the unconformity exposed in the hanging wall in 1315 CGO are interpreted as palaeo-slide scars. The step-like inflections in the unconformity represent the trailing margins from which slide blocks were released. The occurrence of calcite-cemented bioclastic limestone strata in the footwall to these palaeofractures implies that the geometry of the unconformity was controlled by the diagenetic state of the sediments and is consistent with the conclusions of Gawthorpe and Clemmey (1985). The bioclastic

strata were selectively cemented by calcite owing to the occurrence of bioporosity and the ubiquity of crinoid ossicles. Sliding was facilitated by the frequent occurrence of argillaceous interlayers within the Shaley Pales. The argillite beds acted as slip planes along which sliding was concentrated. Brittle failure of the strata at cemented horizons released the slide blocks and produced local, angular relief on the unconformity. Evidence for fractured but undisplaced Shaley Pales was shown in Photo. 22.

The transport of the Boulder Conglomerate over the unconformity resulted in the surficial brecciation and erosion of the substrate. Slide scars in the unconformity are likely to have influenced the flow direction and depositional site of the Boulder Conglomerate. Preservation of the palaeorelief on the unconformity, as demonstrated by the step-like inflections, suggests that the flow of the Boulder Conglomerate decelerated rapidly upon encountering its half graben depositional site: erosion of the unconformity by the Boulder Conglomerate was minimal.

The absence of the A.B.L. Group in the hanging wall of the T Fault proves that these sediments were not intersected by the fault. This is consistent with the fault-controlled, and therefore spatially-restricted, distribution of the A.B.L. Group. Evidence for the deposition of the A.B.L. Group after the Shaley Pales sliding event is demonstrated in drillcore. Photo. 26 shows the depositional contact of the Shaley Pales with the underlying Pale Beds (location A) and the contact of the Argillaceous Bioclastic Limestone with the Shaley Pales (location B). The 12 m thickness of Shaley Pales is considerably less than their estimated depositional thickness of 100 m. The remnant Shaley Pales are characterised by plastically deformed strata (Photo. 26, location C) and polished shale beds. These correspond to the local detachment surfaces of

Gawthorpe and Clemmey (1985). Evidence for the deposition of the A.B.L. Group after the sliding event is provided by the depositional attitude of the Argillaceous Bioclastic Limestone which overlies the decimated Shaley Pales substrate (Photos. 26 and 27).

The Shaley Pales immediately beneath the contact with the Argillaceous Bioclastic Limestone is often marked by a breccia zone (Photo. 26, location B). The breccia comprises clasts of Shaley Pales which have been rotated in an argillaceous matrix. These breccia zones are interpreted as exhumed slide planes, as deduced from their monomict Shaley Pales clast composition and petrographic equivalence to the tectonic breccia zones associated with the major slide planes (Photo. 25). The processes of brecciation and exhumation are interpreted, therefore, as being genetically related. Low angle sliding of the Shaley Pales generated intrastratal breccia zones. These were exhumed as palaeo-detachment surfaces upon transport of the slide blocks basinwards, prior to the deposition of the A.B.L. Group.

Description of the Boulder Conglomerate

Plan 1 shows the detailed mapping of the Boulder Conglomerate from 1315 CGO. The Boulder Conglomerate overlies the unconformity and is depositionally contiguous across the fault trace. The geometry of the Boulder Conglomerate comprises stratiform megabreccia units which are interbedded with laminated argillaceous calcarenite-calcsiltite; the latter are collectively referred to here as the *interbeds* . Both the Boulder Conglomerate and interbeds infill depressions in the unconformity and as such are of limited lateral extent: the margins of these beds pinch out. Successive beds, both breccia units and interbeds, exhibit greater lateral continuity and can be traced over horizontal distances of up to 50 m.

The dip of the bedding is subhorizontal. The thicknesses of both the interbeds and breccia units vary laterally. Interbed thickness varies from 0 m to 1.5 m. Reduced thicknesses of the interbed occur in association with i) topographic highs on the unconformity, ii) concave, erosive bases of the breccia units, iii) the protrusion of outsized clasts from the upper and basal contacts of the breccia units. The contact of the breccia unit with the interbeds is charaterised by the development of a bedding-parallel shear zone within the interbed (Photo. 28).

Fining upwards grading within the interbeds produces graded laminae up to 5 mm thick (Photo. 29). Grain size grades from medium sand (calcarenite) to silt (calcsiltite). The only identifiable grains are angular bioclast fragments and rare siliciclastics. The dark brown colour is a function of the argillite content. The interbeds are characterised by the intense development of concretions (Photo. 28). Laminae in the interbeds is deflected about the concretions; the concretions contain relatively uncompacted sediments and the edge of the concretions exhibit the incipient development of stylolites (Photo. 30). Shearing of the interbeds has resulted in rotation of the concretions within a matrix of plastically-deformed argillaceous calcarenite (Photo. 28). The occurrence of mineralisation associated with the concretions and the implications for its lithostratigraphic timing are considered in detail in Chapter 11.

The geometry of the breccia beds is a series of stacked lenses of varying lateral extent. The bases of the beds are concave up. Individual beds lie with erosive contact on the underlying breccia and/or argillaceous calcarenite. In the absence of interbeds, successive breccia beds are difficult to define owing to their similar morphology. Two breccia types were recognised:

i) Polymict breccia: Shaley Pales, Pale Beds, Waulsortian Limestone and ore are present as granule to boulder-sized clasts (Photos. 31 and 32). The petrography of the ore boulders is considered in Chapter 9. The breccia unit is very poorly sorted, with clasts up to 8 m wide, and is clast supported. Matrix is either rare or absent. Where present, matrix is represented by argillaceous calcsiltite and/or a composite of degraded limestone and ore, siliciclastic and diagenetic sand grains and argillite (Photos. 33 and 34). The contact of the polymict breccia with underlying interbed is marked by a thin zone of plastic interpenetration of these two matrix types (Photos. 35 and 36). The occurrence of mineralisation in the matrix is related to the petrography of the P.B.O. in Chapter 7; the implications of the reworked mineralisation for the lithostratigraphic timing of the C.G.O. are discussed in Chapters 9 and 11.

ii) Pale Beds breccia: infills depressions in the unconformity and attains local continuity where the unconformity is level. The bed(s) are composed of sub-rounded cobbles and boulders of oolitic limestone. The breccia is clast-supported and matrix-deficient, although argillaceous calcarenite-calcsiltite from the overlying interbed infills the irregular top surface and has percolated downwards into the upper level of this open--textured breccia.

The Boulder Conglomerate is deposited unconformably against the T Fault scarp. The contact of the Boulder Conglomerate with the fault plane is sharp (Photo. 13). The breccia immediately above the fault possesses a sheared, fault-parallel fabric. This tectonic deformation is manifested microscopically as the alignment of the matrix at clast edges (Photo. 37).

Interpretation

The Navan Group autochthon, Waulsortian Limestone and ore were reworked in variable proportion as rock avalanches. Deposition of the Boulder Conglomerate post-dated the major displacement on the T Fault which exposed the Navan Group in its footwall: the Boulder Conglomerate was deposited unconformably in the half graben defined by the T Fault. Short, southwards transport distance is proved by the para-autochthonous depositional site/local source of the Boulder Conglomerate and its textural immaturity. The deposition of the Boulder Conglomerate as a megabrecia within the regional slump scar created by catastrophic collapse of the slope is in accordance with Mullins et al. (1986). These authors described the "landward retreat of precipitous, high relief carbonate escarpments" which were generated in response to "catastrophic slope failure". The intraslope basin was the depositional site for "megabreccia debris sheets" derived from failure of the steep canyon-like walls.

Reworking of the Waulsortian Limestone as clasts within the rock avalanches proves that the development of Boulder Conglomerate occurred after the deposition of the stratigraphically highest lithofacies of the A.B.L. Group. By extrapolation, the catastrophic extensional tectonism which exhumed the autochthon and created the depositional setting of the Boulder Conglomerate must also have post-dated the deposition of the Waulsortian Limestone. This conclusion is supported by the tectonic and depositional absence of the A.B.L. Group in the hanging wall of the T Fault.

Reworking of the Waulsortian Limestone to the exclusion of stratigraphically older facies of the A.B.L. Group proves that the underlying sequence was not intersected by the structural level

unconformity in the source region of the Boulder Conglomerate. The absence of the sub-Waulsortian Limestone lithologies is interpreted as a result of the structural control on the stratigraphic distribution of the A.B.L. Group. Photo. 38 shows the intersection of Waulsortian-type limestone overlying the Pale Beds to the north of Zone 2. The limestone is petrographically identical to the Reefoid Argillaceous Bioclastic Limestone described in Chapter 4 (Photos. 4 and 6). Interbedding of reworked bioclastic limestone with in-situ bioclastic limestone and argillite confirms the Waulsortian affinity and excludes its interpretation as Boulder Conglomerate. The bedding of the limestone is sub-perpendicular to the vertical drillcore axis, indicating a sedimentary palaeodip. The absence of the Argillaceous Bioclastic Limestone is interpreted as depositional: the stratigraphic transition to increasingly limestone-rich strata resulted in the onlap of the Waulsortian onto the locally subsided autochthon.

Failure of the basin walls generated rock avalanches which were transported southwards. The avalanches decelerated rapidly on reaching the basin floor and came to rest. Early deposition infilled depressions in the unconformity. Succeeding beds developed greater lateral continuity as sediment supply increased and a level substrate was created. Channelisation of the rock avalanches is indicated by their erosive bases and stacked depositional geometry: the half graben was the locus of deposition for multiple avalanches.

The interbedding of the breccia units with argillaceous calcarenite-calcsiltite proves the episodic nature of the reworking. The interbeds represent the background hemipelagic sedimentation and record protracted periods of uninterrupted, low energy deposition. The variation in thickness of the interbeds is a function of:

i) irregularity of the unconformity,

ii) irregularity of the underlying breccia bed owing to its poor sorting, and

iii) erosion by the succeeding breccia.

Early, i.e. seafloor diagenesis is indicated by:

i) the preservation of hemipelagic sediment as interbeds to the breccia units. Completely unlithified sediment would be plastically deformed and reformed as matrix to the succeeding breccia: evidence for this is limited and is restricted to upper structural, and probably stratigraphic, level of the underlying interbed.

ii) the development of concretions with early diagenetic signature.

The paucity of matrix to the breccias indicates that the Navan Group autochthon and Waulsortian Limestone were in an advanced state of lithification. Production of matrix resulted from:

i) downward percolation of hemipelagic sediments into the upper level of the breccia substrate;

ii) reworking of unlithified siliciclastic and diagenetic sand and argillite in association with the rock avalanches;

iii) erosion of the hemipelagic sediments by the rock avalanches.

Post-depositional extensional tectonism is represented by shearing of the Boulder Conglomerate against the T Fault scarp. The effects of relative movement between the breccia units are demonstrated by the development of sheared lithological contacts. Evidence for tectonism during early diagenesis is provided by the rotation of concretions within a plastic matrix.

Post-depositional displacement on the T Fault is minor and is proven by the subhorizontal, i.e. palaeodip of the Boulder Conglomerate and its interbeds. Regional tilting of the autochthon to the southwest evidently occurred prior to the deposition of the Boulder Conglomerate

and represents an earlier phase in the extensional tectonism. It is speculated that this tilting triggered the delamination of the Shaley Pales.

5A.2.2 1330 CGO

Description

The Boulder Conglomerate exposed on 1330 level is deposited unconformably against the T Fault scarp. The exposure is 15 m vertically above the Boulder Conglomerate exposed in 1315 CGO. Boulders of Waulsortian Limestone, up to 12 m long, and cobble to boulder-sized clasts of bioclastic limestone occur in a matrix of carbonate mud (Photos. 39 and 40). The breccia is clast supported. The appearance is chaotic and structureless: no bedding or depositional structure could be distinguished.

Interpretation

Lithified Waulsortian Limestone and bioclastic limestone and carbonate mud were reworked into the half graben depositional site defined by the T Fault. The chaotic structure and textural immaturity are characteristic of locally derived and rapidly deposited debris flow(s).

The Boulder Conglomerate on 1330 Level is 15 m above that exposed on 1315 Level. The vertical transition from matrix-deficient, polymict and Pale Beds breccia types to Waulsortian Limestone and bioclastic limestone breccia implies a change of source and/or sedimentation patterns. This is consistent with the incorporation of contemporaneous carbonate mud as matrix.

5A.2.3 1285 Block 40 HWD

Description

Fig. 10 shows the underground mapping from 1285 Block 40 HWD. The steep dip of the strata here afforded exposure of the full stratigraphic extent of the Boulder Conglomerate. The Boulder Conglomerate is deposited unconformably over 7 m of Shaley Pales. The Shaley Pales overlie the basal Navan Group with faulted contact. The Shaley Pales are sheared and possess a fault-parallel fabric. The unconformity is irregular and possesses up to 1 m of relief developed where inflections into the unconformity are associated with large boulders in the overlying Boulder Conglomerate. The Boulder Conglomerate is characterised by three distinct lithofacies: in ascending stratigraphic order these are represented by:

1) Pale Beds and Waulsortian Limestone breccia

Up to 18 m of Pale Beds and Waulsortian Limestone breccia overlie the Shaley Pales with a sharp contact. The breccia is clast supported. Sorting is extremely poor with clast size ranging from granule to boulder. The structure of the breccia units is chaotic: sub-rounded Waulsortian Limestone boulders, up to 8 m in diameter, occur in juxtaposition with smaller fragments of Waulsortian Limestone, Pale Beds and ore (Photo. 41). The significance of the latter with regard to the lithostratigraphic timing of the mineralisation is dealt with in Chapter 9.

There are two grades of matrix: coarse and fine. The coarse matrix comprises angular granules and pebbles of oolite (Photo. 42). The fine matrix is composed of comminuted limestone, siliciclastic sand and argillite (Photo. 42). Arenaceous "clasts" exhibit plastic deformation by adjacent Pale Beds and/or Waulsortian Limestone clasts. Their amoeboid

shapes render them transitional between clast and matrix (Photos. 43 and 44).

Bedding within this lower facies of the Boulder Conglomerate is exhibited by the presence of an argillaceous interbed to the breccia units. The interbed varies in thickness from 0 m to 4 m. It is concretionary and contains scattered cobbles. The basal contact of the interbed is defined by the upper, irregular surface of the lower megabreccia unit. The upper contact is defined by the erosive base of the succeeding megabreccia.

2) Carbonate Mud

This lithofacies overlies the Pale Beds and Waulsortian Limestone breccia and is associated with pyrite. The occurrence of non-pyrite lithologies were noticed and sampled extensively. This permitted the identification of primary and reworked sediments.

Two sub-lithofacies were identified. In ascending stratigraphic order, these are represented by:

a) bioclastic carbonate mud (Photo. 45). This sub-lithofacies directly overlies the Pale Beds and Waulsortian Limestone breccia. The contact is sharp but irregular as it is defined by the upper surface of the Lithofacies 1. Bedding is defined by bioclastic laminae within the carbonate mud (Photo. 46). The bioclasts are represented by ostracods, calcispheres and bryozoa fragments. Stylolites within this sub-lithofacies are bedding-parallel. Pyritisation of Lithofacies 2a) is stratiform and occurs as selective replacement to the bioclastic horizons (Photo 46).

b) brecciated pyrite and limestone in a matrix of carbonate mud and argillite. The carbonate mud matrix predominates and supports cobble--sized clasts of oolite (Photo. 47), angular clasts of pyrite, mudstone intraclasts and crinoid ossicles (Photo. 48). The pyrite clasts possess a

laminated and or stalactitic fabric which are truncated and rotated. The subordinate argillite matrix exhibits plastic interpenetration with the carbonate mud.

The precise contact between a) and b) could not be discriminated owing to the common occurrence of pyrite and its highly oxidised state.

3) Pyrite breccia

The stratigraphically highest lithofacies of the Boulder Conglomerate is represented by clast-supported pyrite breccia. Boulders of pyrite possess long and tangential clast contacts and are delineated by a matrix composed of pyritic argillite (Photo. 49). The boulders are composed of either massive or laminated pyrite; the latter exhibit truncation of the laminae at the clast edge.

Interpretation

Vertical displacement of the Navan Group autochthon in the mine area produced a major omission of the stratigraphy: only 4 m of Pale Beds have been preserved in the footwall, indicating a vertical displacement of c.200 m. The structure across which this stratigraphic omission occurs is the T Fault. The shearing of the hanging wall Shaley Pales is attributed to the extensional faulting. The upper level of the Shaley Pales corresponds to the tectonically-created submarine unconformity. Deposition of the Boulder Conglomerate erosively modified the unconformity. This was facilitated by the incomplete lithification of the Shaley Pales, as shown by the loading effects of megaboulders (Figure 10).

Deposition of lithostratigraphically early Boulder Conglomerate is represented by chaotic, texturally immature rock avalanches. These were

locally-derived from the fault-exhumed autochthon and Waulsortian Limestone: the depositional site of the Boulder Conglomerate is para-autochthonous and proximal to the A.B.L. Group. The high energy of the avalanches is indicated by the comminution of the clasts into the matrix. Degradation was facilitated by the presence of sublithified clasts, characteristically the siliciclastics. The Navan Group autochthon was, therefore, heterogeneously lithified: pre-Boulder Conglomerate calcite cementation was selectively associated with the oolitic and bioclastic lithologies.

The episodic nature of the brecciation is proven by the deposition of the thick argillaceous interbed on the irregular top surface of the lower megabreccia. Poor sorting of this lower breccia unit resulted in primary thickness variations of the interbed. Continued reworking is indicated by the presence of lonestone clasts in this hemipelagic interbed. Significant upslope relief on the unconformity/fault scarp is invoked as providing the necessary topographic head to incorporate these outsized clasts.

Incursion of the succeeding megabreccia eroded the argillite and enhanced the primary, depositional thickness variations. The argillite was incorporated into the matrix of the breccia. Partial lithification of the argillite is suggested by development of early diagenetic concretions and its remnant preservation after the megabreccia deposition.

Deposition of carbonate mud indicates a marked change in the sediment supply. Stratigraphically early carbonate mud (Lithofacies 2a) contains evidence for bedding and is interpreted as the product of primary deposition. The pyritised carbonate mud was remobilised and locally deposited (Lithofacies 2b). The mobile carbonate mud behaved thixotropically, transporting Pale Beds cobbles and ripping up the contemporaneous seafloor to produce pyrite and argillite intraclasts.

Unlithified argillite was plastically admixed with the carbonate mud and proves the existence of two types of unlithified, coeval sediment. The source of the Pale Beds cobbles is equivocal: they could be the product of primary erosion of the Navan Group autochthon or reworking of pre-existing Boulder Conglomerate by the carbonate mudflow.

Lithofacies 3) provides evidence for the reworking of a massive pyrite substrate and represents the final event in the depositional history of the Boulder Conglomerate exposed in 1285 Block 40 HWD.

5A.2.4 1330 348S

Description

The upper stratigraphic level of the Boulder Conglomerate was exposed in 1330 348S. It is associated with massive pyritisation, but there were sufficient relict sediments to determine the primary depositional relationships.

The exposure revealed:

i) laminated argillaceous siliciclastic silt (Photo. 50).

ii) mudstone pebble breccia. It is clast supported with minor argillaceous silt matrix (Photo. 51). The matrix is petrographically equivalent to i). The breccia is associated with cobbles of oolite and bioclastic limestone and rare pebbles of sphalerite and galena (Photo. 52).

iii) carbonate mud supporting mudstone pebbles and rounded, bioclastic limestone cobbles (Photos. 53 and 54). The association of stratiform and stratabound pyrite with the carbonate mud is described in detail in Chapter 10.

iv) reworked pyrite and subordinate sphalerite.

v) rhythmically laminated argillite and calcarenite: the Thinly Bedded Unit.

The depositional configuration of i) to iii) is an interbedding (Photo. 55). Bed thickness ranges from decimetre to metre. The effects of boudinage create lateral variations in bed thickness and contiguity owing to the pinch and swell geometry of the bedding. In the most extreme cases, carbonate mud boudins boudins are isolated within i) and/or ii) [Photo. 56]. The basal contact of the micrite beds are characterised by load structures: argillaceous silt is injected into the overlying carbonate mud with flame-like morphology (Photo. 53).

The distribution of Lithofacies iv) is laterally impersistent and confined to the upper stratigraphic level of the Boulder Conglomerate. It comprises a reworked assemblage of pyrite interlayered with subordinate sphalerite and argillite. The clasts and matrix are petrographically equivalent, but are distinguished by their different rheologic-controlled morphologies. The assemblage exhibits a wide range of material behaviour. These are represented by: incipient brittle failure and ductile attenuation (Photo. 57), convolute folding (Photo. 58), and brecciation (Photo. 59).

The Thinly Bedded Unit is deposited over the Boulder Conglomerate and comprises interlayered shale and calcarenite. Bedding is sharply defined and parallel-sided. Evidence for synsedimentary tectonism is represented by extensional microfaults (Photo. 60).

Diamond drilling into the footwall of the C.G.O. intersected clasts of ore in the lower stratigraphic level of the Boulder Conglomerate. The depositional substrate of the Boulder Conglomerate is the Muddy Limestone. The sulphide clasts are represented by pebble-sized fragments of vein-type ore which are clearly truncated at the clast margin (Photos. 61 and 62). The petrography of these clasts and their relationship to the P.B.O is described in Chapter 9.

Interpretation

The Boulder Conglomerate in 1330 348S proves that the Navan area was the depositional focus for sediments produced in a variety of environments.

The deposition of argillaceous silt indicates hemipelagic sedimentation of terrestrially-derived sediments: the Lower Palaeozoic basement was exposed in an unrecognised location to the north.

Hemipelagic deposition was interrupted by the incursion of mudstone breccias in association with reworked limestone and sulphide breccia. The argillaceous silt was eroded and redeposited as matrix. The mudstone pebbles represent intraclasts and indicate reworking of the seafloor, probably related to the event which brecciated and transported the limestone and ore as lithoclasts.

High energy, carbonate mud debris flows eroded the seafloor and entrained the mudstone as intraclasts. Limestone lithoclasts were incorporated en route and supported by the thixotropic carbonate mud. The debris flows were deposited as a series of event beds which interrupted the hemipelagic sedimentation. Rapid deposition of the debris flows and unlithified state of the intraclastic hemipelagic substrate are indicated by the development of basal loading structures.

The effect of post-depositional extensional tectonism is proven by the development of boudinage. The argillaceous interbeds were incompetent and accommodated the boudinage by enveloping the carbonate mud.

The configuration of slump-folded and brecciated interlayered pyrite, sphalerite and argillite overlain by the relatively undisturbed T.B.U. is characteristic of synsedimentary reworking and deformation (Collinson and Thompson, 1982). Stratiform pyrite-sphalerite in

association with laminated argillite was subjected to lateral mass movement and redeposited basinwards above the pyritised seafloor substrate. Mineralisation was pre-slumping: the sulphides were precipitated during sedimentation and remobilised prior to the deposition of the Thinly Bedded Unit. Tectonism and/or sedimentary instability associated with the development of dense, sulphide-rich sediments caused the detachment of the predominantly unlithified substrate and initiated transport. Competent pyrite was brecciated and became admixed with unlithified pyrite, sphalerite and argillite. The transitional character of the deformation is proved by the development of fractures across plastically attenuated pyrite strata. Unlithified stratiform pyrite, sphalerite and argillite were rotated and became entwined. Transport ceased when the sulphide slump experienced compressive stress: the incompetent pyrite-argillite strata were deformed into a series of slump folds.

Evidence for the reworking of sulphide mineralisation prior the events described above is provided by the occurrence of ore fragments throughout the stratigraphic extent of the Boulder Conglomerate. Reworking of mineralisation occurred, therefore, during the entire depositional history of the Boulder Conglomerate. Syn-sedimentary extensional tectonism is regarded as the mechanism which enabled the continuous supply of coeval sediments and lithoclasts into the graben structure defined by the T Fault. This is confirmed by the ubiquitous presence of synsedimentary/early diagenetic extensional deformation features exhibited by the Boulder Conglomerate and T.B.U.

Section B. SEDIMENTOLOGY OF THE THINLY BEDDED UNIT

5B.1 Introduction

The Thinly Bedded Unit (T.B.U.) is stratigraphically located between the Boulder Conglomerate and the base of the Upper Dark Limestone. It is distributed over the mine area and varies in thickness from 0 to 20 m. Maximum thickness of the T.B.U. is developed in the graben structure defined by the T Fault.

5B.2 The Thinly Bedded Unit exposed in 1345 348N

Description

The T.B.U. comprises calcarenite interbedded with laminated shales (Figure 11). Individual bed thickness of these lithologies ranges from 1 mm to 10 cm. The calcarenite beds are composed of well-sorted, bioclastic and pelletal sand of fine and medium grade. Recognisable bioclasts include forams and calcispheres (Photo 63). On the exposure scale, the beds are sharply defined and laterally continuous.

Deviations from the rhythmic interlayering of the shale and calcarenite are rare. In 1345 348N, a 15 cm-thick, erosive-based, fining upward limestone bed was located 1.5 m above the hanging wall of the C.G.O. and was distinguished by its petrographic dissimilarity and its association with sulphide mineralisation. The contact of this bed with underlying shale in the T.B.U. is sharp though with load structures. The composition of the limestone is dominated by ooids and skeletal grains. The ooid nuclei are represented by sand-sized carbonate grains (Photo. 64). Quartz and feldspar sand grains are a minor component. The bioclastic assemblage is diverse and is represented by forams, bryozoa, crinoids, brachiopods, and echinoids.

The bed is poorly sorted with an overall fining upward grading. Grading is petrographically-defined: the basal 3 cm comprises i) disarticulated, fragmented and abraded bryozoa, crinoids, brachiopods and echinoids of pebble and granule size, ii) mudstone pebbles and iii) ooids (Photo 65). The bed exhibits a vertical transition upwards into closely packed calcarenite, comprising ooids and biodebris (Photo. 66). The calcarenite portion of the fining upward bed supports occasional granule to pebble-sized clasts: these are represented by bioclasts, mudstone clasts and plant fragments (Photo. 67). Neil Clarke (pers. comm., 1995) identified the plant matter as having been derived from a Lower Carboniferous swamp environment.

Evidence for extensional deformation of the T.B.U. is pervasive and visible on all scales of observation. On the smallest scale, extensional microfaults vertically offset laminae by <5 mm (Photo. 68). The erosive-based, graded limestone bed and the adjacent T.B.U. macroscopically exhibit the effects of extensional deformation. These are represented by: i) pull-apart and dewatering structures (Photo. 69), ii) boudinage and/or convoluted bedding (Photos. 70 and 71), and iii) bed-scale normal faulting (Photo. 72). The lithostratigraphic timing of the mineralisation associated with the deformed strata is considered in Chapter 11.

Interpretation

Deposition of the T.B.U. records the oscillation between argillite and bioclastic-pelletal calcarenite. The erosive-based, fining upward oolitic-bioclastic bed is interpreted as an event bed which interrupted the deposition of the T.B.U. The event bed is petrographically equivalent to the limestone strata of the Upper Dark Limestones (U.D.L.). The U.D.L. stratigraphically overlies the T.B.U. and interpreted as calcturbidites

(Marchant and Sevastopulo, 1980). The event bed is interpreted, therefore, as heralding the incursion of calcturbidites into the Navan area of the Dublin Basin during the deposition of the T.B.U. The scoured base, sole structures, fining upwards grading and presence of mudstone intraclasts indicate high energy transport and rapid deposition on an unlithified substrate. The event bed demonstrates the features which characterise the Bouma A division and is in accordance with the interpretation of Marchant and Sevastopulo (1980).

The presence of ooids in the event bed provides evidence for the precipitation of calcium carbonate in a wave-swept, shallow marine environment. This is confirmed by the reworking of carbonate matter as ooid nuclei. The enviroment of ooid production must have been palaeogeographically intermediate between the contemporaneous basin floor in the Navan area and the afforested landmass which supplied the plant fragments. Evidence for continued exposure of the Lower Palaeozoic basement is provided by the occurrence of siliciclastic grains. Erosion of the basement was limited and is indicated by the paucity of siliciclastics in the event bed. This is supported by the development of ooids around carbonate sand grains.

The continuation of extensional deformation during the deposition of the T.B.U. is proved by the development of synsedimentary normal faults, boudinage and convoluted strata. The deformation occurred during early diagenesis and is proved by the plastic state of the sediments and the presence of dewatering structures. Microscopic evidence for delay in the diagenesis is provided by the close packed, i.e. compacted, texture of the event bed. The development of convoluted bedding is interpreted as intraformational owing to its association with the boudinage and the contiguity of the deformation in adjacent strata.

Section C. TECTONO-SEDIMENTARY SYNTHESIS OF THE BOULDER CONGLOMERATE AND THINLY BEDDED UNIT

Figure. 12 shows a composite graphic log of the Boulder Conglomerate, Thinly Bedded Unit and Upper Dark Limestone. The Boulder Conglomerate is lithostratigraphically subdivided into Lower, Middle and Upper units. The Lower Boulder Conglomerate is characterised by erosive-based breccia units interbedded with concretionary argillaceous calcarenite-calcsiltite. Lateral persistency of both bed types is related to the amount relief on the depositional substrate: early deposition infilled irregularites in the seafloor unconformity and permitted increased lateral distribution of subsequent strata. The erosive, concave-up bases of the breccia beds and their vertically stacked depositional geometry suggests that the T Fault half graben was the locus of deposition for multiple reworking events.

The breccia beds of the Lower Boulder Conglomerate exhibit the characteristics of rock avalanches: chaotic structure, textural immaturity, matrix deficiency, hummocky surface and deformed substrate (Yarnold, 1993). The absence of volumetrically significant matrix rules out the interpretation of the Lower Boulder Conglomerate as a debris flow complex.

The stratigraphic composition of the clasts in the Lower Boulder Conglomerate comprises Navan Group and Waulsortian Limestone lithologies. Clasts of ore are represented by reworked vein-type and layered mineralisation. The ore fragments are reworked in association with an unlithified matrix composed of diagenetic and detrital sand and argillite.

The composition of the Lower Boulder Conglomerate reflects reworking from local stratigraphy: failure of the fault scar resulted in

reworking of the Navan Group autochthon. Boulders of Waulsortian Limestone were locally reworked from the upper stratigraphic and structural level of the A.B.L. Group. The sedimentology of the individual rock avalanches ranges from monomict (Navan Group only) to polymict (Navan Group and A.B.L. Group) with clast size ranging from granules of comminuted limestone to boulders up to 8 m in length. Correlation of the clast composition with the stratigraphy exposed in the fault scarp and sedimentary immaturity exhibited by the Lower Boulder Conglomerate suggest that the depositional site was fault-controlled and para-autochthonous.

The presence of Waulsortian Limestone clasts in the lithostratigraphically earliest Boulder Conglomerate proves that reworking into graben defined by the T Fault post-dated the deposition and cementation of the Waulsortian Limestone. The graben structure in which the Boulder Conglomerate was deposited is interpreted to have formed after the deposition of the A.B.L. Group. Evidence for the deposition of the A.B.L. Group after an earlier phase of extension-induced mass movement is demonstrated by the deposition of the Argillaceous Bioclastic Limestone over delaminated Shaley Pales. Deposition of the A.B.L. Group within an early sub-basin is proved by the onlap of Waulsortian Limestone onto the mass wasted autochthon. The T Fault represents a later phase of extension. It intersects the autochthon beyond the depositional extent of the A.B.L. Group.

Reworking of the local stratigraphy was episodic and is proved by the deposition of hemipelagic interbeds. The preservation of these interbeds after erosion by subsequent rock avalanches indicates partial lithification. This is confirmed by the development of early diagenetic concretions. Plastic, i.e. soft sediment, deformation of the interbeds is

restricted to a thin zone of plastic entrainment at the base of the breccia beds in which the matrix sediment and substrate sediment exhibit interpenetration textures.

Extensional tectonism after the deposition of the Lower Boulder Conglomerate caused negligible displacement relative to that which tilted and exhumed the Navan Group in the footwall of the T Fault. This is confirmed by the subhorizontal dip of the 1315 CGO which is interpreted as approximating the palaeodip. The effects of post-depositional deformation are manifested as the shearing of the Boulder Conglomerate against the T Fault and the development of slip planes at the contacts of the breccia beds with the hemipelagic interbeds. Evidence for the early diagenetic timing of this deformation is provided by the rotation of the concretions within the interbeds: the unconcreted sediment was compacted, but unlithified and responded plastically.

The Middle Boulder Conglomerate, with its clast-supported fabric and carbonate mud matrix, records a change in the sedimentology of the Boulder Conglomerate. The presence of coeval carbonate mud as matrix to the breccia dictates its interpretation as a debrite. The source of the matrix is unrecognised, but is possibly related to the Waulsortian Limestone lithofacies of the A.B.L. Group. Petrographic analysis of the A.B.L. Group in the Navan area proved the occurrence of carbonate mud (Chapter Four). Study of the Waulsortian Limestone in the Galmoy area demonstrated the existence of carbonate mud in the "Supra-Waulsortian" lithofacies of this fault-controlled "mudbank" (Doyle and Bowden, 1995).

The Upper Boulder Conglomerate is divided in ascending stratigraphic order into sub-lithofacies A and B. Lithofacies A comprises clast-bearing carbonate mud interbedded with laminated, hemipelagic

argillite-siltite. The former are interpreted as low density debrites. Increase in the ratio of carbonate mud to clasts relative to the Middle Boulder Conglomerate indicates a decrease in the reworking of lithified stratigraphy during an increase in the production and/or supply of carbonate mud.

The erosive nature of the debris flows and their viscous rheology are proved by the presence of intraclasts and lithoclasts, and their matrix-support fabric, respectively. Plastic admixing of the carbonate mud with argillite proves that the debris flows were deposited prior to the lithification of a variety of sediment substrates: remobilisation was synsedimentary. Rapid deposition and "freezing" of the carbonate mud is indicated the development of soft sediment loading structures and the matrix support fabric, respectively.

The presence of intraclastic mudstone beds and/or outsized lithoclasts within the hemipelagic interbeds proves that reworking also occurred during a lull in the reworking of carbonate mud. Ore fragments in these breccia beds provide evidence for the continued reworking of mineralisation.

Evidence for the effects of post-depositional extensional tectonism prior to the lithification of Lithofacies A is provided by the development of boudinage associated with the carbonate mud beds.

Lithofacies A is characterised by the association of pyrite with the carbonate mud. Pyrite occurs as replacement to in-situ carbonate mud and as fragments supported by a plastically-deformed carbonate mud matrix. The presence of pyrite fragments which are petrographically equivalent to the pyrite developed as replacement to the carbonate mud debris flows provide evidence for secondary remobilisation of pyritised, but unlithified Boulder Conglomerate. It is possible that the remobilisation

event was related to the extensional tectonism which caused the boudinage.

Lithofacies B is consistently represented by clasts of pyrite--sphalerite-argillite reworked in association with a pyrite-sphalerite--argillite matrix. The rheological properties exhibited by the pyrite--sphalerite-argillite range, therefore, from brittle fragments to unlithified matrix. Both the clasts and matrix possess a layered morphology. This assemblage is interpreted, therefore, as having been locally reworked from a variably lithified, stratiform pyrite-sphalerite-argillite substrate. Reworking is likely to have been induced by active extensional tectonism operating on a dense, unlithified substrate.

The contact of the T.B.U. with the Boulder Conglomerate is sharp and signifies the end of Boulder Conglomerate deposition/remobilisation. Sedimentation of the T.B.U. is represented by the deposition of pelletal-bioclastic calcarenite alternating with shale to produce rhythmic interlayers with sharp contacts. The monotonous interbedding was interrupted by the deposition of an erosive-based, fining-upwards oolitic limestone bed. The latter is petrographically equivalent to the U.D.L. and represents a single Bouma A type depositional event. It is interpreted as an event bed which heralds the incursion of the calcturbidites which were to ultimately fill the Dublin Basin.

The ooid content of the event bed proves the presence of a wave-swept, shallow marine environment. Evidence for contemporaneous subaerial conditions is provided by the reworking of plant fragments from a swamp-type source in association with the event bed. Erosion of the Lower Palaeozoic basement, however, was limited and is manifested as the minor siliciclastic content of this bed. This is consistent with the

lack of energetic fluvial reworking which characterise modernday swamps.

The T.B.U. exhibits extensional deformation of incompletely lithified sediments as manifested by synsedimentary normal faults, boudinage/convoluted bedding and dewatering structures. Continued extensional deformation of the sediments deposited in the graben structure defined by the T Fault confirm the tectonic control of the depositional site.

Compressive deformation of the entire Lower Carboniferous stratigraphy within the A-C-D Fault Complex was the result of the basin inversion during the Variscan Orogeny. The palaeodip of the Boulder Conglomerate exposed in Zone 2 proves that the Lower Carboniferous stratigraphy to the northwest of the A Fault was unaffected by the compression which caused deformation of the stratigraphy within the fault zone. It is possible that the extensional tectonism which ruptured the Navan Group autochthon, thereby creating the depositional site of the Boulder Conglomerate, and the compressional tectonism which resulted in the inversion of this palaeobasin were both focussed on the same crustal lineation(s).

CHAPTER SIX. INTRODUCTION TO THE NAVAN OREBODY

The Navan Orebody is a carbonate-hosted Zn-Pb deposit with total reserves of 69.9 million tonnes combined zinc and lead (Ashton et al., 1986). Mineralisation is divided into the autochthon-hosted Pale Beds Ore (P.B.O.) and the allochthon-hosted Conglomerate Group Ore (C.G.O.). The terms are non-specific with regard to age, character and mineralogy of the mineralisation.

Ninety seven percent of the ore is hosted by the autochthon; average grades are 10.1% Zn (as sphalerite: ZnS) and 2.6% Pb (as galena: PbS). The remaining 3% is represented by the C.G.O. and has average grades of 12.2% Zn and 2.5% Pb. The mineralogy of the C.G.O. is distinct from the P.B.O. Average pyrite (FeS_2) content of the C.G.O. is 23% , with local values up to 50%. Dolomite ($CaMg[CO_3]_2$) occurs as major replacement to the Navan Group and is part of the P.B.O. hydrothermal mineral assemblage (Rizzi, 1992), but is a minor component of the C.G.O. The distribution of ore in the Boulder Conglomerate comprises a lower sphalerite and galena-rich lens and an upper pyritic lens with subordinate sphalerite and galena.

The aspect of the research considered here concentrated on elucidating the morphology, mineralogy and lithostratigraphic timing of the C.G.O. in relation to the overall metallogenesis. The $\delta^{34}S$ isotopic signature of the C.G.O. is compared to the $\delta^{34}S$ survey of the P.B.O. by Anderson (1990).

The Boulder Conglomerate represents a sample of the reworked autochthon, the A.B.L. Group and the contemporaneous sediments. It provides the tectono-sedimentary reference stratum to which the metallogenic evolution of the Navan Orebody can be related. Three

testable hypotheses were constructed to characterise the lithostratigraphic timing of the mineralisation. The predictions of each hypothesis were tested against the evidence afforded by the C.G.O.

6.1 *Hypothesis One: the C.G.O. mineralisation was entirely post-Boulder Conglomerate*

Predictions

There will be no reworked P.B.O. The C.G.O. will not be reworked and will have no early diagenetic signature. Mineralisation should cut across the unconformity. There will be evidence for mineralisation and/or alteration in the fault zones.

6.2 *Hypothesis Two: the C.G.O. mineralisation was entirely pre-Boulder Conglomerate*

Predictions

Mineralisation in the Boulder Conglomerate will only occur as reworked fragments. The ore breccia will be petrographically identical to the P.B.O. The unconformity will truncate the mineralised autochthon, and the proportion of reworked ore in the Boulder Conglomerate will be maximum in the half graben created by the T Fault.

6.3 *Hypothesis Three: Mineralisation occurred syn-Boulder Conglomerate*

Predictions

Ore textures will be controlled by the diagenetic state and fabric of the autochthon and contemporaneous sediments. There will be unequivocal evidence for early diagenetic mineralisation in the Boulder Conglomerate. The C.G.O. and P.B.O. are reworked. The thermo-chemical conditions affecting the Boulder Conglomerate will be different to those

of the autochthon: this difference will be manifested mineralogically and isotopically.

Before presenting the evidence, the character of the mineralisation in the Navan Group and A.B.L. Group are described in Chapters 7 and 8, respectively.

CHAPTER SEVEN. MINERALISATION IN THE NAVAN GROUP

7.1 GENERAL DESCRIPTION

Ore in the Pale Beds is distributed as five stratabound lenses with a stacked geometry (Figures 7 and 8). The configuration of the lenses is stratiform. Cross-cutting mineralisation is represented by large scale vertical coalescence of the lenses and local vein mineralisation. Coalescence of the lenses has produced mineable ore up to 70m thick (Ashton et al., 1995) and the intensity and extent of the P.B.O. mineralisation has rendered primary limestone subordinate in the mineralised autochthon. Sphalerite, galena and dolomite are the volumetrically significant hydrothermal minerals; pyrite and/or marcasite and barite are present locally. The sulphide mineralisation is present as massive, concordant replacement to limestone-rich strata in the Pale Beds and Micrite Unit. The ore is enveloped by the dolomitised autochthon. The dolomitisation possesses a NE-SW-trending, plume-shaped geometry and is interpreted by Rizzi (1992) as the product of fault-controlled, hydrothermal upwelling. The base metals were sequestered from the Lower Palaeozoic basement by crustal convection and the hydrothermal fluids converged upon the extended and fractured Navan Group autochthon (Mills et al., 1987). The development of ore-grade mineralisation and dolomitisation was lithologically-controlled, occurring as replacement to petrographically variable limestone (Anderson, 1990).

The flow of the hydrothermal fluids was concentrated along the lithological contacts presented by limestone-arenite or limestone-argillite. Stratiform caverns were created upon dissolution of the limestone and were the depositional site of laminated diagenetic sediment in association

with dissolutionally reworked siliciclastic grains and argillite. The sedimentary ore comprises sand-grade crystals of sphalerite, dolomite, galena, pyrite, and barite. The diagenetic-detrital laminae exhibit soft sediment deformation textures in association with autoclastically brecciated, mineralised limestone wall rock. The deformation of the diagenetic sediment by the collapsed roof ore is exhibited by loading and injection structures (Anderson, 1990).

7.2 MINERALISATION ASSOCIATED WITH AUTOCLASTICALLY BRECCIATED MICRITE UNIT AND PALE BEDS

7.2.1 Introduction

The P.B.O. is spatially associated with stratiform and stratabound breccia horizons in the Pale Beds and Micrite Unit (Anderson, 1990). Logging of the Boulder Conglomerate confirmed the presence of autoclastically brecciated Navan Group stratigraphy in the footwall of the fault scarp/unconformity. Ashton et al. (1992) refer to the tectonically modified autochthon as the "Close-packed Conglomerate" to reflect the jigsaw fit of the (auto)clasts and the defiency of matrix. Figure 13 shows the graphic log of a typical drillcore intersection of this breccia. The in-situ character of the Close-packed Conglomerate is proved by the preservation of the stratigraphy. Mineralisation is spatially associated with the Close-packed Conglomerate. The objective of this section is to present evidence regarding:

1) timing of the mineralisation in relation to the autobrecciation event(s),

2) factors responsible for mineralisation of the autochthon,

3) the chemical and physical effects of hydrothermal fluids on the autochthon.

The breccias are described according to their stratigraphic level

within the Navan Group autochthon. The subdivisions are:

i) the Micrite Unit,

ii) the lower and middle Pale Beds, and

iii) the upper Pale Beds.

Breccia-associated mineralisation within each of these intervals is described individually. The petrography of the breccias are characterised in accordance with Laznicka (1988): a population of larger size fragments, the **clasts**, is enveloped or infilled by a finer grained **groundmass**. The groundmass comprises particulate matrix and/or a chemically precipitated cement. The matrix *sensu stricto* should be composed of the clastic, fine-grained fraction, whereas the term cement *sensu stricto* refers to the chemically precipitated component. In hydrothermally altered and replaced rocks, such as the Close-packed Conglomerate, the terms converge owing to the presence of "diagenetic sediment" which is petrographically distinct from cement *sensu stricto*. The interclast fraction of the Close-packed Conglomerate is described collectively under the classification of **groundmass** and is interpreted according to its matrix *sensu lato* and cement *sensu stricto* characteristics.

The conclusions are presented as a synthesis in which considerations 1) to 3) are explained. Chapter 9 relates the petrography of the Boulder Conglomerate to the mineralisation associated with the Close-packed Conglomerate/P.B.O.

7.2.2 Previous work

The recognition of the association between mineralisation and the brecciated Pale Beds is not new. After extensive underground mapping of the tectonic-sedimentary-metallogenic relationships, Anderson (1990) interpreted the breccia-associated mineralisation as internally sedimented

within stratiform, hydrothermally-created karst during replacement of a partially lithified host (Figure 14). Rizzi (1992) rejected this, interpreting the mineralisation as the product of hydrothermal fluids exploiting subaerial, karren-type palaeo-emersion surfaces within fully lithified strata (Figure 15). Both authors, however, were in agreement as to the significance of the breccia-associated mineralisation to the development of the P.B.O. The respective claims of Anderson (1990) and Rizzi (1992) are critically evaluated in Section 7.4.

7.2.3 Breccia-associated mineralisation in the Micrite Unit

7.2.3.1 Breccia type A

Description

Clast petrography: Dolomitised pelletal micrite (Photo. 73); dolomite occurs as finely crystalline replacement; the dolomite crystals are non-luminescent.

Groundmass petrography: The groundmass is composite. The first phase comprises brown mud supporting sand to granule-sized clasts of dolomitised pelmicrite and crystals of dolomite (Photo. 74); the dolomite is non-luminescent.

The second phase is exclusively diagenetic and is represented by pyrite and/or calcite. Pyrite is developed as spherules or botryoids. The spherular pyrite is developed along the clast-groundmass interface and contiguously replaces both the clast and matrix (Photo. 75). The botryoids are developed along the margin of secondary fractures which bisect the groundmass (Photo 76). The wallrock limestone is corroded and the botryoids are developed along the fracture/vug margin (Photo 77). The botryoidal pyrite is locally spalled into the contemporaneous void and sparite occludes the remnant porosity (Photos. 77 and 78). Calcite also

occurs without pyrite as cement to secondary fractures which coincide with distribution of the mud-filled fractures (Photo 79). This calcite, however, differs from that which is associated with the botryoidal pyrite: i) the morphology of this calcite is fibrous and the orientation of the fibres is perpendicular to the fracture edge, and ii) the wallrock limestone is uncorroded.

Clast-groundmass relationship: Vertically impersistent fractures define an angular, clast-supported breccia (Photo. 76). The clast edges are sharp. The primary clast edges are discriminated by the mud groundmass. The pyrite-calcite exploits voids represented by secondary fractures and/or corroded oolite. The distribution of the fractures and solution voids coincides with the primary breccia fabric.

Interpretation

In-situ fracturing of the limestone resulted in migration of unlithified, overpressured mud and wallrock fragments as matrix into the fracture network. The Micrite Unit is characterised by the presence of mud interbeds and these are interpreted as the probable source (Photo. 80). This assumption is supported by the development of discordant, mud-filled fractures through limestone adjacent to muddy strata (Photo. 79). Inclusion of dolomitised wallrock in the dolomite-bearing mud proves i) pre-fracturing dolomitisation, ii) unlithified state of the mud and iii) a dilational (extensional) tectonic regime. Dolomite replaced the limestone strata and nucleated in the mud interbeds prior to its injection into the fractures.

Growth of pyrite post-dated injection of the dolomitic mud. Mineralising fluids exploited the clast-groundmass interface and precipitated spherular pyrite. Botryoidal pyrite nucleated in open space

following reactivation of the fracture network and/or dissolution of the limestone. Continued tectonism caused further reactivation and resulted in the brecciation of the pyrite. The remnant porosity was cemented by sparite. The association of pyrite with solutionally-enhanced fracture porosity implies that these particular mineralising fluids were corrosive to limestone.

The development of fibrous calcite as cement to secondary fractures furthermore proves i) syn-diagenesis extensional tectonism and ii) the distribution of secondary fracturing was controlled by the presence of an established breccia fabric.

7.2.3.2 Type B

Description

Clast petrography: Pelletal micrite. The limestone possesses a fenestral fabric; the infill to the fenestrae comprises geopetally deposited micrite with sparite occluding the remnant porosity; the geopetal structures are clearly overturned relative to the subvertical drillcore (Photo. 81). The limestone is heterogeneously dolomitised. The dolomite occurs as i) pervasive replacement by euhedral rhombs (Photo. 82), and ii) coarser, fracture-cementing subhedral rhombs (Photo. 83); the edges of the fractures are non-symmetrical and have an irregular, corroded appearance. The dolomitised micrite and fracture-lining crystals are shattered and overgrown by the succeeding dolomite zone. The overgrowth is contiguous with the cement to the microfractures (Photos. 82 and 83).

Groundmass petrography: Remobilised laminated diagenetic and detrital assemblage (Photo. 84). The diagenetic component is represented by i) fine sand grade, non-luminesecent dolomite grains, and ii) pyrite as

disseminations and brecciated laminae. Detrital sediment is represented by siliciclastic silt and sand, mud and clasts of dolomitised mudstone. The dark colouration of the groundmass is afforded by the presence of disseminated pyrite.

Clast-groundmass relationship: The fracture-cementing dolomite is truncated at the clast edge (Photo. 85). The laminated fabric of the groundmass is plastically attenuated by fragments reworked pyrite (Photo. 86).

Interpretation

Crystallisation of dolomite occurred as replacement to micrite and as growth within unlithified muddy siliclastic strata. The development of fracture porosity in the lithified micrite permitted the growth of coarse dolomite in open space. The non-symmetrical and irregular character of the fracture walls is indicative of corrosion. Microfracturing of the protocrystals and syntaxial overgrowth by later dolomite proves syntectonic dolomitisation.

Autoclastic brecciation of the dolomitised micrite resulted in the injection of the unlithified diagenetic-detrital assemblage as matrix to the breccia: mineralisation evidently preceded remobilisation. Rotation of the clasts is proved by the inverted position of the geopetally-infilled fenestrae. Evidence for the unlithified state of the matrix is provided by the attenuation of its laminated fabric by fragments of reworked pyrite. The tabular morphology of this pyrite suggests that the mineralisation was stratiform. This is consistent with the derivation of the matrix from unlithified, siliciclastic and muddy source strata during mineralisation.

7.2.4 Breccia-associated mineralisation in the lower and middle Pale Beds

7.2.4.1 Type C

Description

Clast petrography: Oosparite. Allochems within the clast exhibit long contacts; the axis of compaction is perpendicular to the subvertical orientation of the drillcore (Photo. 87).

Groundmass petrography: Micrite supporting fine sand grade siliciclastic grains and wallrock limestone (Photo. 88).

Clast-groundmass relationships: The clasts are sharp-edged and angular (Photo. 89); grains at the clast edge are truncated (Photo. 90). Pyrite is developed along the clast-groundmass interface (Photo. 89), contiguously replacing both the clast and groundmass (Photo. 91). The pyritised interface is brecciated and cemented by fibrous calcite (Photo. 92); the fragments exhibit local displacement into the micrite groundmass (Photo. 89).

Interpretation

Unlithified micrite was injected as matrix into fractured, sparite-cemented grainstone. The micrite is petrographically distinguished from the Waulsortian Limestone by the presence siliciclastic sand grains. Cementation of the grainstone occurred after burial as demonstrated by its compacted fabric. Remobilised micrite occurs in vertical proximity to siliciclastic-bearing micrite strata in the Pale Beds. Photo. 93 shows *in-situ* sediment which is petrographically-equivalent to that present as matrix to the autoclasts: potential source strata are local and autochthonous. The autoclasts were rotated as a result of the sedimentary restructuring and is proved by the subhorizontal orientation of the originally vertical axis of compaction.

Mineralising fluids exploited the tectono-sedimentary heterogeneity represented by the clast-micrite interface. Pyrite precipitated as a contiguous replacement of the clast and micrite matrix. Lithification of the groundmass at the time of pyritisation was restricted to the interface, as demonstrated by the brecciation and local displacement of the pyrite into the evidently unlithified micrite. The precipitation of fibrous calcite as cement to the brecciated pyrite proves i) reactivated extensional tectonism, and ii) reactivation of pre-existing tectono-sedimentary interfaces and their exploitation during subsequent diagenesis.

7.2.4.2 Type D

Description

Clast petrography: Dolomitised bioclastic limestone with minor siliclastic sand. Dolomite occurs as highly selective replacement: skeletal grains are unaffected (Photo. 94).

Groundmass petrography: There are two generations of sediment remobilisation. Stage 1) micrite occurs as groundmass to the fractured bioclastic limestone; the micrite supports siliciclastic sand grains and bioclasts (Photo. 95). Dolomitisation is contiguous across the fracture edge and has rendered the contact diffuse; dolomite replacement of the micrite is less intense than the wallrock limestone, but exhibits the same bright red luminescence. The Stage 2) groundmass comprises laminated diagenetic and detrital sediment (Photo. 96). Laminae are defined by grain size and/or compositional variation. The diagenetic fraction includes sand grade dolomite and sphalerite grains and pyrite spherules; the dolomite grains occur as abraded crystals with a bright red luminescence (Photo. 97). The detrital fraction comprises siliciclastic sand grains, mud and dolomitised limestone fragments. The latter possess dolomite which

luminesces with a bright red colour and occurs as selective replacement of the non-bioclast content of the limestone (Photo. 98). The dark colour of the Stage 2) groundmass is afforded by the spherular pyrite and dark brown sphalerite.

Clast-groundmass relationship: The limestone is cut through by the micrite (Photo. 99). The dolomite, which occurs as replacement to the limestone and cross-cutting micrite, is equivalent under C.L. and produces a diffusivity to the limestone-micrite contact. The dolomitised, micrite-veined limestone is fractured (Photo. 99). The dolomitised micrite vein is clearly truncated by the edge of the secondary autoclast (Photos. 100 and 101). The laminated fabric present in the Stage 2) groundmass is sheared and attenuated into parallelism with the side of this refractured, micrite-veined and dolomitised clast (Photo. 101).

The luminescence of the dolomite present in the Stage 2) groundmass is identical to that of the dolomite which replaces the bioclastic limestone-micrite. Furthermore, reworked clasts of dolomitised bioclastic limestone present in the Stage 2) groundmass are petrographically equivalent to the wallrock (Photo. 98).

The interface between the sheared diagenetic-detrital groundmass is marked by a thin calcite vein (Photo. 97).

Interpretation

i) Overpressurised, unlithified micrite was injected as Stage 1) groundmass (matrix) into autoclastically brecciated limestone.

ii) Mineralising fluids exploited the fracture network, causing dolomitisation. Dolomite replacement was selective: bioclasts in the fractured limestone were unaffected and the micrite was only slightly dolomitised.

iii) Dissolution produced hydrothermal cavities: the location of brecciated limestone was critical in directing the flow of hydrothermal fluids through the autochthon.

iv) Precipitation of dolomite, pyrite and sphalerite occurred under conditions of supersaturation within the fluid-filled karst and the crystals were deposited as sediment along with corrosively reworked siliciclastics and mud (Stage 2 matrix). The compositional and grain size variations of the laminae indicate sedimentary conditions. The siliciclastic grains and mud component is interpreted as the insoluble residue after leaching by the corrosive, hydrothermal fluids.

v) Contemporaneity of the Stage 2) matrix with the secondary brecciation is proven by shearing and soft sediment deformation of the unlithified matrix into parallelism with the truncated edge of the dolomitised, micrite-veined limestone. The generation of hydrothermal karst weakened the autochthon: roof collapse resulted in brecciation of the dolomitised limestone and consequent deformational remobilisation of the unlithified internal sediment. The identical C.L. signatures of the replacement and sedimentary dolomites is evidence for paragenetic equivalence. This is supported by the occurrence of wallrock dolomitised bioclastic limestone which have been reworked as fragments into the Stage 2) matrix.

vi) The tectono-sedimentary interface presented by the contact of the secondary autoclast with the Stage 2) matrix was site of dilation and calcite cementation. This reiterates the control of earlier brecciation in directing the flow of fluids through the autochthon during extensional tectonism.

Postscript to Type D

Remobilised ore is frequently encountered as matrix to autoclastically brecciated, dolomitised limestone in the Pale Beds and Micrite Unit. Injection-related deformation ranges from plastically-deformed diagenetic-detrital laminae (Photo. 102) to slurried and brecciated ore in a diagenetic-detrital matrix (Photo. 103).

The diagenetic-detrital laminae are petrographically defined according to i) the ratio of diagenetic to detrital grains, and ii) the grain size (Photo. 104). The diagenetic component is represented by sand grade sphalerite and dolomite crystals and spherular pyrite; the detrital component comprises siliciclastic sand and argillite. The dolomite present in the matrix and as replacement to the host limestone is non-luminescent.

Fragments of remobilised ore within the slurried and brecciated assemblage contain stalactitic pyrite (Photo. 105). Breccia type D is characterised, therefore, by remobilisation of a diagenetic-detrital assemblage which contains evidence for mineralisation in stratiform, fluid-filled open spaces and under the influence of gravity. The similar luminescence of the clast- and matrix-associated dolomites reiterates i) the contemporaneity of the replacement and intrakarst precipitation and ii) the process of autoclastic remobilisation.

7.2.4.3 Type E

Description

Clast petrography: Complete replacement of oolitic limestone by sphalerite and dolomite; quartz nuclei to the ooids possess euhedral overgrowths (Photo. 106); the dolomite crystals are non-luminescent.

Groundmass petrography: Laminated diagenetic and detrital assemblage.

The diagenetic component is represented by silt to sand grade crystals of sphalerite, dolomite and barite and pyrite spherules; the dolomite crystals are non-luminscent. Detrital material is represented by siliclastic sand and mud. Laminae are defined by grain size and compositional variations (Photo. 107).

Clast-groundmass relationship: The clasts of replaced oolite press into, and deform, the groundmass. The diagenetic-detrital laminae at the base of the clast are downwarped and attenuated (Photo. 108); the laminae at the sides of the clast exhibit well-developed flame structures (Photo. 109).

Interpretation

Sedimentary deposition of diagenetic and detrital grains occurred within hydrothermal cavities located beneath intensely replaced oolite. Sedimentation was controlled by fluid chemistry and flow rate. The mud and siliciclastics represent insoluble residue and are the result of corrosive dissolution of the host.

Soft sediment deformation of the laminated internal sediment by the clasts of detached roof rock proves the coexistence of replaced limestone during internal sedimentation. Non-luminescence of the clast and matrix dolomites suggests that both the replacement and sedimentary dolomites are paragenetically-equivalent.

7.2.5 Breccia-associated mineralisation in the upper Pale Beds

7.2.5.1 Type F

Description

Clast petrography: Oobiosparite (Photo. 110).

Groundmass petrography: Siliciclastic sand, fragments of limestone and pyrite spherules. The limestone fragments are petrographically

equivalent to the oobiosparite clasts, but are intensley corroded (Photo. 111). Pyrite is disseminated throughout the matrix and is responsible for the dark colour of the groundmass.

Where the groundmass possesses a slurried appearance, the assemblage also includes: i) granule to pebble-sized fragments of pyrite which range in morphology from botryoidal (Photo. 112) to tabular (Photo. 113), ii) sphalerite-replaced oolite (Photo. 114), iii) fragments of dolomitised mudstone (Photos 115 and 116), and iv) sand grade crystals of dolomite (Photos 117 and 118). The luminscence exhibited by iii) and iv) are identical.

Clast-groundmass relationship: Where the groundmass is relatively undisturbed, the contact with the clast varies from sharp to gradational. Gradational contacts are characterised by intense peripheral dissolution of the clast margin: sparite-cemented allochems are corrosionally truncated and/or intersutured; the dissolution has produced a clast-parallel fabric (Photo. 119). The "streamers" of corroded limestone, where partially attached to the clast, are distinguished from the clast by an obvious dissolutional contact (Photo. 120). The proportion of limestone in the groundmass decreases away from the clast edge. Sharp contacts are present where limestone-deficient groundmass is adjacent to pristine limestone across a corroded contact (Photo. 121).

The occurrence of brecciated sulphides, dolomitised mudstone and dolomite grains in the slurried variation of this groundmass is also associated with the development of a clast-parallel fabric, but is distinguished by the presence of detached and deformed streamers of corroded limestone (Photo. 122).

Interpretation

Isolation of limestone within a predominantly siliciclastic matrix was achieved by dissolution. The siliciclastic sand represents the insoluble residue after leaching of calcite. Dissolution was a peripheral, stoping effect and produced the clast-contouring limestone streamers. Decalcification created the matrix and caused the intersuturing of the corrosionally-reworked limestone clasts.

Corrosional reworking and mineralisation preceeded physical remobilisation of the unlithified matrix. This is proven by the physical mixing of internally-derived sulphide breccia, clasts of dolomitised mudstone, dolomite sand and pyrite spherules in association with corroded limestone and siliciclastic insolubles. Sedimentary restructuring also caused the detachment and deformation of the previously clast--contouring limestone streamers. The viscous rheology and unlithified state of this remobilised matrix is indicated by the matrix support fabric and physical mixing. The clast-parallel fabric developed in the remobilised matrix is interpreted as the result of its shearing against the clast.

The presence of mudstone clasts in the remobilised matrix is indirect evidence for the existence of a precursor mud interbed to the limestone: the processes of corrosion and mineralisation are inferred to have exploited the sedimentary interface represented by the limestone-mudstone contact. Evidence for mineralisation within the consequent hydrothermal porosity is provided by the reworking of stratiform and botryoidal pyrite. Remobilisation is interpreted as the product of solution--induced collapse during active extensional tectonism.

7.2.5.2 Type G

Description

Clast petrography: Arenaceous biosparite (Photo. 123); sparite occurs as infill to biopores (Photo. 124) and as intergrain cement. Dolomite is present as vug fill and replacement. The distribution of the vugs is spatially-associated with the bioporosity-occluding sparite; the margins of the vugs are irregular and the dolomite cement comprises coarse, subhedral, zoned crystals (Photo. 125).

Groundmass petrography: Detrital and diagenetic melange. The detrital fraction is predominant and comprises siliciclastic sand and calcarenite (Photo. 126). Diagenetic grains are represented by dolomite sand and pyrite blebs (Photo. 127). The dolomite grains comprises zoned crystals with non-luminescent cores and an impersistent, outer zone which luminesces bright red.

Clast-groundmass relationship: The clast edges are sharp and can be seen to truncate allochems and the vug-filling calcite-dolomite cement (Photos. 128 and 129). The clast-groundmass interface is fractured and the fracture porosity is cemented by fibrous calcite; the orientation of the fibres is perpendicular to the fracture edges (Photo. 130).

Interpretation

The remobilisation of unlithified siliclastic calcarenite as matrix to fractured bioclastic limestone implies that cementation was lithologically-controlled. Evidence for pre-injection mineralisation is provided by i) the truncation the calcite-dolomite cement stratigraphy, and ii) the inclusion of dolomite crystals and pyrite blebs in the matrix.

Evidence for the post-calcite cementation age of the dolomitisation is proven by the selective development of dissolution vugs associated

with the bioporosity-occluding sparite. The resultant vugs were the sites of crystallisation of coarse dolomite; the subhedral crystallinity of the vug-filling dolomite is indicative of precipitation which was restricted by the presence of a physical interface, i.e. the edge of the pore.

Dilation of the clast-matrix interface by reactivated extensional tectonism is proven by the precipitation of fibrous calcite as cement to the developing fracture.

7.3 SYNTHESIS: DEVELOPMENT OF MINERALISATION IN THE AUTOCLASTICALLY BRECCIATED PALE BEDS AND MICRITE UNIT

1) The presence of unlithified strata in the Pale Beds and Micrite Unit provided a stratiform plumbing system for the throughput of mineralising fluids. Dolomite nucleated in the unlithified argillaceous and/or siliciclastic sediments. Calcite-cemented limestone strata were corroded and dolomitised; precipitation of dolomite occurred within the dissolution vugs.

2) Autoclastic brecciation of the lithified limestone strata caused the local vertical remobilisation of the unlithified, overpressurised sediments. Variably dolomitic argillaceous and siliciclastic sediment and undolomitised micrite migrated into the autoclastic fracture porosity.

3) The development of volumetrically significant mineralisation post-dated the tectonic brecciation-remobilisation event, but was dependent upon its formation. Interlayering of lithified limestone with unlithified strata ensured that the resultant geometry of the primary collapse breccia was stratiform. Mineralising fluids exploited the autoclastically-modified sedimentary interfaces and major ore formation commenced.

4) Dissolution of the limestone by hydrothermal fluids generated stratiform void spaces in the autochthon. Ore minerals precipitated in

fluid-filled cavities under conditions of supersaturation and were deposited internally as diagenetic sediment, during replacement and/or cementation of the host. Replacement by sulphides was lithologically controlled and confined to limestone strata. Evidence for continued dissolution during mineralisation is represented by i) the deposition of insoluble siliciclastic and argillaceous residue as interlaminae to diagenetic sediment on the floor of hydrothermal caverns, and ii) the ubiquity of corrosionally reworked limestone.

5) The structural weakness created by the development of stratiform hydrothermal cavities containing unlithified diagenetic and detrital sediments resulted in secondary autoclastic brecciation upon roof collapse. The internal sedimentary ore was locally remobilised. The dissolution-induced brecciation created further fracture porosity, facilitating the continued input of mineralising fluids and subsequent ore formation.

7.4 DISCUSSION

The conclusions of this research have proven that mineralisation in the Pale Beds and Micrite Unit was the product of primary autoclastic brecciation resulting from stratiform sedimentary and diagenetic heterogeneities within the autochthon. Moore (1989) relates the phenomenon of selective cementation of limestone strata by calcite as the result of the abundance of potential nucleation sites presented by the carbonate allochems; Bathurst (1987) regards retarded lithification of limestone as a function of increasing argillite content.

Mineralising fluids exploited this autoclastic fracture porosity and caused dissolution of the limestone. Solution voids were excavated in lithified strata. Ore minerals precipitated as diagenetic sediment within

hydrothermal cavities during replacement of the host. Failure of the cavity rooves system resulted in secondary collapse brecciation, re-opening the autochthon to mineralising fluids and further ore formation. Mineralisation was stratiform and lithologically and tectonically controlled. These conclusions correspond to those of Anderson (1990).

The conclusions of Rizzi (1992) must be disputed. His criteria for subaerial emersion and subsequent formation of karren-type karst are weak and his reasoning flawed. Evidence to dispute the existence of subaerial exposure in the Navan Group sequence is based on:

1) the meteoric diagenetic environment is characterised by the dissolution of limestone in the upper vadose zone owing to the solubility of calcium carbonate by rainwater. The calcium carbonate removed by dissolution is transported downwards into the lower vadose zone and effects rapid reprecipitation of calcite, i.e. cementation, under conditions of supersaturation (Moore, 1989).

Rizzi (1992) fails to acknowledge the existence of remobilised and therefore unlithified sediment within the Navan Group. This remobilisation is incompatible with the realm of meteoric diagenesis. Furthermore, there is evidence for compacted oolitic strata: a condition related to burial and delayed lithification. Such grainstone strata would undergo selective calcite cementation in the meteoric environment owing to their calcite composition and primary open texture. Rizzi (1992) did not account for the existence of compaction.

2) Rizzi (1992) interpreted the presence of breccia-associated micrite to represent the micritisation of karren-type karst following rapid rise in sea level. This research has shown that the breccia fabric resulted from the fracturing of compacted oolite into angular clasts; unlithified micrite was

locally present within the autochthon and migrated into the low pressure sites afforded by the autoclastically fractured oolite, causing rotation of the autoclasts. Rizzi's (1992) interpretation is dubious since i) the high degree of clast angularity indicates no detectable reworking, ii) the clast edges are unmicritised and exhibit sharply-truncated allochems, and iii) the coexistence of compacted and unlithified limestone sediment is untenable under a regime of meteoric diagenesis.

3) The frequently encountered dark sediment associated with the autoclastic breccia horizons was interpreted by Rizzi (1992) as pedogenic sediment, i.e. soil. Petrographic analysis of this "soil" clearly indicates two modes of formation, neither of which are compatible with a pedogenic origin. Autoclasis of partially dolomitised Micrite Unit caused the sedimentary injection of locally derived, unlithified, dolomitic and pyritic muddy and/or siliciclastic sediment. Disseminated pyrite is the primary cause of the dark colour. Contiguity of matrix with source strata proves local derivation. Dolomitised wallrock was reworked into the matrix: contemporaneity of the brecciation and mineralisation was not considered by Rizzi (1992).

Further petrography on Rizzi's behalf would have shown that the dark sediment associated with the brecciated Pale Beds is composed of interlaminated diagenetic and detrital sediment. The siliciclastic and argillaceous sediment do represent insoluble material, but are the product of hydrothermal dissolution (decalcification) and not pedogenesis. The development of grading within these diagenetic-detrital laminae proves that the sediment was hydraulically sorted and deposited within the stratiform voids described by Anderson (1990). Contemporaneity of the graded ore sediment with the replacement mineralisation is proved by i)

the development of soft sediment deformation textures upon roof collapse, and ii) the equivalent luminescences of the clast and matrix dolomites.

4) Rizzi (1992) regarded the tectonic brecciation-internal remobilisation processes described by Anderson (1990) as "unlikely scenario". Consideration of the economic geology literature, however, reveals frequent references pertaining to the autoclastic remobilisation of unlithified granular ore in association wallrock detritus and argillaceous and siliciclastic insolubles. Anderson (1974) describes the fundamental conditions which must be satisfied for the "ore slurry" hypothesis to be effective. Firstly, mineralisation is developed as stratiform ore lenses after the deposition of the host sediments. Secondly, the ore lenses are water-saturated during burial. Thirdly, fracturing of the strata allows injection of the unlithified ore material into the lower pressure environment offered by the dilated host. Development of the P.B.O. is strikingly resonant with this description, involving stratiform sulphide mineralisation within incompletely lithified sediments during extensional tectonism.

7.5 MINERALISATION IN THE SHALEY PALES

Description

Rizzi (1992) stated that the Shaley Pales were not dolomitised as they lacked the emersion surfaces which he considered instrumental to the mineralisation. In reality, the Shaley Pales are extensively dolomitised. Dolomite commonly occurs as replacement to bioclastic limestone (Photos. 131, 132 and 133).

Ashton et al. (1995) describe vein-type, replacement, cavity-fill and

disseminated Zn-Pb-Fe sulphide mineralisation in the Shaley Pales. The cavity fill sulphides occur as geopetally-laminated floor sediment and stalactites; euhedral honeyblende sphalerite often lines the vug wall. Calcite, dolomite and barite are associated with the sulphide minerals, commonly as the final open space fill to the veins and vugs. Such open space mineralisation is consistently associated with bioclastic limestone strata. Although sulphide mineralisation in the Shaley Pales is rare, there is abundant evidence for intense corrosion of the limestone.

Interpretation

The occurrence of mineralised (dolomitised) Shaley Pales disproves Rizzi's (1992) claim that mineralisation was controlled by the presence of subaerial emersion surfaces. Massive mineralisation does not occur in the Shaley Pales owing to the absence of vertically extensive limestone strata: the P.B.O. occurs as replacement to vertically and laterally extensive limestone strata. Anderson (1990) regarded argillaceous strata in the Pale Beds as having acted as barriers to the vertical movement of ore-bearing fluids. This situation is amplified in the Shaley Pales owing to the high frequency of argillite interbeds and the presence of vertically extensive, argillite-dominated strata.

CHAPTER EIGHT. MINERALISATION ASSOCIATED WITH THE ARGILLACEOUS BIOCLASTIC LIMESTONE GROUP

8.1 INTRODUCTION

Rizzi (1992) stated that the A.B.L. Group was not dolomitised as its porosity was low and it lacked the emersion surfaces which he regarded as conduits for the mineralising fluids. The objective of this chapter is to investigate this claim. It is clear that dolomite and/or sulphide mineralisation is distributed throughout the stratigraphic extent of the A.B.L. Group and so the claim is invalidated. The occurrence of this mineralisation within the three lithofacies of the A.B.L. Group, as outlined in Chapter 4, is described and interpreted.

8.2 MINERALISATION ASSOCIATED WITH THE ARGILLACEOUS BIOCLASTIC LIMESTONE

Description

The A.B.L. comprises bioclastic calcarenite interbedded with variably bioclastic and calcarenitic argillite. All lithological types of the A.B.L. exhibit pervasive, but heterogeneous dolomitisation. There are clear differences, however, in the intensity, crystallinity, mode of occurrence and timing of the dolomite depending upon the host lithology.

The distribution of dolomite within *bioclastic argillite* is restricted to the argillite: the bioclasts are silicified, but are undolomitised (Photo. 134). The dolomite comprises subhedral microrhombs which are distributed throughout the argillite (Photo. 135). Under C.L., the crystals exhibit three distinct zones. These are represented by: i) a core which luminesces medium orange, followed by ii) a bright orange zone, and iii)

an outer non-luminescent zone (Photo. 136).

Dolomite associated with the *bioclastic calcarenite* occurs as i) replacement and ii) cement to open spaces. The replacement dolomite is heterogeneously distributed. Where present, however, the dolomite occurs as selective replacement to the calcarenite: the bioclasts show replacement by silica, but are undolomitised. The dolomite is intensely developed as coarse, hypidiotic mosaics in which the only precursor sediment is represented by variably silicified bioclasts (Photo. 137). Thin-shelled bioclasts within a groundmass of dolomite exhibit the effects of breakage and local offset of the fragments (Photo. 138). The replacement dolomite is dominated by non-luminescent crystals. These sometimes contain a core microcryst which luminesces bright orange (Photos. 139 and 140).

The dolomite present as cement to open spaces within the biocalcarenite occurs in association with a) vugs and b) fractures. Two types of vug were identified: corrosional and intersparite. These both occur in close spatial proximity owing to their association with the biocalcarenite and sparite portions of geopetally-infilled bioclasts. The geopetals are defined by the level upper surface of the biocalcarenite; this is subhorizontal relative to the subvertical axis of the drillcore. Irregularly outlined vugs are distributed throughout the biocalcarenite floor sediment and are infilled by non-luminescent dolomite (Photo. 141). The sparite portion of the geopetal structure comprises coarse, scalenohedral calcite developed on the inner shell walls. The calcite crystals are peripherally corroded and the intersparite porosity is also occluded by non-luminescent dolomite (Photo. 142).

The fractures located within the A.B.L. are steeply dipping, vertically impersistent and confined to the biocalcarenite beds. Photo. 143

shows the coincidence of a dolomite-cemented fracture with the length of bryozoa branch fragment. The fracture transgresses through undolomitised biocalcarenite and is cemented by non-luminescent dolomite.

The dolomite developed within *biocalcarenitic argillite* is the same as that which occurs as replacement of the biocalcarenite. The calcarenite is intensely replaced by a hypidiotopic mosaic of relatively coarse dolomite crystals (Photos. 144 and 145). The dolomite crystals are mostly of the non-luminescent variety, although some do possess medium orange luminescent cores which are succeeded by a bright orange zone. The bioclasts are clearly visible as remnant grains.

Interpretation

The C.L. signature of the dolomite associated with the A.B.L. indicates that there were two major episodes of dolomitisation. Early dolomite formation resulted in the growth of euhedral, zoned microrhombs throughout the argillite and as sporadic replacement to the calcarenite. The bioclasts were unaffected by this replacement, but were silicified.

The succeeding dolomite event resulted in the intense, but heterogeneous, replacement of the calcarenite by non-luminescent dolomite. The crystals coarsened as the replacement ensued and the crystal faces impinged to produce the hypidiotopic mosaic. The bioclasts remained undolomitised. The nucleation of the later, non-luminescent dolomite upon the earlier, zoned type confirms the paragenesis.

The generation of dissolution vugs within the geopetal calcarenite and the corrosion of the overlying sparite is interpreted as showing that: i) acidic fluids permeated through the A.B.L., and ii) there was an early

sparite cement. The peripheral corrosion of the scalenohedral crystals suggests that the throughflow of acidic fluids occurred prior to the occlusion of the remnant geopetal porosity by sparite: the crystal faces were exposed to corrosion. By extrapolation, the development of non-luminescent dolomite as cement to the dissolution vugs and to the corrosionally-modified, intersparite porosity implies that the corrosion and dolomitisation occurring during primary diagenesis of the A.B.L.

Evidence to support this interpretation is provided by the development of vertically impersitent fractures whose distribution is lithologically, and occasionally, bioclastically controlled. Fractures developed in completely lithified stratigraphy would show no such lithologic or bioclast association. The A.B.L. is interpreted, therefore, to have been in a sublithified state during the cementation of these fractures by non-luminescent dolomite.

The earliest post-depositional modification is represented by the breakage of bioclasts. The local offset of the shell fragments is interpreted to be the result of compaction. Dolomitisation must have post-dated the compaction since pre-compaction dolomitisation would have effectively cemented the limestone and preserved the depositional state of the bioclasts. Compaction of the A.B.L. would have resulted from the contemporaneous existence of a sedimentary overburden, implying that the sedimentation rate of the A.B.L. Group was high. The subhorizontal attitude of the geopetal proves that the A.B.L. Group has not undergone any significant rotation. This view is consistent with its interpretation as a carbonate build-up which was locally deposited in a fault-generated sub-basin.

8.3 MINERALISATION ASSOCIATED WITH THE REEFOID ARGILLACEOUS BIOCLASTIC LIMESTONE

Description

The R.A.B.L. is characterised by an increase in the ratio of limestone to argillite: massive bioclastic calcarenite beds are distinguished by millimetric seams of argillite. The limestone beds possess clasts of reworked biocalcarenite. These clasts are distinguished from the petrographically-equivalent matrix under C.L. by the presence of discrete, sharp edged domains whose luminescence differs from that of the matrix (Photo. 146 and 147).

Inspection of the R.A.B.L. in drillcore revealed the presence of irregularly outlined vugs distributed exclusively within the limestone (Photo. 148). The vug fill possesses sedimentary and diagenetic characteristics: the vug margin is defined by a brown assemblage of minerals; this assemblage is heterogeneously distributed on the vug walls, but thickens locally on the floor of the vug; millimetre-sized, dark brown, subhedral crystals are infrequently developed along the walls; the remnant porosity is occluded by a colourless, coarsely crystalline mineral.

Petrographic analysis of the vug fill revealed the presence of a gangue-dominated ore assemblage, comprising sphalerite, dolomite and calcite. The occurrence of this mineralisation is related here to the diagenetic history of the host. The host is composed of sparite-cemented biocalcarenite. The sparite occurs as inter- and intragrain cement (Cct. I). The intergrain sparite is developed as overgrowths to bioclastic grains. Maximum development of these overgrowths is associated with the coarser grains. Where these grains are located close together, the intergrain sparite is contiguous (Photo. 149). The intragrain sparite exhibits the equivalent luminescence, but its distribution is restricted to

biopores (Photo. 150). The bioclastic grains are variably silicified. This silicification affects grains of all sizes, but is most apparent in the coarser fraction (Photo. 151).

The biosparite is cut through by sharp-sided fractures which are cemented by very coarsley crystalline sparite (Cct. II). The distribution of the ore mineral assemblage is spatially associated with dissolution voids developed within the biosparite and/or Cct. II. The size of these dissolution voids ranges from microscopic to macroscopic. Incipient void formation is seen at the interface of Cct. II with the biosparite (Photo. 152). Enhanced dissolution is correlated with the distribution of Cct. II (Photo. 153) and has produced irregular, corrosional terminations to this calcite (Photo. 154). Truncation of Cct. II is most apparent in the basal portion of the vug shown in Photo. 148: both Cct. II and biosparite are clearly truncated (Photos. 155 and 156).

The material which occupies the dissolutional porosity, and which achieves maximum thickness in basal portion of the vug, comprises an accumulation of subhedral crystals of dolomite and occasional sphalerite (Photos. 156 and 157). The dolomite crystals are predominantly non-luminescent, although some do possess brightly luminescent cores (Photos. 153, 154 and 155). This dolomite, and associated sphalerite, is collectively referred to as Dol. I.

The distribution of mineralisation associated with the vug walls is shown in Photos. 158 and 159. The biosparite wallrock is dolomitised. The voidwall is rimmed by coarse, subhedral, non-luminescent dolomite. This dolomite is associated with subhedral, zoned sphalerite and is equivalent to the Dol. I assemblage present in the basal portion of the vug. The coarsest sphalerite crystals are developed on the vug margin and possess euhedral terminations; they are millimetric in size and are

fractured (Photo. 160). The void-rimming, non-luminescent dolomite and sphalerite is overgrown by baroque dolomite which luminesces dull orange. The latter dolomite is distinguished from Dol. I on the basis of its luminescence and saddle morphology; it is designated Dol. II. Dolomite II overgrows Dol. I and is optically continuous with it (Photos. 158 and 159). The remnant porosity is occluded by coarsely crystalline calcite (Cct. III). Calcite III shows zonation in parallelism with the euhedral terminations of the coarse sphalerite crystals. The fractured sphalerite crystals which are still attached to the vug wall are cemented by Cct. III. (Photo. 160).

The occurrence of mineralisation decreases rapidly away from the vug walls and is restricted to the development of zoned dolomite micro--rhombs along seams of argillite (Photo. 150). The biosparite above and below these seams is solutionally modified.

Interpretation

i) reworking of calcite-cemented biocalcarenite in a matrix of primary biocalcarenite indicates synsedimentary calcite diagenesis (Cct. 0) of limestone strata. Extension-related subsidence in the depositional site of the A.B.L. Group is invoked as the mechanism which lowered the basin floor and caused the local reworking of lithified and unlithified biocalcarenite.

ii) the first diagenetic event after the reworking is represented by the overgrowth of sparite (Cct. I) on bioclastic grains; the equivalent calcite was also developed within biopores. The presence of primary bioporosity was limited, however, owing to the fragmented state of the bioclasts.

iii) steeply-dipping fractures developed in the biosparite and were cemented by coarse sparite (Cct. II): fluids saturated with respect to calcium carbonate flowed through fully lithified and extensionally dilated

R.A.B.L.

iv) the interface presented by the Cct. II and biosparite wallrock was exploited by acidic fluids. Dissolution microvugs were selectively developed within the Cct. II.

v) as corrosion ensued, both the wallrock and Cct. II were dissolved and irregular macrovugs were created. The steeply dipping, linear morphology of these fractures and their spatial association with intensely corroded Cct. II implies that the development of these macrovugs was dependent upon the distribution of Cct. II.

vi) mineralising fluids flowed through the dissolution porosity. The corroded biosparite wallrock was replaced by dolomite, and dolomite and sphalerite nucleated on the void walls (Dol. I). Although the majority of the dolomite crystals are non-luminescent, some do possess brightly zoned cores. The latter are possibly equivalent to the microrhombs which are developed along argillite seams. These seams are interpreted as stylolites owing to their association with dissolved and mutually impinged biocalcarenite: dolomitisation occurred after compaction.

vii) the relatively thick assemblage comprising granular dolomite and fragments of zoned sphalerite developed on the floor of the macrovugs is interpreted as a geopetally accumulated diagenetic sediment. Crystallisation within the porosity afforded by the macrovug permitted the growth of coarse crystals of dolomite and zoned sphalerite on the vug wall. The association of sphalerite and dolomite proves their paragenetic equivalence. Evidence for the derivation of this "diagenetic sand" from crystals which were contemporaneously distributed on the vug walls is provided by the predominantly non-luminescent signature of the dolomite and the incipiently fractured state of the zoned sphalerite crystals which are still attached. Those crystals which were completely

fractured became detached and were deposited as diagenetic sediment equivalent to Dol. I.

viii) the composition of the mineralising fluids evolved and coarse crystals of baroque dolomite crystallised on the vug walls (Dol. II).

ix) the remant and intracrystalline fracture porosities were occluded by Cct. III.

8.4 MINERALISATION ASSOCIATED WITH THE WAULSORTIAN LIMESTONE

8.4.1 Preface

Examination of diamond drillcore intersections through the W.L. revealed the frequent presence of saccharoidal dolomite. This dolomite is distinct from the W.L. owing to its dark brown appearance in drillcore and its association with pyritic argillite. The occurrences of dolomite as i) replacement to W.L. breccia, and ii) void fill, are described below and are interpreted in relation to sedimentary fabric and diagenetic history of the W.L.

8.4.2 Dolomite as replacement to W.L. breccia

Description

Photo. 161 shows the development of dark brown, saccharoidal dolomite as replacement to monomict W.L. breccia. The presence of this dolomite is spatially correlated with the distribution of argillite which occurs as matrix to the W.L. clasts (Photos. 162 and 163). The characteristics of the dolomite are described in relation to the petrography of the W.L. breccia:

Clast petrography: biomicsparite. The sparite occurs as coarse crystals of calcite which have nucleated upon bioclasts to produce a radiaxial fringe;

the coarseness of the radiaxial crystals decreases away from the bioclast (Photo. 164).

Matrix petrography: the matrix is composed mostly of argillite with mudstone intraclasts. It possesses a clast-parallel fabric which contours the sharp clast edges (Photo. 165).

Diagenetic characteristics of the matrix: dolomite is developed in the matrix as euhedral crystals which exhibit a range of sizes and C.L. zonation sequences. The coarser crystals possess the greatest number of growth zones, as identified under C.L., and they are commonly deformed. This strain is manifested as i) the elongation of the axis of crystal growth perpendicular to the clast margin, in association with the development of dolomite-cemented microfractures (Photo. 166), and ii) the fracture and local offset of dolomite crystals by calcite veins (Photo. 167).

The development of sulphide mineralisation within the matrix is restricted to the occurrence of pyrite as microcrystalline cubes and irregular blebs. The latter commonly have a shattered appearance (Photo. 168).

The dolomitised and pyritised matrix is traversed by swarms of calcite-cemented fractures (Photo. 169). The calcite possesses a fibrous habit, with the fibres oriented perpendicular to the fracture walls. The veins are developed in parallelism with the clast-parallel fabric in the matrix. Suites of these calcite veins are distinguished by their luminesce. The fractures either cause local displacement of the coarse dolomite crystals (Photo. 167) or they are deflected about such crystals (Photo. 166).

Diagenetic characteristics of the clasts: the primary clast-matrix contact varies from sharp to gradational, according to the contiguity of the dolomitisation across this interface. Sharp contacts are defined by the occurrence of unaltered W.L. adjacent to dolomitic and pyritic argillite

(Photos. 165 and 166). Gradational contacts are defined by the common occurrence of dolomite within the clast and adjacent matrix. The altered W.L. clasts exhibit the effects of intense, peripheral dissolution and/or replacement. Photo. 170 shows the presence of irregular, dissolution vugs within which dolomite occurs as coarse, subhedral crystals; the largest crystals are located within vugs which are distributed in the corroded limestone immediately adjacent to the matrix.

The dolomite present as replacement to the limestone is finer grained and is developed as hypidiotopic mosaics in which W.L. is subordinated to intercrystalline relicts (Photo. 171). Under C.L., both the vug-filling and replacement dolomite exhibit oscillatory zoning which is equivalent to that demonstrated by the matrix dolomite. The distribution of the dissolution and/or replacement is peripheral relative to the clast margin: with increasing distance into the clast, the development of dolomite is restricted to scattered vug fill and/or replacement (Photo. 172).

The altered limestone is fractured. The fractures vary according to their size and cement mineralogy. The smallest fractures are intracrystalline and are represented by micro-brecciated, coarse, vug-associated dolomite (Photos. 173 and 174). The cement to these microfractured crystals is developed in contiguity with the succeeding dolomite zone. Photo. 175 shows the colour negative of Photo. 171, emphasising the presence of a dolomite vein which cuts through intensely dolomitised W.L. and which is in turn truncated by a sparite vein. The dolomite present as fracture cement occurs as syntaxial overgrowths to the earlier replacement dolomite located in the fracture walls.

Interpretation

Mineralising fluids exploited the sedimentary fabric represented by the W.L. breccia. Euhedral crystals of dolomite and pyrite nucleated in the argillite matrix. The flow of the mineralising fluids was directed along clast-matrix interfaces, causing intense peripheral alteration of the W.L. clasts. The limestone was dissolved and the passage of dolomitising fluids through this secondary porosity resulted in the growth of dolomite as occlusions to the dissolution porosity and as replacement to the limestone. The dolomite crystals are colourless in plane polarised light: the dark brown appearance in drill core is related to the presence of intercrystalline argillite. The association of this intercrystalline argillite with the dolomite present as matrix and as occlusions to the dissolution vugs within the limestone implies that the argillite was remobilised from the matrix during the dissolution and dolomitisation. Where the dolomite occurs as replacement to the W.L., or occupies argillite-absent vugs, it is colourless.

The growth of zoned crystals proves that the composition of the dolomitising fluids varied. The greatest number of zones are developed in association with the matrix dolomite, implying that the flow of fluids was focussed through argillite fraction of the breccia. It is possible that the combined effects of interclast compaction of the argillite in association with this directed fluid flow was responsible for the clast-parallel, elongate morphology of the dolomite crystal shown in Photo. 166. The development of pits within contemporaneous dolomite zones and their cementation by the succeeding dolomite event indicates that fluids which were corrosive with respect to dolomite also flowed through the breccia fabric during the dolomitisation.

Evidence for syn-dolomitisation tectonism is seen on the

microscopic and macroscopic scales. Microscopically, this tectonism is represented by the precipitation of dolomite as cement to intracrystalline fractures in contiguity with its syntaxial overgrowth upon the fractured crystal nucleus. The occurrence of dolomite-cemented fractures which cut through intensely dolomitised W.L. provide macroscopic evidence for the existence of syn-dolomitisation tectonism. The brecciation is interpreted as the result of dissolution restructuring and/or continued extension.

The final diagenetic episode is recorded by the precipitation of calcite as cement to fractures. Again, the sedimentary fabric of the W.L. breccia was exploited: dilation of the incompetent argillite resulted in the generation of clast-parallel fractures which were cemented by fibrous calcite. Evidence for multiple dilation events is provided by the variation in luminescence of this calcite. The post-dolomitisation age of this calcite is proved by its cross-cutting and deflected relationships with dolomite crystals in the matrix. The occurrence of sparite as cement to fractures which truncate dolomitised W.L. provides further evidence for the post-dolomitisation age of the calcite. Unlike the fibrous calcite, the precipitation of sparite indicates that the rate of crystal growth was slower than the rate of fracture dilation: the lithified state of the W.L. clasts allowed the fractures to remain open during the flow of calcium carbonate-bearing fluids from which the sparite precipitated.

8.4.3 Dolomite as void fill

Description

The occurrence of dolomite as occlusions to macrovoids within massive W.L. is clearly seen in drillcore. It presents itself as dark brown, saccharoidal dolomite, often in association with coarse, baroque dolomite

(Photo. 176). In hand specimen, the voids are sharp-sided and irregular (Photo. 177). The wallrock is composed of biosparite. The sparite is developed as a coarse, radiaxial fringe to the bioclastic grains; the crystals increase in size away from the bioclast (Photo. 178). Zonation of the radiaxial calcite is defined by concentric variation in its luminescence relative to the bioclast margin. The infill comprises an assemblage of sedimentary and diagenetic material which possess a stratiform, subhorizontal configuration (Photo. 177). In ascending order, these are represented by:

i) argillite

The distribution of the argillite is confined to areas of negative relief on the void floor (Photo. 177). The upper level of the argillite is subhorizontal: the argillite pinches out against the positive floor features, producing rapid thickness changes from 6 mm to 0 mm. The edge of the void is sharp and contours the radiaxial calcite fringe, fragments of which are supported by the argillite (Photo. 179 and 180).

ii) Dolomite A (Dol. A.)

The argillite is overlain by a 2-3 mm thick layer of dolomite which possesses a light brown appearance in hand specimen (Photo. 177). In plane polarised light, Dol. A. comprises a mosaic of coarse, colourless, subhedral crystals; the intercrystalline material is argillite and it is this which imparts the light brown colour to Dol. A. in hand specimen (Photo. 181). Under C.L., the crystals exhibit an intermediate euhedral zone which luminesces brightly; the dully luminescent outer zone represent variably euhedral overgrowths (Photo. 182).

iii) Dolomite B (Dol. B.)

In hand specimen, Dol. B. is represented by a centimetric layer of dark brown saccharoidal dolomite, the upper surface of which is subhorizontal and follows the contours of the top contact of Dol. A. (Photo. 177). In plane polarised light, the dolomite crystals are colourless and form a xenotopic mosaic; argillite occupies the intercrystalline sites and imparts the dark brown colour to Dol. B.; pyrite is a minor component and is disseminated as cubic microcrysts and spherules in interdolomite sites (Photo. 183).

The majority of the crystals luminesce dully, such that individual crystals can only be distinguished under C.L. by the presence of brightly luminescent cores (Photo. 184). The void walls adjacent to Dol. B. are sharp, but irregular and are composed of radiaxial calcite which exhibits replacement by dolomite; isolated fragments of the wallrock are supported by the Dol. B (Photo. 184).

Photo. 185 shows the contact of Dol. A. and B. under C.L. The contact is commonly defined by the presence of disseminated cubic and spherular pyrite (Photo. 186). The void wall adjacent to Dolomites A. and B. comprises radiaxial calcite; this is contiguous with the voidward edge of the calcite fringe which defines the basal argillite.

iv) Dolomite C (Dol. C.)

Dol. C. comprises macroscopic, subhedral baroque crystals developed as a fringe to the remnant void porosity which is contiguous over both the W.L. and the Dol. B. substrate (Photo. 177). The latter possesses a subhorizontal upper surface, over which Dol. C. has overgrown with optical continuity (Photo. 187). Photo. 188 shows the C.L. characteristics of Dol. C. The outermost zone luminesces bright red and

defines the euhedral crystal terminations which characterise Dol. C. Voidwards of this outer zone, the porosity remains unoccluded.

The contact of Dol. C. with the W.L. appears sharp in hand specimen (Photo. 177). Under C.L., however, Dol. C. is shown to have nucleated upon a millimetric dolomite rim (Photo. 189). This dolomite is equivalent to Dol. B., on the basis of i) the predominance of anhedral crystals which luminesce dully and possess brightly luminescing, euhedral nuclei, and ii) the association with pyrite and/or argillite. The contact of this dolomite rim with the W.L. is irregular and shows evidence for replacement. The wallrock comprises the same radiaxial calcite fringe which is present as the void wall to the argillite, Dol. A. and Dol. B.

Interpretation

The void space is interpreted as primary, interbioclast porosity judging from the parallelism of the walls with the concentrically zoned radiaxial calcite fringe. The void filling sequence represents the occlusion of this primary porosity prior to its complete cementation by radiaxial calcite. The development of dolomite is therefore regarded as having occurred during early diagenesis of the W.L. The association of sparite with irregular, often flat-based cavities in variably micritic bioclastic limestone is characteristic of stromatactis (Collinson, 1981), and is in accordance with Tucker (1986), who regards the development of radiaxial calcite as an open space phenomena. The void space is interpreted morphologically and mineralogically, therefore, to represent stromatactis.

The flow of fluids through the void network introduced argillite into the system. This is possibly related to corrosional remobilisation of the argillite from the matrix of W.L. breccia, as described in 8.4.2. The

argillite was deposited under the influence of gravity on the void floor. The distribution of the reworked argillite was controlled by the topography of the void floor, as indicated by its accumulation within depressions and its absence at the apices of the positive features. Fragments of the radiaxial calcite were spalled from the wallrock and subsequently deposited with the argillite.

The composition of the fluids became supersaturated with respect to dolomite. Crystals of Dol. A. nucleated within the void space. These were deposited under the influence of gravity and accumulated over the argillite. The coarse size of the crystals indicates precipitation within open space and under low levels of supersaturation. Evidence for the fluctuation in fluid composition is recorded by the development of zoned crystals. The final anhedral mosaic contrasts with the presence of inner euhedral cores. This suggests that crystallisation continued after the sedimentary deposition of the dolomite crystals and resulted in the mutual impingement of these nuclei. The distribution of argillite in intercrystalline sites implies that the rate of crystal growth exceeded the deposition of argillite.

Increase in the saturation level of the dolomitic fluids resulted in the abundant nucleation of fine grained dolomite. These Dol. B. crystals were also deposited under the influence of gravity, on the contemporaneous void floor, as a diagenetic sediment. The inclusion of fragments of wallrock confirms the sedimentary nature of this predominantly diagenetic assemblage. Although the Dol. B. crystals possess euhedral cores, as defined by the presence of a brightly luminescent innermost zone, the assemblage comprises an idiotopic mosaic of predominantly non-luminescent dolomite. This latter dolomite is developed as overgrowths to the brightly luminescent nuclei:

precipitation of dolomite continued after intial sedimentation and resulted in the impingement of adjacent crystals. Argillite was suspended in the fluid-filled voids and became trapped in the intercrystalline sites.

The light brown and dark brown colouration of the Dolomites A. and B, respectively, reflects the negative correlation which exists between the ratio of intercrystalline argillite and the crystal size. Dol. B. comprises smaller crystals, as a result of which the intercrystalline surface area is considerably greater than for Dol. A. Occlusion of the intercrystal porosity by brown argillite produces dolomite which appears much darker when compared to the more coarsley crystalline Dol. A. The occurrence of disseminated pyrite in intercrystalline sites also contributes to the dark colouration of the layered dolomites. The development of pyrite as cubic microcrystals indicates slow growth from undersaturated, mineralising fluids; it is possible that the flow of these fluids permitted the continued input of argillite. The development of cubic pyrite along the contact between Dolomites A. and B. implies that the mineralising fluids exploited a physical interface. The coincidence of this interface with the bedding plane which separates Dol. A from the stratigraphically younger Dol. B is in accordance with the physical deposition of these diagenetic sediments under the influence of gravity.

The wallrock to the void and the Dol. B. crystal sediment was contiguously replaced and/or overgrown by Dol. B. The diagenetic configuration of the contemporaneous void comprised, therefore, a void-contiguous rim of Dol. B, either as floor sediment or altered Waulsortian Limestone. Dolomite C. nucleated upon the Dol. B substrate and grew over it as a fringe of very coarse, baroque crystals. Evidence for their growth within open space is provided by their coarse size and their euhedral terminations in a voidwards direction. Variation in fluid

composition during the growth of Dol. C. resulted in the development of zoned crystals. The outermost zone contours the crystal edge, voidwards of which the remnant porosity is unoccluded. The precipitation of Dol. C. is interpreted to have sealed the void. Therefore, the final void space represents the remnant, primary, stromatactic porosity after 1) precipitation of radiaxial calcite, 2) deposition of basal argillite, 3) the successive precipitation of Dolomites A., B. and C.

The stratiform morphology and subhorizontal attitude of the sedimentary layers indicate that i) they were geopetally deposited under the influence of gravity, and ii) post-mineralisation tilting of the A.B.L. Group has been negligible.

8.5 SYNTHESIS: DEVELOPMENT OF MINERALISATION IN THE A.B.L. GROUP

Evidence for dolomitisation in the A.B.L. Group is ubiquitous and clearly seen in drillcore. Rizzi's (1992) claim that the A.B.L. Group was undolomitised is shown to be in error: acknowledgement of the association of dolomite with the unequivocally submarine A.B.L. Group would have effectively dismissed his own conclusions which involved the presence of subaerial karst as the control to the development of mineralisation. Rizzi was so enamoured with his findings that he chose to voice them, against the advice of his industrial supervisor (Dr. John Ashton, assistant chief geologist at Tara Mines), at the European Dinantian Environments II conference (University College Dublin, 1994). A reprentative of Crowe Schaffalitzky and Associates enquired if Rizzi had evidence for the distribution of unmineralised palaeokarst outside of the orebody. Rizzi did not and the questioner suggested that the "karst" was created entirely by the mineralising, hydrothermal fluids owing to

the common association of mineralisation with Rizzi's karstic surfaces. In light of the criticism and the growing body of evidence, Rizzi spoke again at the Models for Carbonate-hosted Base Metal Deposits conference (Killarney, 1995); he de-emphasised the presence of subaerial karst and did not qualify his references to "secondary porosity" with a genetic interpretation. This change of opinion is reflected in the titles of his respective presentations: compare "Emersion surfaces within the Dinantian (Courceyan) succession at Navan, Ireland" (1994) with "Sedimentary cyclicity and dolomitisation within the Pale Beds: host rocks to the Navan zinc-lead ore deposit, Ireland" (1995).

Detailed study has revealed that dolomite is extensively developed throughout the entirely submarine A.B.L. Group and it is associated with argillite, limestone and all intermediate lithologies. The modes of occurrence of the dolomite are diverse and are represented by replacement, primary pore fill, secondary (dissolution) pore fill, fracture fill and diagenetic sediment.

The development of dolomite is found to be associated with sedimentary, tectonic and diagenetic heterogeneities, indicating that both physical and chemical interfaces were exploited by the mineralising fluids and were the sites of nucleation. Evidence for the frequently corrosive nature of these fluids is provided by the development of dissolution porosity within both the wall rock and dolomite. Evidence for pyrite and sphalerite is scarce, but where present they are paragenetically associated with the dolomite.

Dolomite in the W.L. is characteristically associated with argillite, inspite of the deficiency of this lithology in the limestone. Evidence for remobilisation of argillite from the matrix of W.L. breccia by corrosive, mineralising fluids was presented in 8.4.2. Other possible sources of

argillite include stylolites and mudstone interbeds within the W.L. and contemporaneous clay in the seawater. The former requires dissolution of the limestone. The latter requires interconnection of the void network with the seawater column. In all instances, the existence of a three-dimensional void system is a pre-requisite for the introduction of the argillite and to permit the flow of the mineralising fluids.

There is abundant evidence for the fracturing of individual dolomite crystals within vugs and dolomite-replaced limestone. Cementation of these fractures by dolomite proves that the dolomitisation was syn-tectonic. This tectonism could be the result of continued regional extension and/or the response to dissolution-induced restructuring of the A.B.L. Group. Whatever process(es) caused this tectonism, tilting of the A.B.L. was negligible judging from the occurrence of geopetally-infilled cavities which show the correct way-up and deviate only slightly from the palaeodip.

CHAPTER NINE. EVIDENCE FOR PRE-BOULDER CONGLOMERATE MINERALISATION

9.1 INTRODUCTION

Hypothesis One stated that for the mineralisation to be lithostratigraphically characterised as post-Boulder Conglomerate, the C.G.O. will contain no evidence of reworked P.B.O. and that the ore will not be truncated by the unconformity. Using underground exposure and diamond drillcore this chapter addresses this hypothesis.

9.2 EVIDENCE FOR PRE-BOULDER CONGLOMERATE MINERALISATION IN UNDERGROUND EXPOSURE

9.2.1 1390 340S

Description

Photo. 190 shows stratiform P.B.O. truncated by the unconformity. The mineralisation comprises crustiform sphalerite, galena, pyrite and barite with pyrite as replacement to the wall rock.

The Boulder Conglomerate overlying the unconformity adjacent to the vein comprises clasts of oolitic limestone and fenestral micrite in a matrix of argillaceous calcsilt. There is no evidence for post-depositional, diagenetic mineralisation of the breccia. Instead, mineralisation is present as pebble to boulder-sized fragments in the Boulder Conglomerate. The clasts are petrographically equivalent to the in-situ mineralisation, being composed of vein-type sphalerite, galena, marcasite and/or pyrite and barite (Photo. 191); boulders of fenestral micrite exhibit stratiform replacement by pyrite which is truncated at the clast edge (Photo. 192).

Interpretation

Stratiform vein mineralisation was established in the Pale Beds prior to the deposition of the Boulder Conglomerate. The mineralisation developed as infill to stratiform voids and replacement to the limestone wallrock. The mineralised Pale Beds was eroded by the rock avalanche so that fragments of ore and host rock were reworked into the Boulder Conglomerate. The scarcity of ore fragments reflects on the restricted spatial development of the mineralisation. The presence of reworked oolitic limestone and fenestral micrite in association with clasts of ore indicates a lower Pale Beds/Micrite Unit source for the Boulder Conglomerate.

9.2.2 1285 Block 40 HWD

Description

Three lithofacies were mapped in 1285 Block 40 HWD (Figure 10). The lowermost lithofacies comprises Pale Beds and W.L. breccia and boulders of vein-type mineralisation (Photo. 41). Mineralisation associated with open space is represented by i) linear fractures lined with sphalerite, and ii) centimetric voids lined with sphalerite. The latter contain millimetric laminae composed of sphalerite and/or barite (Photo. 193) and which are distributed along only one side of the void and are parallel to this contact with the wall rock (Photo. 41).

Both the fractures and voids possess irregular outlines. The wallrock comprises oolitic limestone which has been replaced by an assemblage comprising sphalerite, pyrite, barite, dolomite and silica. Sphalerite replacement predominates along the margins and is gradational into pyritised wallrock (Photo. 194). The silica occurs as overgrowths to quartz grains which represent ooid nuclei (Photo. 195).

Colloform sphalerite contours the edge of the replaced oolite and is overgrown by coarse, pale yellow sphalerite crystals which culminate voidwards in euhedral terminations. Coarse calcite crystals are developed along the margin of the void which coincides with the euhedral terminations of this sphalerite (Photo. 196).

The mineralised wallrock, colloform sphalerite and coarse, pale yellow sphalerite are shattered and cut through by a swarm of calcite-cemented microfractures. The sparite crystals, however, are unfractured. The calcite which is developed as cement to these microfractures has a fibrous habit; the fibres are oriented perpendicularly to the microfracture margins (Photo. 197).

The remaining fill to the void comprises an assemblage of sparite and dolomite crystals and argillite. The argillite occurs as matrix to the clast-supported diagenetic grains and delineates the sharp, irregular margin of the attached sparite (Photo. 198). The calcite and dolomite crystals are colourless in plane polarised light: their dark appearance in hand specimen is due to presence of the argillite matrix.

Interpretation

i) fracturing of the oolitic limestone proved that it was brittle and therefore lithified.

ii) corrosive fluids flowed through the fracture porosity, enhancing it and causing the development of dissolution vugs.

iii) the wallrock was replaced by an ore-gangue assemblage comprising pyrite-sphalerite-barite-silica. The replacement of lithified limestone proves that the alteration was effected by diffusion of the mineralising fluids through an impermeable host. The replacement was highly selective, being controlled by the distribution of calcite; quartz grains were

neither replaced nor corroded, but were overgrown by silica.

It is probable that the development of colloform sphalerite as lining to the fractures and dissolution vugs occurred during replacement of the wallrock. The precipitation of sphalerite with a colloform habit is indicative of high levels of supersaturation. The development of laminated microcrystalline sphalerite is interpreted, therefore, as reflecting the deposition of diagenetic silt derived from the colloform-lined walls and/or from direct precipitation in the fluid-filled void. The association of barite with this internal, diagenetic sediment records the periodic influx of fluids bearing seawater sulphate and barium during sulphide mineralisation.

iv) the level of supersaturation decreased and the colloform and laminated sphalerites were overgrown by coarse, euhedral sphalerite. The continued existence of void space is indicated by the euhedral terminations of this sphalerite.

v) extensional tectonism dilated the autochthon and produced swarms of microfractures which cut through the replaced wallrock and sphalerite. The growth of fibrous calcite as cement to these microfractures indicates that dilation and cementation occurred synchronously. Evidence for the growth of sparite crystals on the void walls after the microfracturing event is provided by their unfractured state.

vi) the remnant void space was occluded by an assemblage of sparite and dolomite sand in an argillite matrix. The fragmented state of the sparite grains and their local source on the void walls indicates that they were internally reworked during remobilisation and forceful intrusion of the matrix. The injection of the matrix possibly resulted from restructuring of the autochthon due to dissolution and/or the presence of unlithified strata during extensional tectonism. The occurrence of dolomitic argillite

as insoluble residue within dissolution voids and as dolomitised, but unlithified primary strata was described in Section 7.2, and supports the interpretation of the source as internal to the autochthon.

vii) the mineralised oolite was reworked in association with unmineralised Pale Beds and W.L. as Boulder Conglomerate. Mineralised clasts represent less than 5% (visual estimate) of the lower lithofacies of the Boulder Conglomerate exposed in 1285 Block 40 HWD.

9.2.3 1315 CGO

9.2.3.1 *Introduction*

Examination of the Boulder Conglomerate in the P2 heading of the 1315 CGO revealed clasts of ore associated with clasts of unmineralised Pale Beds and W.L. (Photos. 199, 200 and 32). The breccia is clast-supported; clast size of both the ore and non-ore fragments ranges from granule to boulder. Their shapes vary from angular through subrounded. The matrix is distinguished from the underlying argillaceous calcsilt interbed by its brown colour, sandy texture and association with comminuted ore and limestone (Photo. 200).

Petrographic analysis identified the presence of mineralisation in the matrix and permitted the recognition of three clast types of ore according to the petrography of the precursor limestone and the degree of replacement. These are represented by i) partially replaced oobiosparite, ii) completely replaced oolitic limestone, and iii) completely replaced bioclastic limestone.

9.2.3.2 Partially replaced oobiosparite

Description

Oobiosparite clasts possess elongate, irregularly-outlined voids

with the wall rock replaced by sphalerite and pyrite (Photo. 201). Replacement is complete peripheral to the margin of the void (Photo. 202). With increasing distance into the host, replacement is incipient and is restricted to nucleation of sphalerite microcrysts around allochems and along intercrystalline boundaries (Photo. 203).

The void wall is rimmed by colloform sphalerite and coarse crystals of galena with euhedral terminations into the void (Photo. 204). The void fill comprises an assemblage of diagenetic and detrital grains. The former are represented by silt to sand-sized crystals of sphalerite, barite and calcite, and fragments of colloform sphalerite. Detrital grains comprise sand grade quartz, feldspar and mica, and fragments of replaced and unreplaced limestone. Photo. 205 shows the petrography of the voidfill: limestone fragments, ore fragments and siliciclastic grains are supported by a matrix of calcite microcrysts and subordinate sphalerite and barite.

Interpretation

Corrosive fluids dissolved the oobiosparite and created irregular dissolution voids. Mineralising fluids migrating through the dissolutional porosity diffused into the lithified limestone along interfaces presented by allochem-sparite boundaries and intersparite boundaries, and replaced the wallrock. Colloform sphalerite precipitated along the void wall and so demonstrate the presence of open space.

Dissolution of the host limestone resulted in the release of quartz, feldspar and mica sand grains as insoluble residue. These grains were remobilised as a granular microbreccia into the sulphide-rimmed void in association with a matrix of contemporaneous sphalerite, barite, and calcite crystals. Fragments of colloform sphalerite and replaced limestone were reworked from the wallrock and prove the erosive capability of the

sediment injection. The association of limestone fragments with a matrix dominated by calcite microcrysts implies the mineralising fluids were in equilibrium with the host carbonate prior to the remobilisation.

9.2.3.3 Completely replaced oolitic limestone

Description

The clasts are composed of oolitic limestone which has been completely replaced by sphalerite-galena-barite-dolomite-silica. The ore has a layered fabric which is truncated at the clast edge (Photo. 32). The layers are defined by replaced oolite interlayered with irregular, stratiform voids which are infilled with an assemblage of diagenetic and detrital grains.

Evidence for precursor oolite is rare owing to the intensity and destructiveness of the replacement (Photo. 206). Sphalerite predominates and is intergrown with subhedral galena (Photo. 207). The sulphides are replaced by coarsely crystalline barite and non-luminescent dolomite (Photo. 208).

Colloform sphalerite contours the replaced oolite and delineates the margins of the stratiform voids (Photo. 209). The voids are sub-parallel, possess irregular margins and are interlayered with the replacement mineralisation, thereby creating the planar fabric. The colloform sphalerite is overgrown by non-luminescent dolomite which is truncated at the edge of the contemporaneous void (Photo. 210). The remnant porosity is occluded by an assemblage of diagenetic and detrital grains (Photos. 211 and 212). The detrital component is represented by grains of quartz, feldspar and mica. The diagenetic grains are represented by sand-sized sphalerite. Silty argillite occurs as amoeboid-shaped clasts owing to their deformation by the adjacent grains. The relative

proportions of detrital to diagenetic grains ranges from equal (Photos. 209 and 210) to diagenetic-dominated (Photo. 211); in the latter case, the detrital grains are isolated within and supported by the diagenetic grains.

The replaced oolite and colloform sphalerite are cut through by swarms of calcite-cemented microfractures (Photo. 213). The microfractures are clearly truncated at the edge of the colloform sphalerite (Photo. 214).

Interpretation

The presence of ghost ooids proves the replacement of oolitic limestone. The incipient obliteration of these allochems attests to the destructiveness of the mineralisation process. Destruction of the primary fabric was intensified by the growth of coarse dolomite and barite as secondary replacement.

The development of dissolution voids is proven by the precipitation of colloform sphalerite. The void-rimming colloform sphalerite was also overgrown by coarse, euhedral dolomite. Truncation of these dolomite crystals at the margin of the contemporaneous void was achieved by i) dissolution prior to the internal remobilisation of the diagenetic-detrital assemblage which infilled the remant porosity, and/or ii) mechanical erosion resulting from this remobilisation.

The occurrence of diagenetic and detrital pore-filling sediment proves the existence of unlithified sphalerite crystals within the hydrothermally-produced porosity. Remobilisation is probably related to the dissolution-induced collapse of the autochthon described in Section 7.2. The scarcity of reworked limestone is a result of the intensity of the wallrock replacement at the time of remobilisation. The siliciclastic grains are interpreted as the insoluble residue after dissolution of the wallrock.

The diagenetic grains record the precipitation from solution under conditions of supersaturation within the secondary porosity. The reworking and plastic deformation of silty argillite with this assemblage proves that unlithified, non-limestone strata were involved in the remobilisation, and is in accordance with the conclusions of 7.2.

Evidence for tectonism during the mineralisation is provided by the development of microfractures which cut through the colloform sphalerite but are truncated by remobilised sediment. The calcite cement to these fractures possess a fibrous morphology which indicates that cementation and dilation were synchronous.

9.2.3.4 Completely replaced bioclastic limestone

Description

The clasts comprise bioclastic limestone which has been completely replaced by sphalerite-galena-pyrite-barite-silica (Photo. 215). Detrital quartz and feldspar grains are rare and represent the only unreplaced precursor sediment; the quartz grains commonly possess silica overgrowths. Ghosts of large bioclasts provide the only evidence for precursor carbonate material ; they are represented by crinoids, rugose corals and bryozoa (Photos. 216, 217, 218, 219 and 220). The bioclasts exhibit pseudomorphic replacement by fine-grained orange sphalerite. Replacement of the bioclasts is usually incomplete: the unreplaced portion is characterised by the development of coarse, pale yellow, euhedral sphalerite on the internal walls of biomoulds, with coarse barite occluding the remnant porosity (Photos. 216 to 218).

The replaced limestone possesses irregularly-outlined voids which are infilled with an exclusively diagenetic geopetal sequence (Photo. 221). Barite and sphalerite occurs as finely crystalline floor sediment which is

developed in contiguity with an underlying barite and sphalerite-filled fracture (Photo. 221, location A). The upper contact of the crystalline sediment is level and comprises coarser, stratiform sphalerite and/or barite laminae (Photo. 221, location B).

The void floor and stratiform barite and sphalerite are fractured and locally displaced (Photo. 221, location C). The fracture is cemented by a symmetrical sequence of zoned sulphides (Photo. 222): microcrystalline galena is distributed along the edge of fracture-lining colloform sphalerite and the remnant fracture porosity is occluded by euhedral, pale yellow sphalerite. The fracture-associated sulphide sequence is contiguously developed along margin of the void. The void-lining mineralisation, however, is characterised by the development of i) a thicker colloform sphalerite rim, ii) very coarse, galena crystals which possess voidwards euhedral terminations, iii) anhedral pyrite, iv) coarsely crystalline, euhedral, pale yellow sphalerite, v) coarse barite crystals, and vi) sparite as occlusion to the remnant porosity (Photo. 221).

The void-lining mineralisation and stratiform sphalerite and barite are cut through by microfractures which are sharp-sided and symmetrical (Photos. 221, 223 and 224). The fracture cement is composed of calcite. Under C.L., this calcite luminesces a very bright orange which permits identification of its distribution as a contiguous rim to the contemporaneous void and as intergrain cement to the void-lining sphalerite (Photos. 225 and 226). The colloform sphalerite exhibits replacement by calcite which possesses the same very bright orange luminescence. The remnant porosity is occluded by sparite.

Interpretation

Replacement of the limestone was associated with the generation

of biomouldic and fabric as selective, dissolutional porosities. Mineral paragenesis associated with the biomouldic porosity is simple: i) brown-orange sphalerite pseudomorphed the bioclasts, ii) the unreplaced portion of the bioclasts were susceptible to dissolution and coarse, pale yellow euhedral sphalerite precipitated on the internal walls of the biomoulds, and iii) crystallisation of coarse barite occluded any remnant secondary porosity.

The paragenesis of the dissolution voids is more complicated and protracted. Dissolution of the host produced irregular voids. Open space is proven by the precipitation and geopetal sedimentation of barite and sphalerite crystals as laminae with a level upper surface. The void floor was fractured and the fractures were filled in contiguity with the overlying stratiform assemblage.

The mineralised wallrock and stratiform barite and sphalerite were fractured which allowed mineralising fluids to flow through the fracture-enhanced dissolution porosity. The fractures were cemented by a condensed sequence of sulphides in contiguity with the precipitation of the equivalent sequence along void margins. The degree of crystallinity of the mineralisation was related to the amount of contemporary porosity: coarse galena and a thick, idiotopic rim of coarse, pale yellow sphalerite grew uninhibitedly on the void walls, but the growth of these same minerals in fracture sites was restricted owing to the limited space available.

The final tectonic event recorded in the paragenesis is the microfracturing of the void-rimming mineralisation. Bisection of the sulphide-cemented fractures by these microfractures implies that tectonism exploited pre-existing structural heterogeneities. Calcite precipitated as cement to the microfractures in contiguity with its

development as a rim to the contemporaneous void. The very bright orange luminescence to this calcite, and the calcite present as intergrain cement to the void-rimming sphalerite and replacement to the colloform sphalerite suggests paragenetic equivalence. The remant void porosity was cemented by sparite.

9.2.3.5 Mineralisation as matrix

Description

The matrix to brecciated ore was decribed in Section 5A.2.1 and was shown to comprise a physically admixed assemblage of argillite and diagenetic and detrital sand grains (Photos. 33 and 34). The matrix is petrographically distinct from the underlying argillaceous calcsilt interbed. The difference is emphasised at the basal contact of the breccia unit where there is evidence for ductile interpenetration of the Boulder Conglomerate matrix and argillaceous calcsilt substrate (Photo. 35).

Interpretation

The petrographic contrast and the sedimentary admixing of the transported matrix with the local substrate proves the deformation of unlithified sediments. The matrix comprises an unlithified assemblage of argillite, siliciclastic grains and crystals of sphalerite, dolomite and barite. Reworking of this unlithified matrix in association with the clasts of ore proves their contemporaneity.

9.2.3.6 *Conclusions*

The Boulder Conglomerate exposed in the P2 heading of the 1315 C.G.O. contains evidence for reworked mineralisation as both clasts and matrix. All clast types record evidence for replacement and dissolution of

lithified bioclastic and/or oolitic limestone during active extensional tectonism. The source of the ore is interpreted as the lower Pale Beds/Micrite Unit owing to the petrographic equivalence of the mineralised limestone with the limestone present at this stratigraphic level in the autochthon as identified by Rizzi (1992). The presence of detrital sand and ooids in the reworked ore rules out the possibility of an A.B.L. Group source owing to the absence of these sediments in the Argillaceous Bioclastic Limestone, the Reefoid Argillaceous Bioclastic Limestone and the Waulsortian Limestone.

The matrix is petrographically equivalent to the types of groundmass associated with the autoclastically brecciated autochthon described in Section 7.2. The occurrence of mineralisation in the matrix as diagenetic sand is interpreted, therefore, as representing a sample of either sedimentary ore which had precipitated under conditions of supersaturation within hydrothermally-produced porosity or which had grown within unlithified argillaceous strata within the autochthon. The reworking of this mineralisation as unlithified sediment proves i) unlithified, ore-rich sediment existed during replacement of the Pale Beds/Micrite Unit, and ii) the P.B.O. was reworked into the Boulder Conglomerate prior to the lithification of the ore sediment. The existence of a heterogeneously lithified and decalcified autochthon during active extensional tectonism are regarded by this research as the major factors which contributed to the formation of the Boulder Conglomerate.

The unlithified ore assemblage does not represent reworked synsedimentary mineralisation derived from erosion of the seafloor by the rock avalanches. This is proved by the consistent absence of coarse siliciclastic grains within the limestone-dominated, hemipelgic interbeds to the Boulder Conglomerate.

9.3 EVIDENCE FOR PRE-BOULDER CONGLOMERATE MINERALISATION IN DIAMOND DRILLCORE

9.3.1 Intersection of underground diamond drillcore with pre-Boulder Conglomerate mineralisation in the 3 Zone, Lower Lens

Description

Underground diamond drillholes U8330, U8332 and 8333 intersected clasts of ore in the Boulder Conglomerate. The clasts comprise angular, pebble to cobble-sized clasts of reworked vein-type ore (Photos. 61 and 62). Sphalerite and galena encrust veins which cut through wallrock composed predominantly of sphalerite and barite. The barite in the wallrock is developed as coarse needles with a radial habit. The barite is intergrown with idiotopic clusters of sphalerite. Detrital quartz and feldspar grains are isolated with this diagenetic mesh (Photos. 227 and 228). The remnant intercrystalline porosity is occluded by subhedral, zoned calcite (Photos. 229 and 230). Dissolution of barite prior to the precipitation of the calcite ranges from intense pitting (Photo. 229) to incipient pseudomorphism of coarse barite needles (Photos. 231 and 232); in both cases the intracrystalline porosity created by the corrosion is infilled by the paragenetically later calcite.

The vein wall is irregular and possesses a rim of colloform sphalerite which is intergrown with galena (Photo. 233 and 234). The colloform sphalerite is overgrown by euhedral microcrysts of sphalerite and coarse galena crystals, the latter exhibiting euhedral crystal terminations in a voidwards direction (Photo. 234). The galena crystals are often fractured. The fractures are cemented by calcite which luminesces very bright orange. This calcite is also contiguously developed as a thin rim which demarks the contemporaneous pore space. The remnant porosity is occluded by sparite which exhibits zonation under C.L. Calcite

is also present as a replacement to the colloform sphalerite (Photos. 233 and 234).

Interpretation

The drillcore intersected clasts of reworked vein-type mineralisation. Evidence for the existence of precursor limestone is represented by the spaced configuration of the detrital quartz and feldspar grains: the intervening carbonate was obliterated by the processes of replacement and dissolution. The host rock comprised a crystalline mesh of barite and sphalerite which was then fractured. Mineralising fluids flowed through the fracture porosity and the vein walls were encrusted with sphalerite and galena. The crystallisation of euhedral sphalerite along the edge of the colloform sphalerite implies a decrease in the rate of crystallisation.

The final paragenetic event is represented by calcite. Prior to the precipitation of calcite, however, there is clear evidence for i) corrosion of barite, and ii) microfracturing of the coarse galena crystals along the vein walls. The dissolution and fracture porosities were cemented by calcite prior to the cementation of all remaining pore space by sparite. The zoned, subhedral characteristics of the sparite proves that calcite-bearing fluids flowed through both the intercrystalline pore space present in the wallrock and the remnant pores in the veins and that these fluids varied in composition. It is probable that replacement of the colloform sphalerite took place during this stage of the paragenesis.

The vein-type ore was reworked as fragments and deposited as Boulder Conglomerate. These fragments were derived from pre-existing vein mineralisation in the autochthon and represent samples of pre-Boulder Conglomerate mineralisation.

9.3.2 Evidence for pre-Boulder Conglomerate mineralisation in the Shaley Pales

Introduction

Diamond drillhole N 927 intersected 11.6 m of Boulder Conglomerate, the footwall to which is the unconformity at the stratigraphic level of the Shaley Pales. Evidence for the occurrence of dolomite as replacement to bioclastic limestone strata within the autochthonous Shaley Pales in N 927 was described in Section 7.5 (Photos. 131 to 133). The stratigraphic composition of the clasts in the Boulder Conglomerate comprises Shaley Pales and Waulsortian Limestone. The former predominate and in drillcore appear petrographically equivalent to the autochthonous Shaley Pales, comprising intensely, but heterogeneously dolomitised bioclastic limestone. The distribution of the dolomite within the clasts shows no preferred relationship with the clast edges. Clasts possessing evidence for dolomite were sampled in order to determine the mode of occurrence of the dolomite and its C.L. signature. The dolomites associated with the autochthonous and allochthonous portions of the stratigraphy are compared and the relative timing of the dolomitisation is interpreted in lithostratigraphic terms.

Description

The intensity of dolomitisation associated with the bioclastic limestone ranges from incipient to virtually complete. Incipient dolomitisation is represented by the localisation of the replacement to intergrain sites; the relict bioclasts are relatively undolomitised and for this reason can be easily identified (Photos. 235 and 236). Where the dolomitisation is most intensely developed, evidence for precursor limestone is reduced to i) incipiently replaced, coarse bioclastic grains

(Photo. 237), and ii) the subordinate limestone groundmass where the dolomite rhombs are not in contact (Photo. 238).

Interpretation

The dolomitic clasts present in the Boulder Conglomerate are petrographically equivalent to the dolomitised Shaley Pales substrate. Their occurrence in the allochthon is interpreted as the product of mass wasting of the autochthon. The short transport distance of the reworked material is indicated by the para-autochthonous site of deposition. The inclusion of dolomitised Shaley Pales as clasts within the allochthon provides evidence for the existence of a dolomitised autochthon prior to the deposition of the Boulder Conglomerate.

9.3.3 Evidence for pre-Boulder Conglomerate mineralisation in the A.B.L. Group

9.3.3.1 Clast A

Description

Mineralisation is common in clasts of bioclastic limestone, occurring as infill to macroscopic vugs (Photos. 239 and 240). The characteristics of the wallrock, vug morphology/alteration rim and vug fill are described below:

Wallrock: argillaceous biosparite. The sparite cement occurs as occlusions to primary inter- and intra-bioclast porosity (Photo. 241). Sub-millimetre seams of argillite possess a crenulated shape and coincide with dissolved and mutually impinged bioclasts (Photo. 242).

Vug morphology/alteration rim: the vug is irregular, but possesses a level floor. The clarity of the contact of the vug wall with the fill varies from sharp to gradational according to the lithology of the wallrock.

Coincidence of the vug floor with bioclastic agillite defines a sharp contact (Photo. 243). The remainder of the wall is developed in limestone and the contact is gradational owing to the effects of peripheral dissolution and replacement. Maximum corrosion occurs in intergrain sites, although the adjacent bioclasts are neomorphosed and/or pitted with a diagenetic calcite pore fill (Photos. 244 and 245). Replacement of the vug wall is clearly seen under C.L. as euhedral, non-luminescent dolomite (Photo. 246).

Vug fill: the lower portion of the vug comprises a layered, sedimentary assemblage of diagenetic grains and wallrock. Layering is defined by the consistent vertical variation in the petrography of these sediments across the vug floor. The vug floor coincides with bioclastic argillite and is overlain by fractured and fragmented crystals of zoned sphalerite (Photos. 243 and 247). The sediment overlying and intercalated with the sphalerite grains comprises subhedral to anhedral crystals of dolomite, clasts of sparite and rare fragments of sphalerite. The fabric is grain-supported, with pyritic argillite present in the interstices (Photos. 247 and 248). The dolomite grains luminesce dull red but are intensely pitted; the dolomite developed as infill to the dissolution microvugs luminesces bright red (Photo. 249).

The granular dolomite and sphalerite assemblage is overlain by a layer comprising coarser, subhedral grains of non-luminescent dolomite and fragments of wallrock limestone. The fabric is grain-supported within a matrix of pyritic argillite (Photos. 250 and 251). The dolomite grains possess intracrystalline fractures (Photo. 252).

The dolomitised wallrock and non-luminescent dolomite sediment are overgrown by very coarse, non-luminescent baroque dolomite (Photo. 253). The inter-baroque dolomite remnant vug porosity

is partially occluded by sparite which exhibits two significant zones (Photos. 254 and 255). The early calcite luminesces medium orange and is highly corroded; this dissolution is manifested as the obliteration of crystal terminations, and the production of intracrystal microvugs. The later calcite occludes the intracrystal microvugs and is developed as an optically contiguous overgrowth to the previous calcite. The remnant intercrystal porosity is unoccluded (Photo. 255).

Interpretation

i) fluids bearing calcium carbonate flowed through the primary porosity present within the bioclastic sediment and sparite precipitated as inter- and intra-grain cement.

ii) post-cementation compaction of the limestone was localised to bioclastic argillite and proves the prior existence of a sedimentary overburden. Concentration of argillite by pressure dissolution is shown by the impingement of bioclastic grains adjacent to the stylolites.

iii) corrosive fluids diffused through the lithified and compacted limestone, causing dissolution. The intergrain calcite was preferentially corroded, although creation of dissolutional macrovugs, which are larger in diameter than the bioclasts, proves the corrosive capabilities of the fluids. Coincidence of the vug floor with the stylolitic, bioclastic argillite suggests that the fluid flow was directed by the presence of compositional heterogeneities. This interpretation is supported by the stylolite-parallel attitude of the vug floor.

iv) fluids bearing zinc and reduced sulphur flowed through the vug and effected the precipitation of coarse sphalerite crystals; fluctuation in composition of the fluids resulted in the development of zoned crystals. The distribution of these crystals on the vug floor in association with

their fractured and fragmented state is indicative of internal reworking and redeposition, under the influence of gravity, as sedimentary grains.

v) change in the composition of the mineralising fluids resulted in the precipitation of three major phases of dolomite in the vug. Initially, crystals of dully luminescent dolomite precipitated in the vug system. Evidence for reworking of these crystals as sedimentary grains is provided by their accumulation as a layer on the vug floor in association with fragments of zoned sphalerite and sparite.

The second dolomite is developed as a layer over the earlier dolomite. Evidence for reworking is provided by the fractured state of the crystals and the presence of fragments of wallrock. The coarse crystal size and non-luminescent C.L. signature proves that the hiatus in reworking occurred during changes in the fluid composition and rate of crystallisation. The argillite in the matrix to the laminae is interpreted as the insoluble residue after dissolution of the argillaceous wallrock adjacent to the stylolite.

The final dolomite is *in-situ* and represented by baroque dolomite developed as contiguous overgrowth to the sedimentary dolomite and dolomitised wallrock. The continued open state of the vug is proved by the growth of the baroque crystals to macroscopic dimension and with voidwards euhedral terminations.

vi) the succeeding fluid was supersatured with respect to calcium carbonate and precipitation of sparite resulted in partial occlusion of the remnant, interbaroque dolomite porosity. Fluids corrosive with respect to calcium carbonate then entered the vug and selectively corroded the sparite. Re-introduction of calcium carbonate-supersaturated fluids, however, resulted in the reprecipitation of further calcite which syntaxially overgrew the corroded sparite and infilled dissolution

microvugs.

vii) the mineralised biosparite was reworked into the Boulder Conglomerate as clasts.

The source of the clasts is interpreted as the limestone-dominated lithofacies of the A.B.L. Group. Evidence to support this claim is provided by:

a) the petrographic equivalence of the host limestones, comprising stylolitic, variably argillaceous biosparite with sparite developed as the primary cement to bioclastic grains. The creation of stylolites is consistent with the existence of a sedimentary overburden.

b) the preferential development of dissolution vugs in association with chemical and/or physical heterogeneities present in the limestone as described in Section 8.4.2. The secondary porosity was generated in all cases by corrosive, mineralisation-related fluids, and not by meteoric diagenesis.

c) the vugs seen both *in-situ* and within clasts possess corroded and dolomitised vug walls. The mode of vug fill and its paragenesis are equivalent to the mineralisation associated with the Reefoid Argillaceous Bioclastic Limestone as discussed in Section 8.3. These are represented by the early geopetal deposition of dolomite crystals, fragments of zoned sphalerite and wallrock as floor sediment. The sediment and wallrock were overgrown by baroque dolomite and the remnant porosity was occluded to varying extent by calcite. The association of argillite with the vug fill is interpreted to represent the insoluble material released by the dissolution.

The presence of mineralised Waulsortian-type Limestone as clasts in the Boulder Conglomerate provide evidence for the development of mineralisation in the A.B.L. Group prior to its reworking into the

Boulder Conglomerate.

9.3.3.2 Clast B

Description

Photo. 256 shows the occurrence of mineralisation from within a clast in the Boulder Conglomerate. The mineralisation is described in the context of wallrock, vug morphology and vug fill:

Wallrock: biomicsparite. The calcite is developed as a radiaxial fringe to bioclastic grains.

Vug morphology: the vug is sharply defined by the euhedral terminations of the radiaxial calcite crystals which project into the void (Photos. 257 and 258).

Vug fill: the vug fill comprises dolomite crystals, fragments of sparite and clasts of mudstone in a matrix of pyritic silty argillite (Photos. 258, 259, 260 and 261). The dolomite crystals exhibit a range in size and crystallinity. The crystals are mostly non-luminescent, although they often exhibit a brightly luminescent inner euhedral zone (Photo. 257). The fabric is grain supported.

Interpretation

Definition of the vug margin by the euhedral, voidwards crystal terminations of the bioclast-fringing radiaxial calcite suggests that the comtemporaneous porosity was primary and resulted from the incomplete cementation of stromatactis. Evidence for the occlusion of the remnant porosity, by a remobilised assemblage composed predominantly of dolomite crystals, is provided by the presence of wallrock sparite which has been reworked as clasts. The absence of wallrock replacement indicates that the site of crystallisation of the dolomite was not the

present void and is expected from the introduction of a physically remobilised sediment. Injection of the diagenetic grains abraded the radiaxial calcite fringe and generated sparite clasts. The presence of mudstone grains and pyritic silty argillite as matrix to the remobilised assemblage, neither of which occur in the immediate host, implies that the void system was connected to source whose location was external to the void.

The presence of dolomite crystals as sedimentary laminae within stromatactis was described in 8.4.3. The development of dolomite within the argillaceous matrix to W.L. breccia and as alteration to the adjacent clasts, associated with dissolutionally remobilised argillite was described in 8.4.2. These occurrences of dolomite are developed within *in-situ* W.L. It is probable, therefore, that the dolomite fill described in this section was originally distributed as replacement to the matrix of primary W.L. breccia and was injected into sites of partially-occluded stromatactic porosity within the clasts. Remobilisation is interpreted as the result of corrosion-induced restructuring of the W.L. during active extensional tectonism. The presence of W.L. as clasts in the Boulder Conglomerate which possess dolomite analogous to that observed *in-situ* provides evidence for the development of dolomite in the W.L. prior to its reworking as Boulder Conglomerate.

9.3.3.3 *Conclusions*

Evidence has been presented for the occurrence of dolomite and subordinate sulphide mineralisation both *in-situ* within the A.B.L. Group and as clasts in the Boulder Conglomerate which have been derived from the A.B.L. Group. The dolomite halo to the P.B.O. described by Rizzi (1992), therefore, extended laterally to the northwest and affected the

supra-Navan Group Waulsortian build-up. This regional dolomitisation was in evidence prior to the formation of the Boulder Conglomerate.

9.4 PRE-BOULDER CONGLOMERATE MINERALISATION: CONSTRAINTS AND CONCLUSIONS

The presence of brecciated mineralisation locally reworked from the Navan Group and A.B.L. Group into the Boulder Conglomerate proves the existence of pre-Boulder Conglomerate mineralisation. Hypothesis One, stating that the mineralisation was entirely post-Boulder Conglomerate, must be rejected.

The ore mineral assemblage is represented by sphalerite-galena-pyrite-barite-dolomite-calcite-silica. Volumetrically significant mineralisation is developed as replacement to limestone. The development of mineralisation within open spaces comprises a small percentage of the total ore, but its occurrence as occlusions to dissolution porosity and as encrustations to fracture porosity prove that the mineralising fluids were often corrosive to calcium carbonate and that the Navan area was tectonically active. Collapse of the autochthon is regarded by this research as the effect of extensional tectonism during decalcification. Evidence to support this is provided by the occurrence of unlithified ore sediment which is reworked as matrix to the Boulder Conglomerate and is petrographically equivalent to that described *in-situ* in Chapter 7.

The C.G.O. represents 3% of the Navan Orebody, of which less than 1% constitutes reworked Pale Beds Ore. Although there is evidence for mineralisation which has been reworked from both the Navan Group and A.B.L. Group, this huge disparity can only be interpreted as reflecting on the regionally extensive, but volumetrically insignificant distribution

of the sulphide mineralisation during deposition of the Boulder Conglomerate. Reworking of massive P.B.O. from the lower stratigraphic level of the Navan Group proves that the T Fault had exhumed almost the entire autochthon and that the lowermost ore lens was in an advanced state of formation.

Mills et al. (1987) correlated the lead isotopic characteristics of the 5 ore lenses (5 to 1, in ascending order). The trend to increased dispersion and less radiogenic averages was interpreted as stratigraphic and to represent synsedimentary mineralisation relative to the deposition of the Pale Beds. Although the findings of this research indicate that the mineralisation occurred after the deposition of the Navan Group, the development of epigenetic ore in the basal Pale Beds and its reworking as the lithostratigraphically earliest Boulder Conglomerate does not negate the work of Mills et al. (1987). The data remains sound, but is re-interpreted here to represent stratigraphic epigenesis: the upwelling hydrothermal fluids which scavanged the metals from the crust necessarily encountered the base of the autochthon first. As ore formation continued, the expanding hydrothermal convection cell scavenged metals from deeper parts of the crust. These were tranferred to progressively higher structural levels within the autochthon, developing as stratiform replacement when they encountered virgin limestone.

CHAPTER TEN. EVIDENCE FOR POST-BOULDER CONGLOMERATE MINERALISATION

10.1 INTRODUCTION

The presence of P.B.O. reworked as Boulder Conglomerate demands that Hypothesis One, stating that the mineralisation was entirely post-Boulder Conglomerate, must be rejected. This chapter assesses the C.G.O. for evidence of mineralisation which is shown to unequivocally post-date the deposition of the Boulder Conglomerate.

10.2 1315 CGO

10.2.1 P1S

Description

The Shaley Pales exposed in P1S are composed of bioclastic limestone and arenite as decimetric interbeds; argillite is a minor component and occurs as millimetric interlaminae to the limestone and arenite beds. Sphalerite, galena and pyrite are disseminated throughout the limestone and arenite (Photos. 262 and 263). The distribution of macroscopic mineralisation is confined to altered stratiform horizons which coincide with the bioclastic limestone strata (Photo. 264). Mineralisation is developed as: i) massive stratiform replacement/void fill and ii) fracture cement.

Massive mineralisation is represented by laterally impersistent, stratiform horizons of intensely replaced limestone (Photo. 265). Sphalerite and galena predominate as the replacing minerals; hydrothermal quartz is associated with the sulphides and is distinguished from detrital quartz by its euhedral crystallinity (Photo. 266). Evidence for relict bioclasts is provided exclusively by those which have been silicified.

The sharpness of the contact of the ore horizons with the unreplaced host varies according to the lithology of the adjacent host and the intensity of the replacement. Photo. 267 shows the sharp contact defined by intensely pyritised bioclastic limestone which is overlain by arenite. Sharp contacts also occur within limestone strata and are located where unreplaced limestone occurs adjacent to intensely mineralised limestone. Here, the contact is irregular (Photo. 268) and exhibits local discordance (Photo. 269). Gradational contacts occur where the limestone is incompletely replaced (Photo. 270).

Macroscopic vugs, possessing irregular stratiform morphologies, are distributed throughout the stratiform replaced horizons (Photo. 271). The wallrock comprises intensely replaced limestone. The vug floor is overlain by laminated, stratiform sphalerite which is intergrown with galena; siliciclastic grains are a minor component of the laminae and occur as stratiform concentrations within the sphalerite. Coarse, subhedral galena is developed upon the roof and walls and is overgrown by coarse, pale yellow sphalerite crystals which possess voidwards euhedral terminations. The remnant vug porosity is occluded by a polyminerallic, non-sulphide assemblage comprising non-luminescent baroque dolomite which is intergrown with barite and/or sparite.

Photo. 272 shows the occurrence of mineralisation as cement in fractures perpendicular to bedding which are located in altered limestone strata. The fracture-associated mineralisation exhibits a complex and composite fill. The fracture is sharp but irregular; pyrite occurs as fracture-parallel replacement to the bioclastic limestone wallrock; pyritisation is massive adjacent to the fracture edges and grades into unreplaced bioclastic limestone wallrock (Photo. 273). The fracture walls are encrusted with colloform sphalerite which is intergrown with occasional

coarse, subhedral crystals of galena (Photo. 274).

The colloform sphalerite and pyritised wallrock are locally reworked as fragments into the basal portion of the fracture; the sulphide clasts are supported by a matrix of siliciclastic sand and granular sphalerite (Photo. 275). The porosity in the upper portion of the fracture is occluded by an exclusively diagenetic fill. The colloform sphalerite which encrusts the fracture walls is brecciated and locally spalled; the fractures and reworked colloform sphalerite are cemented by coarse, pale yellow sphalerite which is non-luminescent under C.L. (Photo. 276). In the presence of significant remnant porosity, this latter sphalerite is developed as coarse subhedral crystals which possess euhedral terminations in a voidwards direction. Evidence for the paragenetic equivalence of this sphalerite with that developed as cement to the brecciated colloform type is proved by its contiguity and non-luminescent C.L. signature (Photo. 277). The pyritised limestone, and colloform and subhedral sphalerites are microfractured and cemented by calcite which luminesces bright orange (Photo. 277). The contemporaneous void margin is delineated by a thin zone of bright orange luminescent calcite and the remnant porosity is occluded by coarse sparite which luminesces medium orange (Photo. 277).

Inflections in the unconformity are infilled with polymict Boulder Conglomerate. The Shaley Pales beneath these inflections is brecciated. The stratiform mineralisation in the Shaley Pales cuts across the unconformity, occurring as sphalerite and galena cement and rim replacement to the adjacent Boulder Conglomerate. The brecciated Shaley Pales substrate possesses sphalerite and galena mineralisation as cement to fractures.

Interpretation

Mineralising fluids permeated through the Shaley Pales and selectively altered and replaced the bioclastic limestone strata. Argillite beds acted as vertical permeability barriers to the mineralising fluids, dictating intrastratal fluid movement: the resultant geometry of the mineralisation was lithologically-controlled and stratiform.

The destructiveness of the replacement-dissolution process is attested to by the obliteration of the carbonate allochems. The preservation of silicified bioclastic grains confirms the resistance of silica to dissolution. The development of stratiform vugs within the massively replaced limestone provides evidence for the generation of porosity by the mineralising processes. Sphalerite was deposited as sedimentary laminae on the vug floors in association with siliciclastic grains which were corrosionally reworked from the host. Decrease in the rate of crystallisation effected the precipitation of coarse sphalerite. The fluid composition changed and a gangue mineral assemblage comprising baroque dolomite and barite and/or calcite grew as coarse crystals and occluded the remnant vug porosity.

The presence of fractures perpendicular to bedding located exclusively within bioclastic limestone strata indicates a contrast in competency between the limestone and arenite strata. The development of early calcite cements as crinoidal overgrowths (Photo. 19) and as occlusions to bioporosity (Photo. 20) is used as evidence for the selective cementation of bioclastic strata. Preservation of the open state of the fracture during the passage of mineralising fluids is proven by the precipitation of colloform sphalerite on the corroded fracture walls. The wallrock was replaced by pyrite. Extensional tectonism dilated the fracture and resulted in the injection of siliciclastics and granular sphalerite from

the underlying unlithified and slightly mineralised arenite bed. The pyritised wallrock and colloform sphalerite were brecciated and locally incorporated as clasts within the sphaleritic arenite matrix. The remnant porosity was occluded by an exclusively diagenetic sequence. Crystals of coarse, pale yellow sphalerite precipitated as cement to the brecciated colloform sphalerite and as coarser crystals within the contemporaneous fracture porosity. The wallrock and void-lining sulphides were then re-fractured. The precipitation of brightly luminescent calcite as cement to the microfractures and as a rim to the encrusting sulphides suggests contemporaneity. The remnant porosity was then occluded by sparite. The configuration of the sedimentary and diagenetic components of the fracture fill defines a linear, bedding-perpendicular geopetal structure.

Post-Boulder Conglomerate timing of this mineralisation is proved by the contiguous development of sphalerite and galena across the unconformity and into the Boulder Conglomerate. The Shaley Pales were brecciated by the channelised rock avalanches. The Boulder Conglomerate is petrographically distinguished from the deformed substrate by its polymicticity (Photo. 17). Mineralisation of the Boulder Conglomerate exposed in P1S occurs as interclast cement and peripheral replacement to the clasts. Intersection of the equivalent mineralisation at the lower structural levels offered by the 1315 CGO AC and P2 headings permitted access to the ore. The detailed petrography of ore is described in the next section.

10.2.2 CGO AC and P2

General description

The C.G.O. exposed in the 1315 CGO AC and P2 headings occurs as cement and rim replacement to stratigraphically equivalent, matrix-

-deficient Boulder Conglomerate (Photos. 278 and 279). The mineralisation is characterised by rapid thickness variations owing to the level upper surface and the irregular basal contact of the breccia with the unconformity (Photo. 22). The mineralisation is contiguous across the unconformity, occurring as sphalerite-dominated cement to the Boulder Conglomerate and to fractures in the Shaley Pales substrate (Photo. 22). The contact of the breccia unit with the Shaley Pales unconformity is distinguished by the presence of iron staining. The staining is a recent phenomenon resulting from exposure-related oxidation of the pyritised contact: the Shaley Pales comprise bioclastic limestone which has been replaced by pyrite along the unconformity (Photo. 280).

Mineralisation associated with the interbeds is volumetrically insignificant compared to that hosted by the breccia horizon, occurring as i) laterally persistent, stratiform pyrite horizons and ii) polyminerallic concretions. The former are described in this section owing to their unequivocally epigenetic characteristics. The latter provide evidence for syngenetic mineralisation and are dealt with in the next chapter.

Description of the breccia-hosted mineralisation

Photos. 281 and 282 show the morphology of the mineralisation which is developed as cement to interclast porosity. The detail of this mineralisation is described below:

Host rock: matrix-deficient Boulder Conglomerate. The clasts comprise subrounded to subangular cobbles and boulders of oobiosparite and bio-oosparite.

Vug morphology/alteration rim: the gross morphology of the vugs are defined by the primary interclast porosity. The precise clast outlines cannot be discriminated owing to the effects of peripheral corrosion

and/or replacement. Pyrite, sphalerite and barite locally predominate as the replacing minerals (Photos. 283, 284 and 285). The extent of clast corrosion varies according to the proximity of adjacent clasts. In the absence of an interclast contact, corrosion is manifested as a concentric zone of intensely dissolved limestone. This zone is characterised by the concentration of siliciclastic grains in association with highly corroded, relict limestone (Photo. 286). Where the clasts are in contact, the dissolution zone thins rapidly, but is developed in the adjacent clasts and has resulted in the obliteration of the contact (Photo. 287).

Vug fill: the development of mineralisation varies morphologically and mineralogically according to its location within the vug. The vug floors are consistently overlain by subhorizontal laminae which are composed of finely crystalline sphalerite, galena and barite; the final layer comprises coarse crystals of yellow sphalerite (Photo. 288). The mineralisation developed on the vug walls and roof comprises colloform sphalerite which is intergrown with galena and barite, and rimmed by coarse yellow sphalerite (Photo. 289). Although the floor and wall/roof sequences are mineralogically equivalent, the latter is characterised by an attenuated colloform sphalerite rim which is intergrown with coarser crystals of galena and then rimmed by coarser crystals of yellow sphalerite.

As with the fracture-cementing mineralisation developed in the Shaley Pales exposed in 1315 P1S, the vug-lining mineralisation shows evidence for repeated brecciation. The colloform sphalerite is locally fragmented and cemented by the later pale yellow, coarse sphalerite (Photo. 290). This sequence is brecciated (Photo. 291) and in the presence of sufficient remnant vug space, the sulphide clasts are locally spalled with the final porosity occluded by non-luminescent baroque dolomite which is intergrown with sparite and/or barite (Photo. 292).

Interpretation

The Boulder Conglomerate deposited directly over the unconformity is interpreted to have been derived from the Pale Beds owing to the petrography of the clasts. The lithified state of the clasts permitted the deposition of a sedimentary breccia which possessed an open texture. Mineralising fluids flowed through the primary interclast pore spaces, causing corrosion and replacement of the clast margins. The development of ore minerals in the vug was gravitationally controlled. Microcrystalline sphalerite precipitated with a colloform habit on the walls and roof during deposition of the equivalent sphalerite as geopetal laminae on the vug floor. Both were intergrown with galena, the coarser crystals of which grew on the walls and are interpreted as gravitationally influenced. The subhorizontal attitude of the diagenetic floor sediment provides evidence for the preservation of palaeodip.

Evidence for syntectonic mineralisation is proved by the brecciation and cementation of the vug lining mineralisation. Initially, the colloform sphalerite was fragmented and cemented by coarse yellow sphalerite. Again, the coarsest crystals grew on the walls and roof. The entire sequence was then brecciated. The final fluids were gangue-bearing and the remnant vug and fracture porosities were cemented by baroque dolomite and barite and/or calcite.

Evidence for the post-Boulder Conglomerate timing of the mineralisation is provided by: i) the development of discordant ore as cement to the Boulder Conglomerate in contiguity with replacement to the Shaley Pales and as cement to the fractured unconformity, ii) the equivalent paragenetic and tectonic histories of the mineralisation developed within the Boulder Conglomerate and underlying Shaley Pales, and iii) the coincidence of pyrite replacement with the eroded

unconformity.

Description of laterally persistent, stratiform mineralisation associated with the interbeds

The sedimentology of the hemipelagic unit which overlies the stratiform and stratabound, ore-cemented breccia unit was described in Section 5A.2.1: fining upwards, graded calcarenite to calcsiltite beds up to 2 cm thick are distributed within depressions in the unconformity and as interbeds to the breccia horizons. In underground exposure, pyrite occurs as stratiform laminae up to 1.5 cm thick (Photo. 293). Microscopically, the pyrite occurs as selective replacement of the coarser, basal calcarenite portions of the graded beds (Photo. 294). The intensity of the replacement is variable along strike, ranging from incipient (Photo. 295) to complete (Photo. 296). In reflected light, incipient replacement is represented by microspherular and blebby pyrite (Photo. 297). Where the replacement is complete, the pyrite is massive and the only evidence for precursor sediment is provided by the presence of unreplaced bioclasts and rare siliciclastic sand grains (Photo. 298); the former are consistently represented by spicular grains.

Interpretation

The development of stratiform mineralisation in the interbeds can be qualified as stratabound by lithologic control: the growth of pyrite occurred as selective replacement to the calcarenite portions of graded beds.

Description of mineralisation in the T Fault and footwall

Pale Beds are present in the footwall of the T Fault and exhibit

stratiform replacement of oolitic limestone by sphalerite, galena and dolomite (Photos. 299 and 300; Plan 1). The ore possesses sharp basal contacts which coincide with argillaceous seams, and upper contacts which grade into unmineralised host limestone. With increasing proximity to the fault zone, the proportion of replaced limestone diminishes, and the ore is developed as laterally impersistent stratiform and locally cross-cutting stringer types (Photo. 301). This P.B.O. is contiguously developed up to a distance of 1 m perpendicular the T Fault and is not truncated by the fault (Photo. 302). Although the oolitic limestone present in this fault-parallel zone is intensely altered, sulphide mineralisation is poorly represented. Alteration of the limestone is seen as i) neomorphic degradation of both allochems and cement (Photo. 303), and ii) intense replacement by rosettes of barite (Photos. 304). The altered limestone is cross-cut by impersistent fractures cemented by sphalerite, dolomite and barite (Photo. 14), with pyrite developed as selective replacement to neomorphosed allochems in the fracture walls (Photo. 303). Mineralisation is poorly developed in the T Fault breccia zone, occurring as peripheral replacement to angular clasts of pristine oolite which have been reworked from the footwall (Photo. 305).

Interpretation

Evidence for mineralisation after the formation of the T Fault is provided by: i) the presence of unreplaced oolite clasts which were plucked from footwall into the fault breccia zone and subsequently pyritised, ii) the development of a fault-parallel alteration zone, iii) the cementation of tectonically fractured Pale Beds located in the footwall immediately beneath the T Fault by sphalerite, barite and dolomite, and iv) the absence of tectonically truncated P.B.O.

Mineralising fluids are interpreted, therefore, to have diffused through the autochthon and to have been directed by the structural heterogeneity represented by the T Fault. The chemical environment here was not conducive to major sulphide mineralisation and the limestone was intensely altered but remained largely unmineralised. This process of degrading neomorphism is closely comparable to Bathurst's (1975) documentation of its occurrence in limestones which have been subjected to tectonic stress and/or very low grade metamorphism.

10.3 1330 CGO PS

Description

The Boulder Conglomerate was described in Section 5A.2.2 as clast-supported, comprising boulders of bioclastic limestone in a carbonate mud matrix. Mineralisation is represented by the development of pyrite as replacement to clast-matrix interfaces (Photo. 39).

Interpretation

This pyritisation occurred after the depostion of the Boulder Conglomerate. Diffusion of the mineralising fluids was directed along the physical interfaces presented by clast-matrix boundaries.

10.4 1330 348S

Description

The stratiform character of the sulphide mineralisation shown in Photo. 55 is related to stratabound sulphide replacement of the low density debrites described in 5A.2.4. The intensity of replacement ranges from incipient to complete. Incipient mineralisation is represented by the bedding-parallel pyritisation of the carbonate mud matrix (Photo. 306).

The pyrite occurs as disseminated microspherules whose distribution is associated with neomorphically aggraded carbonate mud The contact with the unneomorphosed/unpyritised host limestone is sharp (Photo. 307). Irregular microvugs, occluded by zoned sparite, are distributed throughout pyritised/neomorphosed carbonate mud. The vug size is positively correlated with the intensity of pyritisation (Photos. 308 to 311).

Intermediate pyritisation of the carbonate mud is represented by coalescence of the stratiform spherular pyrite (Photo. 312). The coalesced pyrite defines the margins to irregular, stratiform vugs which are occluded by a sequence of episodically zoned, subhedral to anhedral calcite; the wallrock to the vugs comprises variably neomorphosed carbonate mud (Photos. 313 and 314).

Where pyrite replacement is most intense, evidence for precursor sediment is restricted to relict bioclastic grains (Photo. 315). The spherular pyrite occurs as clusters which are contiguously rimmed by growth-zoned botryoidal pyrite (Photo. 316). The interbotryoidal pyrite portion is infilled either by sparite (Photo. 316) or a sulphide-gangue sequence. The latter comprises a contiguous rim of microcrystalline sphalerite which is distributed as a thin rim in roof and wall sites and locally thickens over the floors (Photo. 317). This sphalerite is replaced by dolomite and diagenetic quartz (Photo. 318). Coarse subhedral crystals of galena and sphalerite occur as overgrowths to the microcrystalline sphalerite (Photos. 319 and 320). The sphalerite and dolomite are pitted and possess inclusion-rich calcite as replacement and vug fill. The entire sulphide-carbonate sequence is fractured and coarse, subhedral, crystals of zoned calcite, in association with laths of barite, cement the fractures and occlude the remaining pore space (Photos. 321 and 322).

Interpretation

Mineralising fluids permeated through the interbedded sequence of carbonate mud debrites, mudstone pebble breccia and hemipelagic argillaceous silt. Selective alteration of the carbonate mud ensured that the resultant geometry of the ore was stratiform and stratabound. Diffusion of the mineralising fluids through the carbonate mud neomorphically aggraded the host limestone to microspar during the precipitation of spherular pyrite. The fluids were corrosive to calcite and created dissolutional porosity. The irregular vugs were occluded by pyrite and/or sparite.

Evidence for the existence of an interconnected, three dimensional pyrite mesh and the subsequent dissolution of the interpyrite calcite is provided by the precipitation of zoned botryoidal pyrite as contiguous rims to the coalesced spherular pyrite. Sphalerite then precipitated within the interbotryoid porosity, developing as a thin rim on the vug walls and rooves in contiguity with a thicker, geopetal accumulation on the floors. The sphalerite was replaced by dolomite and hydrothermal quartz. Inclusion-rich calcite precipitated as poorly-formed crystals within the void during replacement of the sphalerite and dolomite by calcite. The sequence of mineralisation was fractured and the tectonically enhanced remnant porosity was cemented by zoned sparite and barite.

10.5 POST-BOULDER CONGLOMERATE MINERALISATION: CONSTRAINTS AND CONCLUSIONS

Evidence has been presented for the development of Post-Boulder Conglomerate mineralisation throughout the vertical and lateral extent of the allochthon deposited in the half graben defined by the T Fault. Hypothesis Two, stating that the mineralisation was *entirely* pre-Boulder

Conglomerate, must be rejected therefore.

Mineralisation present in the lower lens of the C.G.O. is stratiform owing to its occurrences as i) cement to the primary porosity afforded by matrix-deficient breccia horizons, ii) selective pyritisation of the coarse portions of graded hemipelagic carbonate strata in the interbeds, and iii) P.B.O. which has been reworked as breccia beds. The latter provide evidence for pre-Boulder Conglomerate mineralisation and was discussed in Chapter Nine. The conclusions of Chapter Nine stated that volumetrically significant P.B.O. must have formed after the deposition of the Boulder Conglomerate owing to its poor representation as clasts in the allochthon. Evidence to support this is provided by the development of laterally contiguous P.B.O. which is not truncated by the T Fault. Instead, the fault zone was the site of intense alteration, suggesting that major ore formation occurred after the regional displacement of the autochthon which produced this regional structural heterogeneity.

The upper lens is dominated by pyrite as replacement to carbonate mud: the development of massive sulphide mineralisation was lithologically-controlled and consequently both stratiform and stratabound. The precipitation of sphalerite, galena and dolomite which are paragenetically later than this pyrite proves that ore formation occurred after the formation of massive pyrite, and was associated with dolomite.

CHAPTER ELEVEN. EVIDENCE FOR SYNSEDIMENTARY MINERALISATION IN THE BOULDER CONGLOMERATE AND THINLY BEDDED UNIT

11.1 INTRODUCTION

Chapters Nine and Ten presented evidence for development of C.G.O. before and after the deposition of the Boulder Conglomerate, respectively. By extrapolation, the gross lithostratigraphic timing of the C.G.O. is inferred to be synsedimentary relative to the Boulder Conglomerate. This chapter provides evidence from both the Boulder Conglomerate and T.B.U. to substantiate this statement.

11.2 EVIDENCE FOR SYNSEDIMENTARY MINERALISATION IN THE BOULDER CONGLOMERATE

11.2.1 1315 CGO

Introduction

The Boulder Conglomerate exposed on 1315 level comprises matrix-deficient breccia units which overlie the unconformity and possess ore as cement to primary, interclast porosity, in contiguity with replacement and fracture cement in the Shaley Pales substrate. The stratigraphically younger breccia is polymict and contains mineralisation derived from the P.B.O. as both clasts and matrix. The interbed to these breccia horizons is represented by graded beds composed of concretionary calcarenite to calcsiltite. Evidence for the early timing of the concretions is provided by the relatively uncompacted state of the sediments within the concretions (Section 5A.2.1). Although these concretions are carbonate-dominated, they characteristically contain sulphide mineralisation. This association is described below and then interpreted in relation to i) the sulphide cementation of the underlying

breccia horizon, ii) the deposition of the succeeding breccia, iii) the pyritisation of the graded beds, and iv) the post-depositional, interstratal shearing of the breccia horizons.

Description

Photo. 323 shows an example of a typical concretion developed within the interbeds to the Boulder Conglomerate. The cores of the concretions contain fish bones which are replaced by euhedral sphalerite and/or galena (Photo. 324). The altered biodebris core is concentrically encased by a zone comprising uncompacted pelletal carbonate mud in which siderite occurs both as cement and replacement (Photos. 325 and 326).

Interpretation

The heterogeneities represented by fish bones were the focus of diagenesis in the interbeds and were selectively replaced by sphalerite and galena. Evidence for the early diagenetic timing of this mineralisation, during the absence of a significant sedimentary overburden is provided by the development of an outer zone comprising uncompacted pelletal carbonate mud which is cemented and replaced by siderite.

Evidence was presented in Chapter Ten for the post depositional cementation of the stratigraphically earliest breccia horizon by an ore-gangue assemblage and the selective pyritisation of the calcarenite portions of graded beds within the interbeds. This mineralisation is re-interpreted as synsedimentary, and as paragenetically equivalent to that developed within the concretions, since:

i) preservation of the interbed after the deposition of the succeeding rock avalanche implies that the substrate was partially lithified and did not reform as matrix to the breccia.

ii) upper contact of the underlying breccia bed is stratiform and uneroded by the succeeding rock avalanches: cementation by sulphides effected its lithification and prevented erosion of the primary depositional contact (Photos. 278 and 279).

iii) interstratal shearing of the Boulder Conglomerate was taken up along the interbeds and resulted in the rotation of the sulphide-carbonate concretions (Photo. 28) and the brecciation of pyritised calcarenite laminae (Photo. 327): mineralisation was synsedimentary and syntectonic.

11.2.2 1330 348S

Description

The sedimentology of the upper stratigraphic level of the C.G.O exposed in 1330 348S was described in Section 5A.2.4 as comprising a reworked assemblage of stratiform pyrite and subordinate sphalerite in association with silty argillite (Photos. 57, 58 and 59). The T.B.U. was deposited upon these brecciated and slump folded sulphide-dominated sediments and is in-situ.

Interpretation

The configuration of slump-folded sediments overlain by undisturbed bedding is characteristic of synsedimentary deformation (Collinson and Thompson, 1982). The variably lithified stratiform sulphides and argillite were subjected to lateral mass movement and redeposited basinwards. The development of stratiform, pyritic C.G.O. is interpreted, therefore, as synsedimentary and pre-slump: mineralisation occurred in the presence of a contemporaneous seafloor and was remobilised prior to the deposition of the Thinly Bedded Unit. Competent pyrite was brecciated and became physically admixed with unlithified sulphides and argillite. Transport ceased

when the sediments encountered a region of the seafloor which possessed a lesser slope and the reworked stratiform mineralisation was folded and/or brecciated.

11.2.3 1285 Block 40 HWD

Description

Lithofacies 2a and 3 of the Boulder Conglomerate were described in Section 5A.2.3. Both contain evidence for reworked pyrite. Clasts of pyrite in the former are supported by a matrix of bioclastic carbonate mud. Clast morphology is characteristically tabular, with the clast margins seen to truncate stratiform and/or stalactitic fabrics within the clast; the interpyrite material present within the clasts is represented by neomorphically aggraded calcite (Photo. 48).

Lithofacies 3 overlies 2a. The breccia is monomict and clast-supported, comprising fragments of stratiform and massive pyrite in a matrix of pyritic argillite (Photo. 49). Lithofacies 3 is overlain by the T.B.U. Bedding in these overlying sedments is undeformed and is stratiform relative to the irregular, though sharp contact which is defined by the upper surface of Lithofacies 3.

Interpretation

Section 10.4 presented evidence for the development of stratiform pyrite in association with neomorphically aggraded carbonate mud. The timing of this mineralisation was classified as post-depositional owing to its occurrence as selective replacement to the carbonate mud component of low density debrites.

Lithofacies 2a of the Boulder Conglomerate mapped in 1285 Block 40 HWD is interpreted to have been reworked from petrographically equivalent

source strata judging by its association of clasts of pyritised/neomorphosed calcite with conglomeratic carbonate mud. Mass movement of this assemblage occurred prior to the cementation of the carbonate mud and is proved by its secondary reworking as matrix to the pyrite clasts. Major stratiform pyritisation is re-interpreted, therefore, to be synsedimentary: pyritisation-related neomorphism of the carbonate mud caused primary cementation of this sediment and occurred during remobilisation of the Boulder Conglomerate.

The remobilisation of massive pyrite and its deposition as Lithofacies 3, stratigraphically above 2a, proves that pyritisation of the seafloor substrate had intensified and was subsequently reworked. The irregular upper surface to Lithofacies 3 is interpreted as the upper depositional limit of the reworked pyrite and corresponds to the contemporaneous seafloor prior to the deposition of the T.B.U.

11.3 EVIDENCE FOR SYNSEDIMENTARY MINERALISATION IN THE T.B.U.

11.3.1 1345 348N

Description

Recognition of the U.D.L. type event bed described in Section 5B.2 was assisted because of its common association with sulphide mineralisation. Sphalerite and galena occur as replacement and vug fill within the oolitic portion of the bed (Photo. 328). Replacement of the oolite is heterogenous and the distribution of vug mineralisation is spatially associated with replaced limestone (Photo. 70). The vugs are irregular and rimmed with coarse crystals of galena which possess euhedral terminations in a voidwards direction. The vug fill comprises i) a layer of sphalerite which overlies the vug floor and possesses a level upper surface, and ii) sparite

occlusion to the remnant porosity (Photo. 329). The mineralised limestone is boudinaged, possessing a pinch and swell geometry. The distribution of the boudins coincides with the presence of the galena-rimmed vugs (Photo. 70). The overlying and underlying sediment is tangentially thinned at the lower and upper contacts with the vug mineralisation (Photo. 329).

Interpretation

The selective replacement of the U.D.L. type interbed suggests that the mineralisation was lithologically controlled. The mineralising fluids were corrosive and dissolution vugs were formed. Galena replaced the vug walls and grew into the vug as coarse, subhedral crystals. Sphalerite precipitated as microcrysts within the vug and were geopetally deposited as sediment on the vug floor. The remnant vug porosity was cemented by sparite.

Although mineralisation occurred after the deposition of the event bed, and overlying T.B.U., evidence for its early diagenetic timing is provided by the plastic deformation of the replaced strata during extensional tectonism. Lithification at the time of boudinage was restricted to the vugs which were cemented by sulphides and sparite, as indicated by the tangential compaction of the unlithified sediments at the apices to these rigid diagenetic heterogeneities. Mineralisation is interpreted, therefore, as early diagenetic and syntectonic.

11.3.2 1330 348S

Description

The occurrence of mineralisation in the T.B.U. was highlighted by the presence of stratiform sulphides which are contained within an erosive-based, concave-upwards depression (Photo. 330). This structure is 20 cm

deep at its axis and thins laterally to give a width of 1.5 m. It is interpreted as a channel because of its morphology and erosive base.

Mineralisation in the T.B.U. beneath the channel is represented by layers composed of sphalerite,pyrite and clay grain which are interlaminated with argillite (Photo. 331). Sphalerite predominates and occurs as mud-sized grains; the pyrite is framboidal and is distributed throughout the sulphidic sediment (Photos. 332 and 333). Evidence for pre-erosion extensional tectonism is provided by the presence of microfaults within the eroded substrate which do not displace the sediments occupying the channel (Photo. 60).

Samples were taken from the axis of the channel, permitting the identification of five intrachannel beds. In ascending stratigraphic order, these are represented by:

Bed 1) polymict breccia: tabular pebbles of silty mudstone and terrestrial plant fragments are set in a matrix of plastically deformed silty argillite and mud-sized sphalerite and framboidal pyrite (Photo. 334). The plant fragments exhibit perfect, three-dimensional preservation by sphalerite and framboidal pyrite (Photos. 335 and 336). The upper surface of this breccia is parallel to the bedding in the T.B.U., but is irregular owing to the poor sorting and angularity of the clasts.

Bed 2) laminated silty argillite.

Bed 3) massive pyrite which possesses a sharp basal contact with Bed 2) and contains no evidence for precursor sediment (Photo. 337).

Bed 4) sulphide breccia: granule to pebble-sized clasts composed of mud-sized sphalerite and framboidal pyrite are set in a compositionally-equivalent matrix; clasts of silty argillite ranging in size from sand to pebble are supported by the sulphides. The contact with Bed 3) is sharp and undulatory (Photo. 337).

Bed 5) sulphide breccia: this is compositionally equivalent to 4), but is distinguished by the presence of plastically deformed sphalerite-framboidal pyrite clasts which exhibit an attenuated tabular morphlogy (Photo. 337). The contact with 4) is sharp and undulatory. The upper contact with the T.B.U. is sharp and irregular, but is bedding-parallel.

Interpretation

i) depostion of the Boulder Conglomerate ceased and the basin became the depositional site of shale and calcarenite. The siliciclastic silt content of the shale represents hemipelagic sediment deposited under conditions of low energy and derived from an exposed Lower Palaeozoic source located distally and to the north. Production of bioclasts continued on the carbonate platform located upslope and to the north. This sediment was frequently remobilised and redeposited in a basinwards direction as limestone interbeds to the shale.

ii) precipitation of sphalerite and framboidal pyrite as sulphide mud which was deposited on the seafloor as authigenic laminae.

iii) synsedimentary extensional tectonism caused the mass movement of the contemporaneous sediments comprising unlithified authigenic sulphide mud, hemipelagic sediment and mineralised plant fragments of terrestrial origin (N. Clarke, pers. comm., 1994). The remobilised sediments locally eroded the seafloor and were deposited on the floor of the channel as Bed 1. The synsedimentary timing of the sulphides is confirmed by the occurrence of uncompacted plant fragments. These were reworked in a matrix which was unlithified and compositionally equivalent to the channel floor sediments.

iv) re-establishment of hemipelagic sedimentation (Bed 2).

v) synsedimentary precipitation of pyrite within the channel (Bed 3).

vi) reactivated tectonism caused the repeated mass movement of variably lithified authigenic sulphide mud. This was deposited over the intrachannel pyrite as Bed 4. The pyrite possessed a viscous rheology and responded plastically.

vii) repeated mass movement and plastic deformation of unlithified, authigenic sulphide mud (Bed 5).

11.4 CONCLUSIONS: DEVELOPMENT OF SYNSEDIMENTARY MINERALISATION IN THE BOULDER CONGLOMERATE AND T.B.U.

Evidence for synsedimentary mineralisation spans the stratigraphic extent of the Boulder Conglomerate and is also present in the Thinly Bedded Unit. Active tectonism during mineralisation is witnessed on the microscopic and macroscopic scales, ranging from in-situ microfracturing to local, mass flow.

Stratigraphically early C.G.O. is dominated by stratiform sphalerite and galena mineralisation developed as cement to primary porosity and peripheral clast replacement to matrix-deficient breccia units. The contiguous development of ore as cement to the Boulder Conglomerate and as replacement to the underlying Shaley Pales proves that mineralisation of the allochthon and T Fault hanging wall was coeval.

The upper C.G.O. is dominated by pyrite as selective replacement to carbonate mud. Evidence for the early diagenetic timing of this pyritisation is provided by the reworking of petrographically equivalent pyrite as clasts in a matrix of unlithified carbonate mud. The stratigraphic increase in the amount of reworked pyrite records the intensification of the pyritisation with time.

On the basis of petrographic and sedimentologic evidence, the timing of the C.G.O. is interpreted as synsedimentary relative to the deposition of

the Boulder Conglomerate and to have occurred during extensional tectonism. The next chapter assesses the validity of this interpretation through the sulphur isotope signature of the C.G.O.

CHAPTER TWELVE. SULPHUR ISOTOPE ANALYSIS OF THE CONGLOMERATE GROUP ORE

12.1 OBJECTIVES

The C.G.O. was classified in Chapter 11 as synsedimentary to early diagenetic. This interpretation was based on petrologic evidence. Hypothesis Three stated that for this interpretation to be valid, the C.G.O. would have to yield isotopic evidence for the precipitation of sulphide minerals on or near the seafloor. For this purpose, the stable isotopes of sulphur were analysed at the Scottish Universities Research and Reactor Centre in order to i) understand the spatial and temporal isotopic evolution of the C.G.O., ii) determine the source of the sulphur associated with the sulphide mineralisation, and iii) characterise the likely chemical reactions related to, and generating, the mineralisation.

12.2 METHOD

The $\delta^{34}S$ data was acquired from samples of pyrite, sphalerite and galena which were obtained from the underground exposures of the C.G.O. referred to in this thesis. Prior to analysis, all samples were petrographically/paragenetically characterised using thin sections; sample mineralogy and purity was verified by XRD.

Acquisition of the $\delta^{34}S$ data was two stage:

1) 5-10 mg of monominerallic sulphide powders were obtained using a diamond-tipped dentist's drill to establish the mesoscopic $\delta^{34}S$ signature of pyrite, sphalerite and galena. The size of the drillbit required for sample extraction was selected according to the resolution of the ore texture. Duplicate samples were analysed to establish the repeatability of the $\delta^{34}S$ values obtained.

2) microscopic laser ablation of polished blocks provided $\delta^{34}S$ data on the smallest scale available in the United Kingdom at the time of research, permitting samples of 500 microns^2 to be analysed. The samples selected for ablation included those in which i) there was insufficient sample for conventional analysis; ii) the ore texture was beyond the resolution of the finest drillbit; and iii) samples which exhibited directional zoning. For the latter samples $\delta^{34}S$ were used to monitor the isotopic evolution of the sulphur as precipitation occurred. Laser analyses were instrumental in ascertaining the microscopic $\delta^{34}S$ paragenesis of the C.G.O.

Conventional analysis, therefore, provides an insight into the bulk $\delta^{34}S$ of the C.G.O., whereas the laser technique supplies information regarding the small scale processes. The laser results were compared to those acquired conventionally to determine the effect of sample size on the $\delta^{34}S$ values.

12.3 SULPHUR ISOTOPES: THEORY AND APPLICATION TO MINERAL DEPOSITS

Sulphur has four stable isotopes, the respective average abundances of which are given in brackets: ^{32}S (95.02%), ^{33}S (0.75%), ^{34}S (4.22%), and ^{36}S (0.02%) [Macnamara and Thode, 1950]. ^{32}S and ^{34}S are the two most abundant isotopes and differ in mass by about 6%. The results are reported as permil (‰) difference from a primary standard as follows:

$$\delta^{34}S = \frac{(^{34}S/^{32}S)\ \text{sample} - (^{34}S/^{32}S)\ \text{standard}}{(^{34}S/^{32}S)\ \text{standard}} \times 1000$$

Sulphur from the Cañon Diablo meteorite with $^{34}S/^{32}S = 0.0450045$ (Jensen and Nakai, 1963) is the conventional standard and, by definition, has

$\delta^{34}S$ of 0.00 ‰. Positive and negative $\delta^{34}S$ represent, respectively, enrichment and depletion of ^{34}S relative to this standard. Fractionation occurs when the relative abundance of ^{34}S and ^{32}S is altered. There are two types of reaction which produce sulphur isotope variations. The bacterial reduction of sulphate to hydrogen sulphide by certain anaerobic bacteria is a kinetic effect which results in the enrichment of hydrogen sulphide in ^{32}S. Thermochemical reduction of sulphate is an equilibrium fractionation which occurs in the presence of hydrothermal fluid at temperatures greater than 300-350°C (Ohmoto and Lasaga, 1982); the high temperatures associated with thermochemical fractionation exclude this process from being involved in formation of Irish, carbonate-hosted, zinc-lead deposits which are believed to have formed from hydrothermal fluids with a maximum temperature of 250°C (Samson and Russell, 1983, 1987).

12.3.1 Sulphur isotope fractionation in sedimentary rocks

The most important cause for variations in the isotopic composition of sulphur is the reduction of sulphate ions by anaerobic bacteria such as *Desulfivibrio desulfuricans*, which live in sediment deposited in the oceans and in lakes. These bateria split oxygen from sulphate ions and excrete H_2S which is enriched in ^{32}S relative to the sulphate. It is a non-equilibrium reaction which involves the oxidation of organic matter and is expressed as:

$$2(CH_2O) + 2H^+ + SO_4^{2-} \dashrightarrow H_2S + 2H_2CO_3$$

The degree of isotope fractionation by bacteria is inversely proportional to the rate of sulphate reduction, which is in turn controlled by temperature or sulphate concentration or both. The isotopic composition of H_2S liberated by bacteria depends also on the magnitude of the sulphate reservoir. In an open sytem, the sulphate reservoir is infinite and the $\delta^{34}S$ will remain constant, assuming no change in bacterial metabolism. In a

closed system on the other hand, where the sulphate reservoir is limited, its isotopic composition will change due to the preferential removal of ^{32}S as H_2S. The irreversible loss of ^{32}S from the system means that the residual sulphate becomes enriched in ^{34}S. As a consequence, the $\delta^{32}S$ value of the sulphide will also change as a function of time because the enrichment in ^{32}S relative to the standard will be diminished even though the fractionation factor with respect to sulphate remains constant. Enrichment in ^{32}S up to 50‰ has been observed in the Black Sea (Vinogradiv et al., 1950). Such large fractionations are not always achieved and intermediates are produced. Claypool et al. (1980) estimate the $\delta^{34}S$ of Lower Carboniferous seawater sulphate to be +19‰. Assuming the species of anaerobic bacteria which existed during the Lower Carboniferous could mediate the enrichment in ^{32}S seen to occur in the present day natural environment, then the production of sulphides containing negative $\delta^{34}S$ values is expected.

12.3.2 Recent work on bacteriogenic sulphate reduction

Canfield and Thamdrup (1994) have shown that in bacterial systems which are open to sulphate, cycles of fractionation accompanying the bacterial disproportionation of S^0, followed by sulphide oxidation, can generate the large ^{34}S depletions of marine sedimentary and water column sulphides. They propose that "through a repeated cycle of sulphide oxidation to S^0 and subsequent disproportionation, sulphides may be generated that are much more depleted in ^{34}S than those produced in the initial reduction of sulphate to sulphide".

12.4 PREVIOUS WORK

The $\delta^{34}S$ values for sulphide minerals present in the Navan deposit range from -38‰ to +14‰ (Anderson et al., 1986, 1987). The data possesses a bimodal distribution about 0‰: modes occur at -15‰ and +15‰, with the bulk of the ore at Navan containing sulphur enriched in ^{32}S (Anderson, 1990). Anderson (1990) interprets this data to represent the involvement of two sources of sulphur in the formation of sulphide mineralisation at Navan. The population containing sulphide minerals enriched in ^{32}S was the dominant sulphur source. This was derived through reduction of Lower Carboniferous seawater sulphate ($\delta^{34}S$ of +19%; Claypool et al., 1980) by anaerobic bacteria. The population represented by sulphide minerals containing sulphur enriched in ^{34}S is interpreted by Anderson (1990) to show the presence of hydrothermal sulphur which was leached from pyrite present in the Lower Palaeozoic lithologies below the deposit. Anderson (1990) regards the sulphide at Navan to have resulted from fluid mixing: the predominance of the bacteriogenic sulphide is reflected in the bulk of the ore containing sulphur which is enriched in ^{32}S.

In a sulphur isotope study of the Silvermines deposit, Coomer and Robinson (1976) and Greig et al. (1971) established a range of $\delta^{34}S$ from -45 to +10 . The data exhibits a bimodal distribution, with modes for the Lower and Upper G zones occurring at 0‰ and -20‰, respectively. Coomer and Robinson (1976) interpret that two sources of sulphur were involved in the formation of the Silvermines deposit. Sulphide minerals which possess isotopically negative $\delta^{34}S$ are also interpreted to have formed by the combination of the base metals with sulphur produced by the reduction of Lower Carboniferous seawater sulphate by anaerobic bacteria. The sulphides present in the population which clusters around 0‰ contain sulphur enriched in ^{34}S, and are interpreted to have incorporated sulphur whose

source was seated deep in the basement. Ore formation occurred when the hydrothermal fluids, containing base metals and sulphur mixed with bateriogenic sulphur present in the Lower Carboniferous seawater. Coomer and Robinson (1976) suggest that the upwards vertical transition to more negative $\delta^{34}S$ is an isotopic zonation which reflects proximity to the Lower Carboniferous seafloor. They state that "if the Upper G orebody did not form on the seafloor, this change was probably caused by progressive mixing with seawater".

12.5 $\delta^{34}S$ ANALYSIS OF THE C.G.O.

12.5.1 Introduction

Figure 16 shows the total $\delta^{34}S$ datasets for pyrite, sphalerite and galena in the C.G.O. Histograms are then presented in Figure 17 to demonstrate the relationship between the stratigraphic position and $\delta^{34}S$ of these sulphides. The data is interpreted in relation to the sedimentary and diagenetic history of the Boulder Conglomerate and Thinly Bedded Unit.

12.5.2 Total $\delta^{34}S$ dataset for the C.G.O.

Description

Figure 16 shows $\delta^{34}S$ data obtained for pyrite, sphalerite and galena. The majority (92%) of the C.G.O. sulphides exhibit isotopically negative $\delta^{34}S$. Pyrite has an inhomogeneous distribution of $\delta^{34}S$, values of which ranges from -40‰ to +1‰. $\delta^{34}S$ of sphalerite ranges from -41‰ to -7‰. The distribution $\delta^{34}S$ for sphalerite is bimodal; the means of the two populations are -38‰ and -11‰. Galena exhibits the narrowest $\delta^{34}S$ range (-17‰ to +6‰) and has mean of -8‰.

Interpretation

Relative to the $\delta^{34}S$ value of Lower Carboniferous seawater sulphate of +19‰ (Claypool et al., 1980), the minimum $\delta^{34}S$ values for pyrite (-40‰), sphalerite (-41‰) and galena (-14‰) show that iron, zinc and lead combined with sulphur which was fractionationed by up to 59‰, 60‰ and 33‰, respectively. The only viable process which could have fractionated sulphur to the extent shown by the sulphide minerals of the C.G.O. is the reduction of sulphate by anaerobic bacteria in a relatively open system. The range of $\delta^{34}S$ reflects the production of intermediates which result from variations in the rate of sulphate reduction, the availability of oxidisable organic matter, temperature, species of bacteria and population density, mixing with sulphur produced in a closed system or derived from hydrothermal leaching of the basement.

The submarine setting of the Boulder Conglomerate satisfies the environmental criterion that seawater provided the infinite reservoir of sulphate for reduction by anaerobic bacteria. Sulphate reduction by is mediated at, and a short distance beneath, the seafloor (Curtis, 1987): petrographic and isotopic evidence converge in defining the C.G.O. as synsedimentary relative to the deposition of the Boulder Conglomerate.

12.5.3 Lithostratigraphic distribution of $\delta^{34}S$ in the C.G.O.

Description

Figure 17 presents the $\delta^{34}S$ data for the C.G.O. according to the relative stratigraphic location of the mineralisation in the Boulder Conglomerate, as identified in underground exposure. The lithofacies of the Boulder Conglomerate and the range of $\delta^{34}S$ for the associated mineralisation is shown in Figure 12.

<u>$\delta^{34}S$ of the C.G.O. in the Lower Boulder Conglomerate</u> (Figure 17a)

The mineralisation occurs as replacement to the Shaley Pales, as cement and/or replacement to the breccia beds, as replacement to the interbeds, and as clasts of P.B.O. The minimum $\delta^{34}S$ for sulphide minerals is -21‰. The mean values for pyrite, sphalerite and galena are -8‰, -10‰ and -10‰, respectively. Pyrite exhibits a range of 22‰ compared to 14‰ for galena and 4‰ for sphalerite. The broad range demonstrated by pyrite and galena is afforded by the occurrence of a cluster of values about 0‰. $\delta^{34}S$ of sulphides developed as replacement to the Shaley Pales and the interbeds fall within the range of values exhibited by the sulphides present as cement/replacement to the breccia beds.

<u>$\delta^{34}S$ of the C.G.O. in the Middle Boulder Conglomerate</u> (Figure 17b)

Pyrite occurs as replacement to the carbonate matrix of clast-supported debris flows. $\delta^{34}S$ of this pyrite ranges from -31‰ to -20‰ and has a mean of -28‰.

<u>$\delta^{34}S$ of the C.G.O. in the Upper A Boulder Conglomerate</u> (Figure 17c)

Mineralisation occurs as replacement of low density, carbonate mud debris flows. Clusters of spherular pyrite replaces the carbonate mud and are overgrown by botryoidal pyrite (Photo. 316). The edge of the pyrite botryoids are overgrown by sphalerite and galena (Photo. 319). $\delta^{34}S$ of the pyrite ranges from -32‰ to -35‰. Laser analysis showed that $\delta^{34}S$ of the spherular pyrite is -32‰ compared to values of -34‰ and -35‰ for the botryoidal pyrite overgrowths; conventional analysis of a combined pyrite sample produced $\delta^{34}S$ of -33‰, which equates to the mean of the pyrite population. The paragenetically later sphalerite and galena possess $\delta^{34}S$ signatures which are distinct from the pyrite. The $\delta^{34}S$ of sphalerite ranges

from -18‰ to -7‰; galena contains sulphur which is enriched in ^{34}S, ranging from -17‰ to +6‰. This is shown in the mean $\delta^{34}S$ values of -13‰ and -10‰ for sphalerite and galena, respectively.

$\delta^{34}S$ of the C.G.O. in the Upper B Boulder Conglomerate (Figure 17d)

The Upper B facies of the Boulder Conglomerate comprises reworked sulphides. It is the stratigraphically highest facies of the Boulder Conglomerate. Values of $\delta^{34}S$ for pyrite range from -40‰ to -30‰; the mean value for pyrite is -33‰. Sphalerite which is plastically deformed in association with the reworked pyrite exhibits $\delta^{34}S$ of -23‰. A single $\delta^{34}S$ analysis for reworked pyrite from 1285 HWD falls within the range exhibited by the reworked pyrite exposed in 1330 348S.

$\delta^{34}S$ of the sulphides in the Thinly Bedded Unit (Figures 17e and f)

The T.B.U. was deposited contiguously over the Upper A and B facies of the Boulder Conglomerate. Sulphides occur as laminae and channel-filling debris flows. The $\delta^{34}S$ of sphalerite ranges from -41‰ to -37‰; the mean value for sphalerite is -39‰. The $\delta^{34}S$ of pyrite is constant at -39‰, giving a mean value which is the same as the sphalerite.

Interpretation

The sulphur isotope data presented in Figure 17 shows that the major sulphur source for the C.G.O. was bacterially reduced seawater sulphate which had a $\delta^{34}S$ value of +19‰ (Claypool et al., 1980). The system was open during the deposition of the Boulder Conglomerate and the T.B.U., permitting the continued production of sulphur which was enriched in ^{32}S. It is not possible to state unequivocally what caused the variation in $\delta^{34}S$ fractionation. Possible factors include: the species of bacteria, population

density, metabolic rate, temperature, the availability of oxidisable organic matter, mixing with fluid containing sulphur enriched in ^{34}S.

Evidence for the existence of fluids containing isotopically distinct sulphur is provided by the sulphides minerals developed as replacement to carbonate mud in the Upper A facies of the Boulder Conglomerate (Photo. 319). The narrow range of $\delta^{34}S$ (32‰ - 35‰) of the pyrite reflects the precipitation of sulphides during the production of isotopically homogeneous, bacterial sulphur in an open system. The isotopic signature of the paragenetically later sphalerite and galena is distinct from the pyrite: galena contains sulphur relatively enriched in ^{34}S, and sphalerite and galena contain sulphur which is relatively unenriched in ^{32}S compared to the earlier pyrite. The ore mineral assemblage indicates that fluids containing bacteriogenic sulphur mixed with hydrothermal sulphur and/or sulphur produced in a partial closed system.

12.6 CONCLUSIONS: CONVERGENCE OF ISOTOPIC AND PETROLOGIC EVIDENCE

The overwhelmingly negative $\delta^{34}S$ signature of the C.G.O. indicates that open sytem bacterial reduction of contemporaneous seawater sulphate was instrumental in the formation of sulphides. Hypothesis Three, stating that the formation of the C.G.O. occurred during deposition of the Boulder Conglomerate, survives both isotopic and petrologic scrutiny.

12.6.1 Possible chemical reactions associated with the mineralisation and their metallogenic implications

Production of sulphide by anaerobic bacteria:

$$2(CH_2O) + 2H^+ + SO_4^{2-} \dashrightarrow \mathbf{H_2S} + 2H_2CO_3 \quad (1)$$

Formation of base metal sulphide minerals:

$$Zn^{2+} + H_2S \text{ ---> } \mathbf{ZnS} + 2H^+ \quad (2)$$

$$Pb^{2+} + H_2S \text{ ---> } \mathbf{PbS} + 2H^+ \quad (3)$$

$$FeS + H_2S \text{ ---> } \mathbf{FeS_2} + H_2 \quad (4)$$

The sulphide produced in reaction (1), when combined with Zn, Pb and Fe, results in the formation of sphalerite, galena and pyrite, respectively. Reactions (2) and (3) are acidifying since hydrogen ions are released upon reaction of the Zn and Pb with H_2S. The physical manifestation of this acidification is represented by the dissolution of calcium carbonate, evidence for which is ubiquitous throughout the limestone of the mineralised Navan area. The acidifying reactions provide chemical evidence which converges with the petrographic evidence (Chapters 7 and 8) to show that Rizzi's hypothesis, involving meteoric diagenesis in the formation of secondary porosity, is not viable.

The effects of reactions 1-4, therefore, generated a positive feedback system which permitted continued and enhanced metallogenesis in the Navan area: the bacterial production of H_2S was instrumental in the formation of base metal sulphides, and the precipitation of Zn and Pb sulphides produced acidic fluids which corroded the carbonate host, permitting further growth of sulphides in the dissolution pores.

Mineralisation in the Navan area epitomises, therefore, the Gaia theory of Lovelock (1962): biological activity has ability to extensively modify the contemporaneous enviroment in a coevolution of content and context. Large scale production of sulphide by bacteria created an effective sink for upwelling, hydrothermally-derived base metals. For this reason, the localised production of bacterial sulphur was a controlling factor in the formation of the C.G.O. in particular and the Navan Orebody in general. The

massive production of sulphur depleted in ^{34}S implies that the chemical factors essential for the metabolism of anaerobic bacteria (organic matter, sulphate, iron) were not limiting. The continued survival of the bacterial colony could possibly represent the ecological response to the mineralisation since the continuous precipitation of sulphide minerals prevented the concentration of metals reaching toxic levels.

CHAPTER THIRTEEN. SYNTHESIS OF MINERALISATION

13.1 THE LITHOSTRATIGRAPHIC TIMING OF THE C.G.O. AND ITS RELATIONSHIP TO THE P.B.O.

In metallogenic terms, the objective of this research was to provide unequivocal evidence to determine the lithostratigraphic timing of Europe's largest Zn-Pb oreboby. This was achieved by applying and integrating fundamental, and often elementary, geologic and isotopic principles. Chapter Two presented the questions which stimulated the metallogenic aspects of this research. The questions and their answers are presented below.

1) Was the deposition of the Boulder Conglomerare syngenetic or epigenetic relative to the formation of the C.G.O.?

The key factors which enabled this question to be answered were i) the collection and preparation of a representative population of samples, and ii) the determination of the requisite scale of observation. On the basis of the petrographic information generated during the course of the research, the lithostratigraphic timing of the C.G.O. was **syngenetic relative to the deposition of the Boulder Conglomerate and T.B.U.** Evidence to prove this is provided by:-

a) the growth of sulphides associated with the early diagenetic cementation of interbeds to stratigraphically early, clast-dominated Boulder Conglomerate (Photos. 28, 293-298, 323-327). The primary, interclast porosity of the breccia beds was cemented by sulphides, barite, sparite and dolomite; the clast edges experienced peripheral corrosion and replacement (Photos. 22, 278, 279, 281-292).

b) the pyritisation and secondary remobilisation of unlithified carbonate mud debris flows in the upper Boulder Conglomerate during extensional tectonism (Photos. 48, 49, 55, 56-59, 306-322).

c) the development of sulphides as rigid diagenetic heterogeneities within unlithified U.D.L.-type event beds in T.B.U. during extensional tectonism (Photos. 70 and 329).

d) the precipitation of sphalerite and framboidal pyrite as authigenic sulphide mud during the replacement of plant fragments. The authigenic sediments were reworked as sulphide debris flows during extensional tectonism (Photos. 331-337).

The gross stratiform morphology of the C.G.O. is related, therefore, to:

- the cementation of breccia beds by sulphides.
- the selective replacement of carbonate strata by sulphides.
- mass movement of the replaced strata and subsequent redeposition as a sedimentary assemblage *sensu stricto*.
- the precipitation of authigenic sulphide sediment as laminae within the T.B.U.

Although the occurrence of authigenic sediment provides evidence for the direct precipitation of sulphides from the ore-related fluids on the seafloor, this type of mineralisation is volumetrically insignificant. The majority of the ore occurs as **replacement to carbonates** and **occlusion to primary and/or secondary porosity**; the generation of secondary porosity is restricted to carbonate strata and confirms the solubility of $CaCO_3$ in the presence of the ore fluids. The volume of sulphide mineralisation present as C.G.O. is related, therefore, to sediments which possessed the primary

compositional and porosity properties: **the existence of the requisite precursor sediments determines the potential for economic mineralisation.**

2) <u>What is the $\delta^{34}S$ signature of the C.G.O.?</u>

The C.G.O. is dominated by **biogenic sulphur** derived by the reduction of seawater sulphate by anaerobic bacteria in an open system. The presence of biogenic sulphur is consistent with the development of the C.G.O. during sedimentation since the criteria for a contemporaneous seawater sulphate source and the existence of a sediment-seawater interface for the hydrologic and/or diffusive input of H_2S containing sulphur enriched in ^{32}S are satisfied.

3) <u>What is the relationship of the C.G.O. to the P.B.O.?</u>

Major ore developed in the autochthon as replacement to petrographically varied carbonate lithologies, the regional stratiform depositional shape of which dictated that gross morphology of the ore was stratiform (Figures 7 and 8). Deviations from this configuration are represented by the precipitation of the ore mineral assemblage within ore-related dissolution vugs and unlithified detrital strata; the unlithified state of the detrital sediments was either primary or the product of dissolutional reworking. Brecciation of the replaced limestone host strata resulted in the injection of the diagenetic-detrital sedimentary assemablage as matrix to the autoclasts, as described in Chapter 7. Evidence for tectonic, in-situ brecciation prior to ore formation is provided by the injection of unmineralised sediment as matrix to locally fragmented and rotated carbonate strata. This primary autobreccia fabric was exploited by the mineralising fluids and proves that the presence of both tectonic and sedimentary/diagenetic interfaces controlled the subsequent flow and/or

diffusion of these fluids through the autochthon. Injection of the unlithified ore assemblage records evidence for the gravitational restructuring of a variably lithified and vuggy autochthon.

Evidence for pre-Boulder Conglomerate mineralisation is provided by the truncation of P.B.O. by the unconformity and the occurrence of P.B.O. which has been reworked as stratigraphically early Boulder Conglomerate. The clasts are petrographically equivalent to in-situ P.B.O. present at low structural and stratigraphic levels in the footwall scarp of the T Fault. The matrix is identical to the detrital-diagenetic sediment which was recognised as matrix to the autobrecciated Pale Beds. The para-autochthonous setting of the reworked P.B.O. proves that reworking was confined to the half graben defined by the T Fault (Figure 8). The unlithified state of the reworked matrix proves that the deposition of the Boulder Conglomerate occurred during the formation of the P.B.O. (Photos. 33-36). The amount of reworked P.B.O. in the Boulder Conglomerate is disproportionately small when one considers its local fault scarp source in relation to the volume of mineralisation hosted by the autochthon: the rock avalanches evidently sampled an immaturely mineralised autochthon; it is probable that the mass movements were related to the gravitational restructuring of the autochthon, facilitated by the heterogeneously lithified nature of the Navan Group strata during continued extensional tectonism.

Major ore formation within both the autochthon and allochthon commenced after the displacement of the stratigraphy by the T Fault and occurred during the deposition of the Boulder Conglomerate in the half graben produced by this tectonism. This tectonic-sedimentary-metallogenic theme was portrayed in its completeness in the 1315 exposure of the C.G.O. (Plan 1). The P.B.O. is not truncated by the T Fault. Instead, sulphide mineralisation occurs as i) cement to the tectonically brecciated footwall

(Photos. 13 and 14), ii) rim replacement to unmineralised clasts present in the fault zone (Photo. 305), and iii) replacement of the footwall which becomes more intense away from the T Fault and/or fault scarp unconformity (Photos. 299-301); the zone between the fault breccia and major ore is fault parallel and comprises neomorphically degraded limestone which is massively replaced by barite but contains only disseminated sulphides (Photos. 302-304). The Boulder Conglomerate immediately overlying the unconformity is cemented by sulphides in contiguity with replacement and/or fracture-cementing mineralisation within the Shaley Pales beneath the unconformity in the hanging wall of the T Fault (Photos. 16, 22 and 262-277).

The $\delta^{34}S$ signature of the P.B.O. is a bimodal distribution about zero permil, which Anderson (1990) interprets as the mixing of bacterially depleted sulphur with hydrothermal sulphur derived from the upwelling metalliferous fluids. The Boulder Conglomerate was the site of massive bacterial sulphur production and is invoked as the contemporaneously and locally derived source of depleted sulphur which contributed to the formation of the P.B.O. and C.G.O.

4) Why is the Waulsortian Limestone relatively unmineralised?

The A.B.L. Group was deposited in response to an episode of submarine extensional tectonism. Normal faults striking NE-SW displaced the Navan Group to the northwest. The limited vertical displacement by these faults is proved by the presence of Shaley Pales in both hanging walls and footwalls. Increasingly carbonate-dominated sediments accumulated unconformably upon the down-warped Navan Group. Evidence for early diagenetic calcite cementation and syntectonic-synsedimentary deposition of the Waulsortian Limestone is provided by the mass movement of biosparite

in a carbonate mud matrix. There is no mineralisation associated with either the clasts or matrix present in this monomict breccia.

Waulsortian Limestone containing dolomite and minor sulphides, and dolomitised Shaley Pales, are present as clasts within the Boulder Conglomerate deposited in the half graben defined by the T Fault: the Navan area was the site of regional hydrothermal alteration which occurred after the deposition of the A.B.L. Group and before the mass movement of all pre-exisiting lithologies into the basin created by the later catastrophic phase of extension which produced the T Fault. Regional dolomitisation resulted from the flow of ore-related fluids into strata located laterally and vertically with respect to the developing P.B.O. The compositional and textural characteristics of the A.B.L. Group and Shaley Pales permitted the ubiquitous dolomitisation. The lack of major sulphide mineralisation within the Shaley Pales and A.B.L. Group resulted from i) the absence of contemporaneous sulphidic sediments deposited unconformably over the Shaley Pales and A.B.L. Group, and ii) the presence of argillaceous interbeds throughout the Shaley Pales and within the basal A.B.L. Group acted as vertical permeability barriers, precluding the ascent of the metalliferous fluids.

13.2 COMPARISON WITH OTHER IRISH DEPOSITS

The Navan Orebody is anomalous when compared to other Irish Zn-Pb deposits, e.g. Silvermines, Tynagh, and Lisheen, because the majority of the ore occurs as epigenetic replacement to the Navan Group and the syngenetic portion is not associated with the Waulsortian. In all cases, however, mineralisation is spatially related to the normal fault which causes maximum vertical dsiplacement of the Lower Carboniferous stratigraphy;

the syngenetic ore is developed in association with the contemporaneous sediments which were deposited in the half graben.

In stratigraphic terms, the position of the ore is explained by the broadly contemporaneous, i.e. mid-Dinantian, timing of the mineralisation in relation to the distribution of i) the Waulsortian Limestone and ii) the shallow marine carbonate succession deposited conformably over the Old Red Sandstone. The distribution of the Waulsortian Limestone ranges from thick and laterally continuous in the southwest of the Irish Midlands to sporadic bioclastic limestone build-ups in the northeast (Figure 3; Lees, 1964; Gray, 1986). The potential for mineralisation hosted by the Waulsortian in the southwest is increased, therefore, owing to its greater lateral, and possibly stratigraphic, distribution.

The Old Red Sandstone is succeeded by shallow marine limestones. Although the latter are contiguous throughout the Irish Midlands, the succession thickens considerably to the north (Figure 3). The potential for mineralisation hosted within Navan Group-equivalent sediments, therefore, is increased to the north.

If one applies this tectono-sedimentary template to the Silvermines deposit, for example, it is obvious that the scarcity of ore within the footwall to the Silvermines Fault is related to preservation of Old Red Sandstone (the Basal Clastics) and Lower Palaeozoic lithologies (the Silurian greywackes) in the horst block, as a result of fault-related omission of the stratigraphy (Figure 18). These lithologies contain only disseminated and fracture-filling mineralisation since their non-limestone composition prevented the development of major ore as epigenetic replacement. The presence of epigenetic mineralisation within the Silvermines deposit is located in the hanging wall to the Silvermines fault: the Lower G Zone comprises

sphalerite and galena occurring as replacement, cavity fill and fracture fill to hydrothermally dolomitised oolitic limestone (Figure 18; Andrew, 1986).

The Upper G Zone is located within limestone strata deposited in the hanging wall to the Silvermines Fault and represents the syngenetic portion of the Silvermines deposit. The ore is developed at the base of the Waulsortian Limestone and is characterised by stratiform massive pyrite and debris flows comprising clasts of mineralised and unmineralised Waulsortian Limestone in a matrix of sulphides, dolomite and fine rock debris (Boyce et al., 1984; Andrew, 1986).

On the basis of petrographic evidence, the Lower and Upper G Zones are analagous with the P.B.O. and C.G.O., respectively. The epigenetic ore of the Lower G Zone is hosted in hanging wall owing to the absence of limestone strata in the footwall. The syngenetic ore provides evidence for mineralisation during reworking of the Waulsortian Limestone into the half graben created by the Silvermines Fault. The thickening of the A.B.L. Group across this fault implies that sedimentation was influenced by localised subsidence. The earliest evidence for major displacement is provided the reworking of Waulsortian Limestone and ore as debris flows into the half graben: the Silvermines Orebody formed during the episode of normal faulting which resulted the mass movement of the mineralised Waulsortian Limestone into the half graben created by the Silvermines Fault (Andrew, 1986).

The equivalence of the C.G.O. with the Upper G Zone, and of the P.B.O. with the Lower G Zone is reflected in the spatial distribution of $\delta^{34}S$. The epigenetic portion of both orebodies are characterised by sulphur which is relatively enriched in ^{34}S (Anderson, 1990; Coomer and Robinson, 1976). The C.G.O. and the Upper G Zone, on the other hand, are associated with sulphur enriched in ^{32}S. This isotopic zonation is interpreted by Coomer and

Robinson (1976) to represent the progressive mixing of hydrothermal fluids, containing metals and sulphur enriched in ^{34}S, with Lower Carboniferous seawater containing biogenic sulphur. Petrologically and isotopically, therefore, the Silvermines and Navan deposits are analogous.

13.3 METALLOGENIC MODEL

The Navan Orebody is classified as a "composite deposit" (Laznicka, 1985) owing to the paragenetic equivalence of the P.B.O. with the C.G.O. The P.B.O. represents the epigenetically mineralised autochthon; the C.G.O. is the laterally equivalent, syngenetically mineralised allochthon. It is this bipartite spatial and temporal division of the mineralisation which characterises Irish-type deposits (Hitzman and Large, 1978).

The formation of mineralisation is in accordance with Russell (1983) and is summarised:

i) extensional tectonism raised the geothermal gradient and permitted the ascent of hydrothermal fluids which leached metals and sulphur from the crust. Bischoff et al. (1981) reported the concentration of heavy metals, as chloride complexes, when brines of varying salinities and temperatures were reacted with greywacke. Experimental evidence shows, therefore, the potential for saline fluid to leach metals from the geosynclinal lithologies present in the Lower Palaeozoic Basement and to transport them as chloride complexes.

ii) the fluid flow was directed by major crustal lineaments related to the Caledonoid structural grain. As the upwelling fluid intersected the upper level of the crust, fluid flow was focussed into extensionally faulted strata.

iii) the half graben generated by the extension was site of prolific bacterial reduction of seawater sulphate. Mixing of the metalliferous, hydrothermal fluids with biogenic sulphur in the seawater resulted in the precipitation of

sulphide minerals. It is probable that the growth of the bacterium reflects the ecological response to the inundation of a sediment-seawater system with hot, metalliferous fluids.

The development of ore grade mineralisation was controlled by the presence of vertically and laterally extensive limestone strata. The fluids permeated into the host sediments located in both the faulted autochthon and the contemporaneous sediments deposited in the half graben. Major ore formation occurred as epigenetic replacement of the autochthon during replacement and/or cementation of limestone-rich strata in the Boulder Conglomerate. The hydrothermal fluids were corrosive to calcite and generated secondary porosity which assisted the flow of the fluids into the host limestone. The syngenetic timing and isotopically negative $\delta^{34}S$ signature of the C.G.O. define the Boulder Conglomerate as a zone of major bacterial sulphur production.

13.4 EXPLORATION GUIDELINES

The conclusions of this research state that in order for base metal sulphide mineralisation to achieve the magnitude exemplified by the Navan Orebody, four fundamental requirements must be satisfied: metalliferous, hydrothermal fluids must mix with bacterially-produced sulphide in the presence of extensionally faulted carbonate strata which is of sufficient volume to host an economic deposit. All four factors must co-exist spatially and temporally, or significant mineralisation will not occur.

It is critical to appreciate that although Irish base metal sulphide mineralisation is often associated with Waulsortian Limestone, the presence of Waulsortian Limestone is not essential to mineralisation: all limestones possess equal capacity for replacement owing to their calcium carbonate composition. This is exemplified by the Navan Orebody, Europe's largest

zinc-lead mine, where neither the epigenetic nor the syngenetic ore is hosted by Waulsortian Limestone: the occurrence of the A.B.L. Group in proximity to the mineralisation at Navan was incidental.

The common factor to all Irish-type orebodies is the presence of major normal faults which displace Lower Carboniferous limestone stratigraphy. The exploration target areas are second order half grabens developed in limestone stratigraphy during the Lower Carboniferous. Proximity to major normal faults is indicated by i) vertically displaced strata associated with stratigraphy omitted across fault planes/zones, ii) rapid thickness and facies variations across the fault, and iii) the presence submarine unconformities. The syn-/post-faulting sediments deposited unconformably over the floor of the half graben are represented by megabreccias which have been derived from upslope by mass wasting of the fault scarp, and the contemporaneous sediments. The sedimentology of the megabreccia is dictated by the composition and diagenetic state of the horst block and the contemporaneous sediments. The presence of black, organic-rich (hemi) pelagic strata as interbeds to the megabreccia indicate anoxia within the basinal sediments and the potential for the reduction of seawater sulphate by anaerobic bacteria.

REFERENCES

Anderson, I.K., Boyce, A.J., Russell, M.J., Fallick, A.E., Hall, A.E. and Ashton, J.H. (1986). Textural and sulphur isotopic support for Lower Carboniferous sedimentary exhalative base metal deposition at Navan, Ireland. *Terra Cognita*, **6**, 133.

Anderson, I.K., Ashton, J.H., Boyce, A.J., Fallick, A.E. and Russell, M.J. (1987). A sulphur isotope overview of the Navan Zn-Pb orebody, Ireland. Mineral Deposits Studies Group A.G.M., Newcastle upon Tyne.

Anderson, I.K. (1990). Ore depositional processes in the formation of the Navan zinc-lead deposit, Ireland. *Unpublished Ph.D Thesis*, University of Strathclyde.

Anderson, R. A. (1974). Slurry injection of vein materials in the Coeur D'Alene district. *Economic Geology*, **69**, 414-415.

Anderton, R., Bridges, P.H., Leederm M.R. and Sellwood, B.W. (1985). *A dynamic stratigraphy of the British Isles, a study of crustal evolution.* George, Allen and Unwin, London.

Andrew, C.J. (1986). The tectono-stratigraphic controls to mineralisation in the Silvermines area, County Tipperary, Ireland. In: *The geology and genesis of mineral deposits in Ireland.* Eds. Andrew, C.J., Crowe, R.W.A., Finlay, S., Pennell, W.M. and Pyne, J.F., The Irish Association for Economic Geology, Dublin.

Andrew, C.J. and Ashton, J.H. (1985). Regional setting, geology and metal distribution patterns of the Navan Orebody. *Transactions of the Institute of Mining and Metallurgy, Section B: Applied Earth Science.* **94**, B66-B93.

Ashton, J.H., Downing, D.T. and Finlay, S. (1986). The geology of the Navan orebody. In: *The geology and genesis of mineral deposits in Ireland.* Eds. Andrew, C.J., Crowe, R.W.A., Finlay, S., Pennell, W.M. and Pyne, J.F., The Irish Association for Economic Geology, Dublin.

Ashton, J.H., Black, A., Geraghty, J., Holdstock, M. and Hyland, E. (1992). The geological setting and metal distribution patterns of Zn-Pb-Fe mineralisation in the Navan Boulder Conglomerate. In: *The Irish minerals industry, a review of the decade, 1980 to 1990*. Eds. Bowden, A.A., Earls, G., O'Connor, P.G. and Pyne, J.F., The Irish Association for Economic Geology, Dublin.

Barker, A.J. and Gayer, R.A. (1985). Caledonian-Appalachian tectonic analysis and the evolution of related oceans. In: *The Tectonic Evolution of the Caledonide-Appalachian Orogen*, p126--165. Ed. Gayer, R.A. Earth Evolution Sciences, Vieweg, Braunschweig.

Bathurst, R.G.C. (1987). Diagenetically enhanced bedding in argillaceous platform limestone: stratified cementation and selective compaction. *Sedimentology*, **34**, 749-778.

Berner, R.A. (1970). Sedimentary pyrite formation. *American Journal of Science*, **268**, 1-23.

Bischoff, J.L., Radtke, A.S. and Rosenbauer, R.J. (1981). Hydrothermal alteration of greywacke by brine and seawater: roles of alteration and chloride complexing on metal solubilisation at 200 and 350°C. *Economic Geology*, **76**, 659-676.

Boast, A.M., Coleman, M.L. and Halls, C. (1981). Textural and stable isotopic evidence for the genesis of the Tynagh base metal deposit, Ireland. *Economic Geology*, **76**, 27-55.

Boyce, A.J., Anderton, R. and Russell, M.J. (1983). Rapid subsidence and early Carboniferous base metal mineralisation in Ireland. *Trans. Inst. Min. Metal.*, **92**, 55-66.

Canfield, D.E. and Thamdrup, B (1994). The production of 34S-depleted sulphide during bacterial disproportionation of elemental sulphur. *Science*, **266**, 1973-1975.

Claypool, C.E., Holser, W.T., Saki, I.R. and Zak, I. (1980). The age curves for sulphur and oxygen isotopes in marine sulphate and their mutual interpretation. *Chemical Geology*, **28**, 199-260.

Clifford, J.A., Ryan, P. and Kucha, H. (1986). A review of the geological setting of the Tynagh orebody, County Galway. In: *The geology and genesis of mineral deposits in Ireland.* Eds. Andrew, C.J., Crowe, R.W.A., Finlay, S., Pennell, W.M. and Pyne, J.F., The Irish Association for Economic Geology, Dublin.

Collinson, J.D. and Thompson, D.B. (1982). *Sedimentary structures.* George, Allen and Unwin, London.

Coomer, P.G. and Robinson, B.W. (1976). Sulphur and sulphate-oxygen isotopes and the origin of the Silvermines deposits, Ireland. *Mineralium Deposita*, **11**, 155-169.

Cope, J.C.W., Guion, P.D., Sevastopulo, G.D. and Swan, A.R.H. (1992). The Carboniferous. In: *Atlas of Palaeogeography and Lithofacies.* Eds. Cope, J.C.W., Ingham, J.K. and Rawson, P.F., Geological Society Memoir No. 13.

Curtis, C.D. (1980). Diagenetic alteration in black shales. *Journal of the Geological Society of London*, **137**, 189-194.

Dahlstrom, C.D.A. (1970). Structural geology in the eastern part of the Canadian Rocky Mountains. *Bull. Can. Pet. Geol.*, **18**, 332-406.

Doyle, E. and Bowden, A.A. (1995). Carboniferous basin development in Ireland, evidence from the Galmoy area. In: Models for carbonate-hosted base metal deposits. I.A.E.G. weekend course, May, 1995.

Drobner, E., Huber, H., Wachtershauser, G., Rose, D. and Stetter, O. (1990). Pyrite formation linked with hydrogen evolution under anaerobic conditions. *Nature*, **346**, 742-744.

Feely, H.W. and Kulp, L. (1957). Origin of Gulf Coast sulphur deposits. *Bull. Am. Ass. Petr. Geol.*, **41**, 1802.

Ford, R.W. (1957). Sulphur isotope effects in chemical and biological processes. *Ph.D Thesis*, McMaster University, Hamilton, Canada.

Gardiner, P.R.R. (1975). Plate tectonics and the evolution of the southern Irish Caledonides. *Sci. Proc. Roy. Dub. Soc. (Series A)*, Vol.5, 385-396.

Gawthorpe, R.L. and Clemmey, H. (1985). Geometry of submarine slides in the Bowland Basin (Dinantian) and their relation to debris flows. *Journal of the Geological Society of London*, **142**, 555-565.

Greig, J.A., Baadsgard, H., Cumming, G.L., Folinsbee, R.E., Krouse, H., Ohmoto, H., Sasaki, A. and Smejkal, V. (1971). Lead and sulphur isotopes of the Irish base metal mines in Carboniferous carbonate host rocks. In: *Proceedings of the IMA-IAGOD Meetings 1970*. Joint Symposium Volume (Tokyo), Society of Mining Geologists of Japan, Special Issue 2, 84-92.

Harrison, A.G. and Thode, H.G. (1957). The kinetic isotope effect in the chemical reduction of sulphate. *Transactions of the Faraday Society*, **53**, 1648-1651.

Harrison, A.G. and Thode, H.G. (1957). Mechanism of the bacterial reduction of sulphate from isotope fractionation studies. *Transactions of the Faraday Society*, **54**, 84-92.

Hitzman, M.W. and Large, D. (1986). A review and classification of the Irish carbonate-hosted base metal deposits. In: *The geology and genesis of mineral deposits in Ireland.* Eds. Andrew, C.J., Crowe, R.W.A., Finlay, S., Pennell, W.M. and Pyne, J.F., The Irish Association for Economic Geology, Dublin.

Jensen, M.L. and Nakai, N. (1963). Sulphur isotope meteorite standards: results and recommendations. In: Biogeochemistry of Sulphur Isotopes. *Proc. Nat. Sci. Found. Symp., Yale Univ., April, 1962*, 1-15.

Johnston, J.D., Collar, D., Miller, G. and Critchley, M.F. (in review). Structural controls of Irish carbonate-hosted base-metal deposits. In: *European Dinantian Environments*. Eds. Jones, G., Somerville, I.D. and Strogen, P., Special Publication of the Geological Society of London.

Jones, G.V. and Brand, S.F. (1986). The setting, styles of mineralisation and mode of origin of the Ballinalack Zn-Pb deposit. In: *The geology and genesis of mineral deposits in Ireland.* Eds. Andrew, C.J., Crowe, R.W.A., Finlay, S., Pennell, W.M. and Pyne, J.F. The Irish Association for Economic Geology, Dublin.

Jones, G.E. and Starkey, R.L. (1957). Fractionation of stable isotopes of sulphur by micro-organisms and their role in the deposition of native sulphur. *Applied Microbiology*, **5**, 111-115.

Kaplan, I.R. and Rafter, T.A. (1958). Fractionation of stable isotopes of sulphur by Thiobacilli. *Science*, **127**, 517-518.

Kaplan, I.R., Rafter, T.A. and Hulston, J.R. (1960). Sulphur isotope variations in nature: application to some biogeochemical problems. *N.Z.J. Sci.*, **3**, 338-361.

Kaplan, I.R. and Rittenberg, S.C. (1964). Microbiological fractionation of sulphur isotopes. *Journal of General Microbiology*, **34**, 195-212.

Kemp, A.L.W. and Thode, H.G. (1968). The mechanism of the bacterial reduction of sulphate from isotopic fractionation studies. *Geochim. Cosmochim. Acta*, **32**, 71-91.

Large, D.E. (1980). Geological parameters associated with sediment-hosted, submarine exhalative Pb-Zn deposits: an empirical model. *Geological Journal*, **40**, 59-129.

Laznicka, P. (1985). Concordant versus discordant ore deposits and ore transformations. In: *Handbook of Stratabound and Stratiform Ore Deposits*, Volume 11, p149. Ed. Wolf, K.H., Elsevier, Amsterdam.

Laznicka, P. (1988). Breccias and coarse fragmentites: petrology, environments, associations and ores. *Developments in Economic Geology*, Spec. Publ. 25, p57. Ed. Laznicka, P., Elsevier, Amsterdam.

Leake, B.E. (1978). Granite emplacement: the granites of Ireland and their origin. In: *Crustal Evolution in Northwest Britain and Adjacent Regions*. Eds. Bowes, D.R. and Leake, B.E. Geol. J. Special Issue 10. Seal House Press.

Lees, A. (1964). The structure and origin of the Waulsortian (Lower Carboniferous) reefs of west central Eire. *Philosophical Transactions of the Royal Society of London*, **B247**, 483-531.

Libby, D.J. (1985). The Tara Mines story. *Transactions of the Institute of Mining Metallurgy: Mining Industry*, **94**, A1-A41.

Love, L.G. (1967). Early diagenetic iron sulphide in recent sediments of the Wash (England). *Sedimentology*, **9**, 327-352.

Macnamara, J. and Thode, H.G. (1950). Comparison of the isotopic constitution of terrestrial and meteoric sulphur. *Phys. Rev.*, **78**, 307.

Marchant, T.R. and Sevastopulo, G.D. (1980). The Calp of the Dublin District. *Irish Journal of Earth Science*, **3**, 195-320.

Max, M.D., Ryan, P.D. and Inamdar, D.D. (1983). A magnetic deep structural geology interpretation of Ireland. *Tectonics*, 2, 431-451.

McKerrow, W.S. and Soper, N.J. (1989). The Iapetus Suture in the British Isles. *Geology Magazine*, **126**, 1-8.

Mills, H., Halliday, A.N., Ashton, J.H., Anderson, I.K. and Russell, M.J. (1987). Origin of a giant orebody at Navan, Ireland. *Nature*, **327**, 223-225.

Moore, C.H. (1989). *Developments in Sedimentology 46: Carbonate diagenesis and porosity*, p16. Ed. Moore, C.H., Elsevier, Amsterdam.

Mullins, H.T., Gardulski, A.F. and Hine, A.C. (1986). Catastrophic collapse of the west Florida carbonate platform margin. *Geology*, **14**, 167-170.

Nakai, N. and Jensen, M.L. (1960). Biogeochemistry of sulphur isotopes. *J. Earth Sci.*, **8**, 174.

Nakai, N. and Jensen, M.L. (1964). The kinetic isotope effect in the bacterial reduction and oxidation of sulphur. *Geochim. Cosmochim. Acta*, **28**, 1983-1912.

Nolan, S.C. (1989). The style and timing of Dinantian syn-sedimentary tectonics in the eastern part of the Dublin Basin. In: *The role of tectonics in Devonian and Carboniferous sedimentation in the British Isles.* Eds. Arthurton, R.S., Gutteridge, P. and Nolan, S.C., Yorkshire Geological Society Occasional Publication No.6

Ohmoto, H. and Rye, R.O. (1979). Isotopes of sulphur and carbon. In: Geochemistry of hydrothermal ore deposits. Ed. Barnes, H.J., Wiley Interscience, N.Y., 509-567.

Pattrick, R.A.D. and Polya, D.A. (1993). *The mineralisation and geological evolution of the British Isles. In: Mineralisation in the British Isles.* Eds. Pattrick, R.A.D. and Polya, D.A. Chapman and Hall, London.

Philcox, M.E. (1984). Lower Carboniferous Lithostratigraphy of the Irish Midlands. *Special Publication of the Irish Association for Economic Geology.*

Philcox, M.E. (1989). The mid-Dinantian unconformity at Navan, Ireland. In: *The role of tectonics in Devonian and Carboniferous sedimentation in the British Isles.* Eds. Arthurton, R.S., Gutteridge, P. and Nolan, S.C., Yorkshire Geological Society Occasional Publication No.6.

Pickering, K.T., Bassett, M.G. and Siveter, D.J. (1988). Late Ordovician-early Silurian destruction of the Iapetus Ocean: Newfoundland, British Isles and Scandinavia - a discussion. *Trans. Roy. Soc. Edin.: Earth Sci.*, **79**, 361-382.

Plant, J.A. (1986). Models for granites and their mineralising systems in the British and Irish Caledonides. In: *The geology and genesis of mineral deposits in Ireland.* Eds. Andrew, C.J., Crowe, R.W.A., Finlay, S., Pennell, W.M. and Pyne, J.F., The Irish Association for Economic Geology, Dublin.

Redmond, P. (1995). Structural controls on mineralisation and dolomitisation at the Lisheen Zn-Pb deposit, Co. Tipperary, Ireland. In: Models for carbonate-hosted base metal deposits. I.A.E.G. weekend course, May, 1995, 16-18.

Rizzi, G. (1992). The sedimentology and petrography of Lower Carboniferous limestones and dolomites; host rocks to the Navan zinc-lead ore deposit, Ireland. *Unpublished Ph.D Thesis*, Glasgow University.

Russell, M.J. (1978). Downward excavating hydrothermal cells and Irish-type ore deposits: importance of an underlying thick Caledonian prism. *Transactions of the Institute of Mining and Metallurgy: Applied earth science*, **87**, B168-B171.

Samson, I.M. and Russell, M.J. (1983). Fluid inclusion data from Silvermines base metal-barite deposits, Ireland. *Trans. Inst. Min. Metall.*, **B92**, 67-71.

Samson, I.M. and Russell, M.J. (1987). Genesis of the Silvermines zinc-lead-barite deposit, Ireland: fluid inclusions and stable isotopic evidence. *Econ. Geol.*, **82**, 371-394.

Sevastopulo, G.D. (1981). The Lower Carboniferous. In: *The geology of Ireland*. Ed. Holland, C.H. Scottish University Press, Edinburgh.

Soper, N.J. (1988). Timing and geometry of collision, terrane accretion and sinistral strike-slip events in the British Caledonides. In: *The Caledonian-Appalachian Orogen*. Eds. Harris, A.L. and Fettes, D.J. Geological Society Special Publication, **38**, pp. 481-492.

Thode, H.G., Kleerekoper, H. and McElcheran, D. (1951). Isotope fractionation in the bacterial reduction of sulphate. Research, **4**, 581.

Thode, H.G., Monster, J. and Dunford, H.B. (1961). Sulphur isotope geochemistry. *Geochemica Cosmochemica Acta*, **25**, 159-174.

Thode, H.G. and Monster, J. (1963). The sulphur isotope abundances in evaporites and in the ancient oceans. *Vernadsky Memorial Volume, II*, Moscow.

Yarnold, J.C. (1993). Rock avalanche characteristics in dry climates and the effect of flow into lakes: insights from mid-Tertiary sedimentary breccias near Artillery Peak, Arizona. *The Geological Society of America*, **105**, 345-360.

Zhou, J. (1985). The timing of calc-alkaline magmatism in parts of the Alpine-Himalayan collision zone and its relevance to the interpretation of Caledonian magmatism. *Journal of the Geological Society of London*, **142**, 309-317.

Appendix A. Collar co-ordinates of the surface diamond drillholes referred to in the text.

Drillhole number	Northing	Easting
N156	9422.5	9787.3
N158	9452.1	9452.9
N170	9584.0	9420.3
N191	9359.9	9299.0
N261	9146.8	8476.2
N307	9511.2	9268.5
N647	9355.0	9015.6
N654	9226.3	9059.3
N689	9722.6	9017.5
N743	9779.3	8732.7
N793	9668.8	8509.1
N823	9270.2	8336.7
N873	9227.7	7700.3
N912	9496.4	7884.2
N927	8837.4	8469.8
N1012	8831.8	8548.9
N1016	9580.9	7799.5
N1023	9044.2	7318.4
N1027	8648.0	8054.0
N1030	8987.4	7375.1
N1039	9212.7	7884.3
N1064	8871.1	7717.9
N1072	9192.6	9651.8
N1109	9096.7	9549.4
N1137	8297.5	8391.0
N1149	8513.1	7533.9
N1156	9022.6	7382.1
N1174	7382.2	10980.5
E13	8365.1	10301.4
E14	8065.0	10200.0

Appendix B. Table of $\delta^{34}S$ results for sulphide minerals in the C.G.O.

P=pyrite S=sphalerite G=galena

Lab. No.	$\delta^{34}S$	Ml.	Sample location and details
SA2057	-39.51	P	1330 348S; laminated pyrite in T.B.U.
SA2058	-40.83	P	1330 348S; reworked pyrite
SA2062	-17.38	S	1330 348S; rim to pyrite botryoid
SA2064	-30.61	P	1330 348S; reworked pyrite
SA2065	-33.77	P	1330 348S; replaced carbonate mud
SA2067	-7.49	S	1330 348S; rim to pyrite botryoid
SA2068	-9.38	S	1330 348S; rim to pyrite botryoid
SA2069	-12.37	S	1330 348S; rim to pyrite botryoid
SA2070	-13.27	G	1330 348S; rim to pyrite botryoid
SA2071	+6.62	G	1330 348S; rim to pyrite botryoid
SA2073	-15.00	P	1315 P1S; replaced Shaley Pales
SA2074	-9.29	P	1315 P1S; interclast cement
SA2075	-1.44	G	1315 P1S; replaced Shaley Pales
SA2076	-21.85	P	1315 CGO AC; interclast cement
SA2077	+1.51	P	1315 CGO AC; interclast cement
SA2079	-9.29	G	1315 CGO AC; interclast cement
SA2080	-2.76	P	1315 P2; lamina in interbed to B.C.
SA2081	-11.60	P	1315 P2; interclast cement
SA2082	-21.01	P	1315 P2; ore boulder
SA2084	-11.84	G	1315 P2; ore boulder
SA2085	-39.97	P	1330 348S; channelised pyrite in T.B.U.
SA2086	-39.83	P	1330 348S; channelised pyrite in T.B.U.
SA2087	-9.42	S	1315 CGO AC; interclast cement
SA2088	-10.53	S	1315 P2; interclast cement
SA2089	-9.65	S	1315 P1S; fracture cement in Shaley Pales
SA3431	-37.00	S	1330 348S; lamina in T.B.U.
SA3432	-26.66	P	1330 CGO; clast-matrix replacement
SA3435	-12.32	S	1315 CGO AC; interclast cement
SA3437	-32.29	P	1330 348S; reworked pyrite
SA3439	-29.41	P	1330 CGO; clast-matrix replacement
SA3441	-37.92	S	1330 348S; channelised sphalerite in T.B.U.
SA3442	-9.51	S	1315 P2; interclast cement
SA3444	-13.67	P	1315 P2; interclast cement
SA3449	-31.00	P	1285 HWD; reworked pyrite
SA3450	-0.04	P	1285 HWD; ore boulder

SA3453	-9.37	G	1315 CGO AC; interclast cement
SA3454	-12.33	G	1315 P2; interclast cement
SA3455	-20.61	P	1330 CGO; clast-matrix replacement
SA3456	-12.88	G	1315 P2; sulphide concretion
SA3458	-9.93	S	1315 P1S; replaced Shaley Pales
SA3459	-10.18	S	1315 P1S; replaced Shaley Pales
SA3460	-9.32	S	1315 P1S; replaced Shaley Pales
SA3469	-9.72	S	1285 HWD; ore boulder
SA3470	-41.33	S	1330 348S; channelised sphalerite in T.B.U.
SA3483	-23.60	S	1330 348S; reworked sphalerite
SA3485	-40.91	S	1330 348S; channelised sphalerite in T.B.U.
SA3486	-39.91	S	1330 348S; channelised sphalerite in T.B.U.
SA3488	-32.43	S	1330 348S; channelised sphalerite in T.B.U.
SA3489	+5.52	G	1330 348S; rim to pyrite botryoid
SA3490	+1.97	P	1315 CGO AC; interclast cement

The integration of petrologic and isotopic data from the Boulder Conglomerate to determine the age of the Navan orebody, Ireland.

Volume II Figures and Photographs

by

Colin Victor Ford, B.Sc, M.Sc.

Thesis submitted for the degree of Doctor of Philosophy in the Faculty of Science, Department of Geology and Applied Geology, University of Glasgow.

August 1996.

Table 1. Overview of the geological setting of the Navan area and the mineralisation hosted by the Pale Beds and Boulder Conglomerate.

Host	PALE BEDS (P.B.O.)	BOULDER CONGLOMERATE (C.G.O.)
Age	Lower Dinantian: Courceyan	Mid-Dinantian: Chadian
Sedimentology	Limestone interbedded with sandstone and shale.	Carbonate debris flows interbedded with shale. Clast composition is dominated by Courceyan and Chadian lithologies; there is evidence for reworking of the Lower Palaeozoic basement.
Mineralisation	Stratabound and locally stratiform ore lenses. Major ore and associated dolomite occurs as replacement to limestone and trends NE-SW. Other styles of mineralisation include cement to fractures and in-situ breccia zones, and cavity fill. The fractures trend NE-SW. The cavities contain sedimentary ore which exhibits soft sediment deformation.	Stratiform and stratabound pyrite lenses which are variably associated with minor, cross-cutting ore. At stratigraphically low positions, ore occurs in reworked limestone as clasts and groundmass. Mineralisation associated with the clasts is represented by massive ore, fracture cement and concentrically-replaced clast margins.
Depositional setting	The post-Caledonian Dublin Basin. The basin axis trends NE-SW and represents the Iapetus suture zone.	Local basin created by normal faults of late Courceyan to Chadian age. The faults trend ENE and dip to the SSE.
Sources of information: Andrew and Ashton (1985), Ashton et al. (1986), Anderson (1990), Ashton et al. (1993)		

FIGURES

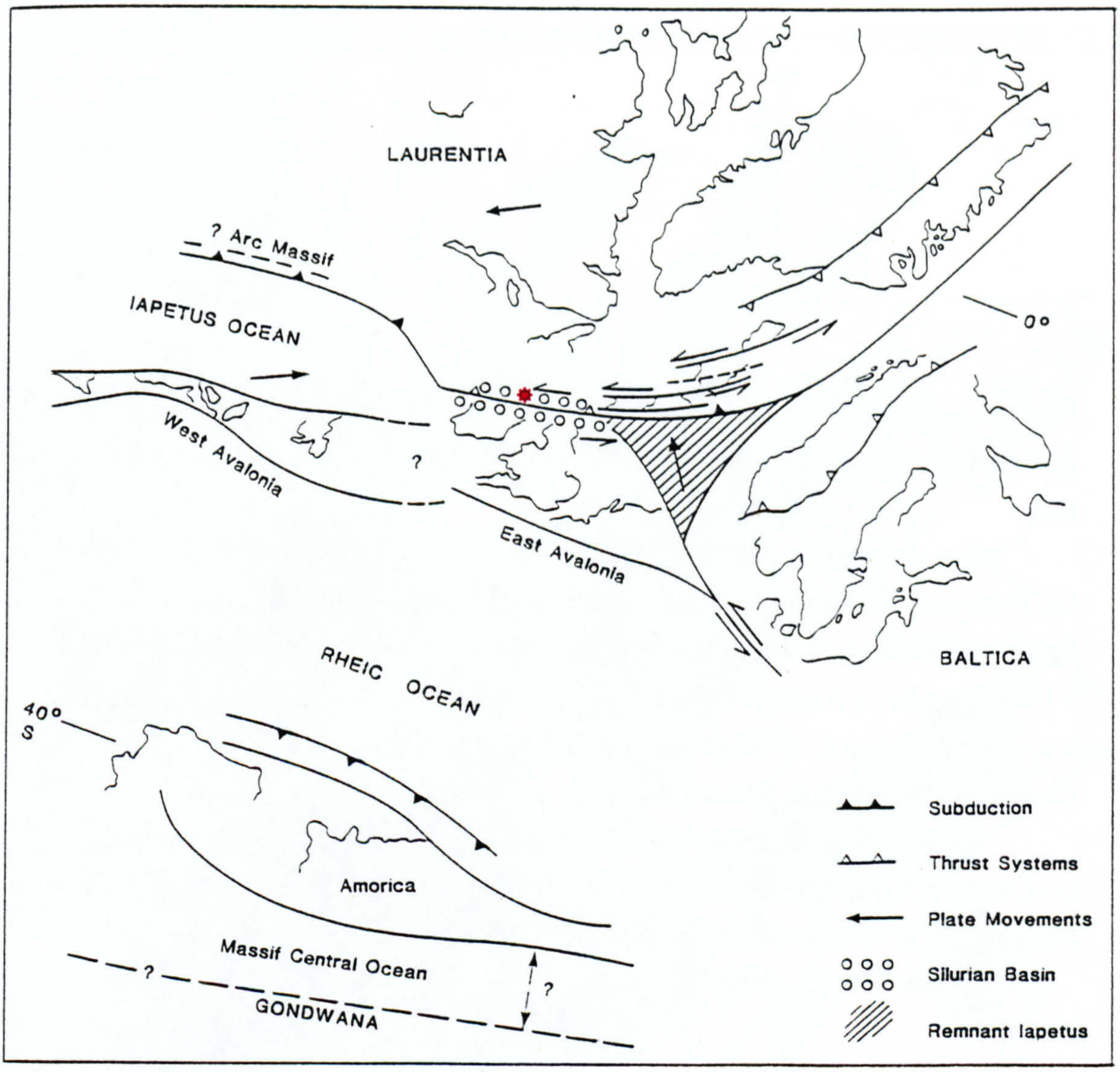

Figure 1. Tectonic influences and plate positions in the British Isles region at 435 Ma.; the approximate palaeosite of Navan is shown by the red star (based on Barker and Gayer, 1985; Pickering *et al.*, 1989).

Figure 2. Distribution of major exposed and hidden NE lineaments and granites in Britain and Ireland. The location of Navan is shown by the red star.

Lineaments: OIT=Outer Isles Thrust; MT=Moine Thrust; GCF=Great Glen Fault; HBF=Highland Boundary Fault; LF=Leannan Fault; FCL=Fair Head-Clew Bay Linear; SUF=Southern Uplands Fault; VL=Virginia Linear; **NTL=Navan-Tipperary Linear;** SIL=Southern Ireland Lineament; GWL=Graignamanagh-Wicklow Linear; WL=Wexford Linear; MSL=Meanai Strait Line.

Granites: Ca=Carnsore; Co=Corvock; Cr=Crossdoney; D=Donegal; G=Galway; L=Leinster; N=Newry; O=Oughterard; Om=Omey; Ox=Ox Mountains; R=Roundstone; S=Saltees; T=Tyrone.

(From Plant, 1986; after Gardiner, 1975; Leake, 1978; Max *et al.*, 1983).

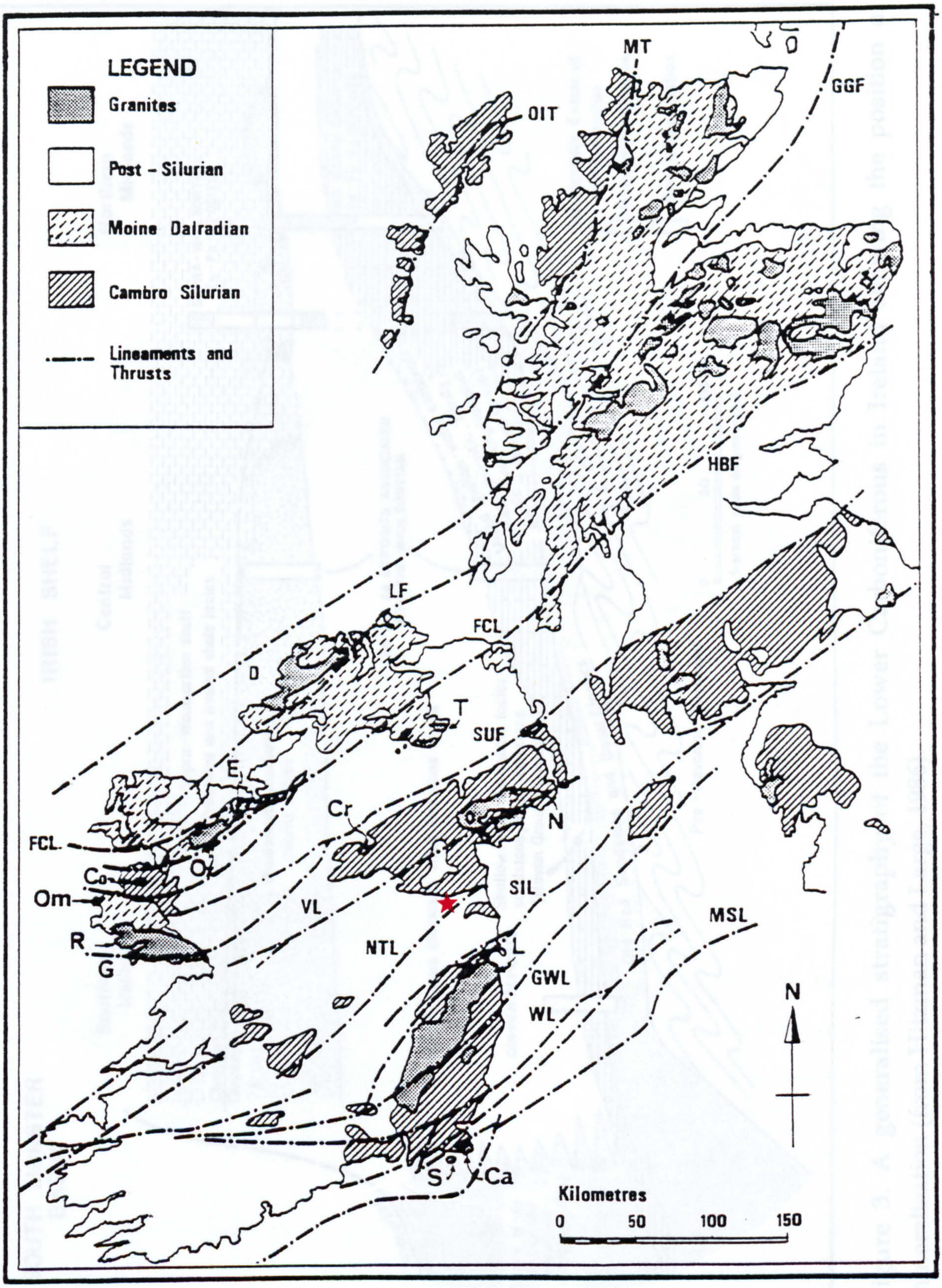
LEGEND
Granites
Post – Silurian
Moine Dalradian
Cambro Silurian
Lineaments and Thrusts
MT
OIT
GGF
HBF
LF
FCL
D
T
SUF
E
Cr
N
FCL
O
Co
Om
VL
SIL
MSL
R
G
NTL
L
GWL
WL
N
S
Ca
Kilometres
0
50
100
150

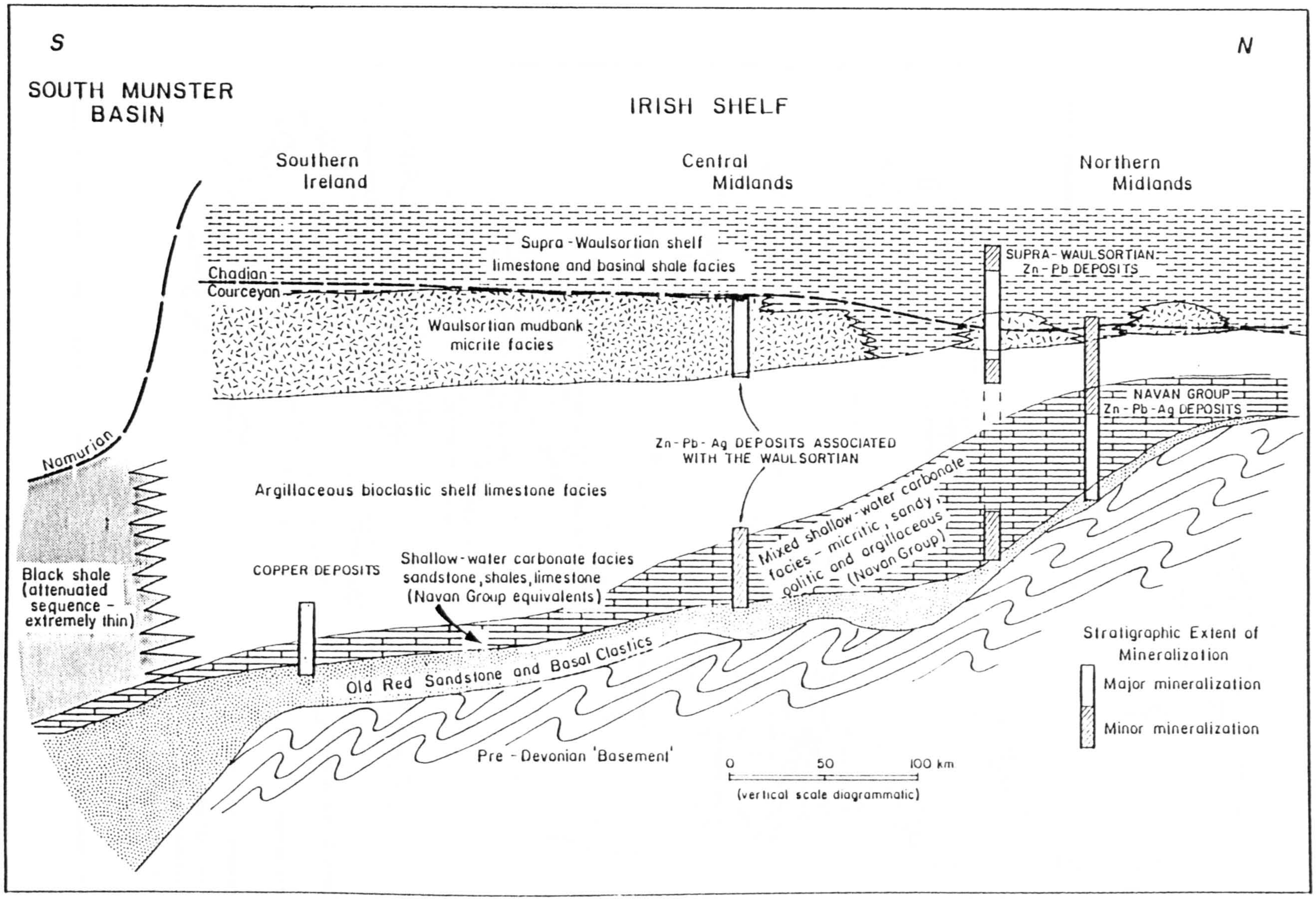

Figure 3. A generalised stratigraphy of the Lower Carboniferous in Ireland showing the position of mineralisation (from Hitzman and Large, 1986).

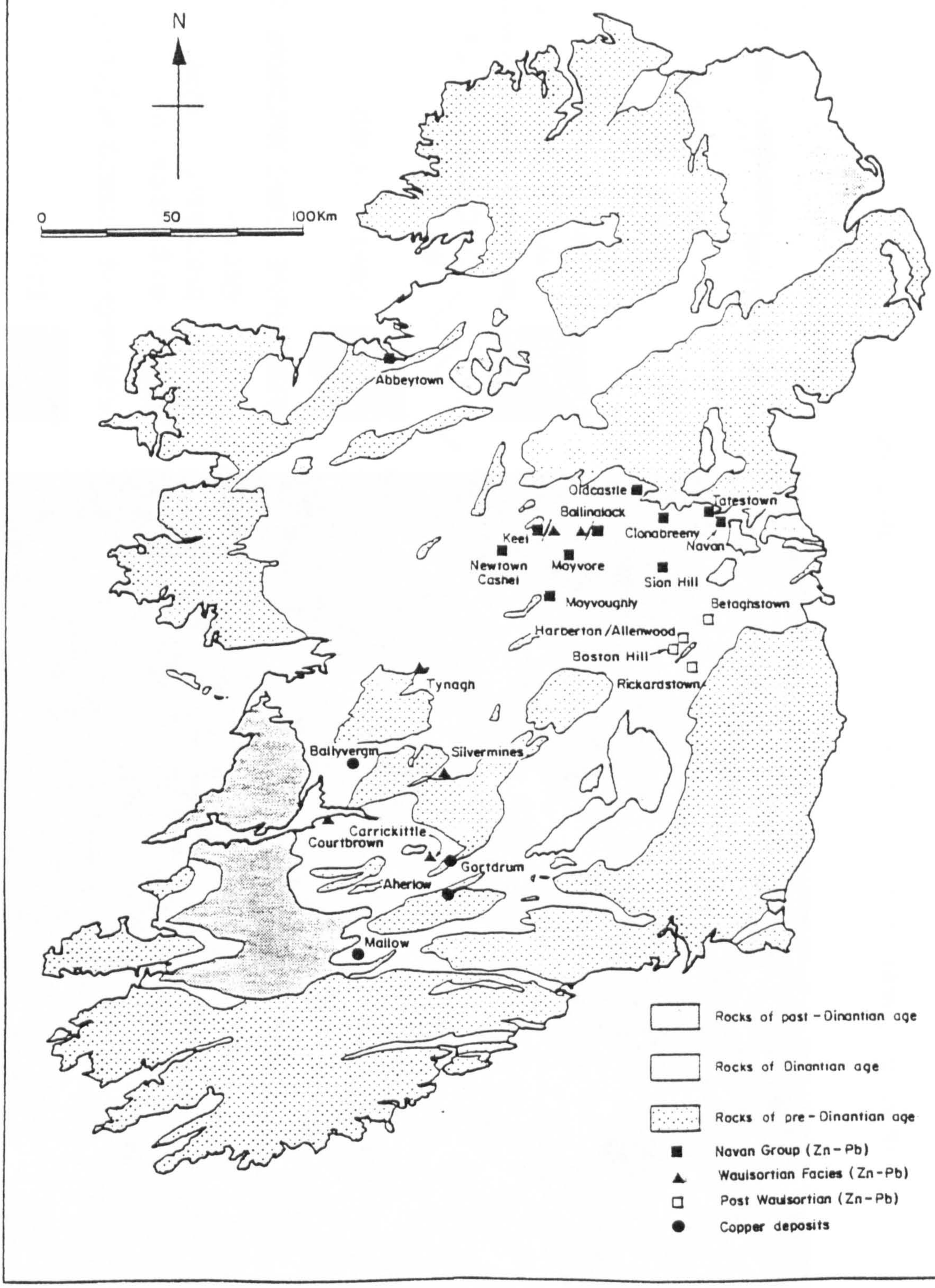

Figure 4. Simplified geological map of Ireland showing the location of mineral deposits (From Hitzman and Large, 1986).

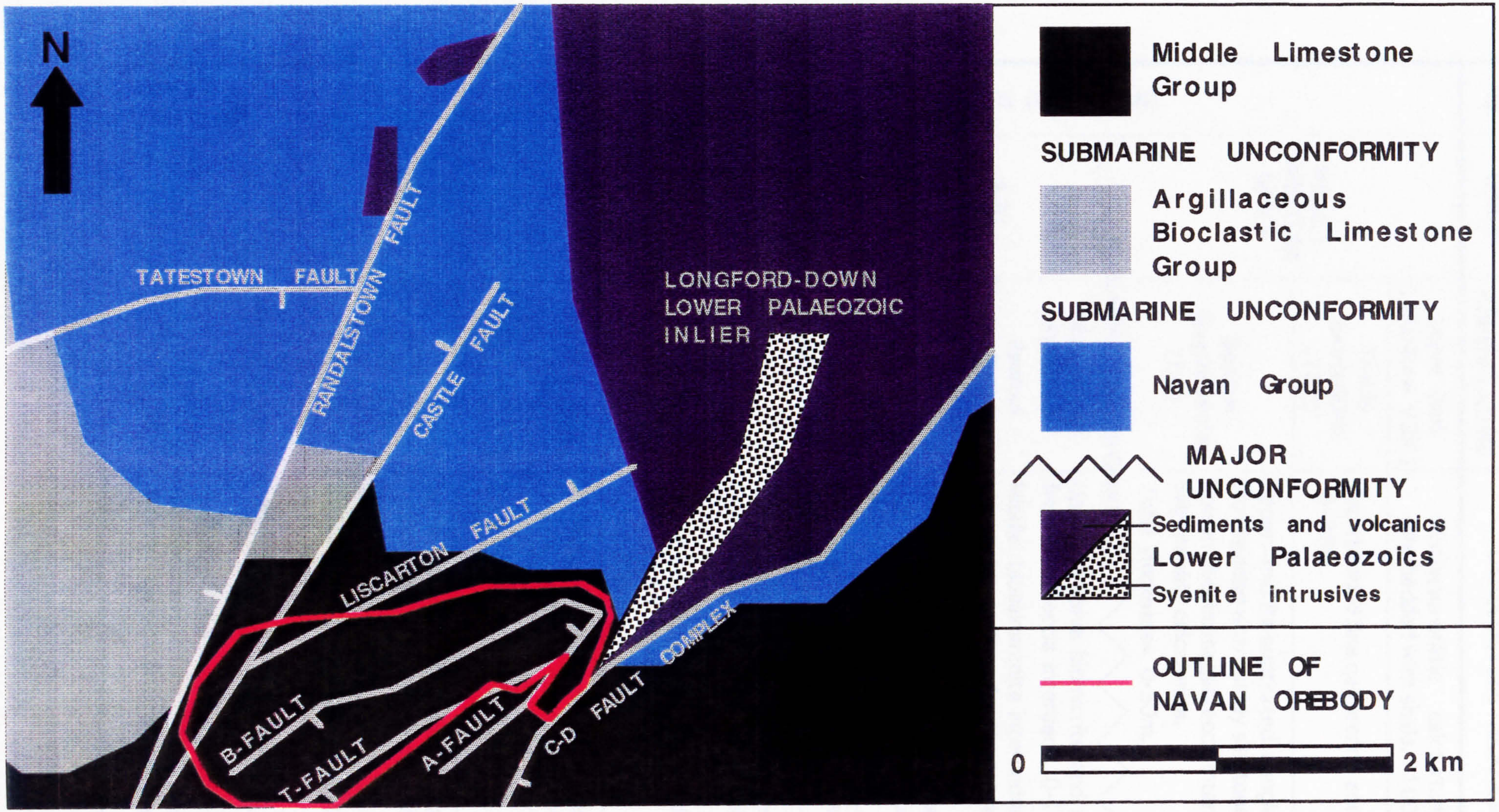

Figure. 5. Simplified geology of the Navan area (after Ashton *et al.*, 1986).

AGE	GROUP	LOCAL NOMENCLATURE	LITHOLOGY and THICKNESS
LOWER CARBONIFEROUS (DINANTIAN)	MIDDLE LIMESTONE GROUP	Upper Dark Limestone (UDL)	Bioclastic-oolitic calcturbidites interbedded with shale. >1000m.
		Thinly BeddedUnit (TBU)	Interbedded fine calcarenite and shale. 0-20m.
		Boulder Conglomerate (BC)	Upper: micrite-supported conglomerate interbedded with muddy siltstone. Lower: chaotic megabreccia interbedded with muddy calcarenite. Total thickness= 0-50m.
	SUBMARINE UNCONFORMITY		
	A.B.L. GROUP	Waulsortian Limestone	Upper: massive biomicrite and sparite; frequent breccia interbeds. 0-175m.
		Reefoid Argillaceous Bioclastic Lst	Middle: biocalcarenite interbedded with bioclastic argillite; frequent breccia interbeds. 0-185m.
		Argillaceous Bioclastic Lst	Lower: bioclastic calcarenite interbedded with bioclastic argillite. 0-100m.
	SUBMARINE UNCONFORMITY		
	NAVAN GROUP	Shaley Pales (SP)	Interbedded bioclastic limestone, calcarenite and argillite. 100m.
		Pale Beds (PB)	Upper: oolite content reduced; bioclastic limestone interbedded with arenite and argillite. Lower: oobiolimestone interbedded with micrite and argillite. Total thickness= 200m.
		Micrite Unit (MU)	Variably bioclastic, oncolitic and oolitic micrite; argillite interbeds. 0-60m.
		Muddy Limestone (ML)	Muddy, bioclastic micrite. 10-20m.
		Laminated Beds (LB)	Laminated dark siltstones and argillite interbedded with arenite and calcarenite. 30-45m.
		RedBeds (RB)	Beddedconglomeratesandarenites. 0-45m.
	MAJOR UNCONFORMITY		
LOWER PALAEOZOIC		Lower Palaeozoics (LP)	Shales, silstones and grits with Ordovician volcanics. Cut by late Silurian syenite and lamprophyre intrusions. Base not known.

Figure 6. Simplified stratigraphy of the Navan area
(Modified after Andrew and Ashton, 1985).

Figure 7. Isometric view of serial, NW-SE strike sections across the Navan Orebody; section spacing increased to enhance visibility (Diagram courtesy of John Ashthon, Tara Mines Ltd.).

ISOMETRIC VIEW OF SERIAL, NW-SE STRIKE SECTIONS ACROSS THE NAVAN OREBODY

(SECTION SPACING INCREASED TO ENHANCE VISIBILITY)

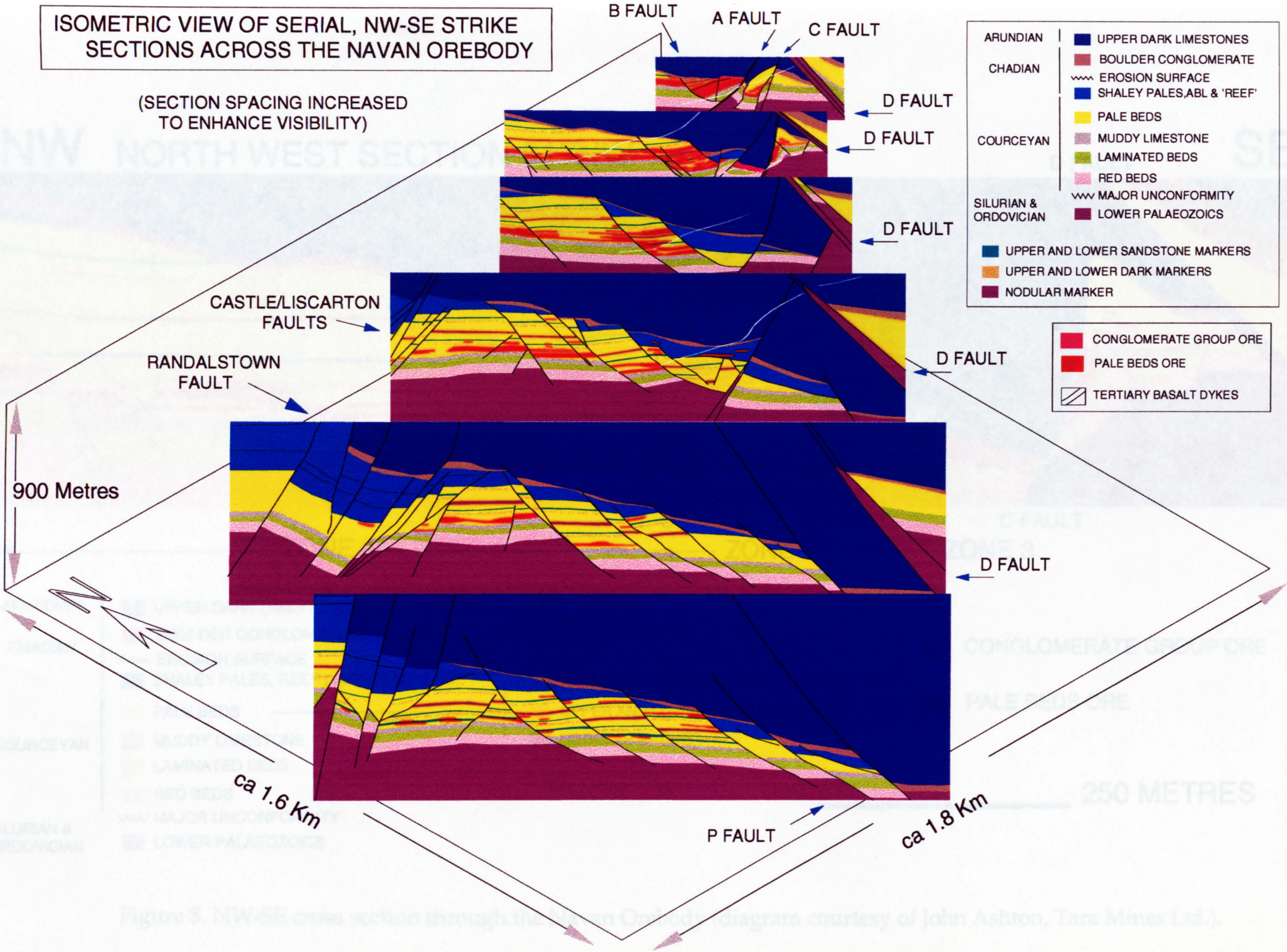

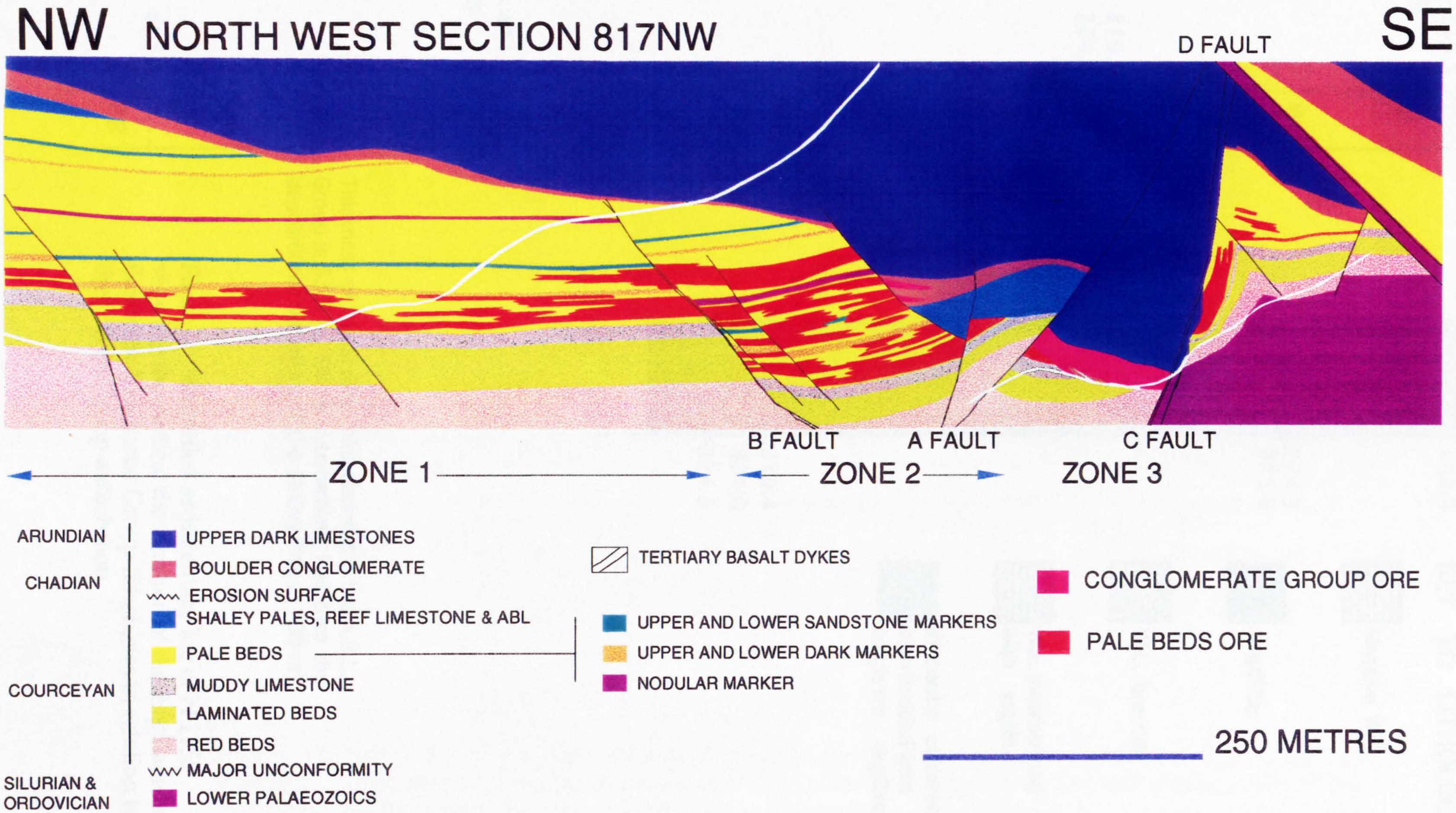

Figure 8. NW-SE cross section through the Navan Orebody (diagram courtesy of John Ashton, Tara Mines Ltd.).

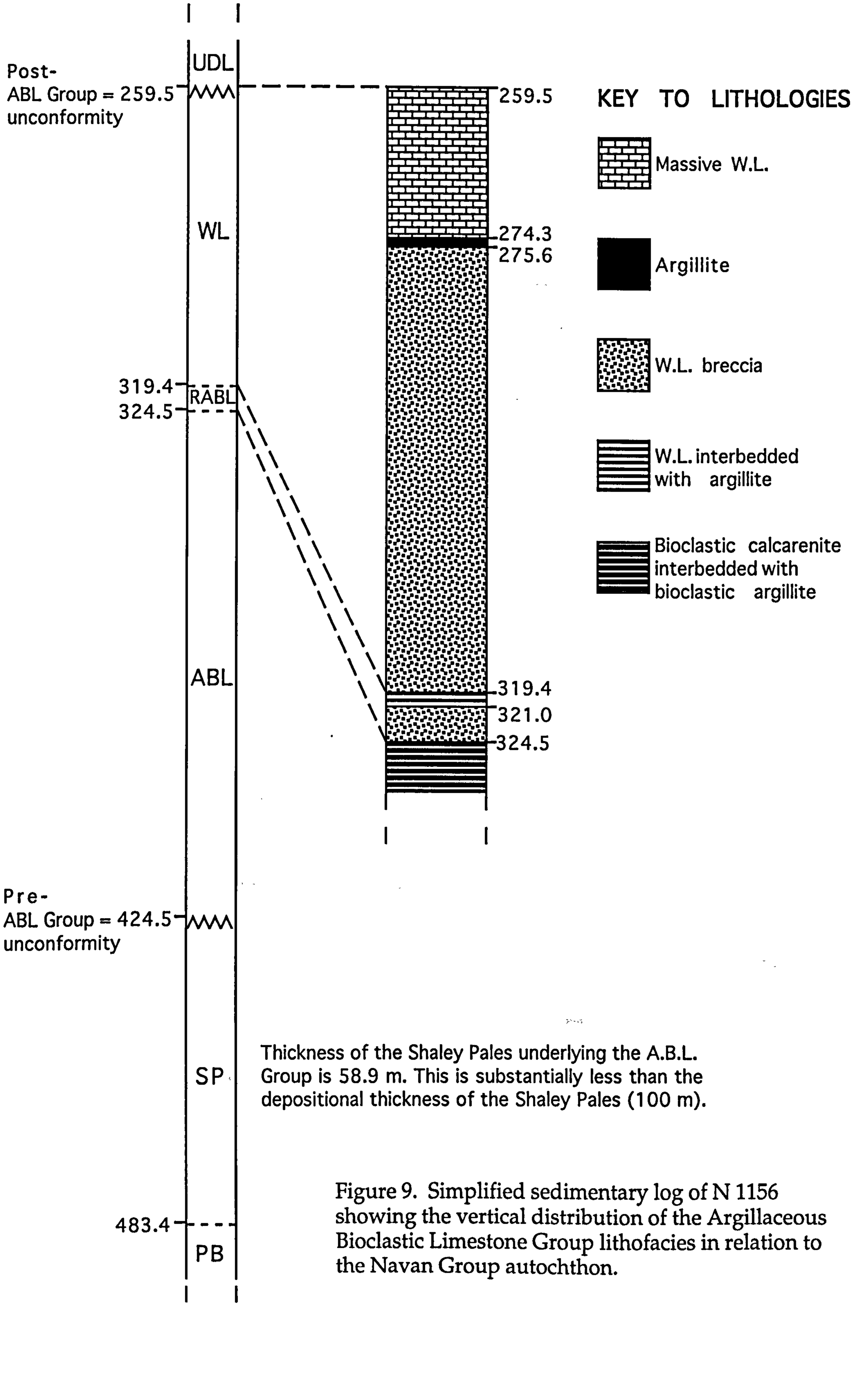

Figure 9. Simplified sedimentary log of N 1156 showing the vertical distribution of the Argillaceous Bioclastic Limestone Group lithofacies in relation to the Navan Group autochthon.

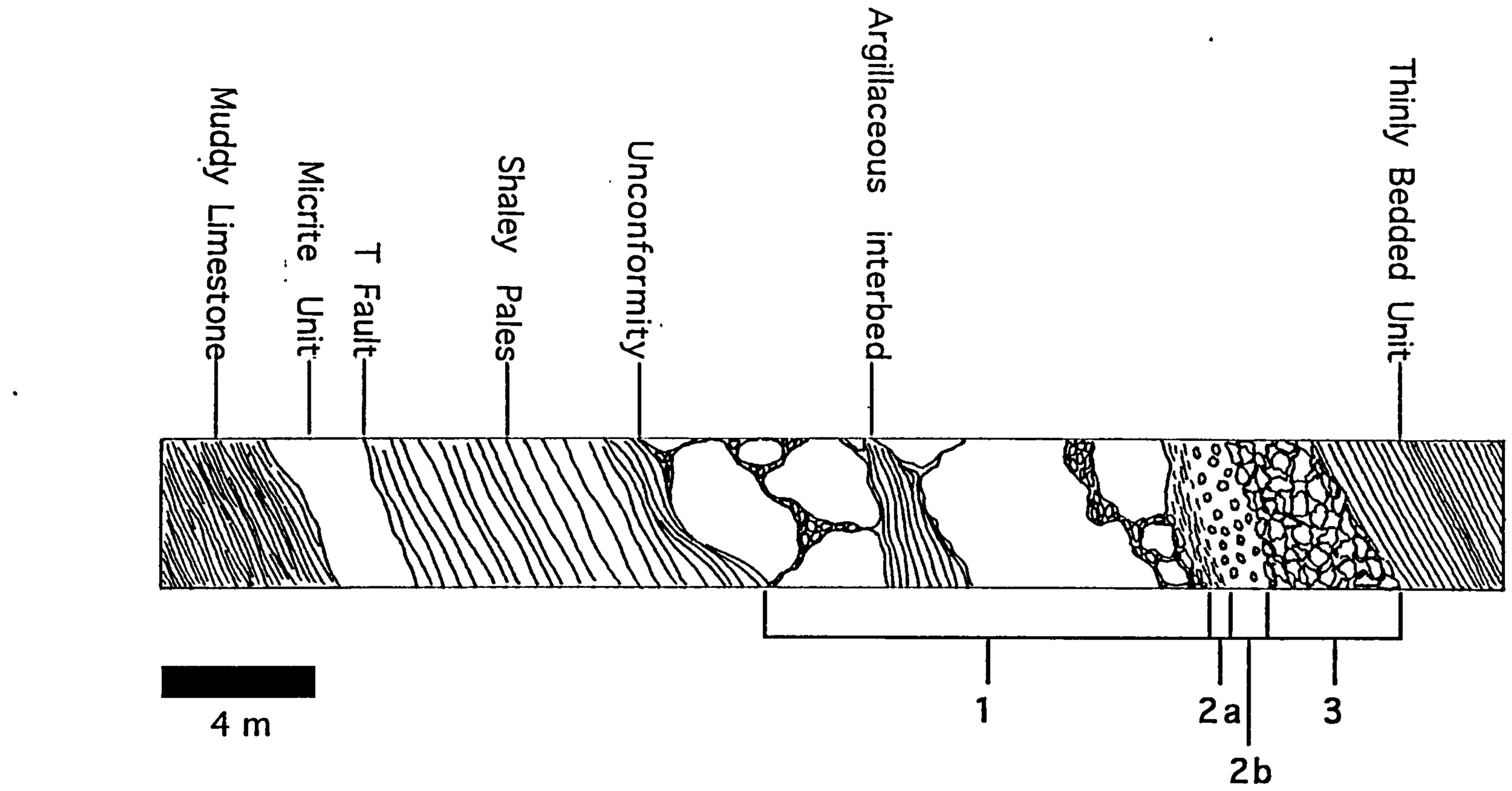

Figure 10. Summary of the sidewall mapping of the stratigraphy exposed in the 1285 HWD Block 40 heading. Variscan compression is responsible for steep dip, permitting the full stratigraphy of the Boulder Conglomerate to be seen as a dip section. The boulders greater than 0.5 m in diameter present in Lithofacies 1 are drawn to scale.

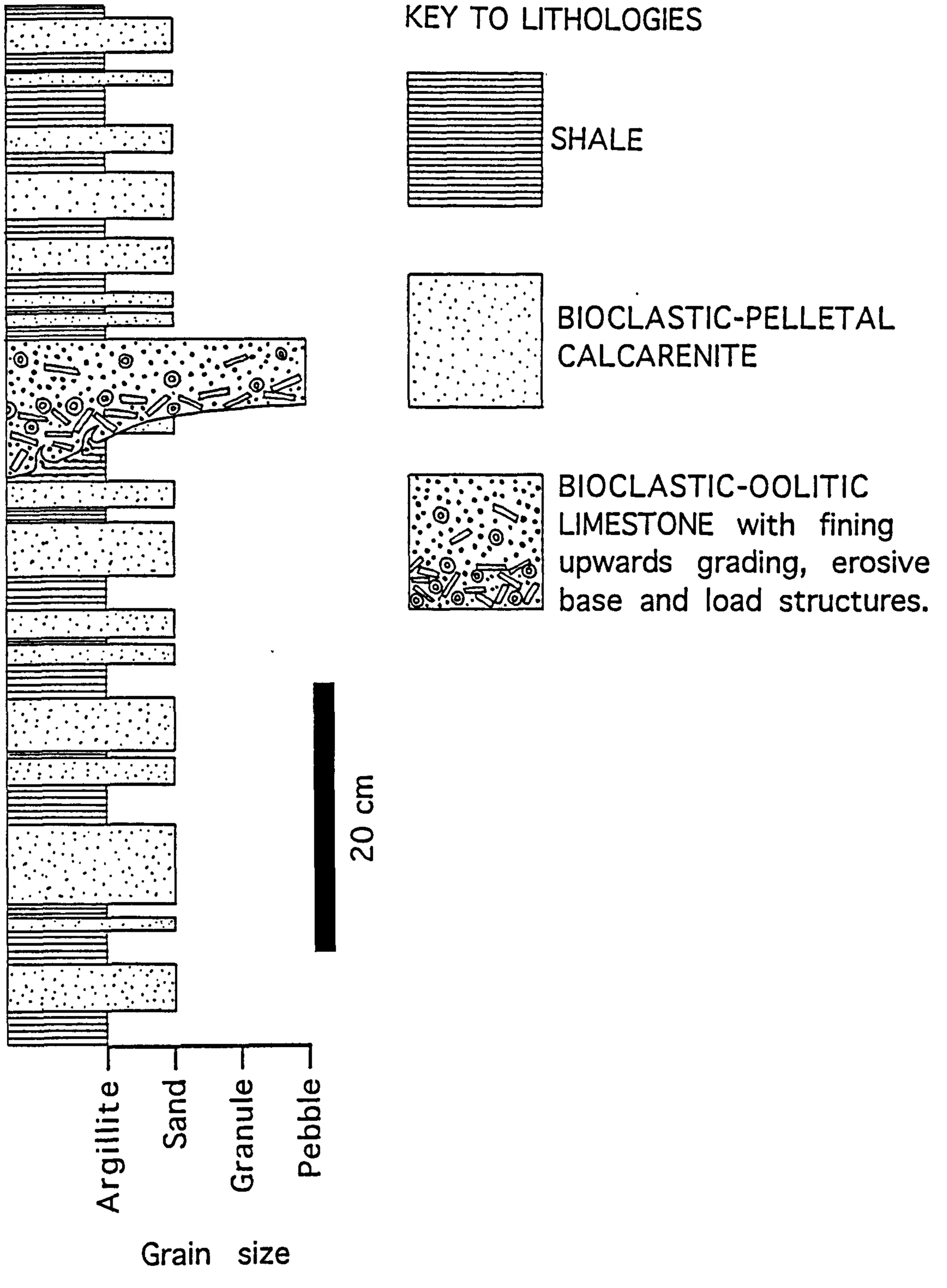

Figure 11. Schematic sedimentary log of the Thinly Bedded Unit exposed in the 1345 348N heading.

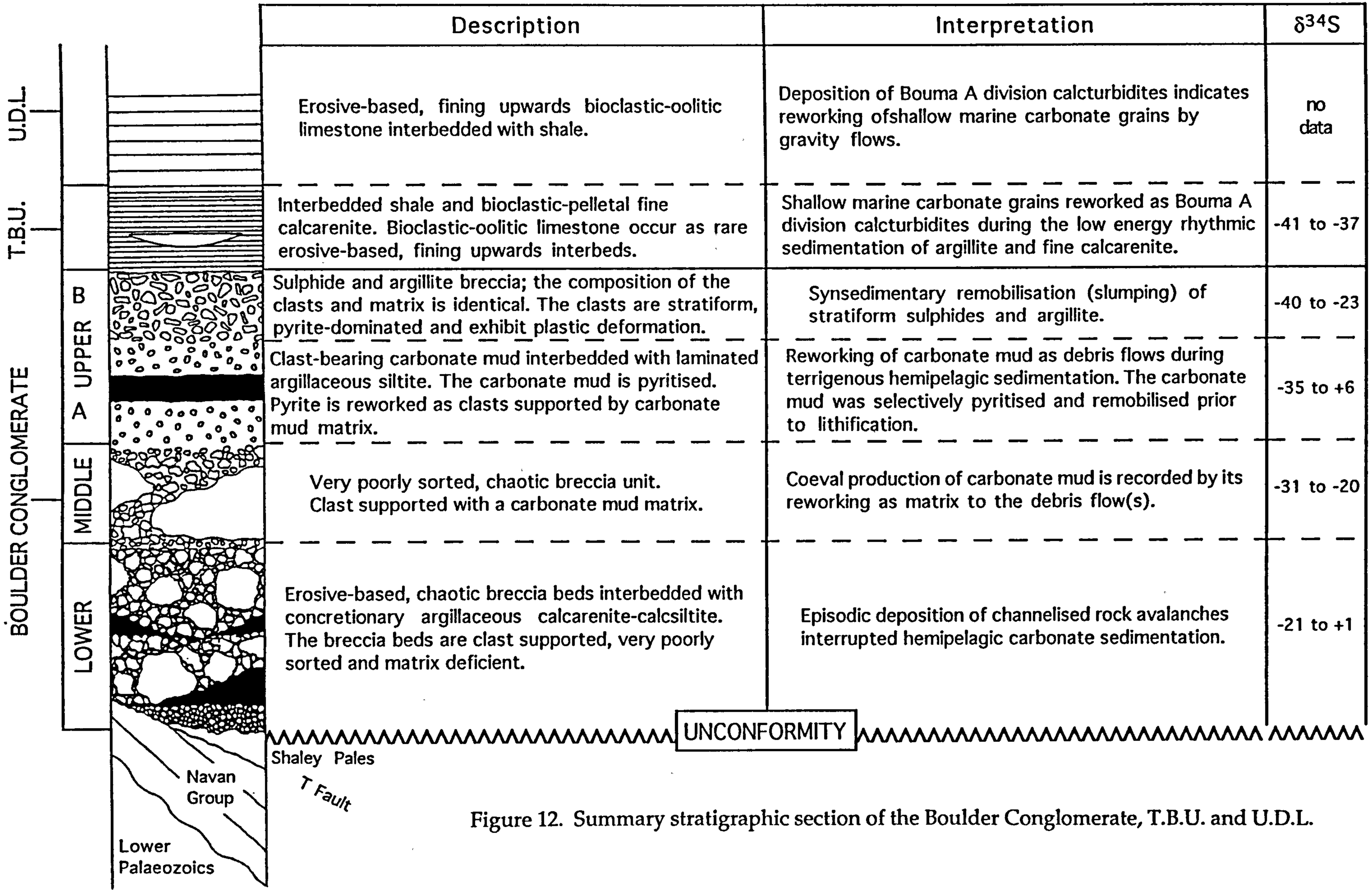

Figure 12. Summary stratigraphic section of the Boulder Conglomerate, T.B.U. and U.D.L.

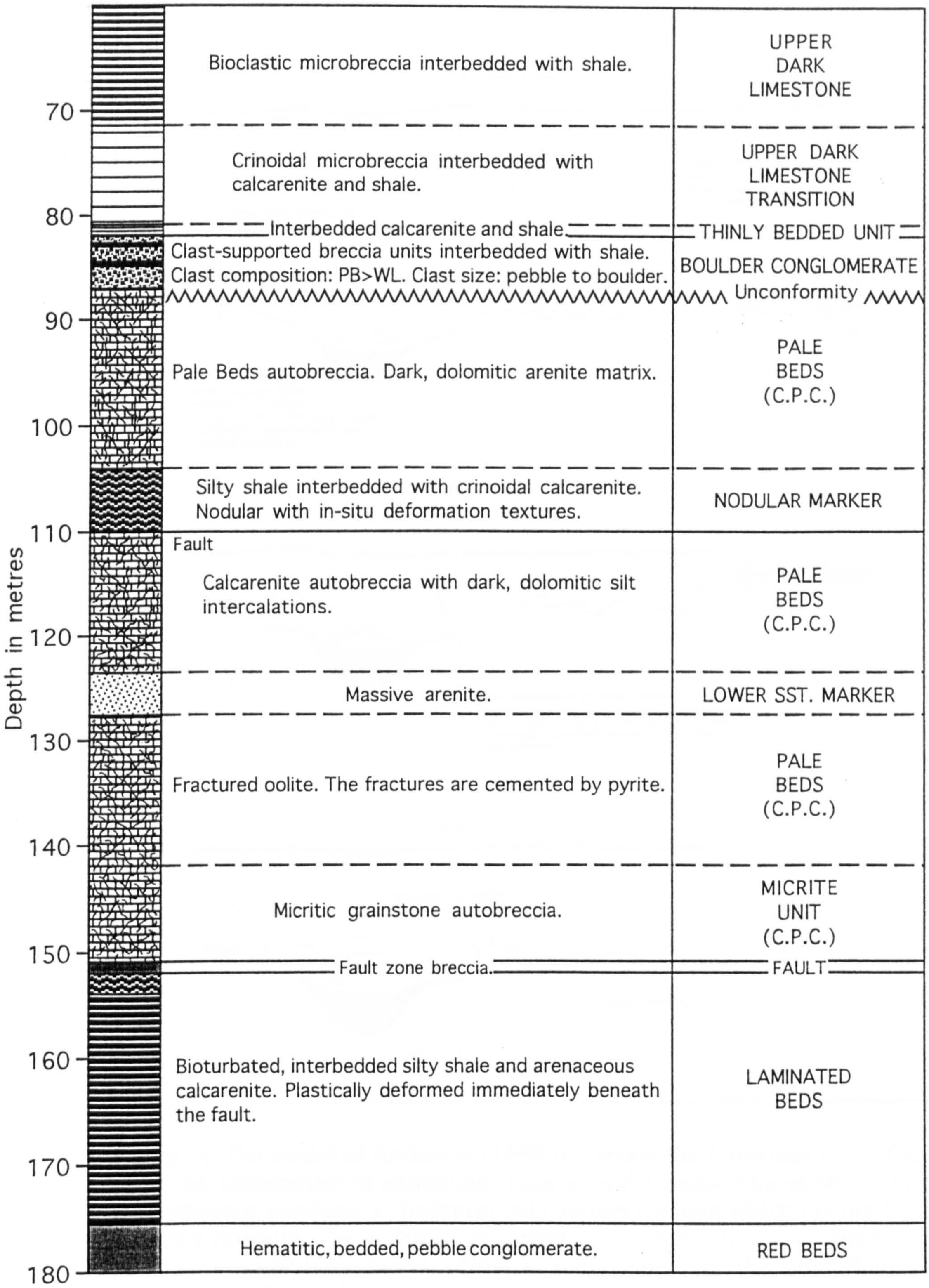

Figure 13. Graphic log of diamond drill hole N1072 showing the occurrence of the Close--Packed Conglomerate in the Pale Beds and Micrite Unit present in the Navan Group autochthon (Original log summary by John Ashton, Tara Mines Ltd.).

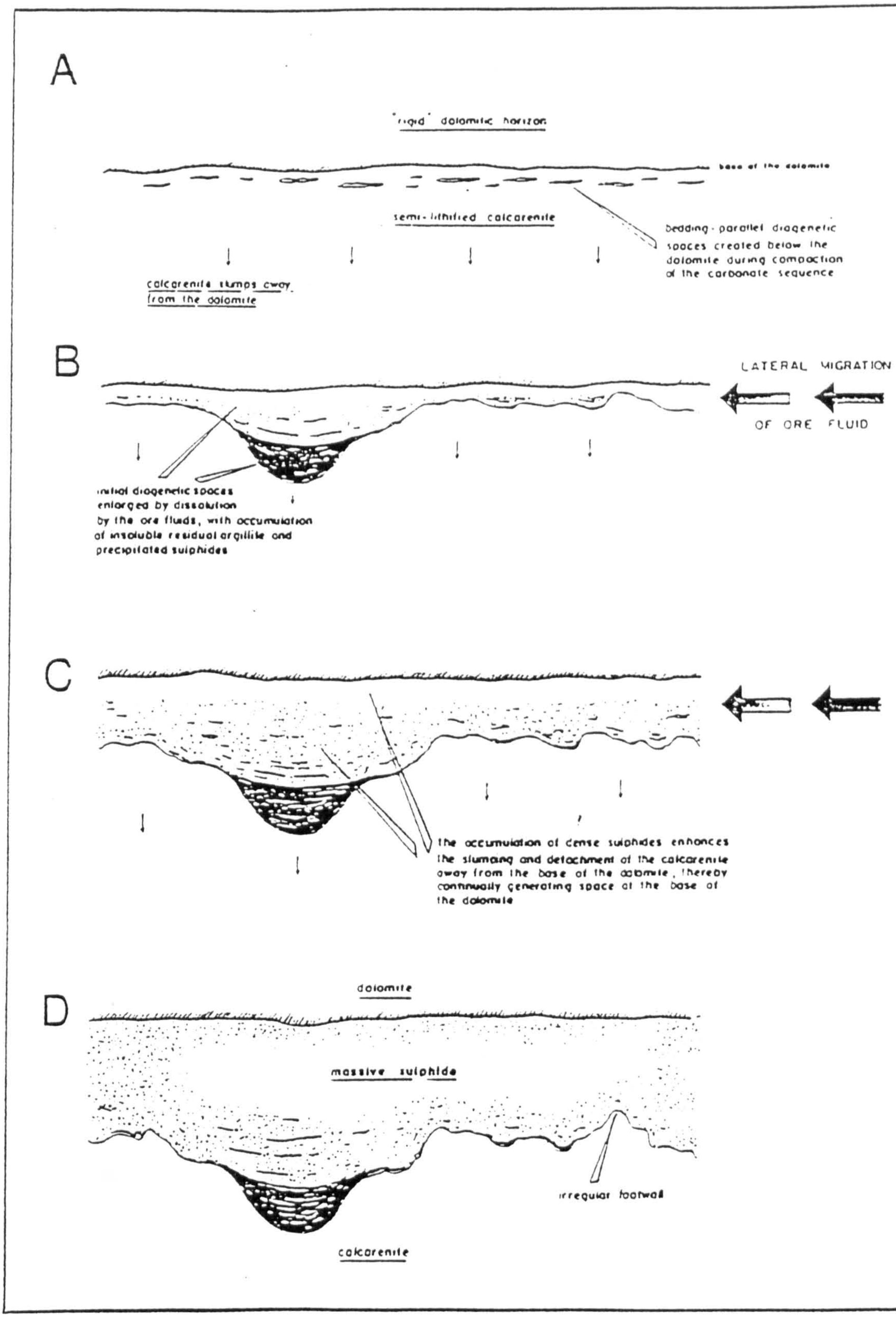

Figure 14. The model of Anderson (1990) to explain the formation of the Pale Beds Ore. Detachment of unlithified strata from dolomitised limestone during mineralisation produces a stratiform void system through which the ore fluid migrates laterally. The wallrock is corroded, enlarging the void space and producing insoluble residue which is redeposited on the void floor in association with sulphide minerals precipitated in the void. Collapse of the void roof after Stage D causes the remobilisation of this unlithified, laminated sediment and produces a stratiform breccia fabric.

Figure. 15. Diagrammatic reconstruction of a "palaeokarst surface" created during deposition of the Pale Beds (from Rizzi, 1992). Dissolution of lithified limestone by meteoric fluids produces a pedogenic breccia on the karst surface and subsurface cavities which are connected to the surface. Siliciclastic silt and sand, derived through dissolution and erosion, are deposited in depressions on the karst surface and enter into the subsurface cavities; the sedimentary structures indicate hydraulic transportation. Rizzi (1992) interpreted the higher permeability of this non-carbonate sediment which characterises the numerous palaeokarst surfaces present in the Pale Beds and Micrite Unit as the control to the formation of the Pale Beds Ore.

Th
10
Va
Co

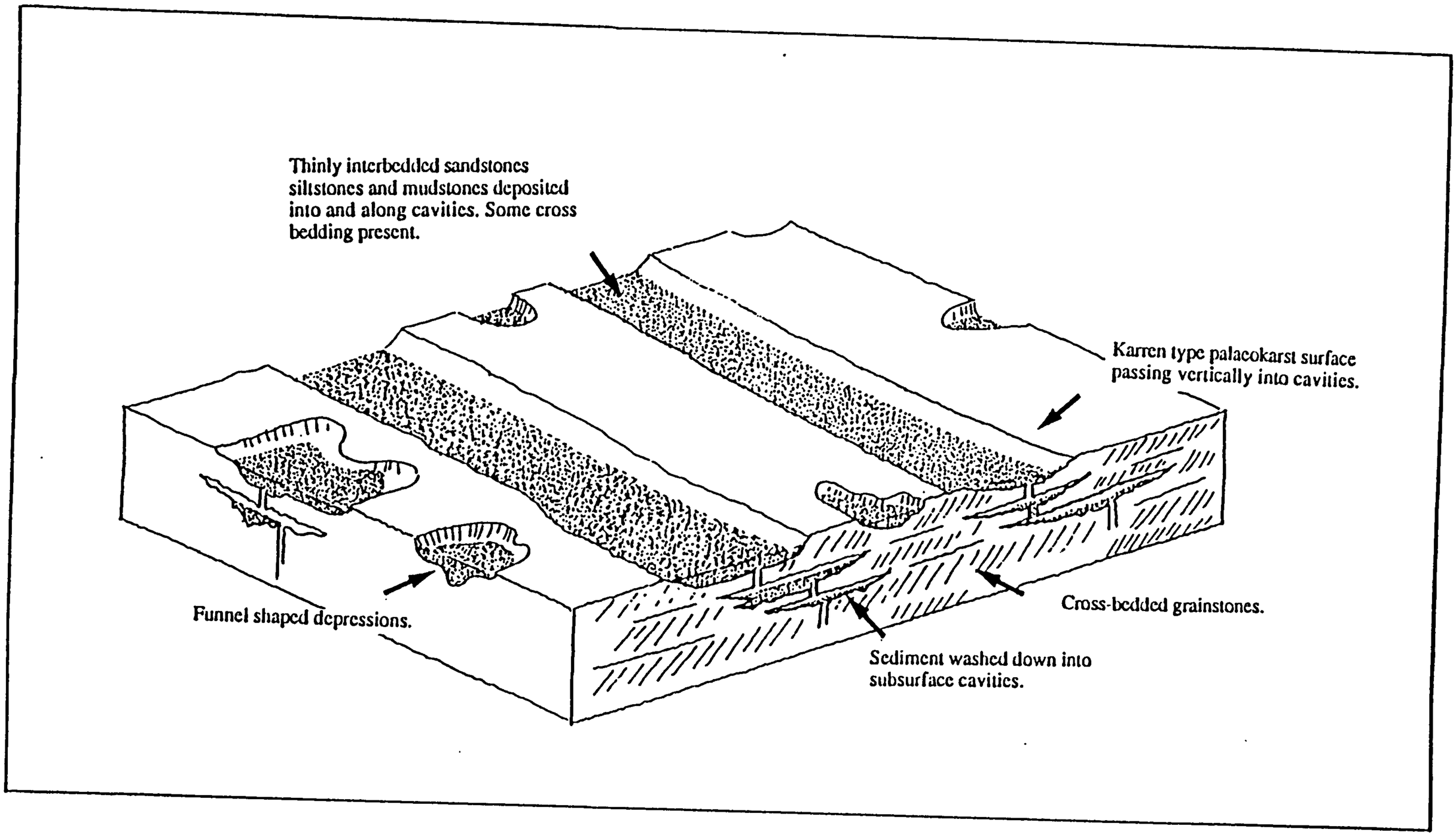
Thinly interbedded sandstones siltstones and mudstones deposited into and along cavities. Some cross bedding present.
Karren type palaeokarst surface passing vertically into cavities.
Funnel shaped depressions.
Cross-bedded grainstones.
Sediment washed down into subsurface cavities.

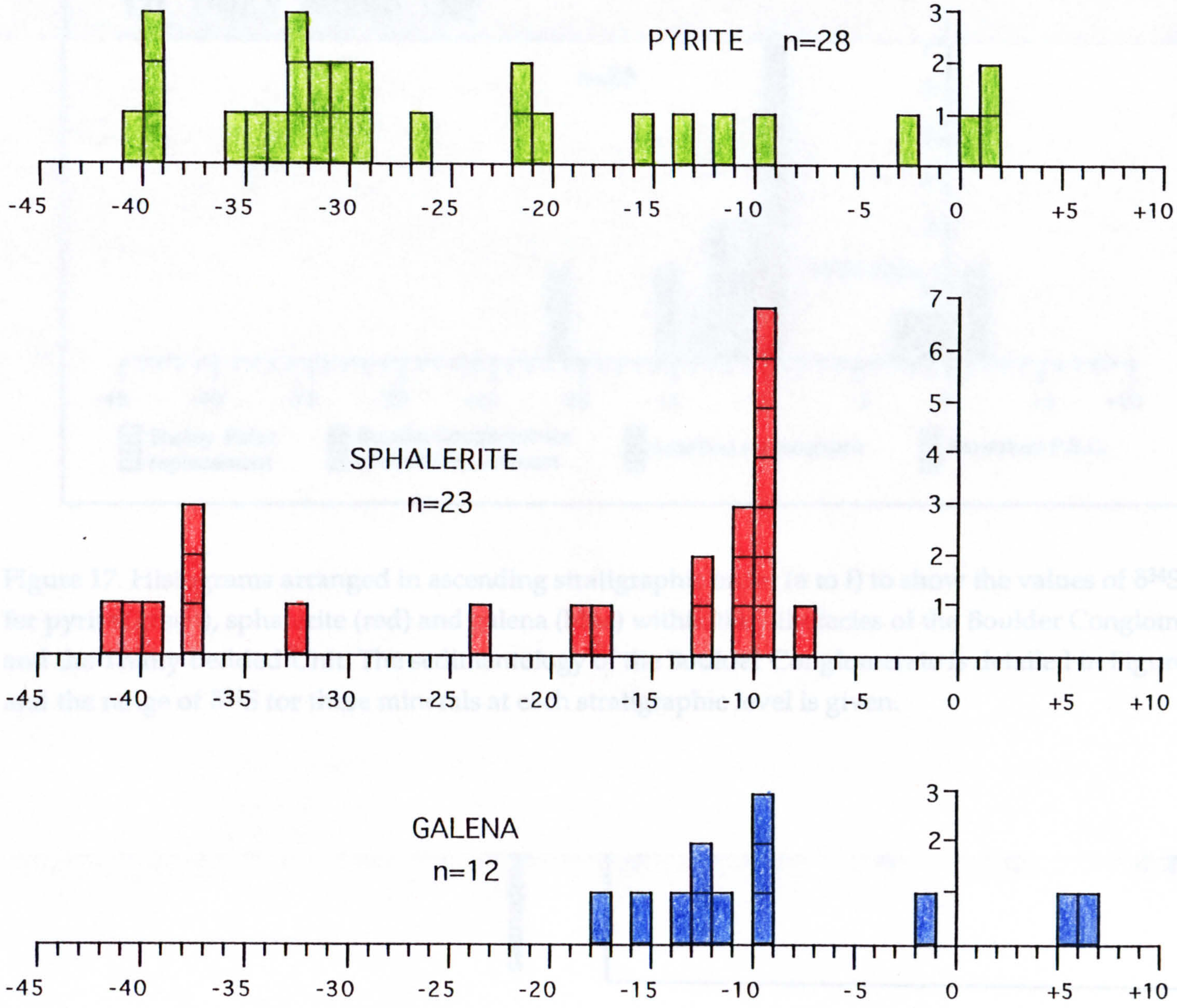

Figure 16. Histograms showing the total $\delta^{34}S$ datasets for analyses of pyrite, sphalerite and galena from the C.G.O.

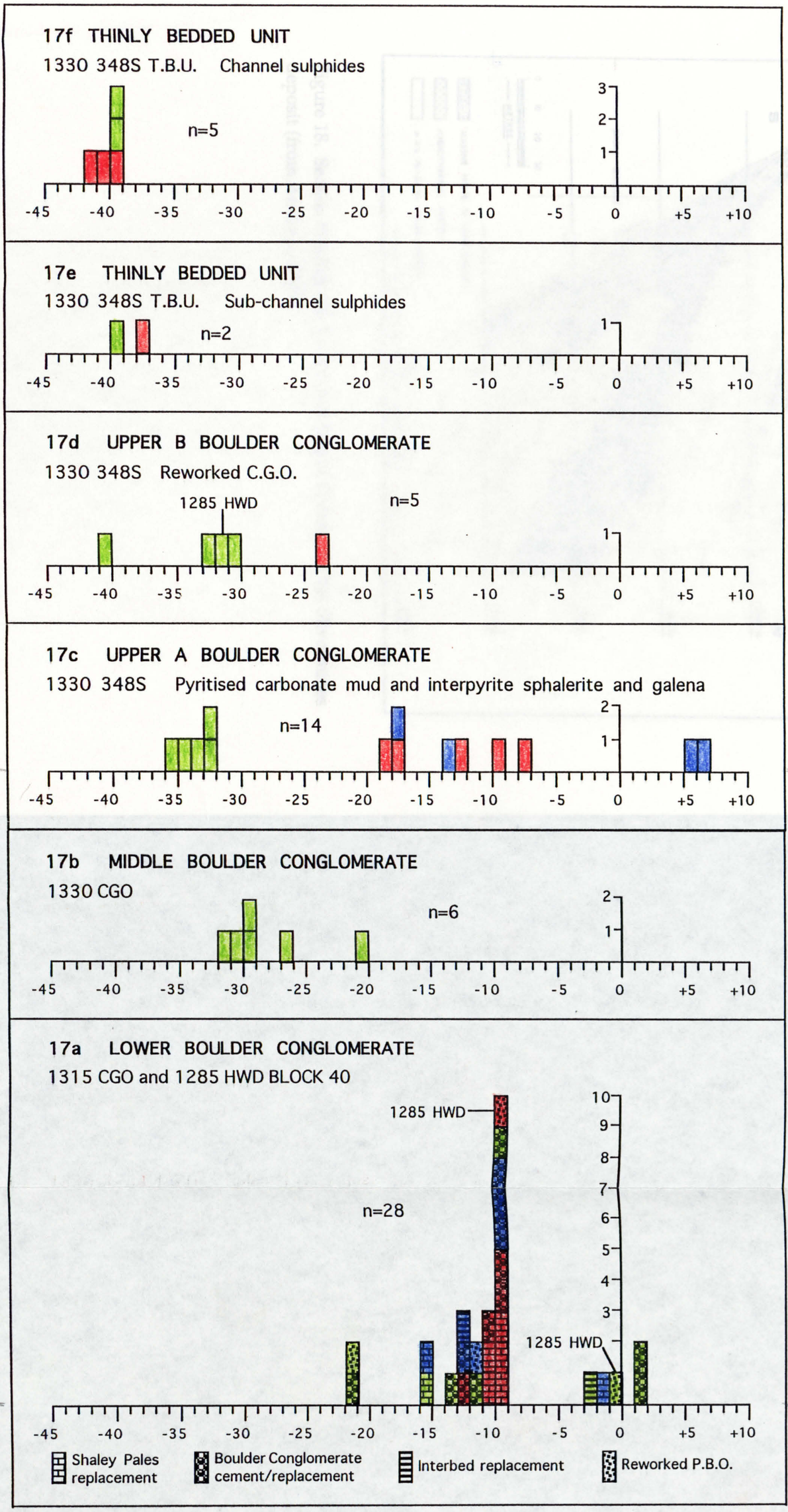

Figure 17. Histograms arranged in ascending stratigraphic order (a to f) to show the values of $\delta^{34}S$ for pyrite (green), sphalerite (red) and galena (blue) within the lithofacies of the Boulder Conglomerate and the Thinly Bedded Unit. The sedimentology of the Boulder Conglomerate is detailed in Figure 12 and the range of $\delta^{34}S$ for these minerals at each stratigraphic level is given.

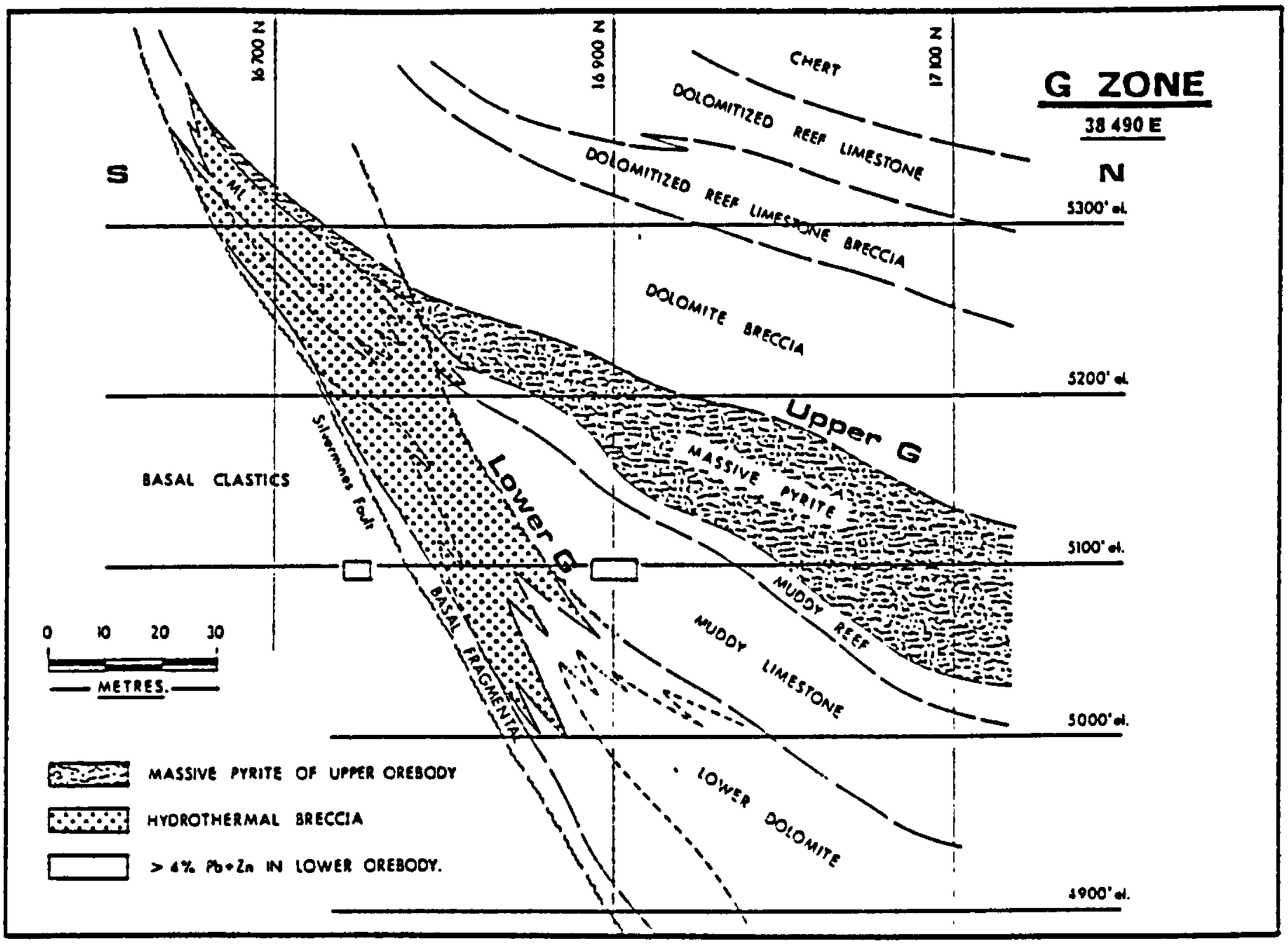

Figure 18. Section through the Lower and Upper G zones of the Silvermines deposit (from Andrew, 1986).

PHOTOGRAPHS

Photo. 1. Drillcore intersection through the Argillaceous Bioclastic Limestone Group showing the stratigraphic transition to increasingly carbonate-dominated lithologies (N1016).

Photo. 2. The Argillaceous Bioclastic Limestone facies in drillcore (N1156).

Photo. 3. Articulated crinoid stem within an argillaceous interbed of the Argillaceous Bioclastic Limestone (N1039).

1

2

3

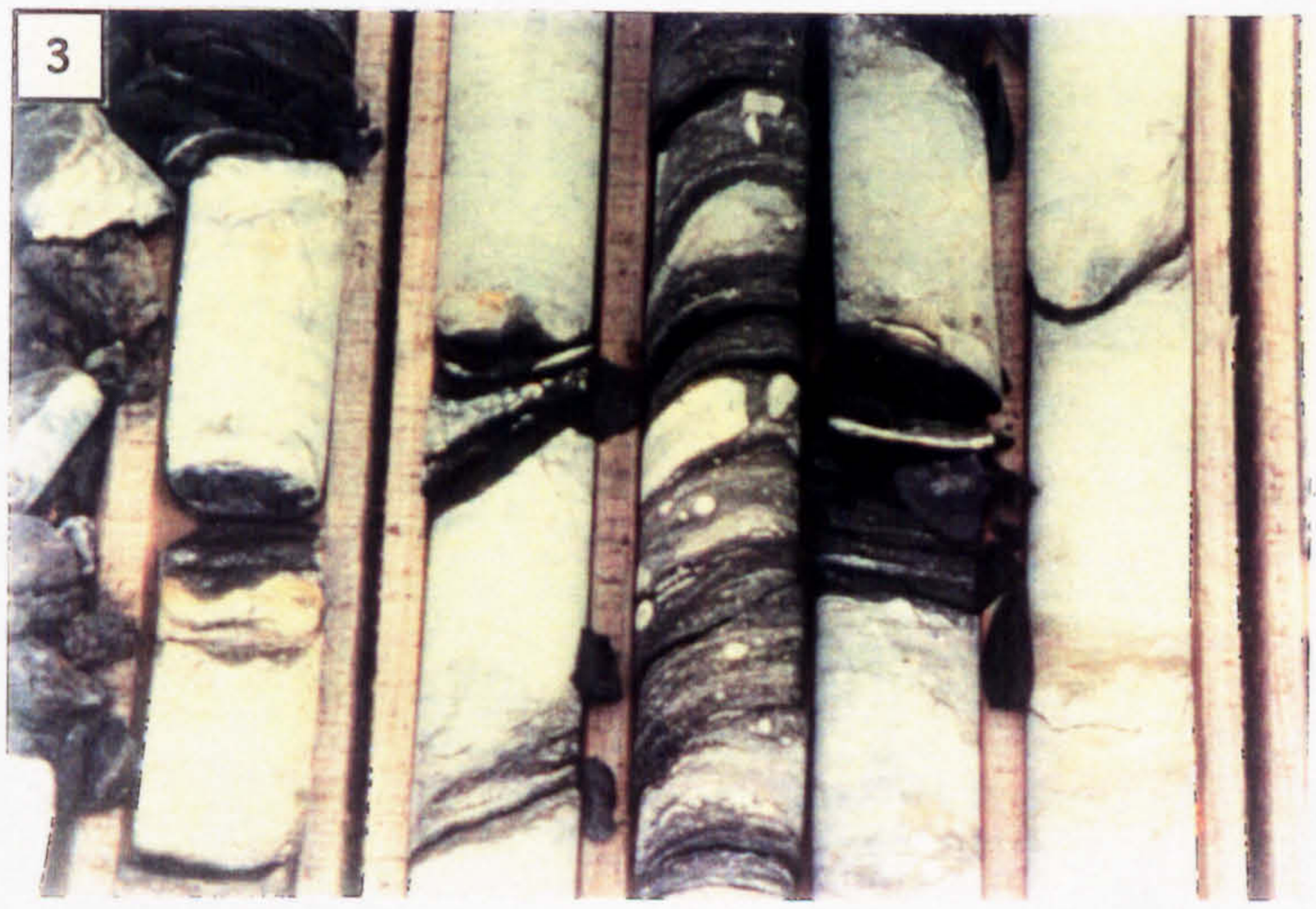

Photo. 4. Crinoidal limestone with millimetric argillite interlayers; the latter are frequently defined by broken drillcore (N912).

Photo. 5. Crinoidal argillite interbed to a limestone-dominated interval of the Reefoid Argillaceous Bioclastic Limestone (N1023).

Photo. 6. Breccia subfacies of the Reefoid Argillaceous Bioclastic Limestone (N1030).

Photo. 7. Bryozoa fragments supported by a matrix of pelletal carbonate mud (PPL; N873, 303.25 m).

Photo. 8. Crinoid ossicle possessing syntaxial sparite overgrowth; the sparite-cemented limestone is truncated by calcite micro-veins (CL; N873, 265.4 m).


4

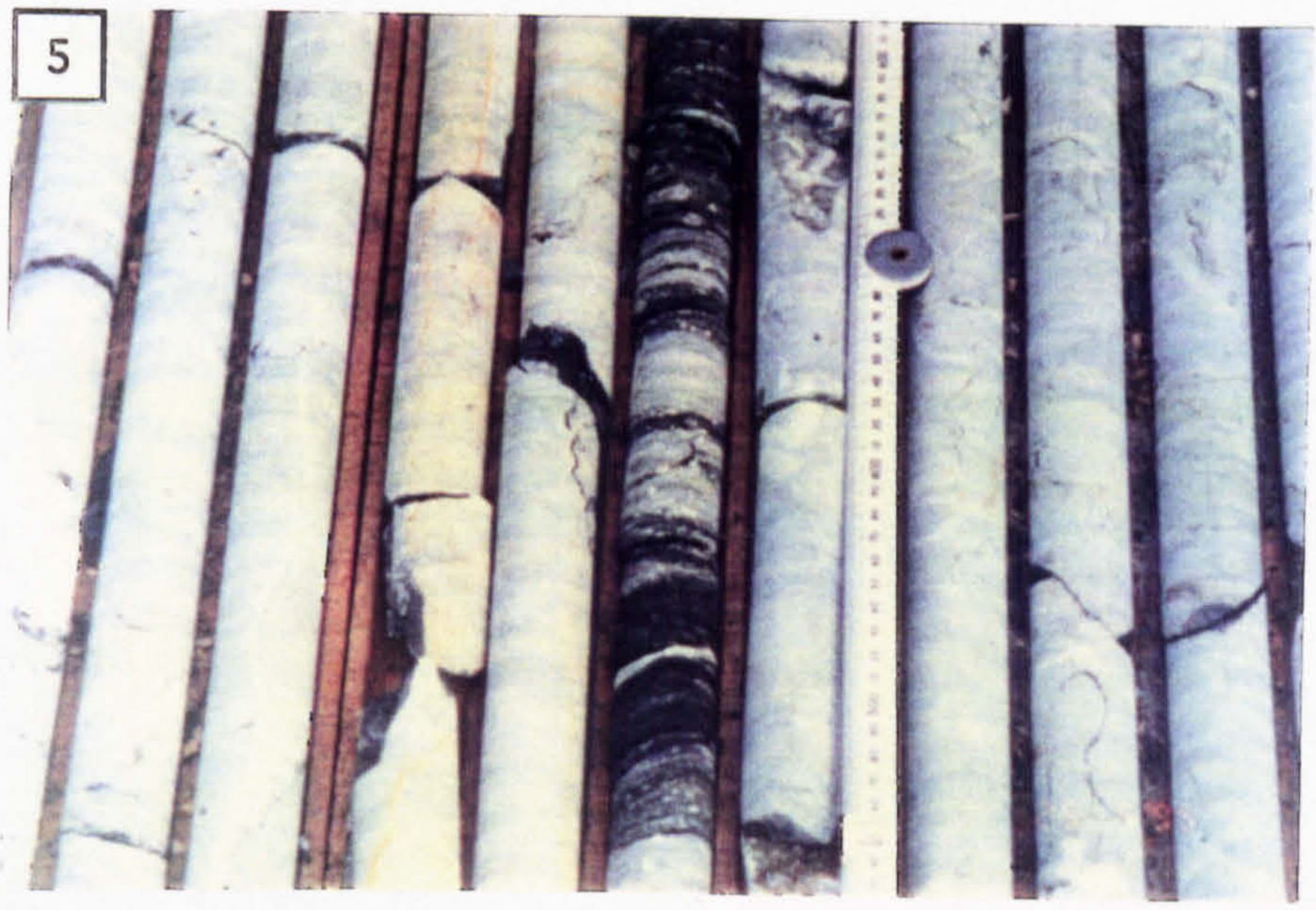
5

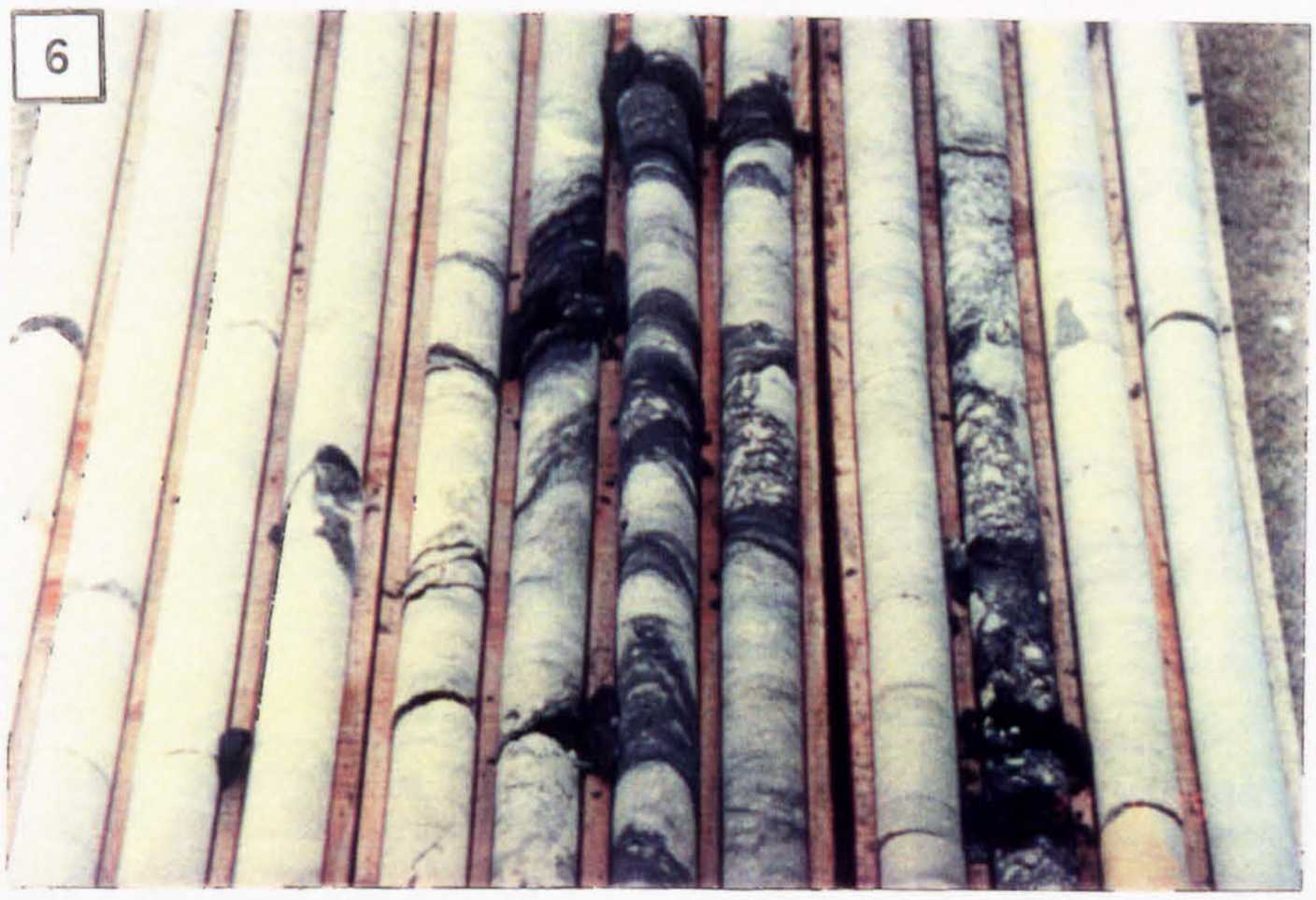
6

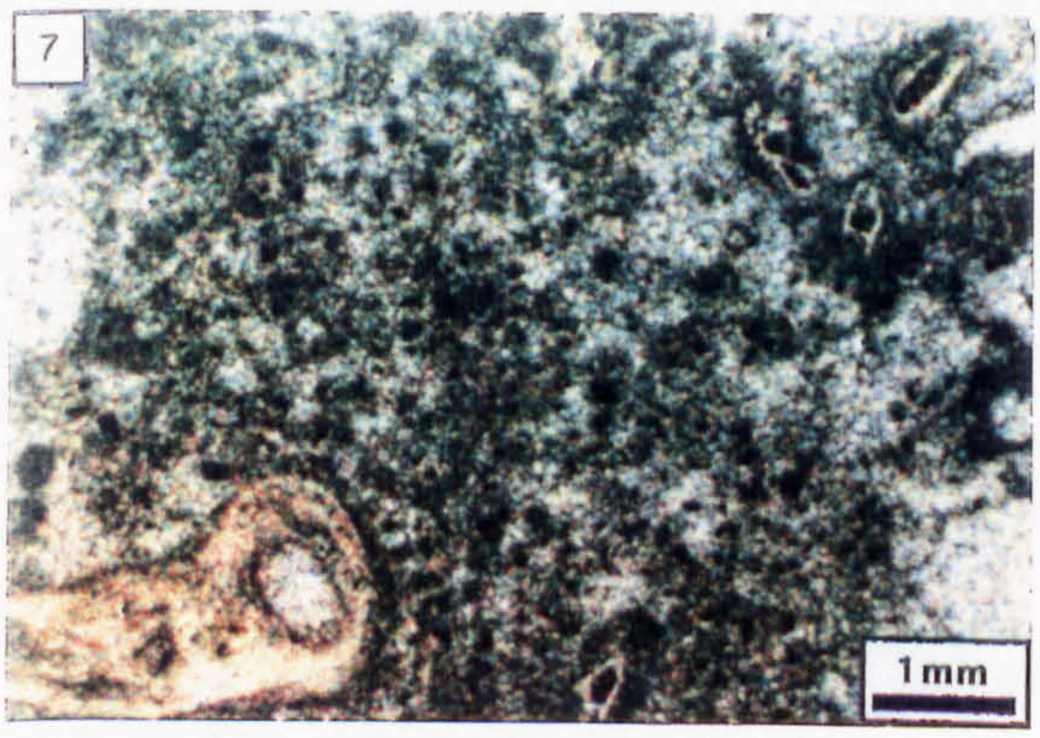
7
1 mm

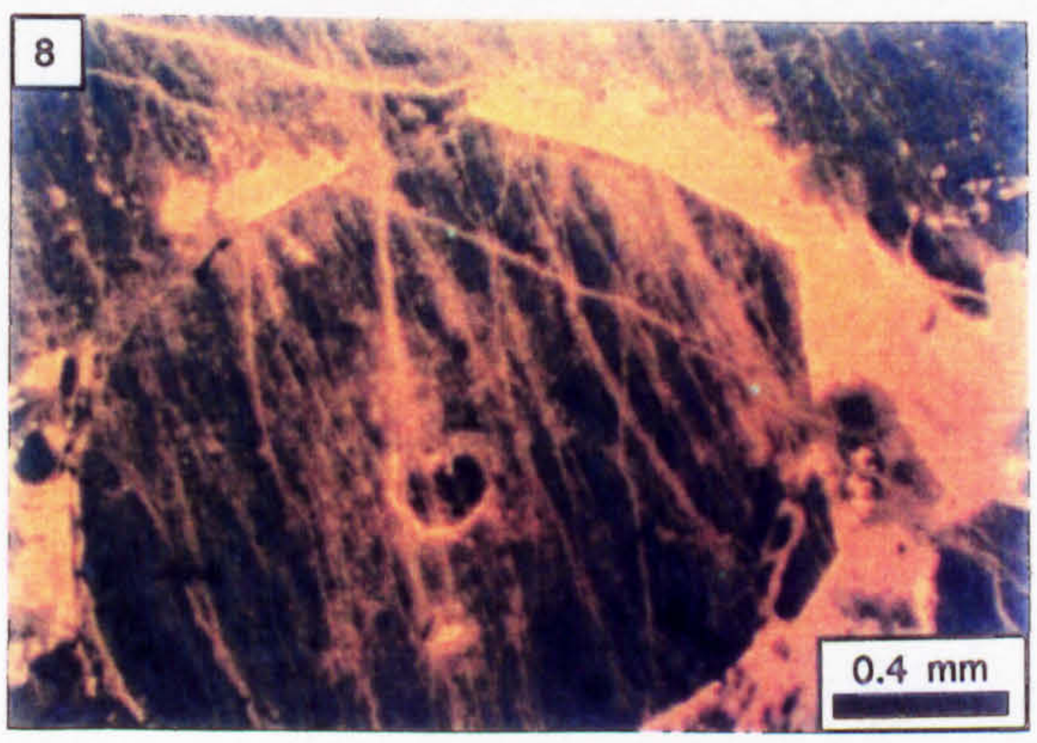
8
0.4 mm

Photo. 9. Mudstone pebble in contact with bioclastic carbonate mud clast (PPL; N873, 303.25 m).

Photo. 10. Clast-supported, monomict Waulsortian Limestone breccia; the dark sediment which defines the limestone clasts is argillite (N1156, 277.6--295.3 m).

Photo. 11. Bioclastic carbonate mud clast in carbonate mud matrix (PPL; N873, 303.25 m).

Photo. 12. Distinction of the clast and carbonate mud matrix shown in Photo. 11 under CL; calcite micro-veins cut across the breccia fabric (N873, 303.25 m).

Photo. 13. East sidewall of the P1N heading showing fractured Pale Beds (1), fault zone breccia (2), the T Fault scarp/unconformity (3), and the Boulder Conglomerate (4); 25 cm ruler for scale.

9

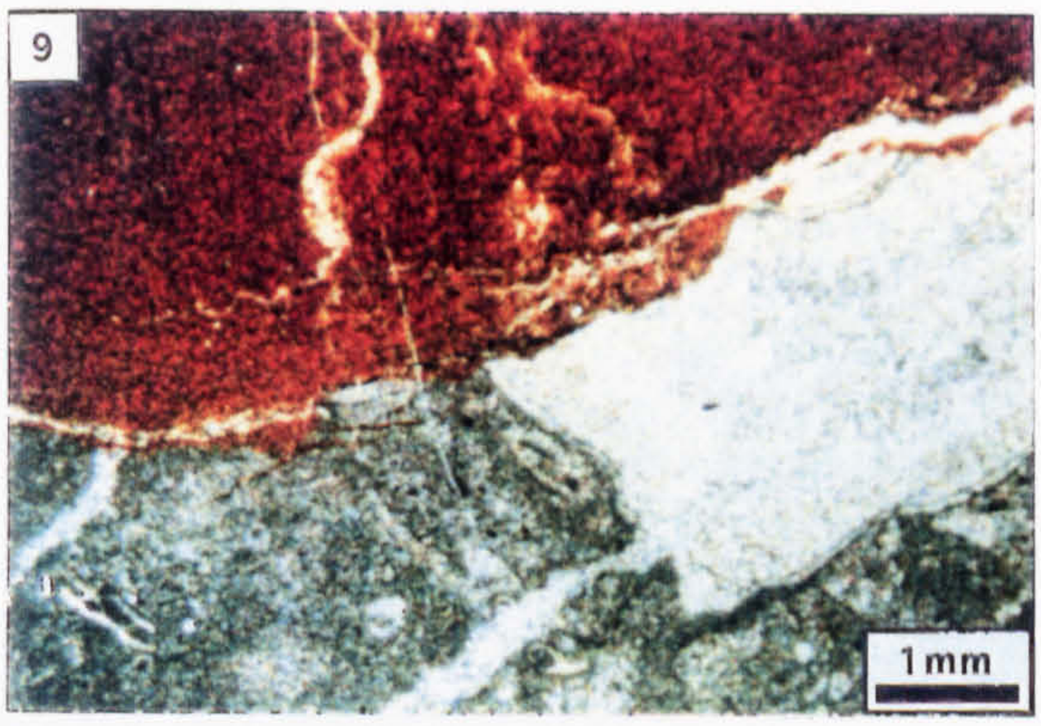

10

11

12

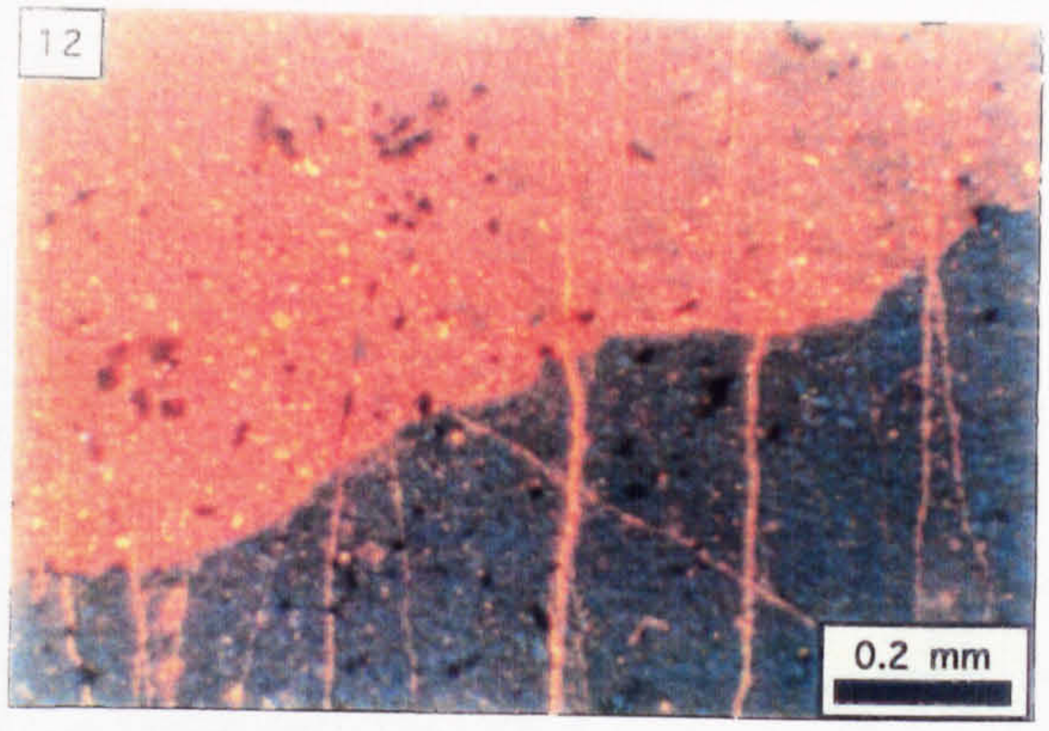

13

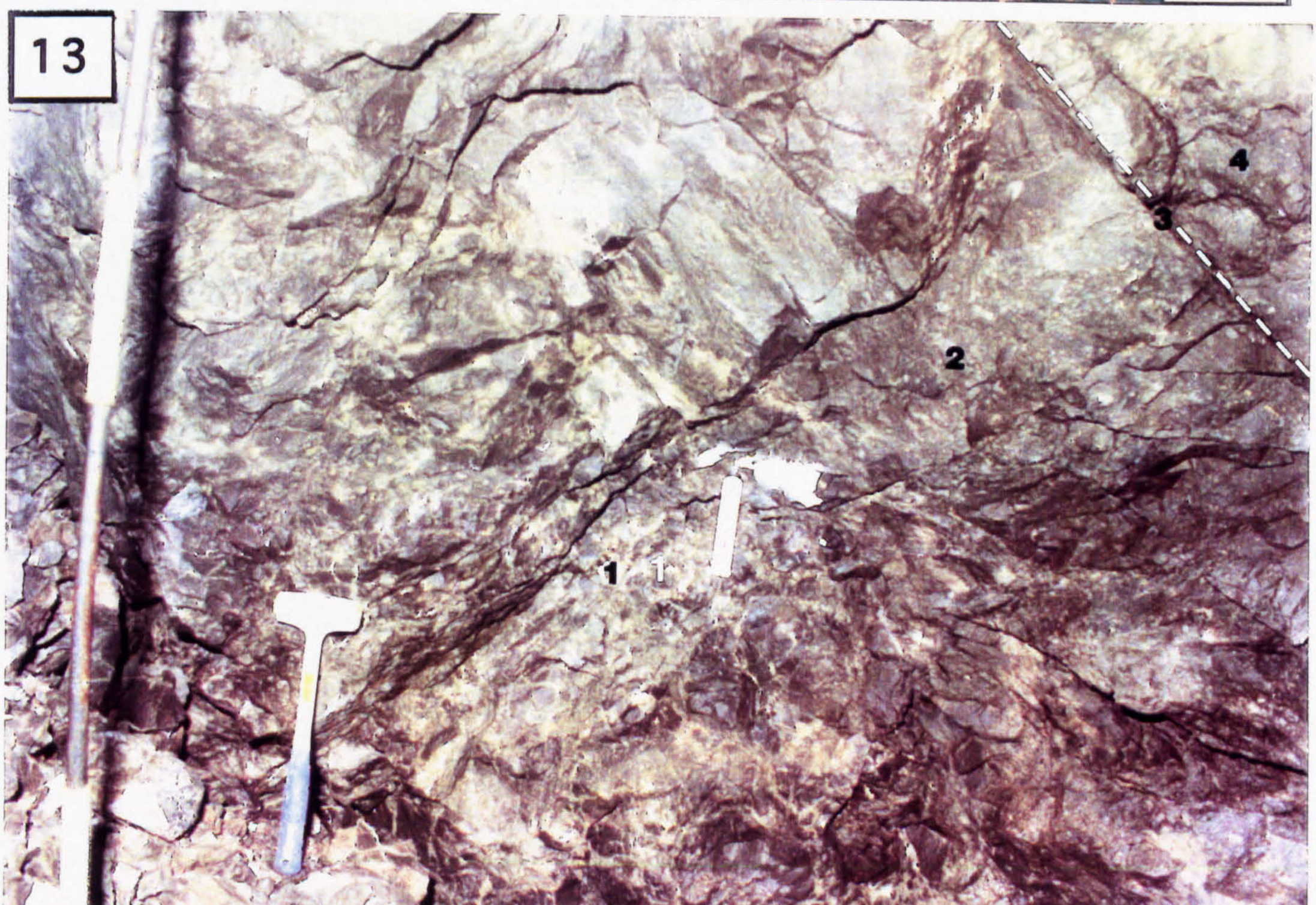

Photo. 14. Polished specimen of fractured Pale Beds from location 1 in Photo. 13.

Photo. 15. Petrography of the fault zone breccia showing a clast of oolitic limestone in a matrix of siliciclastic sand (sample from location 2 in Photo. 13; PPL).

14

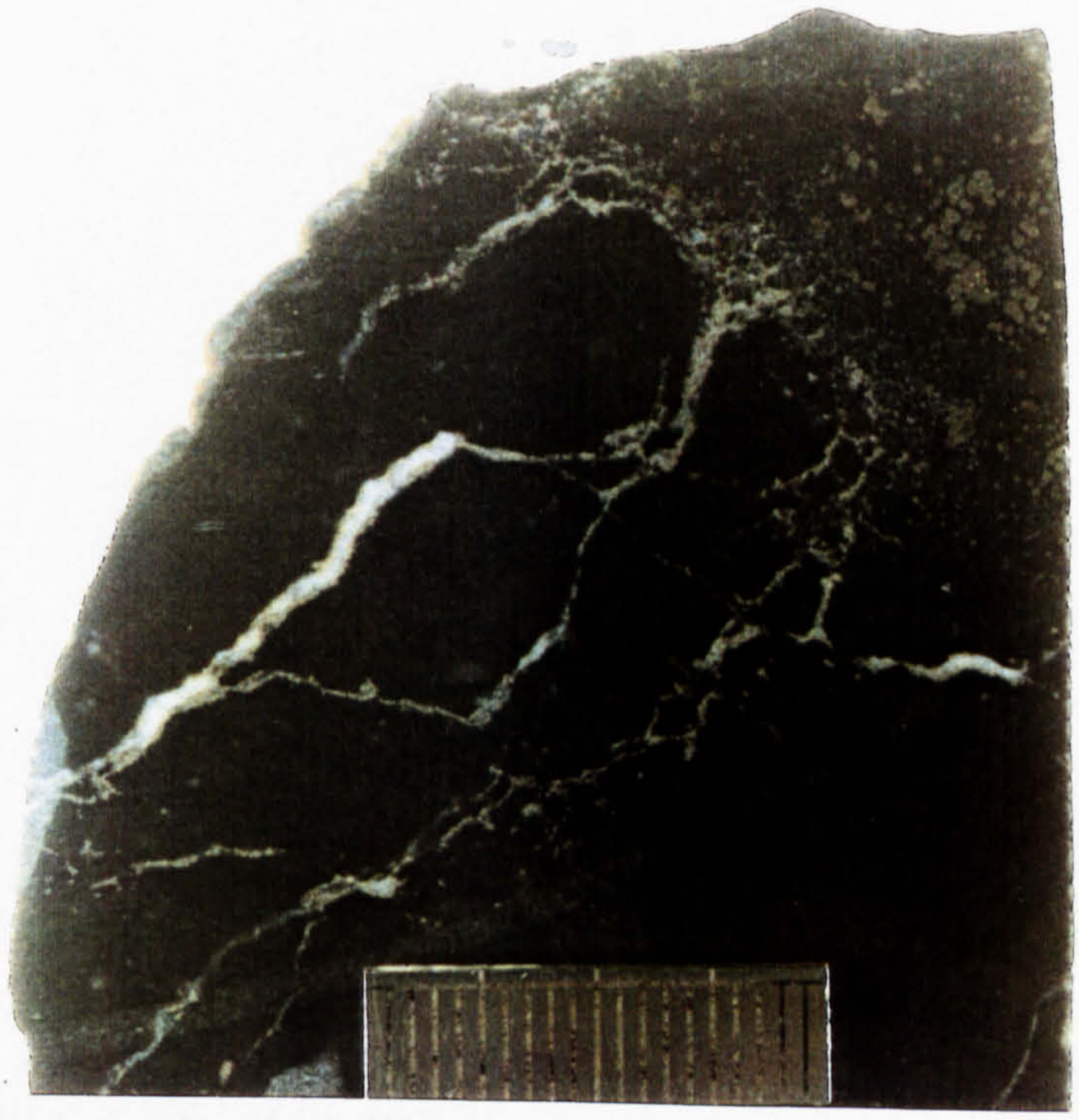

15

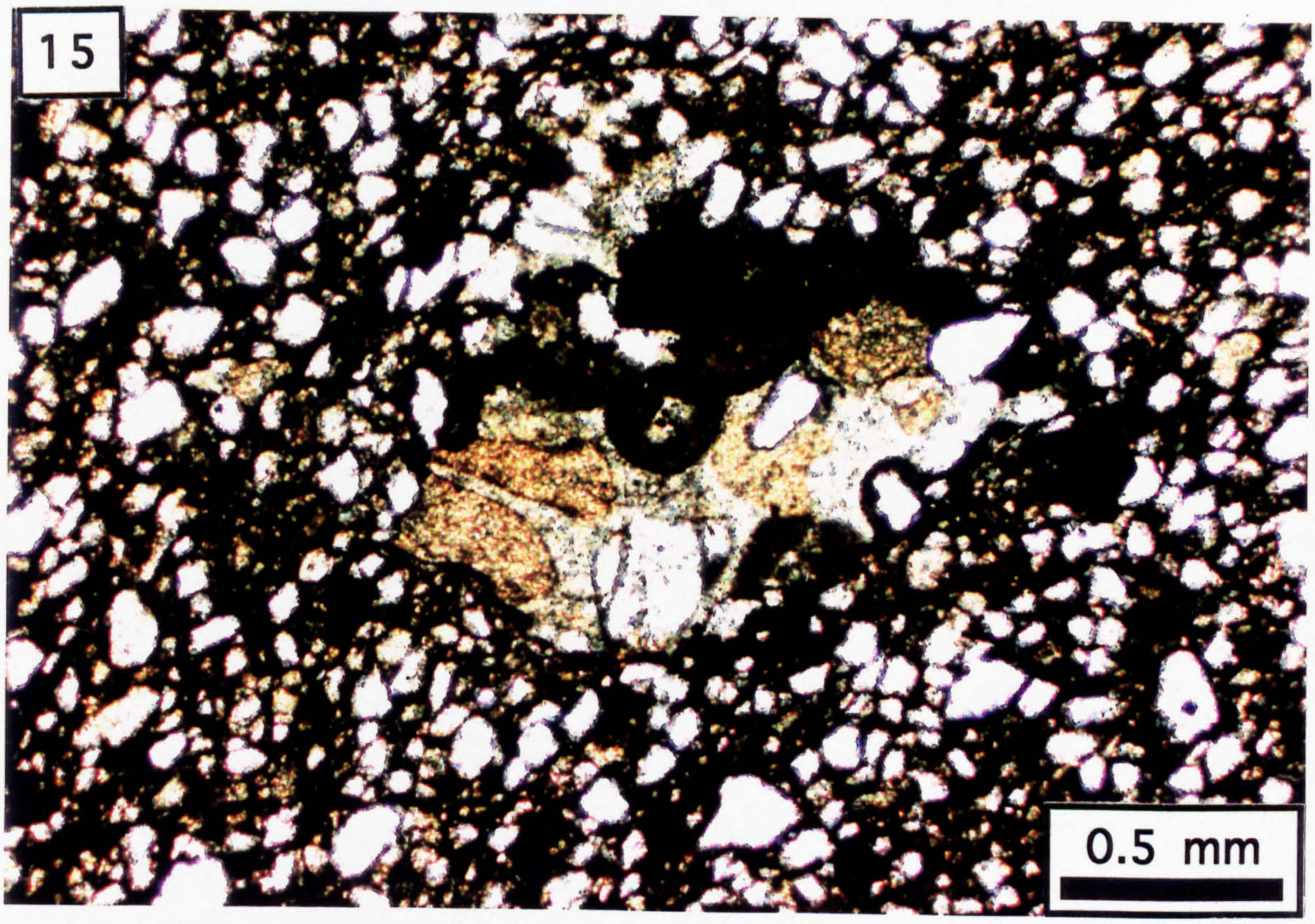

Photo. 16. Underground photograph showing the west sidewall of the P1S heading. Boulder Conglomerate overlies the unconformity, infilling an irregular embayment developed in the Shaley Pales substrate (1). The Boulder Conglomerate comprises clast-supported breccia units (2) interbedded with argillaceous calcsiltite (3).

Photo. 17. Oolitic limestone clast from the breccia unit present in location 2 in Photo. 16 (PPL).

16

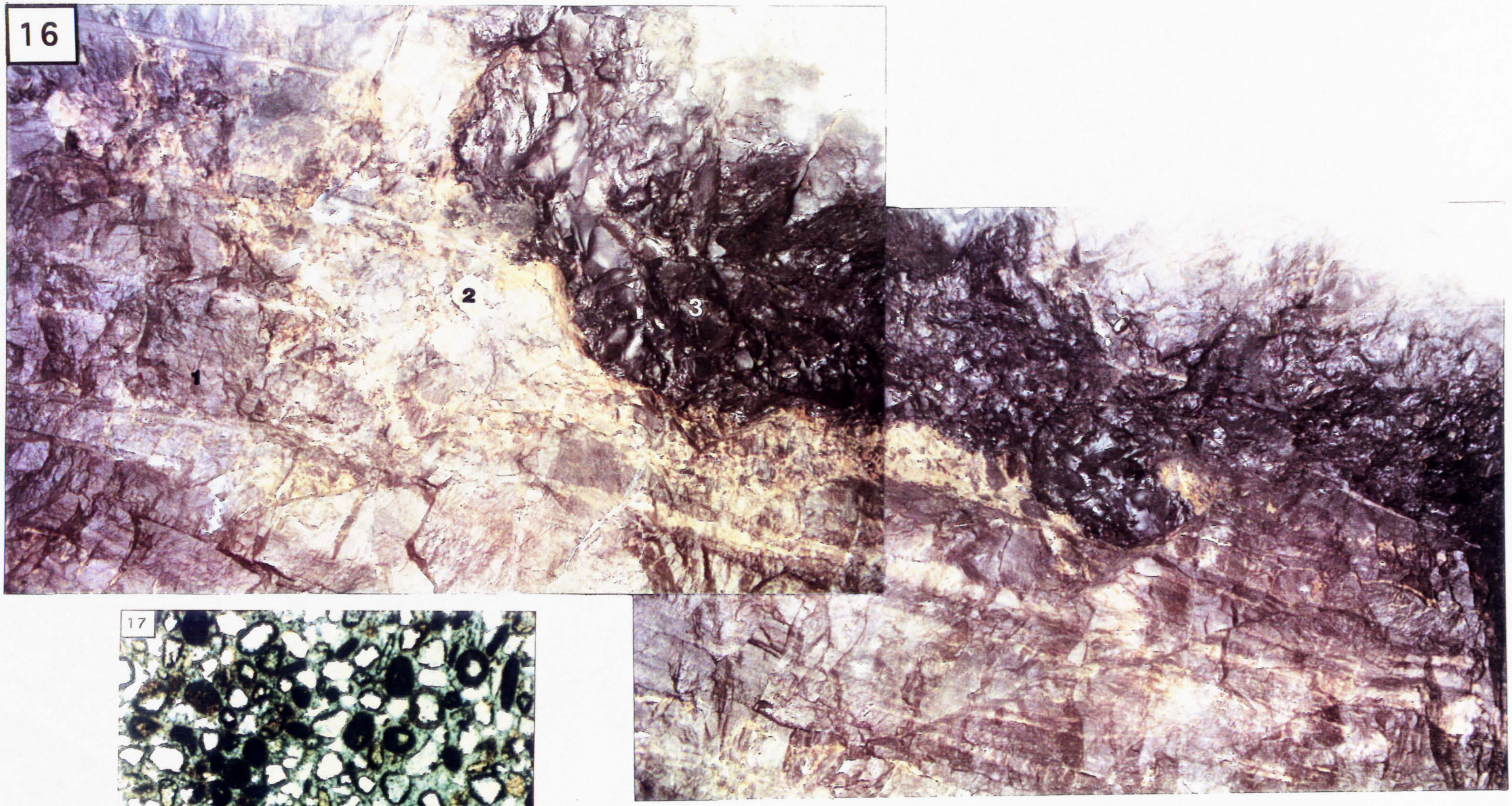

17

Photo. 18. Step-like inflection in the unconformity (U) at the intersection of P1S with CGO AC. The breccia bed deposited over the Shaley Pales is polymict and contains angular boulder of Waulsortian Limestone (w).

Photo. 19. Crinoid ossicle showing a syntaxial sparite overgrowth; the dark portion of the photomicrograph is the edge of the slide (CL; sample from P1S).

Photo. 20. Sparite occlusion to bioporosity (CL; sample from P1S).

Photo. 21. Underground photograph showing a sheared argillite interbed in the Shaley Pales (west sidewall of P1S; 25 cm ruler for scale).

18

19

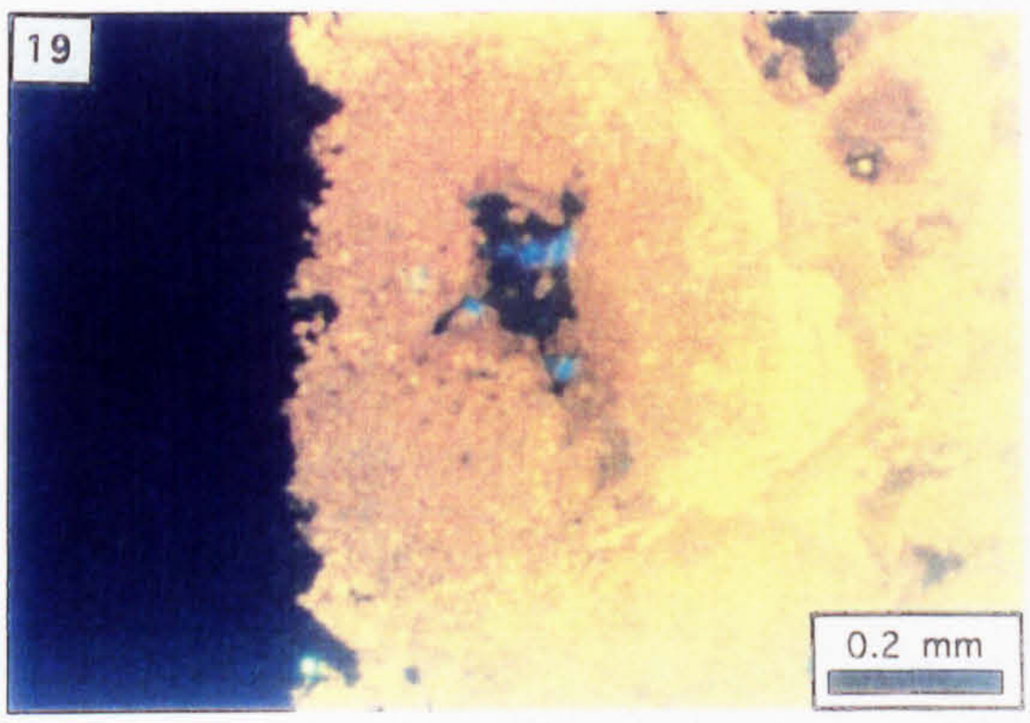

20

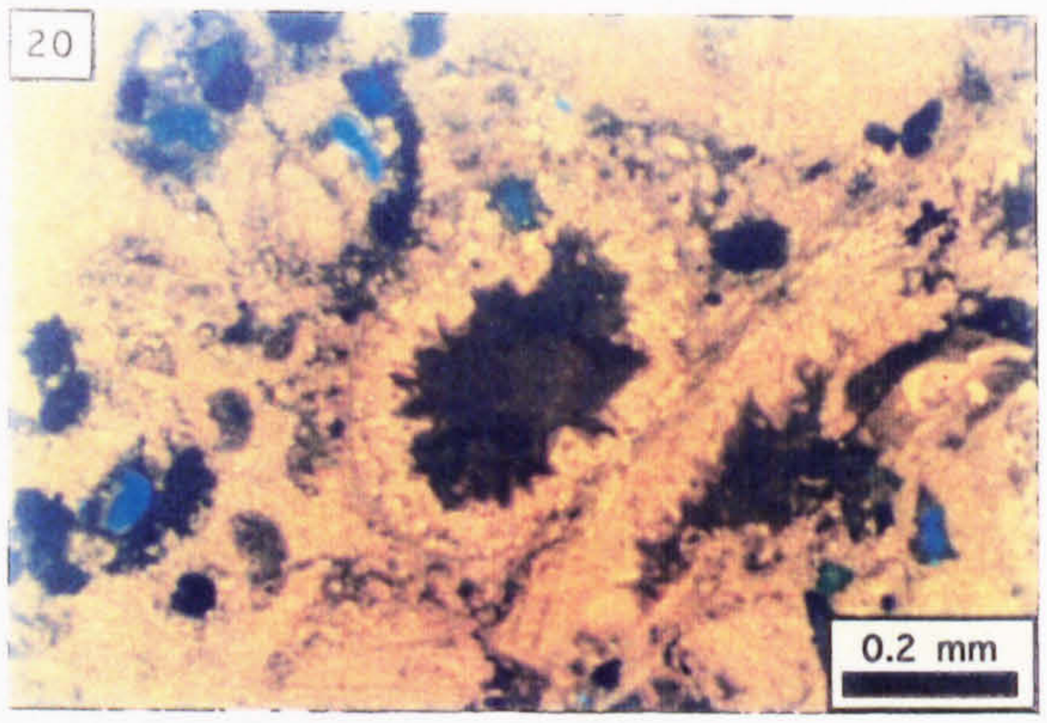

21

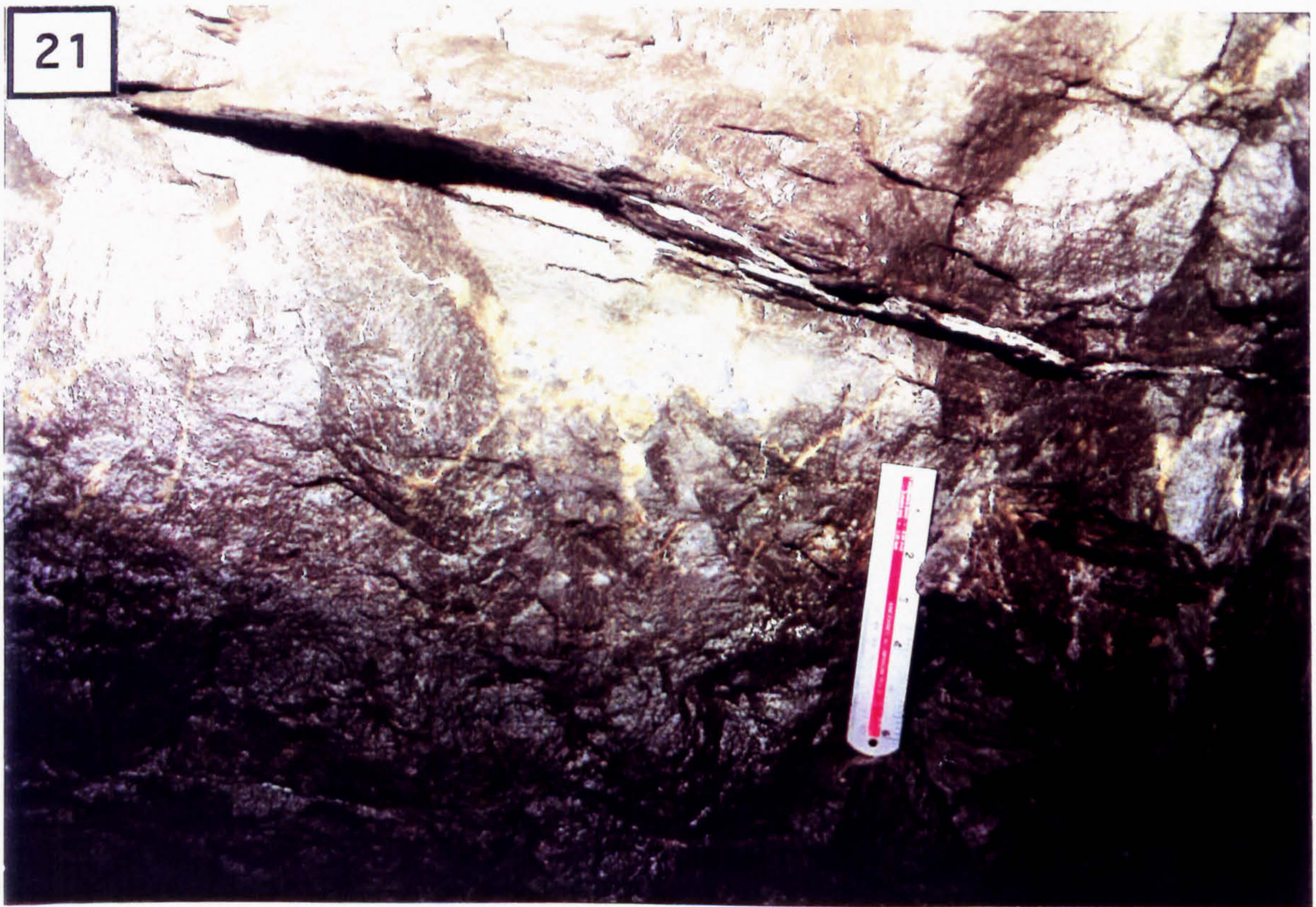

Photo. 22. West sidewall of the P2 heading showing a subvertical fracture located in the Shaley Pales (1) which is truncated by the unconformity (2) and overlain by Boulder Conglomerate (3).

Photo. 23. Fault breccia comprising clasts of Pale Beds and Micrite Unit, derived from the footwall and hanging wall, respectively (N1012, 523.9 -528.9 m).

Photo. 24. Deformed strata within the Shaley Pales (N1192).

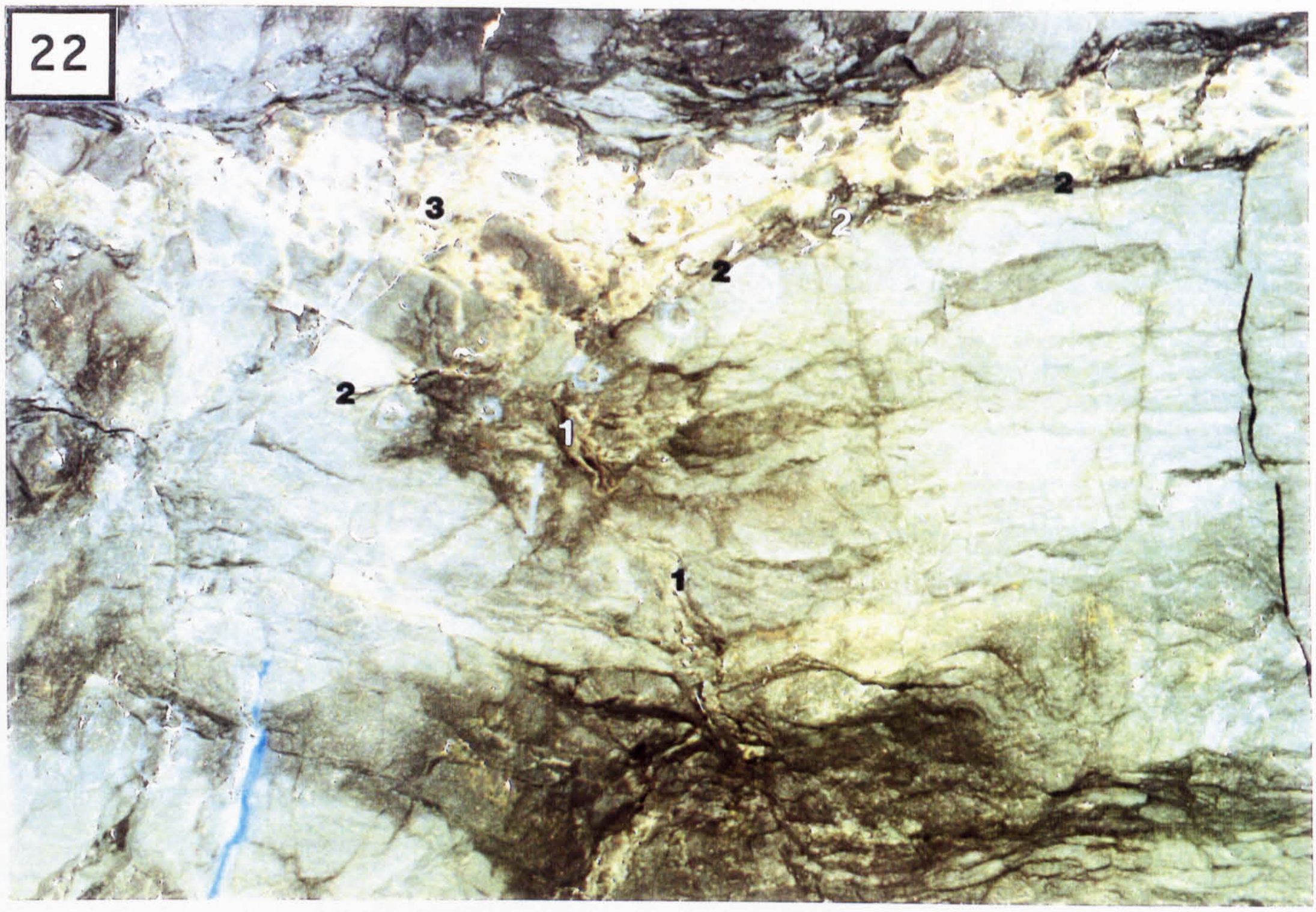
22
3
2
2
2
2
1
1

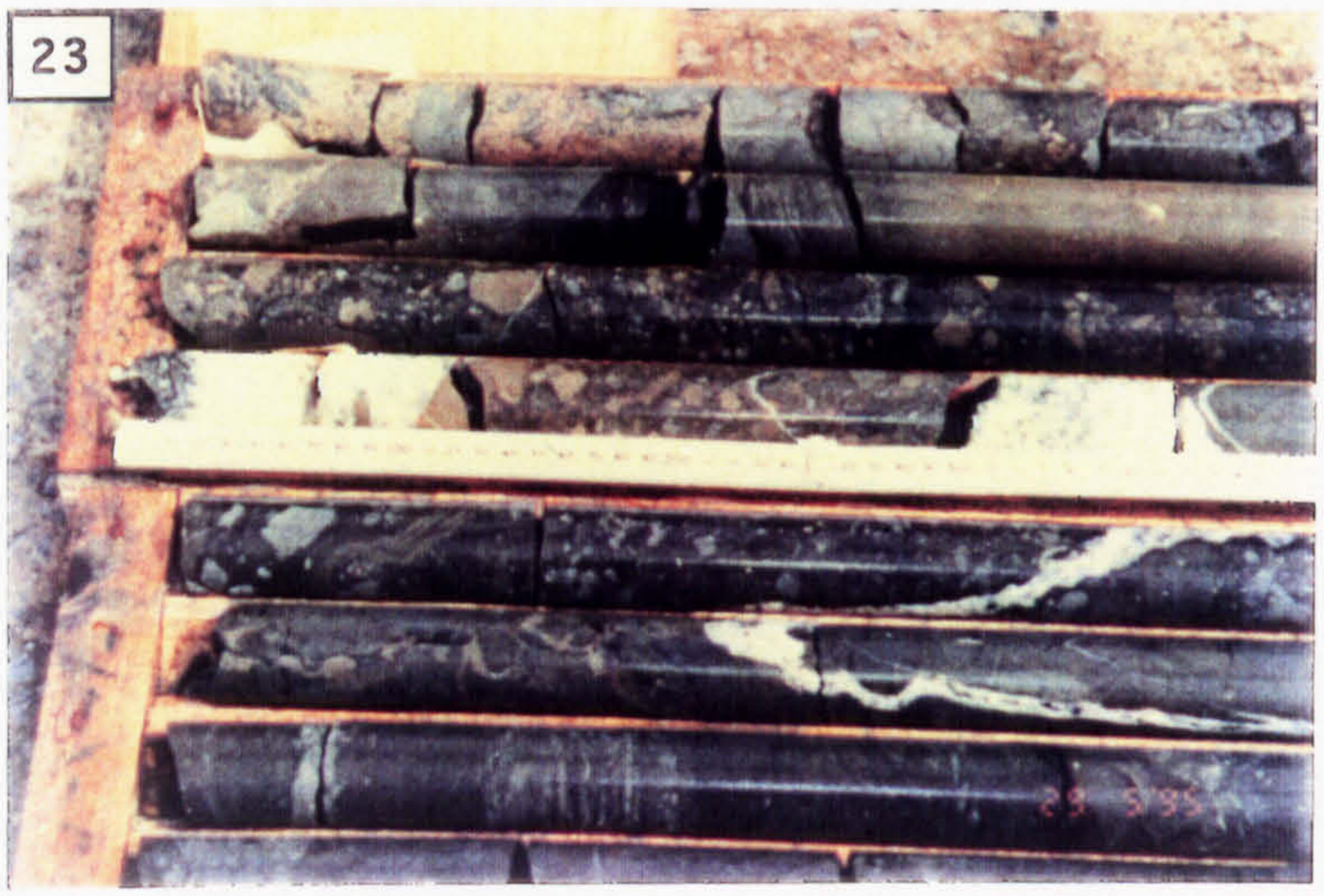
23
29 5'95

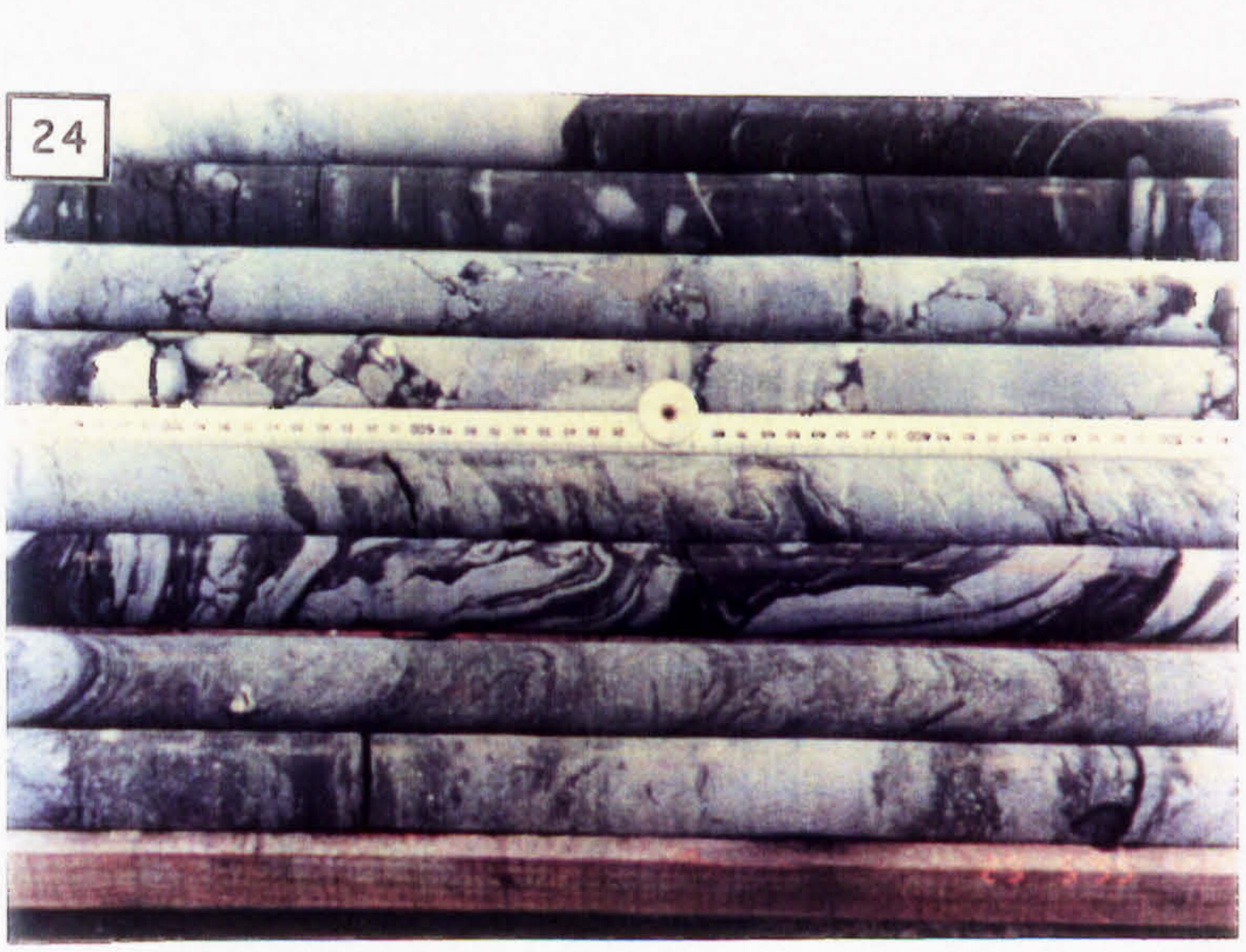
24

Photo. 25. Breccia zone within the Shaley Pales coincident with repeated Shaley Pales stratigraphy (N1027).

Photo. 26. Diamond drillcore sequence showing: A=the contact of the Shaley Pales with the Pale Beds; B=the contact of the A.B.L. with the Shaley Pales; C=sheared and tilted Shaley Pales strata (N1064).

Photo. 27. Argillaceous Bioclastic Limestone overlying sheared Shaley Pales; bedding in the former is undeformed and perpendicular to the sub-vertical axis of the drillcore (N1149).

25

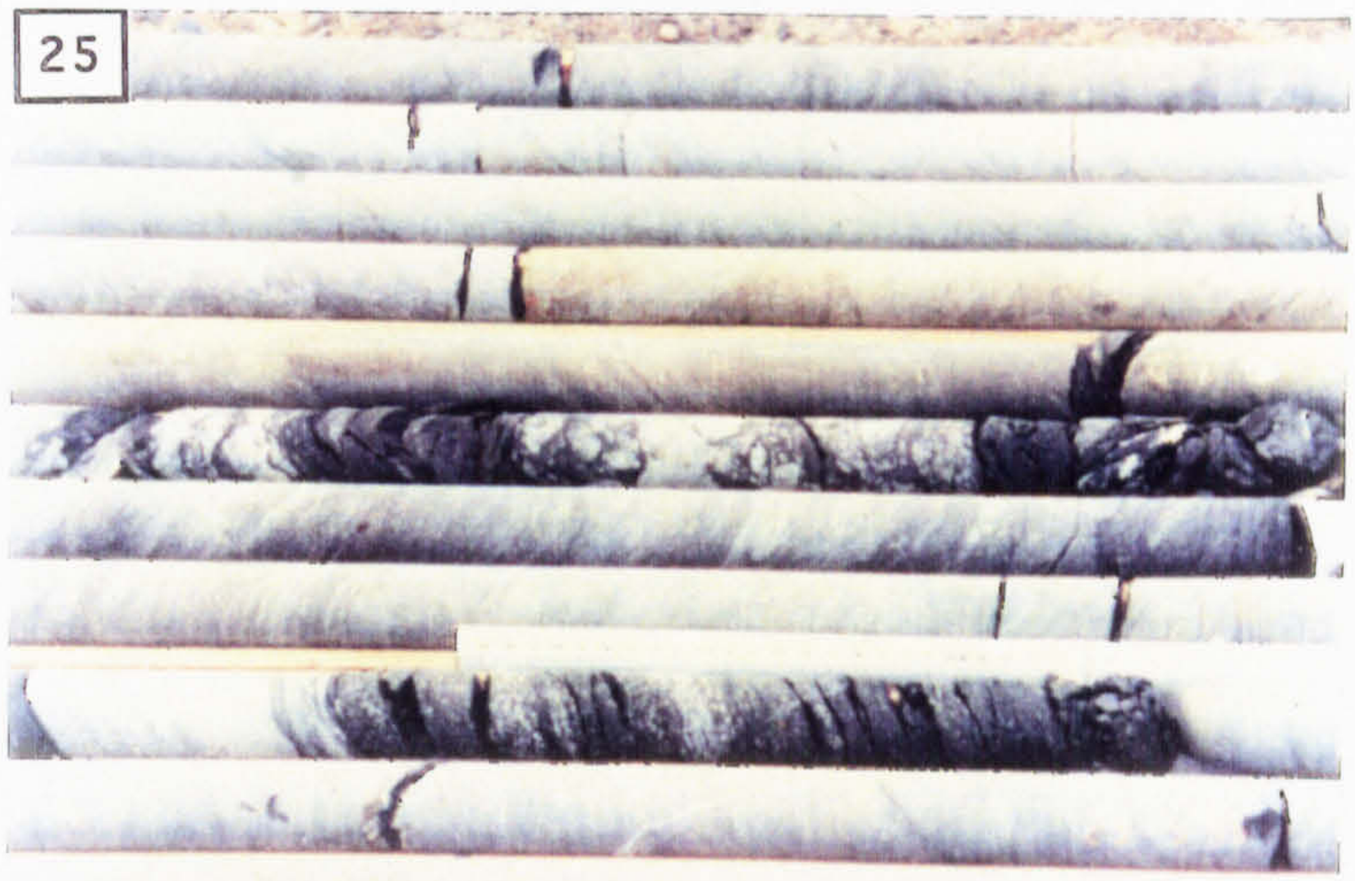

26

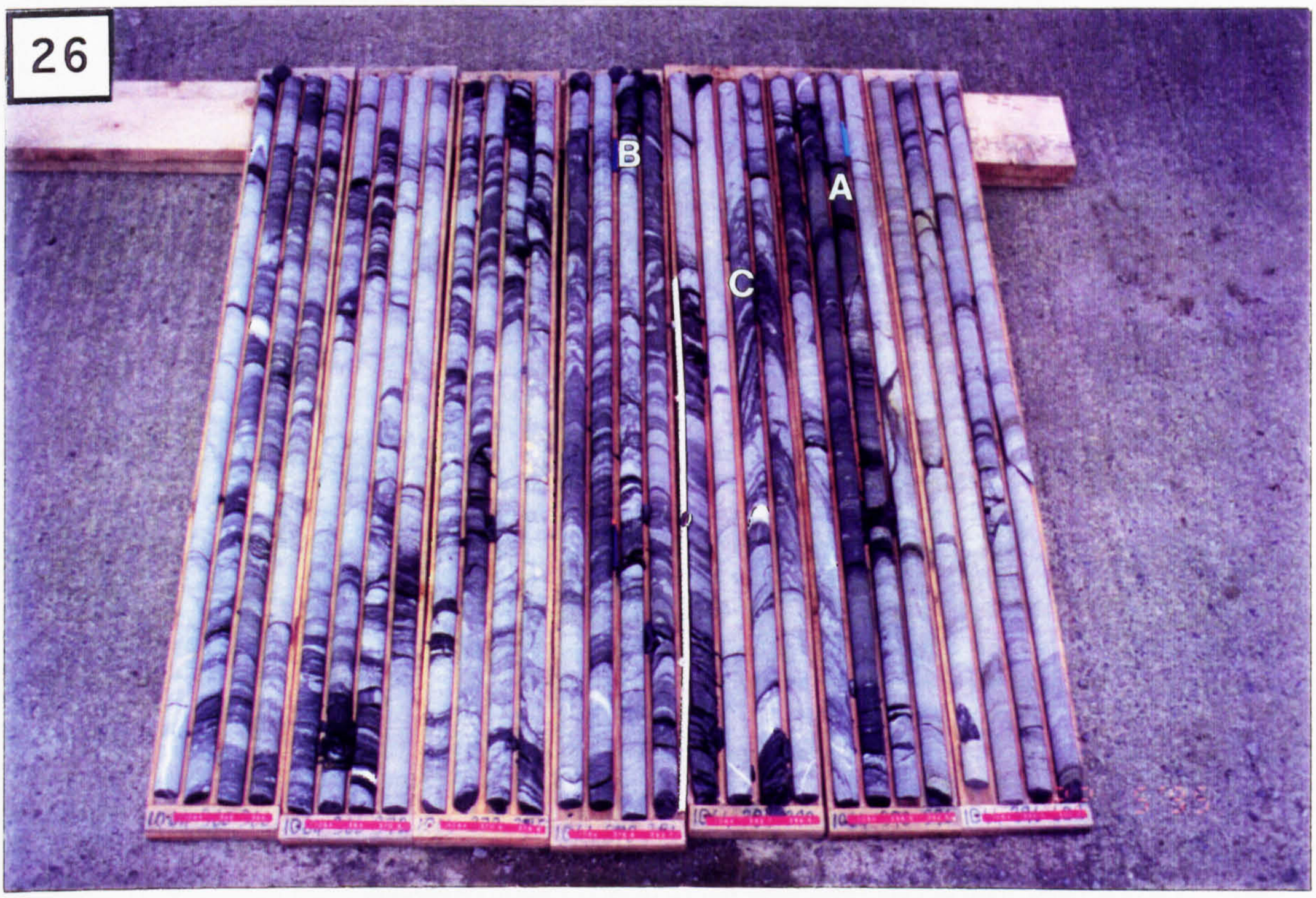

27

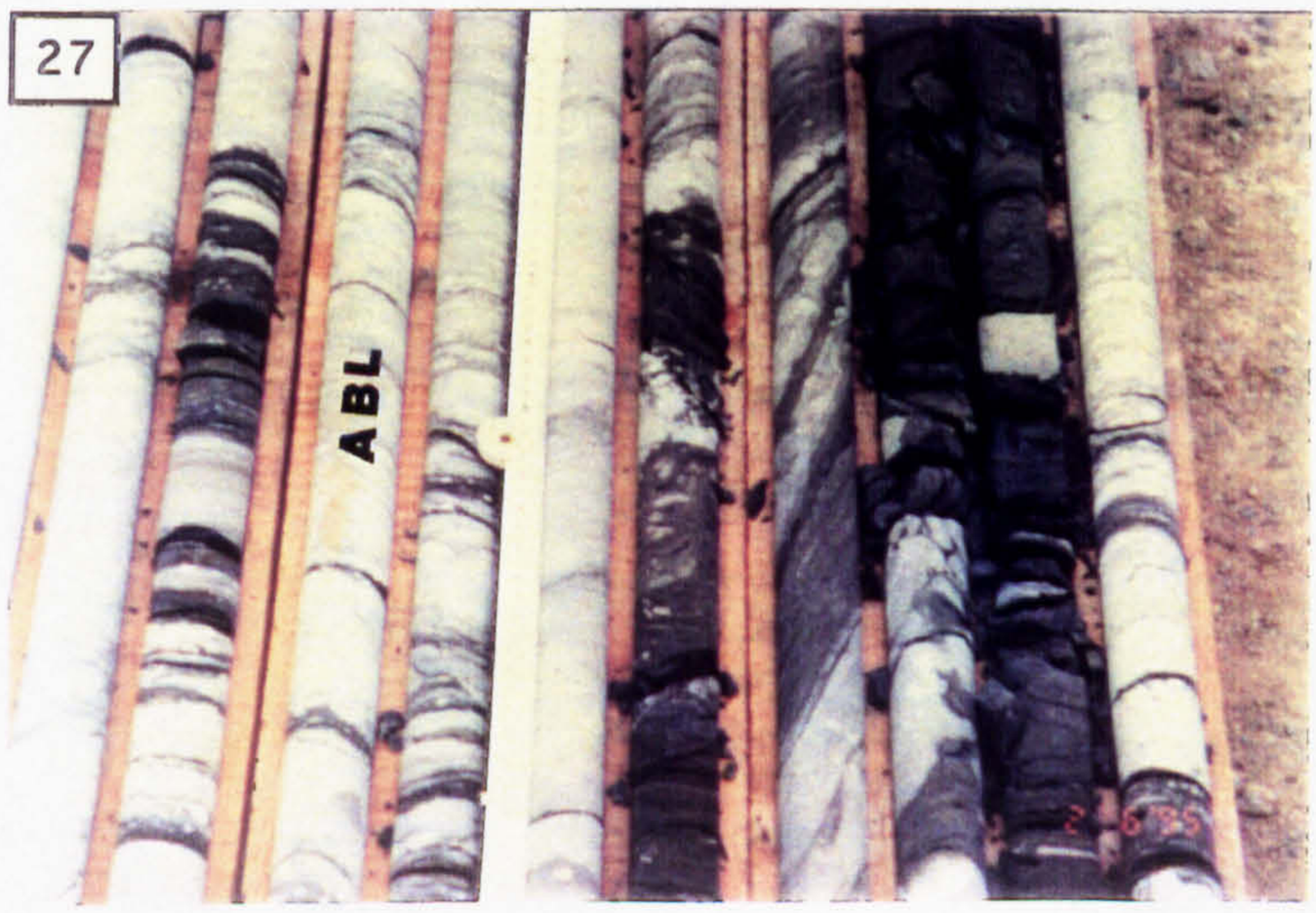

Photo. 28. Underground photograph of the Boulder Congomerate exposed on the north side of CGO AC: concretionary argillaceous calcsiltite (1) occurs as a subhorizontal interbed to stratiform breccia units (2); the interbed adjacent to the breccia strata exhibits a contact-parallel fabric (3) [25 cm ruler for scale].

Photo. 29. Graded laminae of the interbed (PPL).

Photo. 30. Stylolitic upper contact of a concretion from the interbed with the overlying, compacted sediment (PPL).

Photo. 31. Polymict breccia from the P2 heading; the light grey, angular clast is Waulsortian Limestone (pen for scale).

28

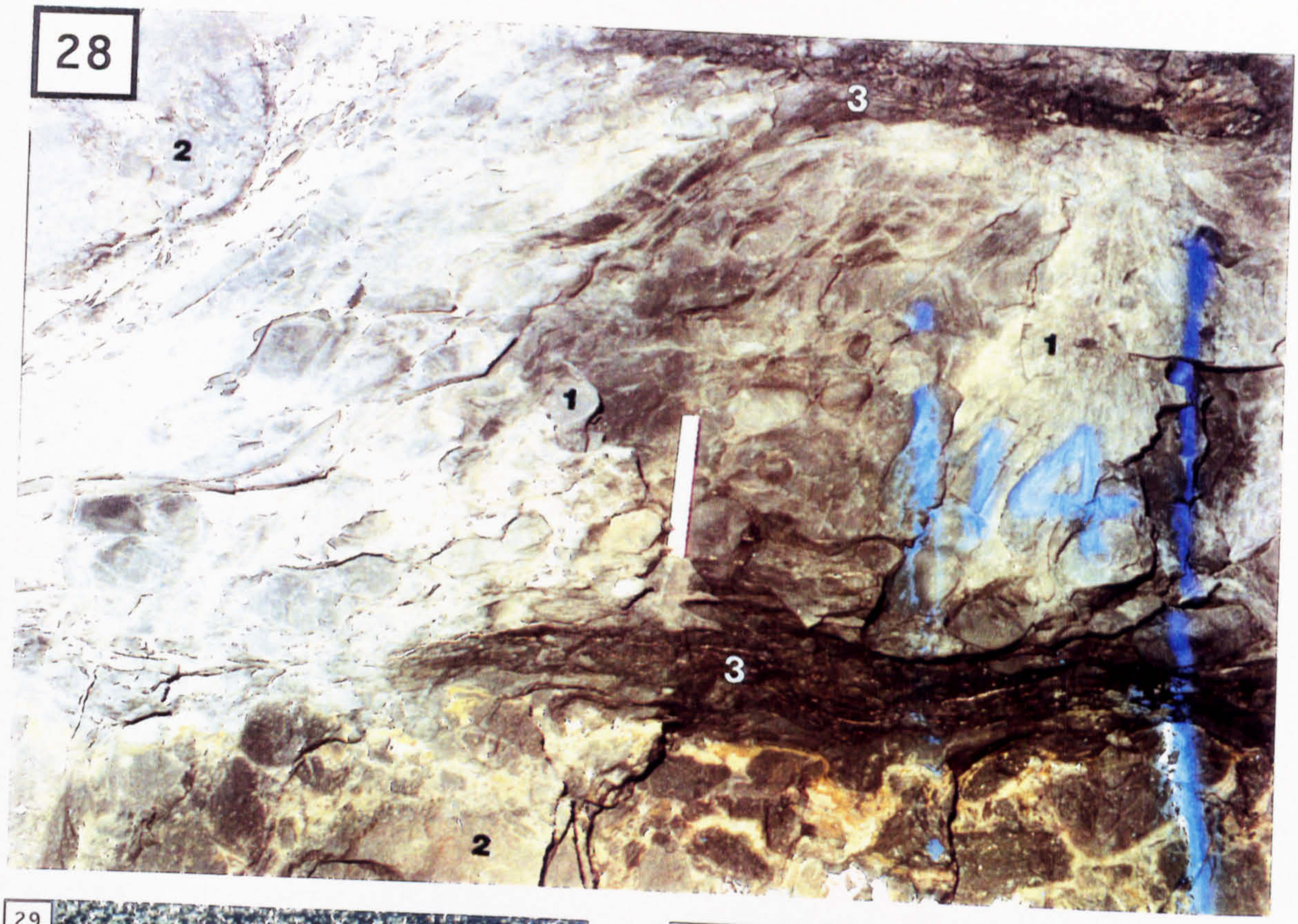

29

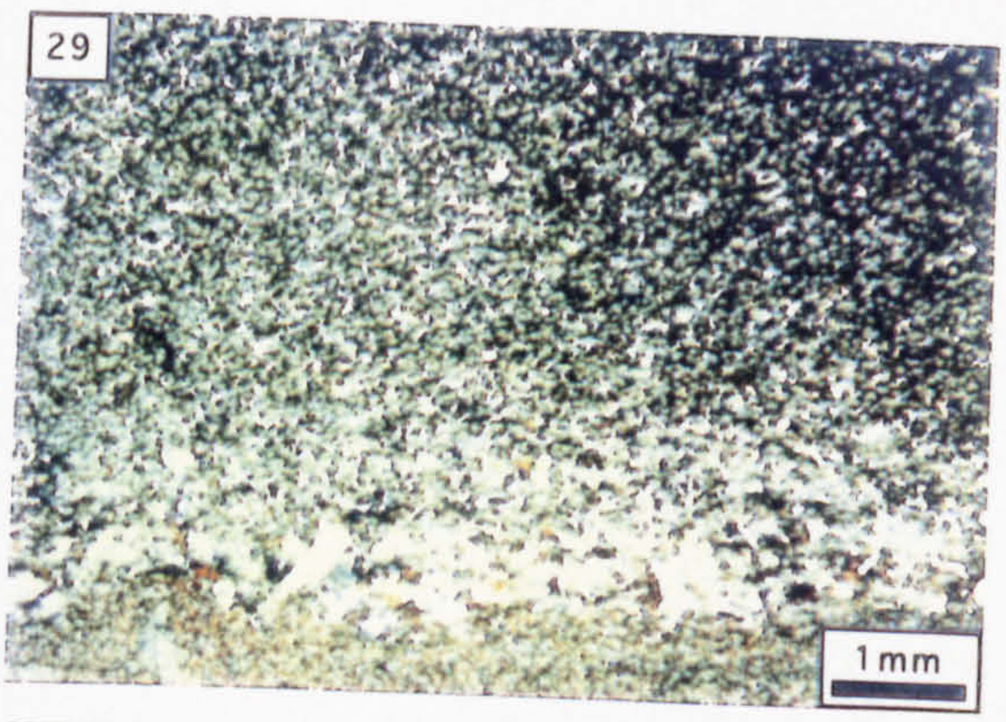

30

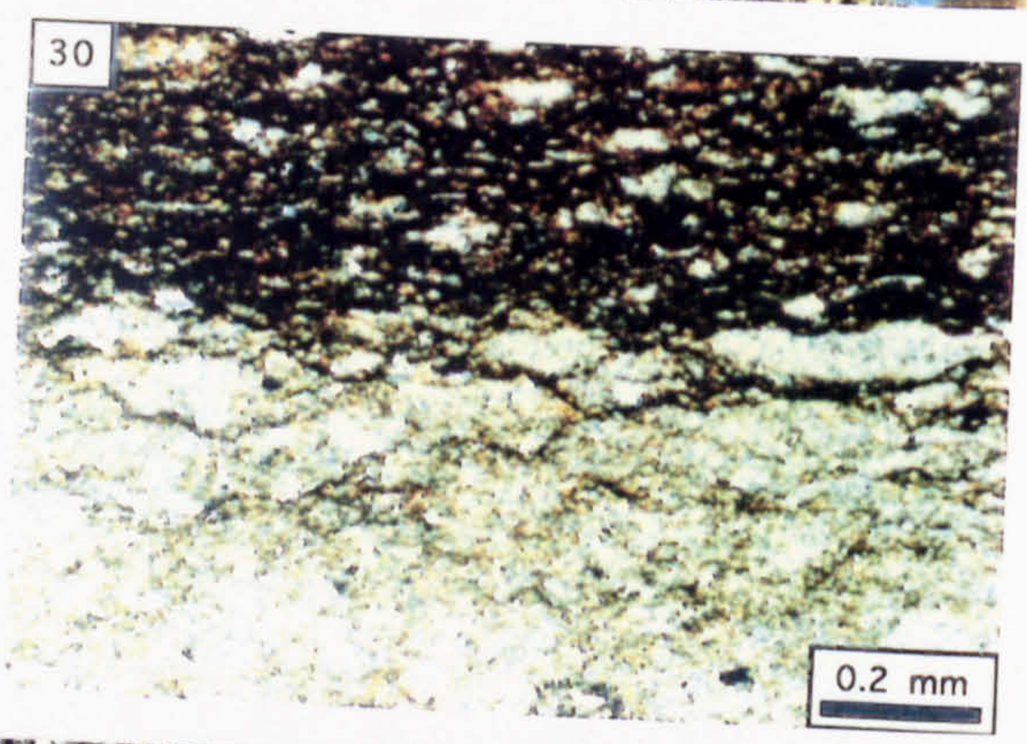

31

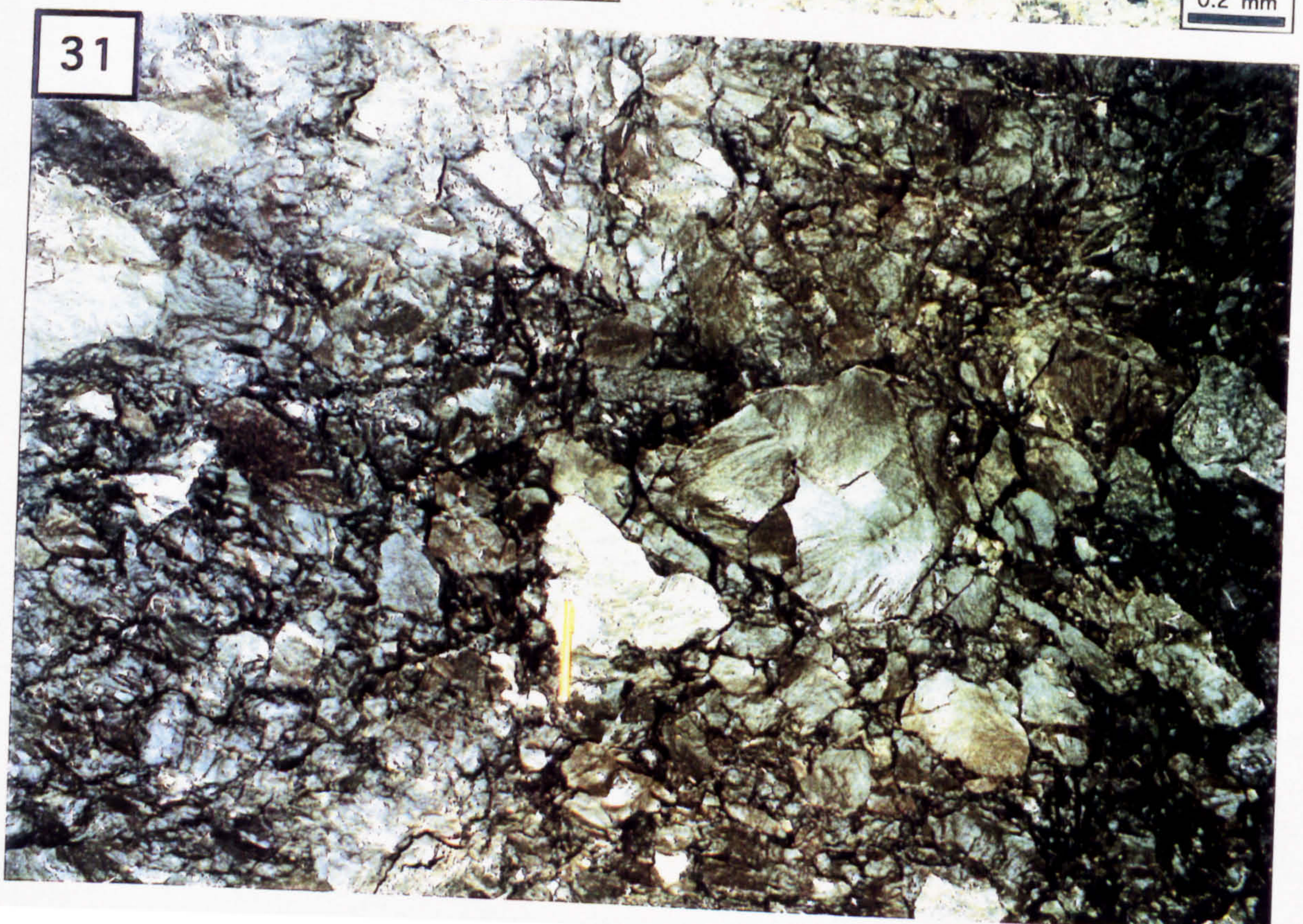

Photo. 28. Underground photograph of the Boulder Congomerate exposed on the north side of CGO AC: concretionary argillaceous calcsiltite (1) occurs as a subhorizontal interbed to stratiform breccia units (2); the interbed adjacent to the breccia strata exhibits a contact-parallel fabric (3) [25 cm ruler for scale].

Photo. 29. Graded laminae of the interbed (PPL).

Photo. 30. Stylolitic upper contact of a concretion from the interbed with the overlying, compacted sediment (PPL).

Photo. 31. Polymict breccia from the P2 heading; the light grey, angular clast is Waulsortian Limestone (pen for scale).

Photo. 32. Polished slab from the P2 heading showing an ore boulder; notice the presence of a stratiform fabric which is truncated at the clast edge (cm-ruler for scale).

Photo. 33. Matrix to the Polymict breccia showing grains of siliciclastic sand (1), comminuted limestone (2), dolomite (3), sphalerite (4) and pyrite (5), set in a background of argillaceous (calc)siltite (PPL).

Photo. 34. Contact of an oolitic limestone clast with the matrix shown in Photo. 33; the light grey grains present in the latter are sphalerite (RL).

Photo. 35. Contact of the Polymict breccia with the underlying interbed; notice the plastic sediment interpenetration structures developed between the interbed (A) and the ore-bearing matrix (B).

28

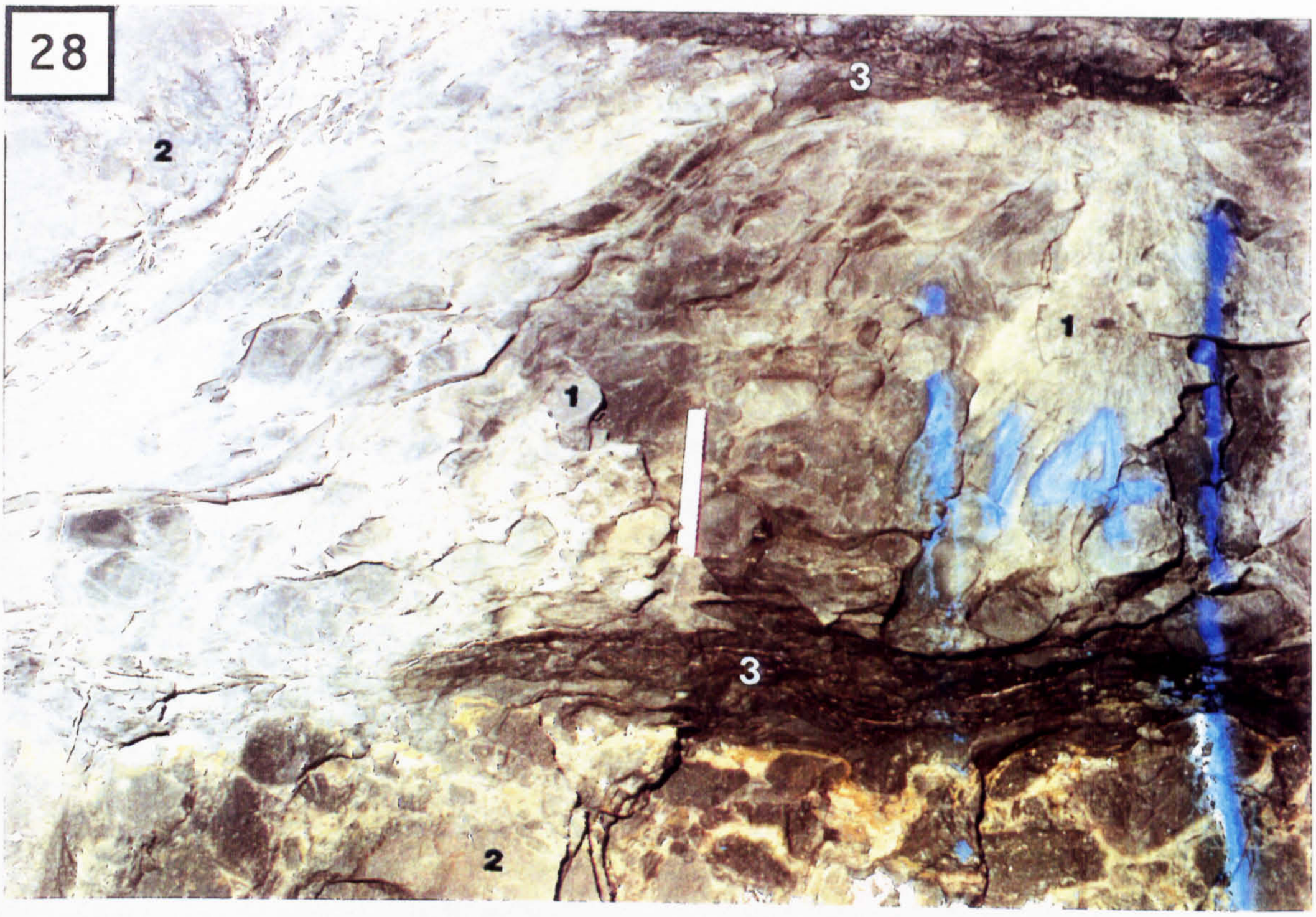

29

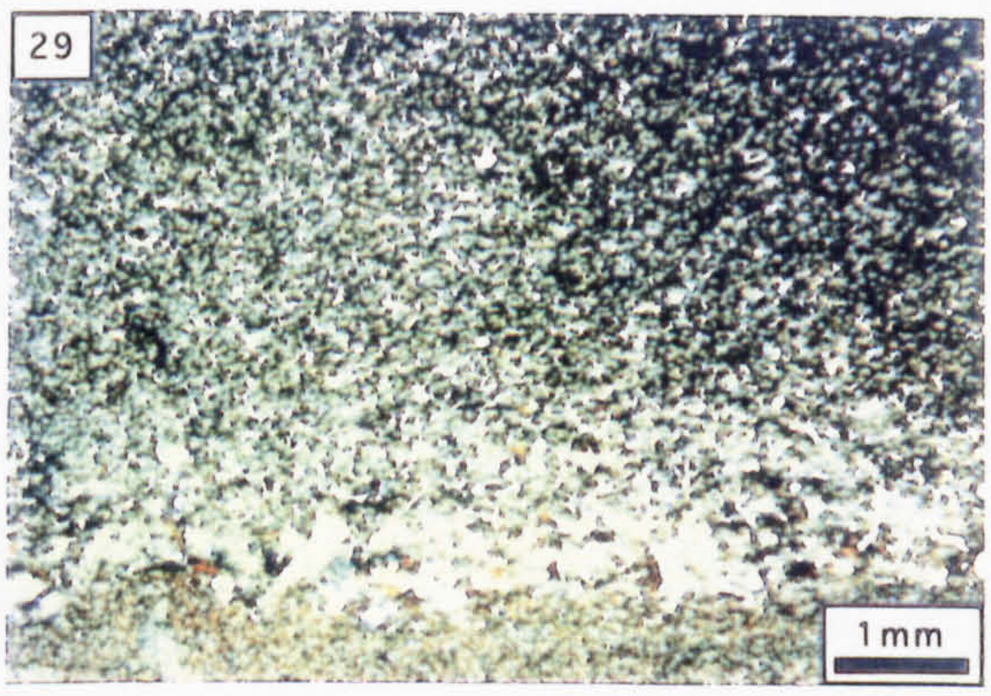

30

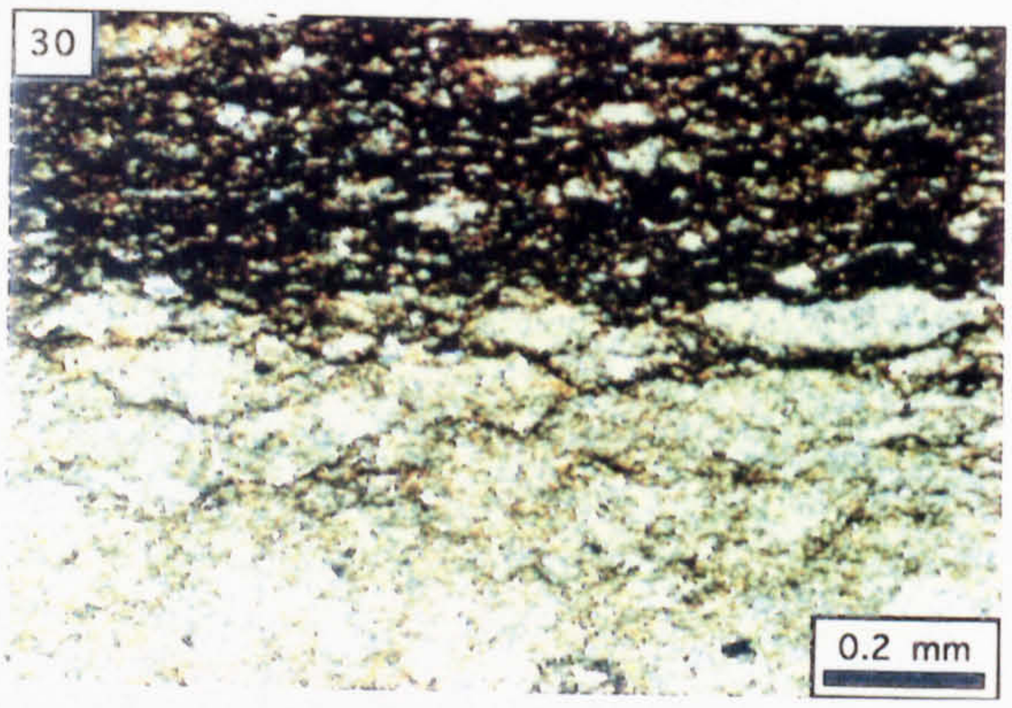

31

32

33

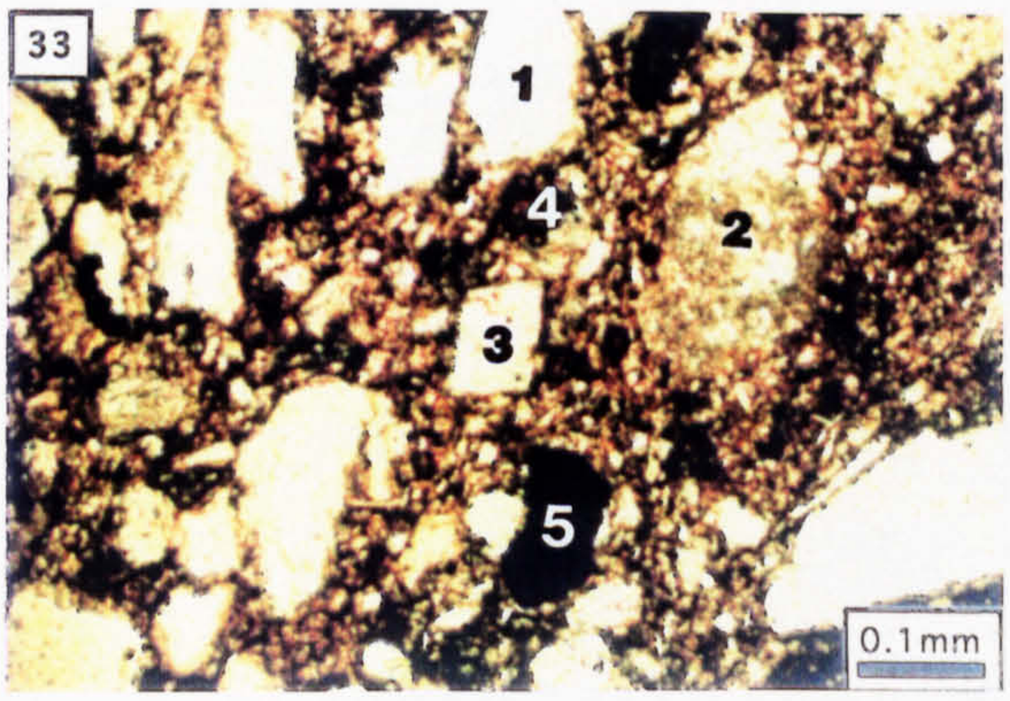

34

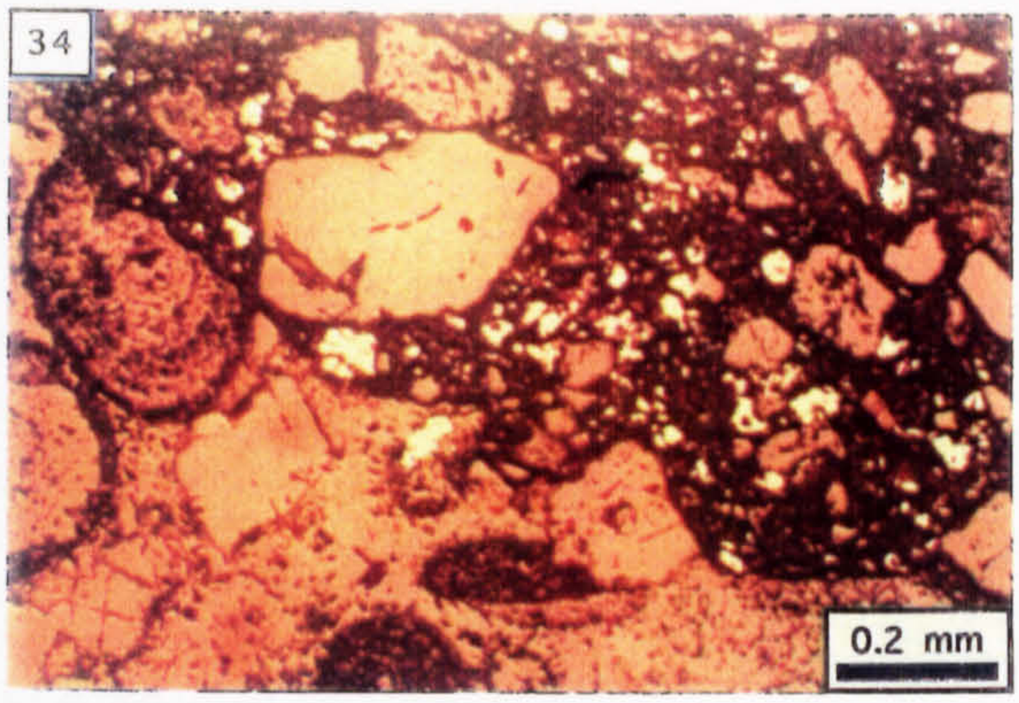

35

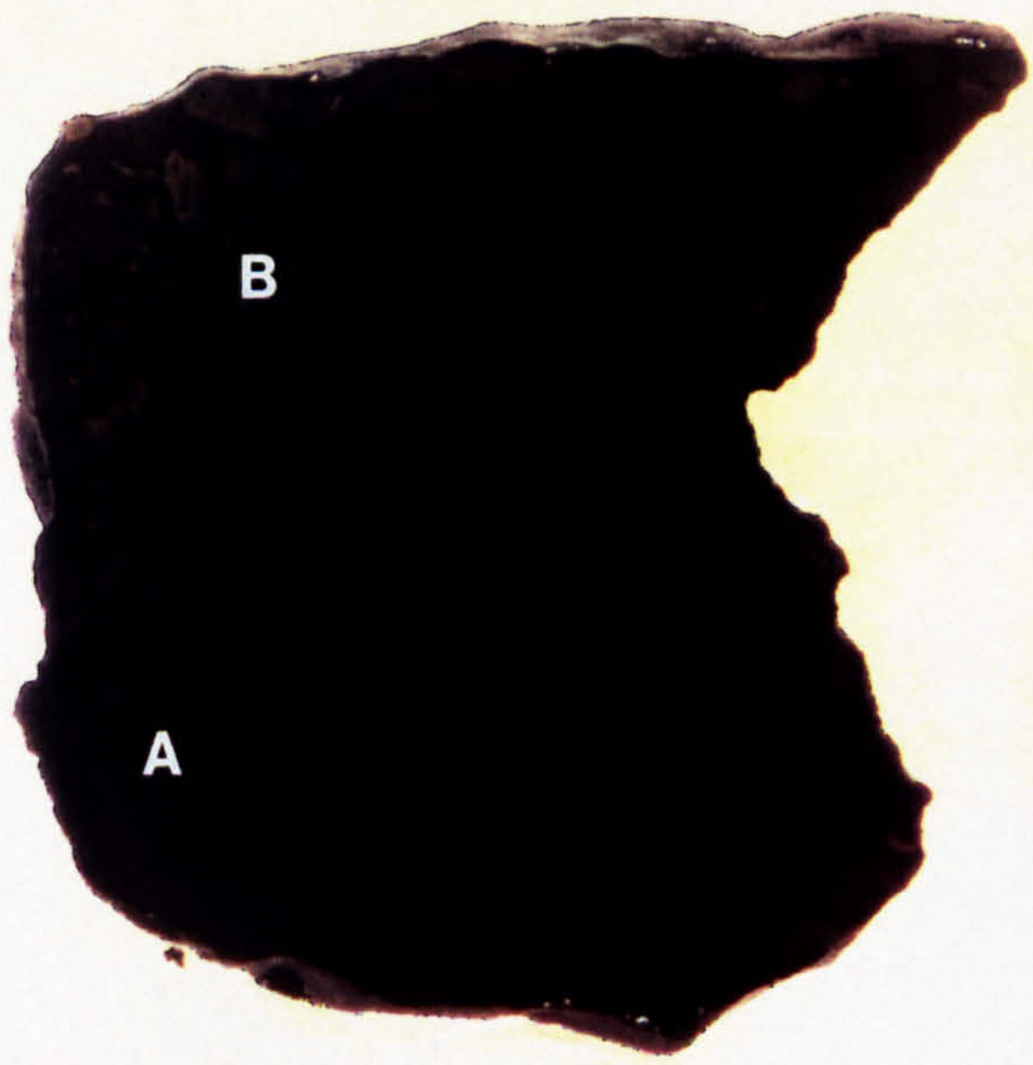

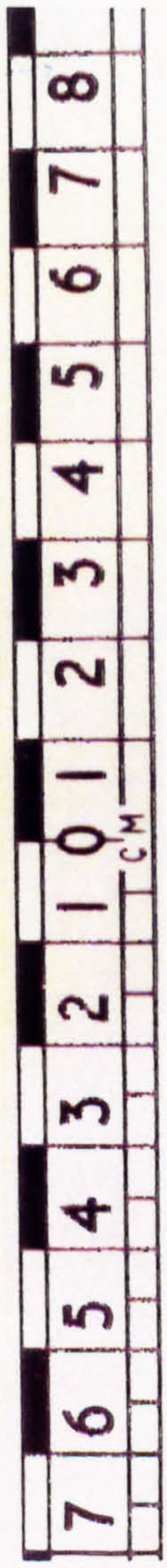

Photo. 36. Thin section of the plastically interpenetrated sediments shown in Photo. 35; A=deformed interbed, B=matrix to Polymict breccia (PPL).

Photo. 37. Clast-matrix contact of the Boulder Conglomerate deposited upon the T Fault scarp/unconformity exposed in the P1N heading. Notice the clast-parallel fabric developed in the matrix (XPL).

Photo. 38. Contact of Waulsortian-type limestone with the Pale Beds in N689.

Photo. 39. Polished slab of Boulder Conglomerate from 1330 CGO; pyrite occurs as replacement to the clast-matrix interfaces (2 cm scale bar).

Photo. 40. Carbonate mud matrix to Boulder Conglomerate exposed in 1330 CGO (PPL).

36

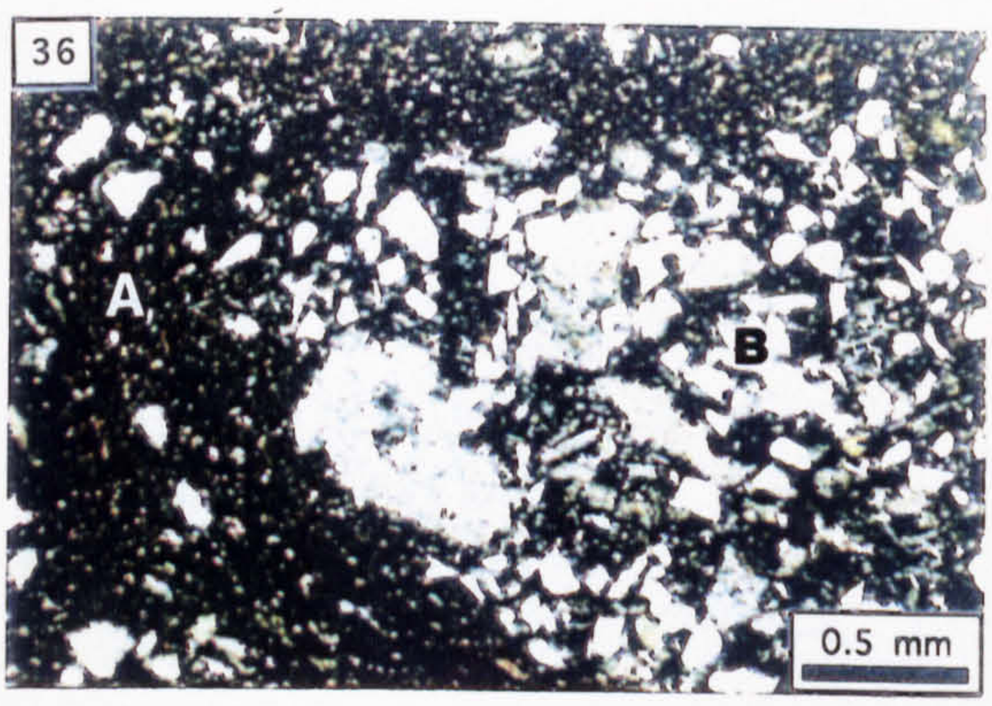

37

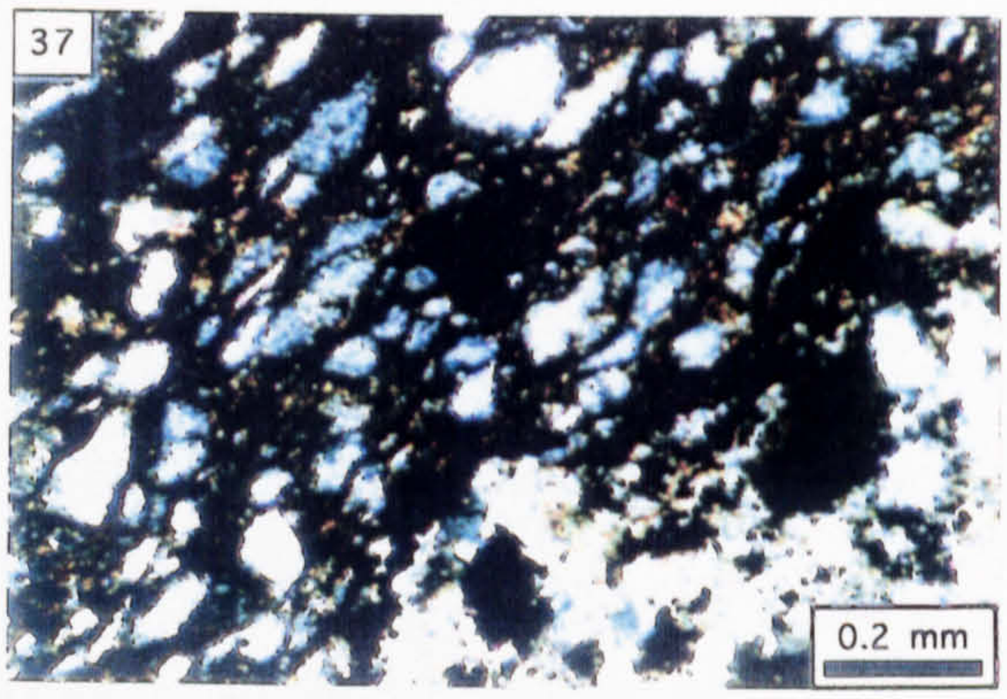

38

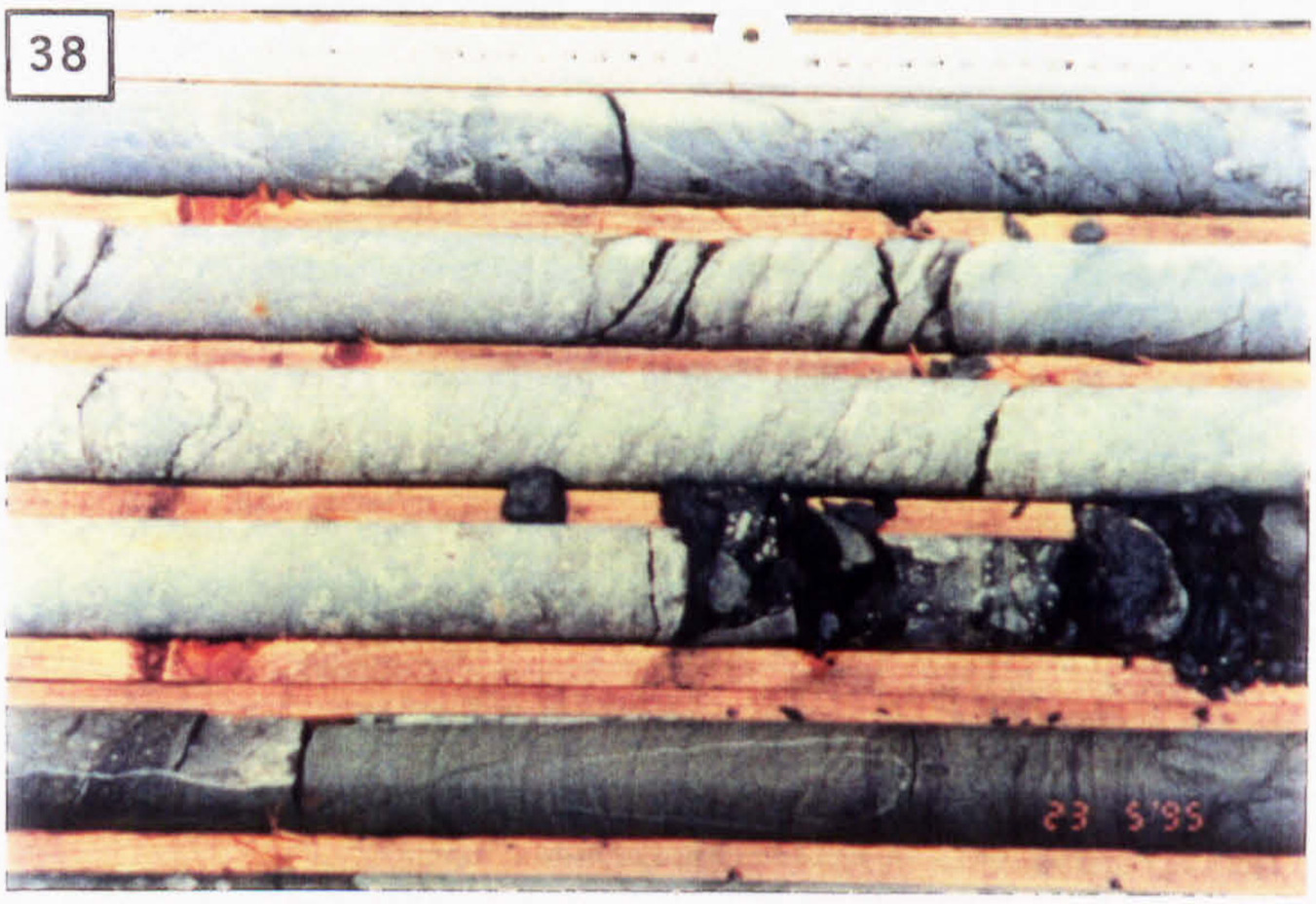

39

40

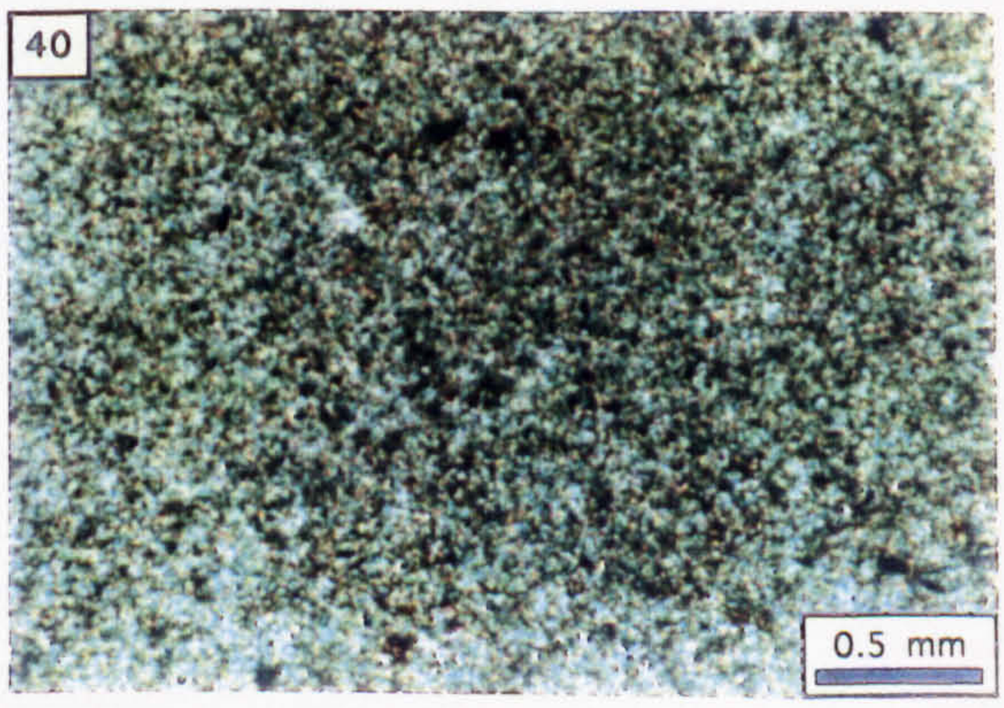

Photo. 41. Ore fragment located in Lithofacies 1 of the Boulder Conglomerate in 1285 Block 40 HWD; F=fracture-filling mineralisation, L=laminated mineralisation, O=replaced oolite as wallrock to F and L (2 cm scale bar).

Photo. 42. Matrix to Lithofacies 1 comprising granules of oolitic limestone in a submatrix of siliciclastic sand and argillite (PPL).

Photo. 43. Polished slab showing an amoeboid-shaped clast (a) [2 cm scale bar].

41

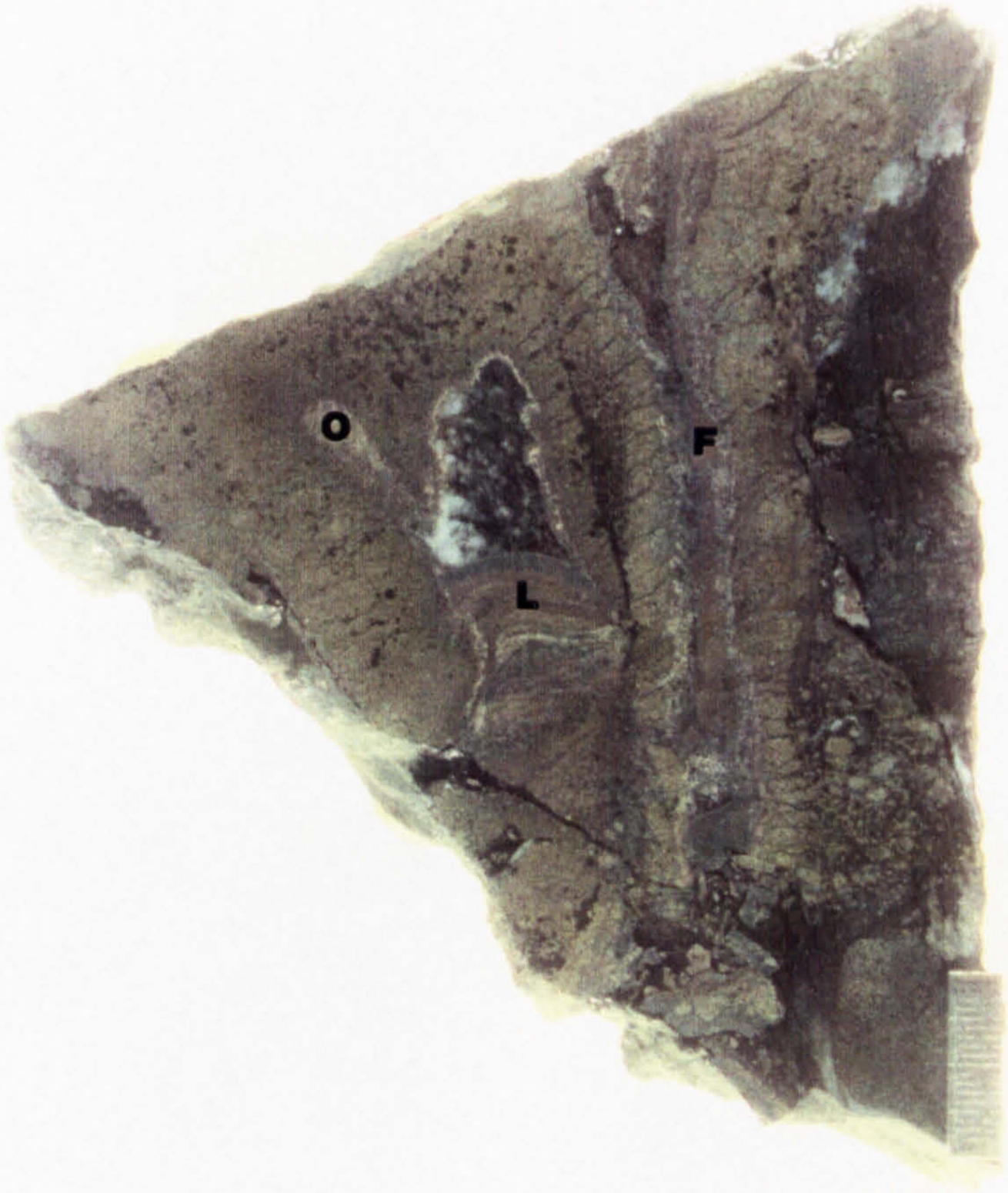

42

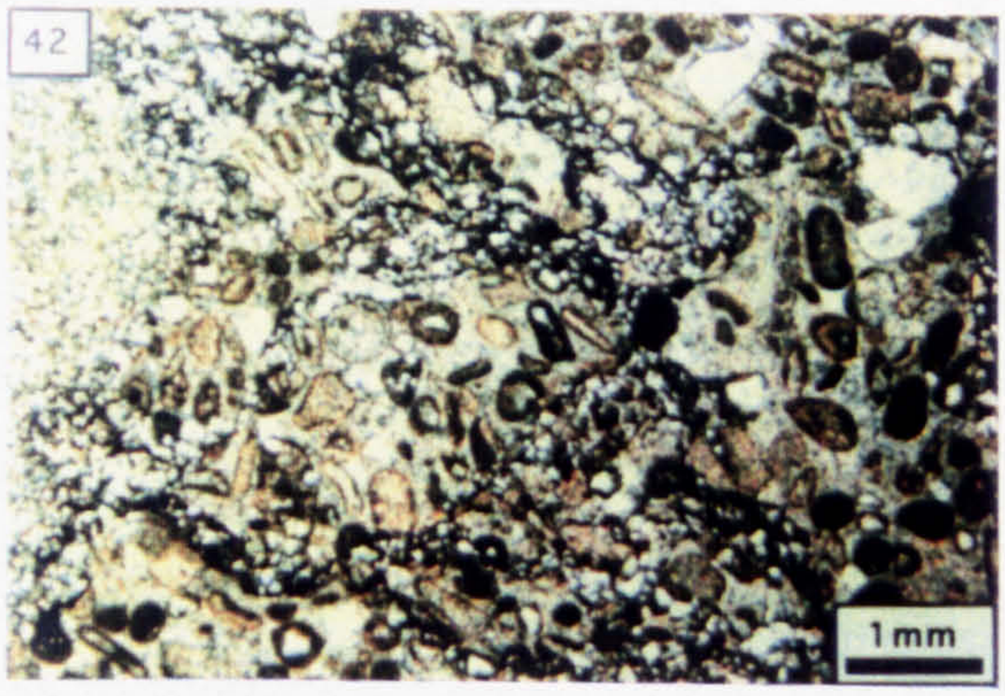

43

Photo. 44. Thin section showing the arenaceous composition of an amoeboid clast (A) [PPL].

Photo. 45. Lithofacies 2a comprising carbonate mud (PPL).

Photo. 46. Pyritised bioclastic layer present in Lithofacies 2a (PPL).

Photo. 47. Lithofacies 2b showing an oolitic limestone clast supported in a matrix of carbonate mud (PPL).

Photo. 48. Polished slab from Lithofacies 2b showing pyrite (p), mudstone (m) and crinoidal debris (c) as clasts which are supported by a carbonate mud matrix (2 cm scale bar).

44

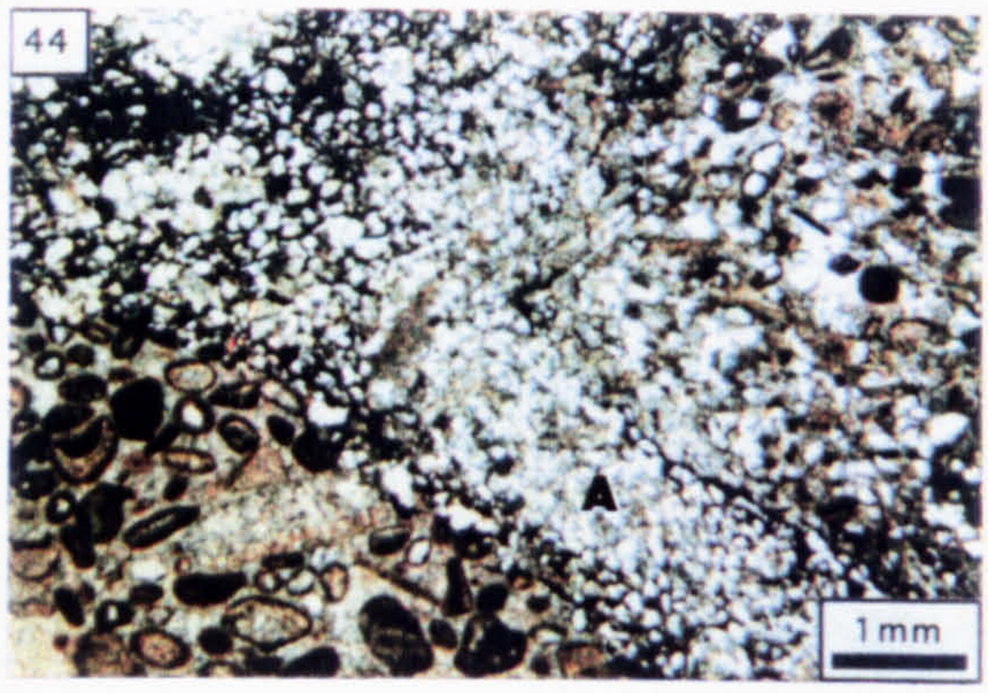

45

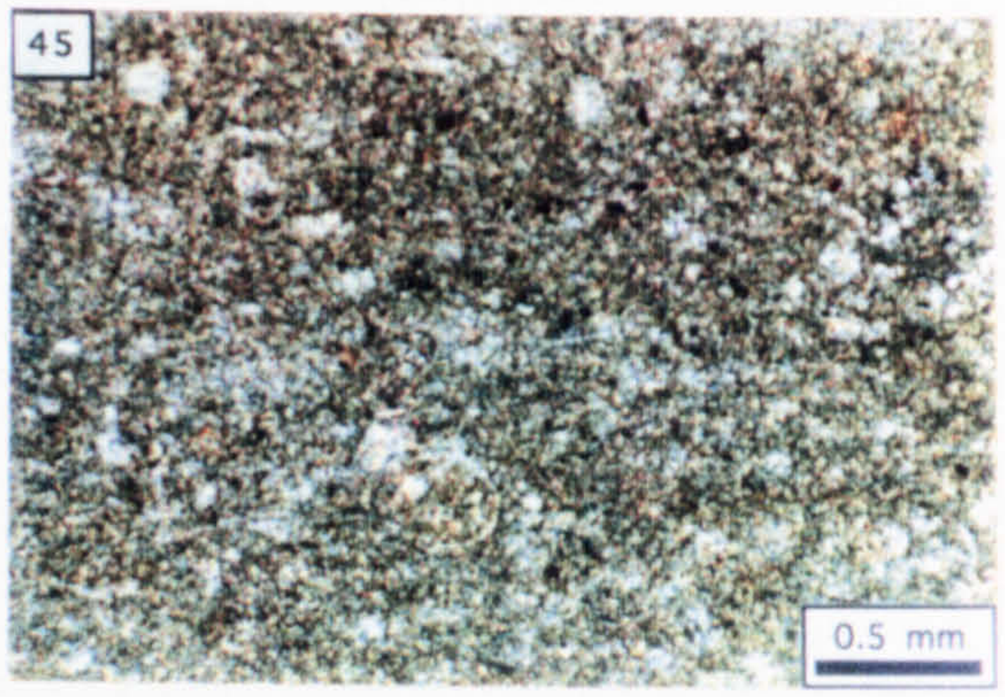

46

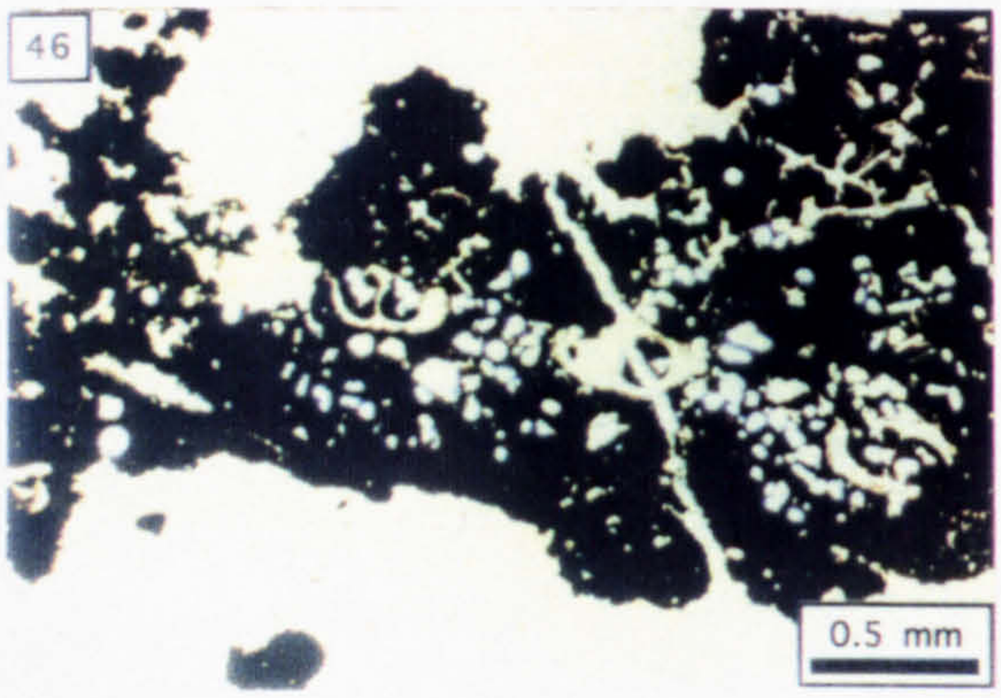

47

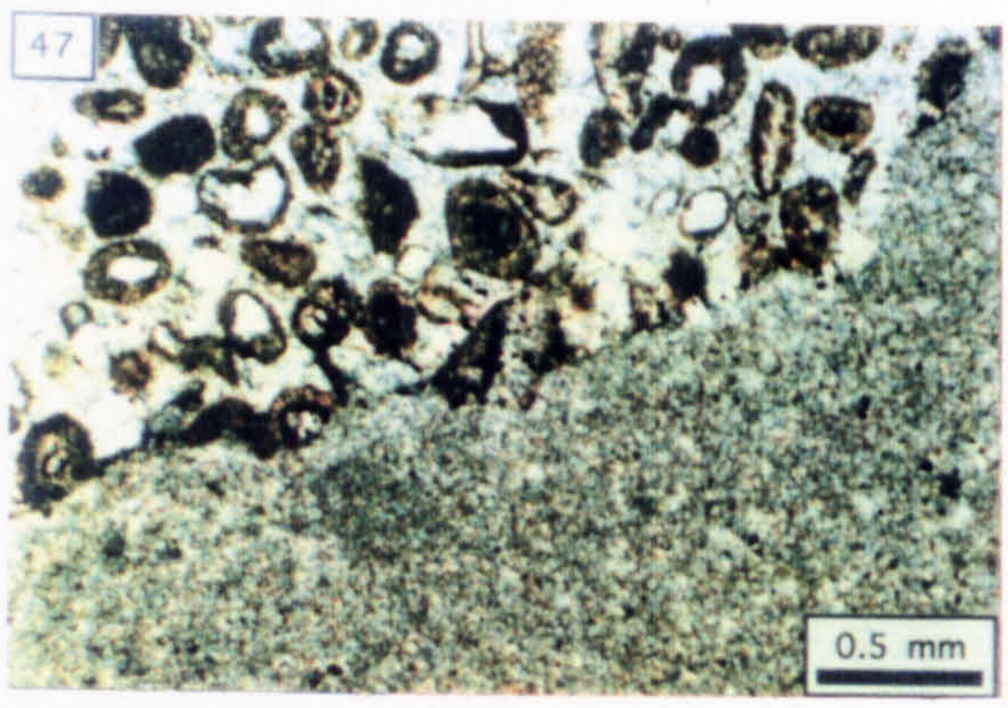

48

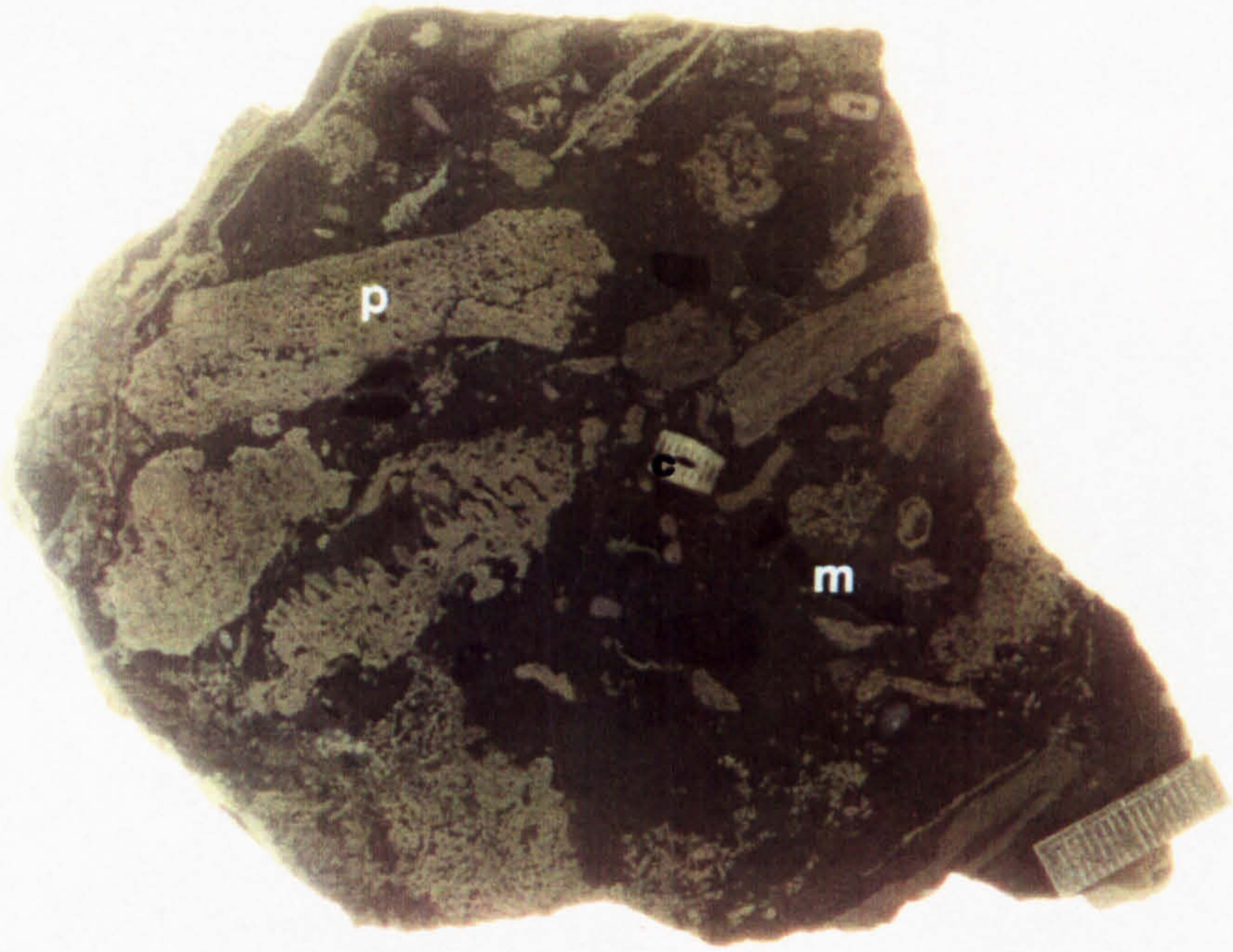

Photo. 49. Polished slab from Lithofacies 3 showing clast-supported pyrite breccia (2 cm scale bar).

Photo. 50. Argillaceous siliciclastic silt (PPL).

Photo. 51. Mudstone pebble in a matrix of plastically deformed argillaceous silt; notice the clast-parallel fabric developed in the matrix (PPL).

Photo. 52. Clast of sphalerite and galena from a mudstone pebble breccia bed (scale bar graded in millimetres and 0.5 cm).

Photo. 53. Polished slab of a carbonate mud boudin exhibiting basal load structures.

Photo. 54. Bioclastic limestone cobble supported by calcisphere-bearing carbonate mud (PPL).

49

50

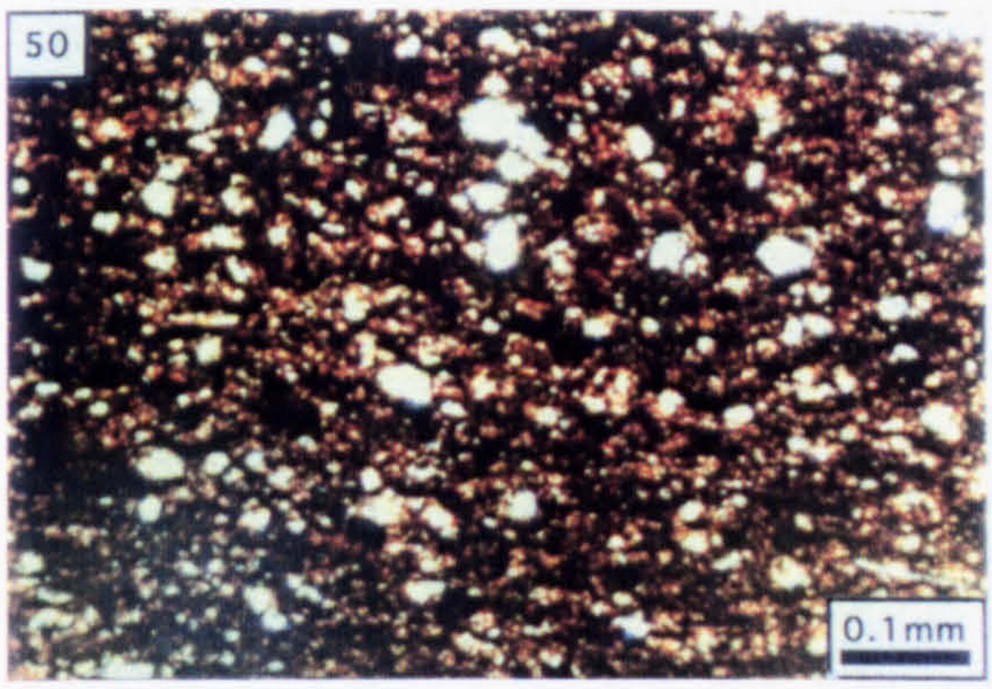

51

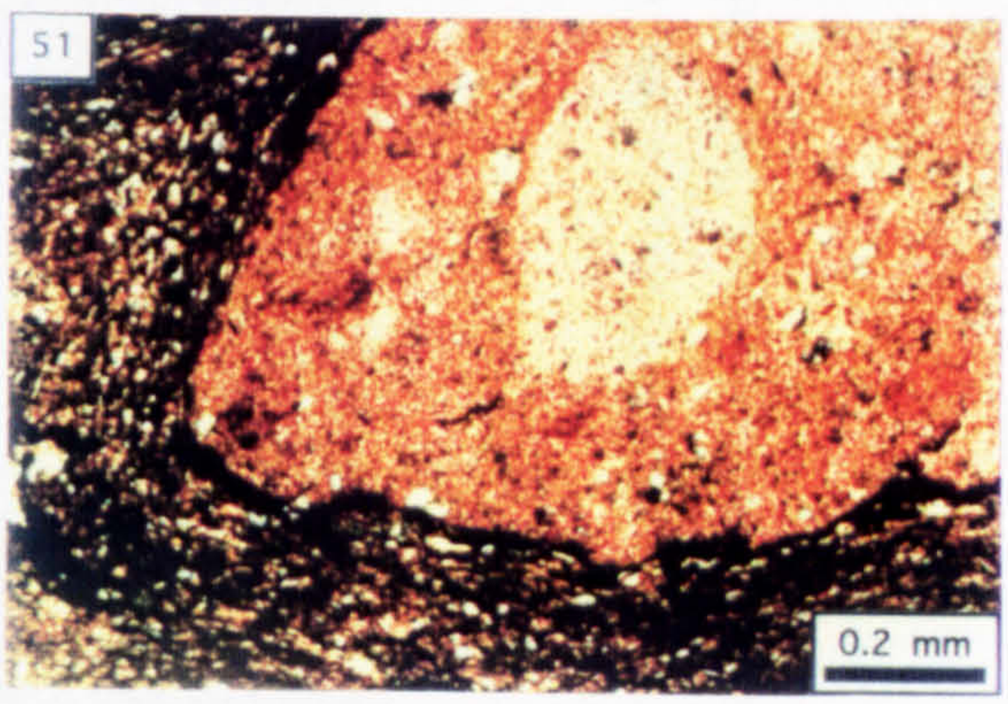

52

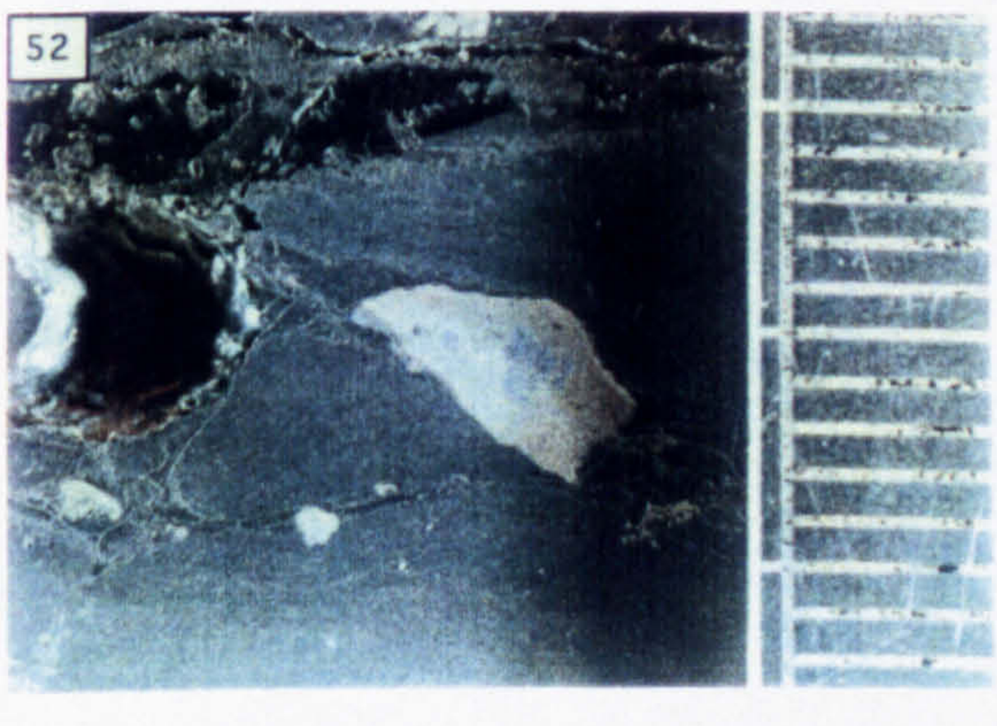

53

54

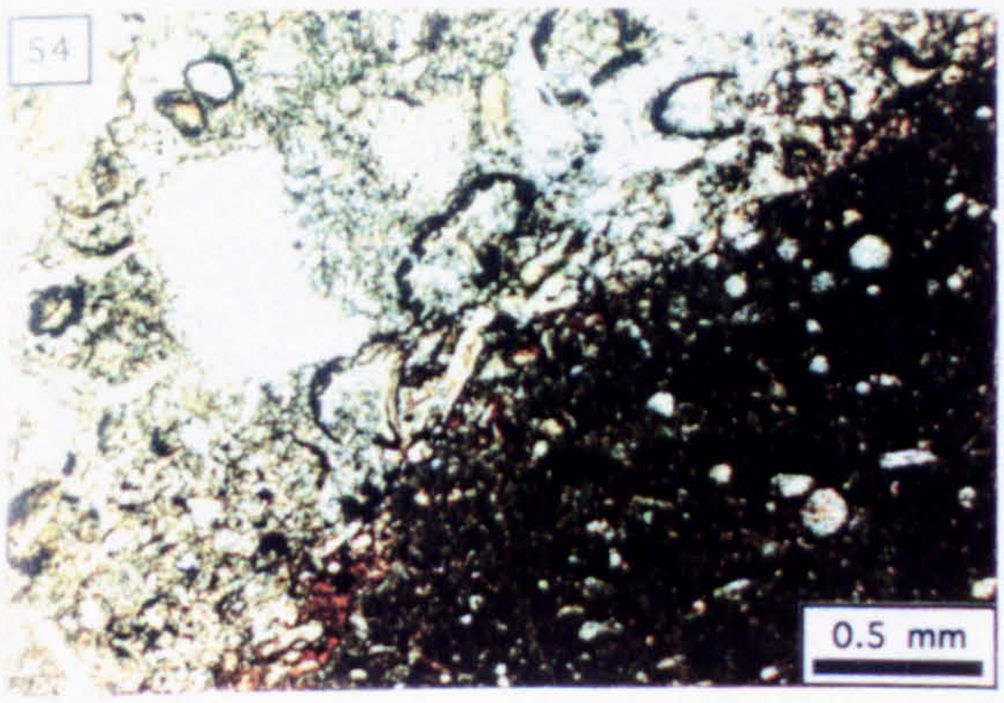

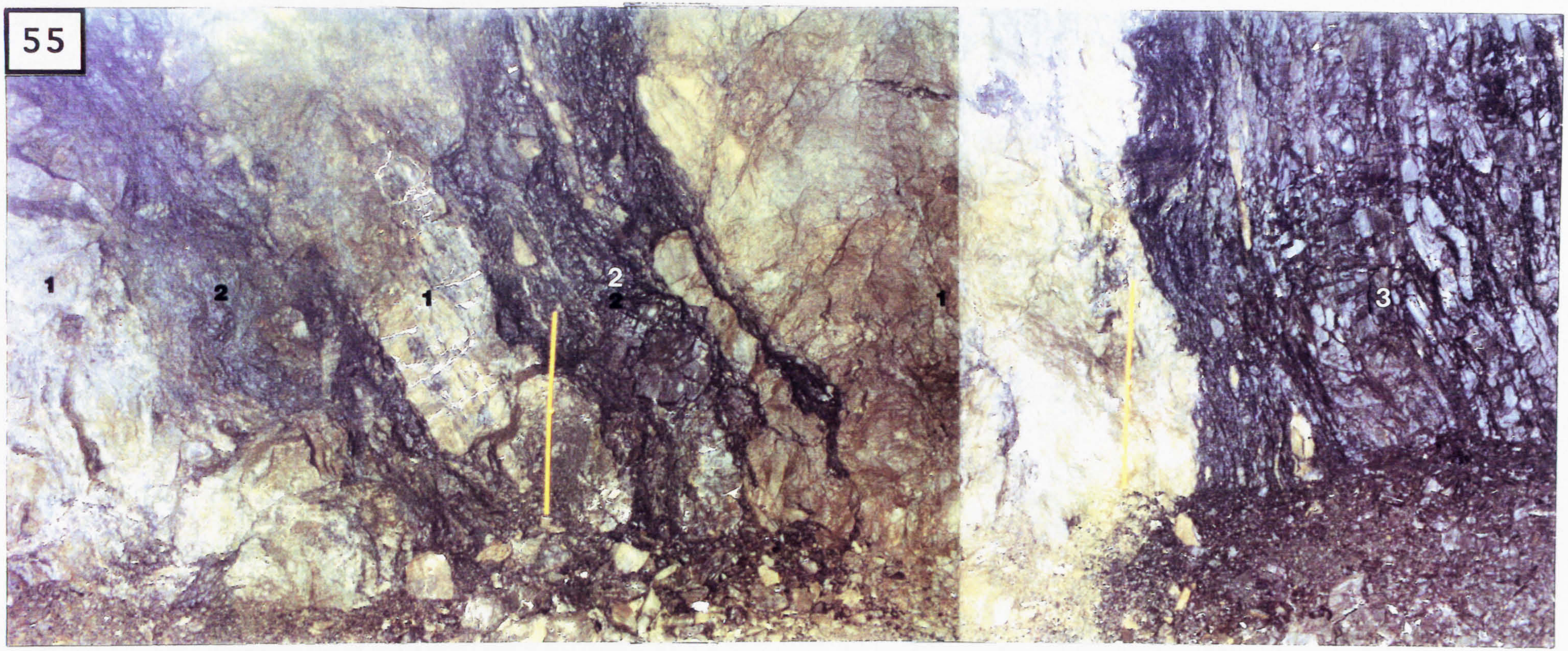

Photo. 55. Underground photograph of the 1330 348S exposure. 1=pyritised carbonate mud, 2=laminated argillaceous silt with mudstone pebble breccia interbeds, 3=Thinly Bedded Unit (1 m ruler for scale).

Photo. 56. Pyritised carbonate mud boudin within mudstone pebble-
-bearing argillaceous silt (25 cm ruler for scale).

Photo. 57. Polished slab showing an attenuted and fractured pyrite layer; notice the truncation of the underlying laminated pyrite and sphalerite, and the presence of clastic pyrite and sphalerite in the overlying sediments.

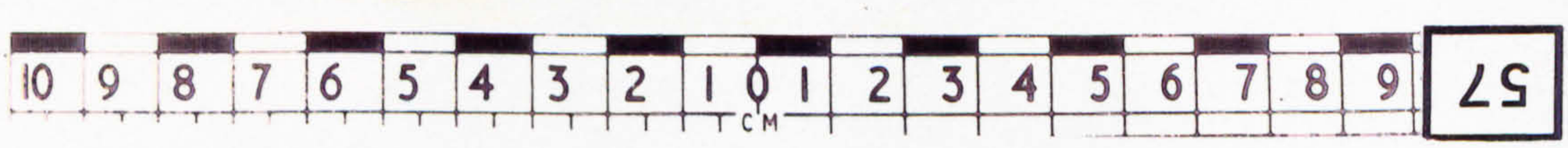
10 9 8 7 6 5 4 3 2 1 0 1 2 3 4 5 6 7 8 9
CM
57


56

Photo. 58. Slump-folded stratiform pyrite, sphalerite and argillite (2 cm scale bar).

Photo. 59. Brecciated pyrite, sphalerite and argillite in a matrix of pyrite.

58

59

Photo. 60. Extensionally microfaulted interlayered shale and calcarenite of the T.B.U.; C=channelised sulphides containing a mineralised plant fragment (p) [scale bar graded in millimetres and 0.5 cm].

Photo. 61. Clast of sphalerite and galena (U8333, 7.3m).

Photo. 62. Clast of ore from U8330, 19.5m.

Photo. 63. Pelletal and foramiferal limestone from a typical calcarenite bed in the T.B.U. (PPL).

Photo. 64. Oolitic grains present in the erosive-based, fining-upwards bed in the T.B.U. exposed in 1345 348N (PPL).

Photo. 65. Mudstone clasts (brown grains) and bioclasts (light grains) from the micro-breccia located at the base of the fining-upwards bed (PPL).

60

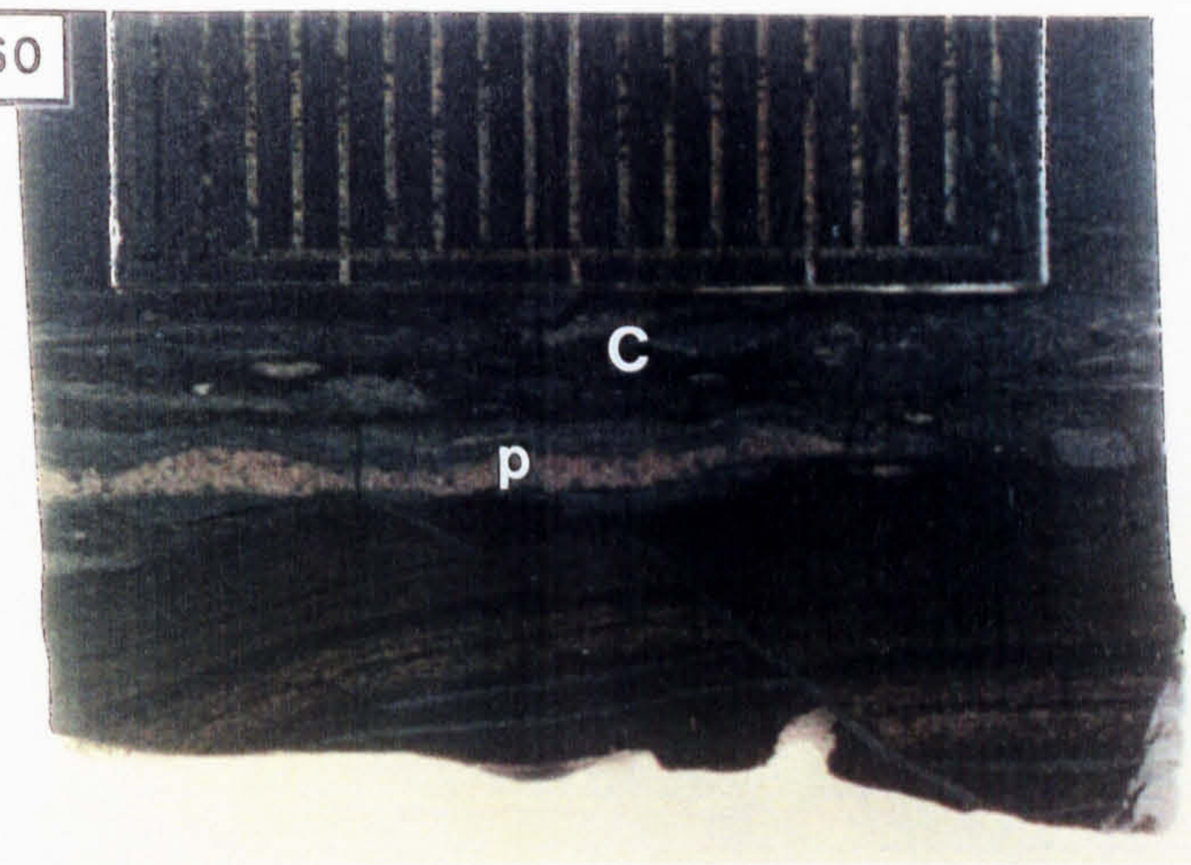

61

62

63

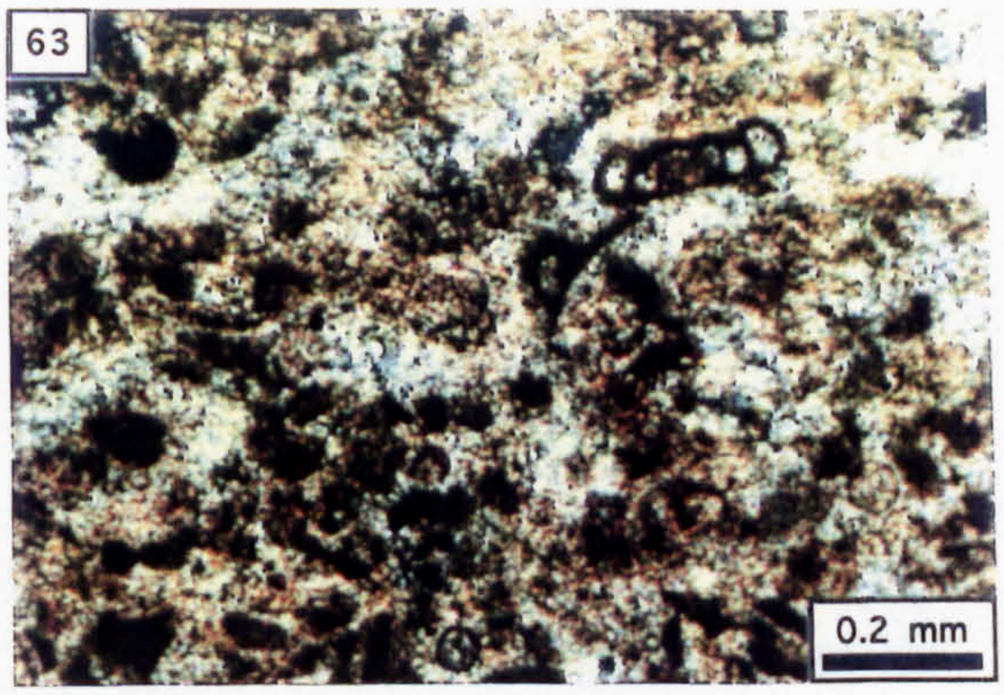

64

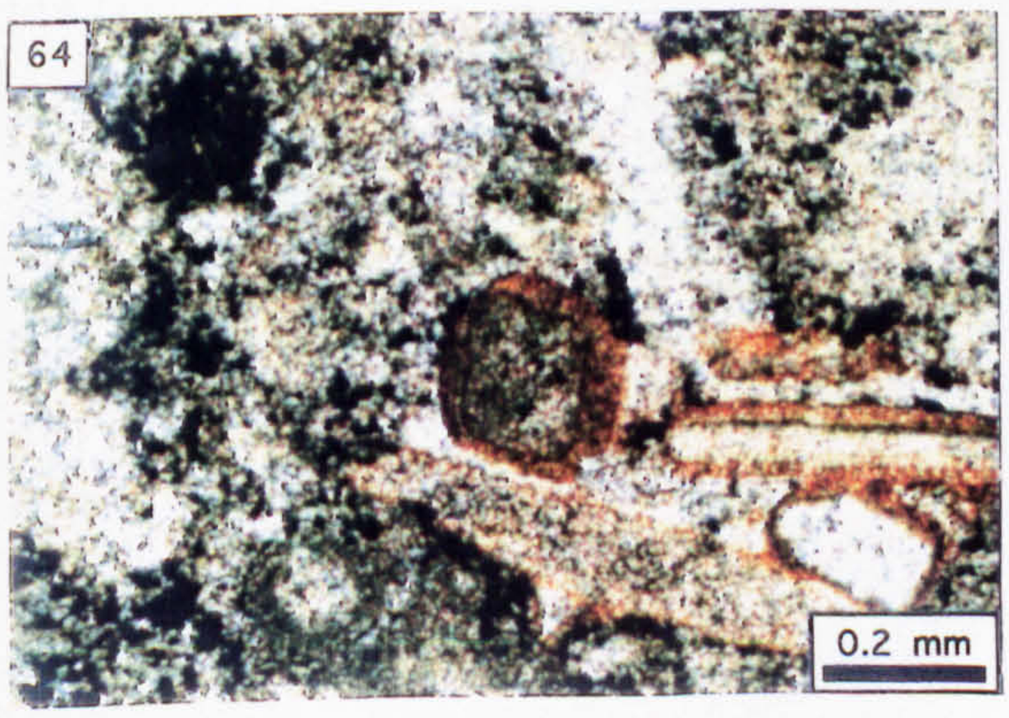

65

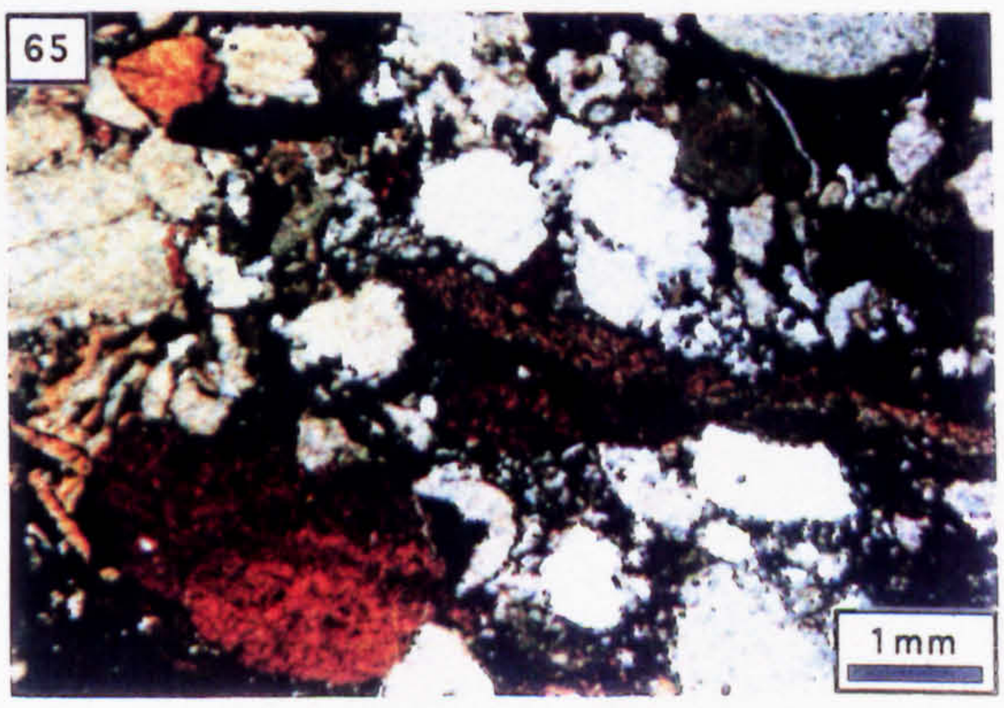

Photo. 66. Petrography of the calcarenite portion of the fining-upwards, erosive-based bed (PPL).

Photo. 67. Plant fragment replaced by calcite and barite (XPL).

Photo. 68. Polished slab showing offset of the T.B.U. by extensional microfaults (2 cm scale bar).

Photo. 69. Polished slab showing extended and dewatered T.B.U. strata (2 cm scale bar).

66

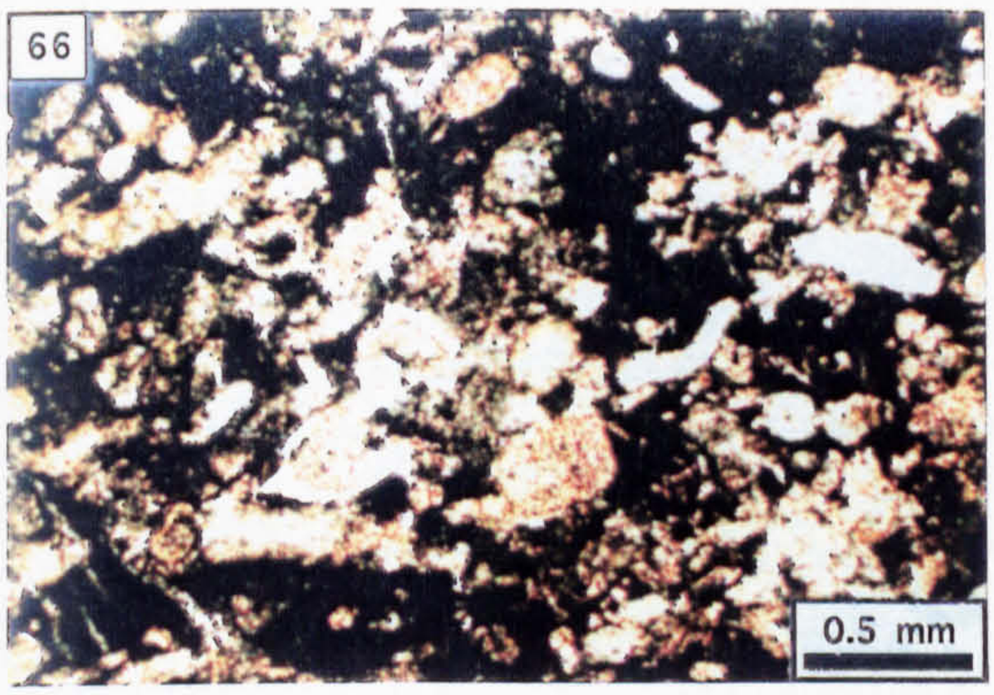

67

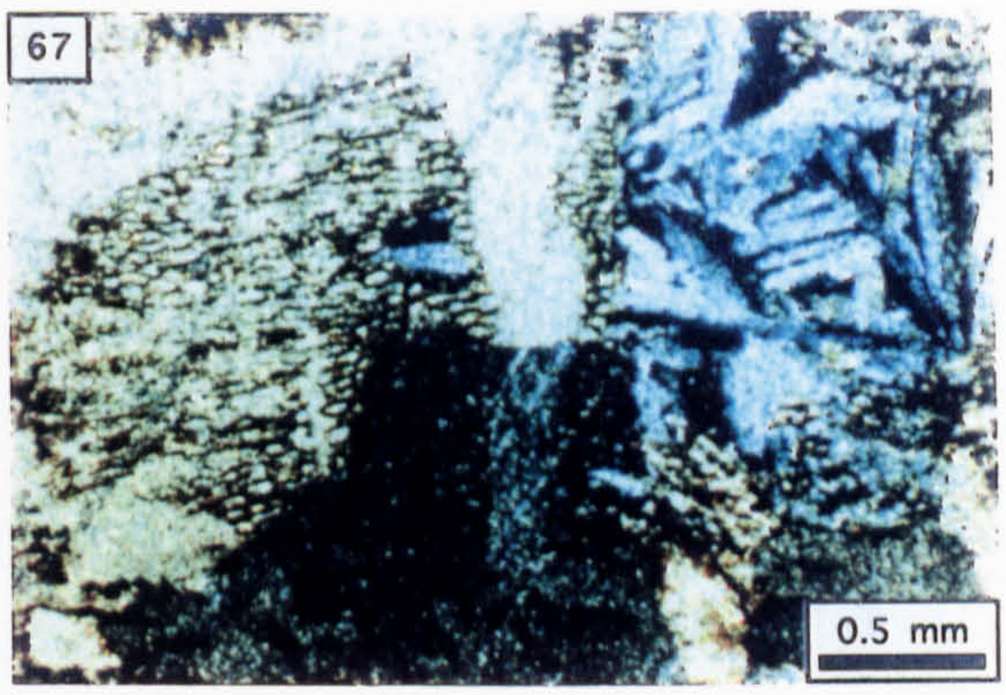

68

69

Photo. 70. Polished slab showing boudinaged oolitic limestone; notice the vug-filling mineralisation (v) contained within the boudin (2 cm scale bar).

Photo. 71. Polished slab showing boudinaged and convolutely folded oolitic limestone (2 cm scale bar).

Photo. 72. Polished slab of the fining upwards bed showing ductile, extensional displacement (2 cm scale bar).

Photo. 73. Dolomite replacement to pelletal micrite (N1174, 779.6 m; PPL).

70

71

72

73

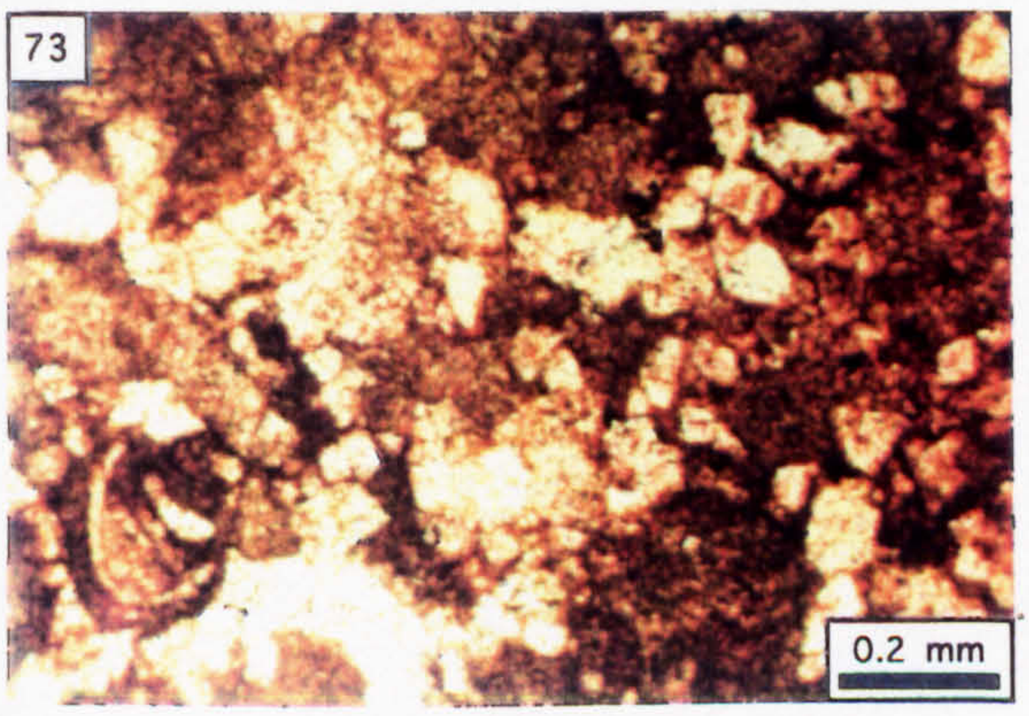

Photo. 74. Mud supporting euhedral dolomite crystals and clasts of dolomitised pelmicrite (N1174, 779.6 m; PPL).

Photo. 75. Clast-groundmass interface showing contiguous replacement by spherular pyrite (N1174, 779.6 m; PPL).

Photo. 76. 36.5 mm-diameter drillcore showing clasts of pelmicrite in a mud matrix; the mud is fractured and pyrite occurs along the the fracture walls; the remnant fracture porosity is occluded by sparite (N1174, 779.6 m).

Photo. 77. Detail of the drillcore shown in Photo. 76: botryoidal pyrite occurs as cement to fractured mud and as a rim to corroded pelmicrite; the pyrite is brecciated and cemented by sparite (N1174, 779.6 m).

74

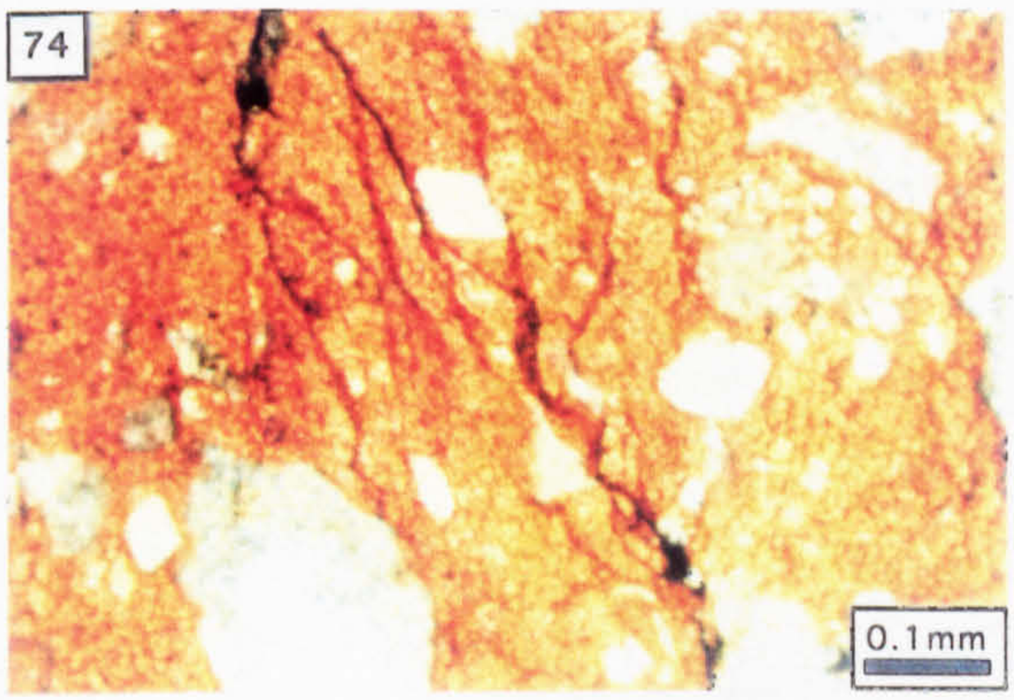

75

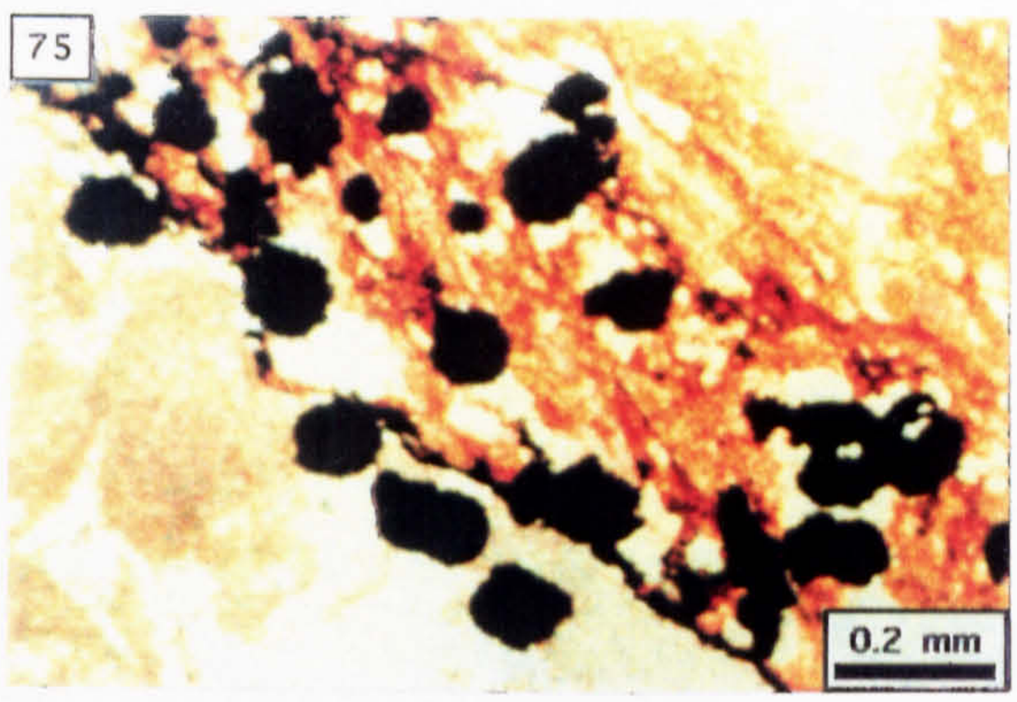

76

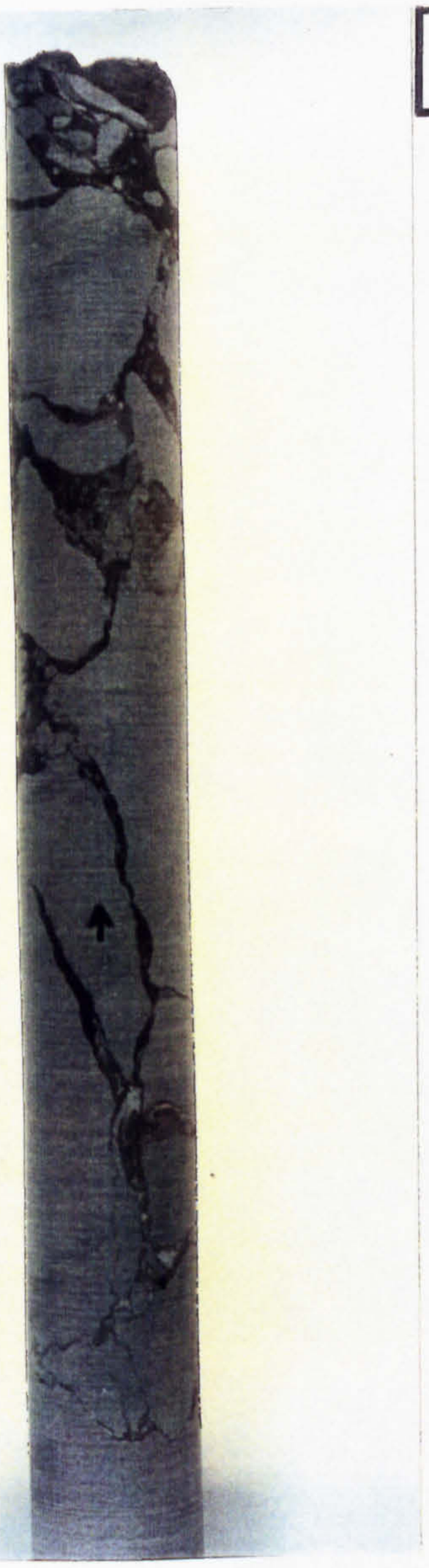

77

Photo. 78. Brecciated botryoidal pyrite cemented by sparite (N1174, 770.0 m).

Photo. 79. Fractured pelletal micrite interbedded with mudstone; the fracture contains mud which is bisected by fibrous calcite (E14, 592.5 m).

Photo. 80. Mudstone interbed to the Micrite Unit in E13, at 469.6 m.

Photo. 81. Rotated clast composed of fenestral pelmicrite (PPL; N1109, 183.4 m).

Photo. 82. Dolomitised pelmicrite; the vertical dark line to the left is a hole in the slide (CL; N1109, 183.4 m).

Photo. 83. Coarse, fracture-filling dolomite in pelmicrite (CL; N1109, 183.4 m).

78

79

80

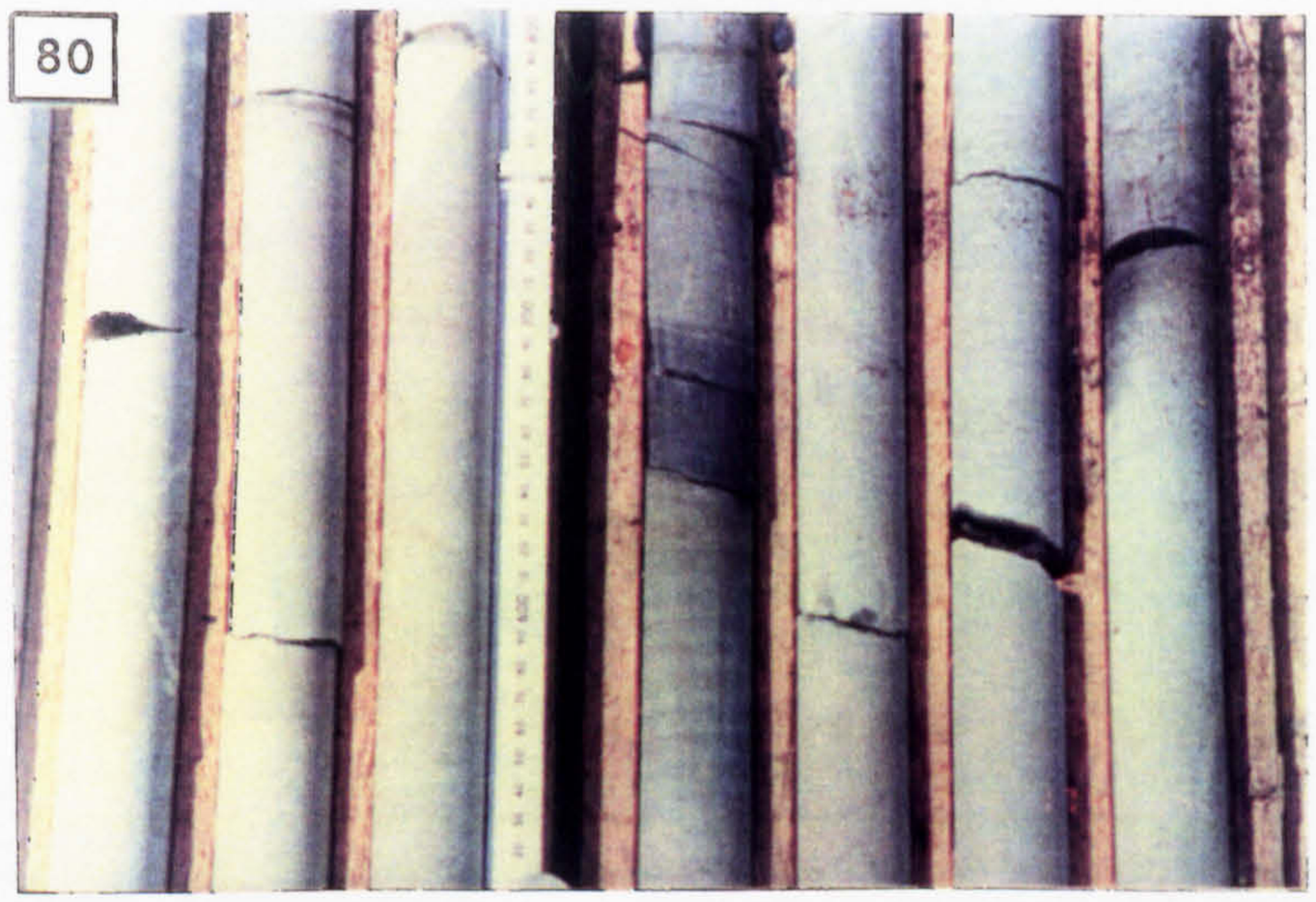

81

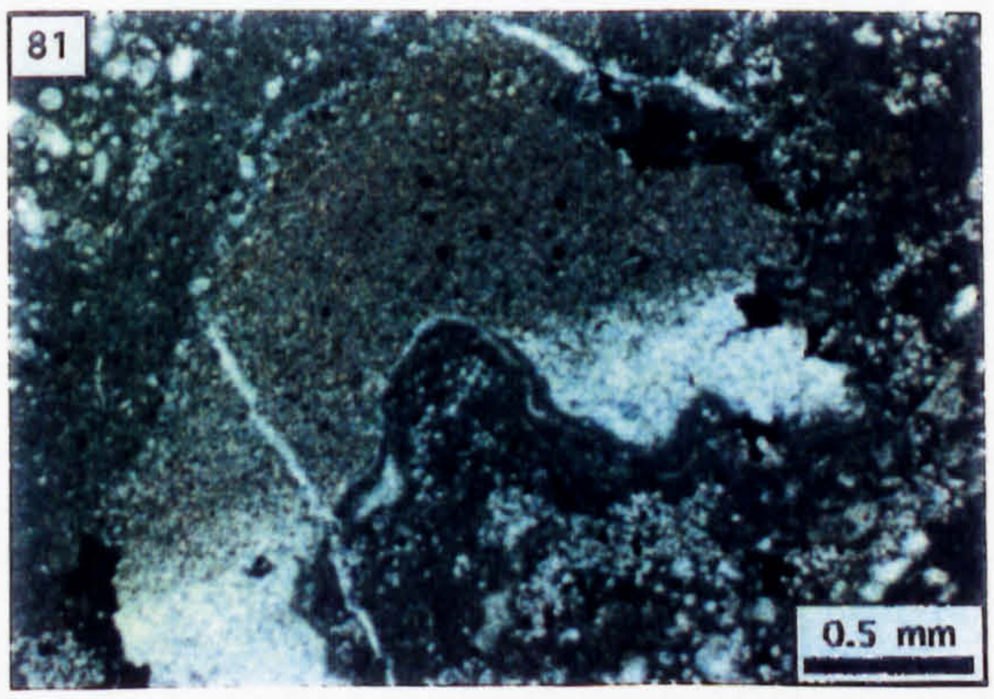

82

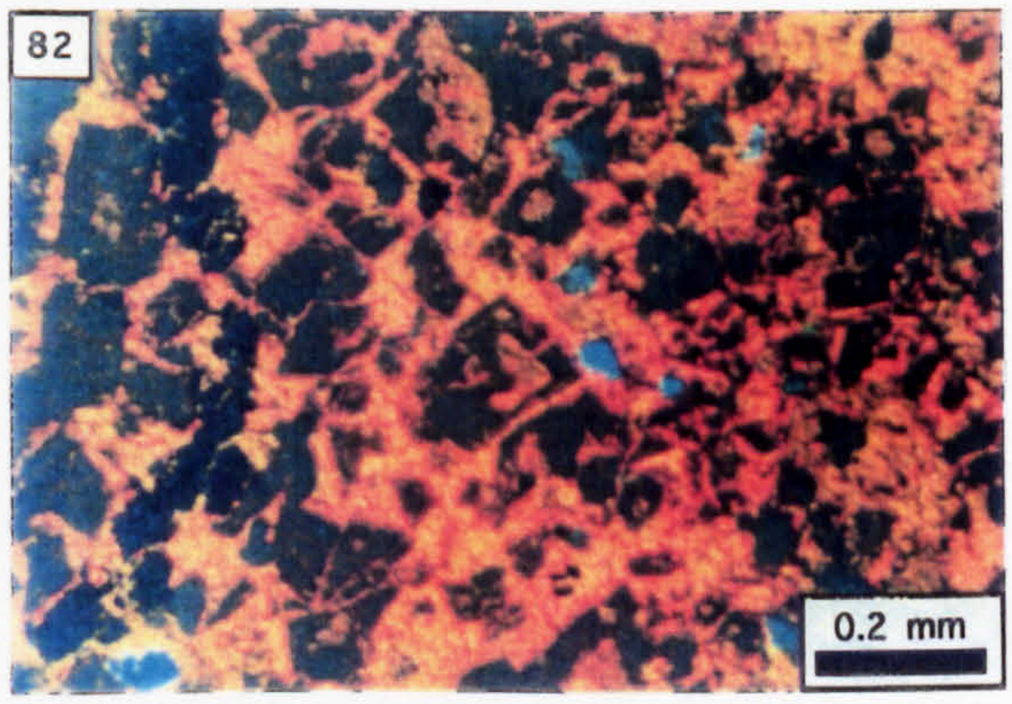

83

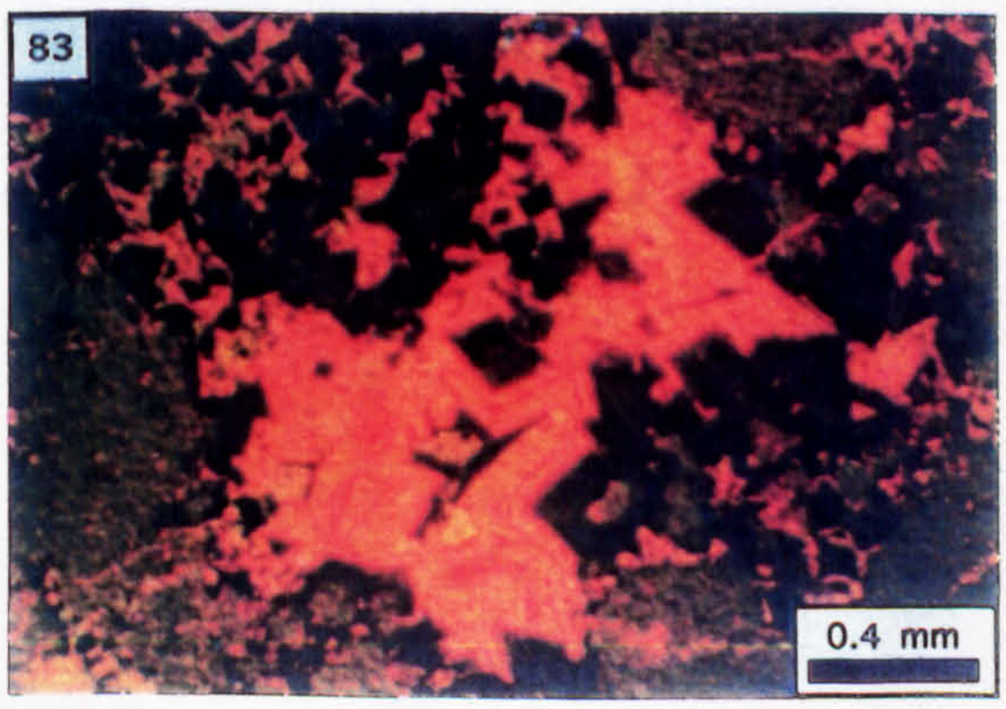

Photo. 84. Split and polished drillcore showing the groundmass to breccia type B; note the presence of deformed pyrite laminae (2 cm scale bar; N1109, 183.4 m).

Photo. 85. Truncation of the fracture-cementing dolomite at the clast edge (CL; N1109, 183.4 m).

Photo. 86. Laminated silty argillite of the groundmass showing plastic attenuation by a clast of pyrite (PPL; N1109, 183.4 m).

Photo. 87. Clast of compacted oolitic limestone; notice that the axis of compaction has been rotated through 90^0 (PPL; N170, 83.1 m).

Photo. 88. Micrite groundmass supporting siliciclastic grains (PPL; N170, 83.1 m).

84

85

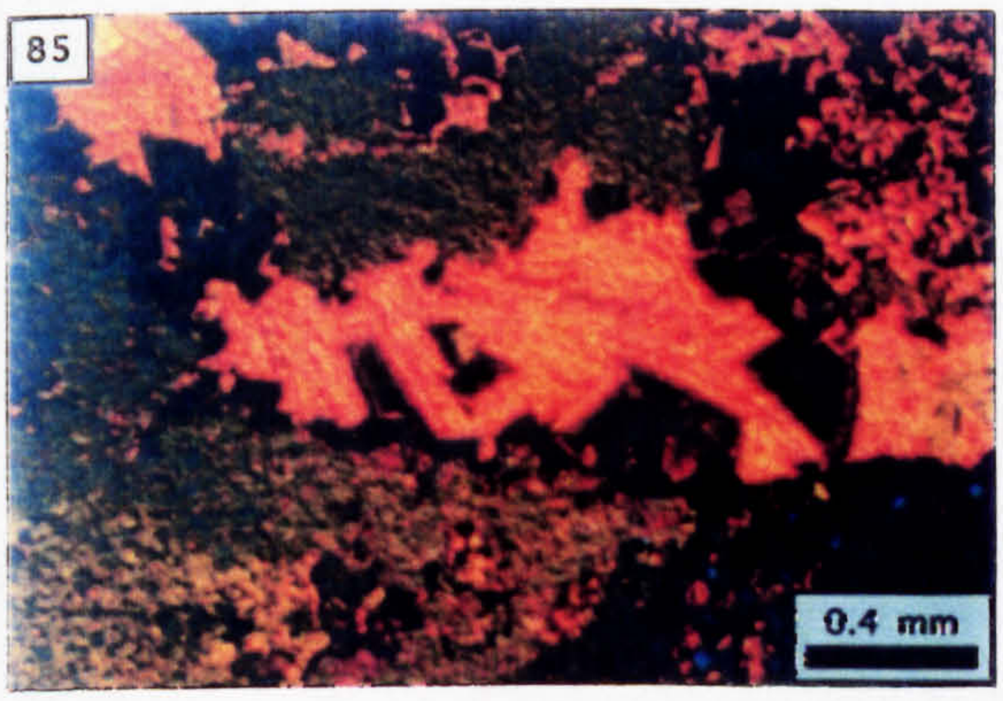

86

87

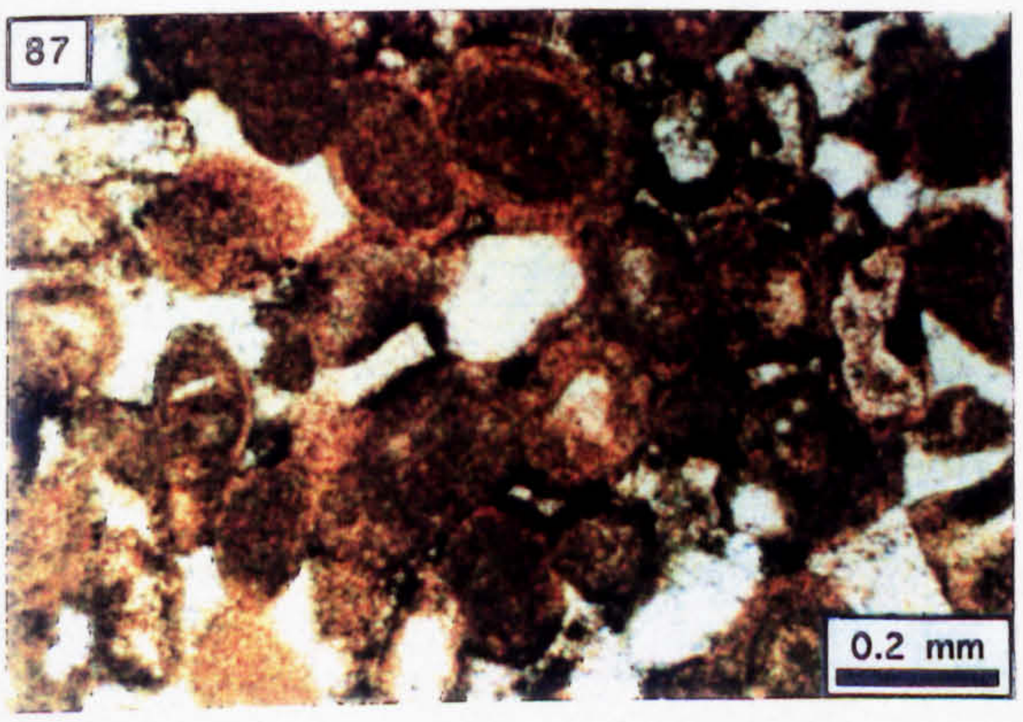

88

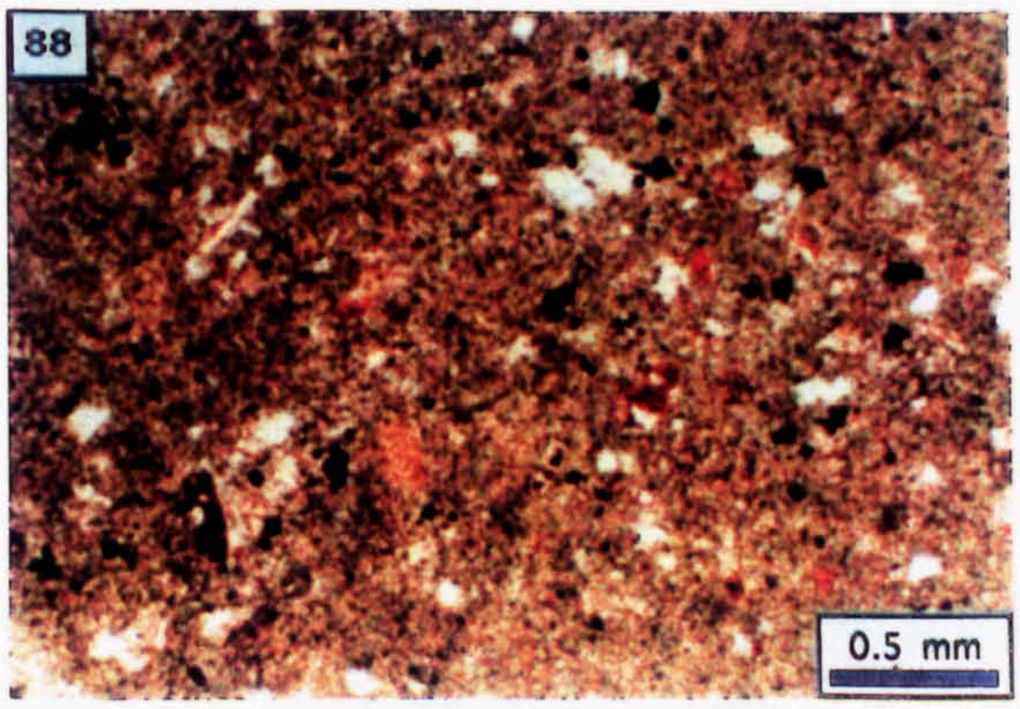

Photo. 89. Petrography of the Type C breccia in drillcore; c=clast, m=micrite, p=pyrite, ct=calcite (N170, 83.1 m; 2 cm scale bar).

Photo. 90. Petrography of the clast edge showing sharply truncated ooids; the micrite occurs as interclast sediment (PPL; N170, 83.1 m).

Photo. 91. Clast-groundmass interface showing contiguous replacement by pyrite (PPL; N170, 83.1m).

Photo. 92. Fibrous calcite (F) cementing brecciated pyrite at the clast-groundmass interface (PPL; N170, 83.1 m).

Photo. 93. *In-situ* siliciclastic sand-bearing micrite strata located at 90.6 m, in N170 (PPL).

Photo. 94. Unreplaced bioclastic grains (orange) within dolomitised limestone (CL; N165, 69.3 m).

Photo. 95. Siliciclastic sand-bearing micrite (1) occupying fracture in dolomitised bioclastic limestone (2) [PPL; N156, 69.3 m].

89

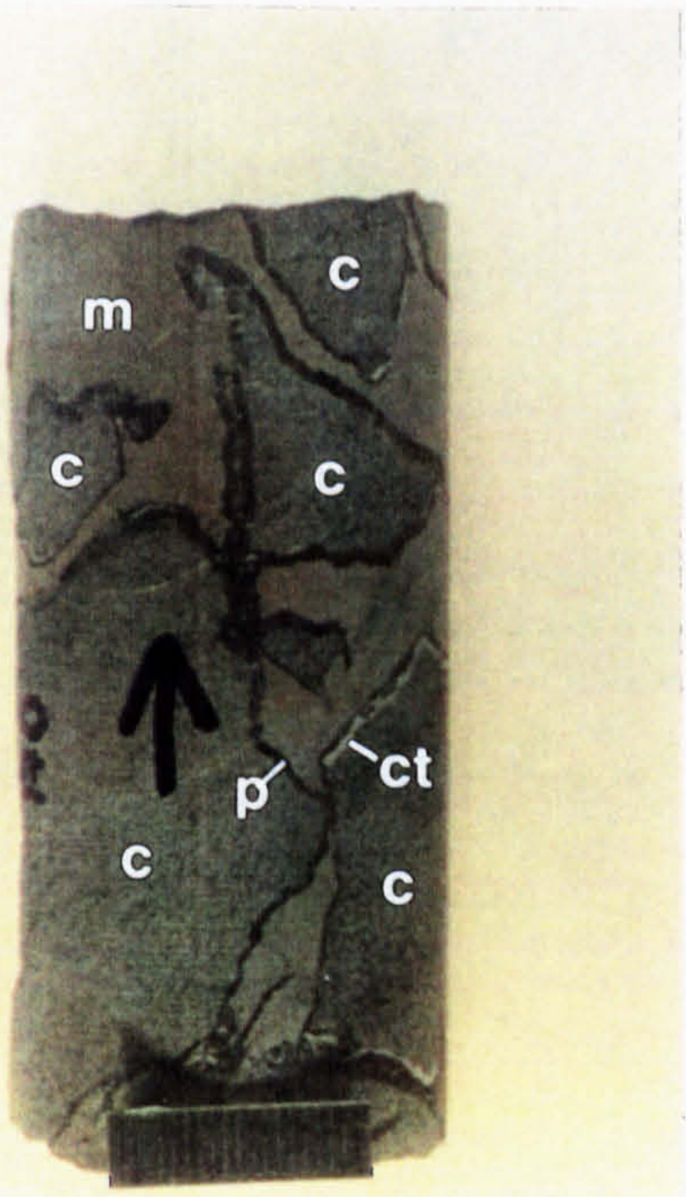

90

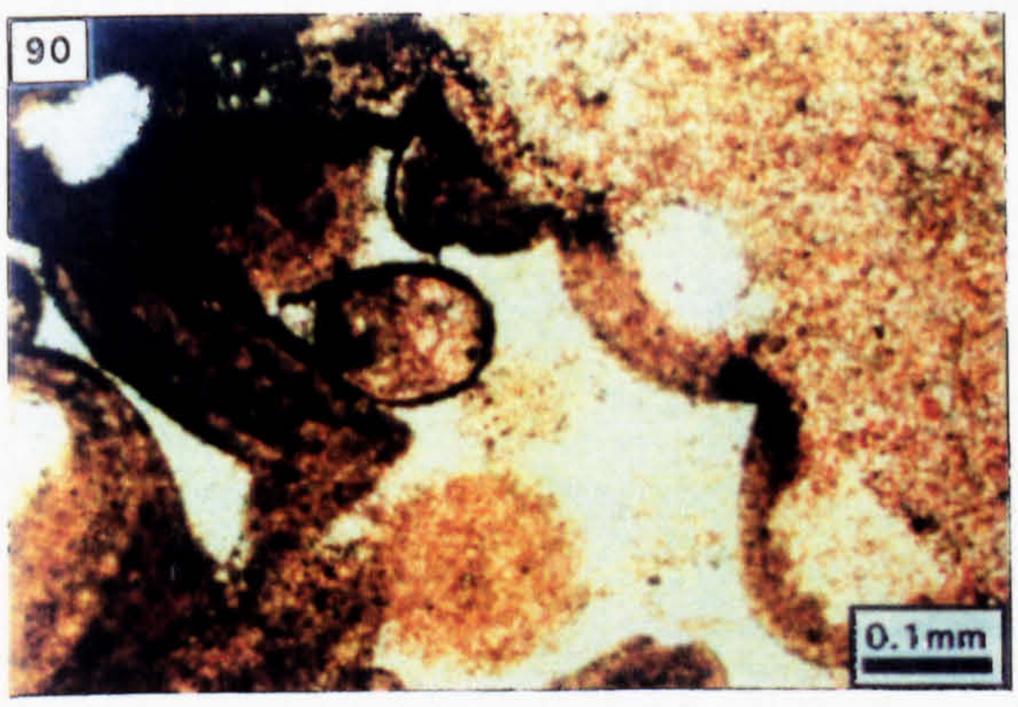

91

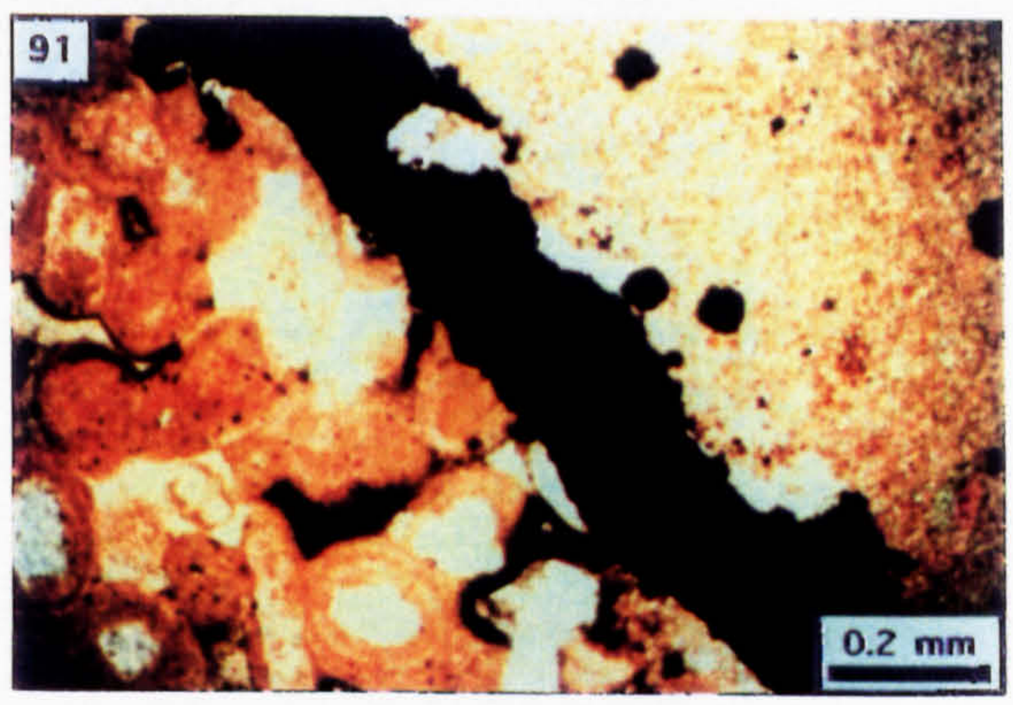

92

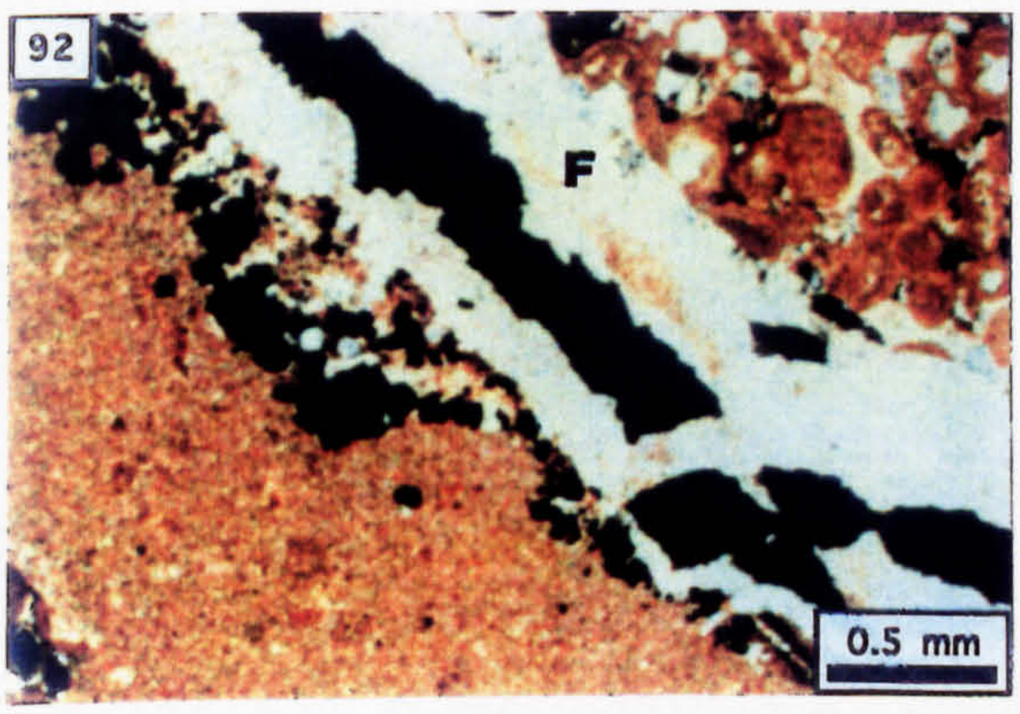

93

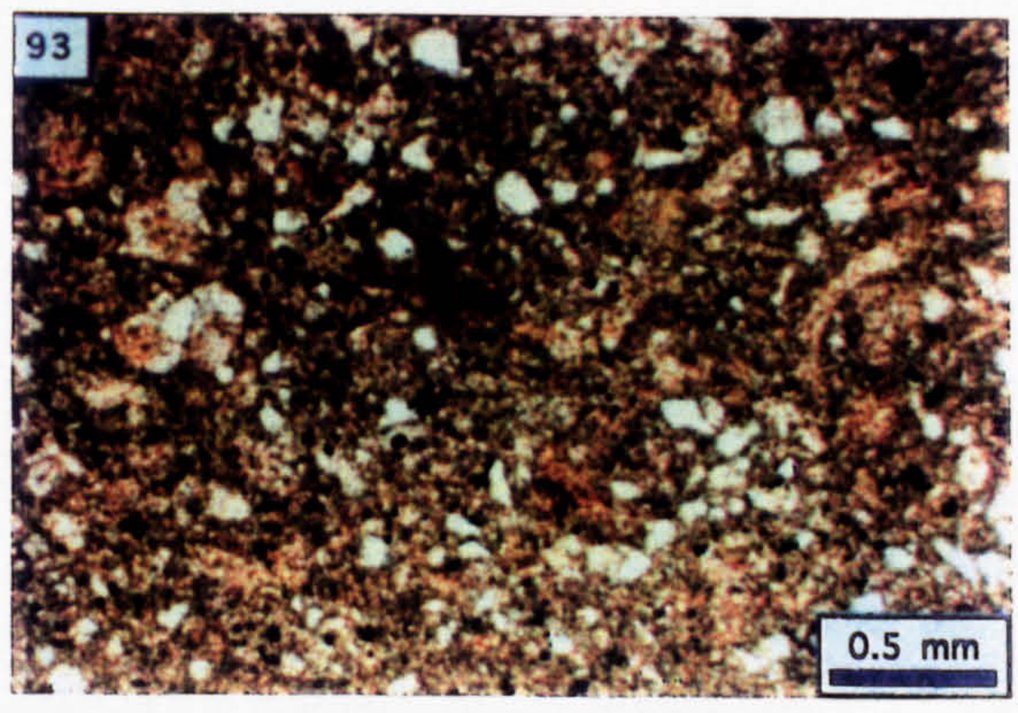

94

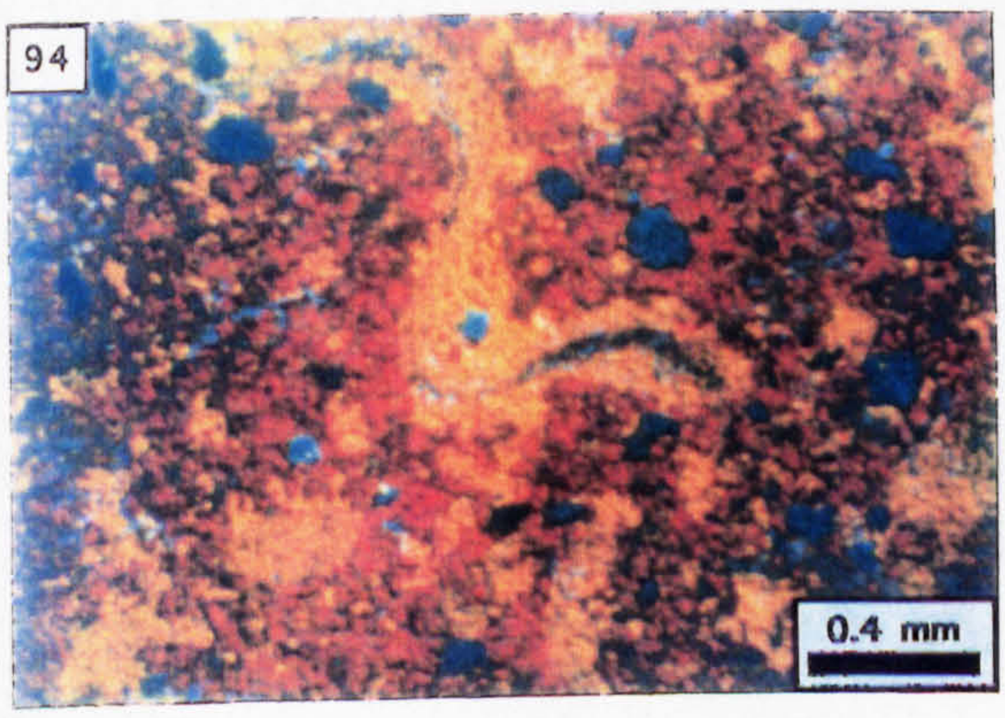

95

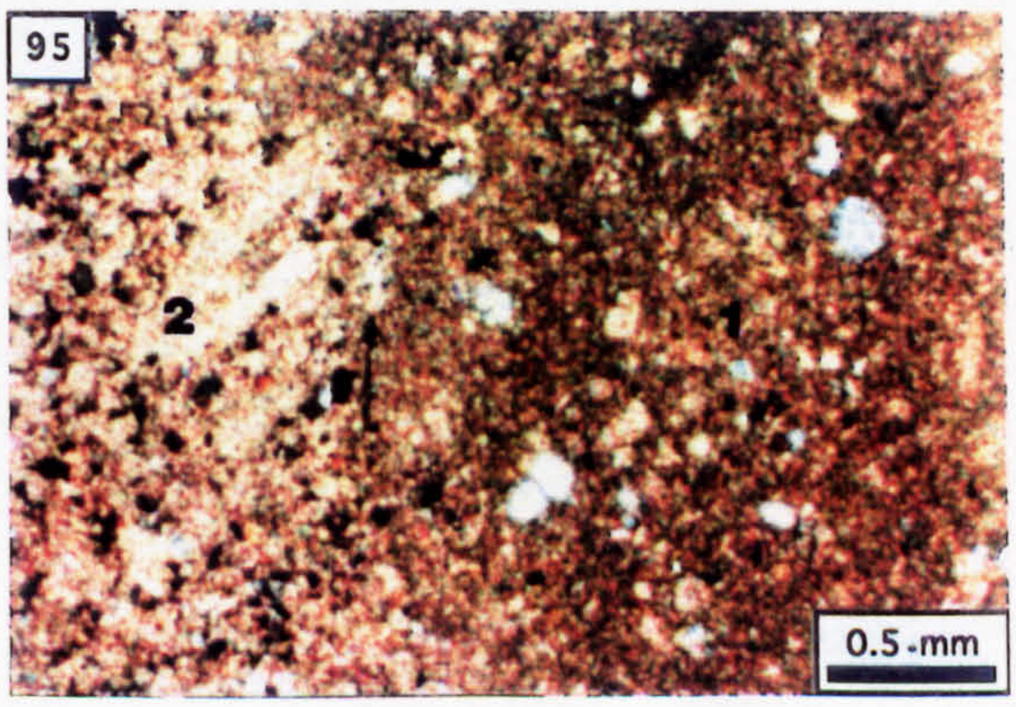

Photo. 96. Laminated diagenetic and detrital sediment (PPL; N156, 69.3 m).

Photo. 97. Remobilised Stage 2 groundmass adjacent to dolomitised bioclastic limestone; the grains in the former which luminesce red are dolomite; the clast-groundmass interface is marked by a calcite vein (CL; N156, 69.3 m).

Photo. 98. Clast of dolomitised bioclastic limestone within the Stage 2 groundmass (CL; N156, 69.3 m).

Photo. 99. Drillcore showing dolomitised bioclastic limestone cut through by micrite [m] (2 cm scale bar; N156, 69.3 m).

Photo. 100. Truncation of the micrite vein (M) at the edge of a dolomitised bioclastic limestone (B) clast; diagenetic and detrital laminae of the Stage 2 groundmass (2) are sheared into parallelism with the clast edge (PPL; N156, 69.3 m).

Photo. 101. Black and white photo-negative of a thin section showing the Stage 2 groundmass (2) deformed against the side of a clast comprising dolomitised bioclastic limestone; notice the micrite vein (M) which is truncated at the clast edge (width of view is 36.5 mm; N156, 69.3 m).

Photo. 102. Plastically deformed diagenetic-detrital laminae occurring as matrix to autoclastically brecciated Pale Beds (2 cm scale bar; N158, 138.6 m).

96

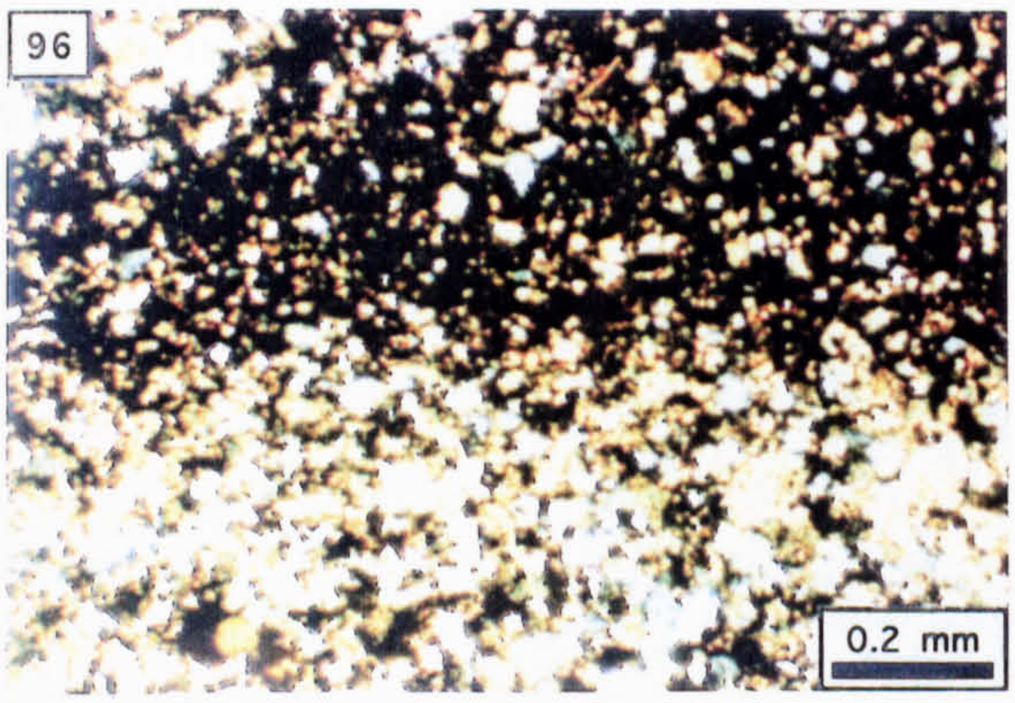

97

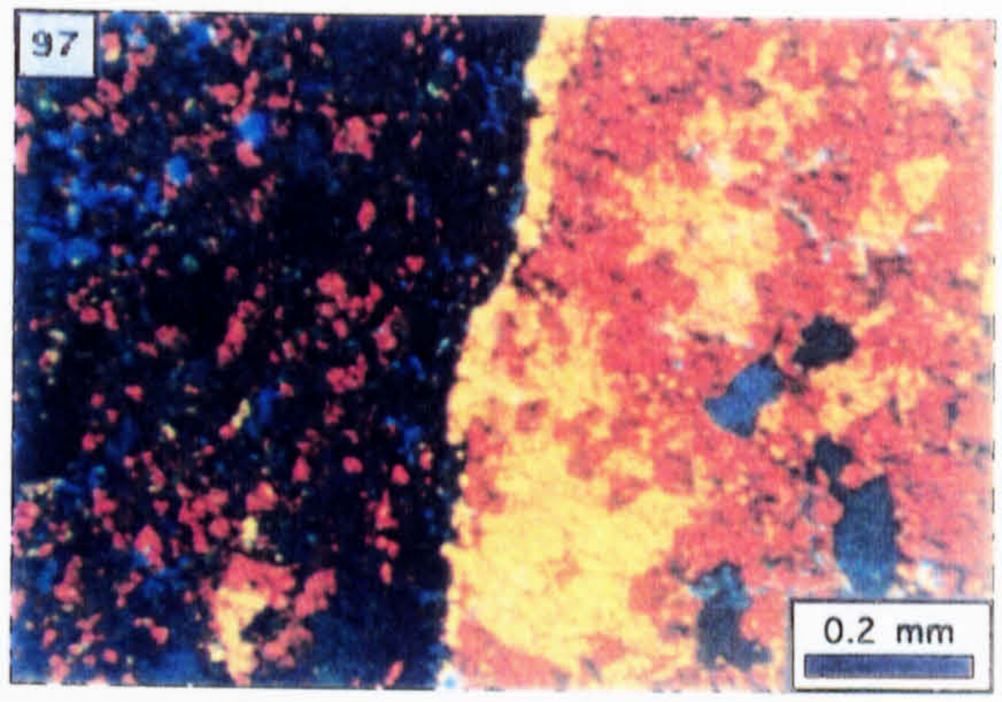

98

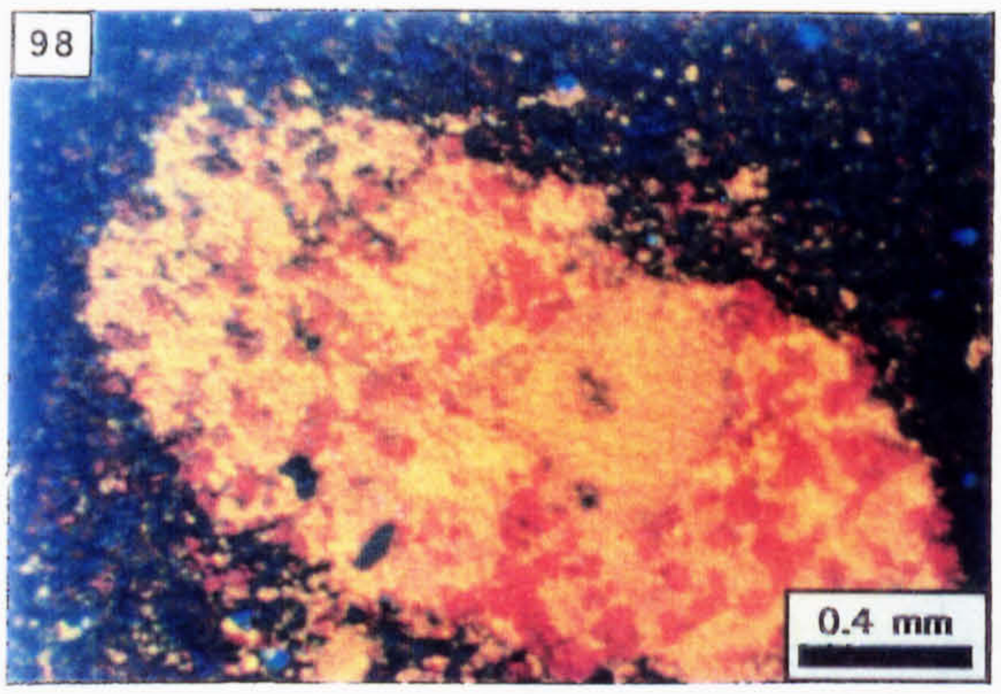

99

100

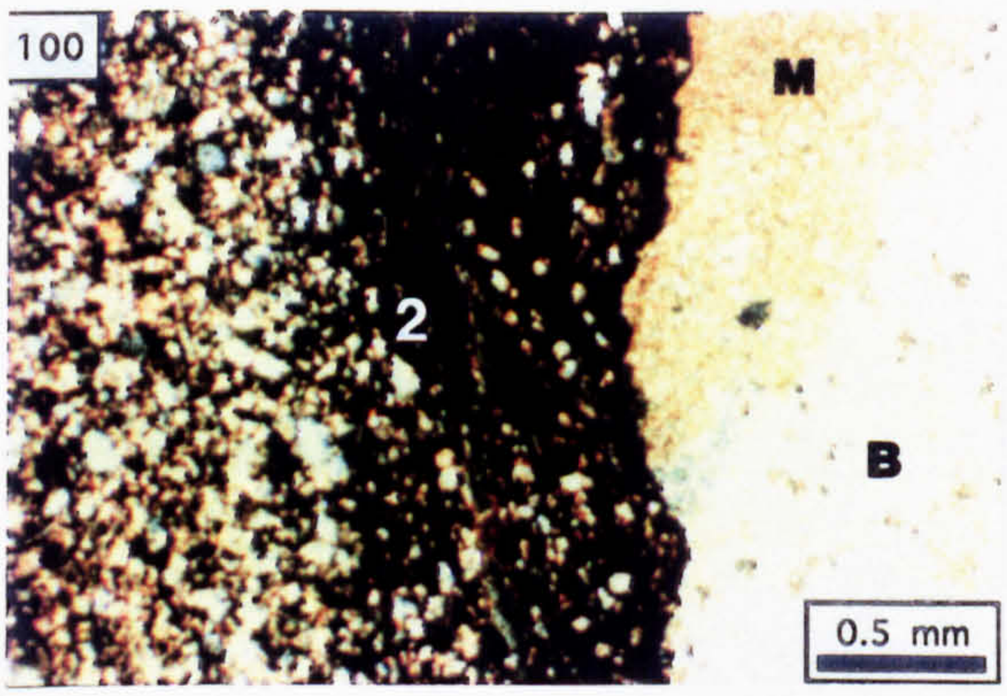

101

102

Photo. 103. Ore slurry-breccia as matrix to autoclastically brecciated Pale Beds (2 cm scale bar; N307, 118.0 m).

Photo. 104. Laminated diagenetic-detrital sedimentary assemblage present as matrix to autoclastically brecciated Pale Beds (PPL; N158, 138.6 m).

Photo. 105. Remobilised ore clast containing stalactitic pyrite [asterisks] (2 cm scale bar; N307, 118.0 m).

103

104

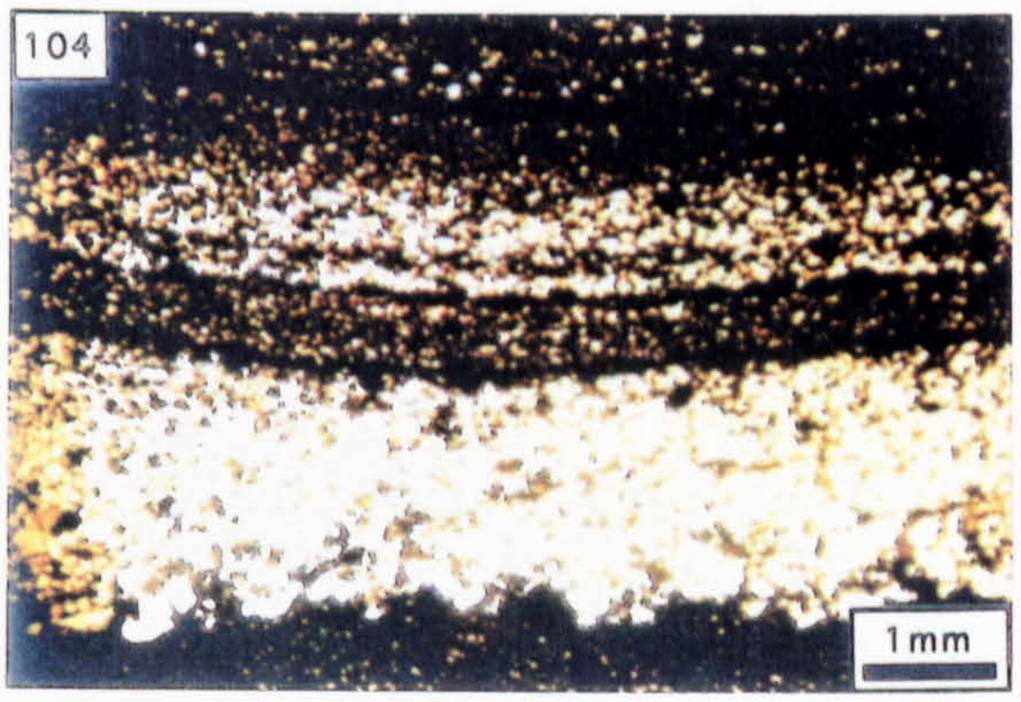

105

Photo. 106. Oolitic limestone replaced by sphalerite; the white grains are unreplaced siliciclastics (PPL; N158, 150.8 m).

Photo. 107. Laminated diagenetic-detrital sediment occurring as groundmass to clasts of replaced oolite (PPL; N158, 150.8 m).

Photo. 108. Black and white photo-negative of a thin section showing laminated diagentic-detrital sediment of the groundmass which is downwarped and attenuated at the base of a clast composed of replaced oolite (O) [width of view is 36.5 mm; N158, 150.8 m].

Photo. 109. Flame structures defined by compositional variations in the groundmass and created by the loading effects of clasts of replaced oolite (2 cm scale bar; N158, 150.8 m).

Photo. 110. Oobiosparite of the upper Pale Beds (N261, 242.9 m).

Photo. 111. Groundmass to the oobiosparite clast shown in Photo. 110 showing clasts of highly corroded limestone supported by a matrix of siliciclastic sand; the dark, intergrain sediment is composed of pyritic argillite (PPL; N261, 242.9 m).

106

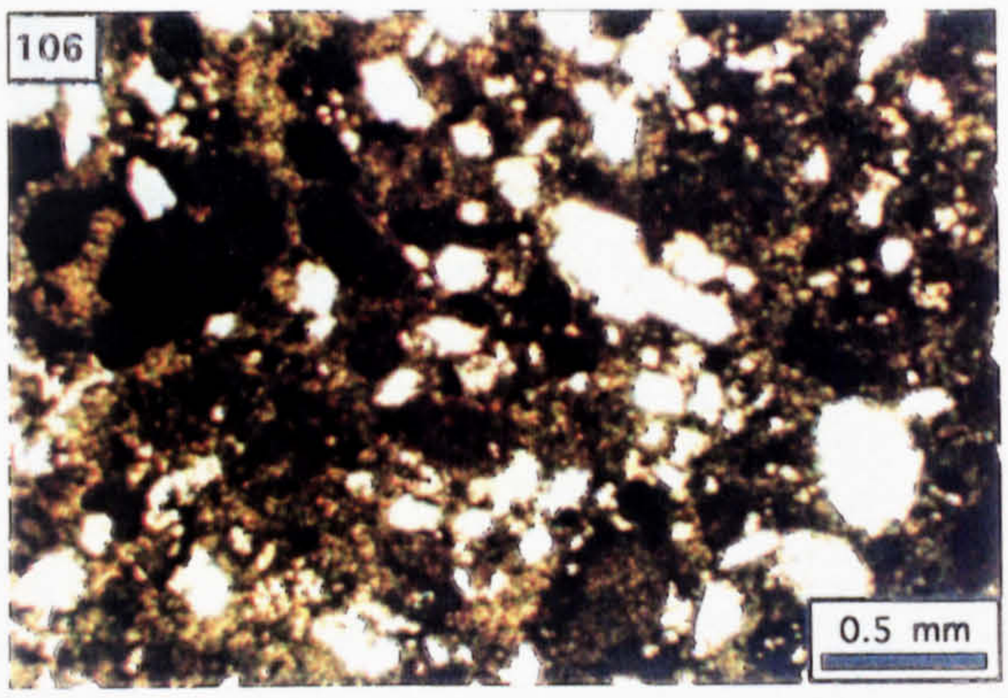

107

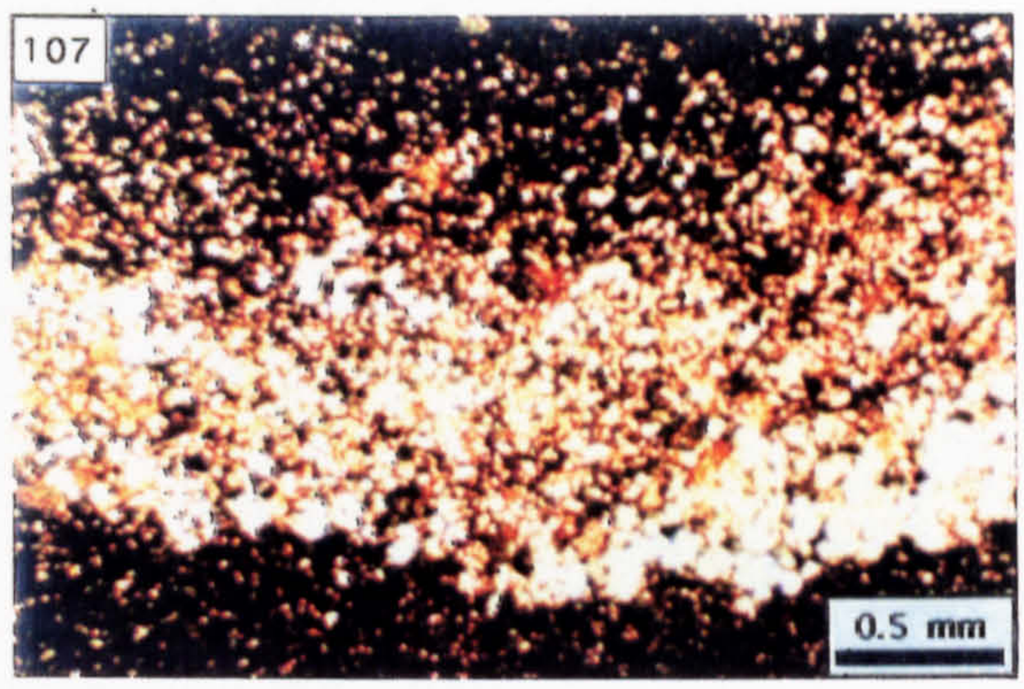

108

109

110

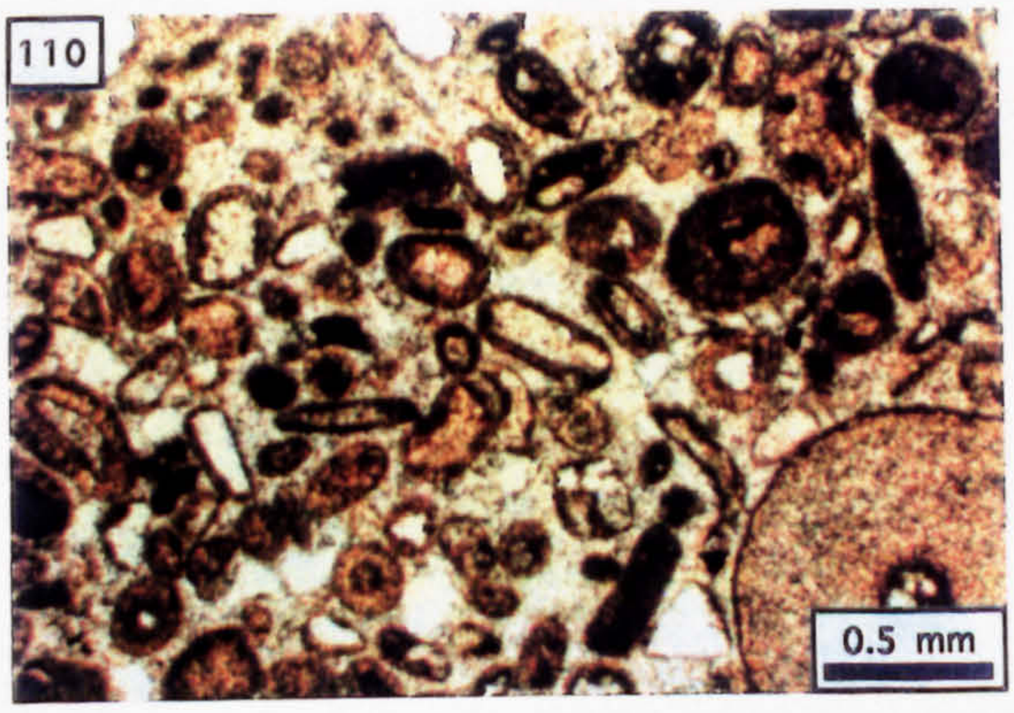

111

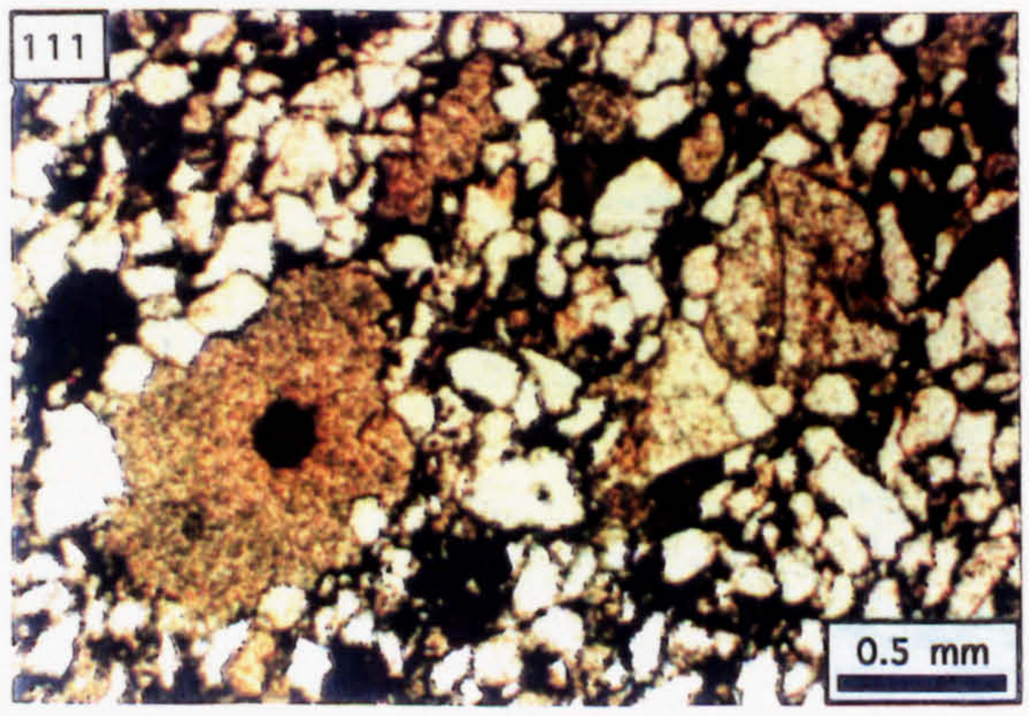

Photo. 112. Clast of botryoidal pyrite, the matrix to which is shown in Photos. 114-118 (scale bar graded in millimetres; N654, 207.5 m).

Photo. 113. Tabular pyrite (p) and mudstone (m) breccia (N654, 206.6 m).

Photo. 114. Clast of sphalerite-replaced oolite (O) supported by pyritic mud and siliciclastics (N654, 207.5 m).

Photo. 115. Tabular clast of dolomitised mudstone supported by spherular pyrite, mud, siliciclastic sand and dolomite (CL; N654, 207.5 m).

Photo. 116. As Photo. 115 but PPL.

Photo. 117. Petrography of the matrix showing dolomite crystals associated with siliciclastic sand, spherular pyrite and mudstone clasts (CL; N654, 207.5 m).

Photo. 118. As Photo. 117 but PPL.

Photo. 119. Gradational clast-groundmass contact; C=clast (PPL; N261, 242.9 m).

112

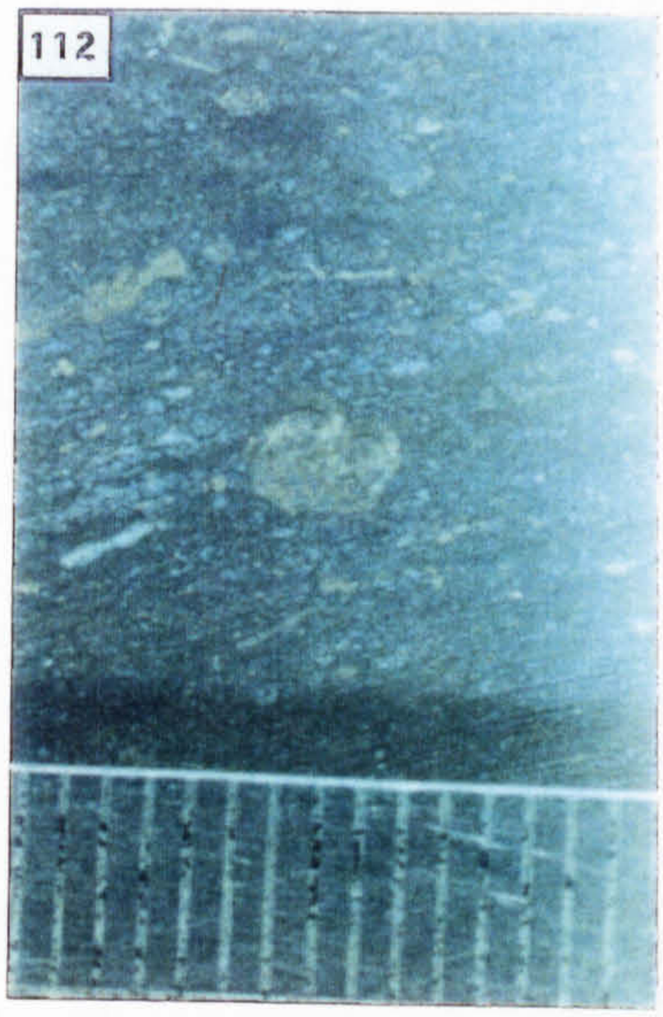

113

114

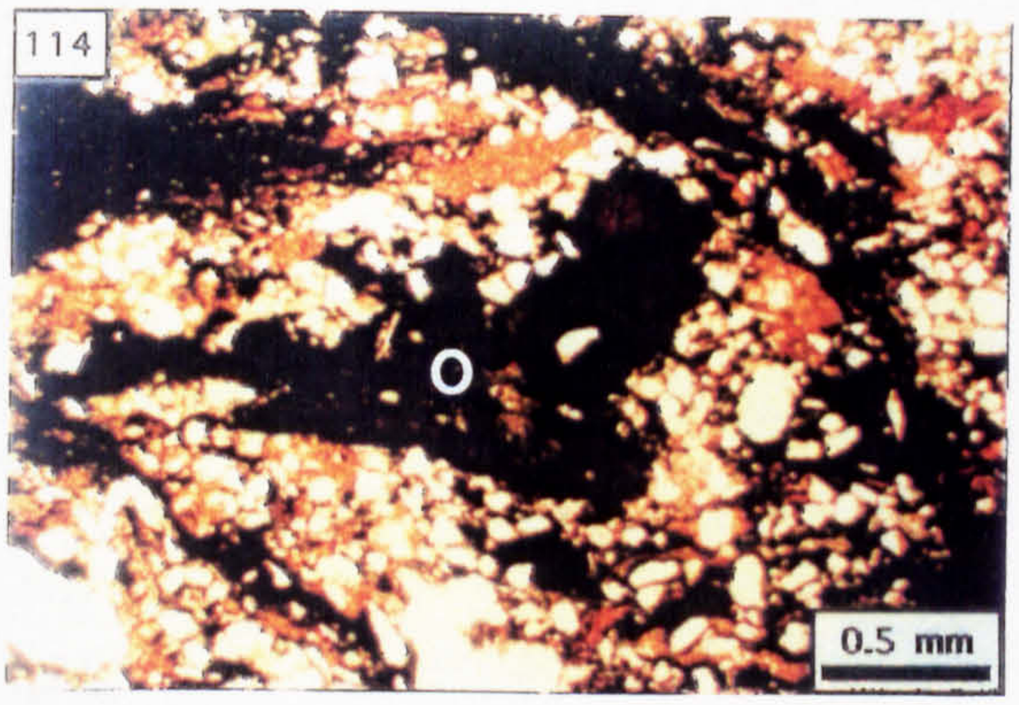

115

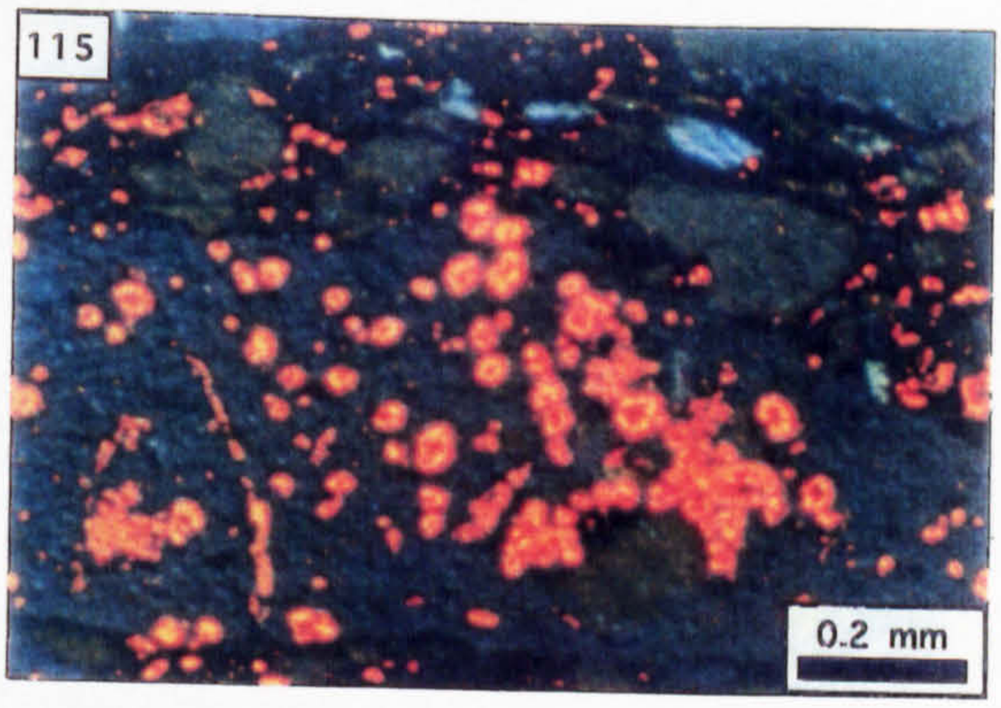

116

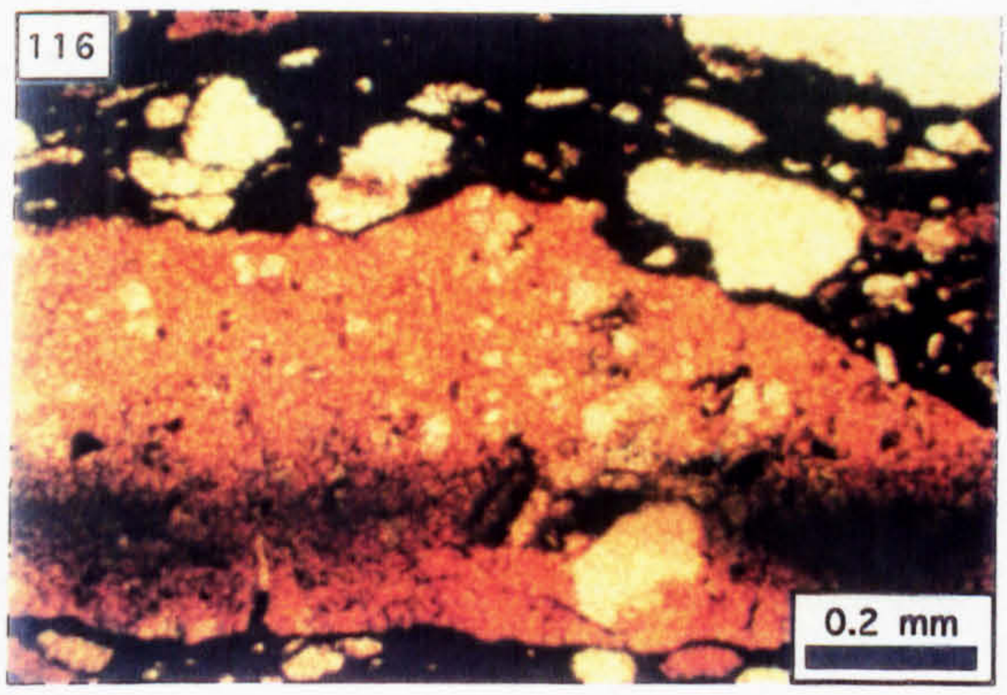

117

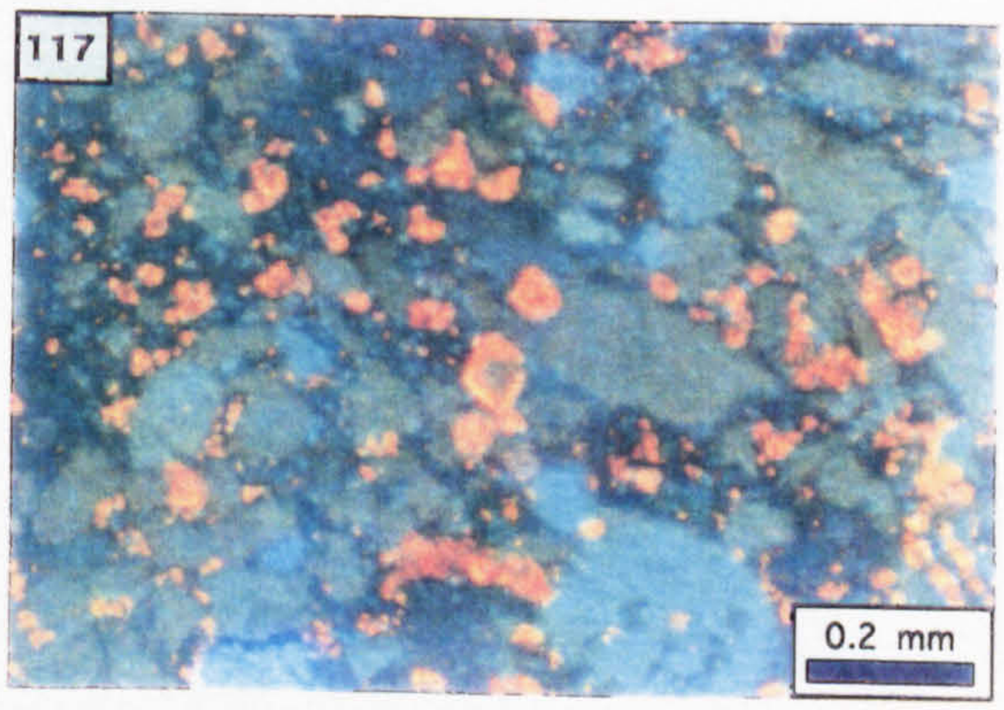

118

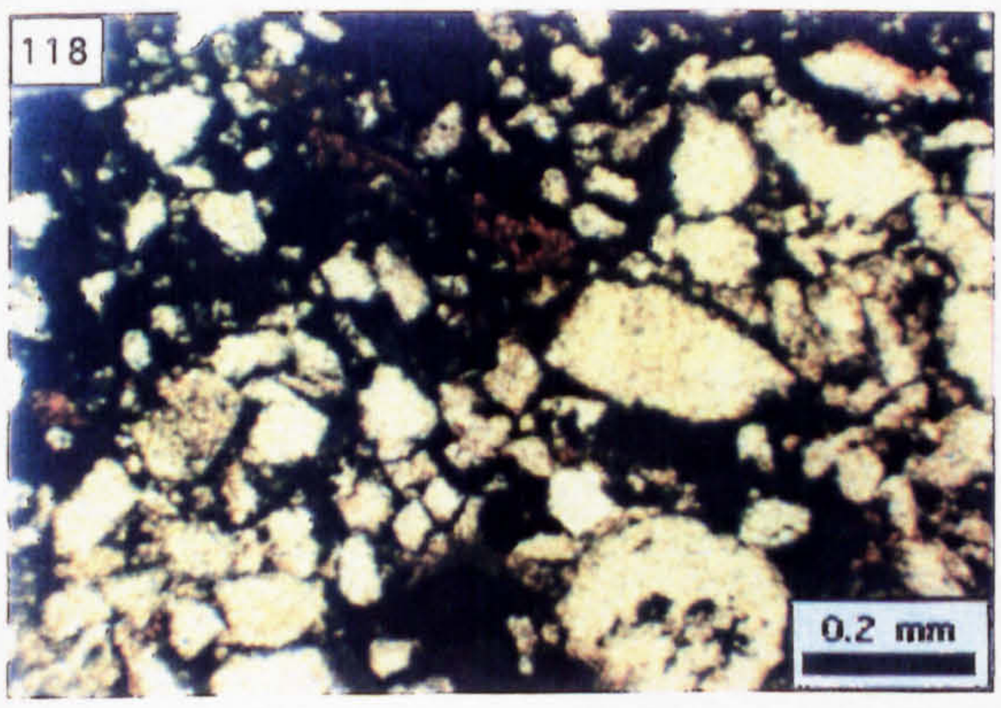

119

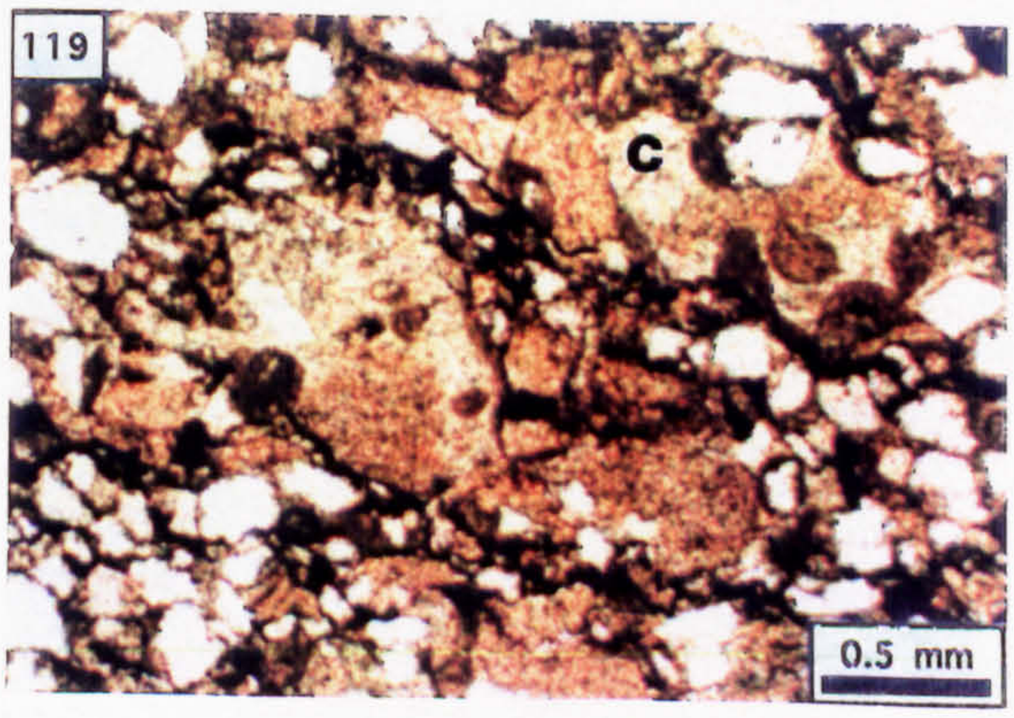

Photo. 120. Dissolved contact of a limestone "streamer" (S) with a clast of oobiolimestone (C); notice the concentration of siliciclastic grains along the interface (PPL; N261, 242.9 m).

Photo. 121. Pristine limestone adjacent to a groundmass comprising corroded limestone and siliciclastic sand (PPL; N261, 242.9 m).

Photo. 122. Drillcore showing the presence of detached and deformed limestone streamers within a groundmass of (dolomitised) mudstone, siliclastic sand, dolomite crystals and sulphide clasts; C=limestone clast, S=limestone streamer, G=groundmass (2 cm scale bar; N654, 270.5 m).

Photo. 123. Arenaceous biosparite clast (PPL; N191, 139.9 m).

Photo. 124. Zoned sparite occluding a biopore within the arenaceous biosparite clast shown in Photo. 123 (CL; N191, 139.9 m).

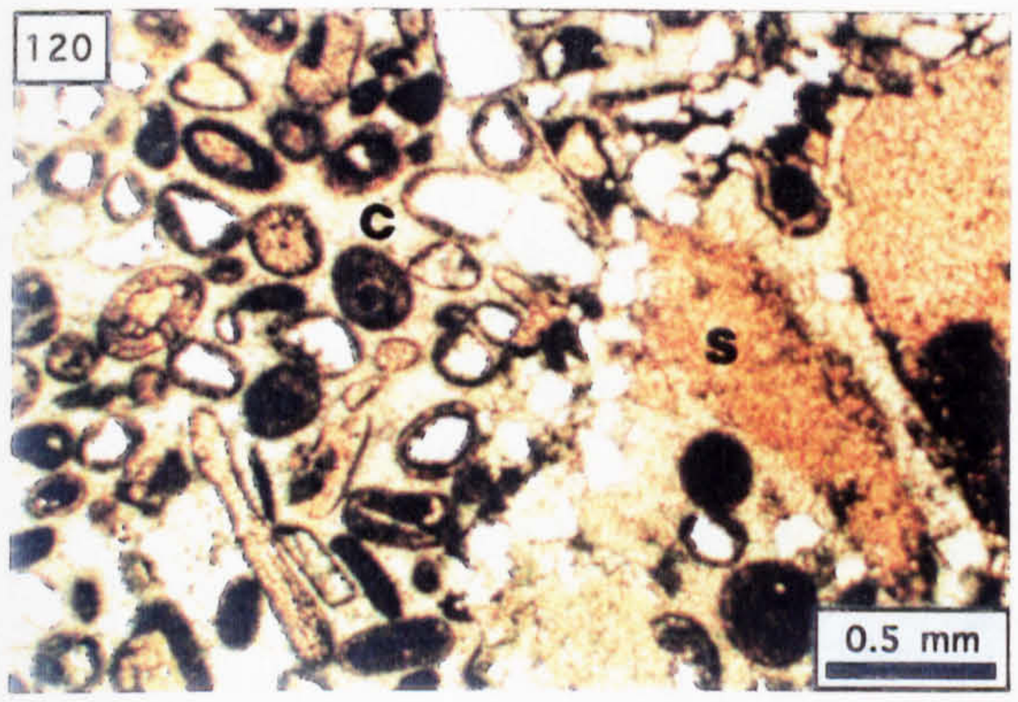
120
C
S
0.5 mm

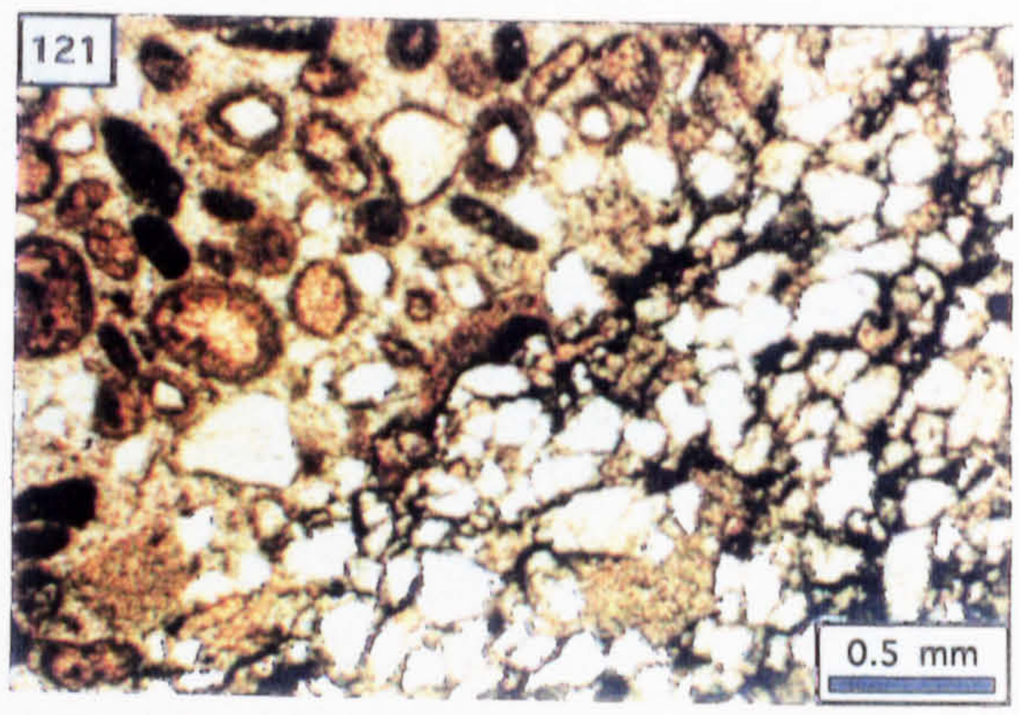
121
0.5 mm


122
C
S
S
S
G
S

123
0.5 mm


124
0.4 mm

Photo. 125. Subhedral, zoned dolomite occluding an irregular vug within bioporosity-occluding sparite (CL; N191, 139.9 m).

Photo. 126. Siliciclastic groundmass to the arenaceous biosparite clast (PPL; N191, 139.9 m).

Photo. 127. Drillcore showing clasts of pyrite (p) contained within the groundmass (G) to clasts of arenaceous biosparite (C) [2 cm scale bar; N191, 139.9 m).

Photo. 128. Biopore-filling sparite truncated at the clast edge (XPL; N191, 139.9 m).

Photo. 129. Detail of the truncated sparite and intra-sparite dolomite (CL; N191, 139.9 m).

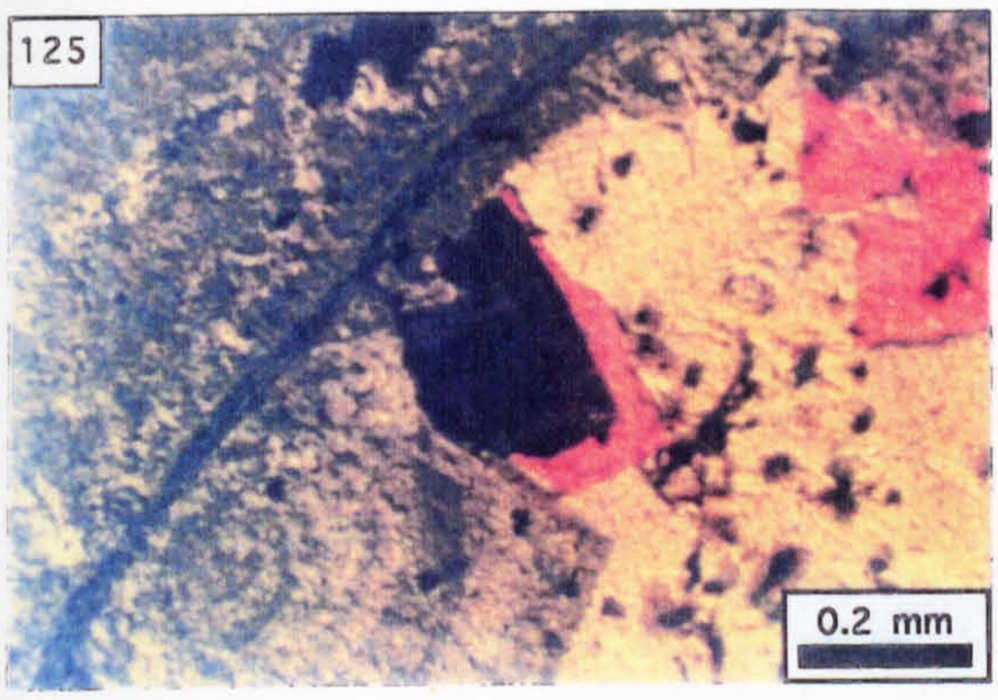
125
0.2 mm

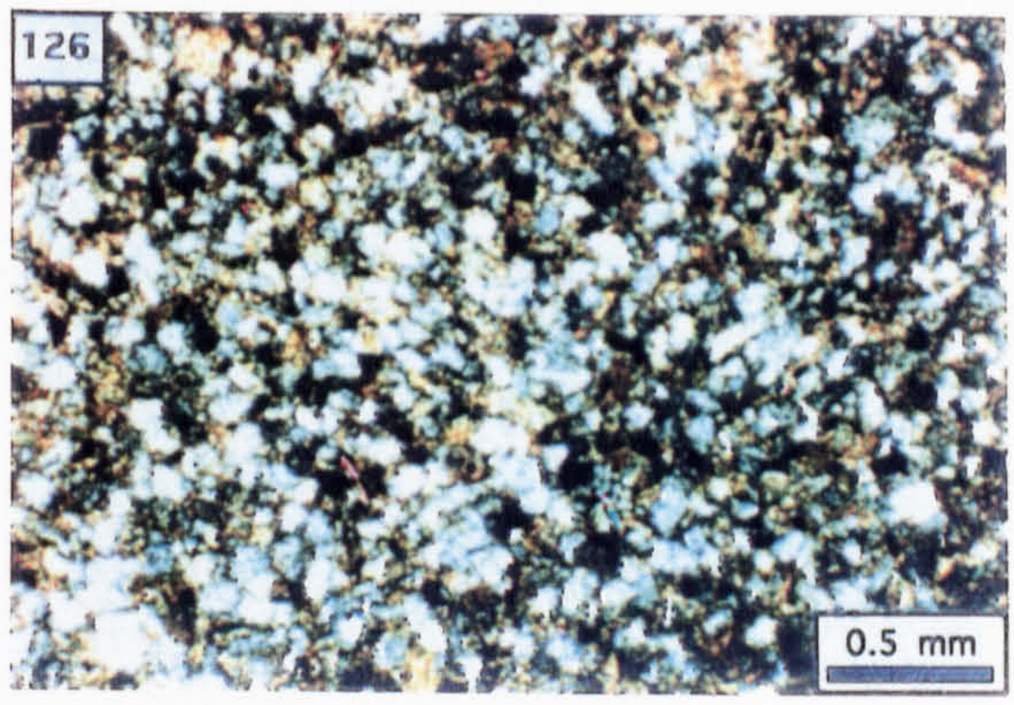
126
0.5 mm

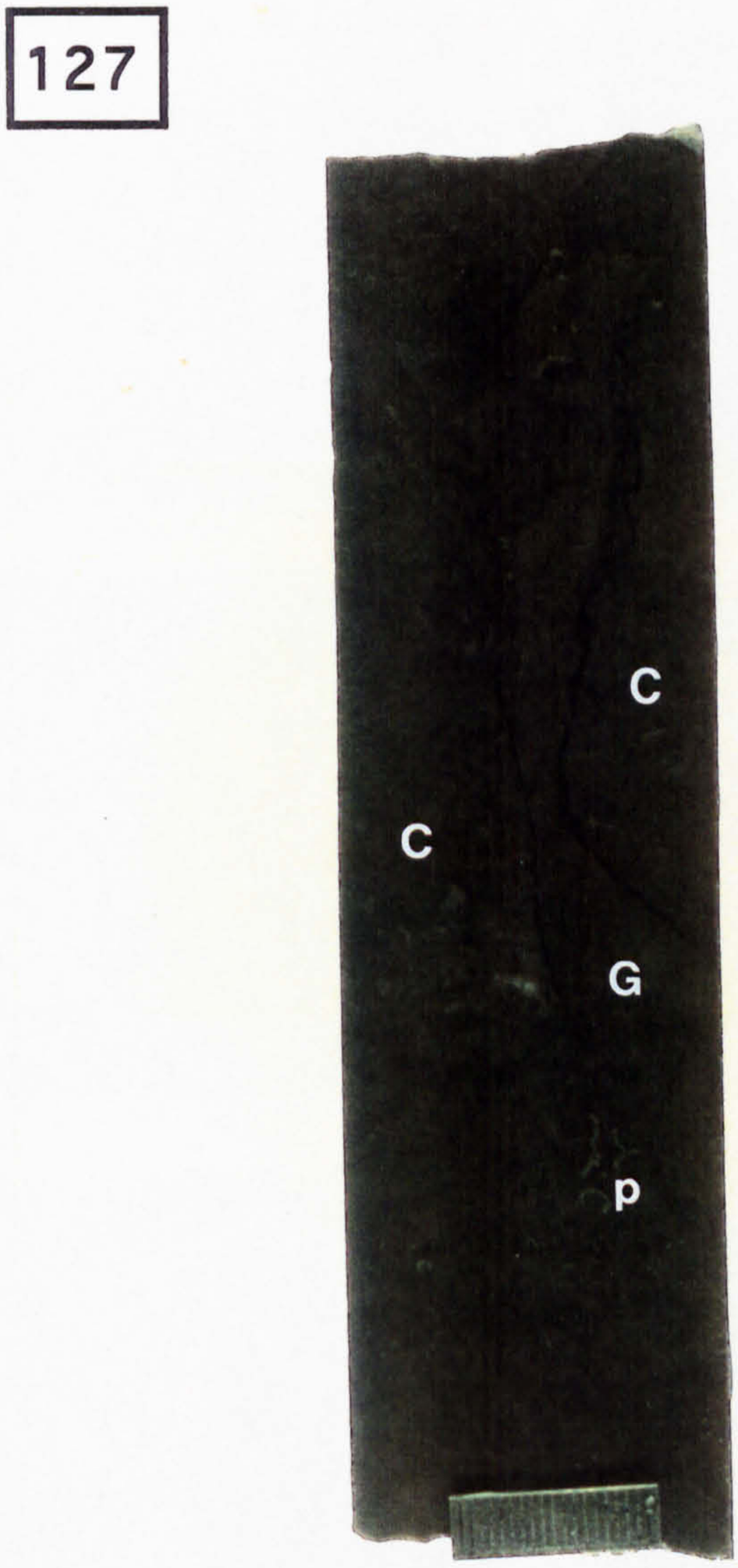
127
C
C
G
p

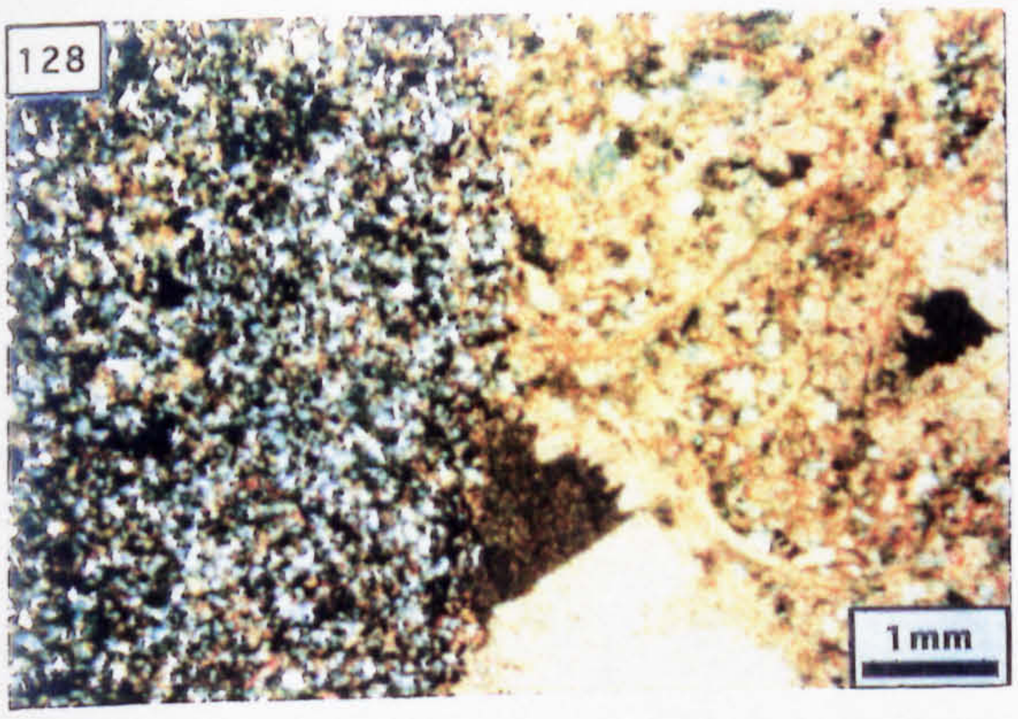
128
1 mm

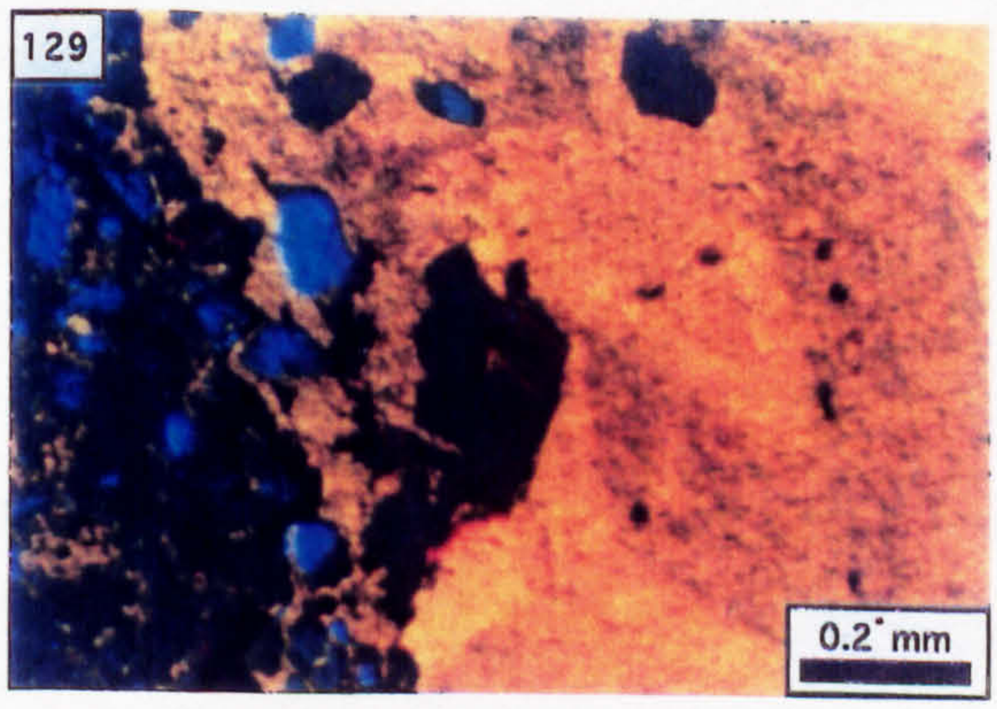
129
0.2 mm

Photo. 130. Fibrous calcite vein (V) located along the clast-groundmass interface (PPL; N191, 139.9 m).

Photo. 131. Selectively preserved bryozoa fragment within otherwise intensely dolomitised bioclastic limestone (CL; N927, 356.2 m).

Photo. 132. Relict bioclasts in intensely dolomitised bioclastic limestone (CL; N927, 356.2 m).

Photo. 133. As Photo. 132 but PPL.

Photo. 134. Silicified bioclasts within bioclastic argillite of the Argillaceous Bioclastic Limestone; S=silica (PPL; N743, 23.4 m).

Photo. 135. Euhedral dolomite rhombs in argillite (PPL; N743, 23.4 m).

Photo. 136. CL zonation of the dolomite associated with the argillite; S=silica replacement to crinoid ossicle (N743, 23.4 m).

Photo. 137. Silicified bioclasts within dolomitised calcarenite (XPL; N743, 23.4 m).

Photo. 138. Fractured shell fragment within dolomitised calcarenite (XPL; N743, 23.4 m).

Photo. 139. Calcarenite replaced by dolomite possessing brightly luminescent cores (CL; N743, 23.4 m).

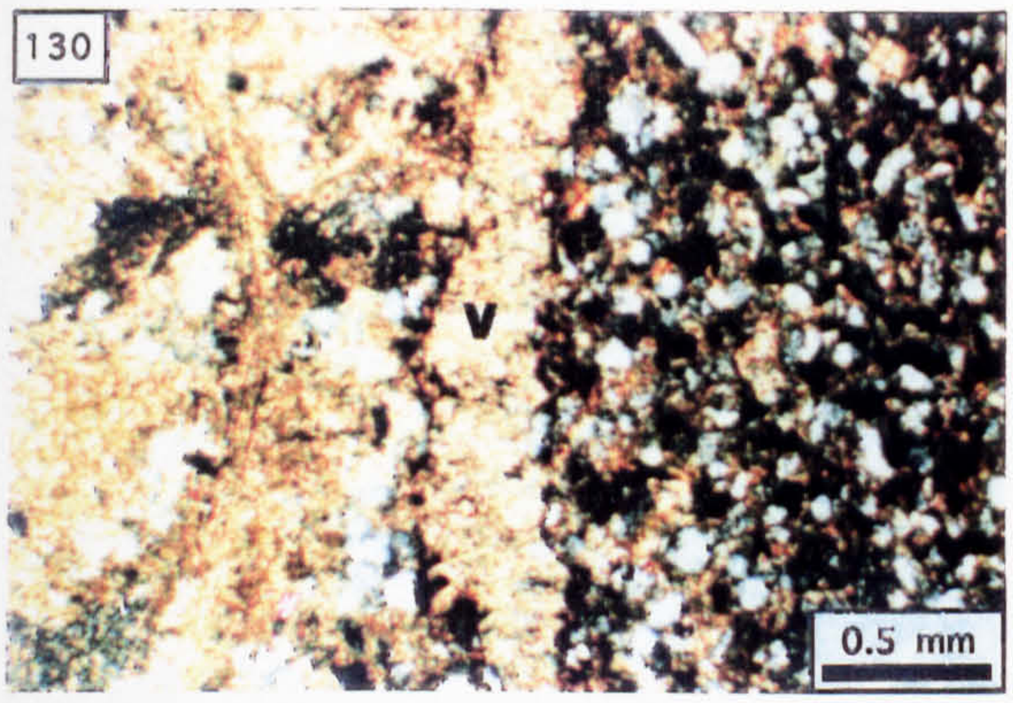
130
V
0.5 mm

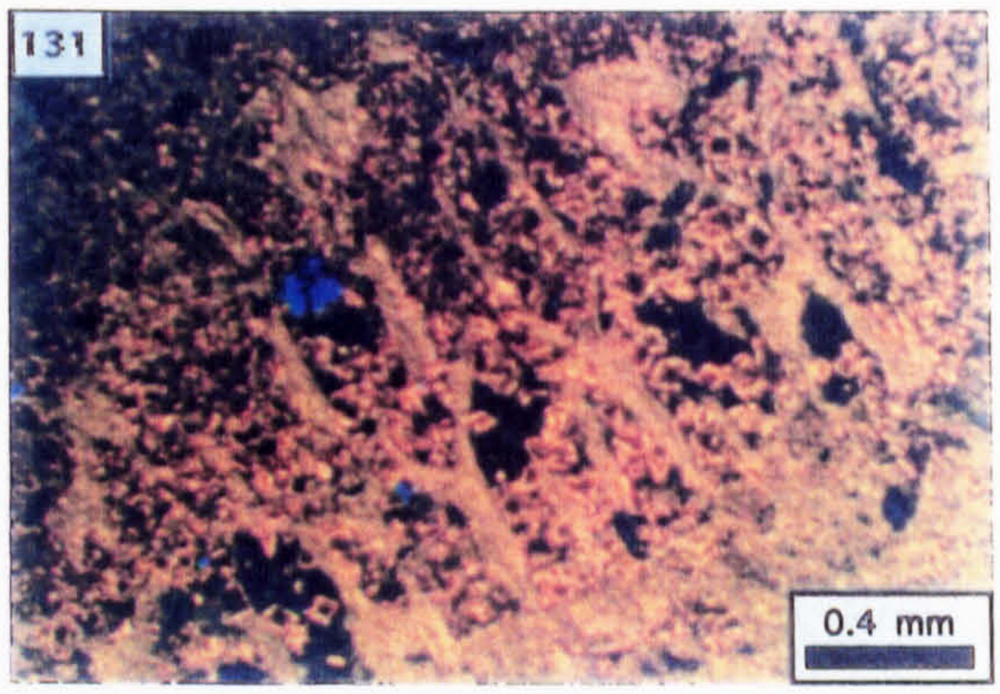
131
0.4 mm

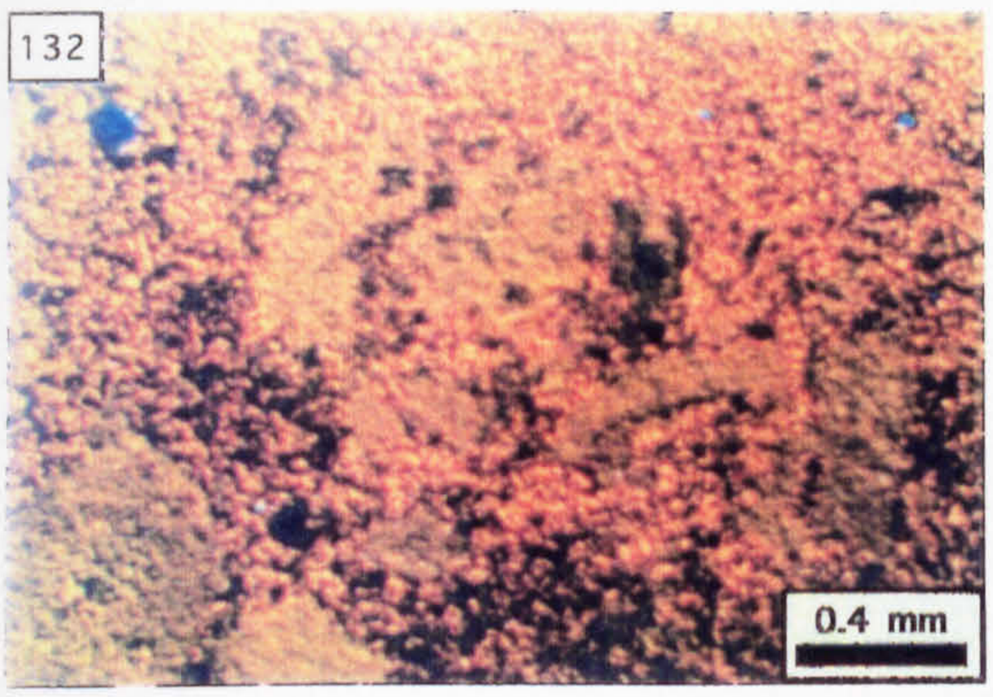
132
0.4 mm

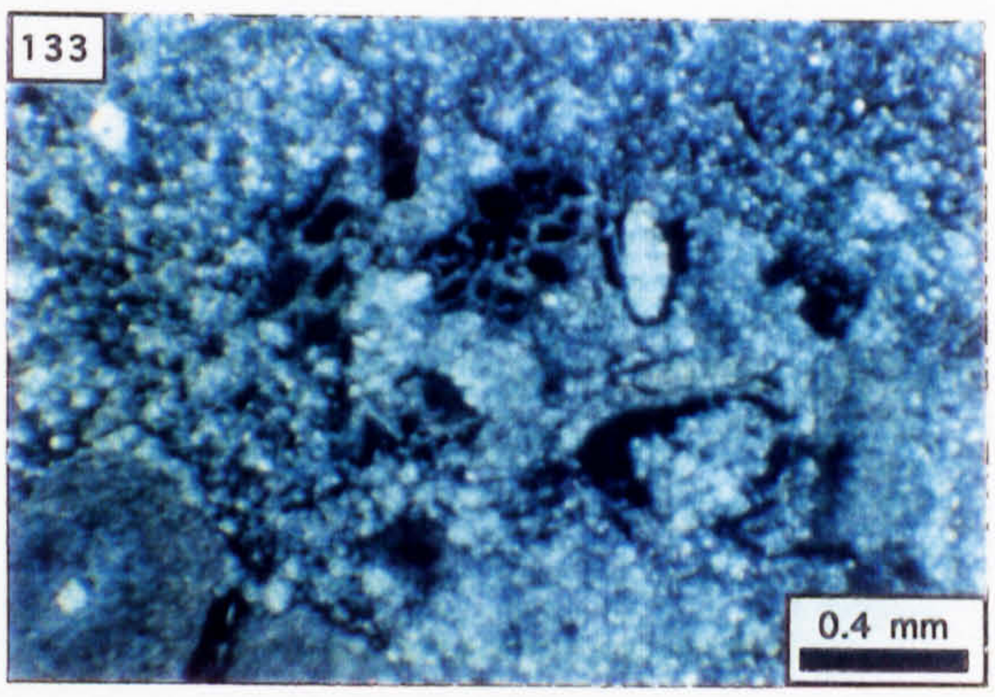
133
0.4 mm

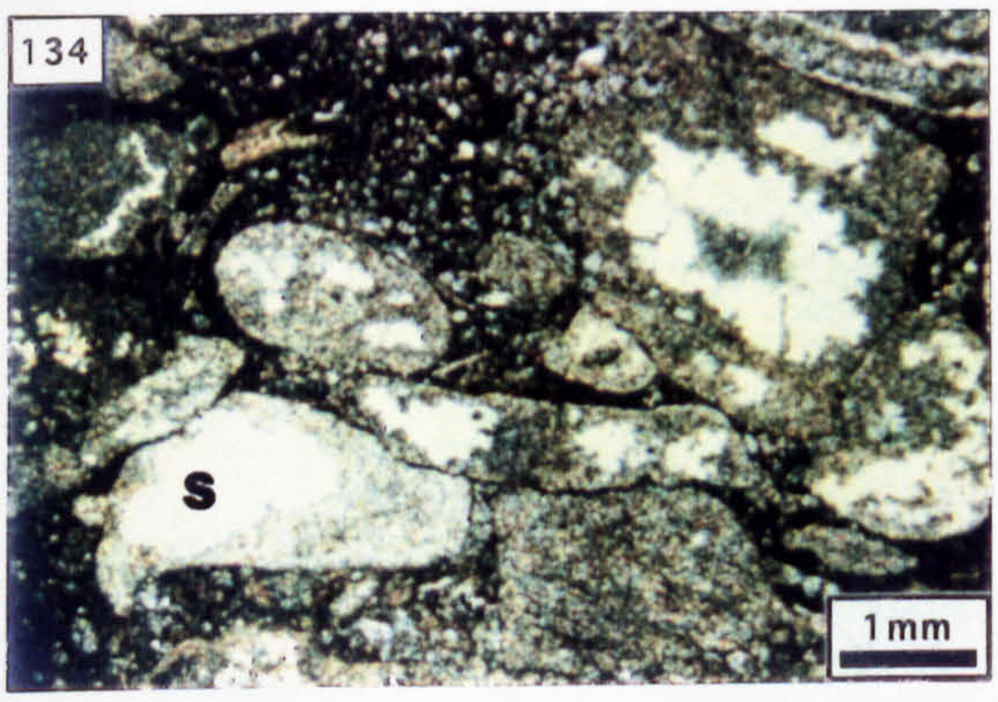
134
S
1mm

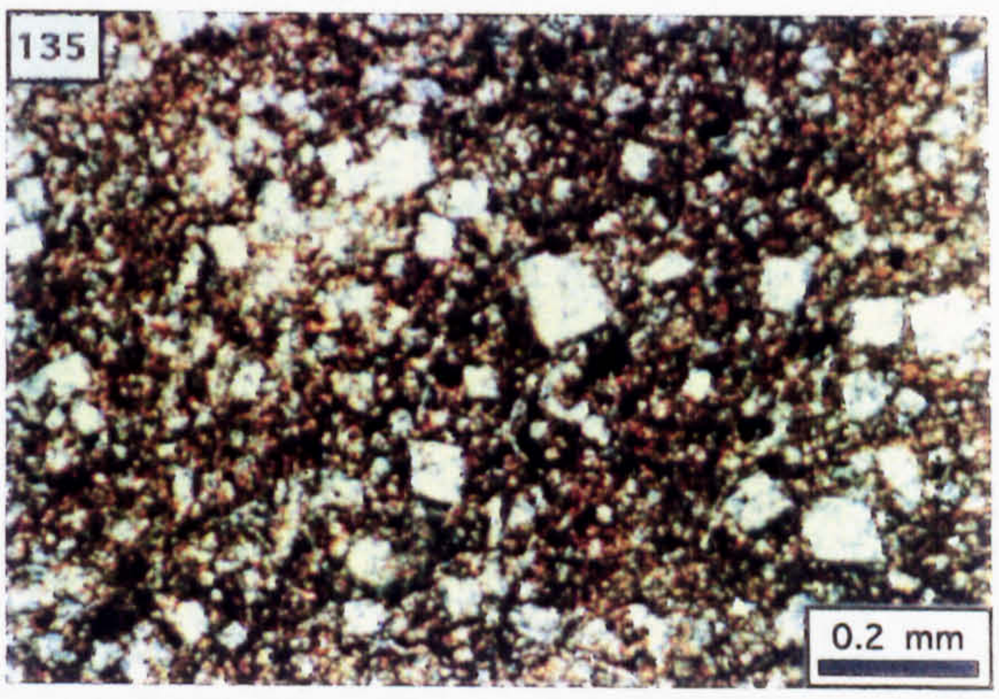
135
0.2 mm

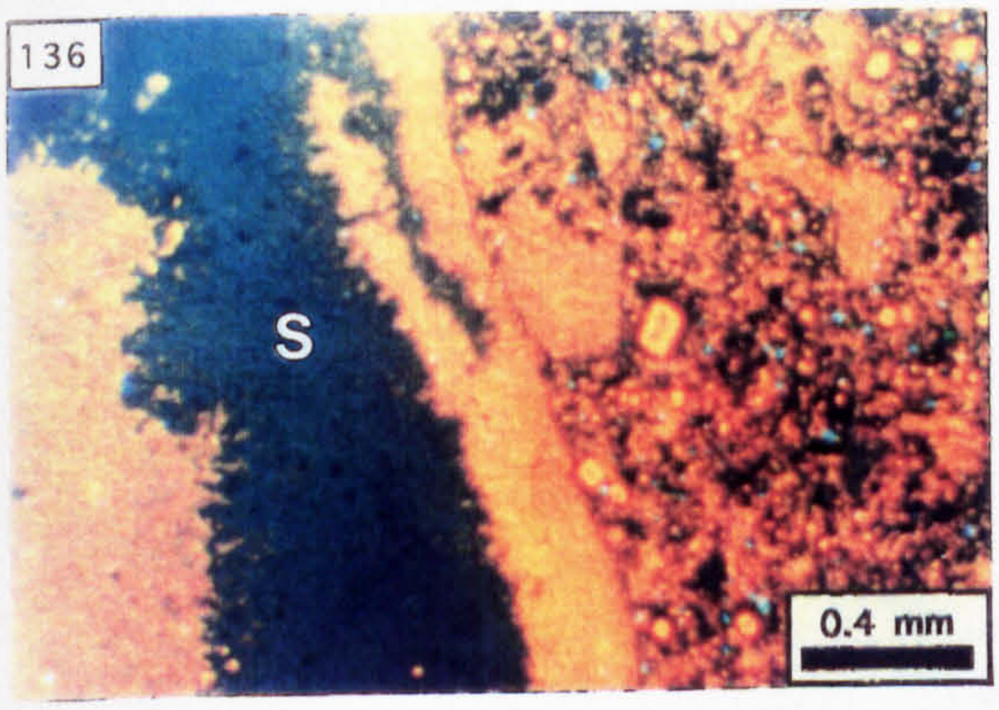
136
S
0.4 mm

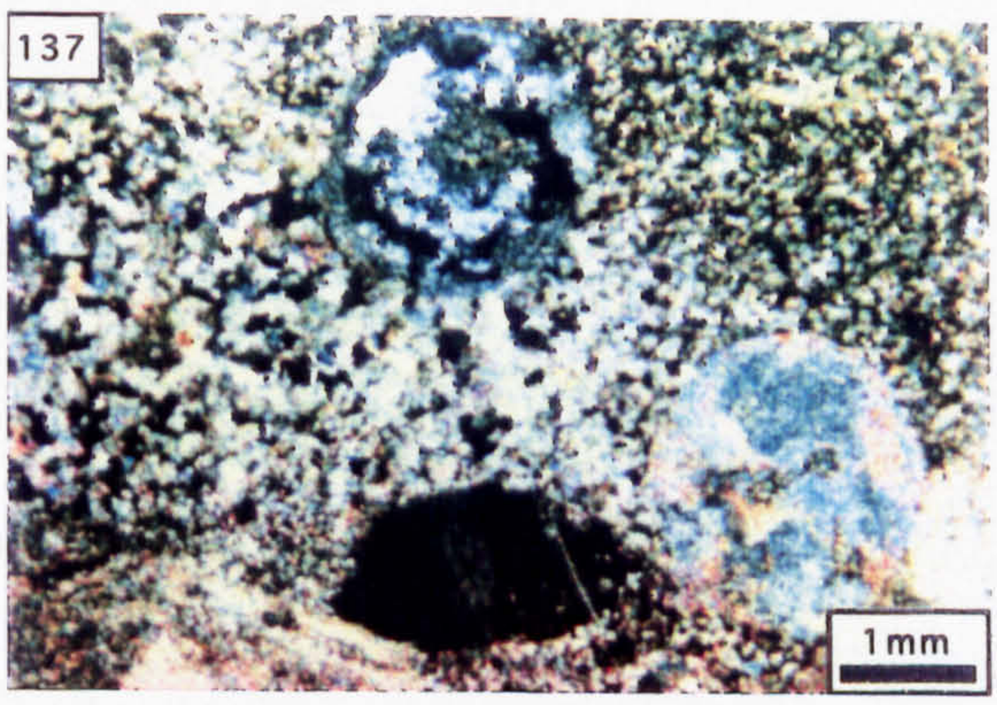
137
1mm

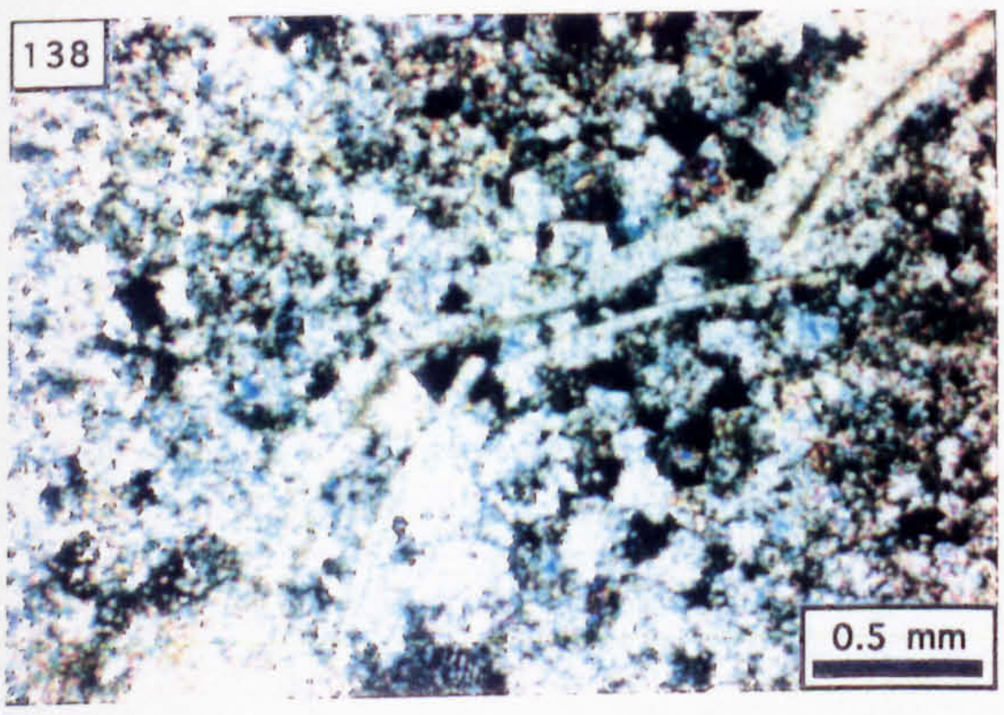
138
0.5 mm

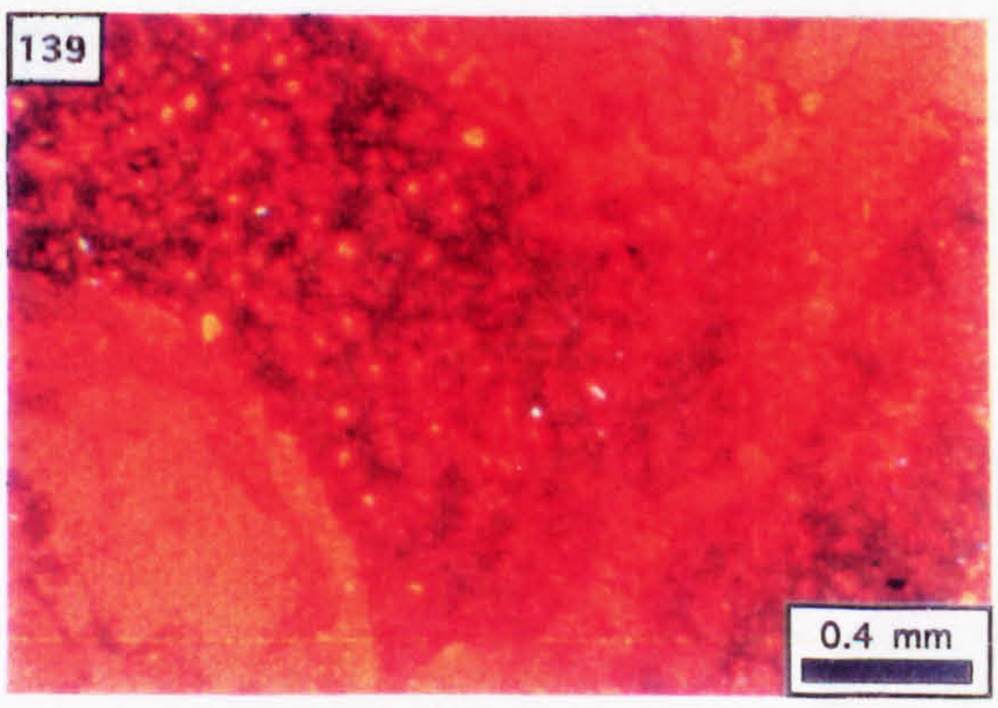
139
0.4 mm

Photo. 140. As photo. 139 but XPL.

Photo. 141. Irregular, dolomite-filled vugs (d) located within biocalcarenite which occurs as sediment on the floor of a bioclast (CL; N743, 23.4 m).

Photo. 142. Corroded scalenohedral crystals of calcite (c) located on the internal bioclast wall (b) in the absence of biocalcarenite; dolomite (d) occludes the pore space defined by the calcite (CL; N743, 23.4 m).

Photo. 143. Dolomite cement to an impersistent fracture located in undolomitised biocalcarenite; notice the coincidence of the fracture with the bryozoa fragment (PPL; N743, 23.4 m).

Photo. 144. Dolomite replacement to biocalcarenitic argillite; the dark line is the CL stage (PPL; N743, 23.4 m).

Photo. 145. As Photo. 144 but CL.

Photo. 146. Clast of biocalcarenite (A) supported by a matrix of biocalcarenite (CL; N261, 215.7 m).

Photo. 147. As Photo. 146 but PPL.

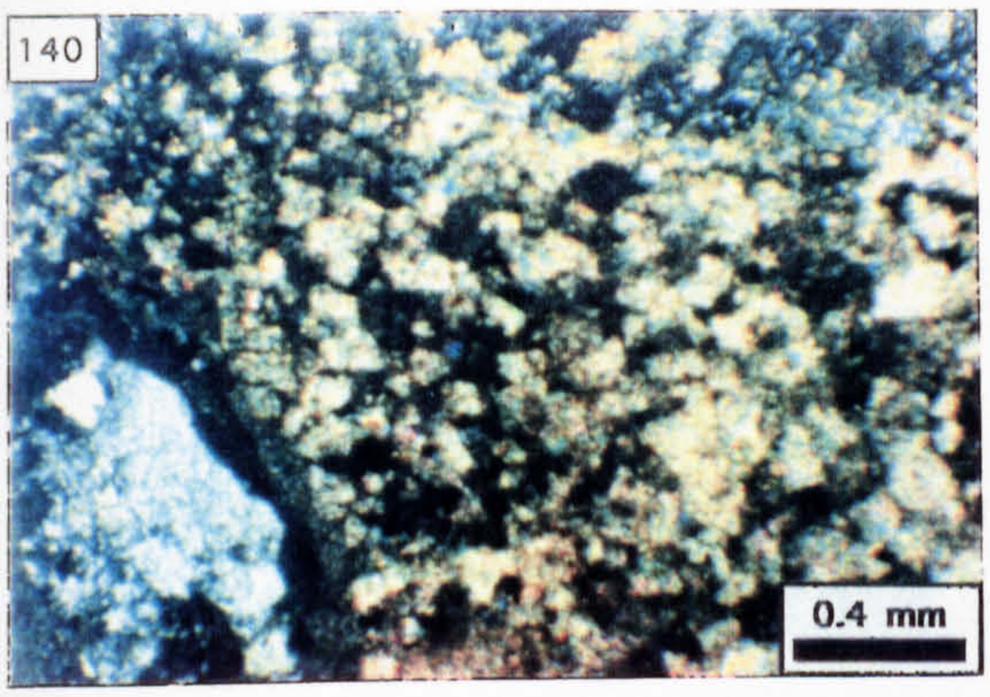
140
0.4 mm

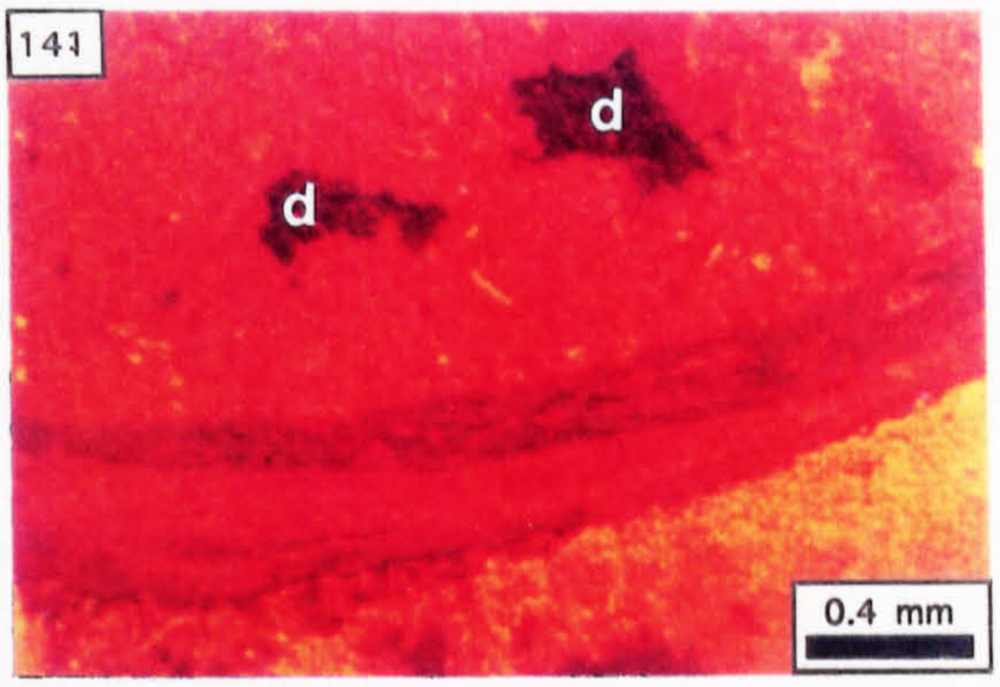
141
d
d
0.4 mm

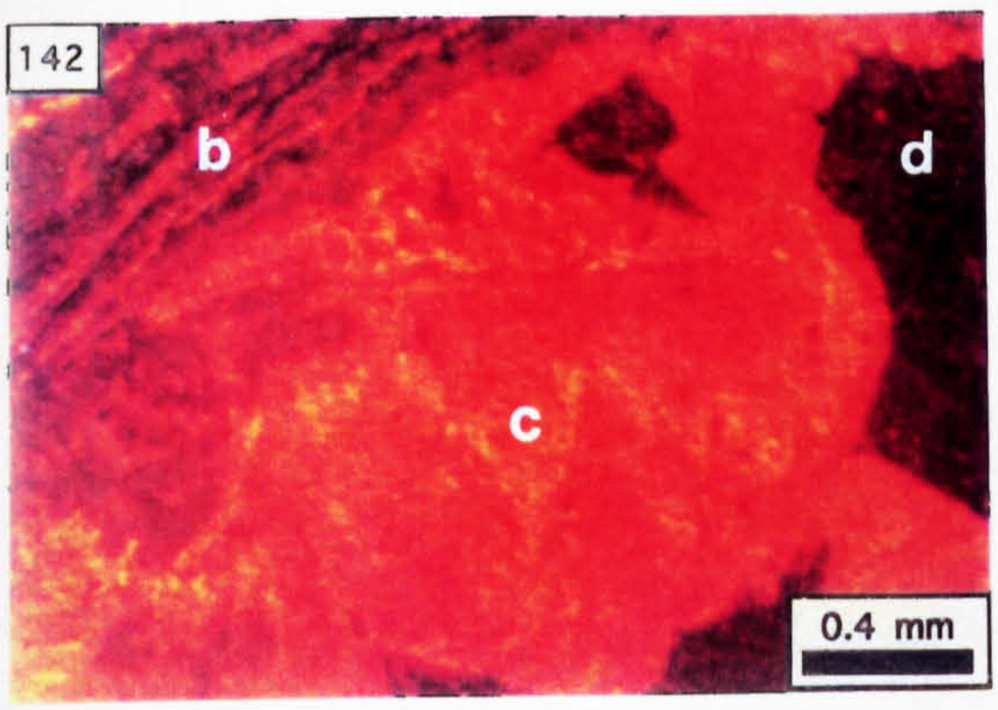
142
b
d
c
0.4 mm

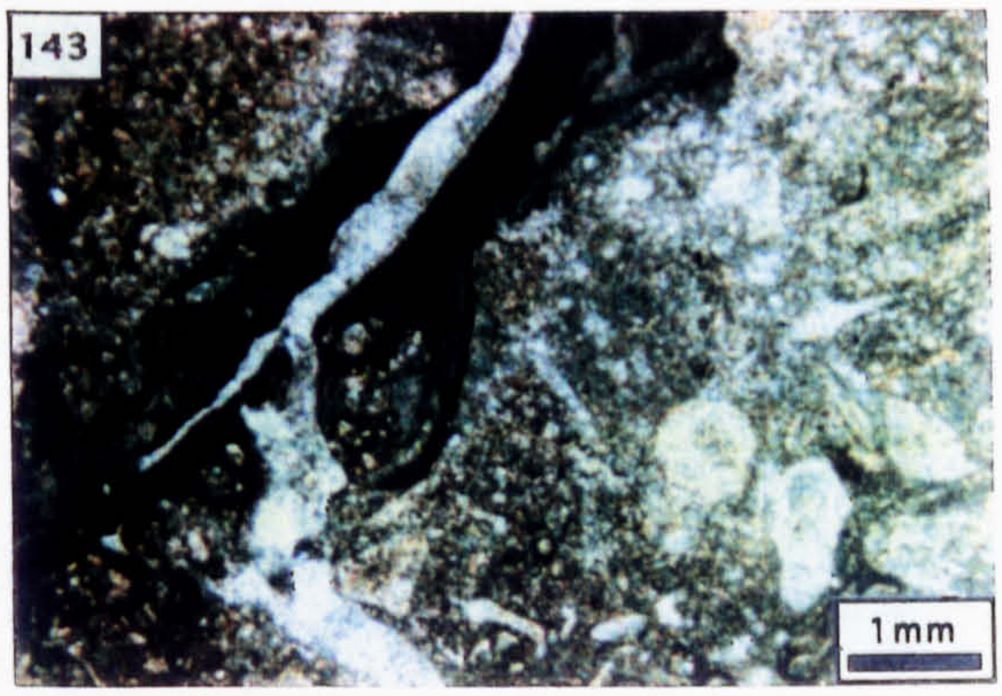
143
1mm

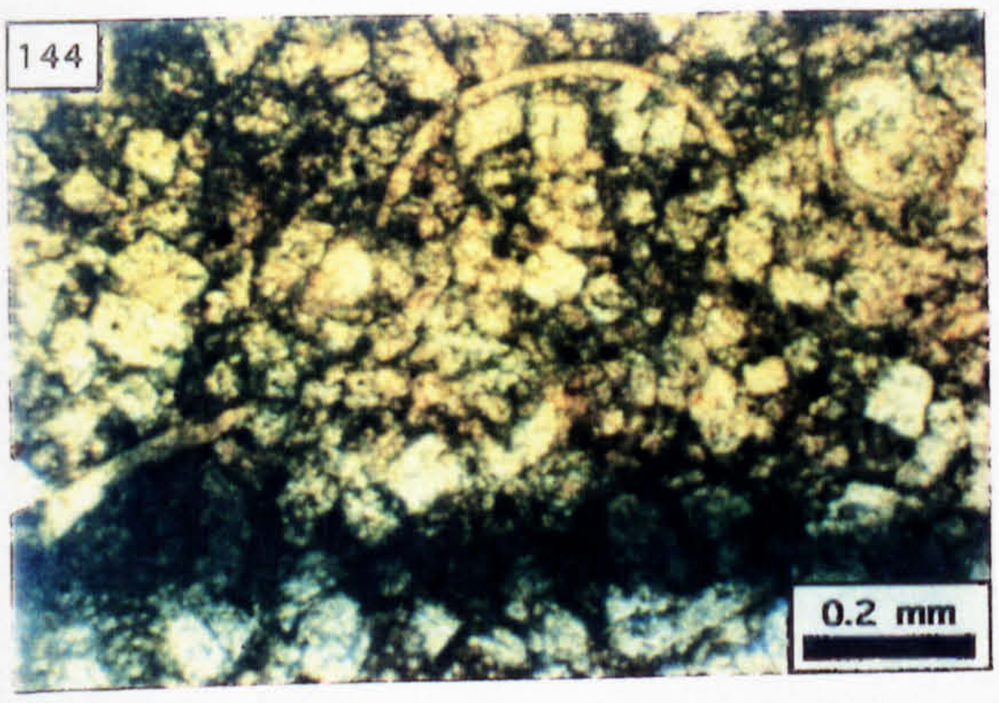
144
0.2 mm

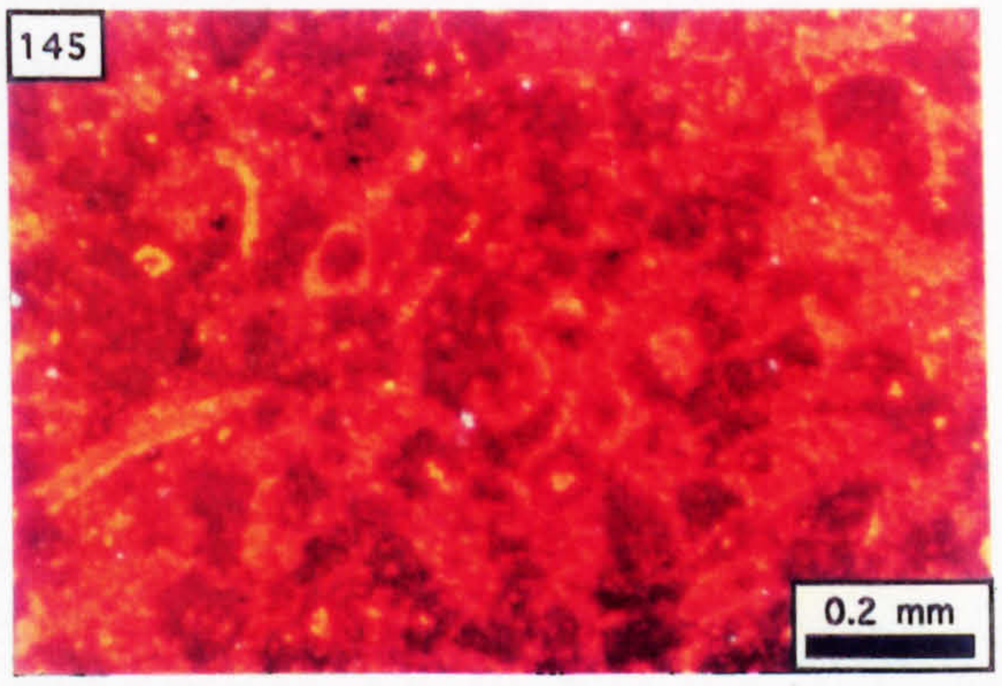
145
0.2 mm

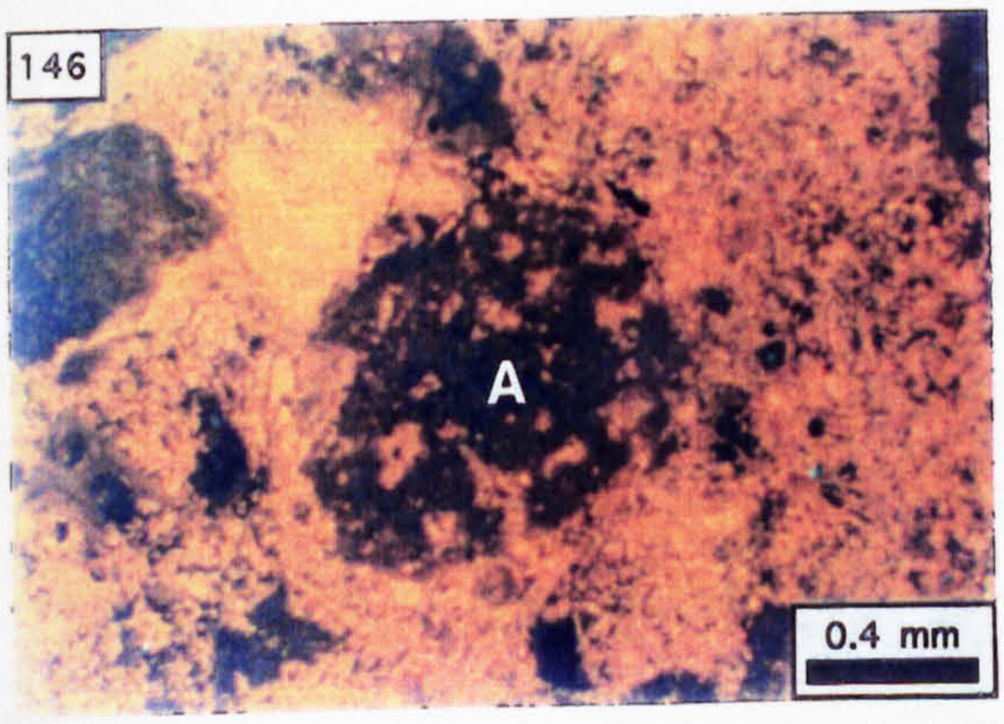
146
A
0.4 mm

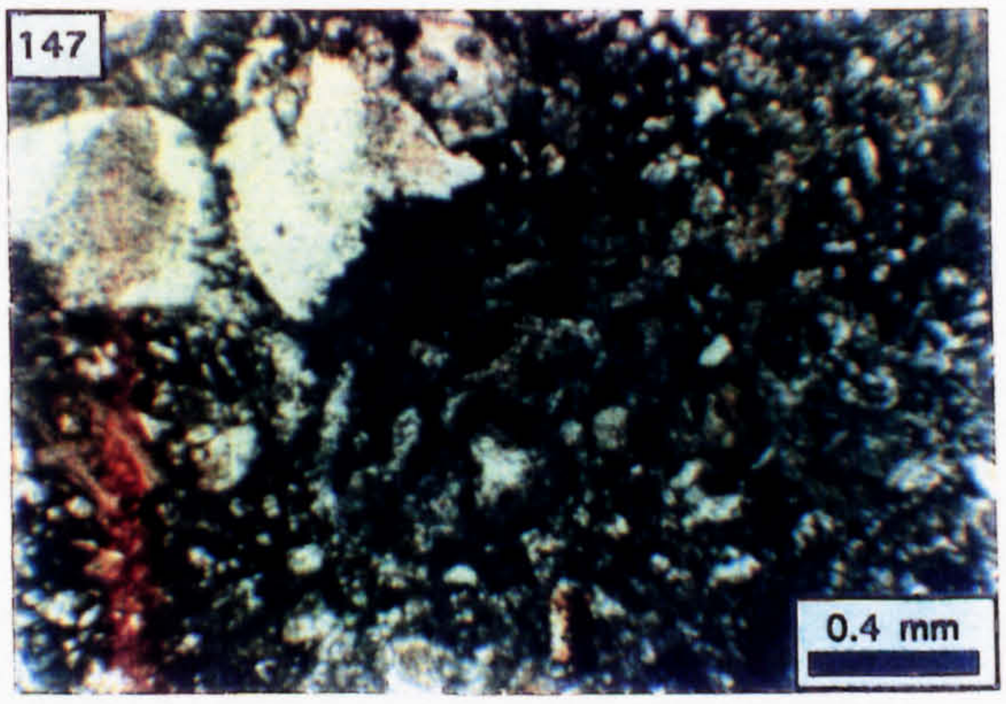
147
0.4 mm

Photo. 148. Drillcore showing vug-filling mineralisation in Reefoid Argillaceous Bioclastic Limestone (N261, 215.7 m).

Photo. 149. Sparite developed as an interbioclast cement (CL; N261, 215.7 m).

Photo. 150. Sparite occlusion to a biopore; note the presence of dissolved bioclasts in contact with the subhorizontal argillite seam (a) [CL; N261, 215.7 m].

Photo. 151. Coarse bioclastic grains showing replacement by silica (PPL; N261, 215.7 m).

Photo. 152. Irregular, dolomite-filled vugs (d) developed along the interface of Calcite II (C) with biosparite (B) [CL; N261, 215.7 m].

148

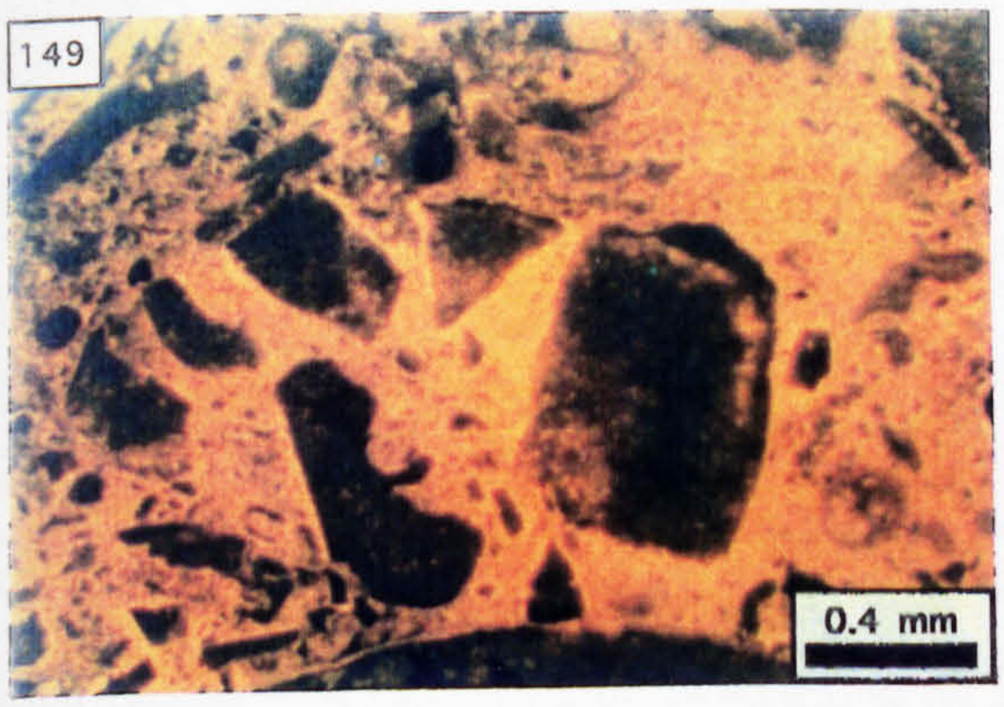

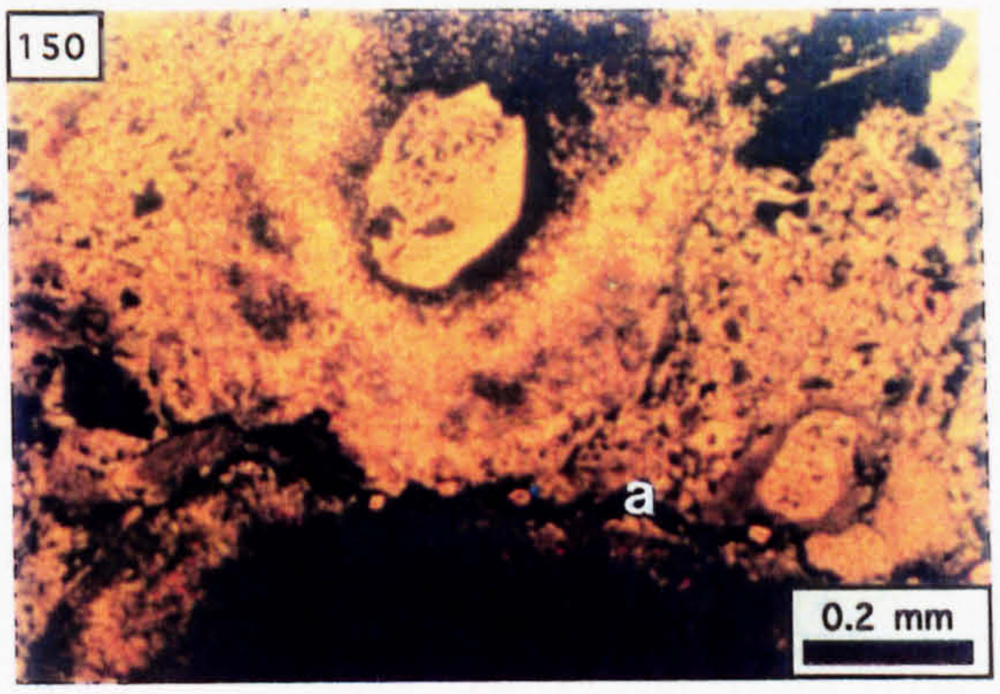

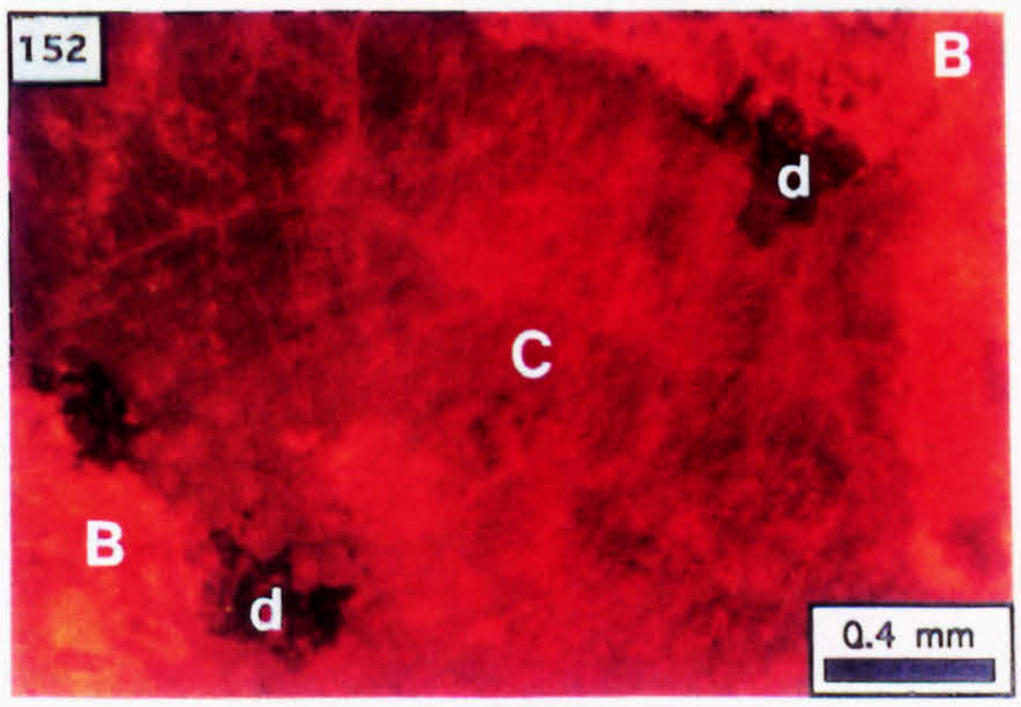

Photo. 153. Calcite II showing the effects of enhanced dissolution; C=Calcite II, B=biosparite, d=dolomite (CL; N261, 215.7m).

Photo. 154. Dolomite (d) infilling a dissolution vug which is preferentially located in Calcite II (C); B=biosparite (CL; N261, 215.7 m).

Photo. 155. Truncation of Calcite II (C) and biosparite (B) at the edge of the vug shown in Photo. 148 (CL; N261, 215.7 m).

Photo. 156. As Photo. 155 but PPL to show the presence of a clast of zoned sphalerite (S) within a matrix of dolomite.

Photo. 157. Dolomite (light grains) and sphalerite (dark grains) occurring as the crystal sediment which occupies the basal portion of the vug shown in Photo. 148 (PPL; N261, 215.7 m).

Photo. 158. Cross section through the vug wall showing dolomitised biosparite (B), Dol. I (1), Dol. II (2) and Cct. III (C) [CL; N261, 215.7 m).

Photo. 159. As Photo. 158 but PPL.

Photo. 160. Calcite cement to intracrystal fractures within a crystal of zoned sphalerite located on the vug wall; the fracture cement is contiguous with the sparite which occludes the remaining vug space (CL; N261, 215.7 m).

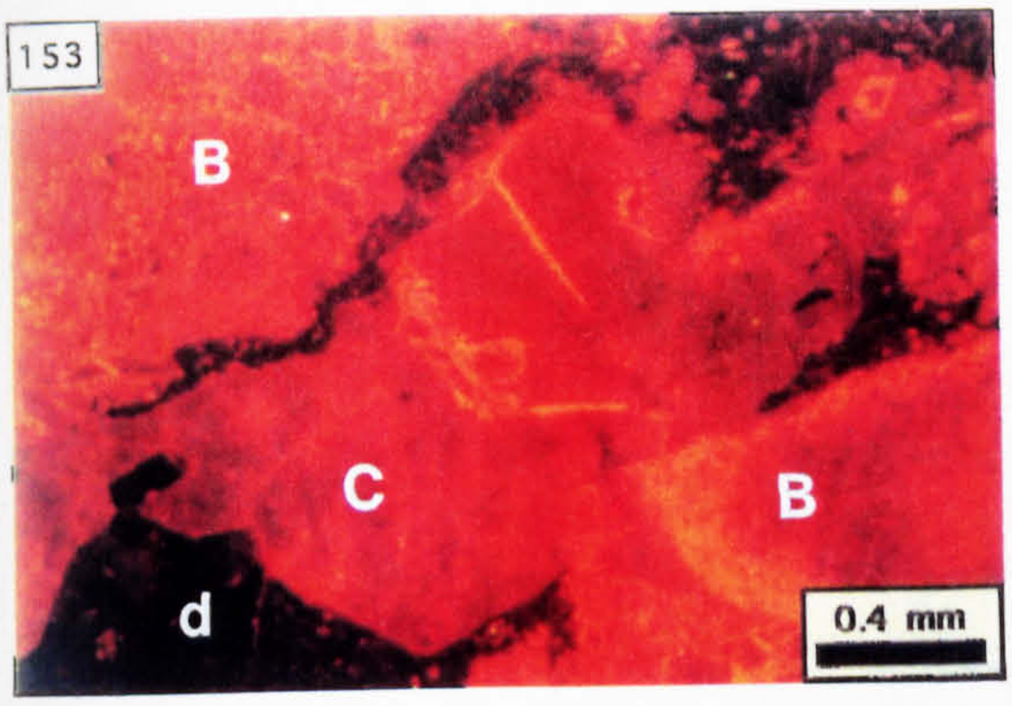
153
B
C
B
d
0.4 mm

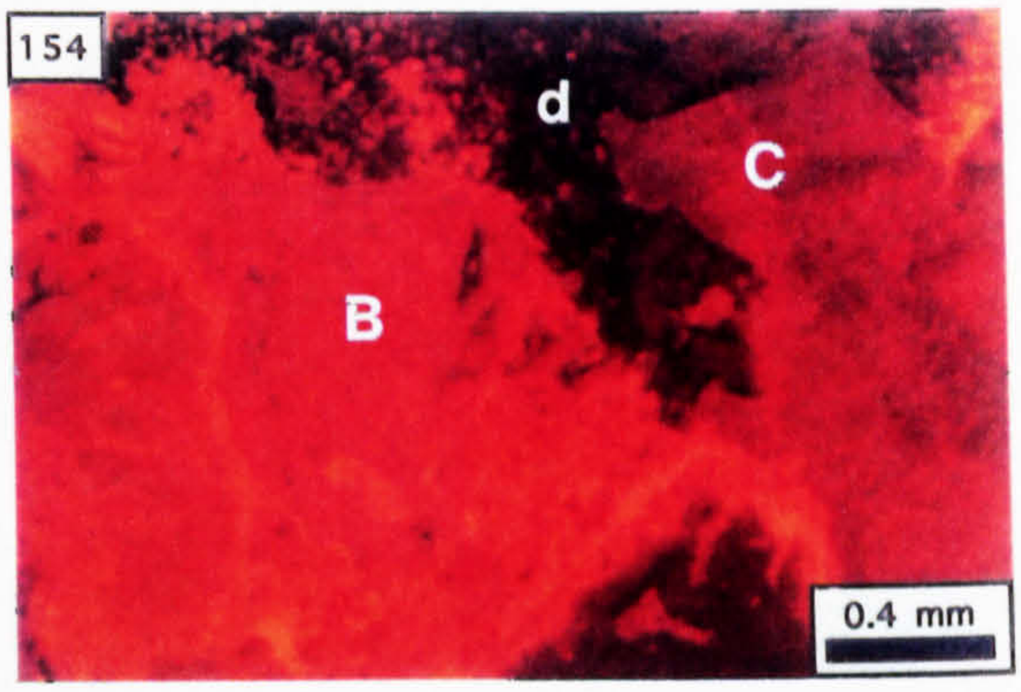
154
d
C
B
0.4 mm

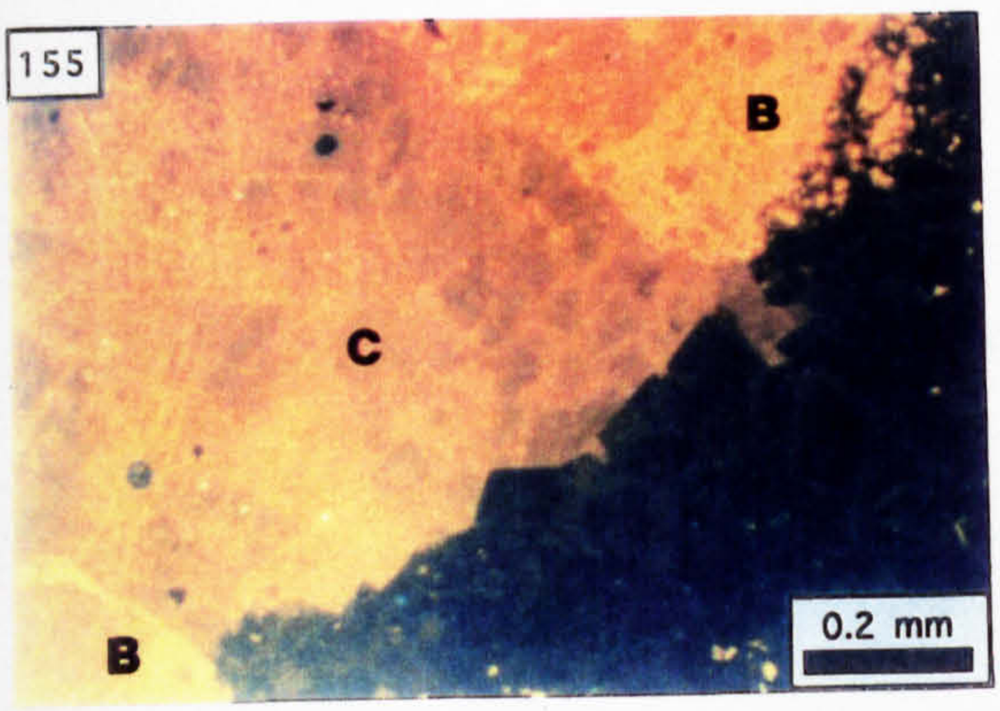
155
B
C
B
0.2 mm

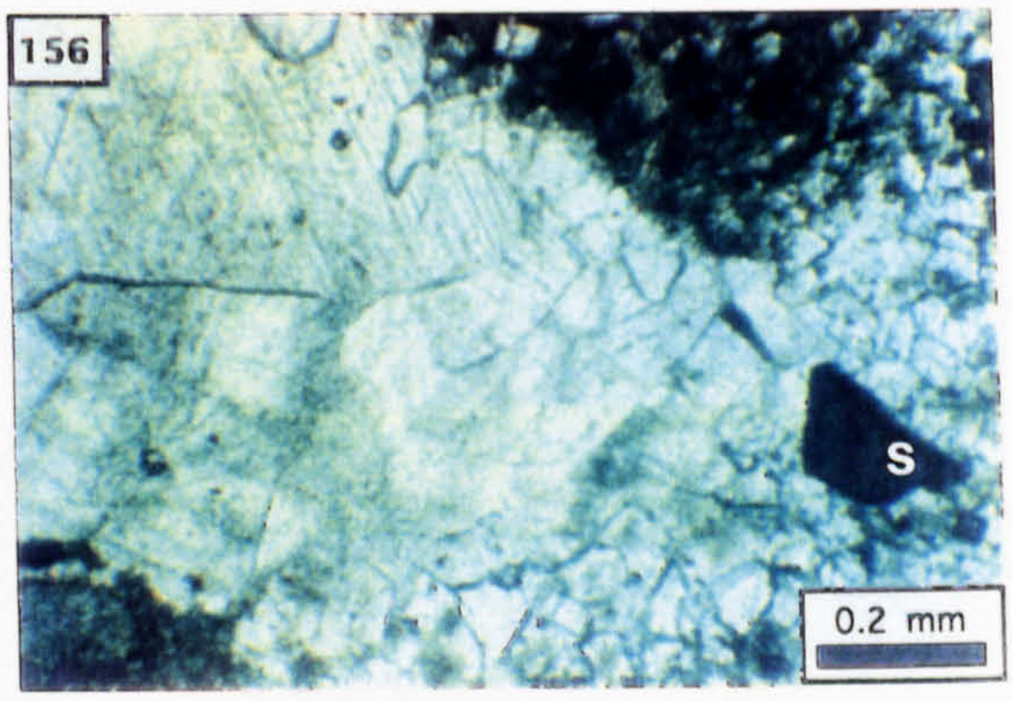
156
S
0.2 mm

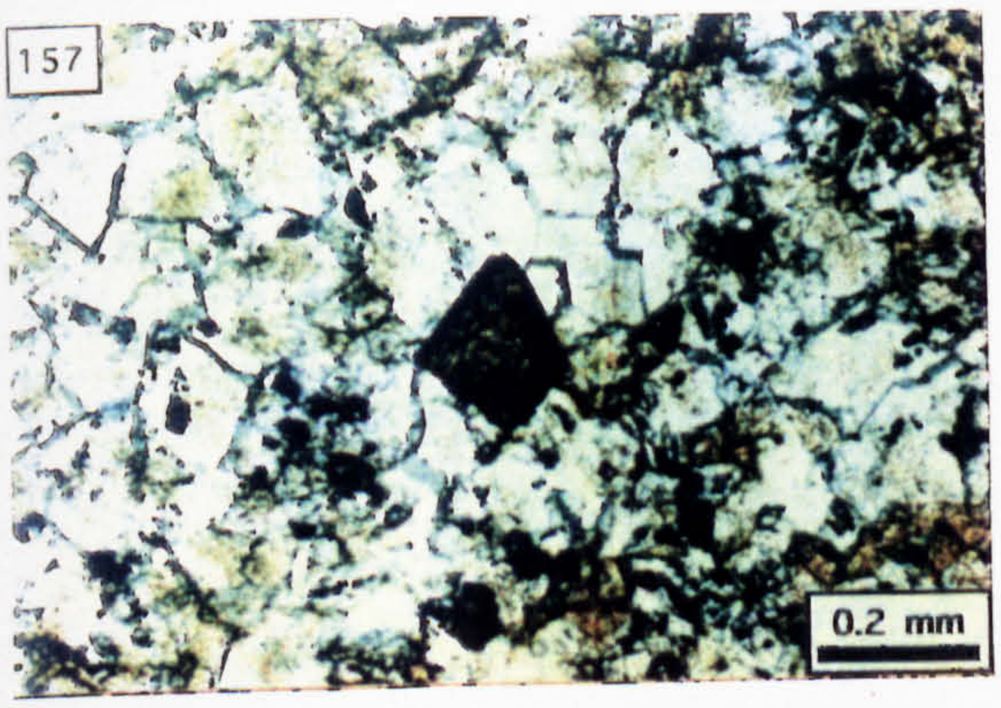
157
0.2 mm

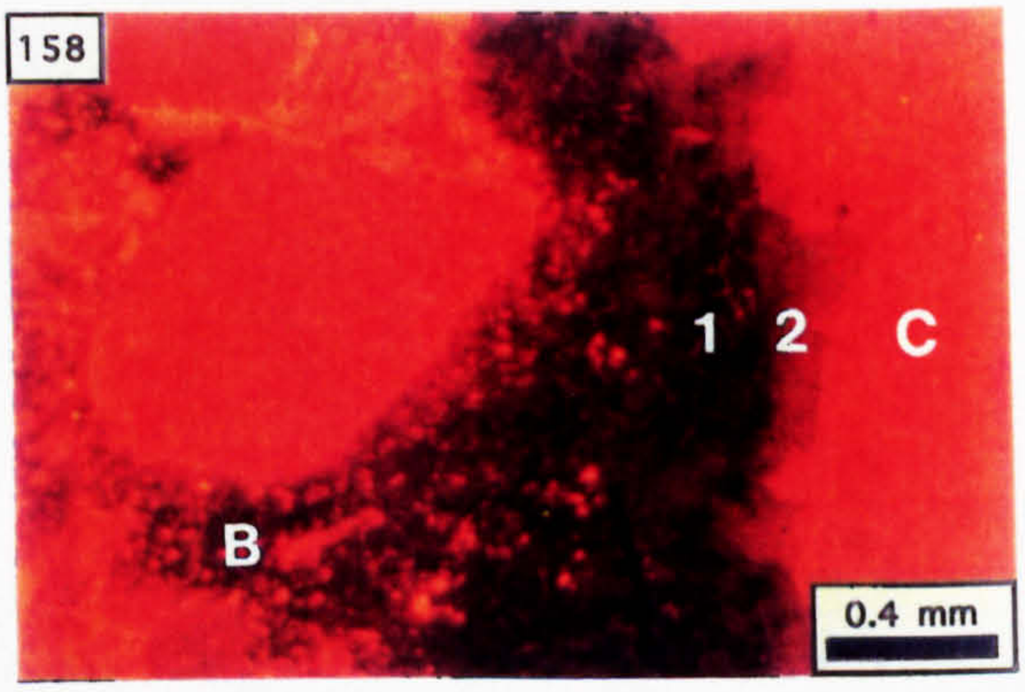
158
1 2 C
B
0.4 mm

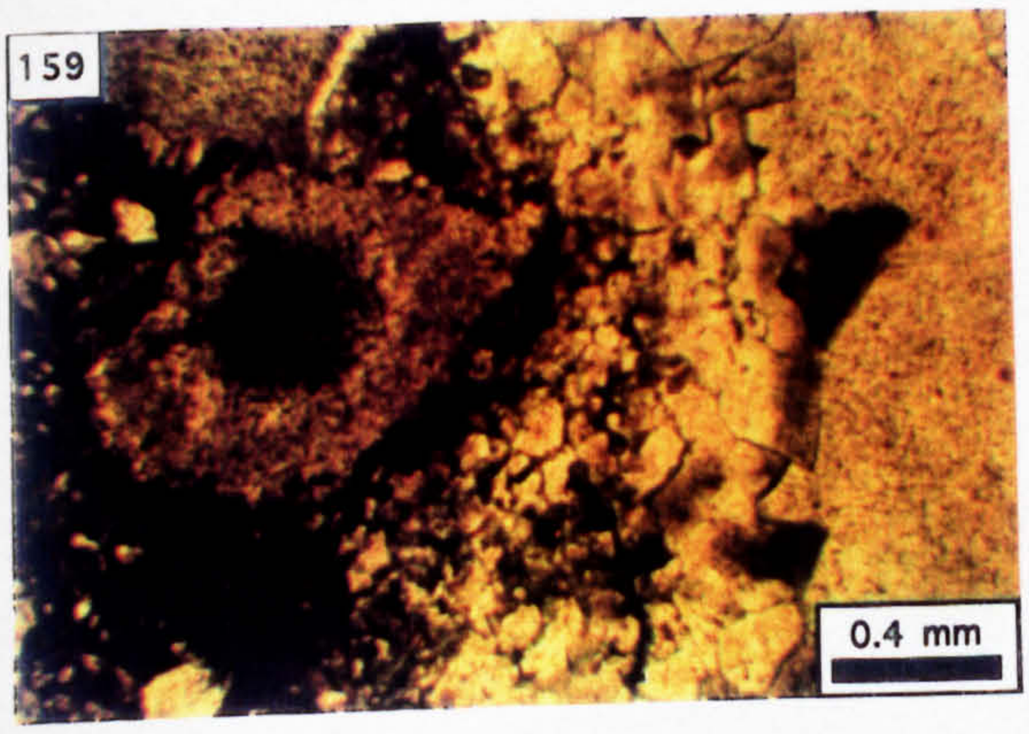
159
0.4 mm

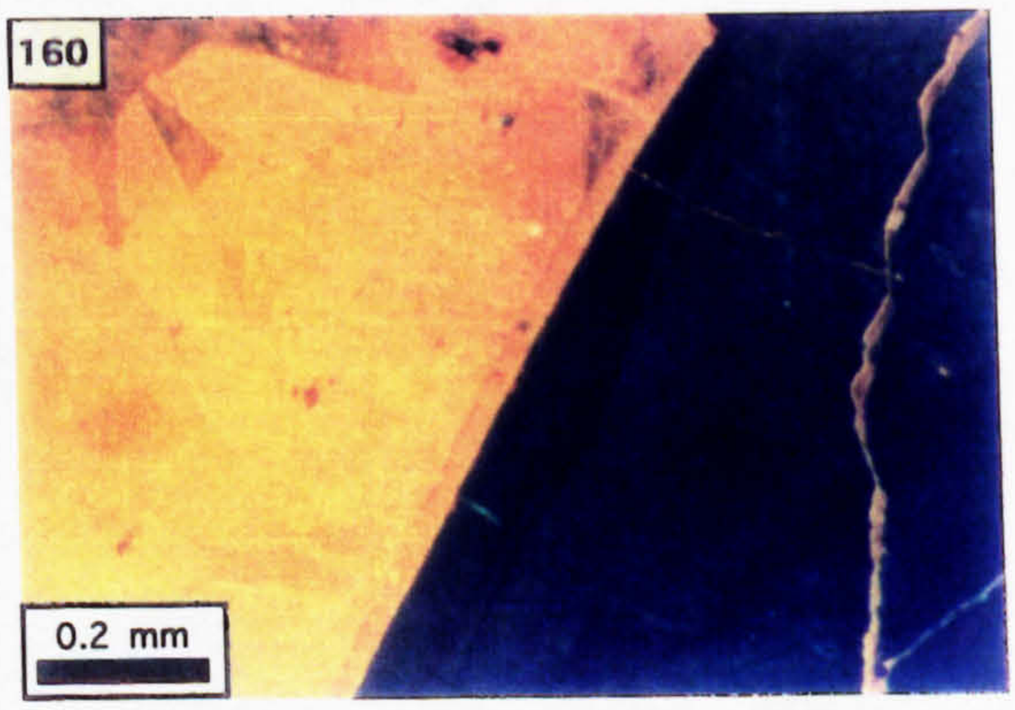
160
0.2 mm

Photo. 161. Wauslortian Limestone breccia in N1016 replaced by dark brown dolomite.

Photo. 162. Waulsortian Limestone breccia showing clasts of limestone in a groundmass of argillite (A) and dolomitic argillite (D) [N793].

Photo. 163. Close up of the Waulsortian Limestone breccia showing the spatial relationship of the dolomitic argillite (D) with argillite (A) in the groundmass to the clasts (N1016).

161

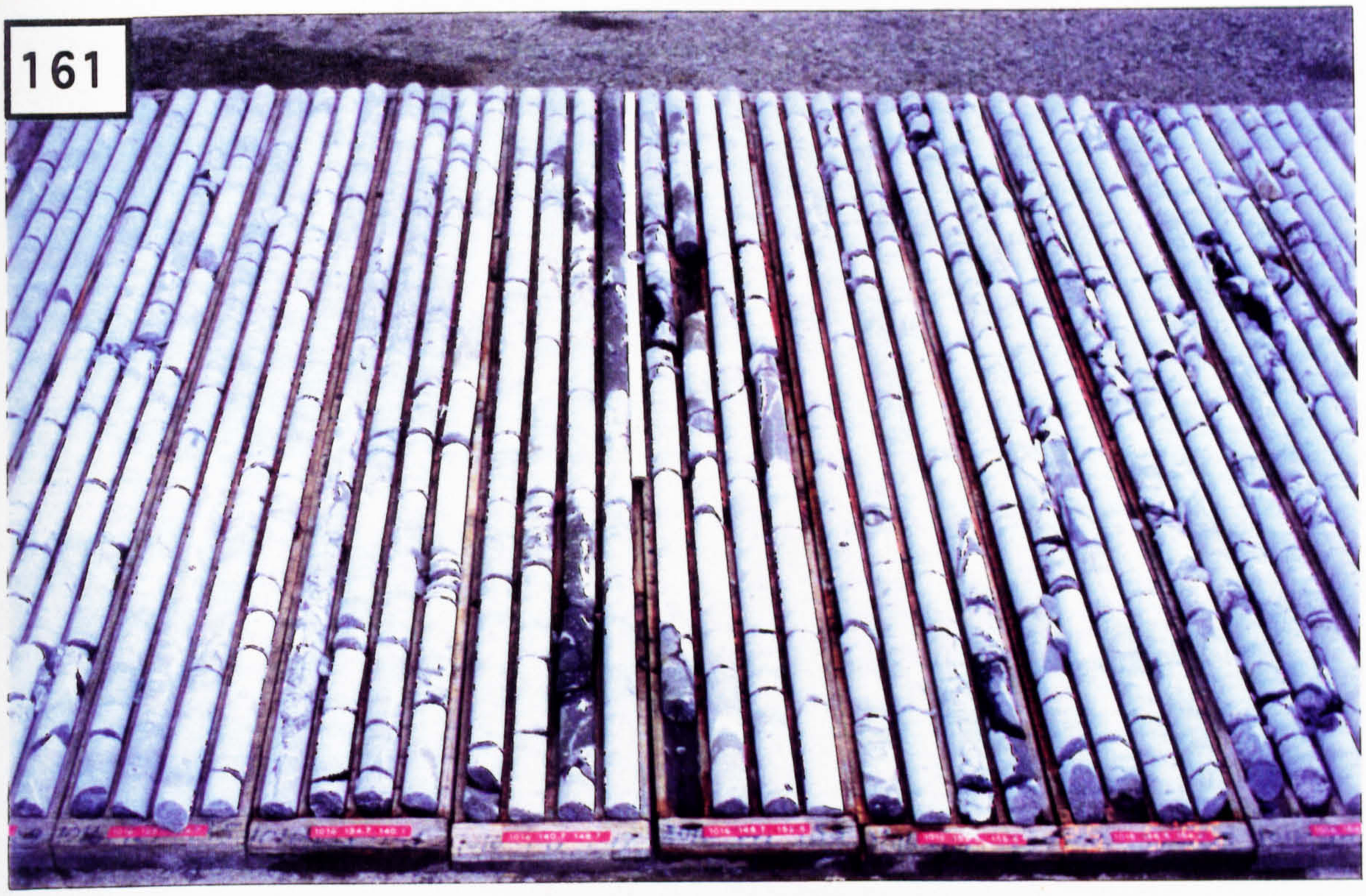

162

163

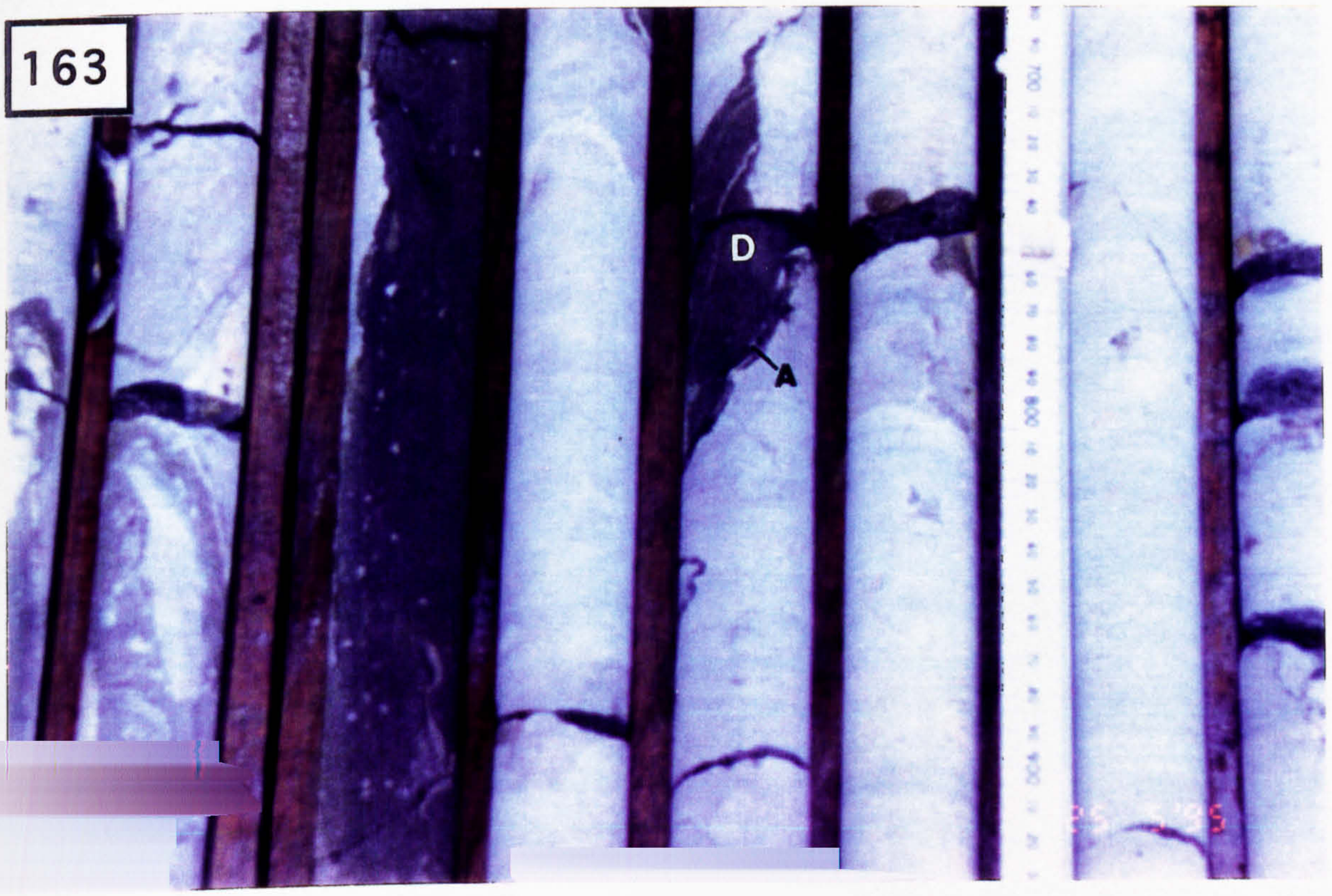

Photo. 164. Clast petrography of the W.L. breccia showing the development of sparite as a radiaxial fringe to bioclasts (XPL; N1016, 143.7 m).

Photo. 165. Matrix to the W.L. breccia showing clasts of mudstone (M) supported by argillite; notice the sharp contact with the clast (C) and the clast-parallel fabric (PPL; N1016, 143.7 m).

Photo. 166. Dolomite associated with the matrix to the W.L. breccia; notice the elongated, clast-parallel shape of the large dolomite crystal and the occurrence of intracrystalline microfractures which are cemented by dolomite; C=W.L. clast (CL; N1016, 143.7 m).

Photo. 167. Dolomite crystals (d) fractured and offset by calcite micro--veins (CL; N1016, 143.7 m).

Photo. 168. Euhedral and blebby pyrite (pale yellow) within the matrix to the W.L. breccia (RL; N1016, 143.7 m).

Photo. 169. Dolomitic and pyritic argillite matrix traversed by fibrous calcite micro-veins in parallelism with the clast edge (CL; N1016, 143.7 m).

Photo. 170. Coarse, subhedral dolomite (d) occupying irregular vugs along the corroded edge of a W.L. clast (C) [CL; N1016, 143.7 m).

Photo. 171. Intensely dolomitised W.L. clast (CL; N1016, 143.7 m).

Photo. 172. Dolomitised sparite from the clast interior (CL; N1016, 143.7 m).

Photo. 173. Detail of Photo. 170 showing intracrystalline microfractures which cut through vug-filling dolomite located along the corroded edge of a W.L. clast (CL; N1016, 143.7 m).

164

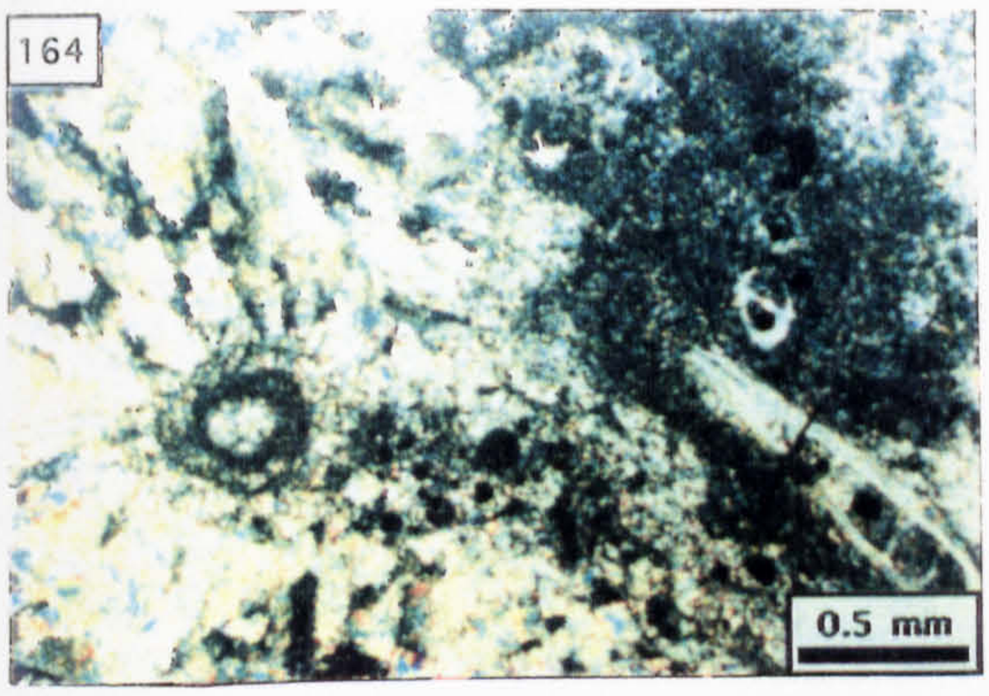

165

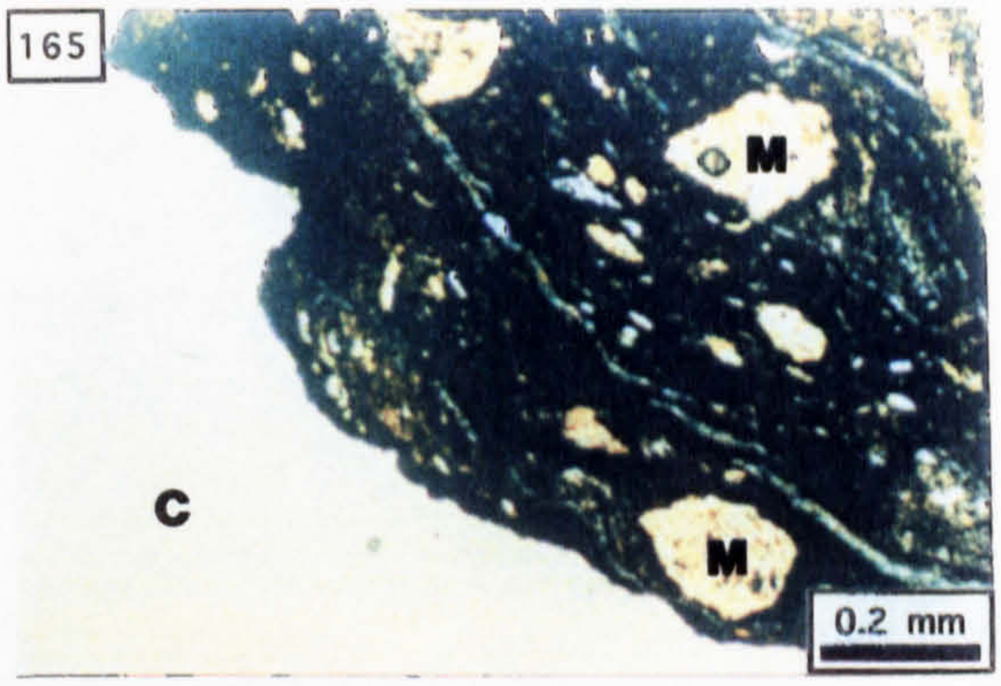

166

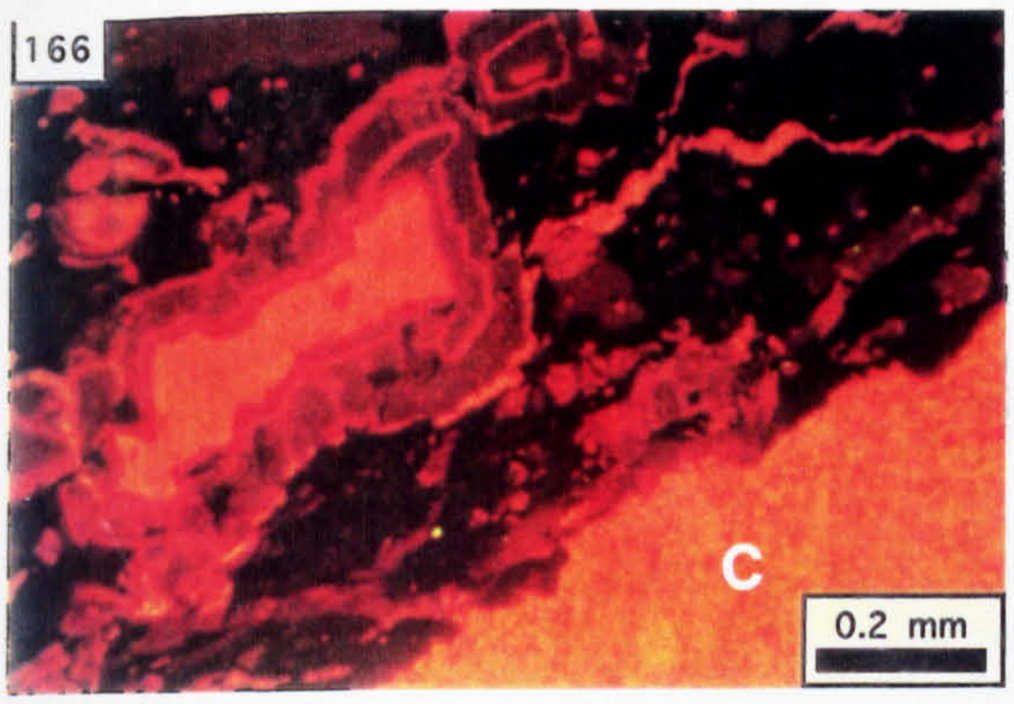

167

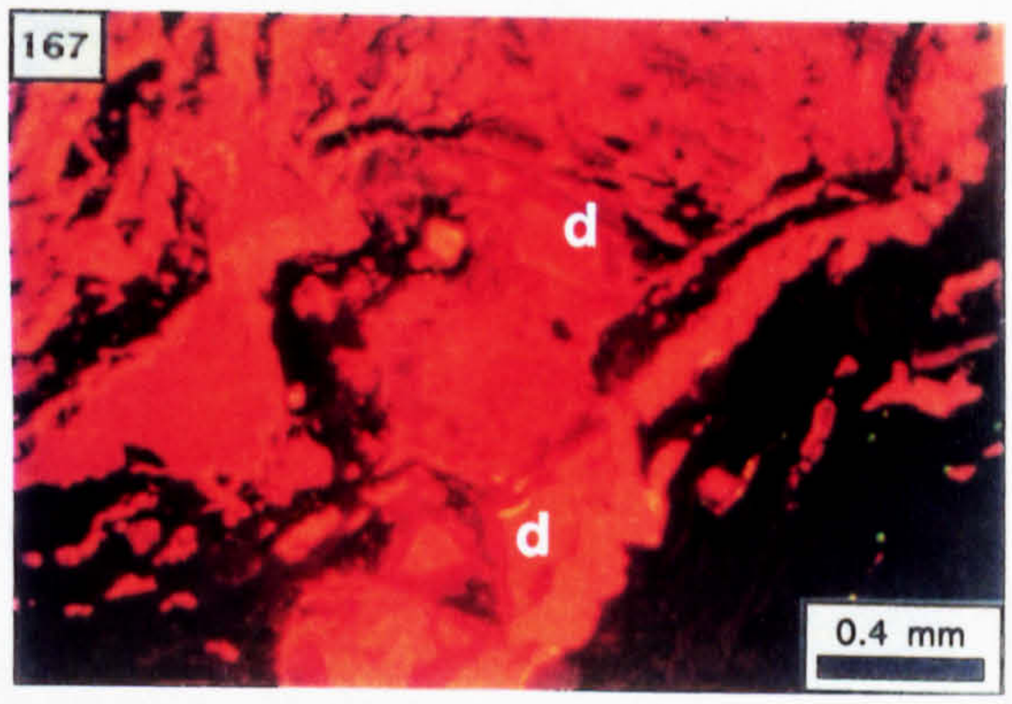

168

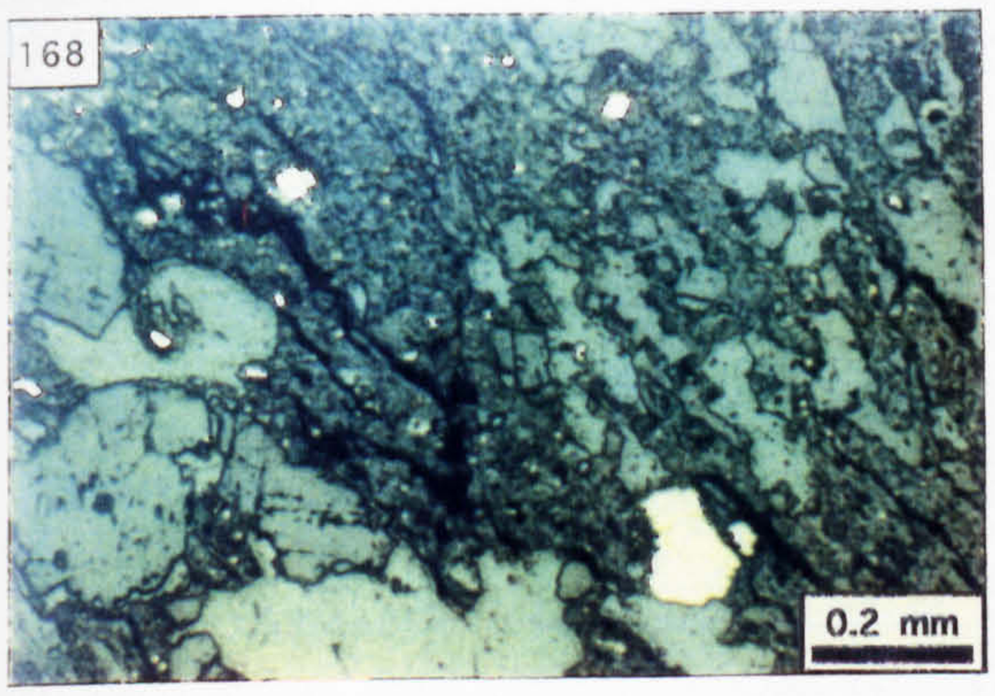

169

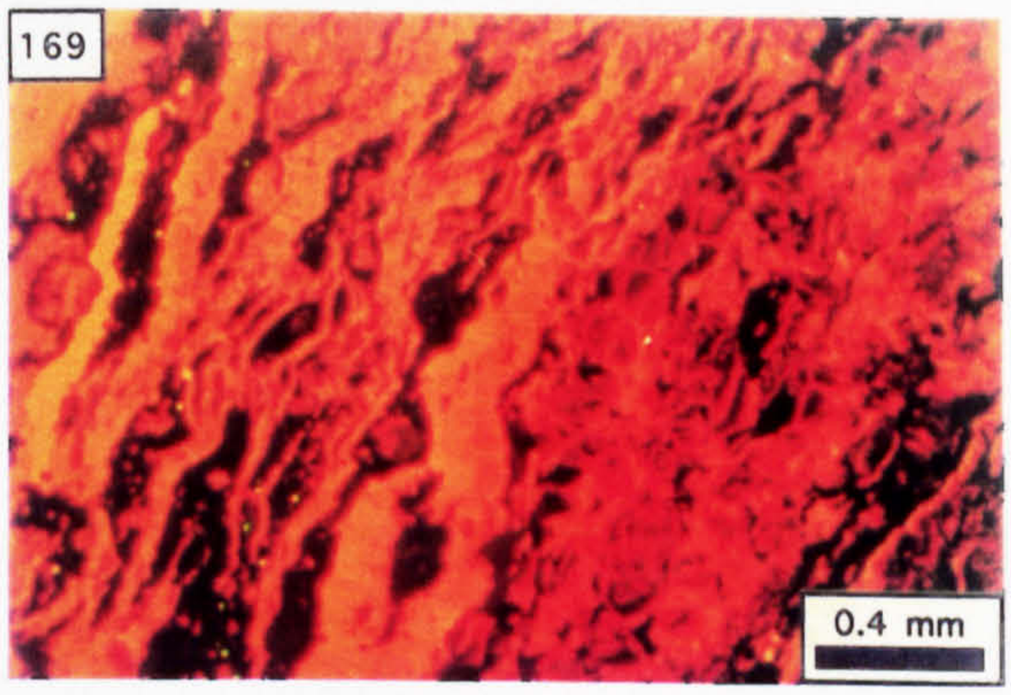

170

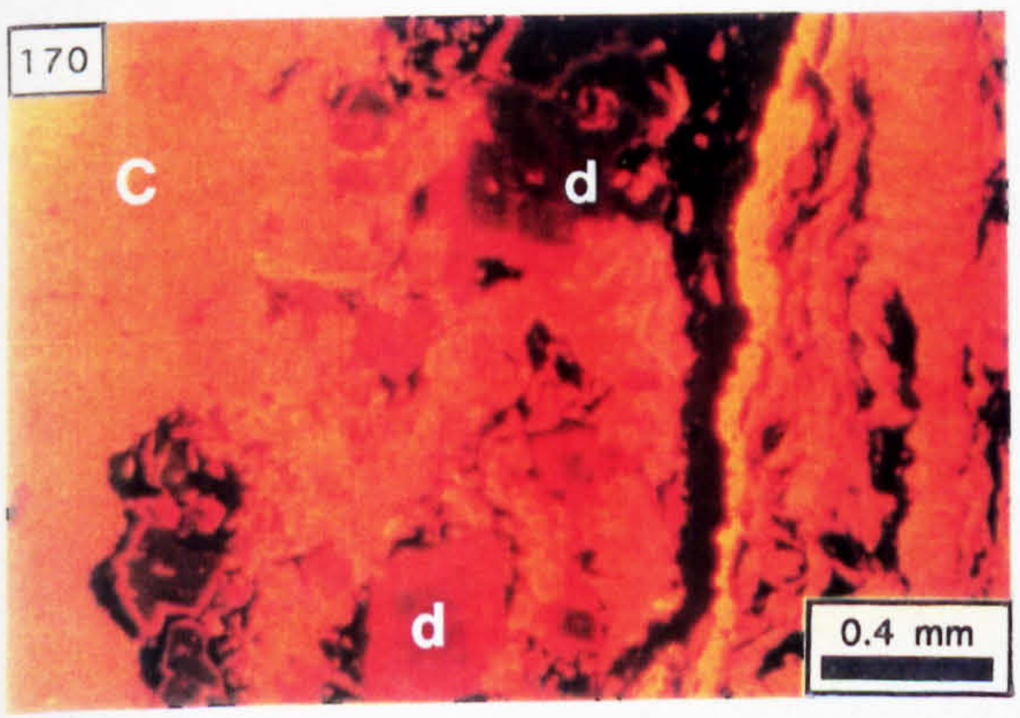

171

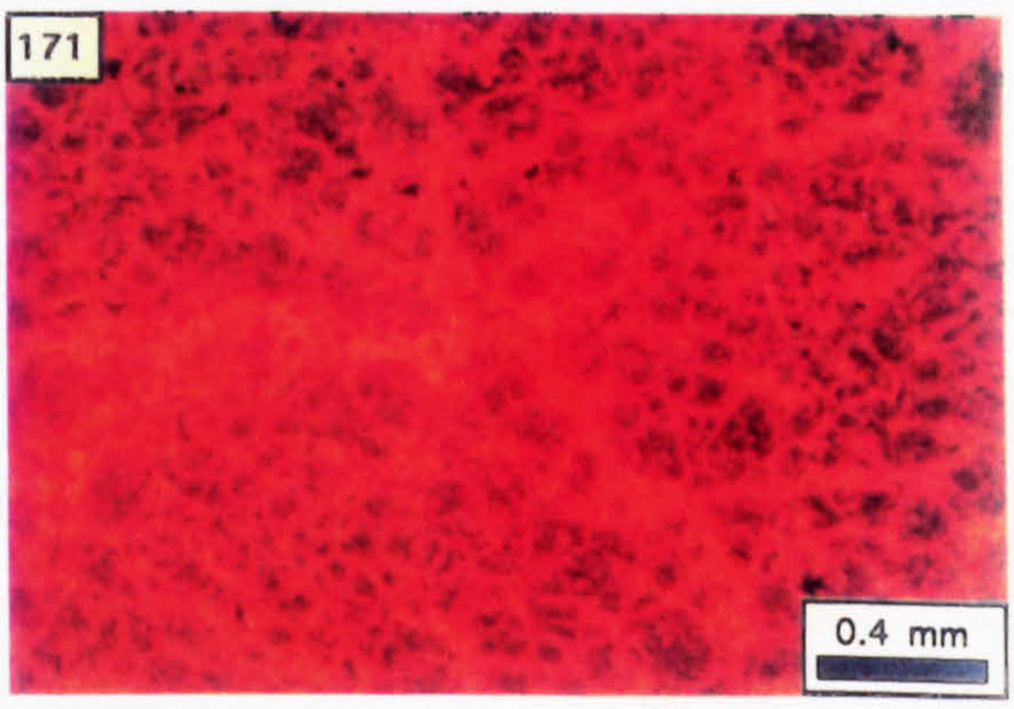

172

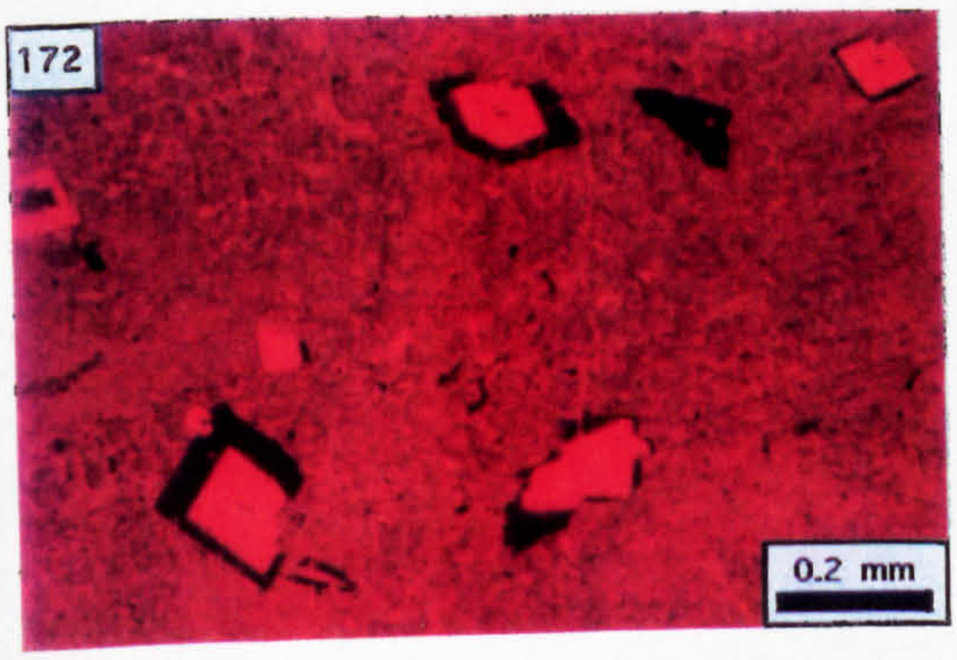

173

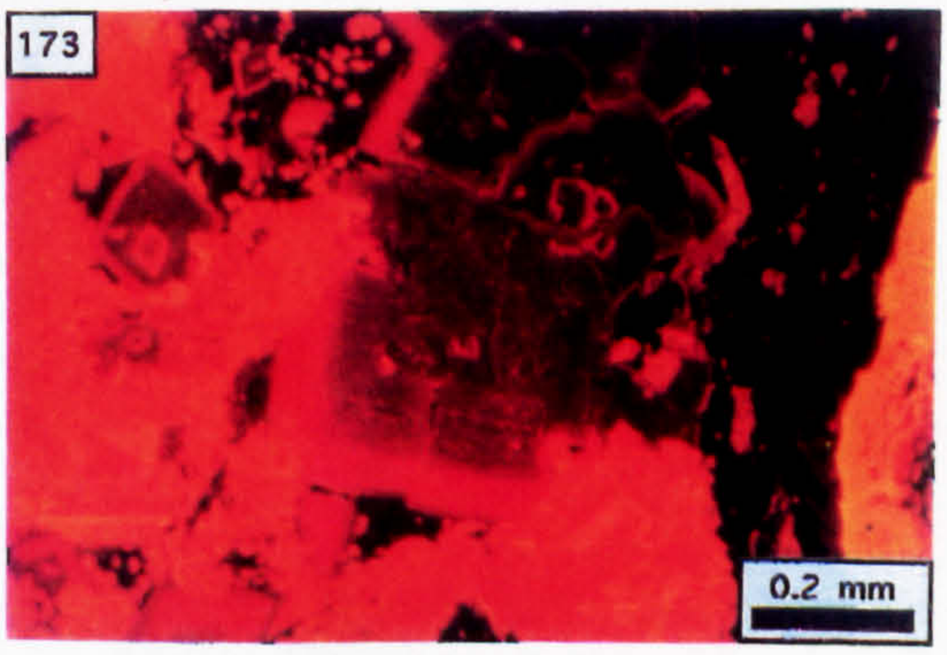

Photo. 174. Microfractured vug-filling dolomite (CL; N1016, 143.7 m).

Photo. 175. Colour photo-negative of Photo. 171 showing a dolomite vein (d) through dolomitised W.L.; the vein dolomite occurs as a syntaxial overgrowth to the dolomite present in the fracture walls. Both dolomites are truncated by a sparite vein (s) [CL; N1016, 143.7 m].

Photo. 176. Void-filling dolomite (V) in 36.5 mm diameter drillcore (N823, 150.5 m).

Photo. 177. Detail of the void-filling dolomite shown in Photo. 176; a=argillite, A=Dol. A., B=Dol. B., C=Dol. C., o=unoccluded porosity, d=dolomite rim (2 cm scale bar).

174

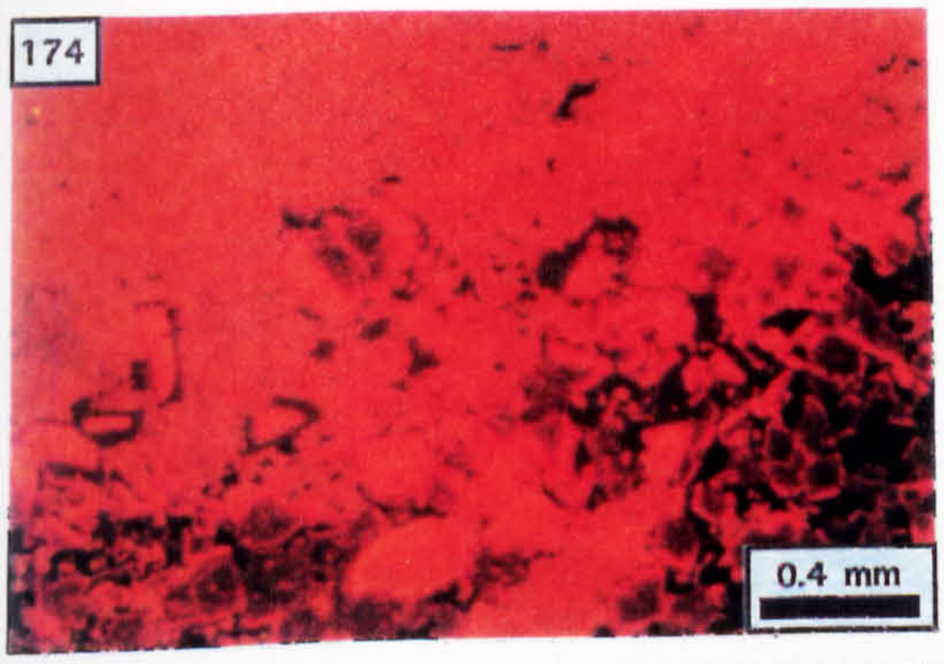

175

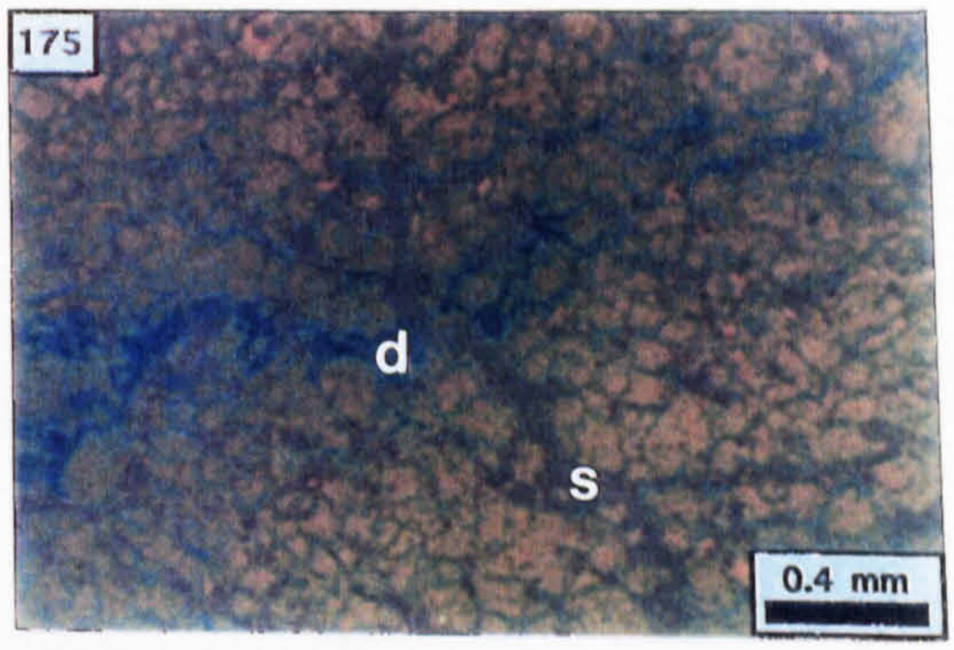

176

177

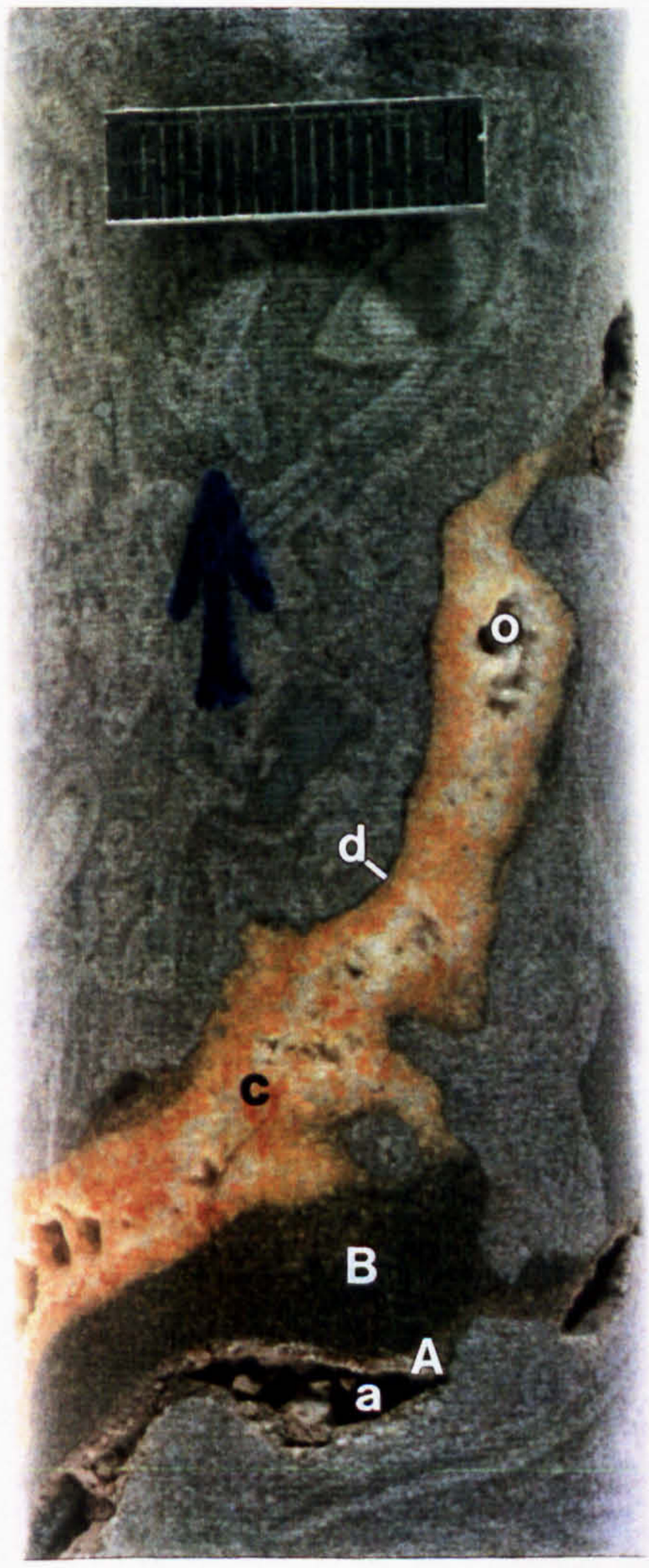

Photo. 178. Petrography of the Waulsortian Limestone wallrock to the void showing radiaxial sparite cement developed as a fringe around bioclasts (PPL; N823, 150.5 m).

Photo. 179. Petrography of the void floor showing fragments of sparite (orange grains) supported by argillite (a); the dark patches are areas where the argillite has been plucked from the thin section during prepation; the void wall comprises radiaxial calcite (r) [CL; N823, 150.5 m].

Photo. 180. As Photo. 179 but XPL to show the perpendicular relationship of the void wall with the axis of the radiaxial sparite fringe.

Photo. 181. Petrography of Dol. A.; the brown, intercrystal sediment is argillite (PPL; N823, 150.5 m).

Photo. 182. CL characteristics of Dol. A.; r=radiaxial sparite wallrock (N823, 150.5 m).

Photo. 183. Petrography of Dol. B.; p=pyrite (PPL; N823, 150.5 m).

Photo. 184. Fragments of sparite (s) supported by Dol. B.; note the irregularity of the radiaxial sparite (r) along the void margin (CL; N823, 150.5 m).

Photo. 185. Subhorizontal contact of Dol. A. with Dol. B. showing their different luminesces (CL; N823, 150.5 m).

Photo. 186. As above but PPL to show the association of pyrite (black grains) with Dol. B. (PPL; N823, 150.5).

Photo. 187. Dol. C. (C) developed as a syntaxial overgrowth to the subhorizontal, upper contact of Dol. B. (B); O=unoccluded porosity (XPL; N823, 150.5 m).

178

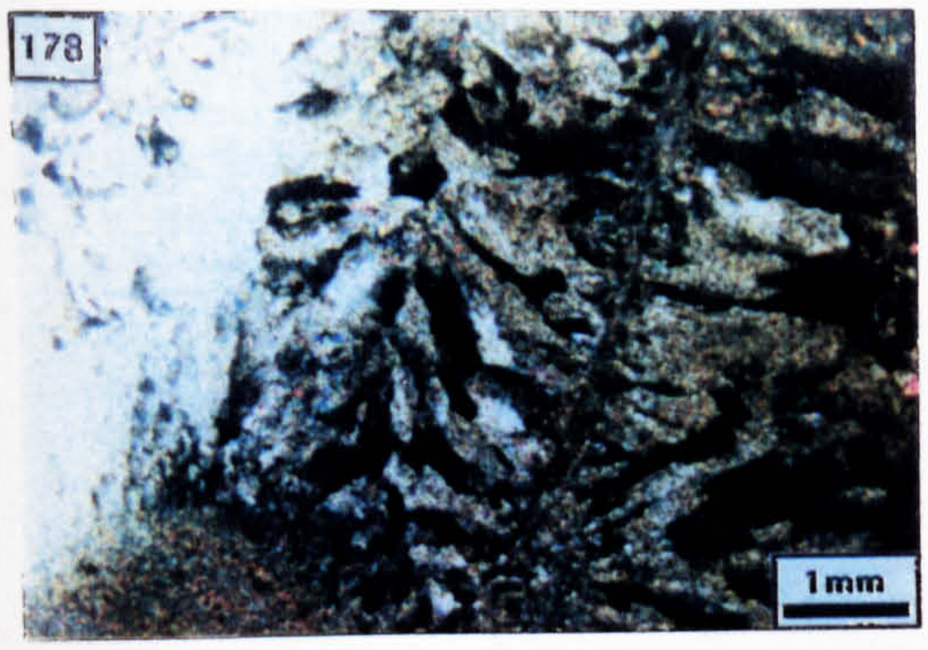

179

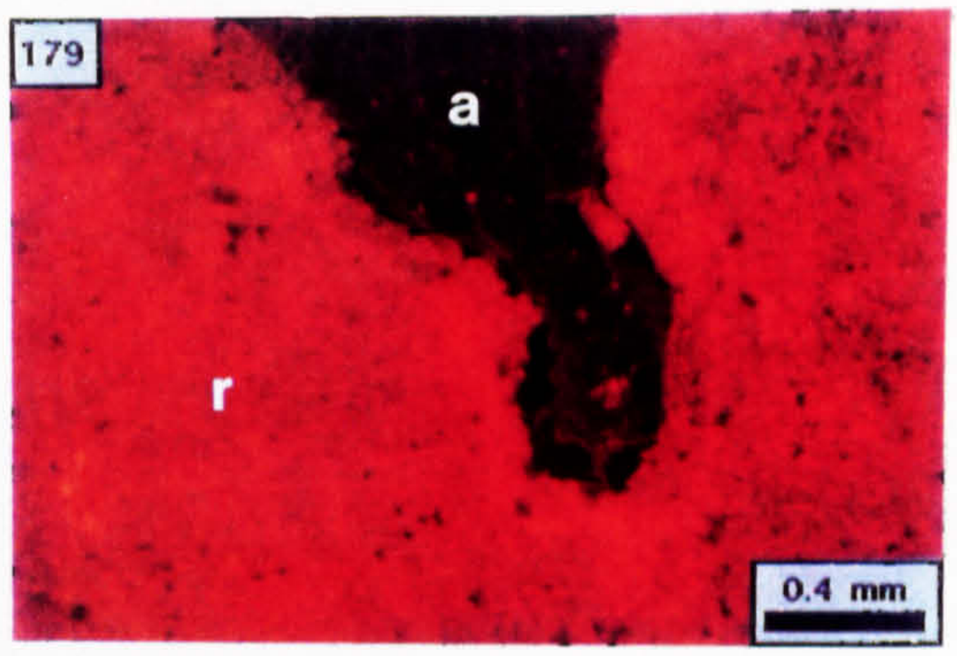

180

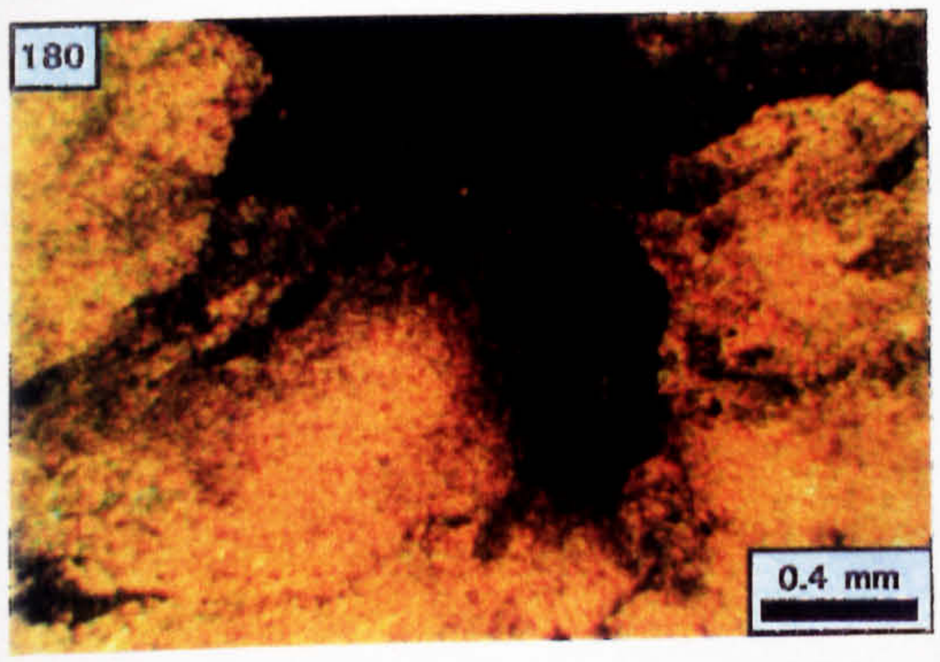

181

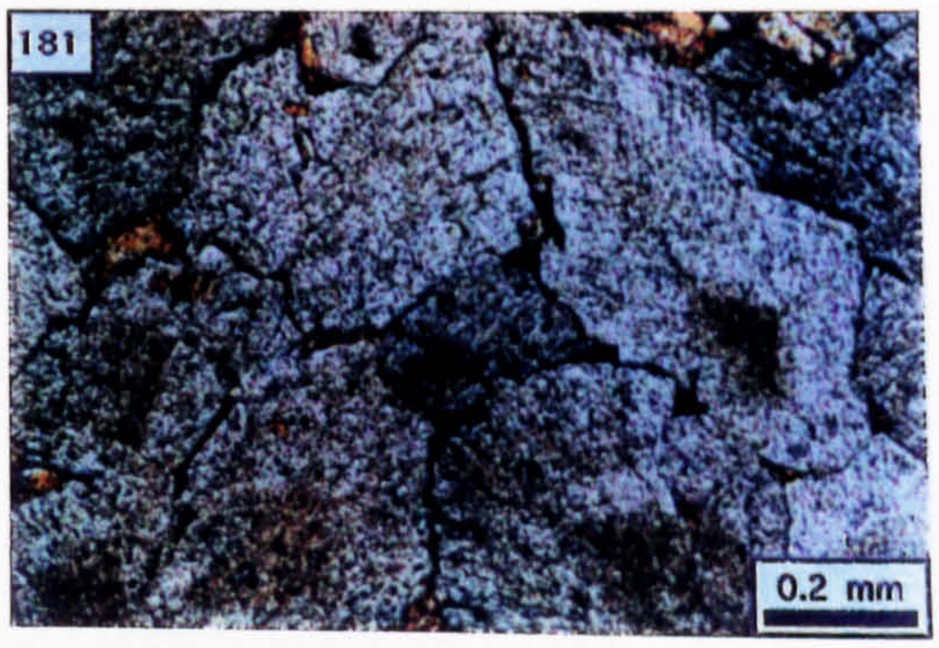

182

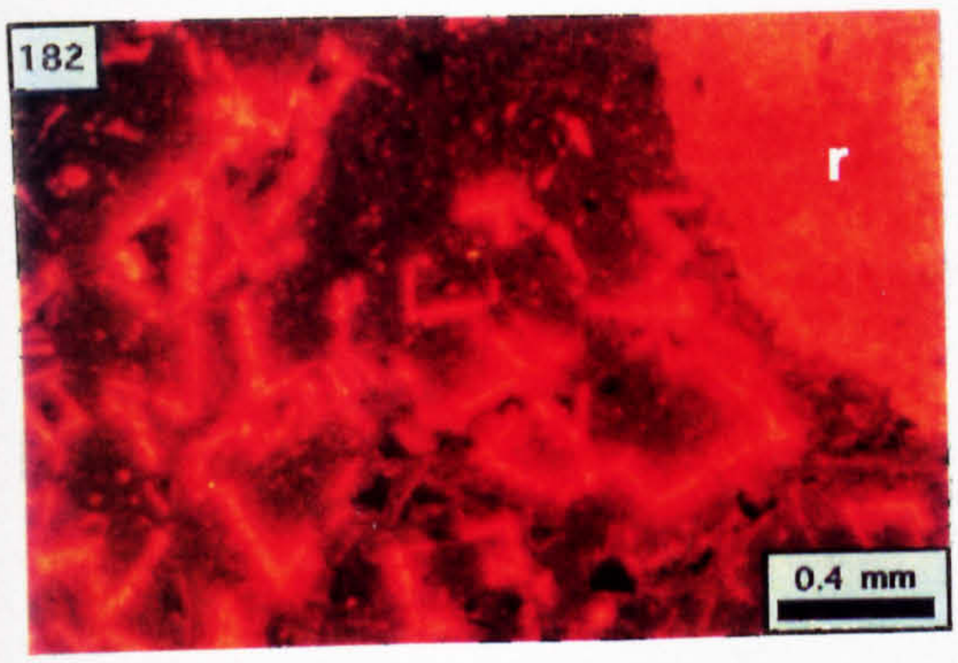

183

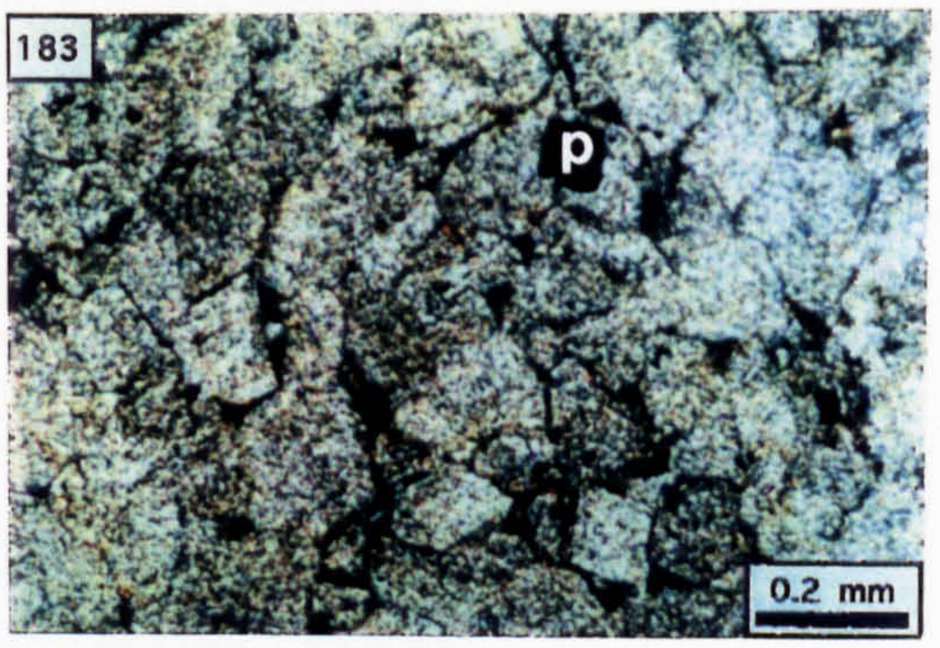

184

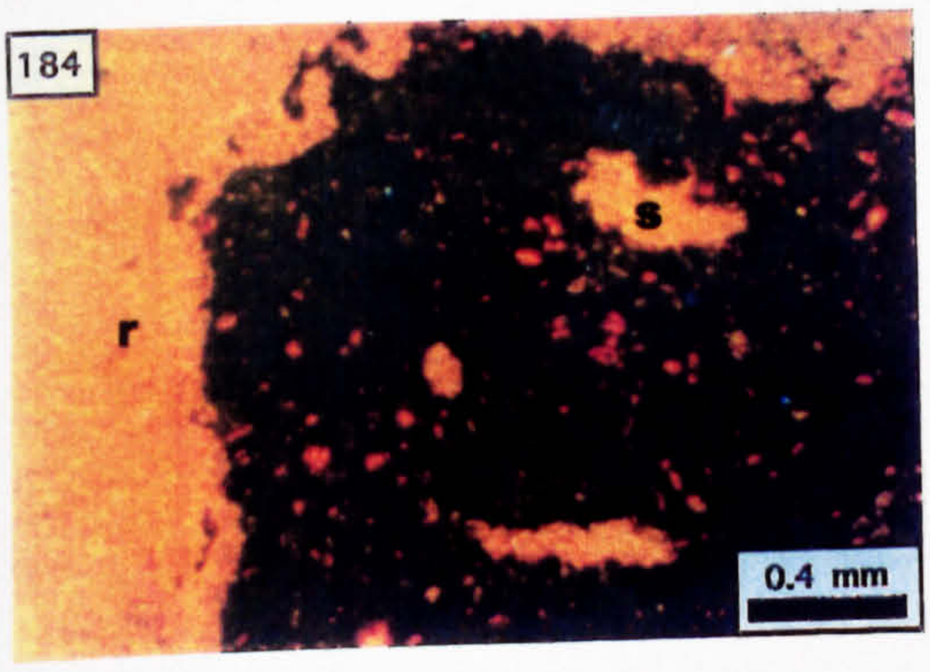

185

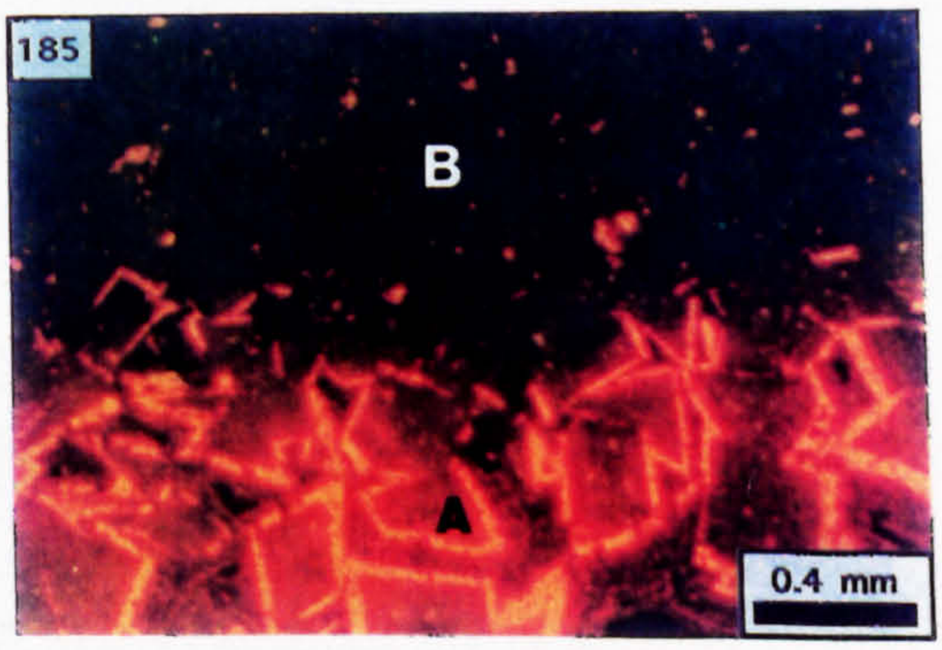

186

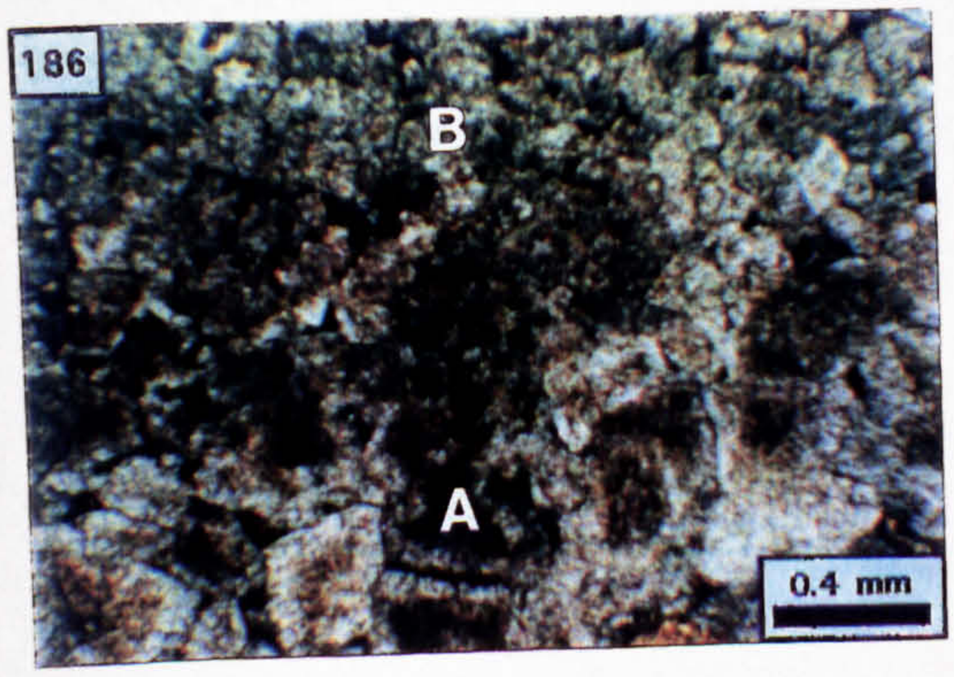

187

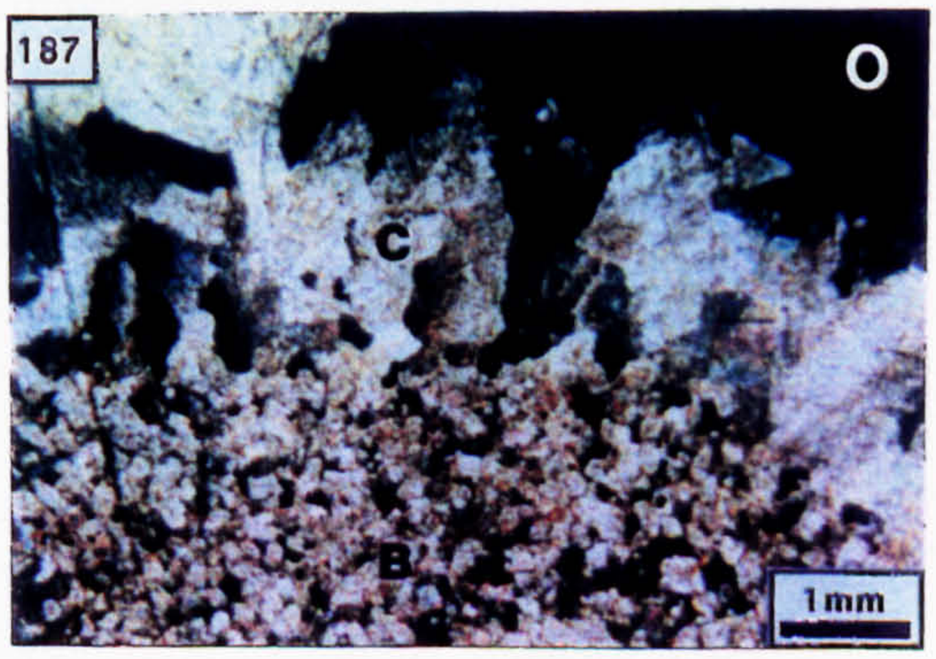

Photo. 188. CL characteristics of Dol. C. (C); B=Dol. B., O=unoccluded porosity (N823, 150.5 m).

Photo. 189. Dolomite rim (d) located between radiaxial sparite wallrock (r) and Dolomite C.; the non-luminescent grains are pyrite (CL; N823, 150.5 m).

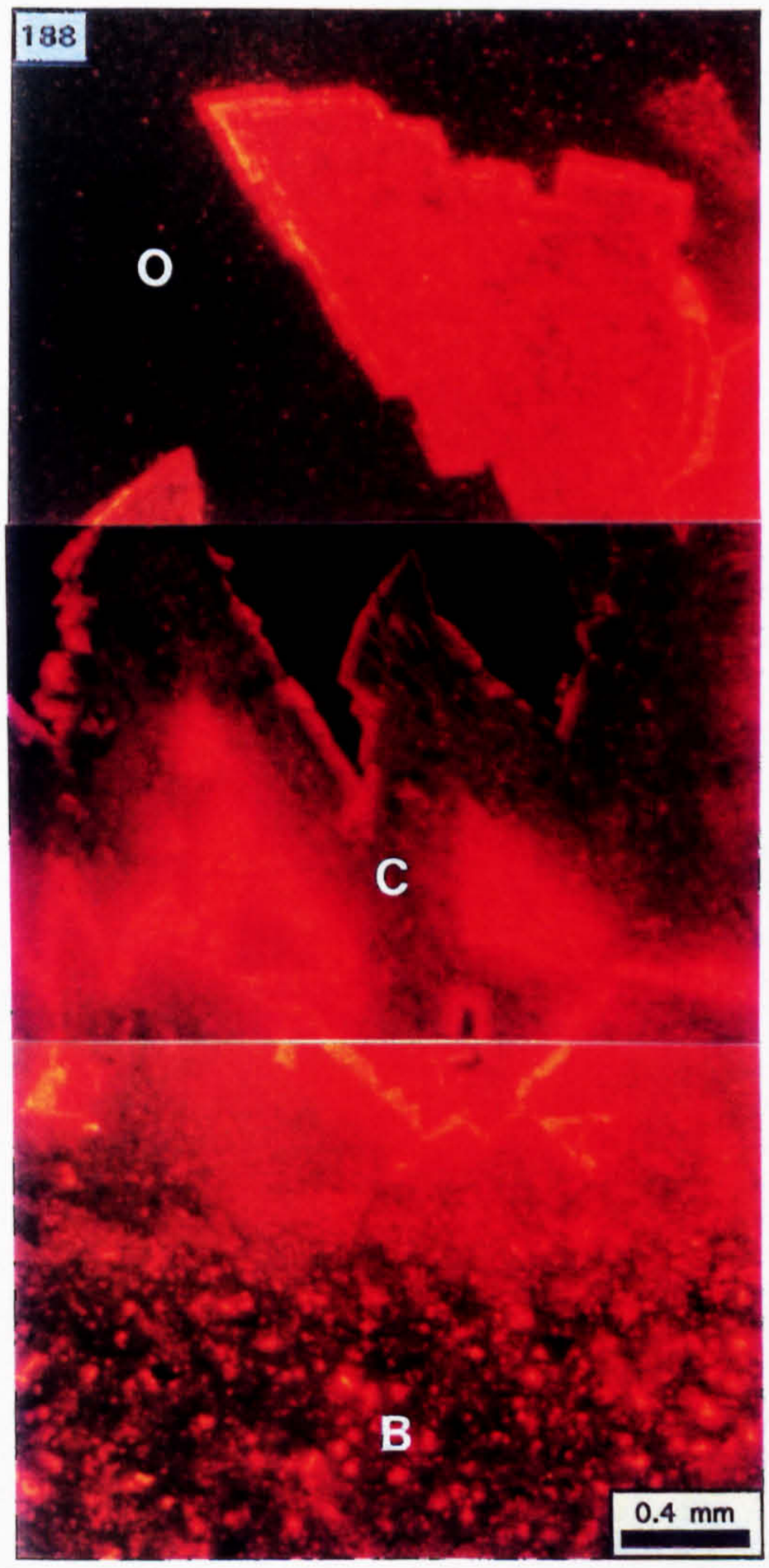
188
O
C
B
0.4 mm

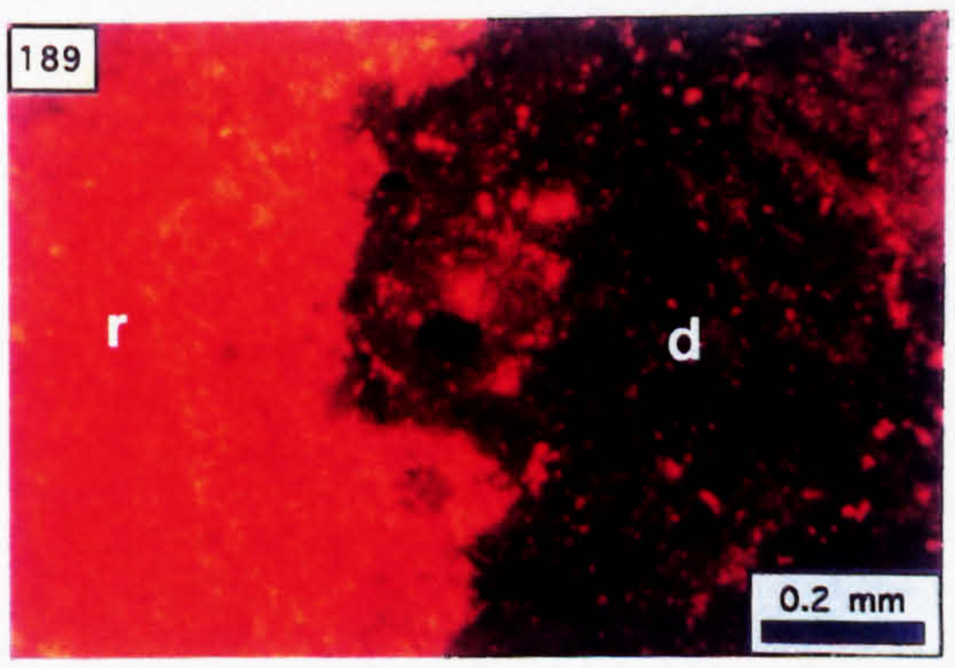
189
r
d
0.2 mm

Photo. 190. Underground photograph from 1390 340S showing Pale Beds Ore truncated by the unconformity and overlain by Boulder Conglomerate; the heading is located in the A-C-D Fault Complex: the steep dip of the unconformity is due to Variscan compression.

Photo. 191. Clast of ore from the Boulder Conglomerate exposed in the 1390 340S heading; notice the calcite veining which cuts across the ore, but is truncated at the clast edge (2 cm scale bar).

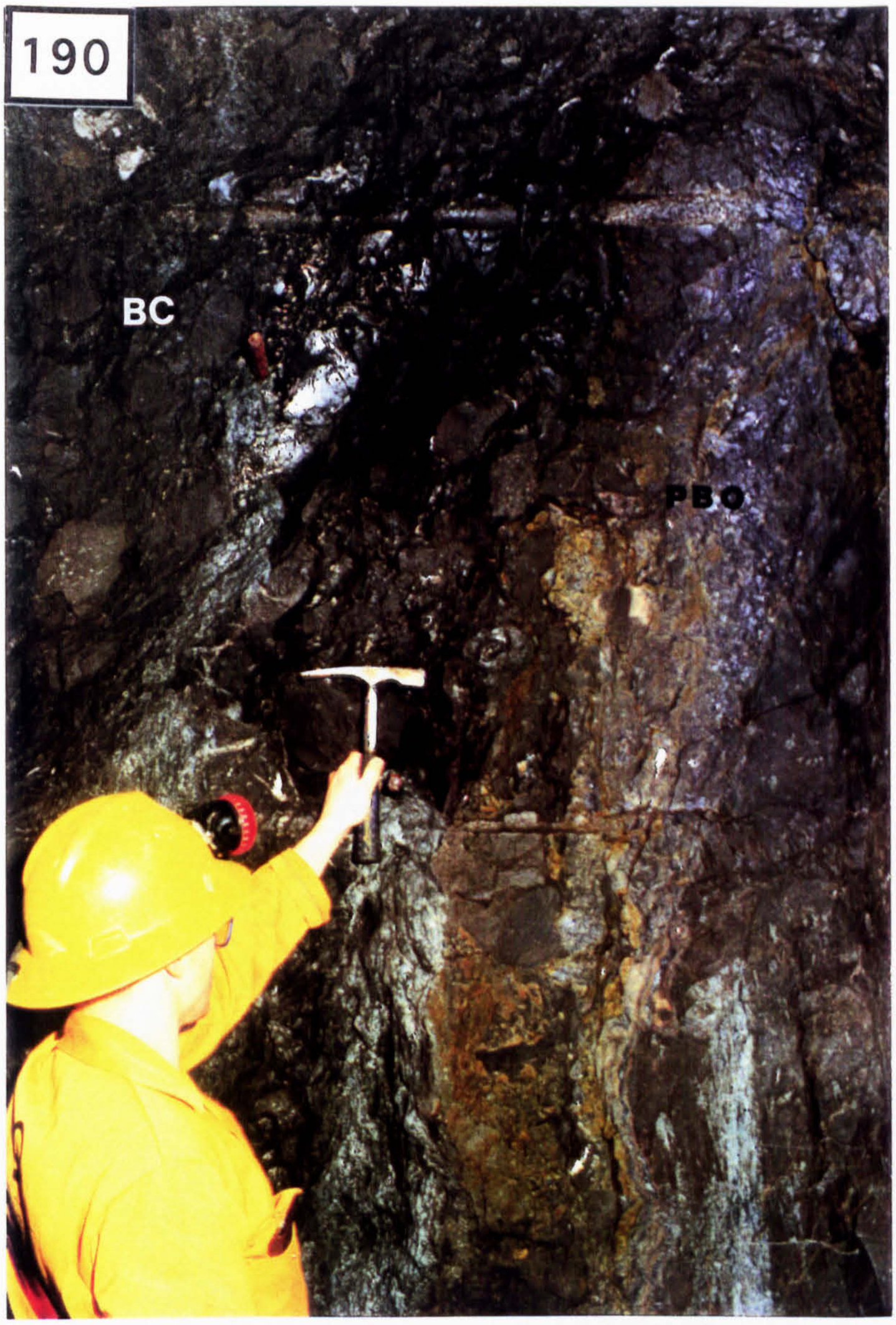
190
BC
PBO


191

Photo. 192. Clasts of micrite within the Boulder Conglomerate exposed in 1390 340S showing stratiform replacement by pyrite.

Photo. 193. Laminated mineralisation from location L in Photo. 41; laminae are defined by the ratio of sphalerite to barite and the colour of the sphalerite (PPL).

Photo. 194. Oolitic limestone replaced by pyrite, sphalerite and barite; the white grains are unreplaced siliciclastics which occur as nuclei to ooids (PPL).

Photo. 195. Silica overgrowth to a detrital quartz grain in the replaced oolite (PPL).

Photo. 196. Section through the void wall showing oolite replaced by pyrite, sphalerite and barite (1) which is overgrown by coarse sphalerite (2) and then sparite (3) [PPL].

Photo. 197. Calcite as cement to microfractures through replaced oolite (PPL).

Photo. 198. Petrography of the diagenetic and detrital assemblage which occludes the final void porosity defined by the margin of the attached sparite: 1=attached sparite, 2=sparite grains, 3=dolomite grains, 4=argillite matrix (PPL).

192

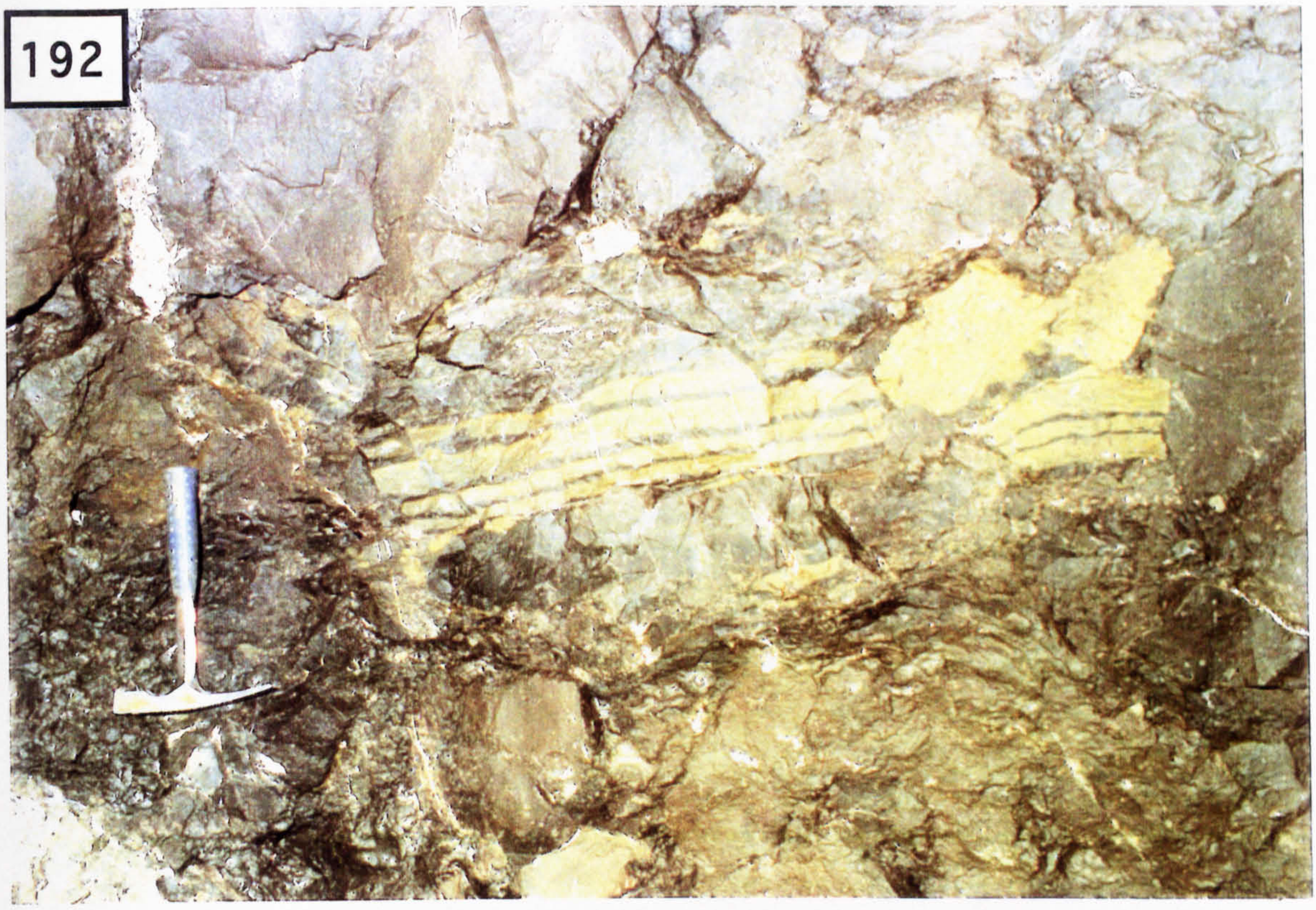

193

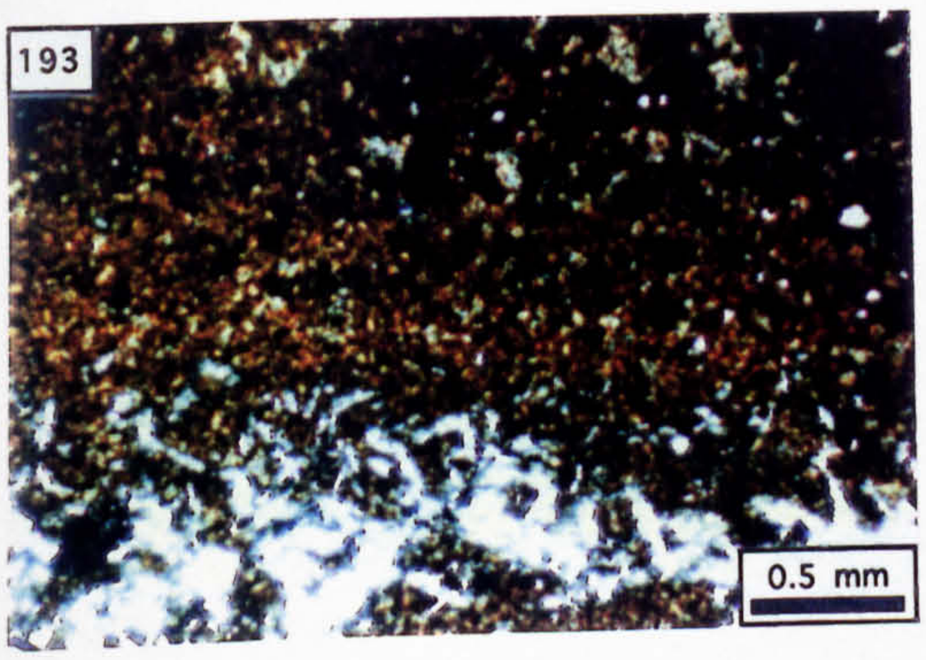

194

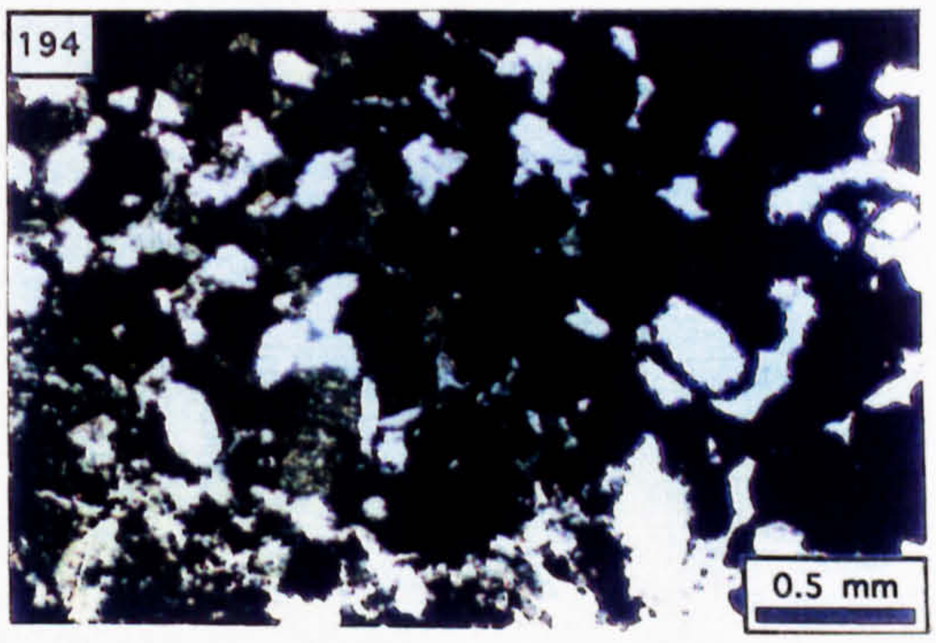

195

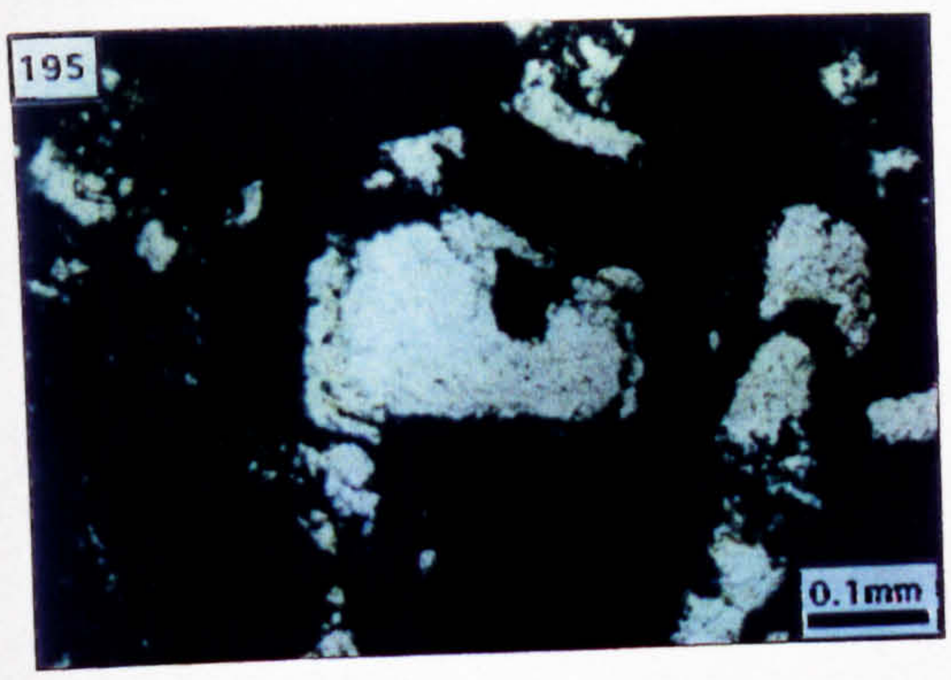

196

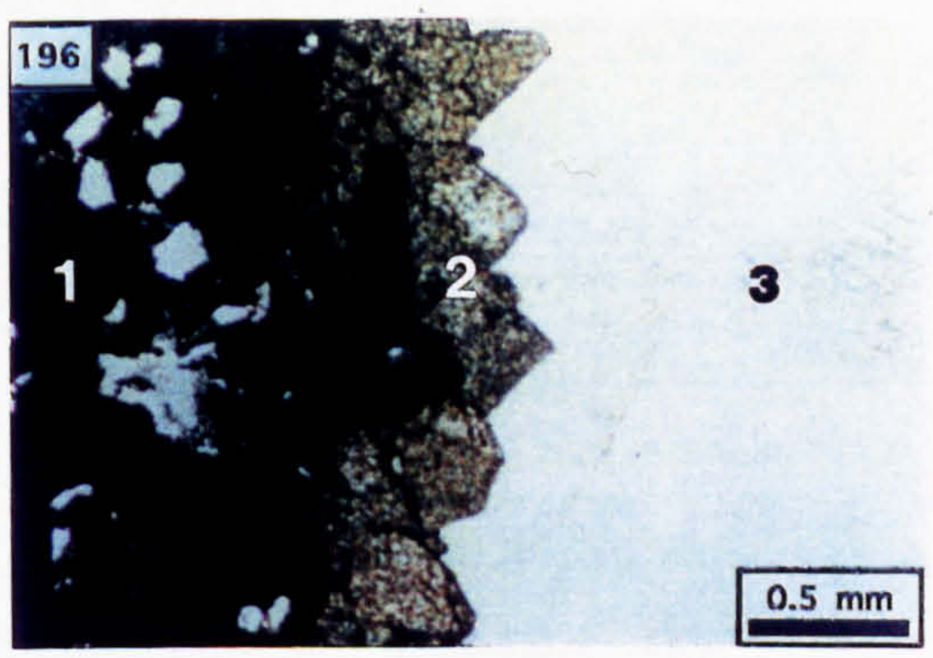

197

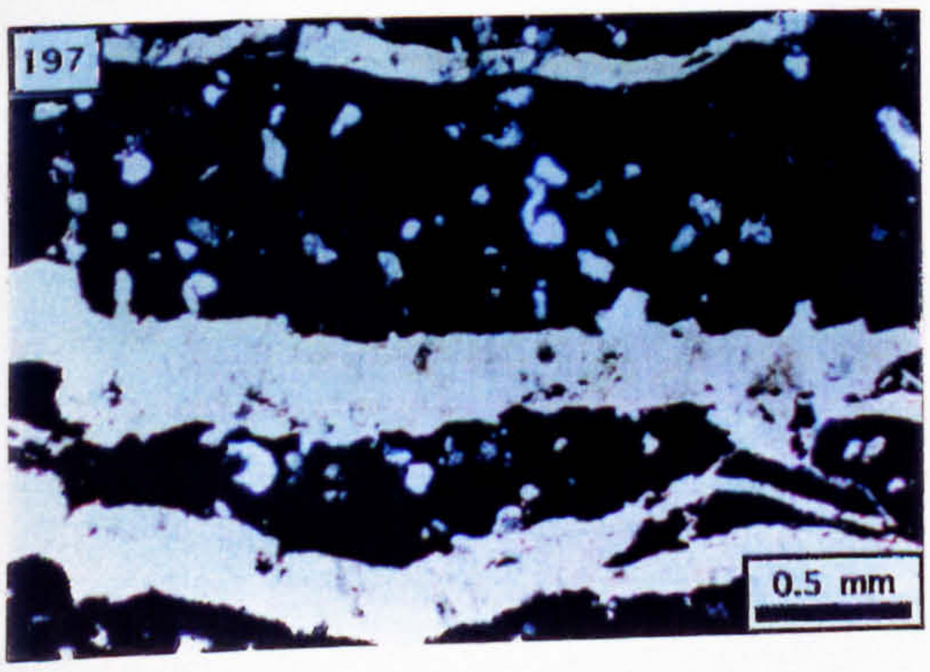

198

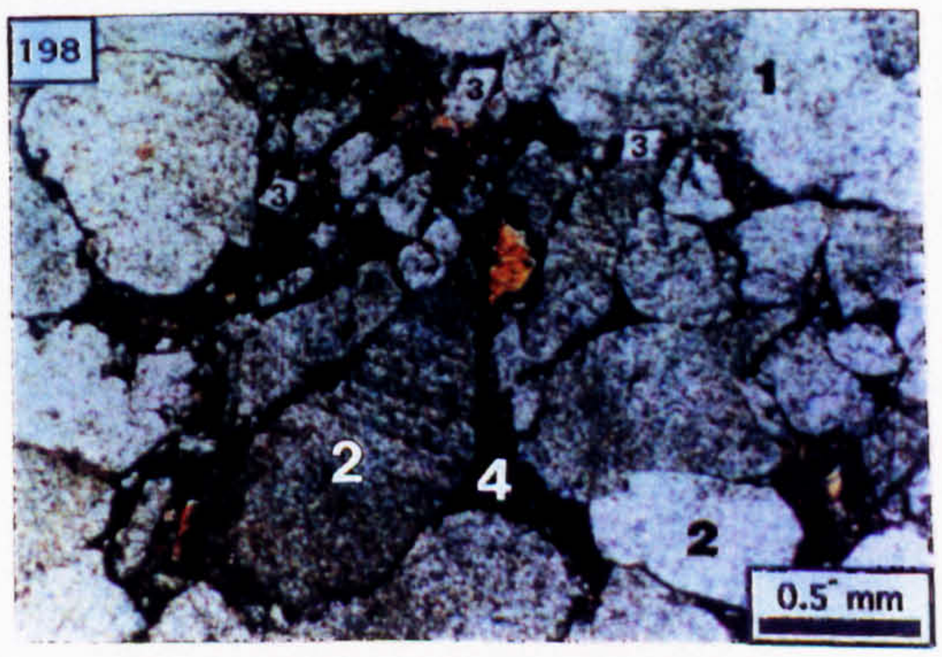

Photo. 199. Underground photograph of the Boulder Conglomerate exposed on the west sidewall of the P2 heading showing clasts of ore (O) from the clast-supported, polymict breccia deposited on the unconformity (U).

Photo. 200. Polished slab from the P2 heading showing clasts of ore and unmineralised Pale Beds (2 cm scale bar).

199

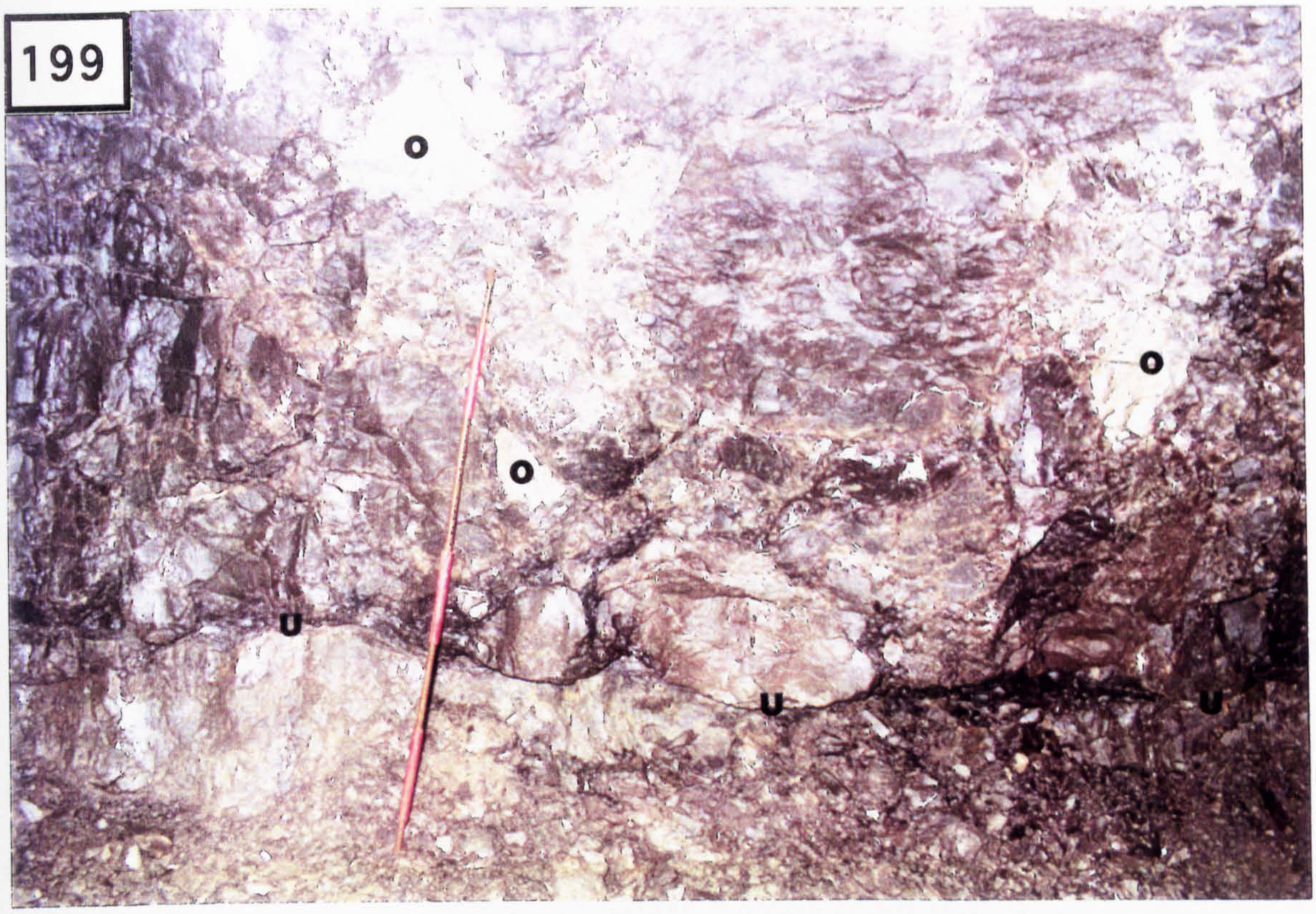

200

Photo. 201. Clast of partially replaced oobiosparite showing the association of mineralisation with an elongate vug (V) [PPL].

Photo. 202. Sphalerite (brown) and pyrite (black) replacement of the oobiosparite adjacent to the vug; the white grains are unreplaced siliciclastic ooid nuclei (PPL).

Photo. 203. Oobiosparite showing sphalerite developed as microcrysts around allochems and along intersparite boundaries (PPL).

Photo. 204. Void-rimming colloform sphalerite (c) and galena (g) [PPL].

Photo. 205. Petrography of the void-filling sediment (PPL).

Photo. 206. Oolitic limestone replaced by sphalerite (brown) and galena (black); the white grains represent unreplaced siliciclastic nuclei to the ooids (PPL).

Photo. 207. Sphalerite intergrown with galena (PPL).

Photo. 208. Dolomite and barite replacement of sphalerite (XPL).

Photo. 209. Colloform sphalerite delineating the void edge (PPL).

Photo. 210. Dolomite replacement (d) of the void-rimming colloform sphalerite; notice the truncated contact of the dolomite crystals adjacent to the void-filling diagenetic and detrital assemblage (PPL).

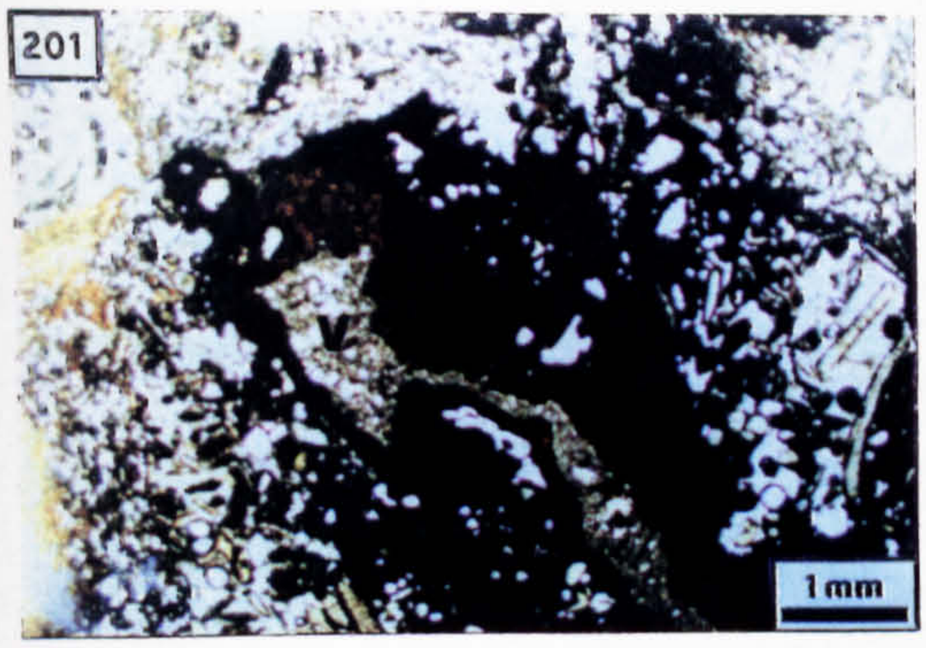
201
1mm

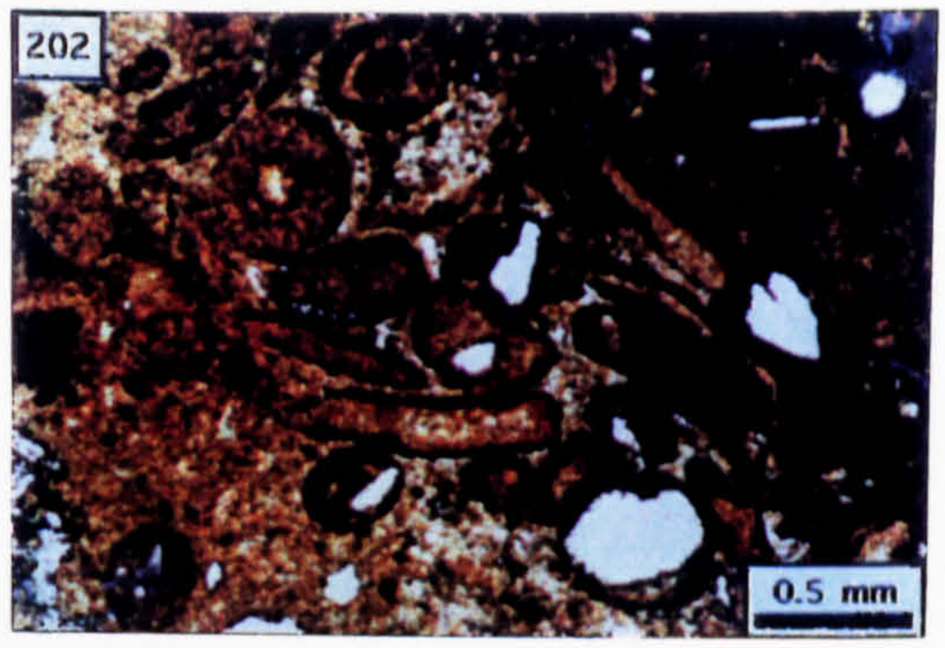
202
0.5 mm

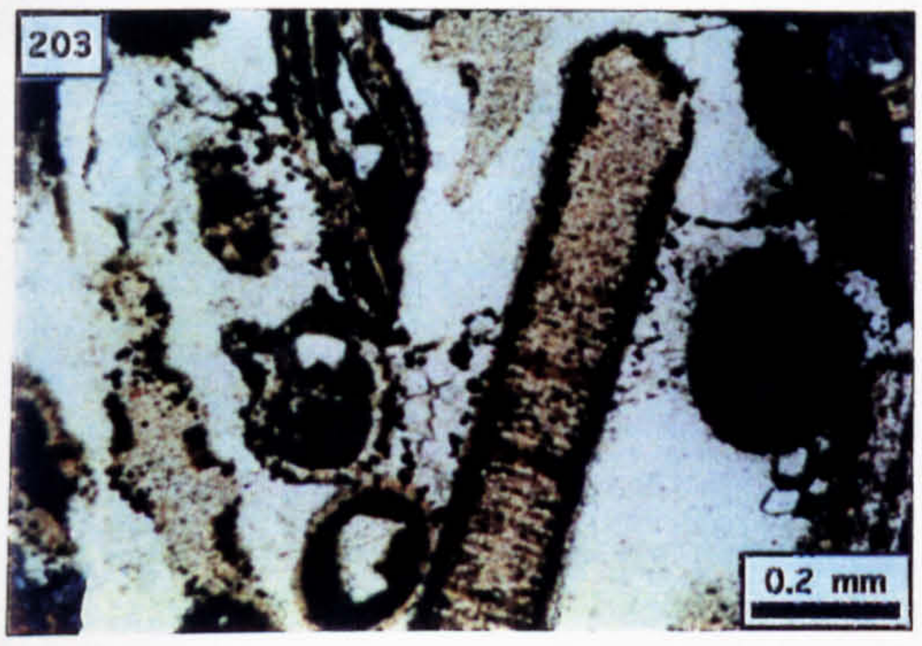
203
0.2 mm

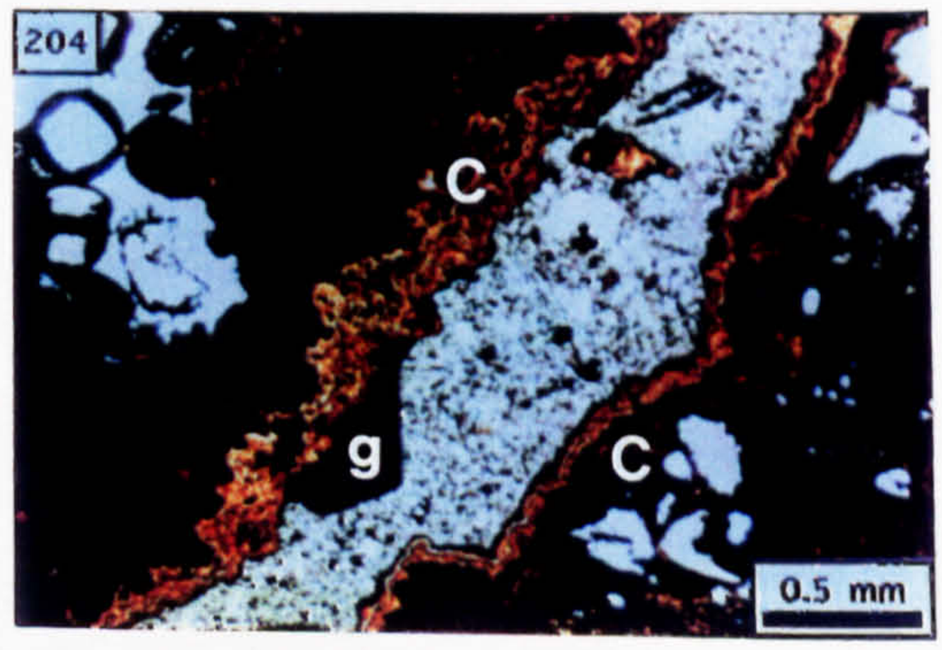
204
C
g
C
0.5 mm

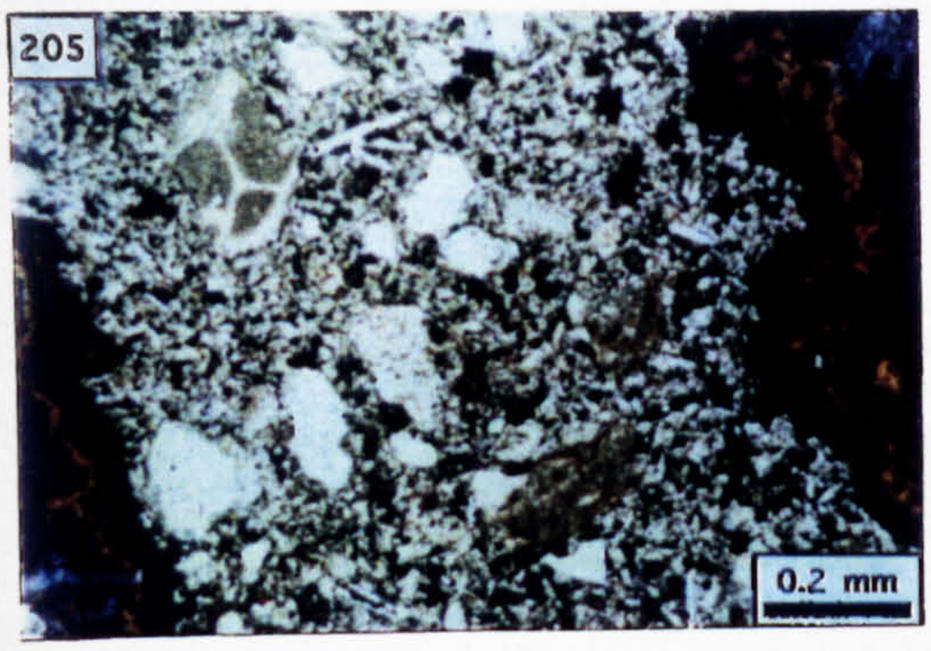
205
0.2 mm

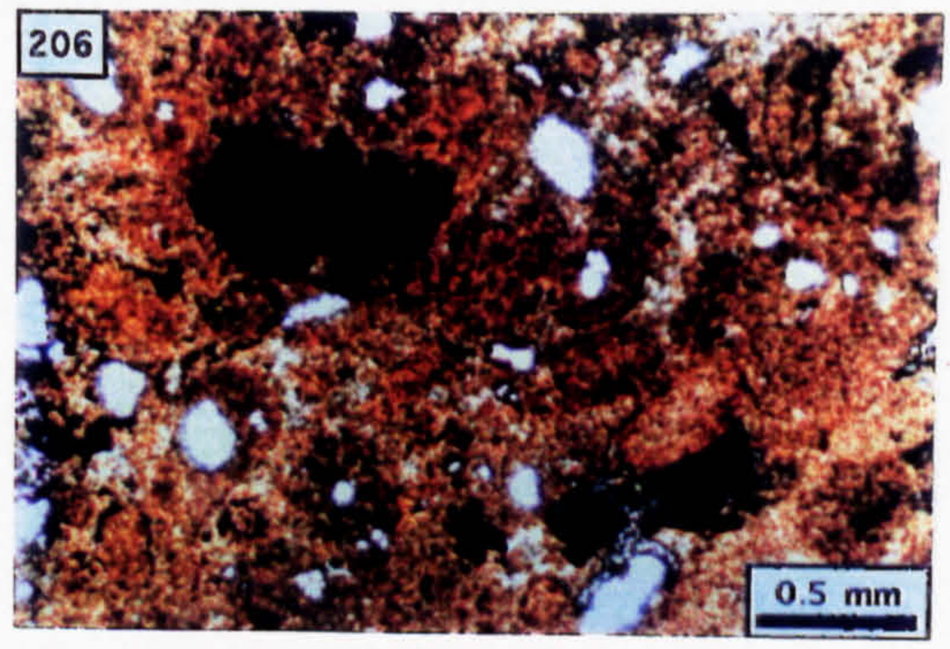
206
0.5 mm

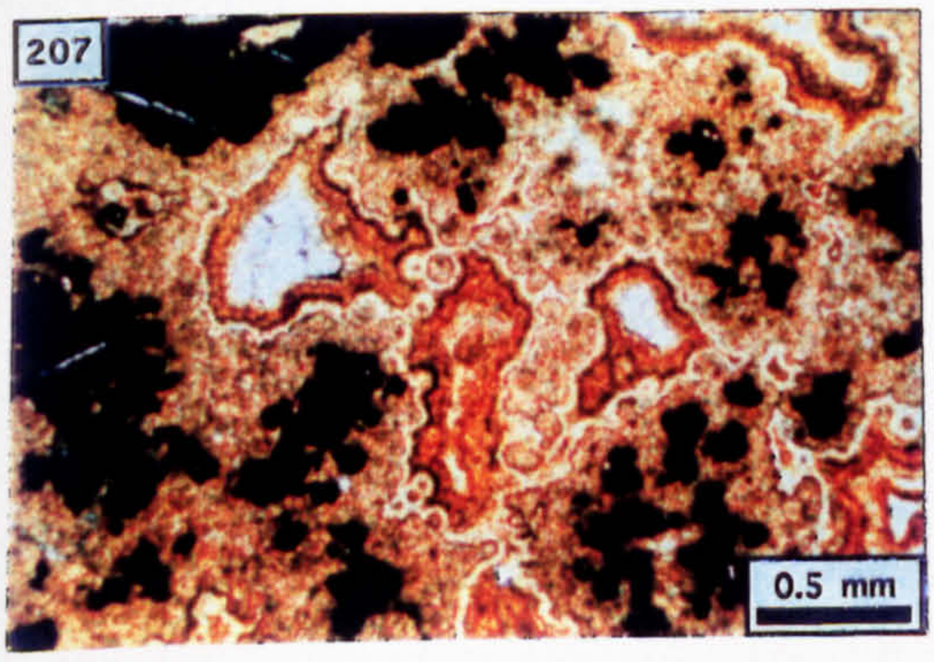
207
0.5 mm

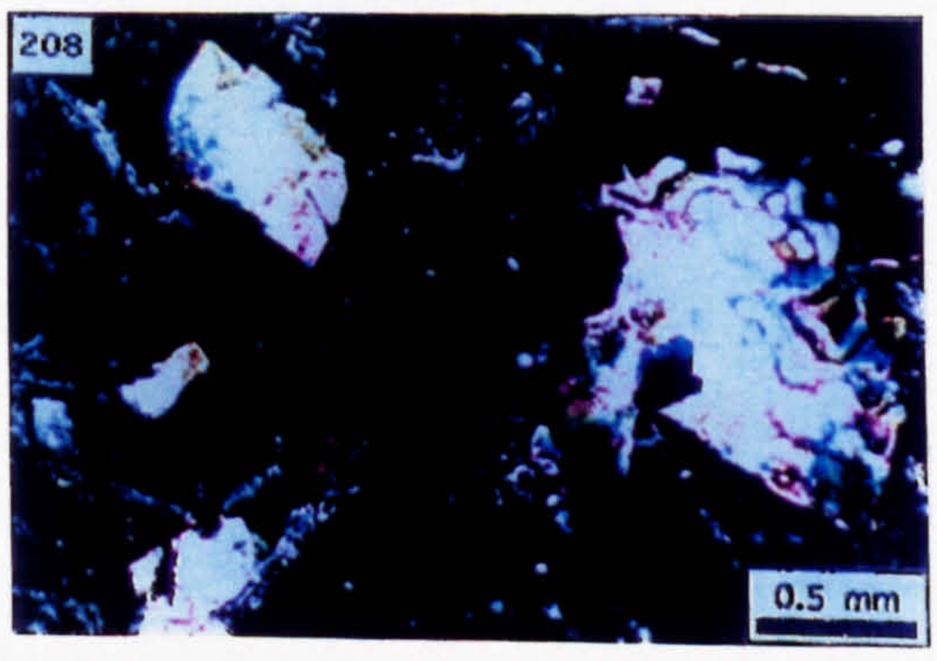
208
0.5 mm

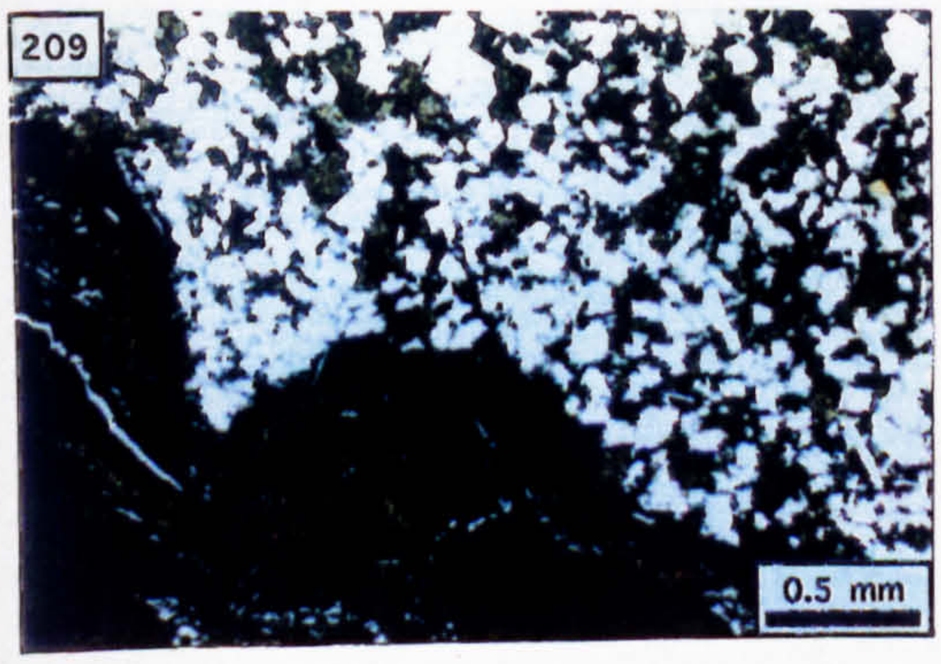
209
0.5 mm

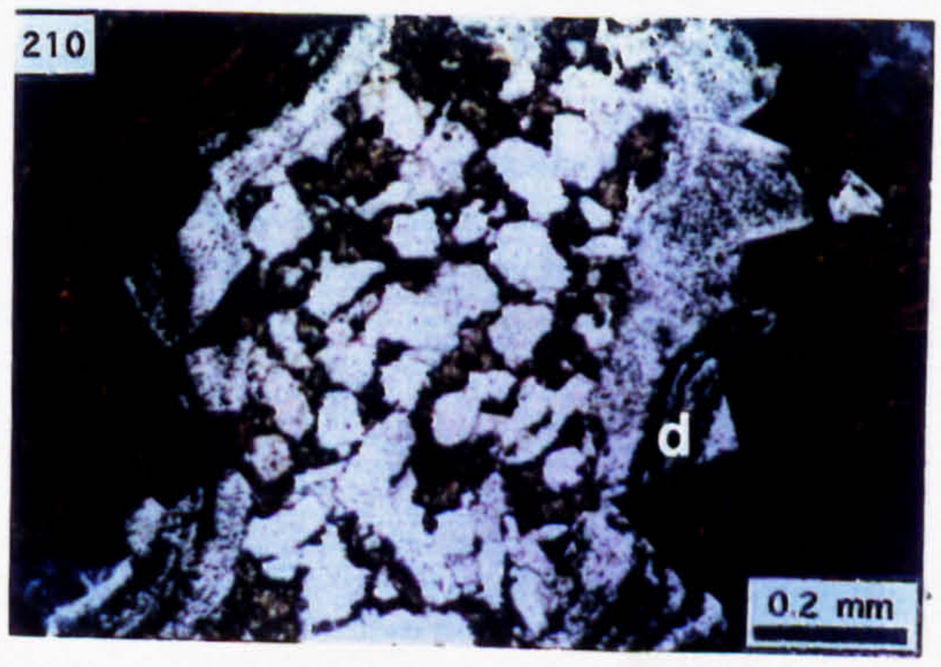
210
d
0.2 mm

Photo. 211. Petrography of the void-filling diagenetic and detrital assemblage: s=siliciclastic grains, z=sphalerite grains, a=silty argillite (PPL).

Photo. 212. As above but XPL.

Photo. 213. Calcite-cemented microfractures cutting through replaced oolite and colloform sphalerite (CL).

Photo. 214. Calcite-cemented microfracture truncated at the edge of the colloform sphalerite (PPL).

Photo. 215. Skeletal galena intergrown with sphalerite as replacement to bioclastic limestone (PPL).

Photo. 216. Longitudinal section of crinoid stem pseudomorphed by orange sphalerite and possessing coarse, pale yellow sphalerite developed on the walls of biomoulds; the remnant biomouldic porosity is occluded by barite (PPL; width of view=4 cm).

Photo. 217. Mineralised crinoidal limestone showing sphalerite as partial infill to biomouldic porosity (z) [PPL; width of view=2.5 cm].

Photo. 218. Rugose corals, replaced by sphalerite and possessing coarse, pale yellow sphalerite developed on the walls of biomoulds; the remnant biomouldic porosity is occluded by barite (b) [PPL; width of view=3 cm].

Photo. 219. Cross section through a solitary rugose coral replaced by orange and pale yellow sphalerites and barite (PPL; width of view=3.5 cm).

Photo. 220. Bryozoa fragments replaced by sphalerite (PPL).

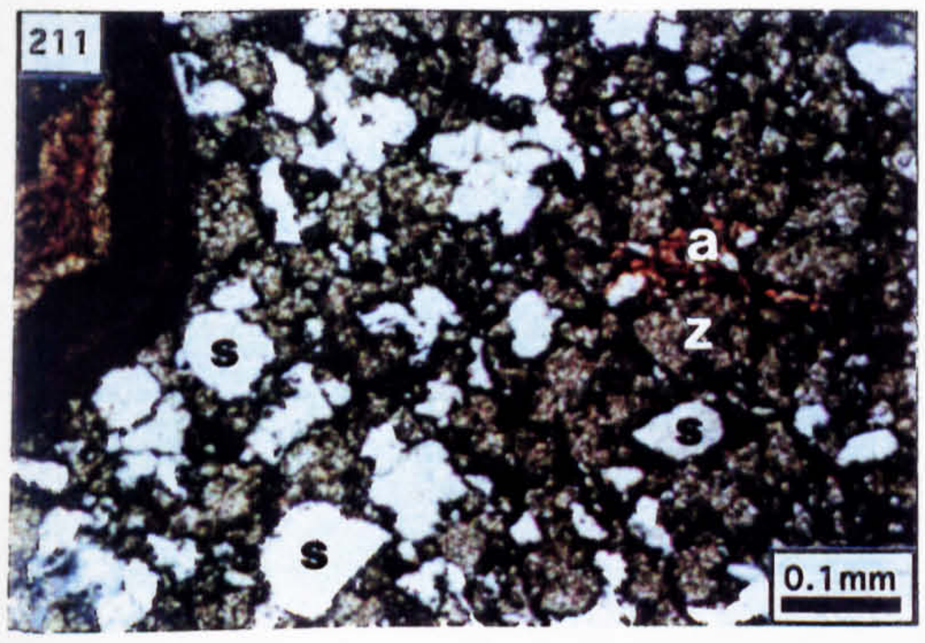
211
a
z
s
s
s
0.1mm

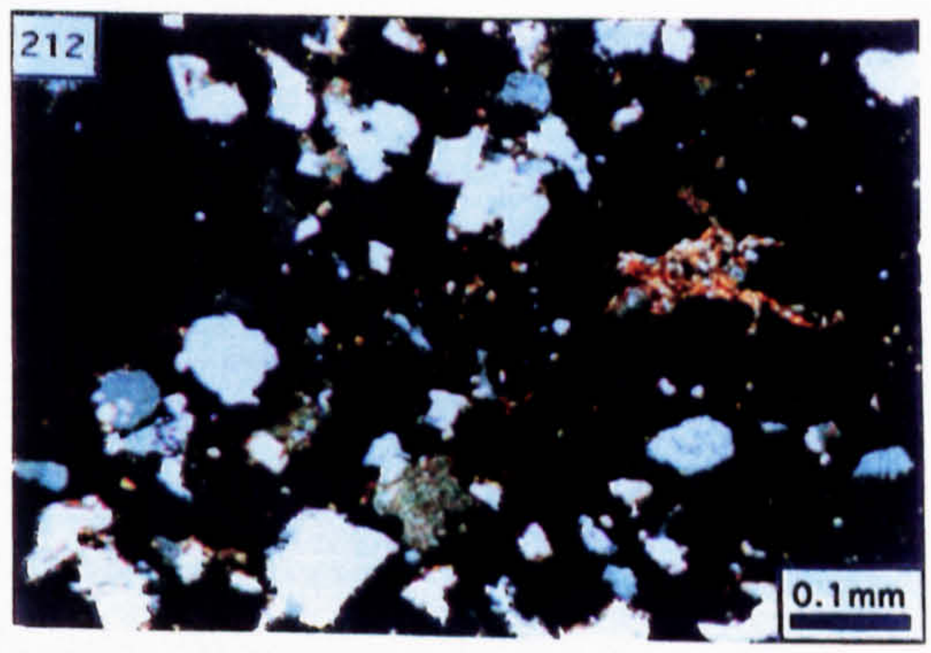
212
0.1mm

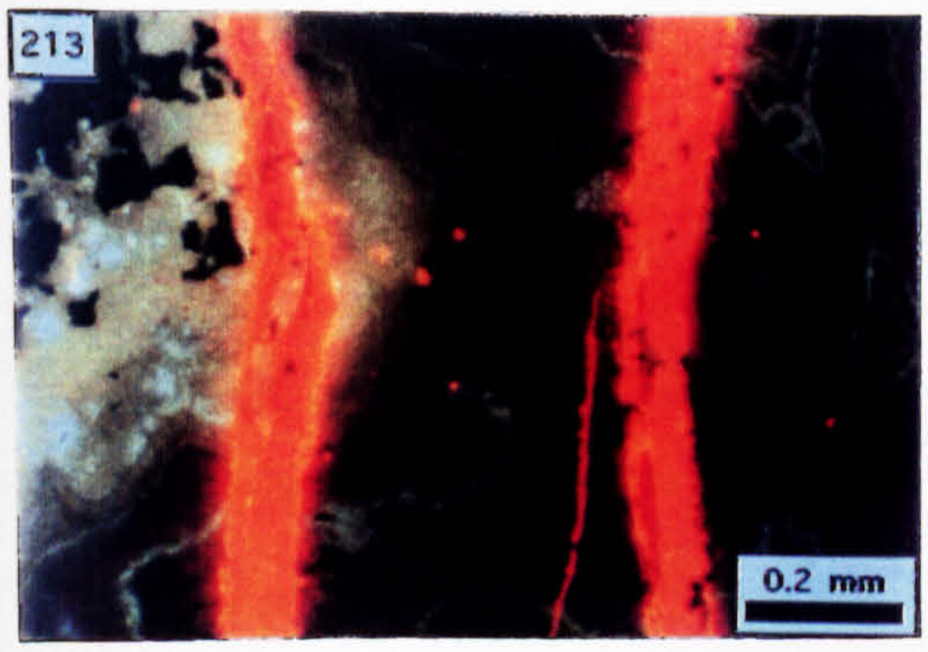
213
0.2 mm

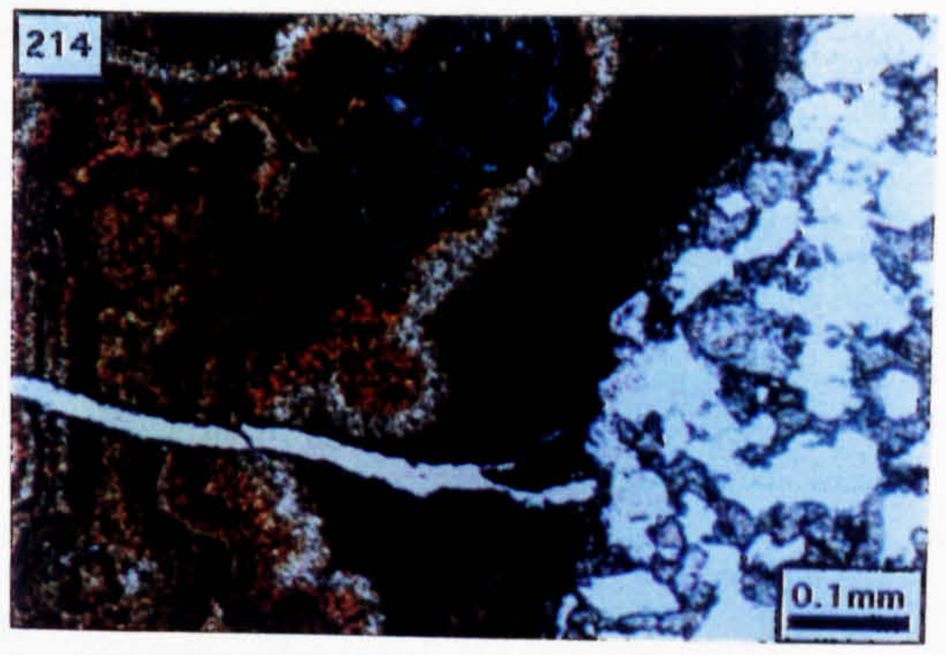
214
0.1mm

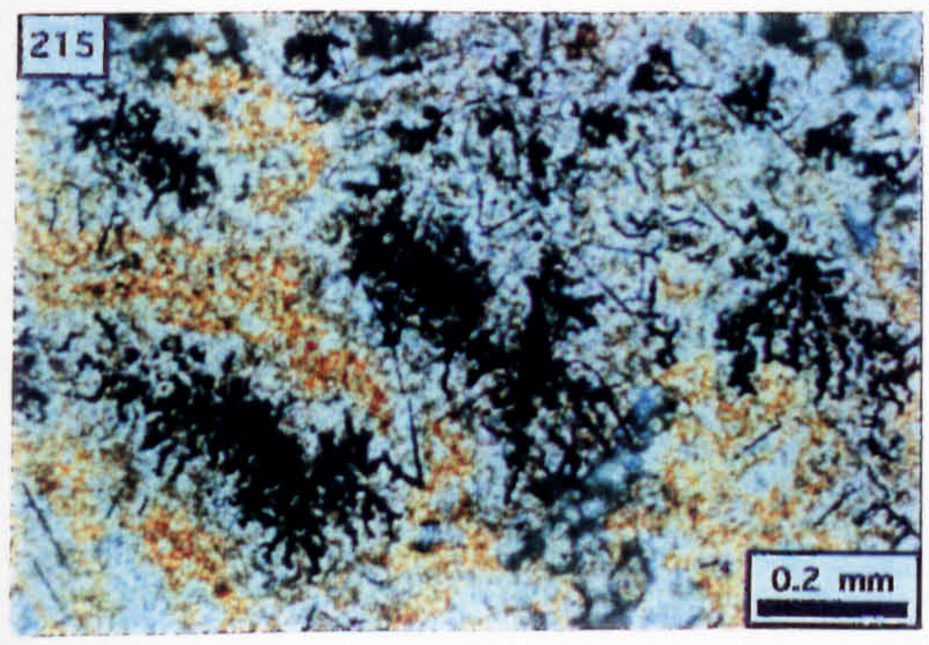
215
0.2 mm

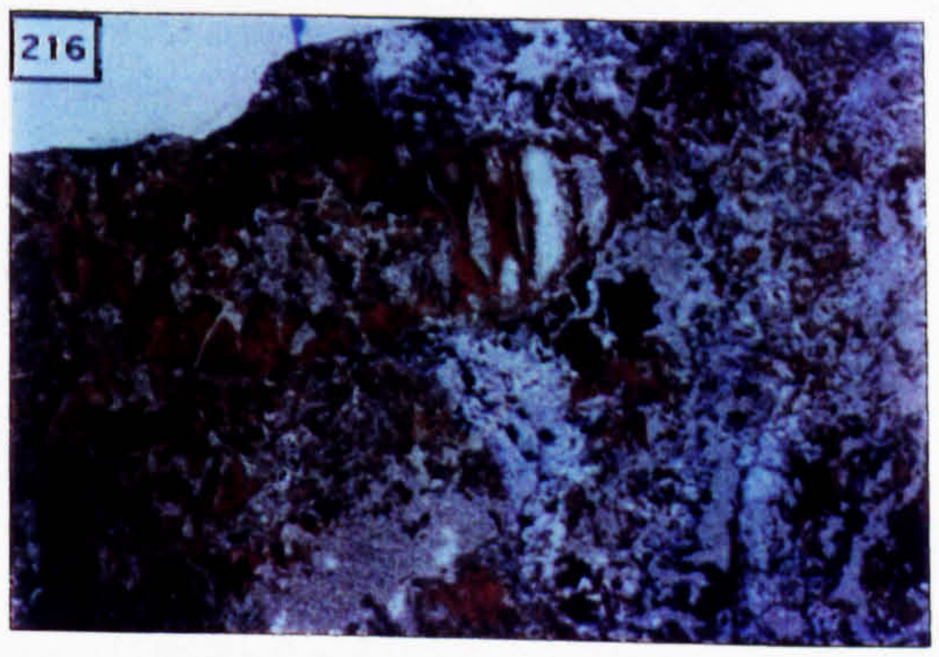
216

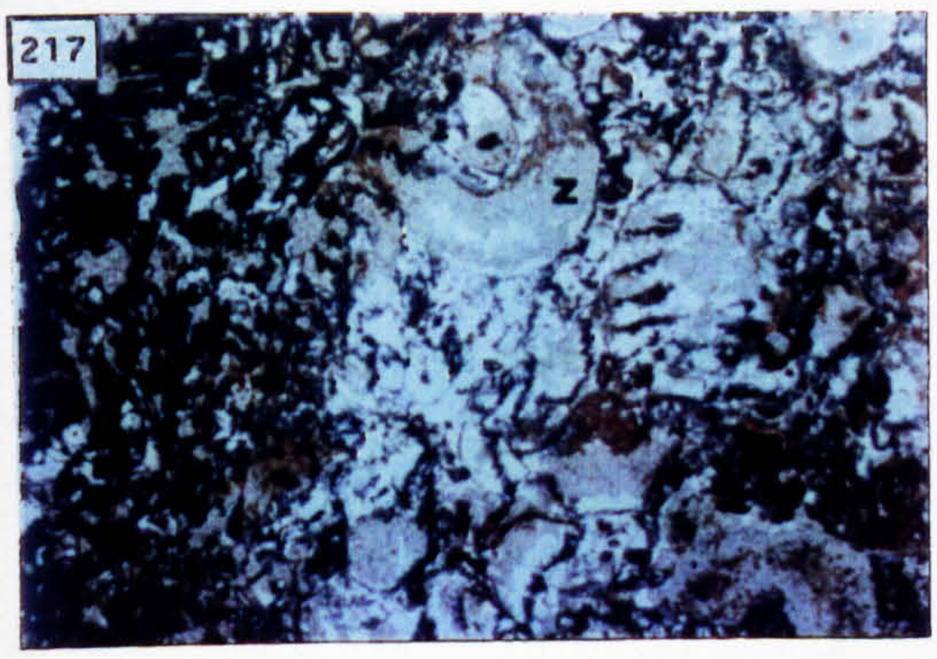
217
z

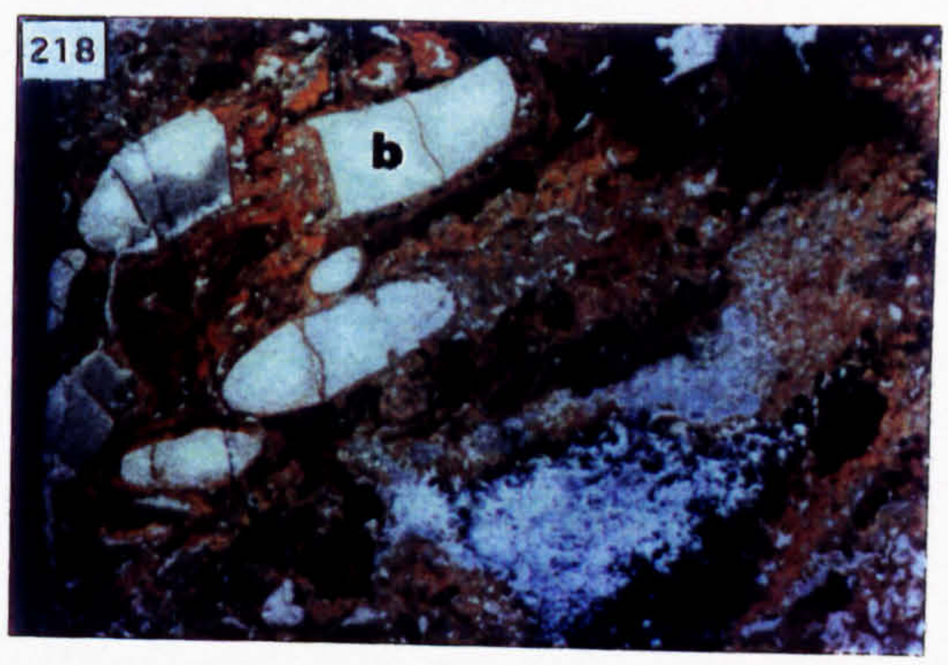
218
b

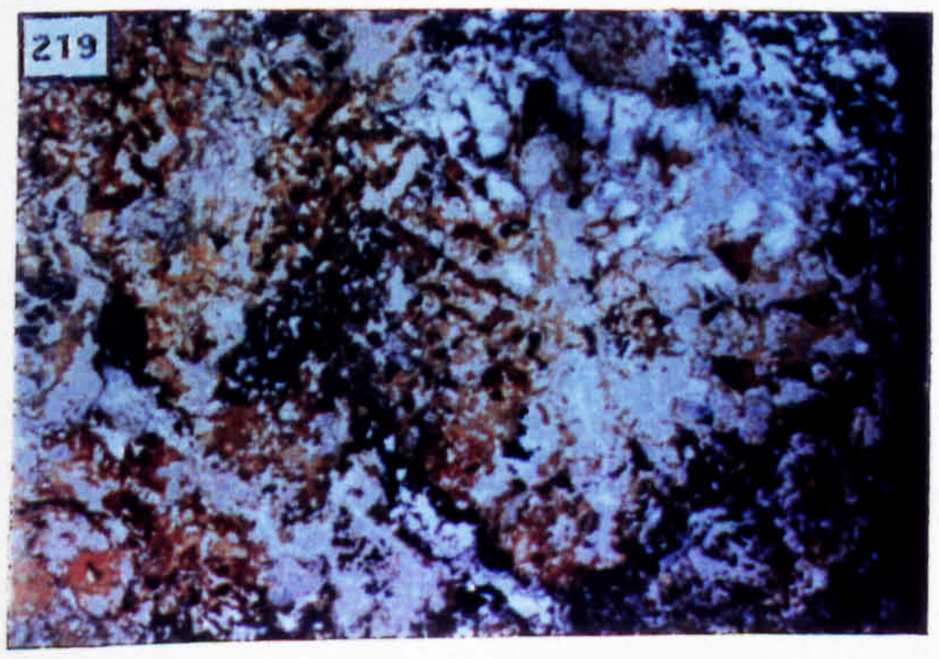
219

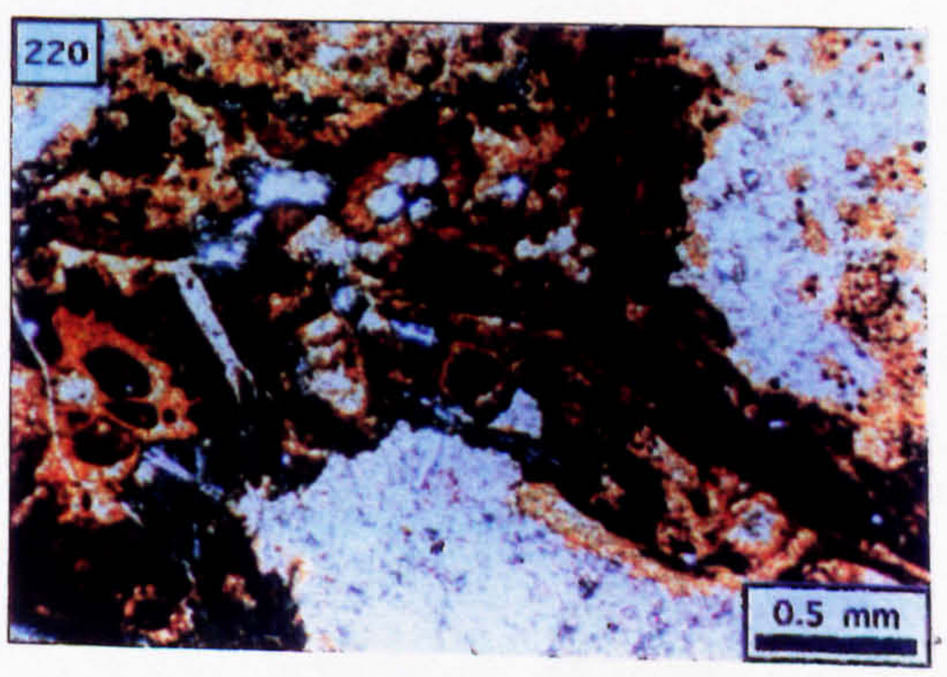
220
0.5 mm

Photo. 221. Petrography of the void-filling mineralisation within clasts of completely replaced bioclastic limestone. A=fine barite and sphalerite, B=laminated coarser sphalerite and/or barite, C=sulphide-cemented fracture through A and B (PPL; width of view=2 cm).

Photo. 222. Detail of the fracture cement from location C in Photo. 221; A=fine sphalerite and barite wallrock, c=colloform sphalerite, g=microcrystalline galena, s=pale yellow sphalerite (PPL).

Photo. 223. Calcite-cemented microfractures cutting through the colloform sphalerite (c), subhedral galena (g) and anhedral pyrite (p) [RL].

Photo. 224. Calcite-cemented microfractures cutting through the colloform sphalerite (c) and coarse, pale yellow sphalerite (s); the latter is developed as a rim to the void in contiguity with the final cement to the fracture shown in Photo. 222 (PPL).

Photo. 225. Bright orange luminescent calcite developed as cement to the microfractures shown in Photo. 224. Note the contiguity of this calcite with the euhedral edge of the coarse, void-lining sphalerite (s); c=colloform sphalerite (CL).

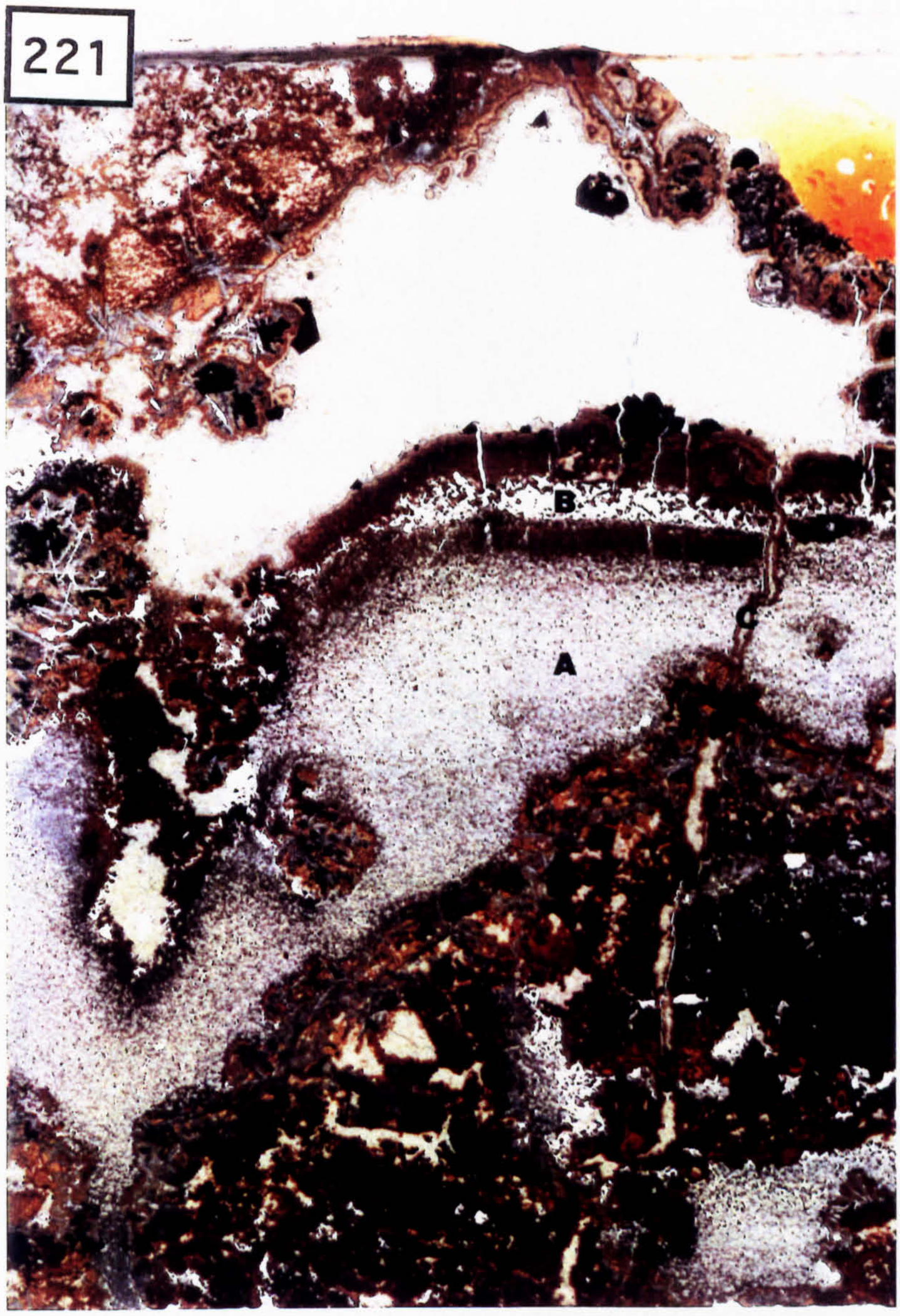
221
B
C
A

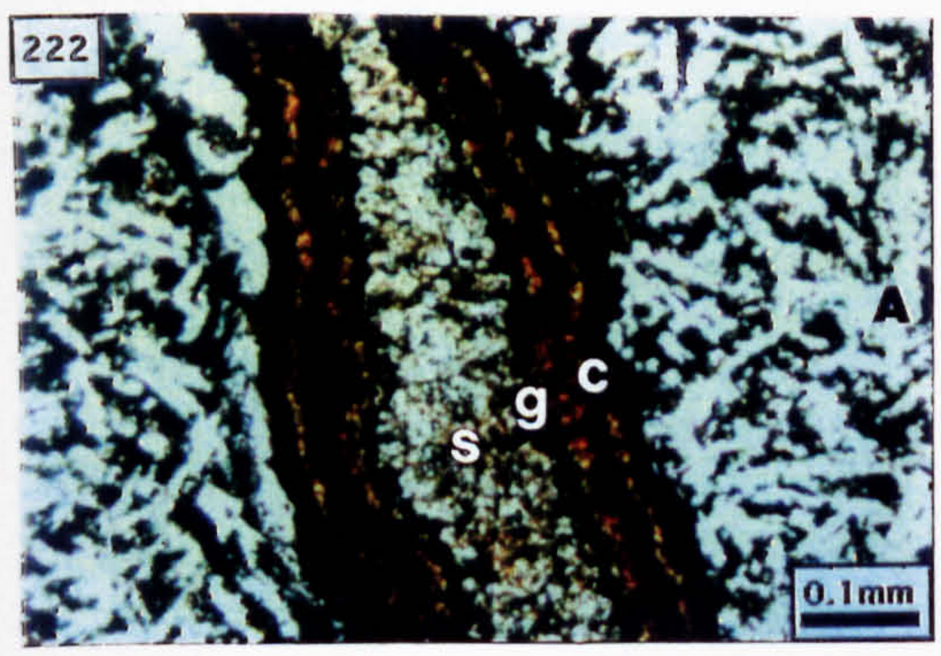
222
A
c
g
s
0.1mm

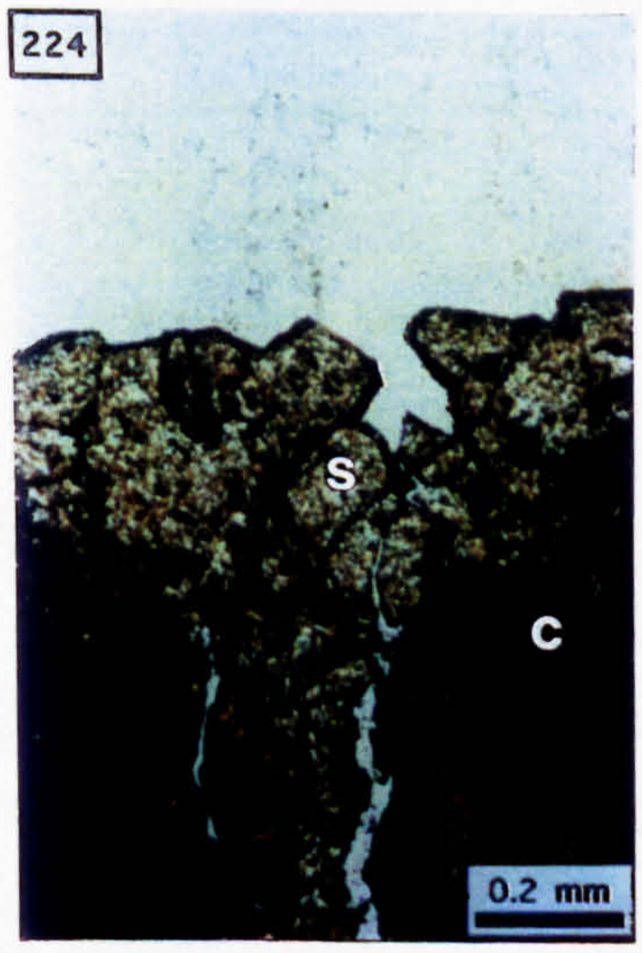
224
S
C
0.2 mm

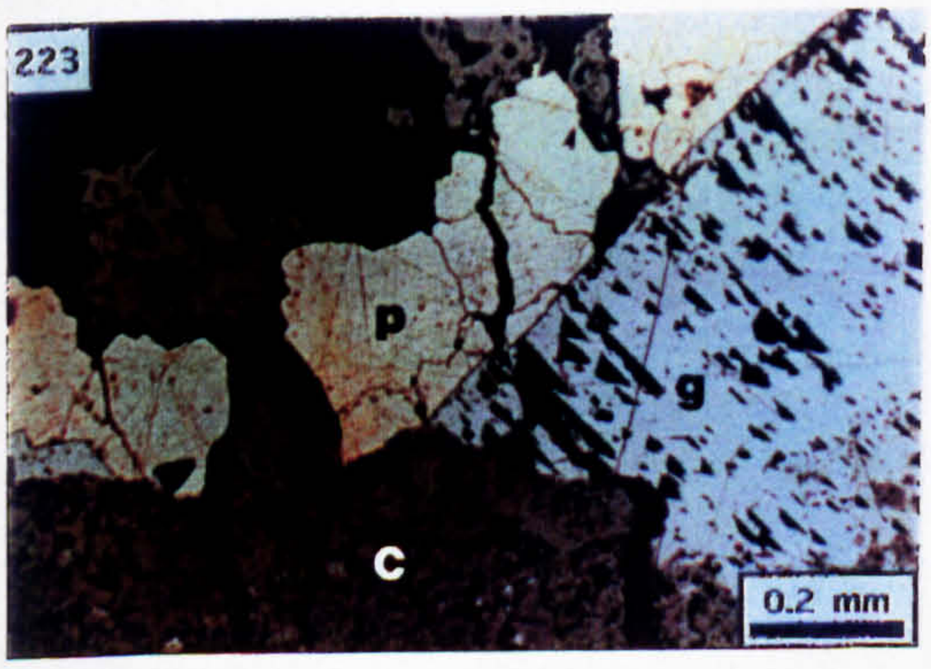
223
P
g
C
0.2 mm

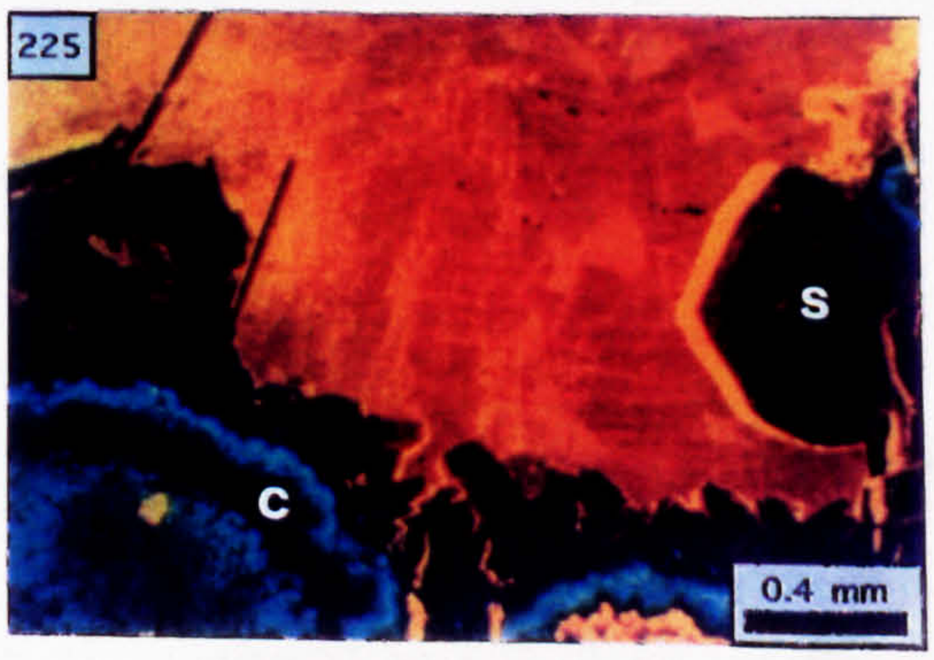
225
S
C
0.4 mm

Photo. 226. Cross section through the void wall showing the association of brightly luminescent calcite with coarse, subhedral sphalerite (s) and colloform sphalerite (c); the remaining void space is occluded by sparite; g=galena overgrowth to the colloform sphalerite (CL).

Photo. 227. Petrography of the vein wall: b=barite, s=sphalerite, c=calcite (CL; U8330, 19.5 m).

Photo. 228. As above but XPL; q=quartz grain.

Photo. 229. Zoned calcite occluding porosity defined by barite (b) and sphalerite (s); notice the occurrence of calcite which infills microvugs in the barite (CL; U8330, 19.5 m).

Photo. 230. As above but XPL.

Photo. 231. Calcite-filled pore defined by barite (b) and sphalerite (s); notice the relict acicular habit of the barite after replacement by calcite and the occurrence of calcite which infills microvugs in the barite (CL; U8330, 19.5 m).

Photo. 232. As above but XPL.

Photo. 233. Petrography of the vein fill showing calcite as replacement to colloform sphalerite (r) and as zoned sparite (S) which occludes pore space defined by the colloform sphalerite (CL; U8330, 19.5 m).

Photo. 234. Petrography of the vein fill at higher magnification showing the occurrence of microcrystalline sphalerite (z) as a rim to the colloform sphalerite (c). Coarse galena (g) partially occludes the vein porosity defined by the sphalerite. Microfractures in the galena are cemented by calcite and zoned sparite (S) infills the remaining pore space (CL; U8330, 19.5 m).

Photo. 235. Clast of Shaley Pales exhibiting selective dolomitisation of the intergrain material: the bioclasts are clearly distinguished as relict grains (PPL; N927, 351.1 m).

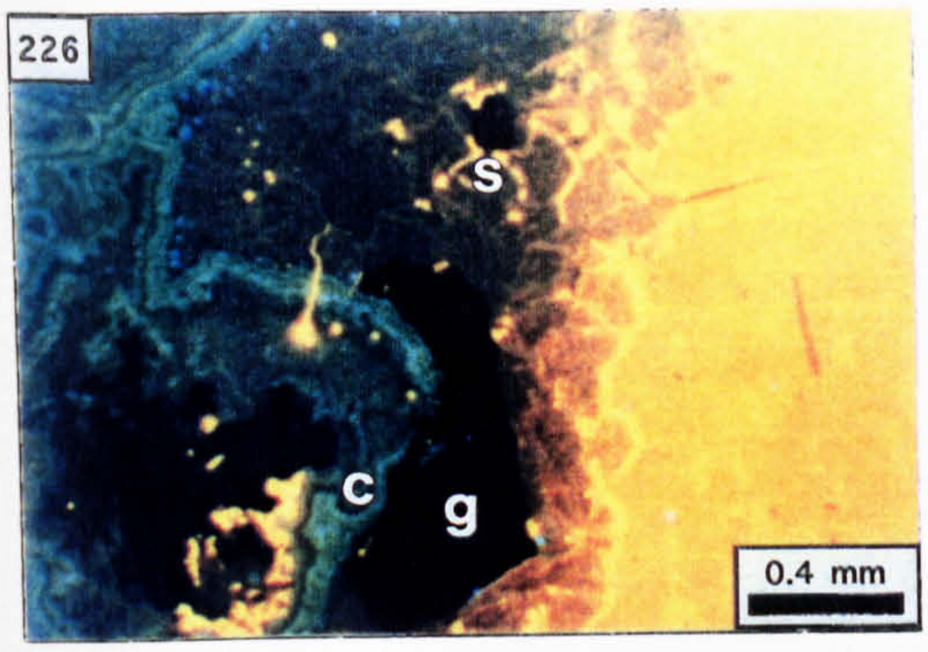
226
s
c
g
0.4 mm

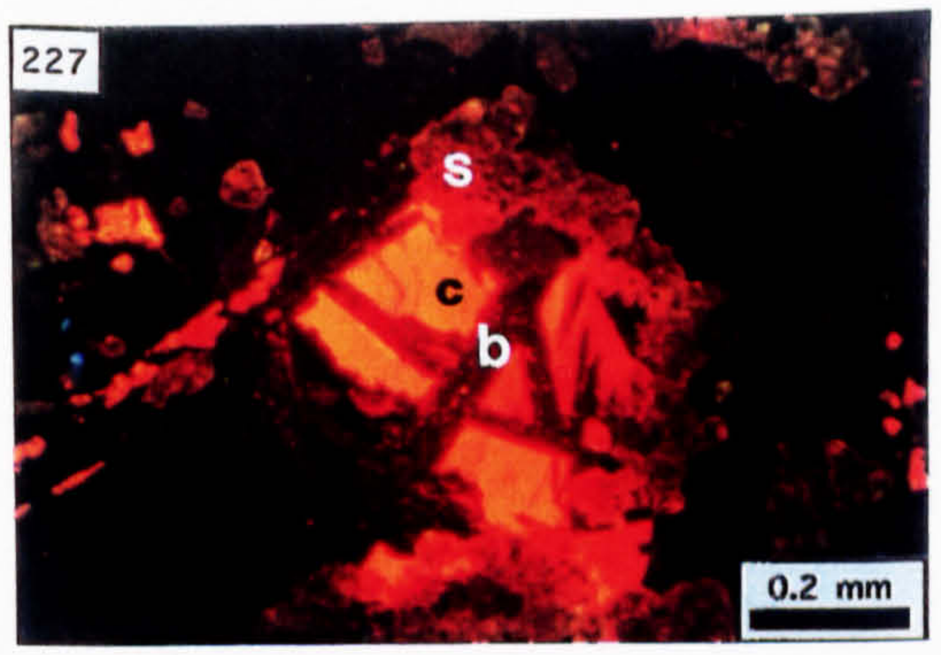
227
s
c
b
0.2 mm


228
q
0.2 mm

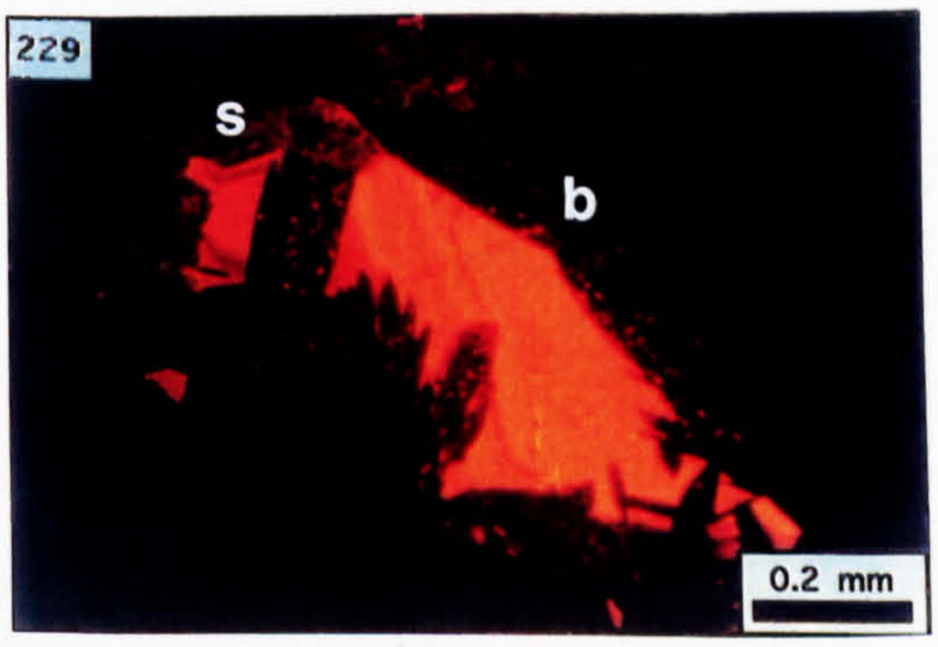
229
s
b
0.2 mm

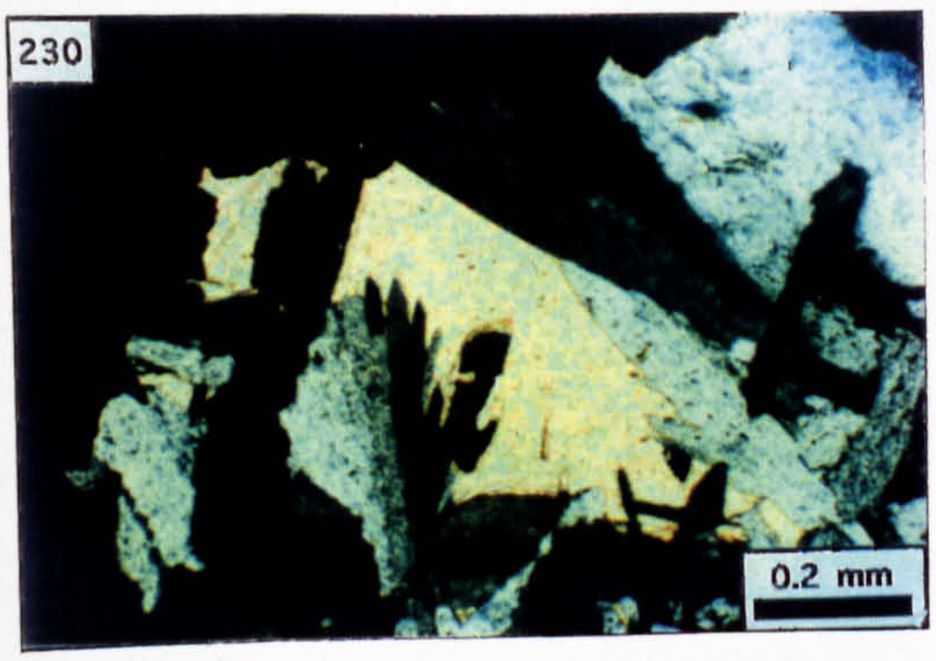
230
0.2 mm

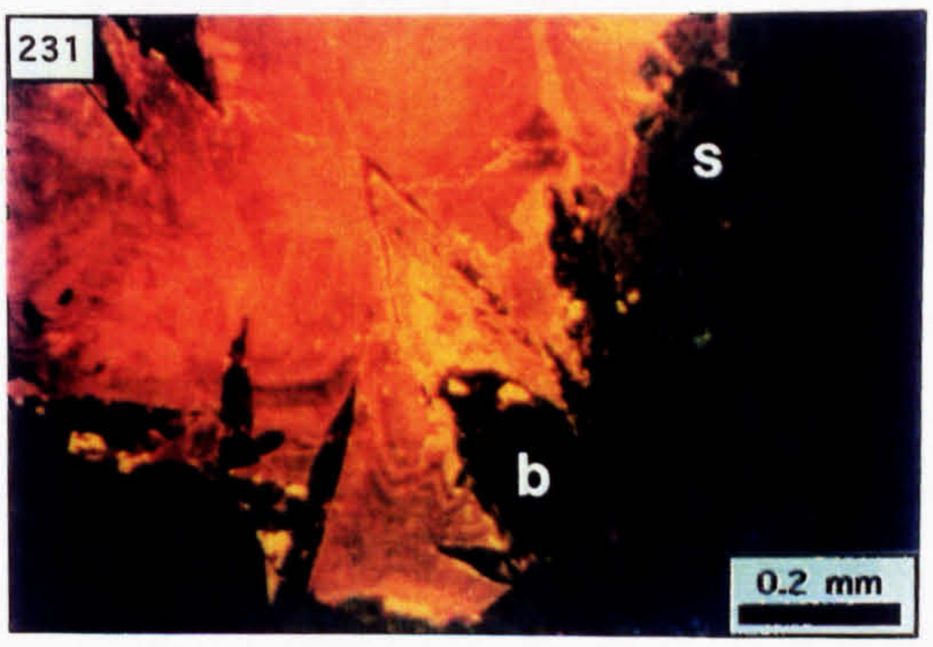
231
s
b
0.2 mm

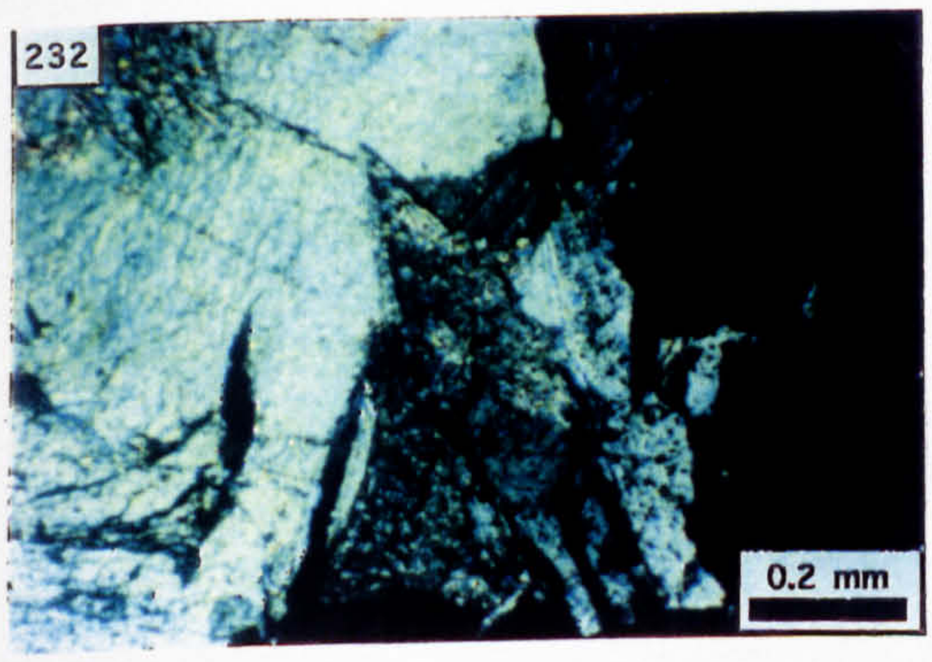
232
0.2 mm

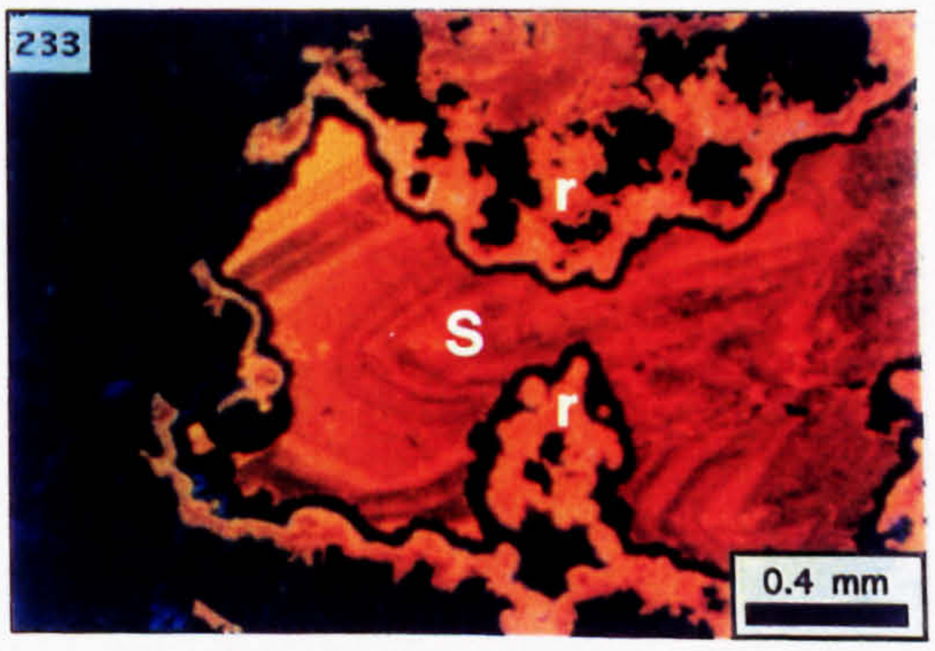
233
r
S
r
0.4 mm

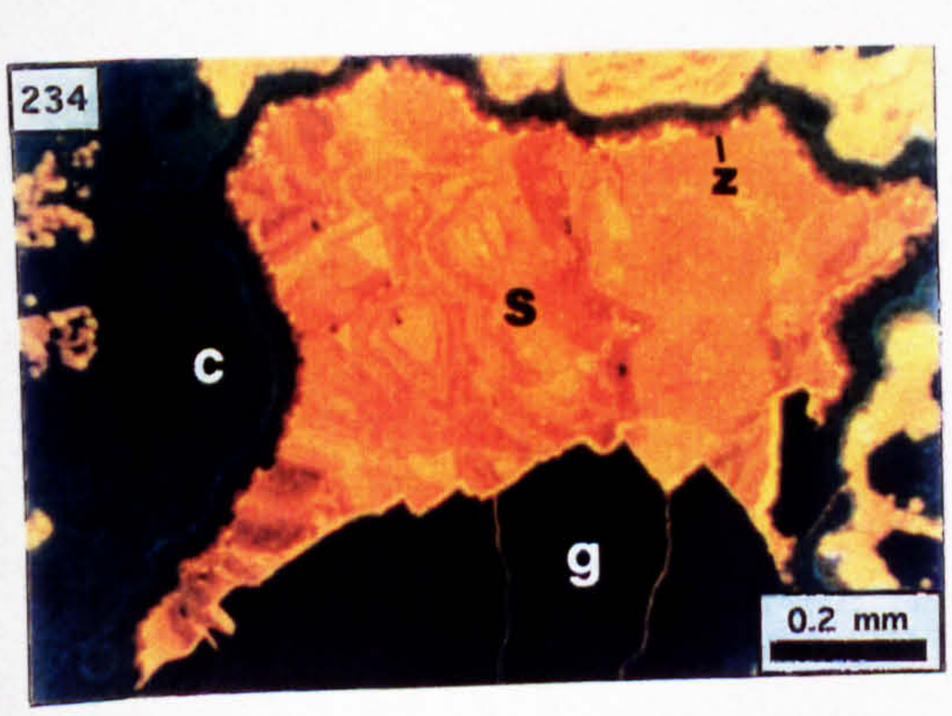
234
z
s
c
g
0.2 mm

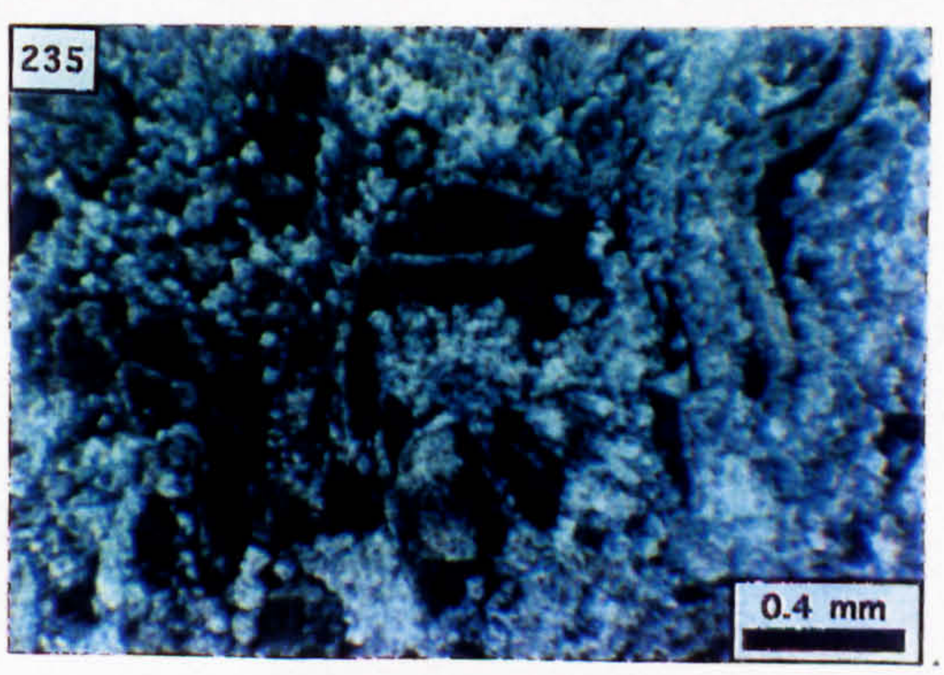
235
0.4 mm

Photo. 236. As above but CL.

Photo. 237. Relict bioclast within intensely dolomitised limestone (CL; N927, 351.1 m).

Photo. 238. CL zonation of the dolomite which replaces the limestone (CL; N927, 351.1 m).

Photo. 239. Vug-filling mineralisation (V) contained within a boulder of bioclastic limestone (N647, vug at 182.43 m).

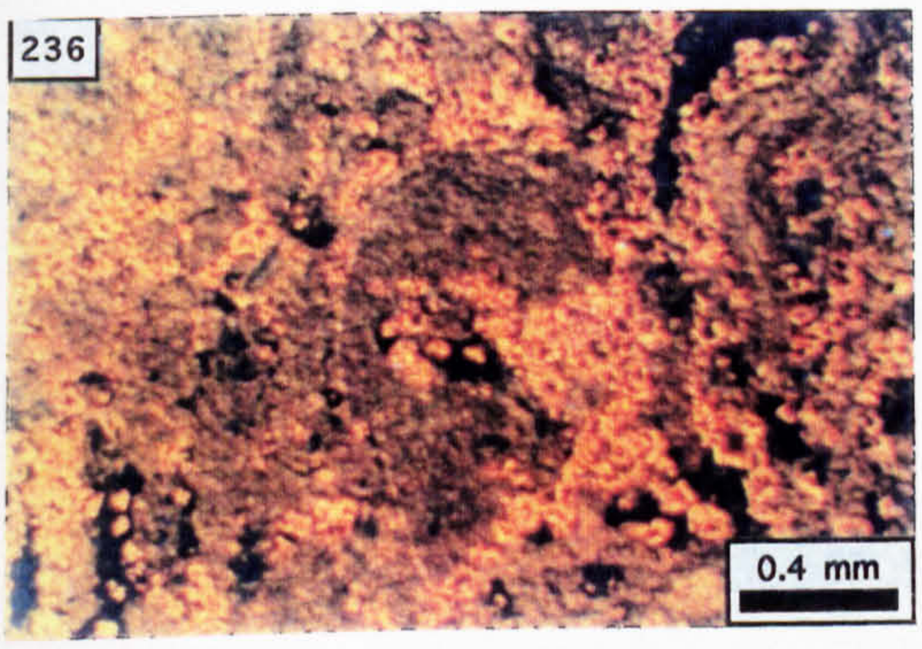
236
0.4 mm

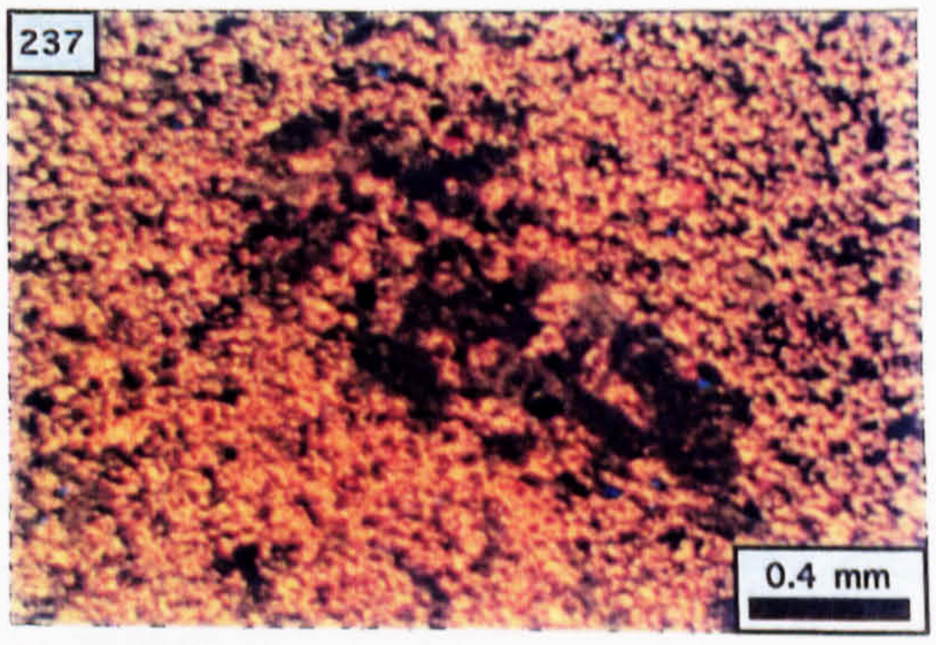
237
0.4 mm

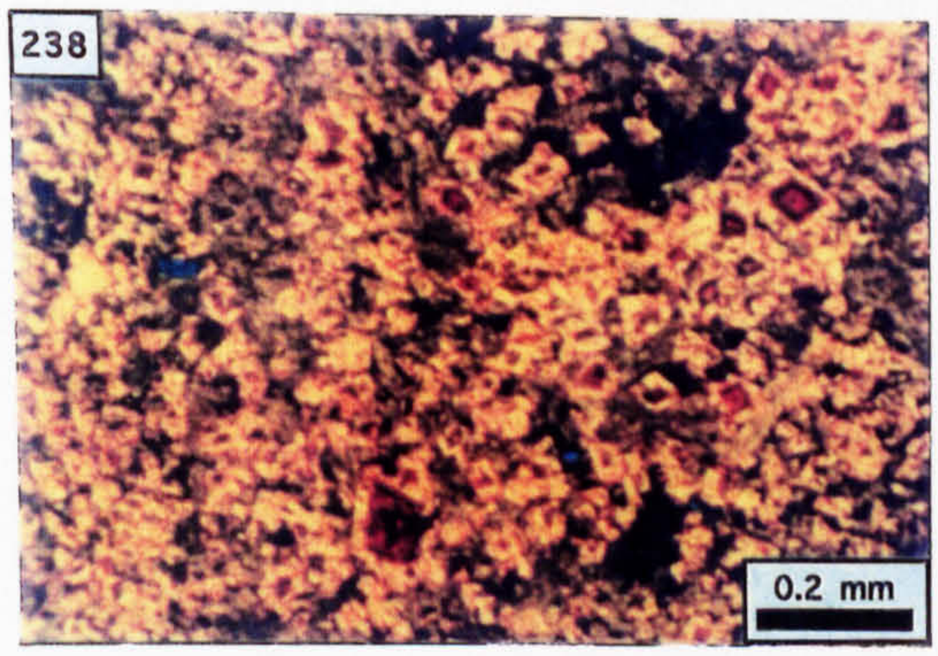
238
0.2 mm

239
V1
26 5'95

Photo. 240. Detail of vug-filling mineralisation present in a boulder of bioclastic limestone (2 cm scale bar; N1192, 494.4 m).

Photo. 241. Sparite as cement to intra-(1) and inter-(2) bioclast porosity (CL; N1192, 494.4 m).

Photo. 242. Crenulated argillite seam (A) coincident with dissolved and mutually impinged bioclasts (PPL; N1192, 494.4 m).

Photo. 243. Petrography of the vug floor showing grains of zoned sphalerite (s) and dolomite (d) lying with sharp contact over bioclastic argillite (b) [PPL; N1192, 494.4 m].

Photo. 244. Petrography of the vug wall showing non-luminescent dolomite (d) infilling an interbioclast dissolution pore (CL; N1192; 494.4 m).

Photo. 245. Non-luminscent dolomite infilling interbioclast dissolution pores in the vug wall (CL; N1192, 494.4 m).

Photo. 246. Euhedral, non-luminescent dolomite replacing the vug wall (CL; N1192, 494.4 m).

Photo. 247. Fractured and fragmented crystals of zoned sphalerite deposited upon the bioclastic argillite vug floor; the inter-sphalerite grains comprise subhedral to anhedral dolomite (PPL; N1192, 494.4 m).

240

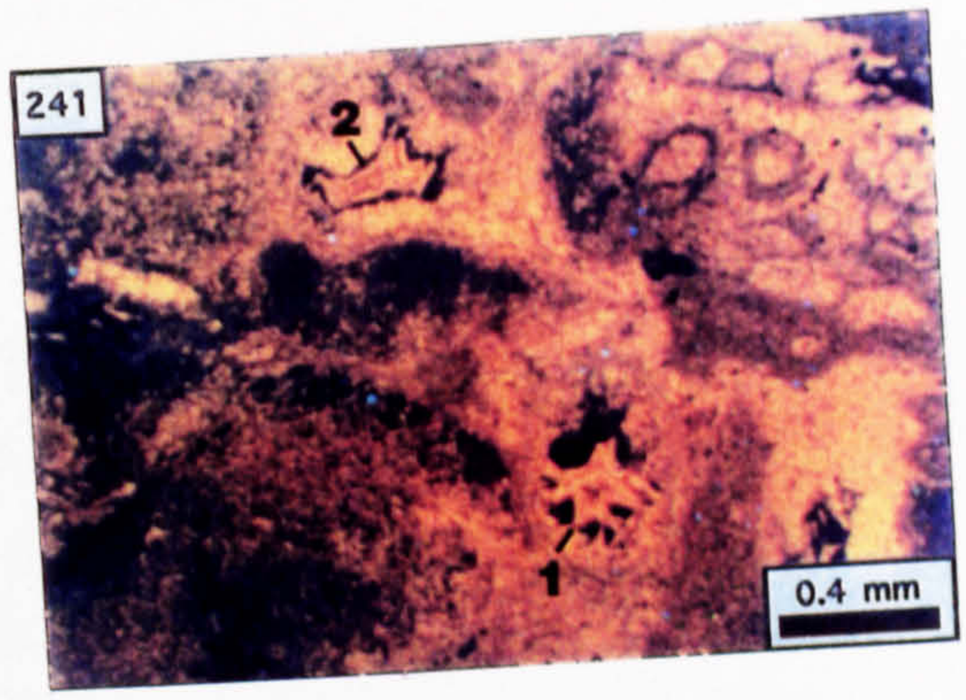
241
2
1
0.4 mm

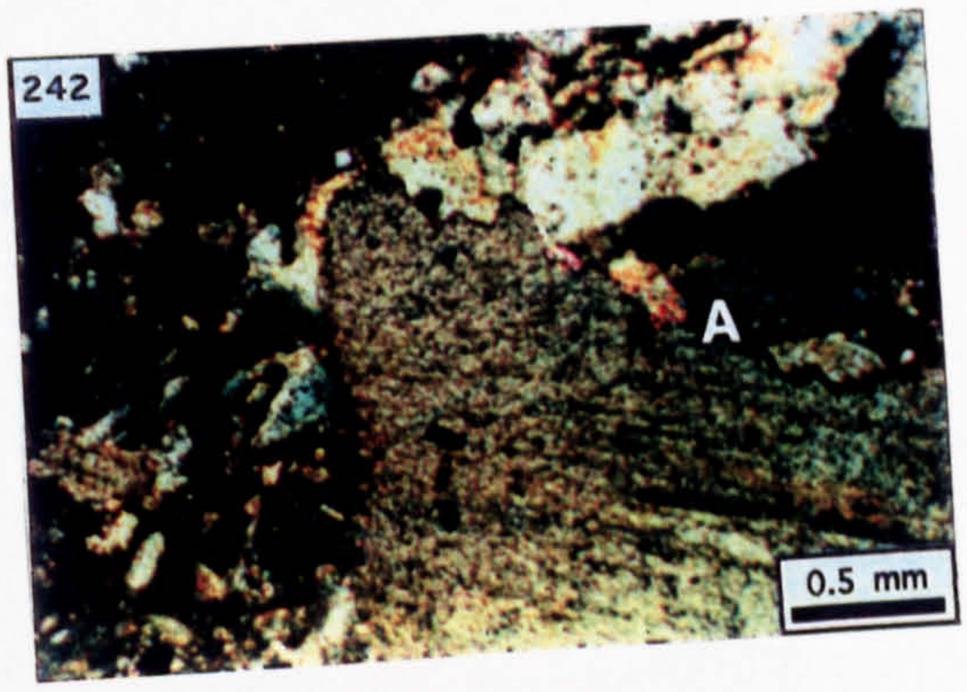
242
A
0.5 mm

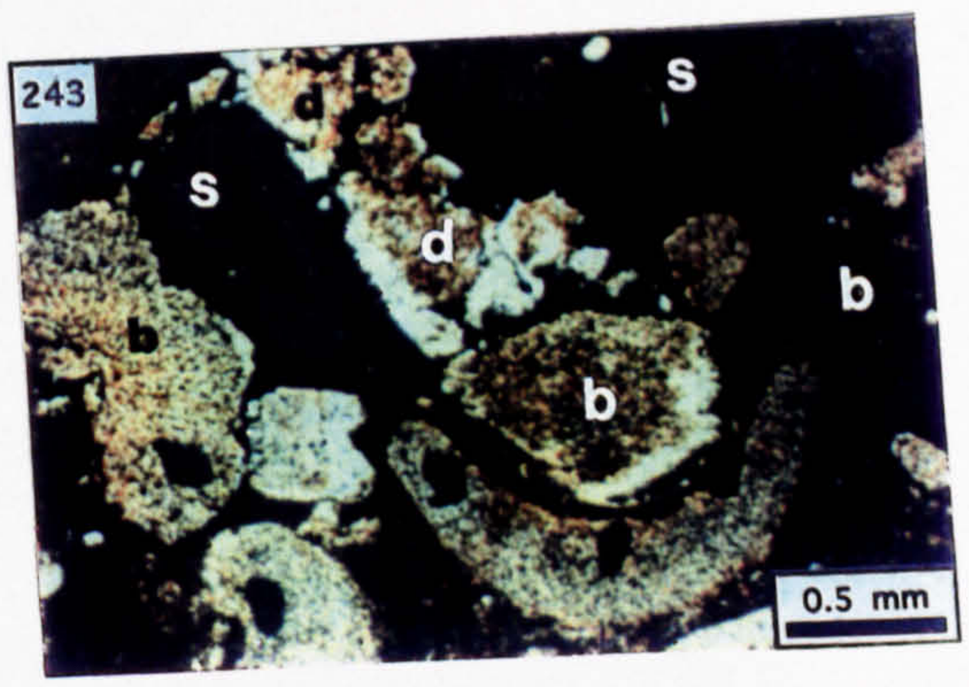
243
d
S
S
d
b
b
b
0.5 mm

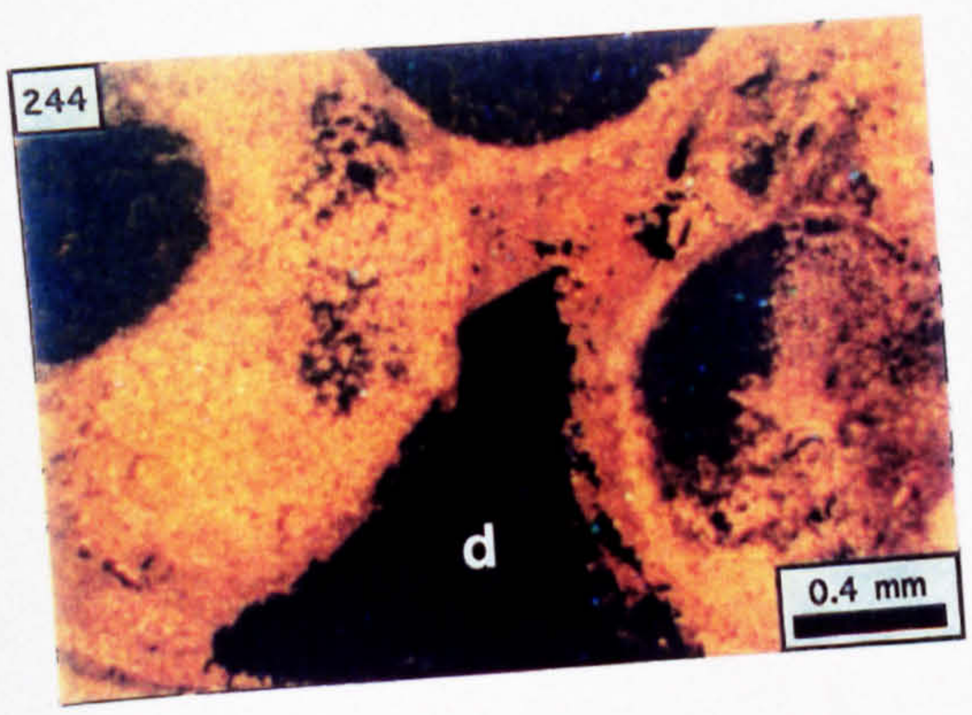
244
d
0.4 mm

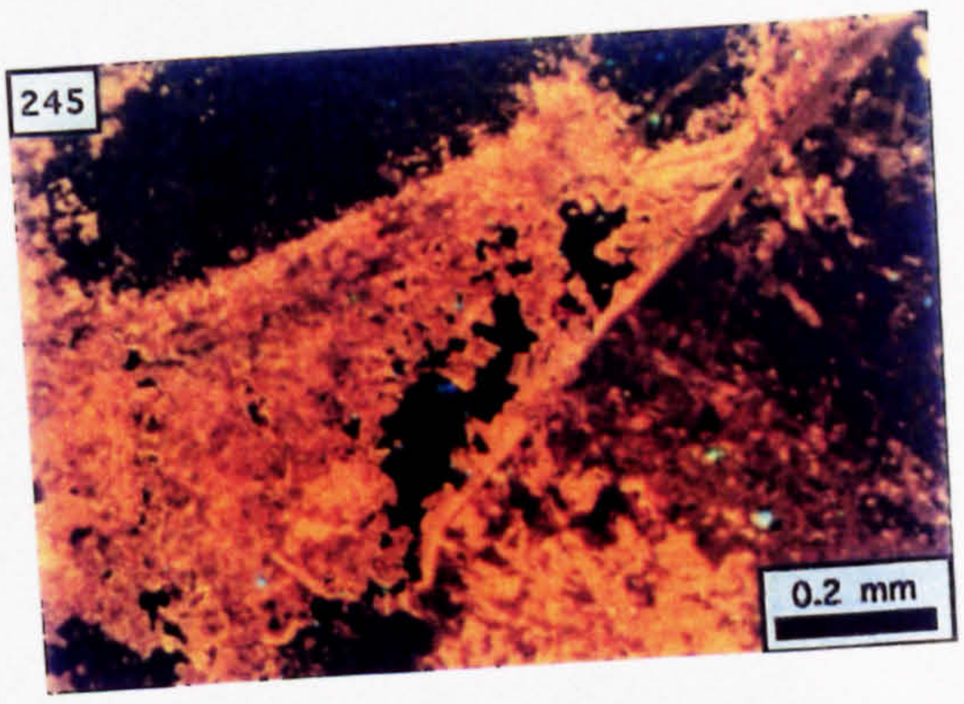
245
0.2 mm

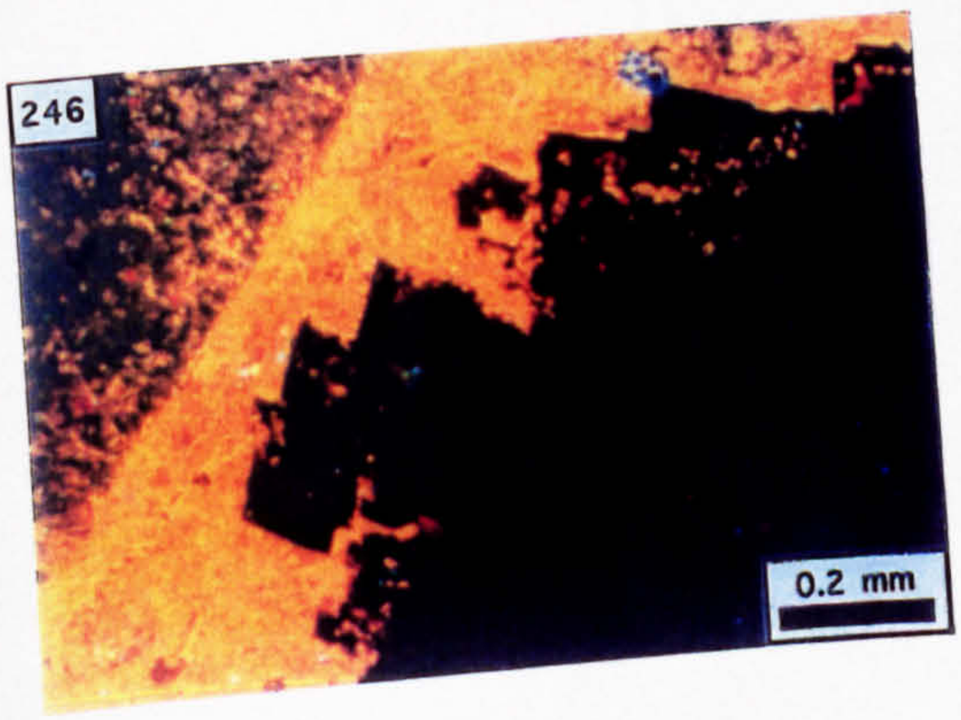
246
0.2 mm


247
1mm

Photo. 248. Fractured sphalerite grain supported by a matrix of subhedral to anhedral dolomite; the dark, interdolomite sediment comprises pyritic argillite (PPL; N1192, 494.4 m).

Photo. 249. As above but CL.

Photo. 250. Clast of wallrock supported by a matrix of subhedral dolomite and pyritic argillite (PPL; N1192, 494.4 m).

Photo. 251. As above but CL.

Photo. 252. Fractured dolomite crystals (RL; N1192, 494.4 m).

Photo. 253. Very coarse baroque dolomite developed as a syntaxial overgrowth to the dolomite shown in Photo. 250 (PPL; N1192, 494.4 m).

Photo. 254. Petrography of the corroded and reprecipitated sparite which partially occludes the interbaroque dolomite porosity (CL; N1192, 494.4 m).

Photo. 255. As above but PPL to show the presence of baroque dolomite (d) and unoccluded pore space (O).

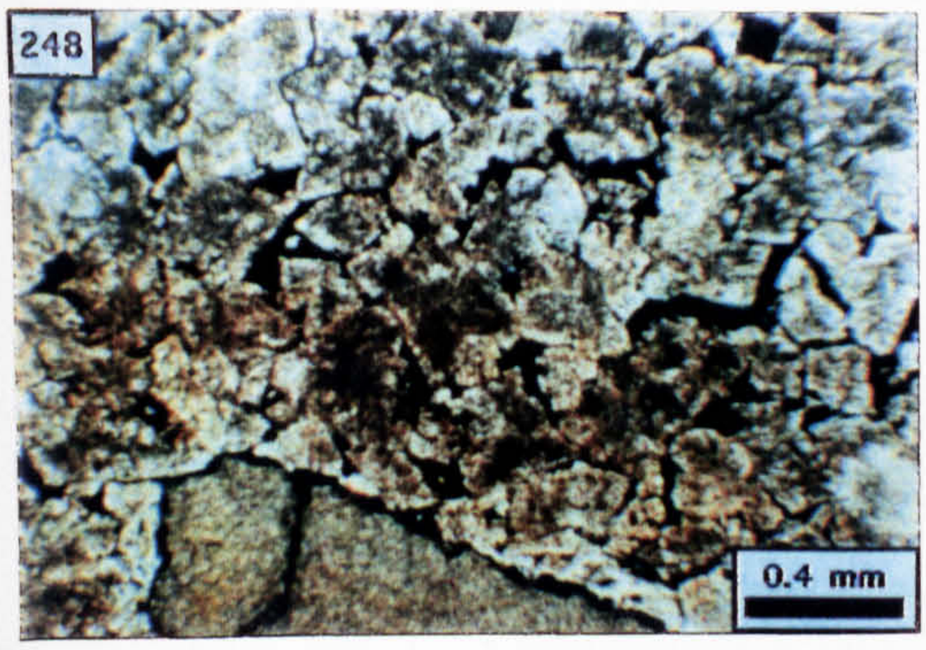
248
0.4 mm

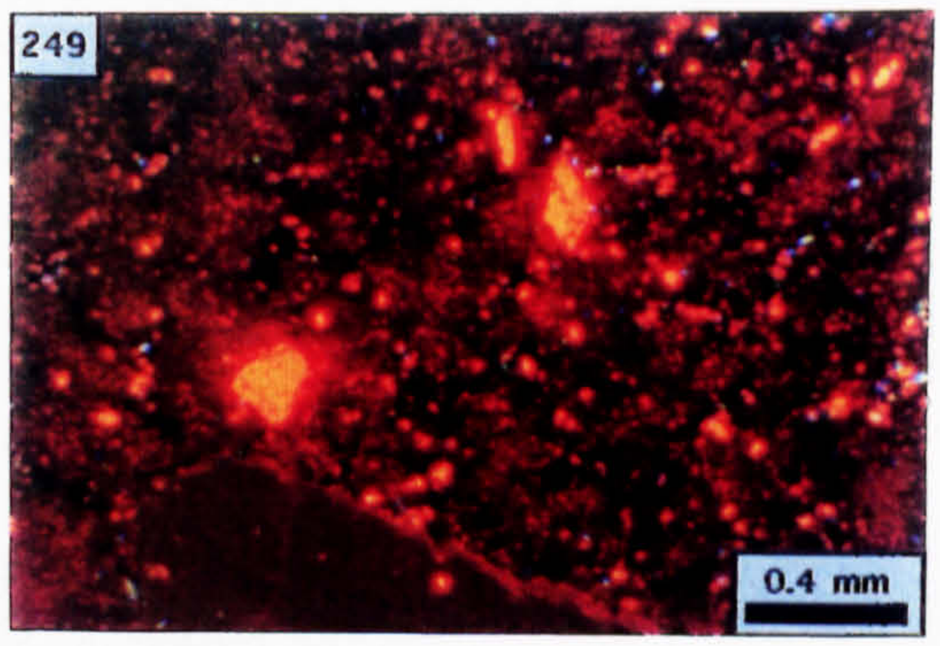
249
0.4 mm

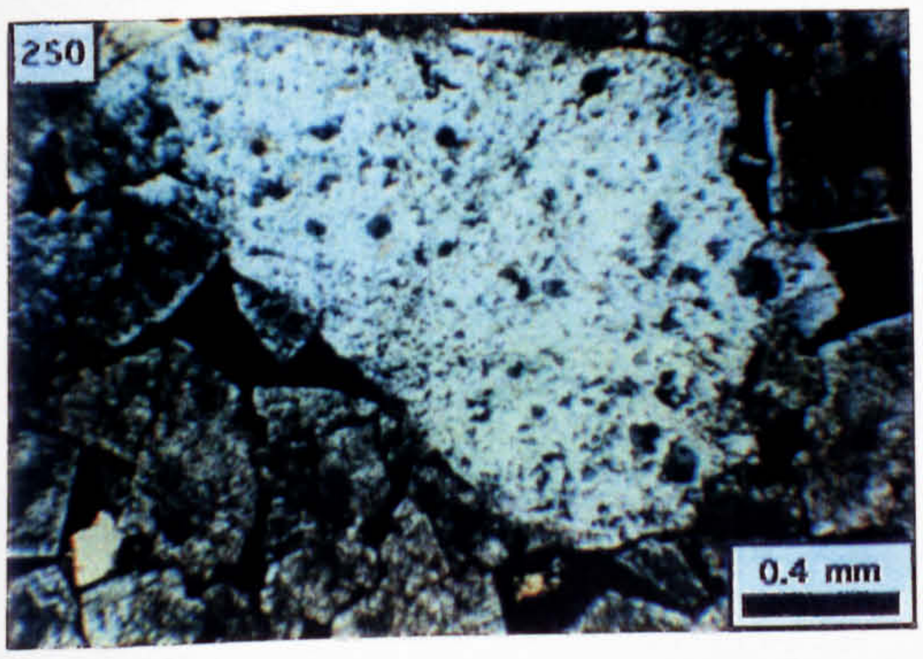
250
0.4 mm

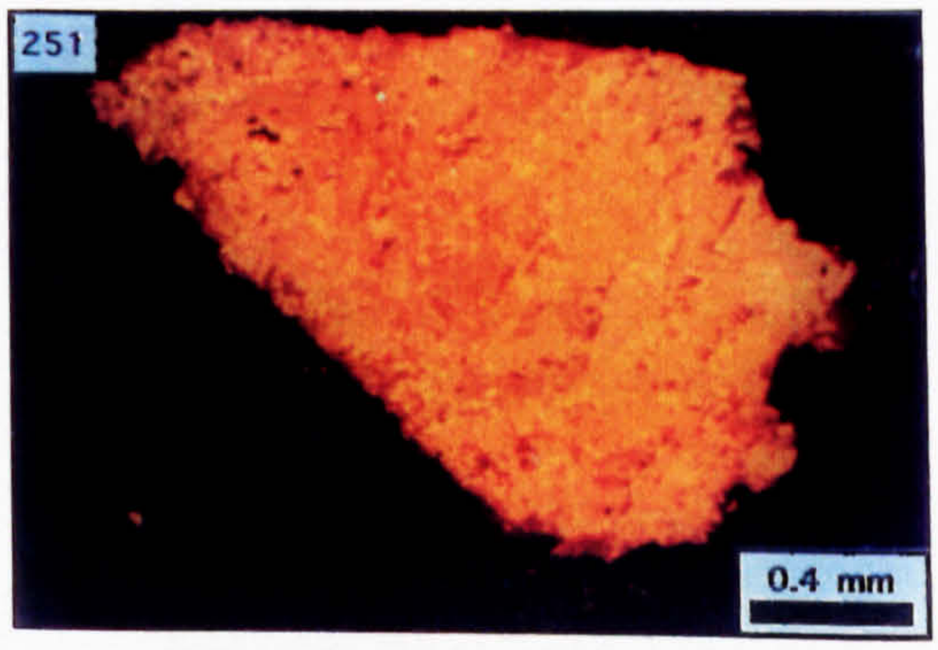
251
0.4 mm

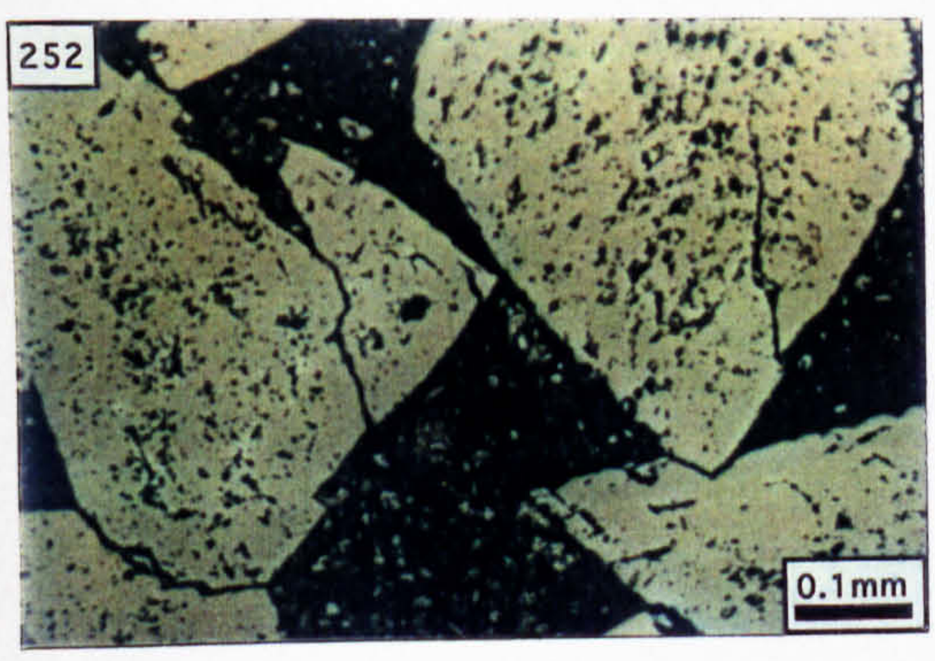
252
0.1mm

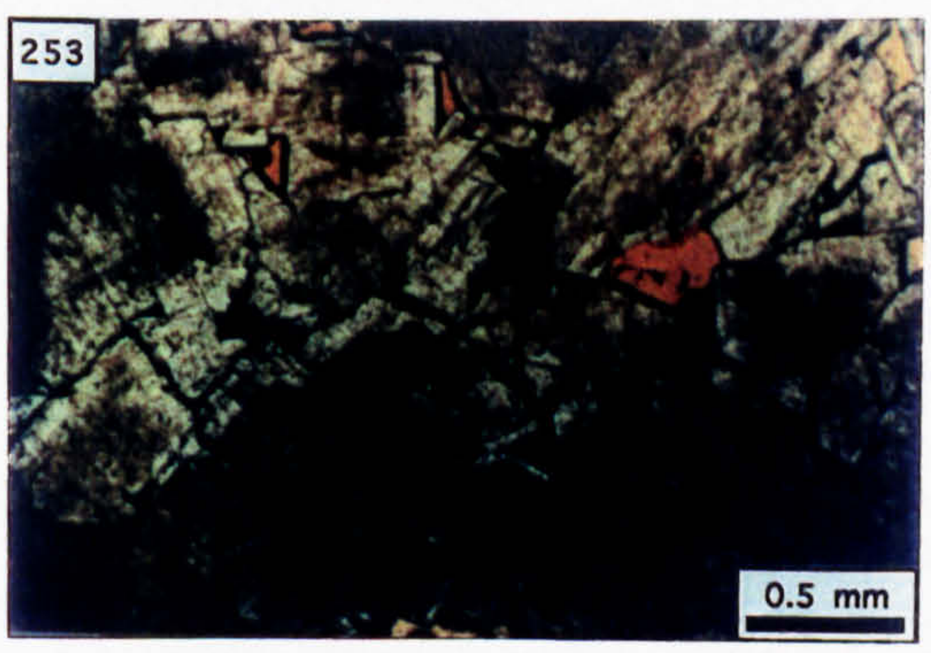
253
0.5 mm

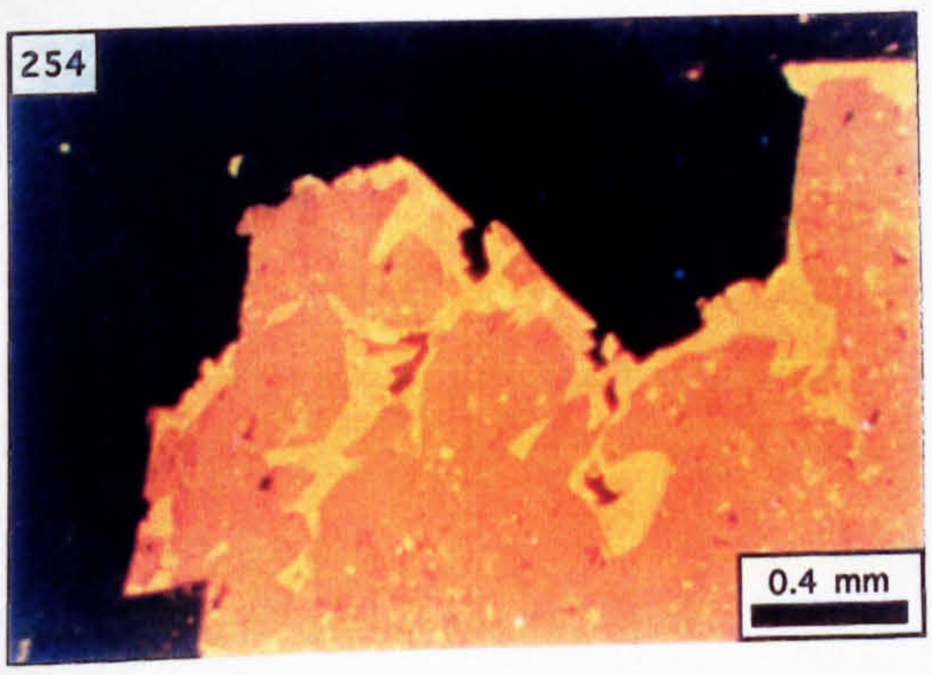
254
0.4 mm

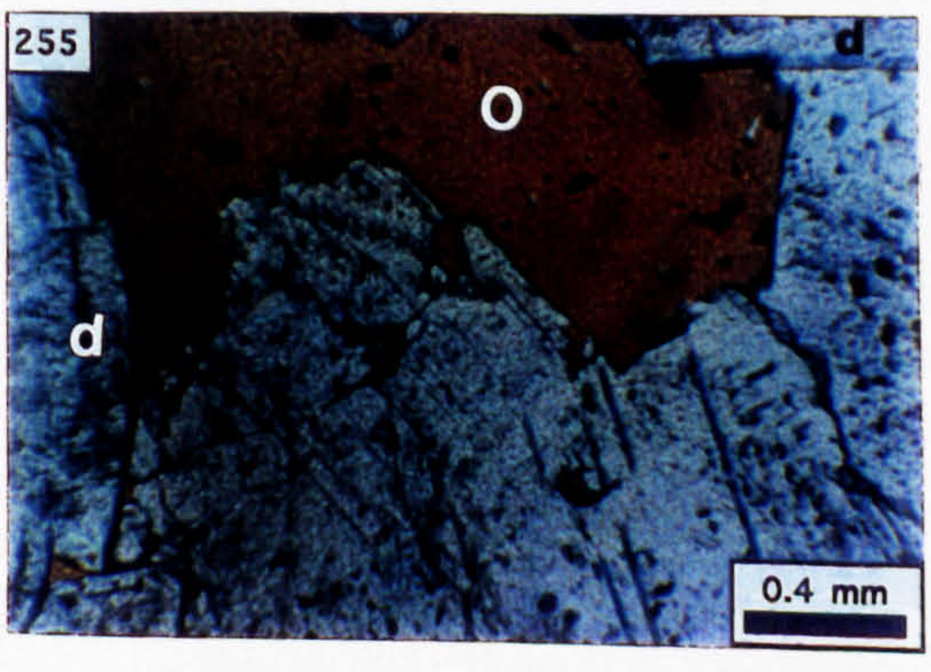
255
O
d
d
0.4 mm

Photo. 256. Dolomite (d) infilling a void lined with radiaxial calcite (r) from a clast in the Boulder Conglomerate; b=biomicrite (2 cm scale bar; N1137, 562.9 m).

Photo. 257. Void margin defined by the euhedral crystal terminations of radiaxial calcite (r); the void fill comprises crystals of non-luminescent dolomite, often with brightly luminescent cores (CL; N1137, 562.9 m).

Photo. 258. As above but XPL; p= pyrite.

Photo. 259. Petrography of the vug fill showing a sparite clast (S) supported by a matrix of dolomite grains; the dark, intergrain material comprises pyritic argillite (PPL; N1137, 562.9 m).

Photo. 260. As above but CL; notice the brightly luminescent, euhedral cores to the dolomite grains (N1137, 562.9 m).

Photo. 261. Mudstone clasts (m) associated with dolomite and pyritic argillite (PPL; N1137, 562.9 m).

Photo. 262. Sulphide mineralisation (dark grains) disseminated in arenite (PPL).

Photo. 263. Sulphide mineralisation (dark grains) disseminated in biosparite (PPL).

256

257

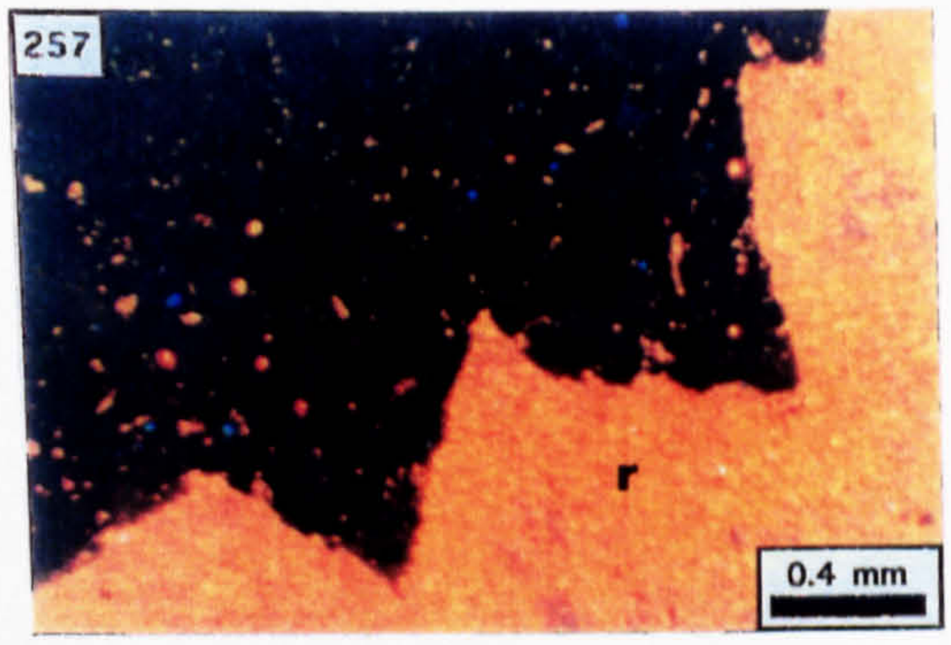

258

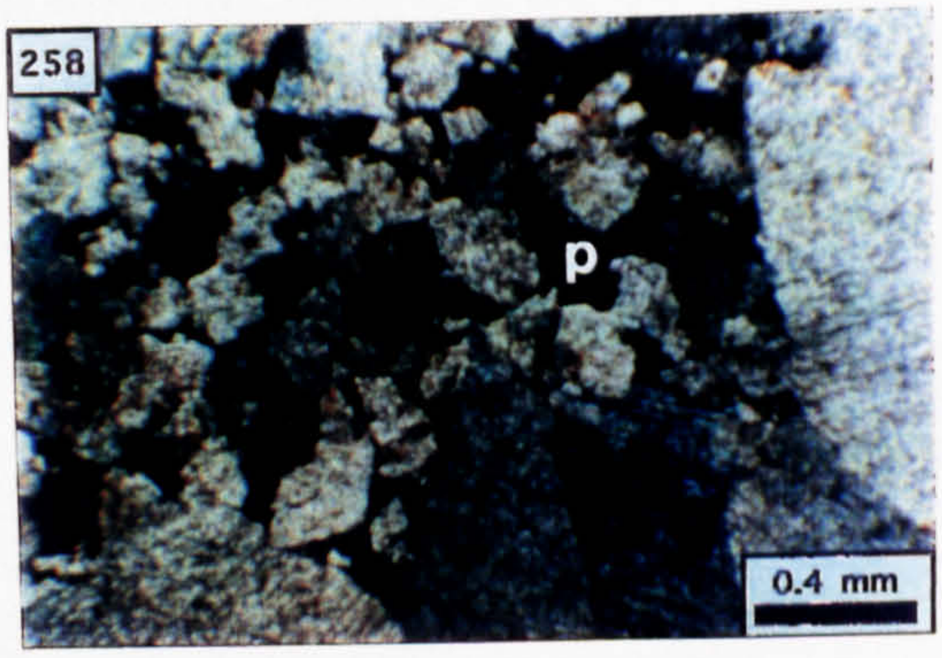

259

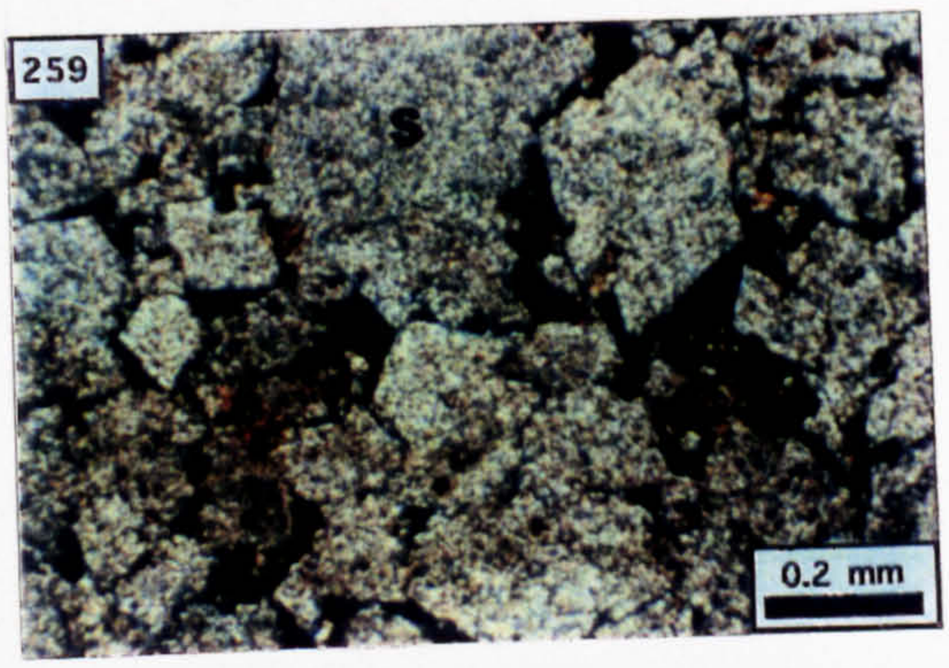

260

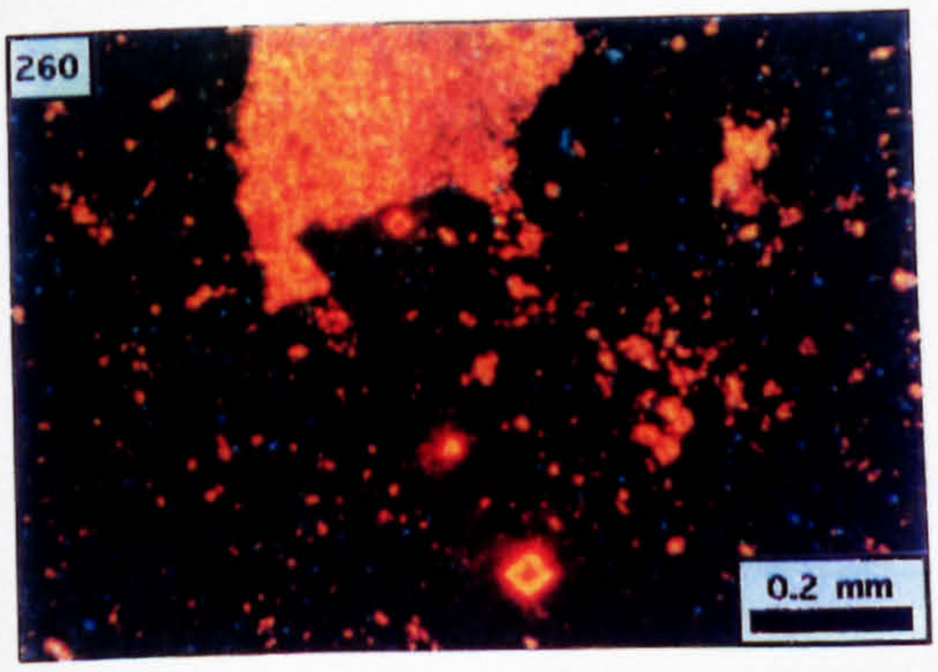

261

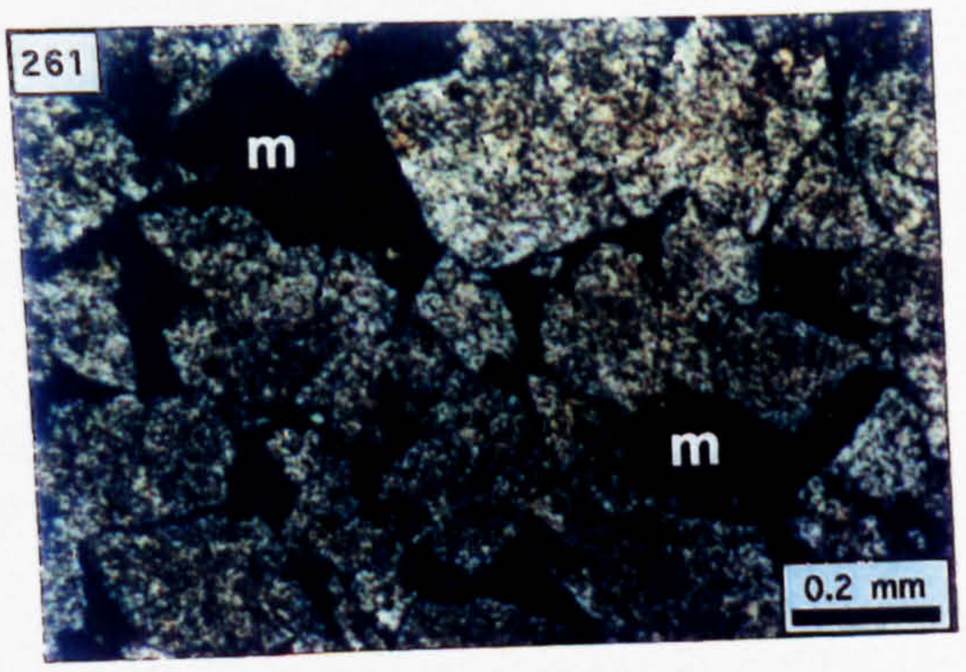

262

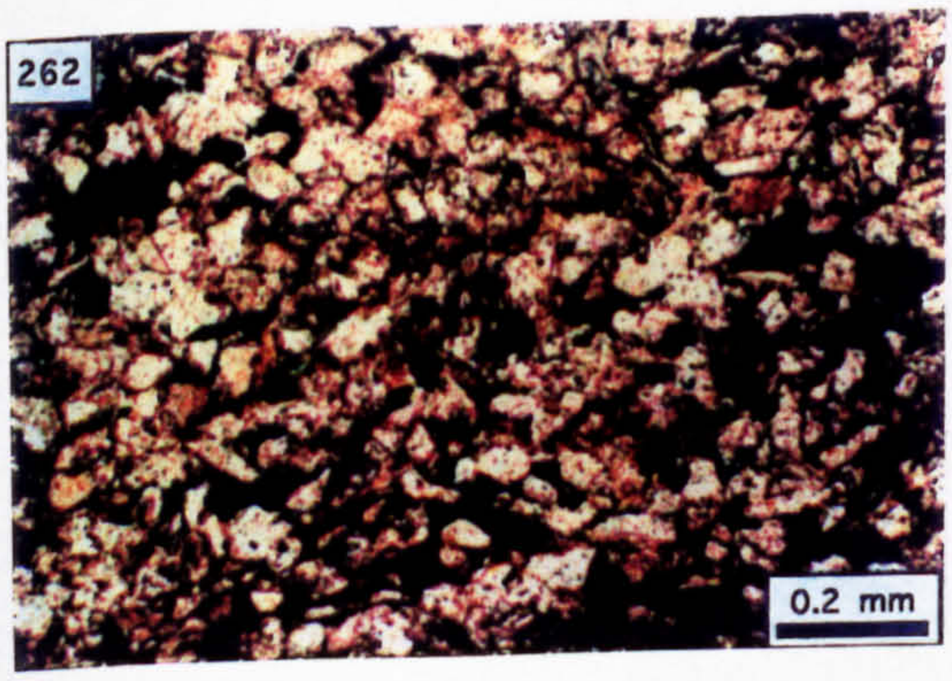

263

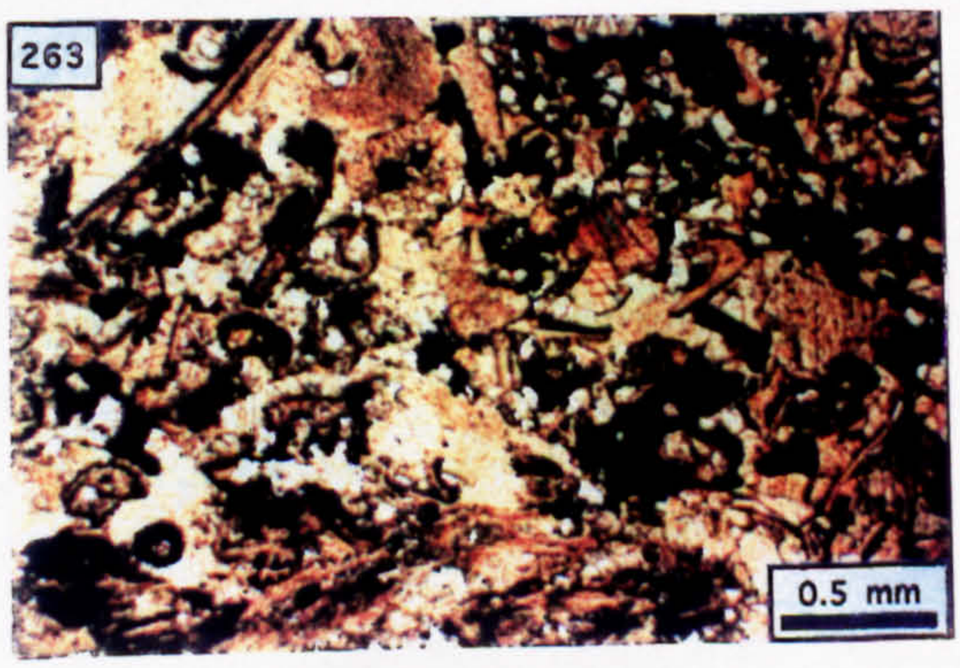

Photo. 264. Underground photograph of the P1S heading, looking south, showing mineralised bioclastic limestone strata (a) in the Shaley Pales beneath the unconformity (U); the back is dry and unwashed.

Photo. 265. Underground photograph of the east sidewall of the P1S heading showing mineralisation developed as stratiform replacement to bioclastic limestone in the Shaley Pales (25 cm ruler for scale).

Photo. 266. Petrography of the replacement mineralisation: g=galena, s=sphalerite, q=hydrothermal quartz (PPL).

Photo. 267. Intensely pyritised bioclastic limestone (B) overlain by relatively unmineralised arenite (A); the white grains present in B are unreplaced detrital siliciclastics [PPL].


264
U

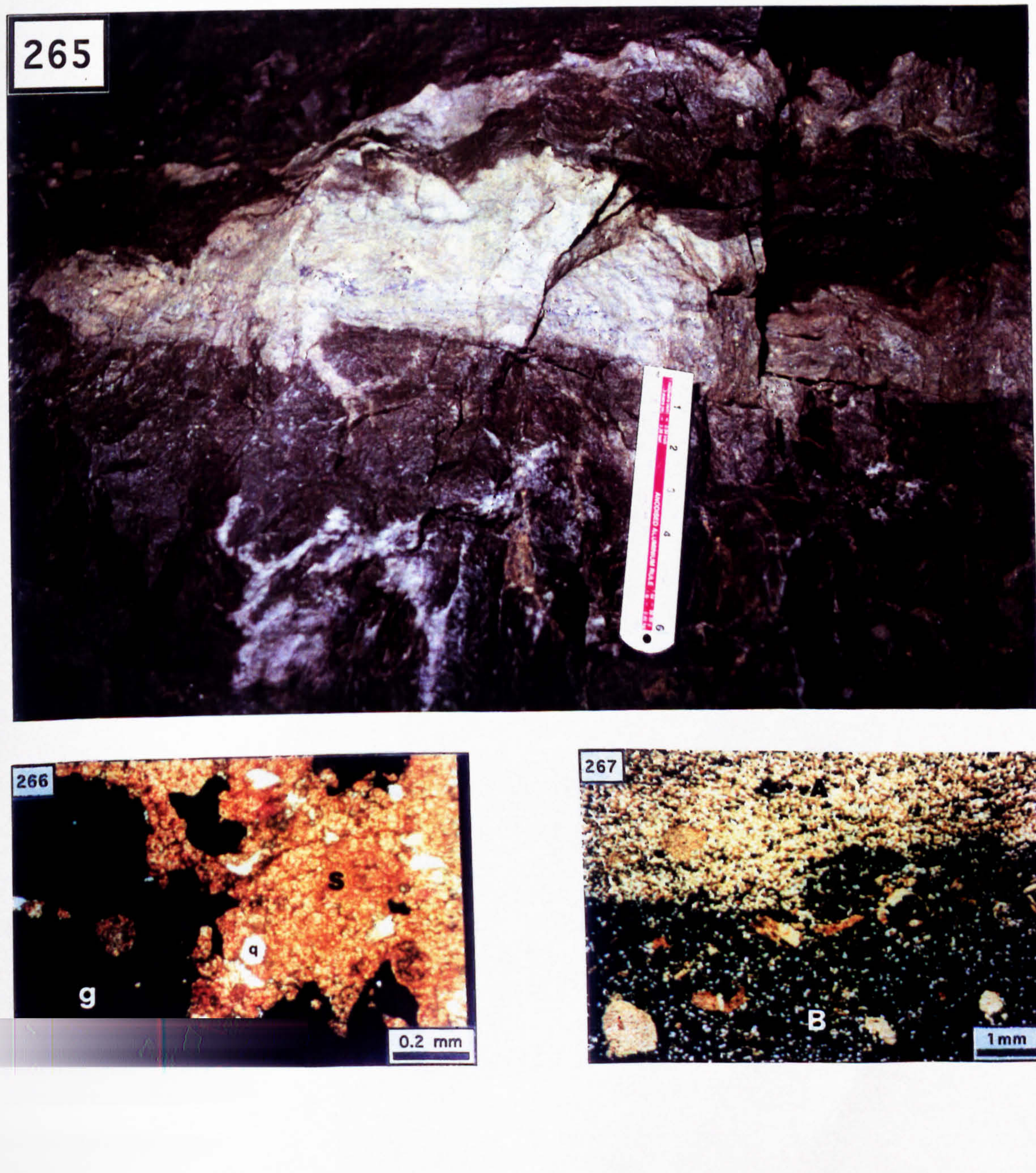
265

266
S
q
g
0.2 mm

267
A
B
1 mm

Photo. 268. Sharp, irregular contact defined by intensely replaced bioclastic limestone (1) overlying unmineralised bioclastic limestone (2) [PPL].

Photo. 269. Replacement mineralisation exhibiting local discordance in relation to a stylolite (s) located in bioclastic limestone (PPL).

Photo. 270. Partially replaced bioclastic limestone (PPL).

Photo. 271. Petrography of the vug mineralisation associated with the replaced bioclastic limestone strata: 1=laminated fine sphalerite containing detrital siliciclastics, 2=coarse, yellow sphalerite, 3=baroque dolomite intergrown with barite (PPL).

Photo. 272. Underground photograph of the east sidewall of the P1S heading showing mineralisation associated with vertically impersistent fractures through replaced bioclastic limestone strata.

Photo. 273. Petrography of the fracture-associated mineralisation: B=unreplaced bioclastic limestone, P=pyritised bioclastic limestone, F=fracture-encrusting colloform sphalerite, S=sediment, C=calcite. The white grains present in the pyritised bioclastic limestone are unreplaced siliciclastic sand grains and partially replaced coarse bioclasts (PPL).

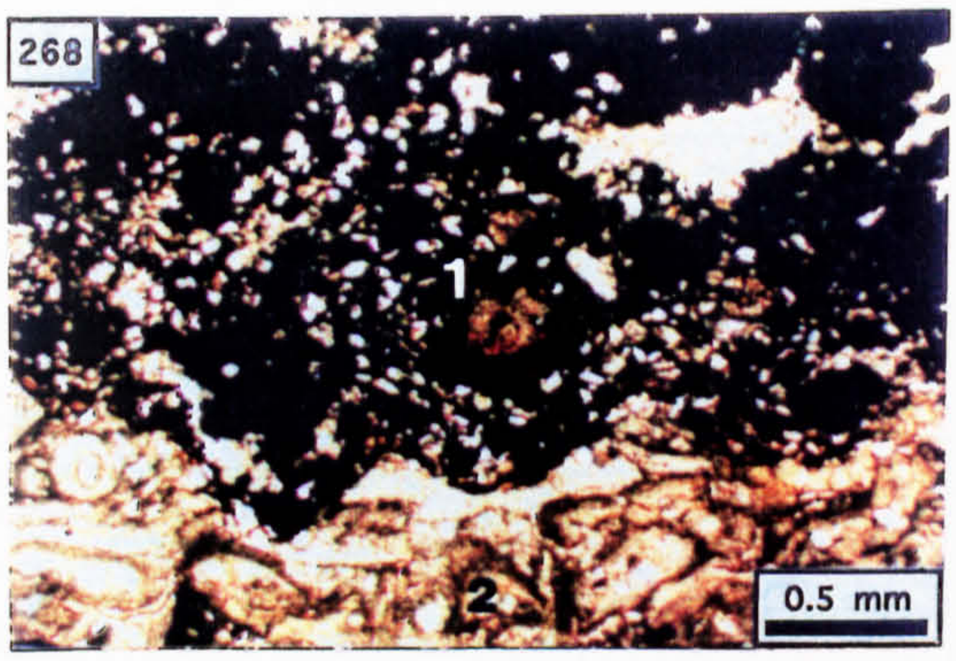
268
1
2
0.5 mm

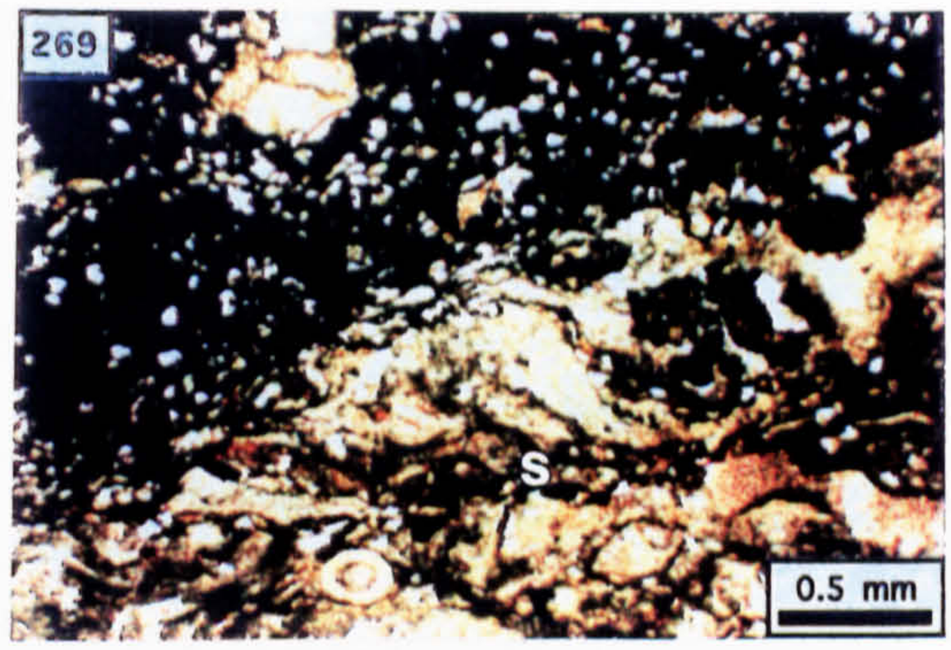
269
S
0.5 mm

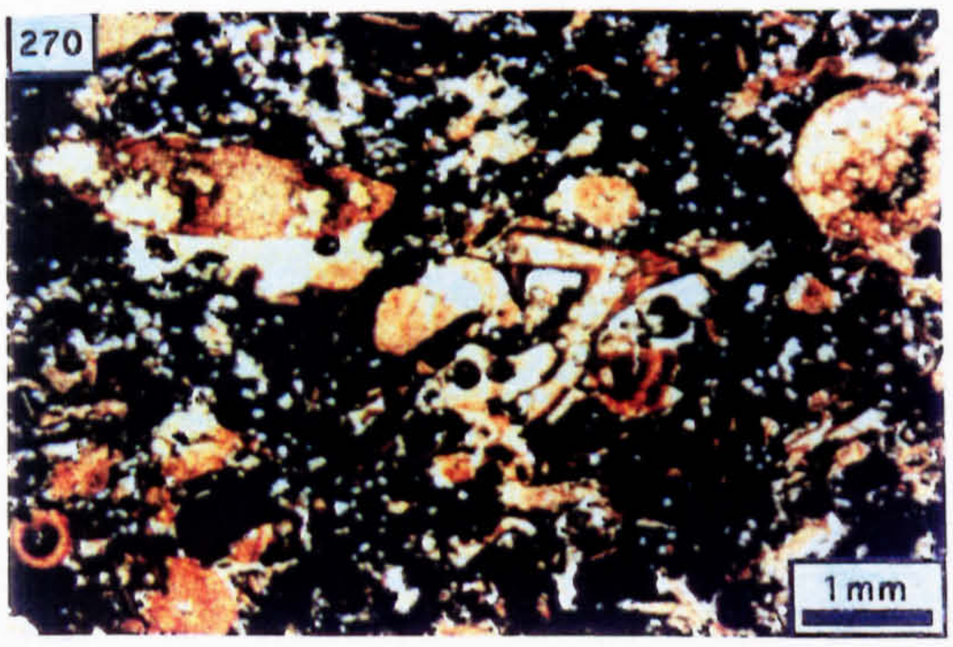
270
1mm

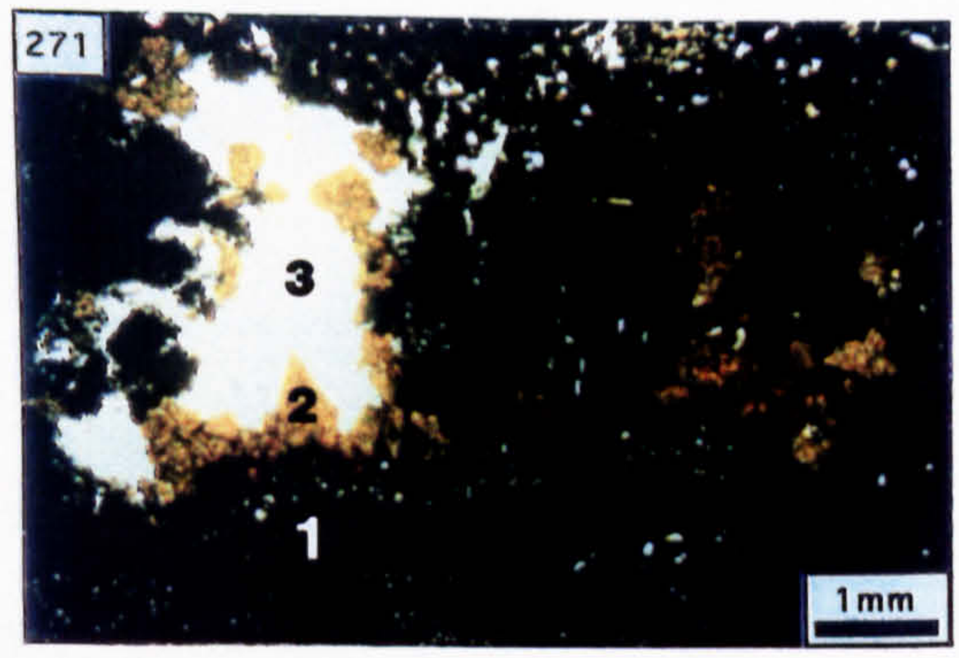
271
3
2
1
1mm


272

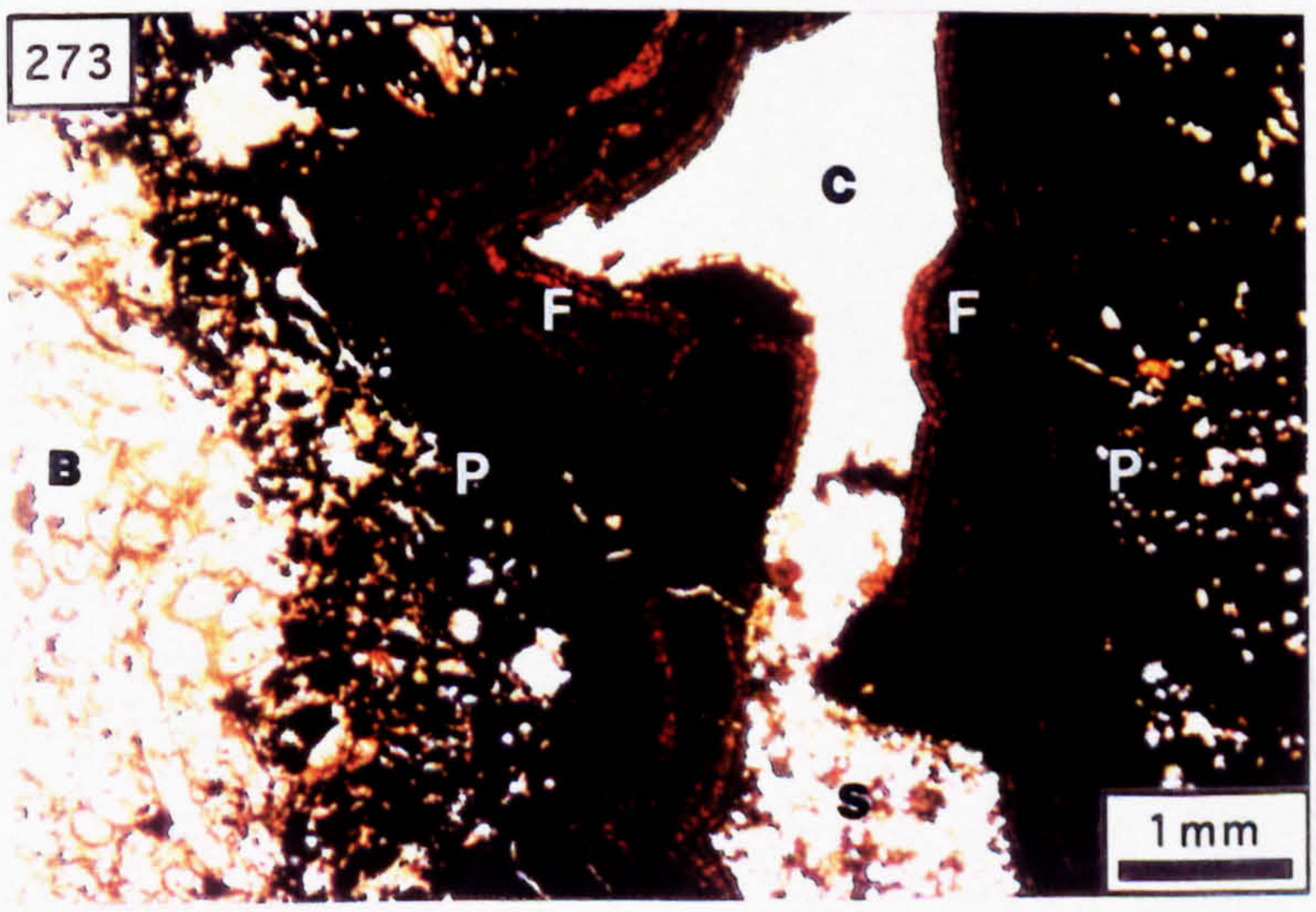
273
C
F
F
B
P
P
S
1mm

Photo. 274. Subhedral galena (g) intergrown with colloform sphalerite and encrusting the fracture wall (PPL).

Photo. 275. Fragment of the fracture wall showing pyritised bioclastic limestone, encrusted with colloform sphalerite; the clast is supported by a matrix of sphaleritic arenite (PPL).

Photo. 276. Brecciated colloform sphalerite cemented by coarse, pale yellow sphalerite; the latter is non-luminescent in C.L. and corresponds to "n" in Photo. 277 (PPL).

Photo. 277. CL photomicrograph of the fracture mineralisation: p=pyritised bioclastic limestone, c=colloform sphalerite, n=non-luminescent sphalerite, s=sparite. Notice the contiguity of the non-luminescent sphalerite with the cement to the microfractured colloform sphalerite.

Photo. 278. Underground photograph of the north sidewall of CGO AC showing mineralisation developed as cement to the breccia bed deposited unconformably over the Shaley Pales; i=interbed to the Boulder Conglomerate (25 cm ruler and hammer for scale).

Photo. 279. Underground photograph of the east sidewall of the P2 heading showing mineralisation as cement to the strike-equivalent breccia unit shown in Photo. 278; U=unconformity, i=interbed to the Boulder Conglomerate.

274

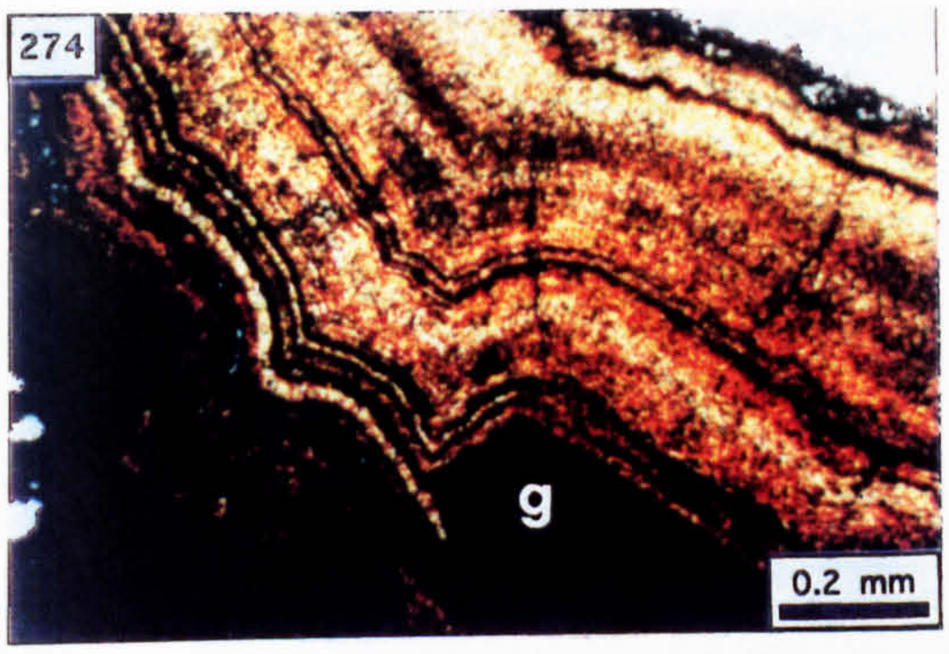

275

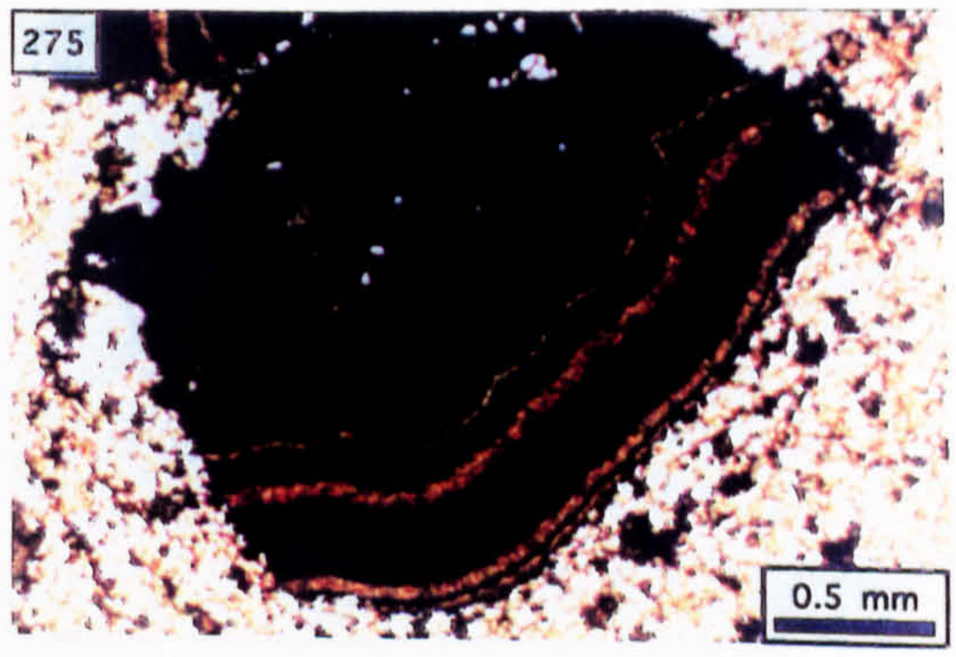

276

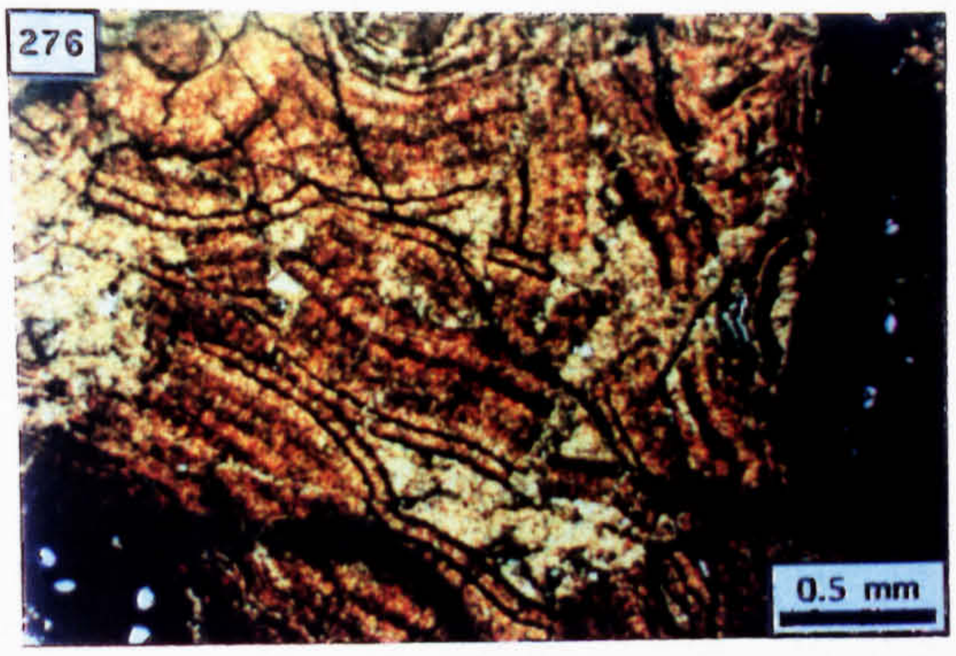

277

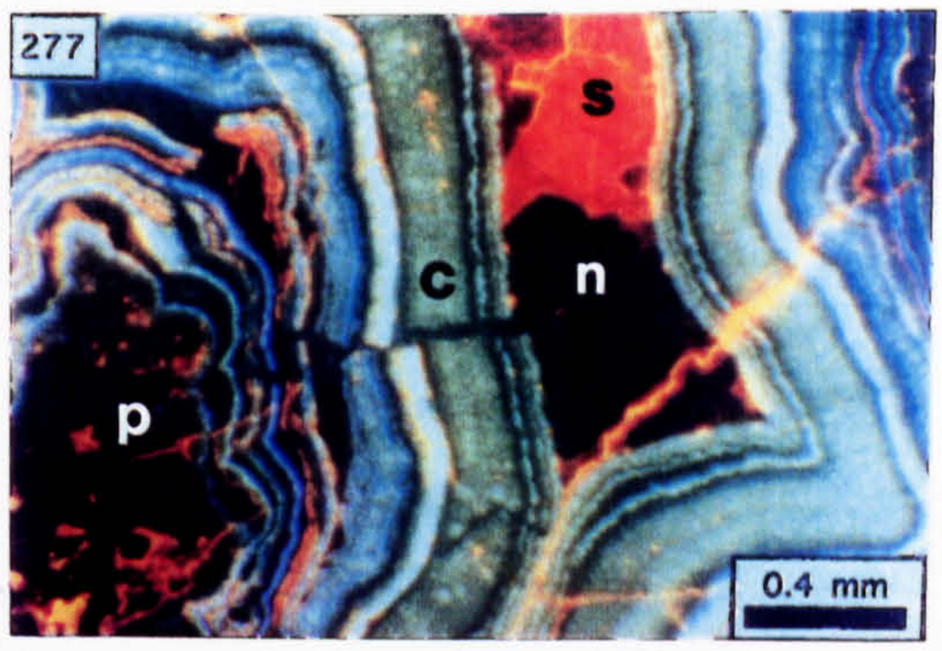

278

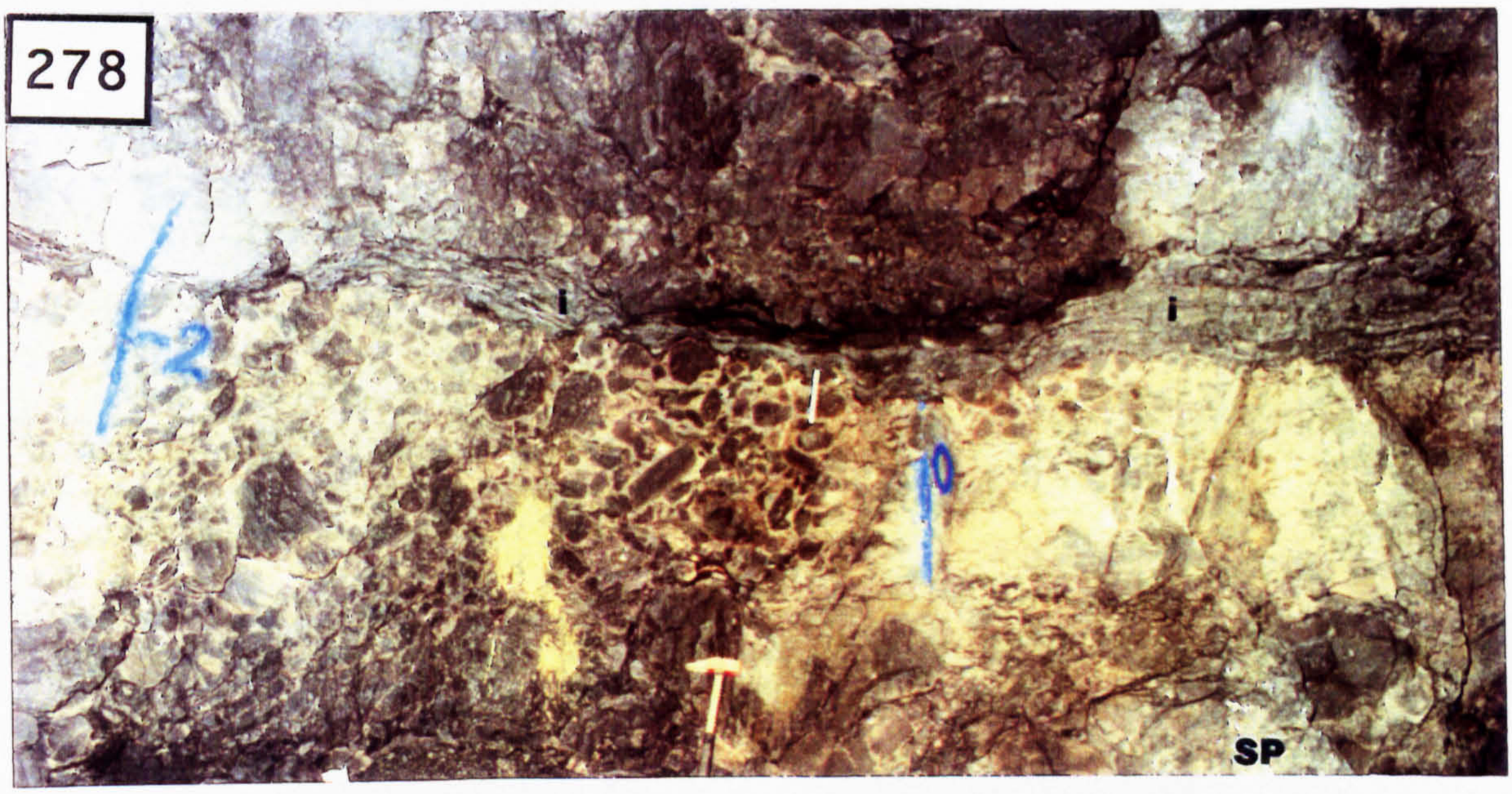

279

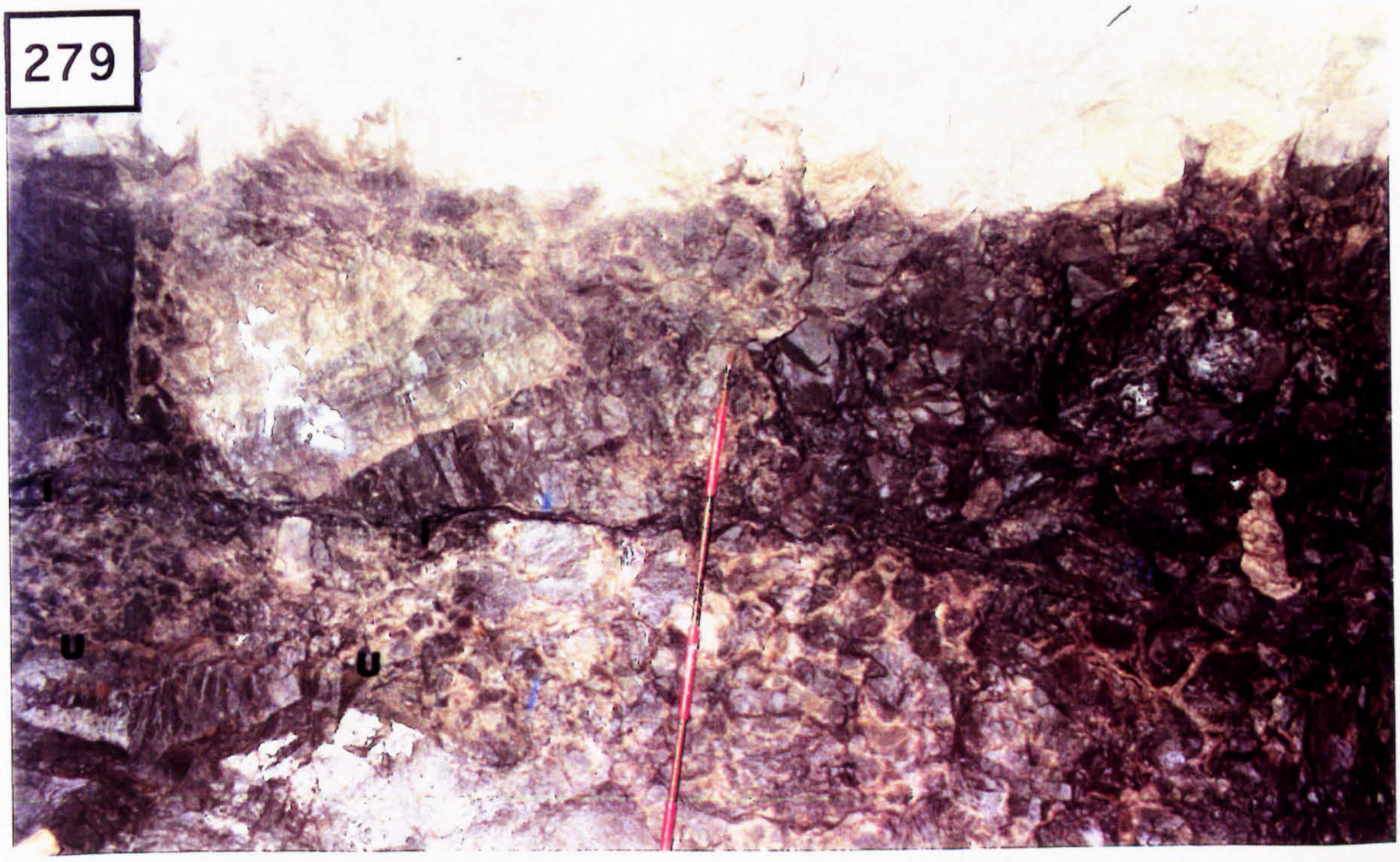

Photo. 280. Pyritised bioclastic limestone from the unconformity (PPL).

Photo. 281. Polished slab showing the petrography of the mineralisation developed as cement to the breccia unit deposited on the unconformity; c=limestone clasts (2 cm scale bar).

Photo. 282. Close-up of Photo. 281 showing the occurrence of mineralisation as interclast cement to limestone clasts; 1=geopetally laminated sphalerite-barite, 2=clast-encrusting sphalerite-galena, 3=rim replacement, 4=brecciated 2, 5=void-occluding baroque dolomite-barite--sparite; notice the obliterated interclast contact at 3a.

Photo. 283. Pyritised rim (P) to a biosparite clast (PPL).

Photo. 284. Rim of oobiosparite clast replaced by sphalerite (S) [PPL].

Photo. 285. Oobiosparite clast showing peripheral replacement by barite (B) and sphalerite (dark grains); q=relict detrital siliciclastic grains (PPL).

Photo. 286. Petrography of the mineralisation developed on the floor of an interclast void showing: 1=unaltered oobiosparite, 2=peripherally altered clast margin, 3=geopetal sphalerite; notice the concentration of detrital siliclastics and the presence of corroded limestone in 2 (PPL).

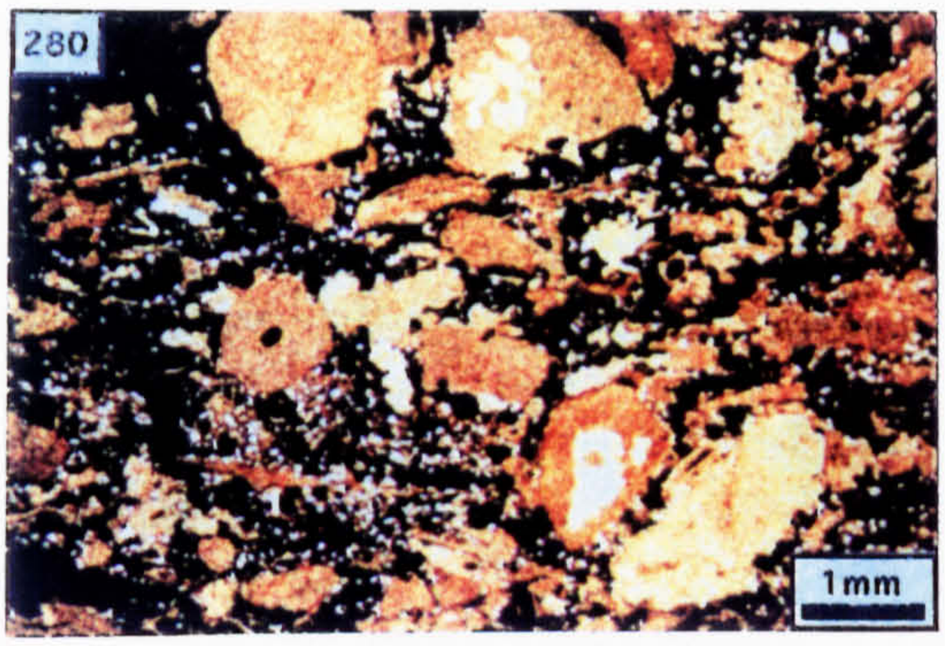
280
1mm

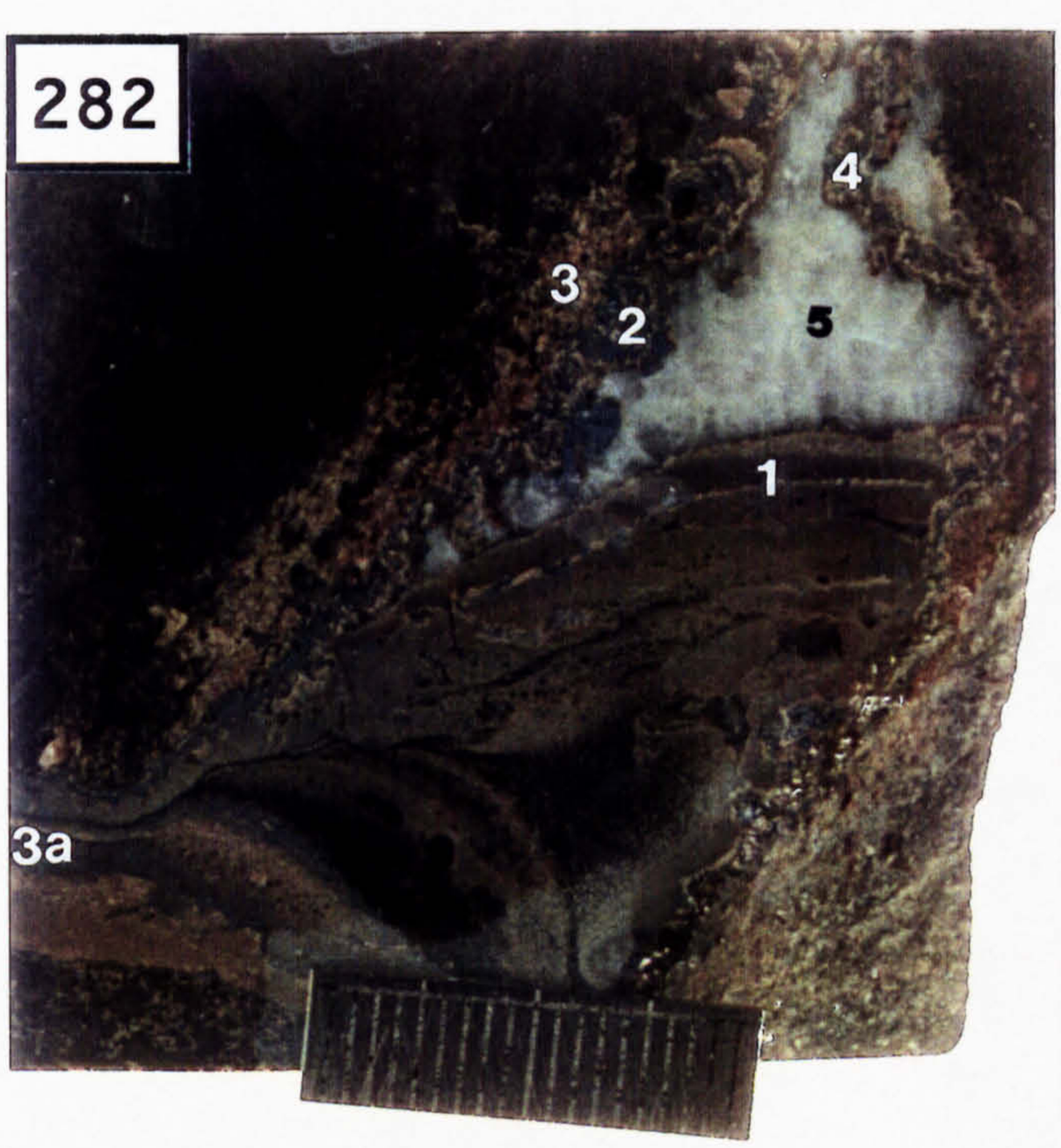
282
4
3
2
5
1
3a


281
C
C
C

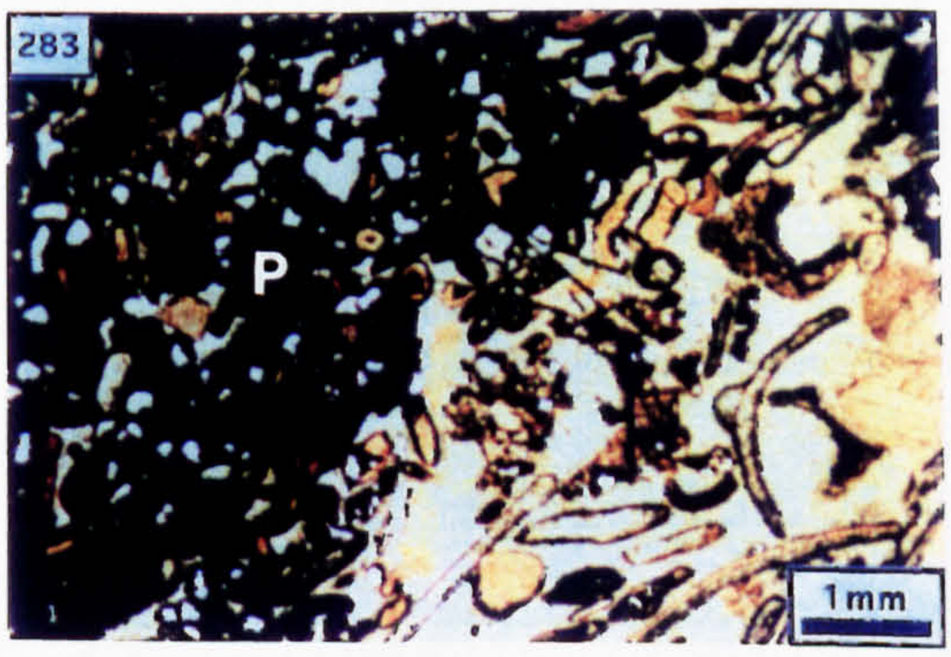
283
P
1mm

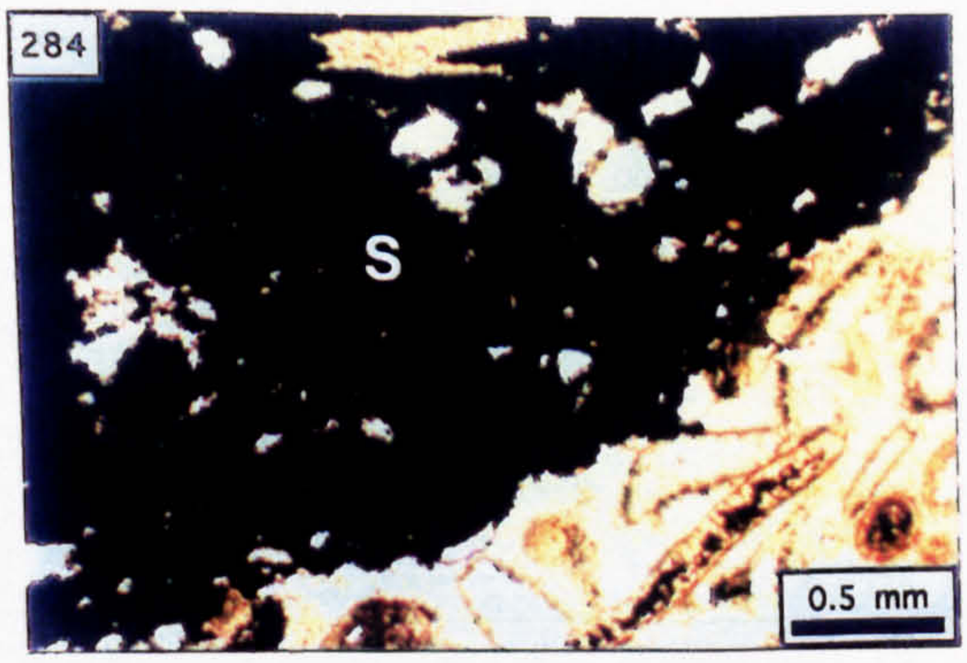
284
S
0.5 mm

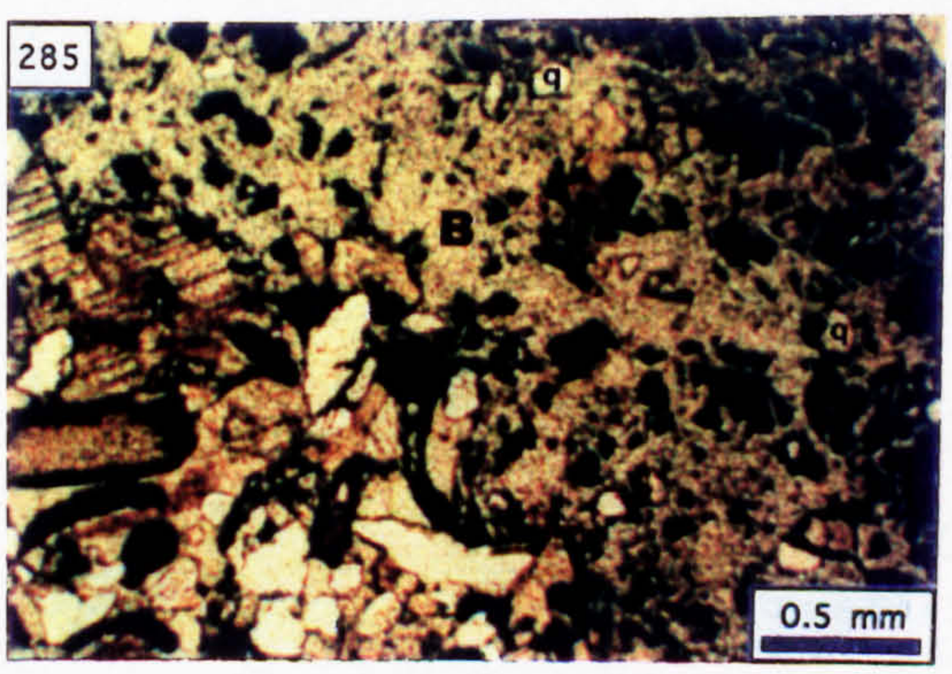
285
q
B
q
0.5 mm

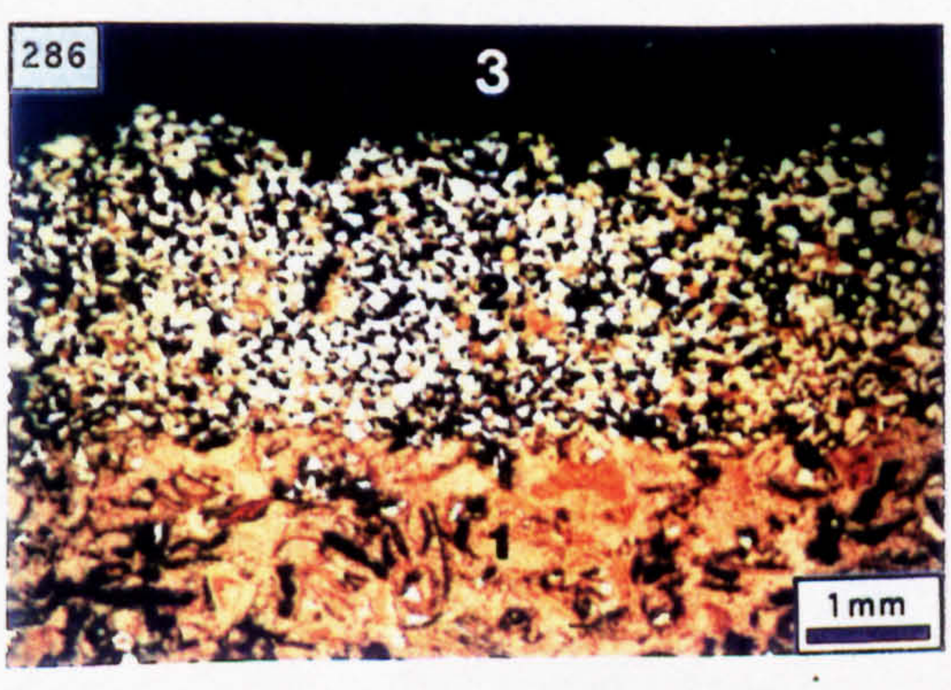
286
3
1
1mm

Photo. 287. Morphology of the corroded clast margins where the clasts (C) are in contact. Sphalerite (S) occurs as cement to the altered clast margins in contiguity with the geopetal sphalerite present on the void floor. The vein which truncates the sphalerite and alteration rim is cemented by fibrous calcite (PPL).

Photo. 288. Mineralisation developed as geopetal laminae on the void floor showing interlaminated microcrystalline sphalerite and barite which is overgrown by coarse, yellow sphalerite (PPL).

Photo. 289. Cross section through void wall showing replaced oolite (O) which is encrusted by colloform sphalerite (C) and then coarse, yellow sphalerite (Y) [PPL].

Photo. 290. Brecciated colloform sphalerite cemented by coarse yellow sphalerite (PPL).

Photo. 291. Brecciated coarse yellow and colloform sphalerites (PPL).

Photo. 292. Brecciated crustiform sphalerite cemented by intergrown baroque dolomite-barite-sparite; the gangue assemblage occludes the remnant interclast porosity (PPL).

Photo. 293. Underground photograph of the P2 heading showing stratiform pyrite (p) within hemipelagic strata overlying the unconformity (U).

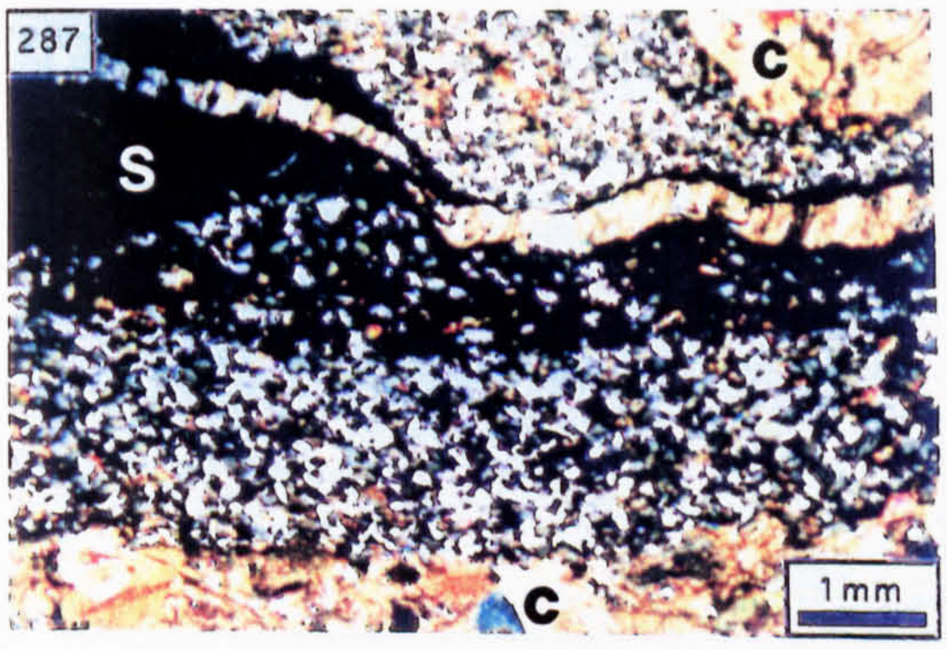
287
S
C
C
1mm

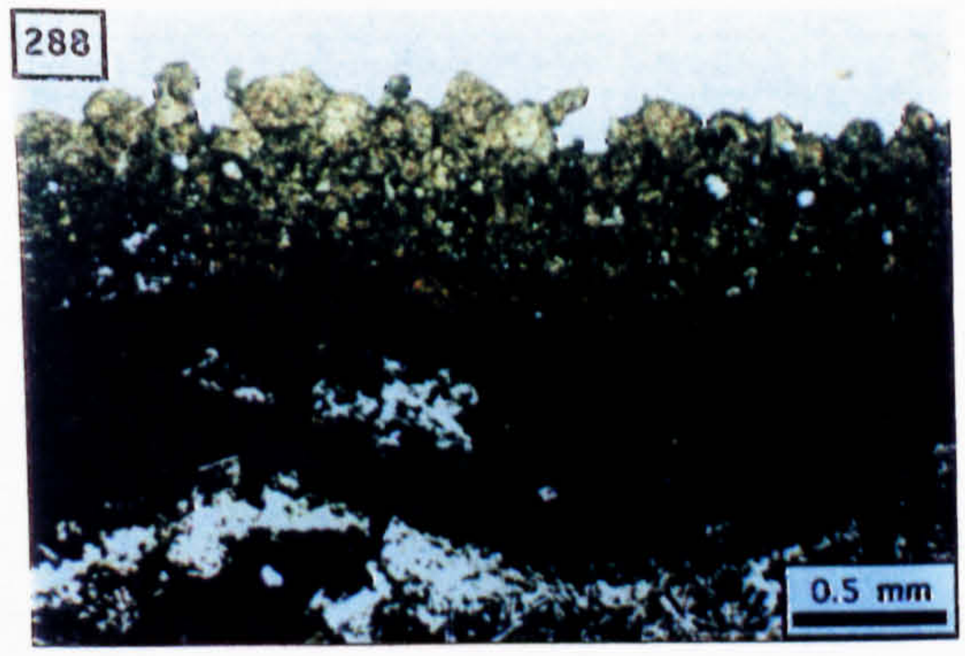
288
0.5 mm

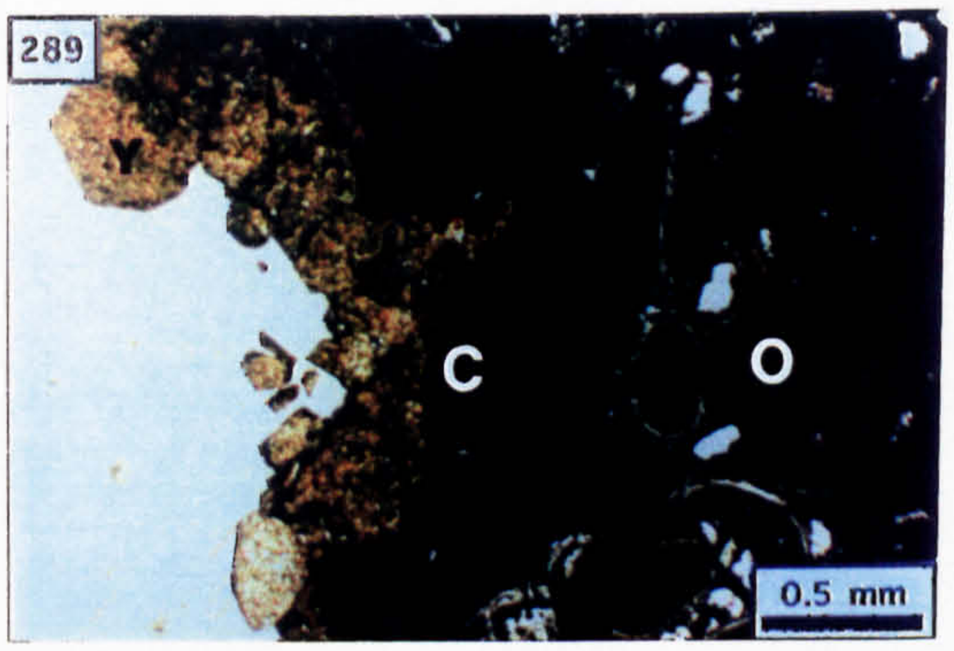
289
Y
C
O
0.5 mm

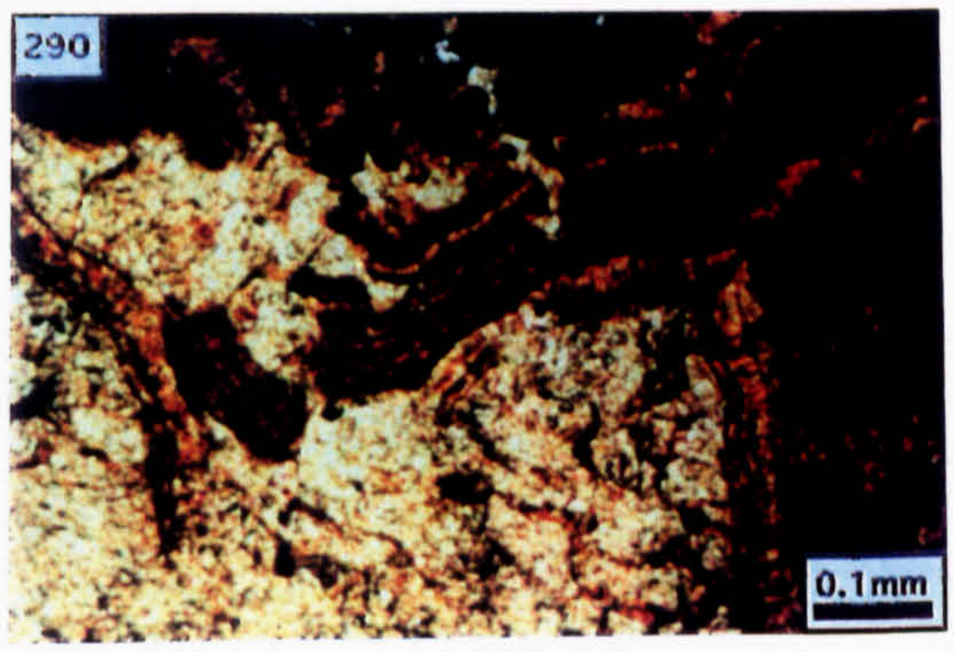
290
0.1mm

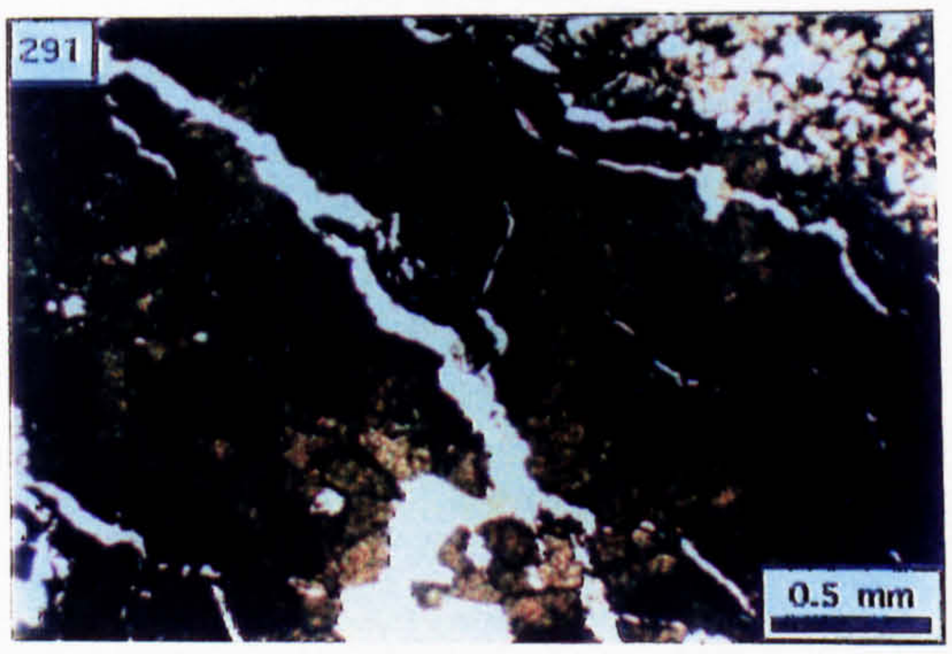
291
0.5 mm

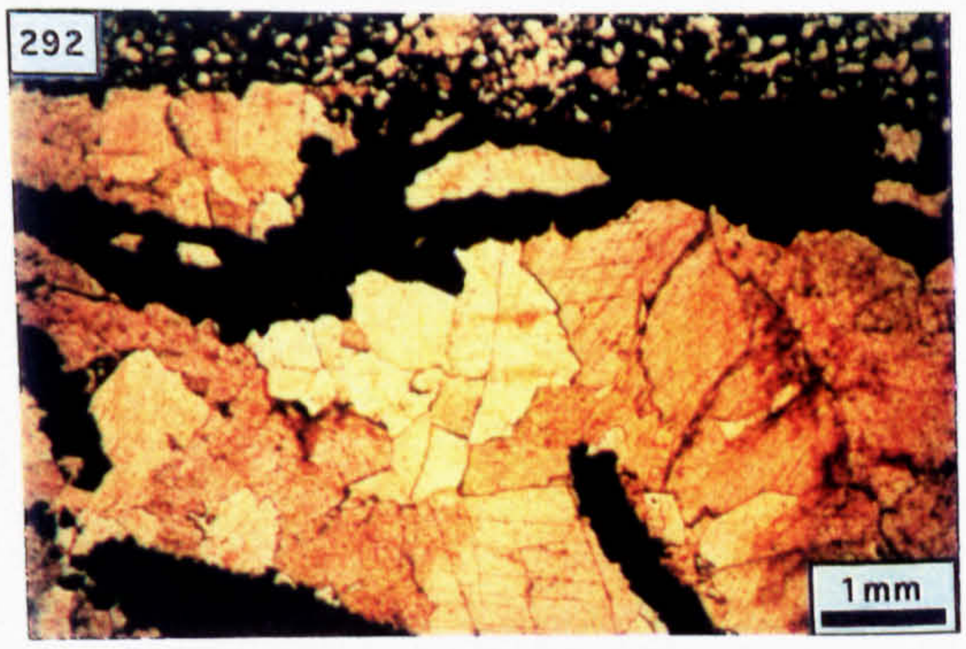
292
1mm

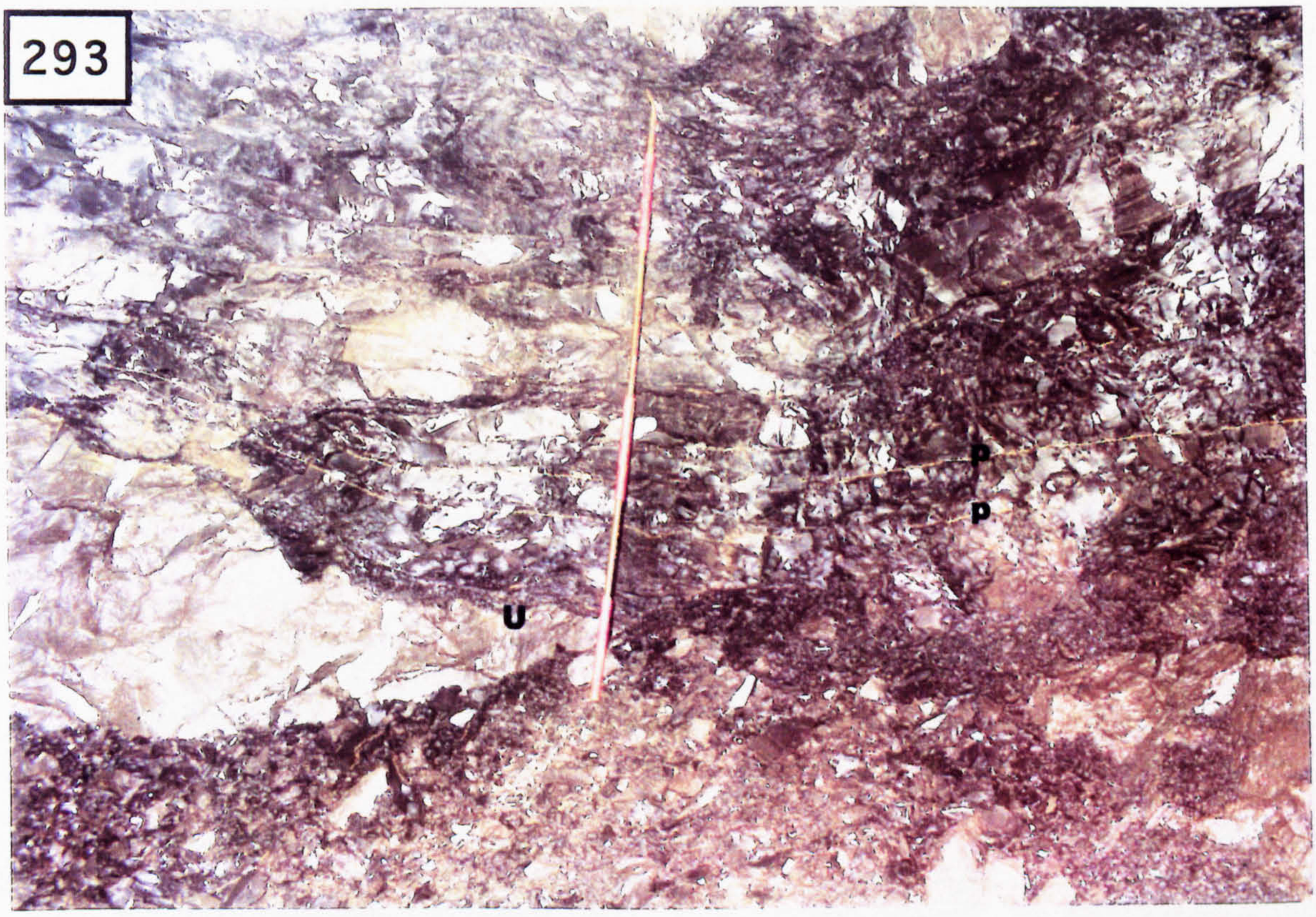
293
P
P
U

Photo. 294. Graded calcarenite to calcsiltite lamination showing replacement of the coarser sediment by pyrite (PPL).

Photo. 295. Incipiently pyritised calcarenite at the base of a graded lamination (PPL).

Photo. 296. Completely pyritised calcarenite (PPL).

Photo. 297. Blebby pyrite containing relict spicular bioclasts (RL).

Photo. 298. Massively pyritised calcarenite containing unreplaced bioclasts (RL).

Photo. 299. Underground photograph showing P.B.O. present in the footwall of the T Fault. The sharp lower contact of the stratiform sphalerite and galena with the unmineralised Pale Beds is marked by a millimetric layer of argillite (25 cm ruler for scale).

Photo. 300. Sample of the mineralisation shown in Photo. 299 showing oolitic limestone replaced by sphalerite and dolomite; the white grains are unreplaced detrital siliciclastics (PPL).

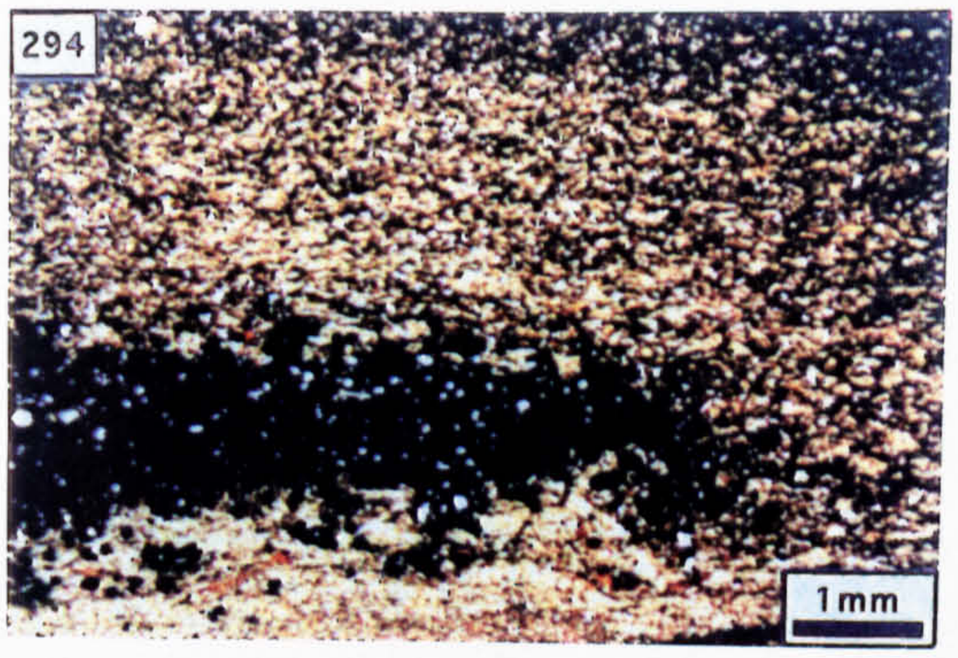
294
1mm

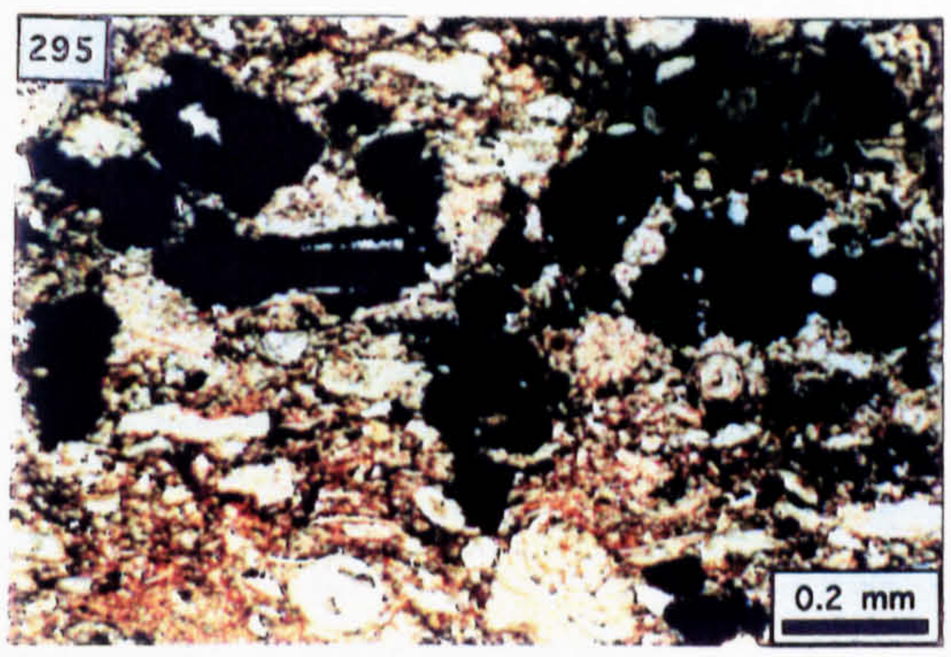
295
0.2 mm

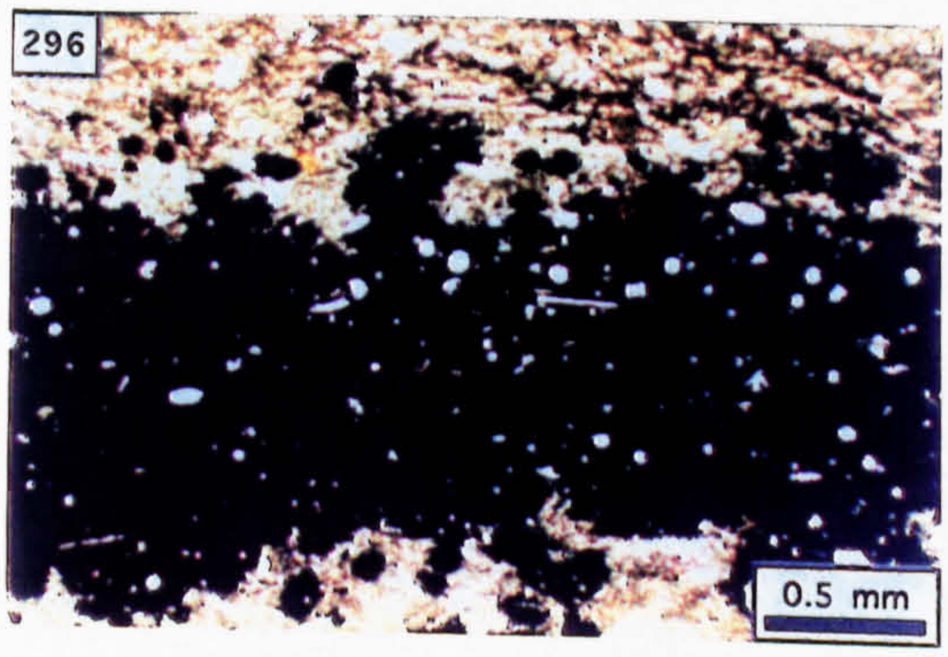
296
0.5 mm

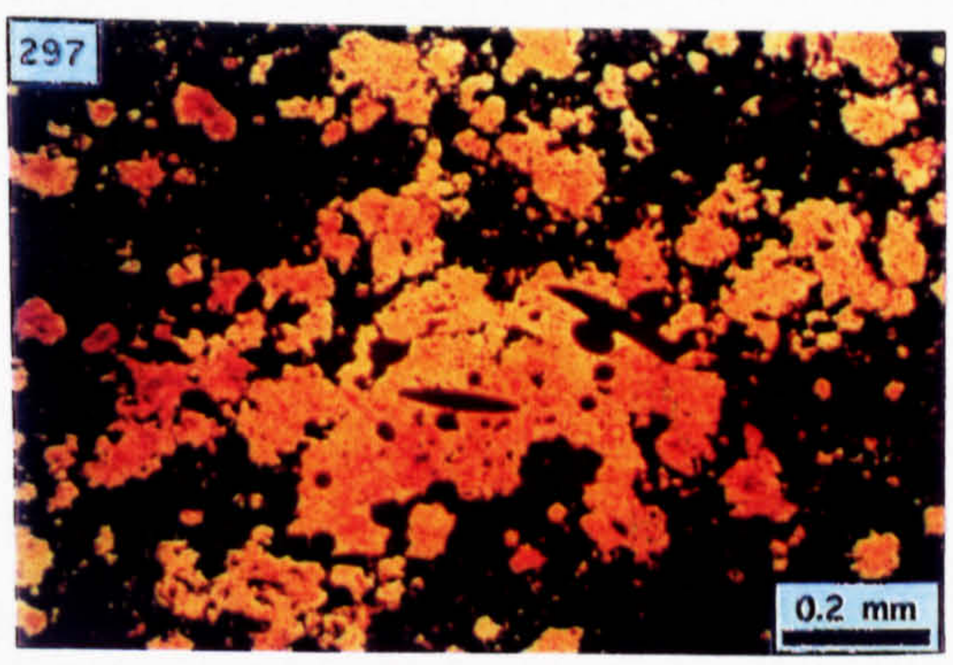
297
0.2 mm

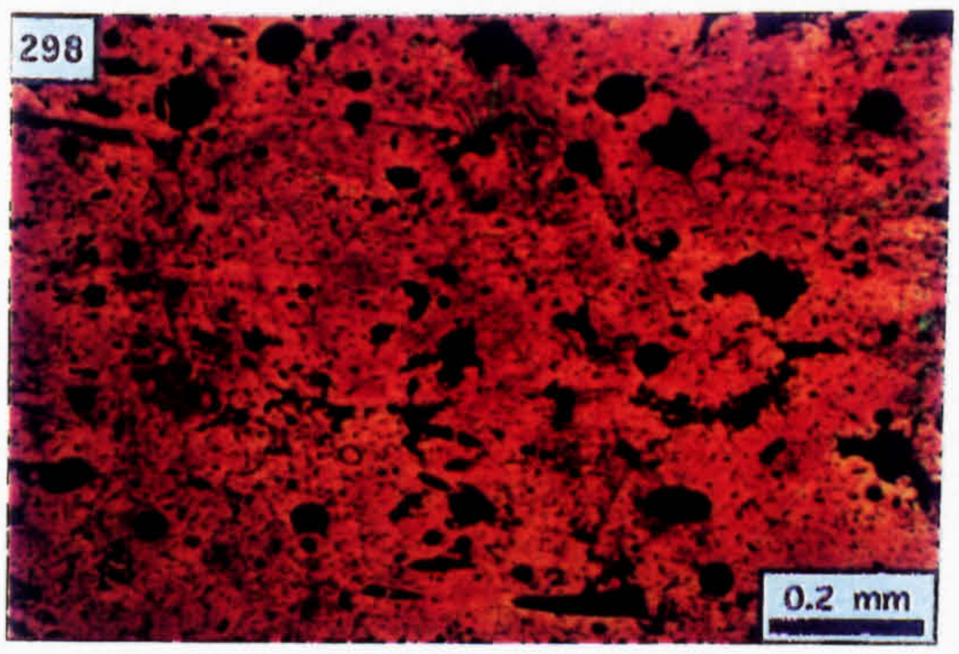
298
0.2 mm

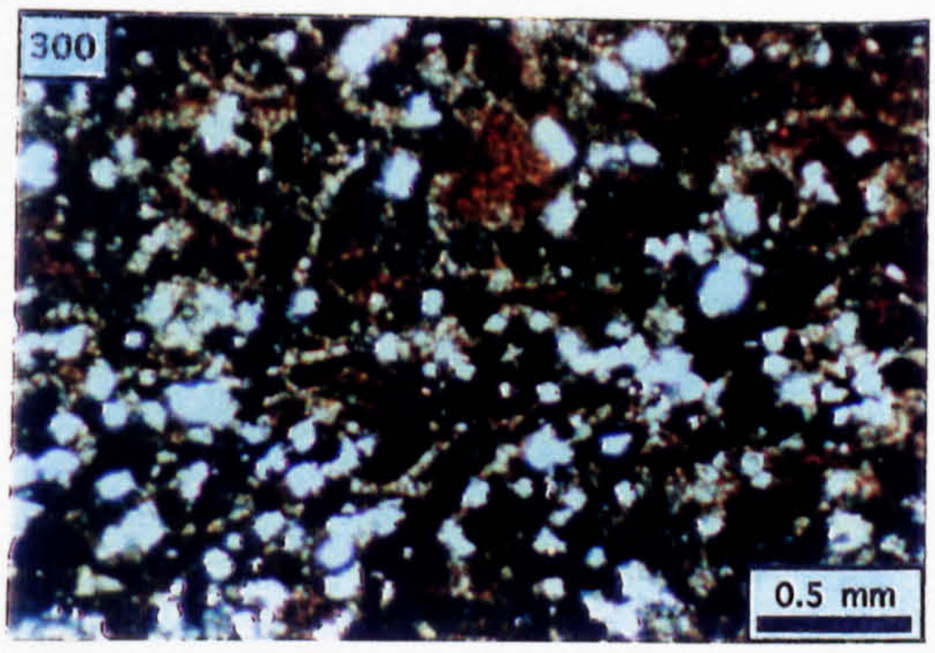
300
0.5 mm

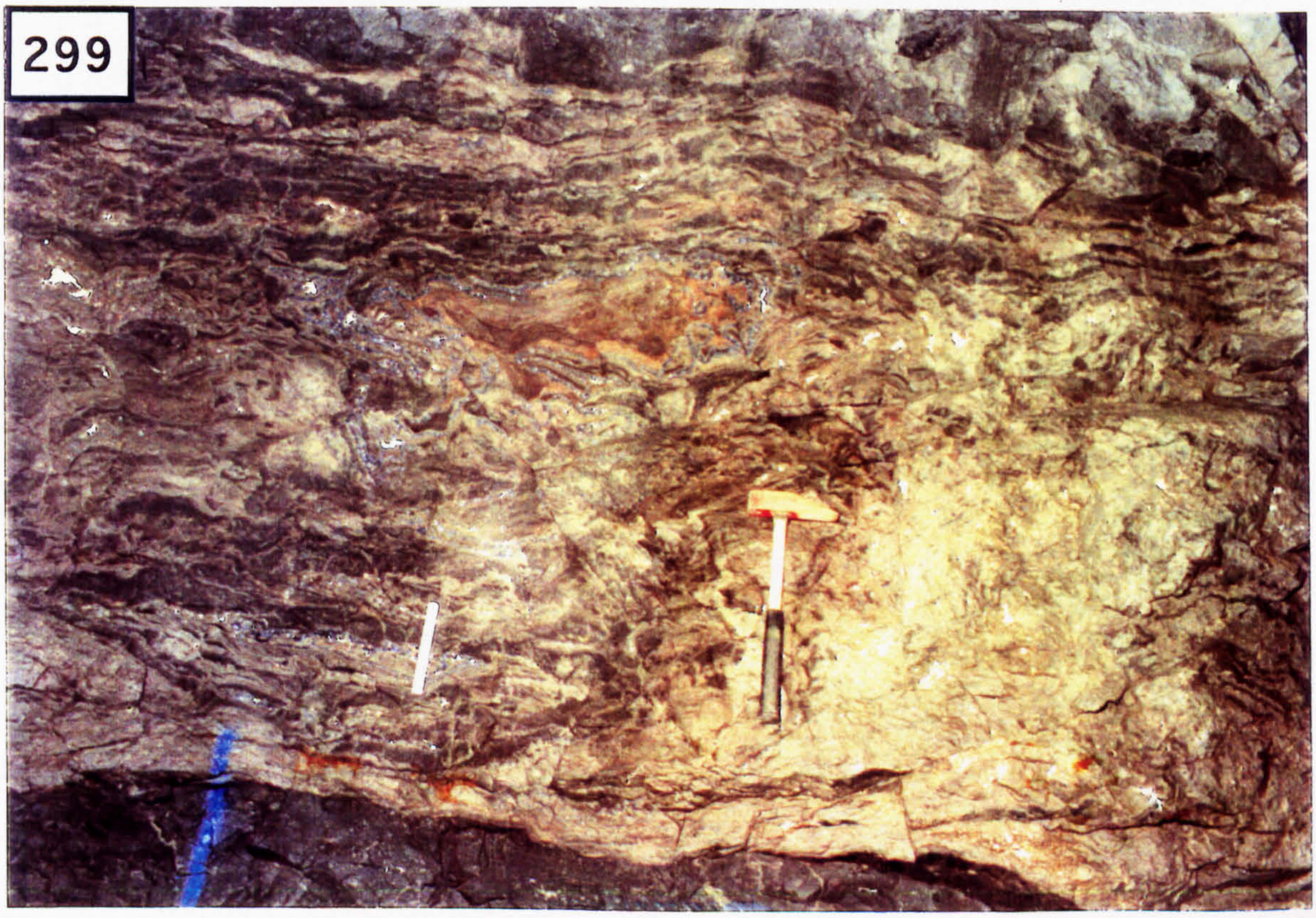
299

Photo. 301. Morphology of the P.B.O. beneath the fault zone (25 cm ruler for scale).

Photo. 302. Undergound photograph showing Boulder Conglomerate overlying the unconformity/T Fault, the P.B.O., and the presence of a fault-parallel alteration zone (A) developed in the Pale Beds beneath the unconformity.

Photo. 303. Neomorphically degraded oolitic limestone from the T Fault alteration zone. Notice the pyritised ooids present in the wall rock to the fracture cemented by sphalerite (f) [PPL].

Photo. 304. Oolitic limestone from the T Fault alteration zone showing replacement by barite; notice the spaced configuration of the unreplaced siliciclastic grains (XPL).


301

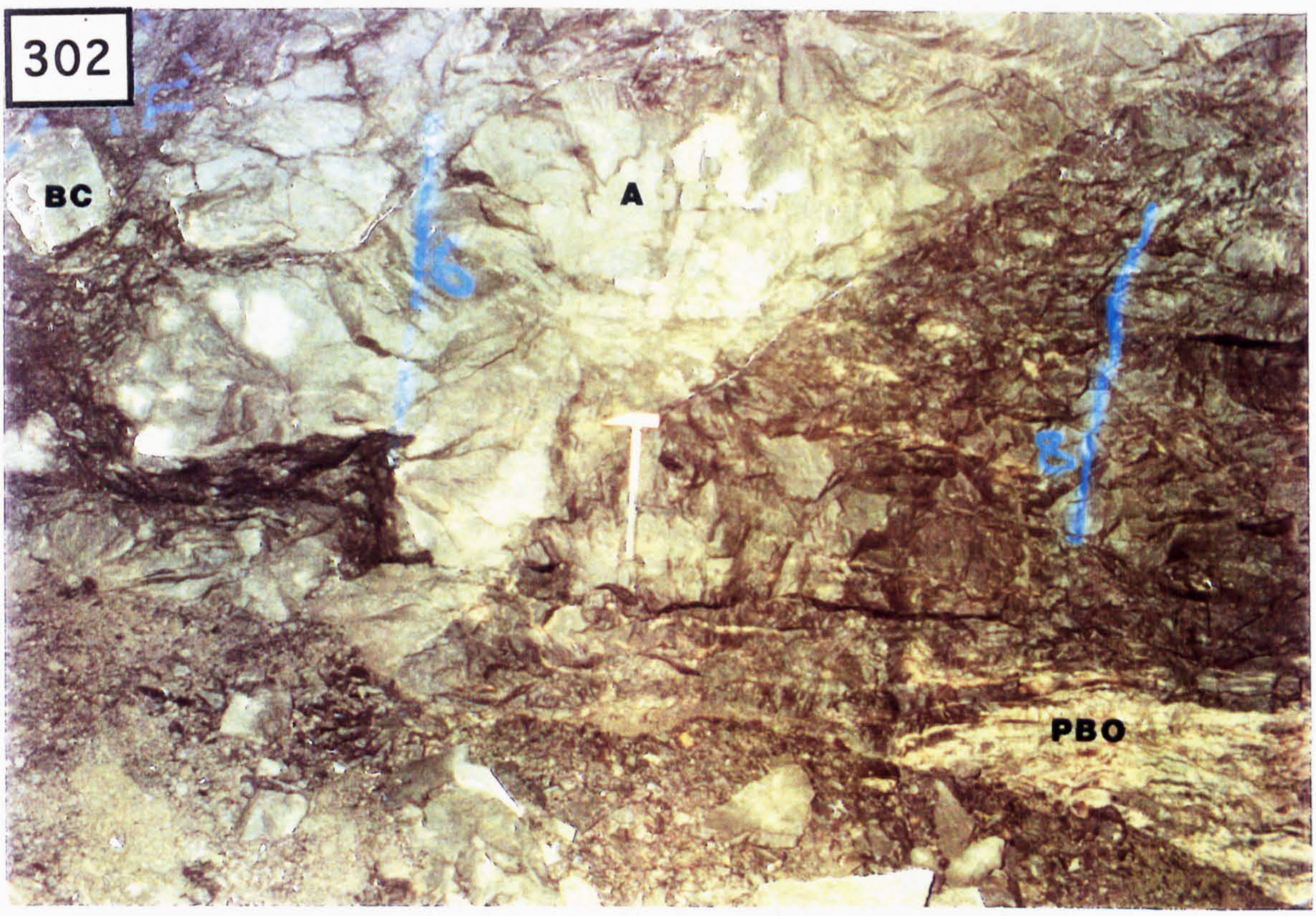
302
BC
A
PBO

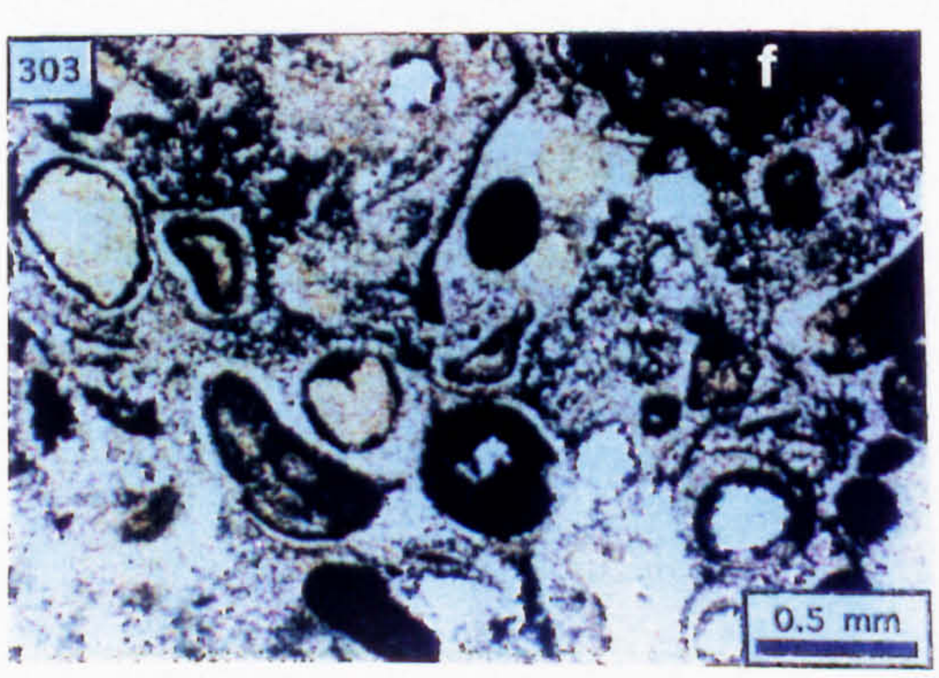
303
f
0.5 mm

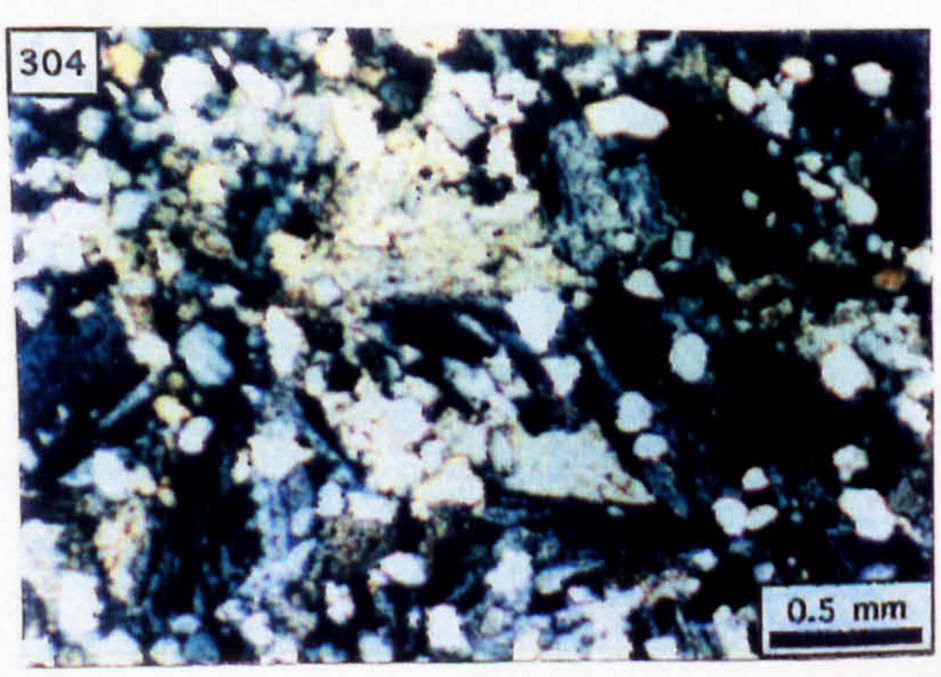
304
0.5 mm

Photo. 305. Clast of oolitic limestone from the T Fault breccia zone showing a pyritised rim (p) [PPL].

Photo. 306. Polished slab showing pyrite developed as stratiform replacement to carbonate mud.

Photo. 307. Microspherular pyrite associated with neomorphically aggraded carbonate mud (PPL).

Photo. 308. Neomorphically aggraded carbonate mud containing microspherular pyrite; b=relict bioclast (PPL).

Photo. 309. As above but CL, showing the presence of zoned sparite as infill to microvugs (z).

Photo. 310. Coarse microspherular pyrite associated with coarse, neomorphically aggraded carbonate mud (PPL).

Photo. 311. As above but CL, showing the presence of coarse, zoned sparite as vug fill.

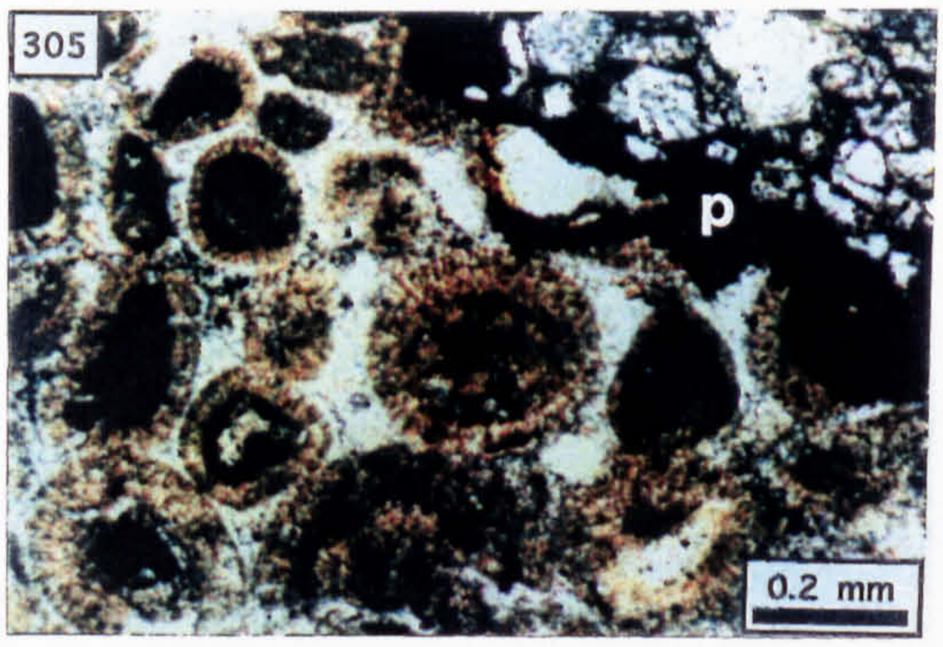
305
p
0.2 mm

307
0.1mm

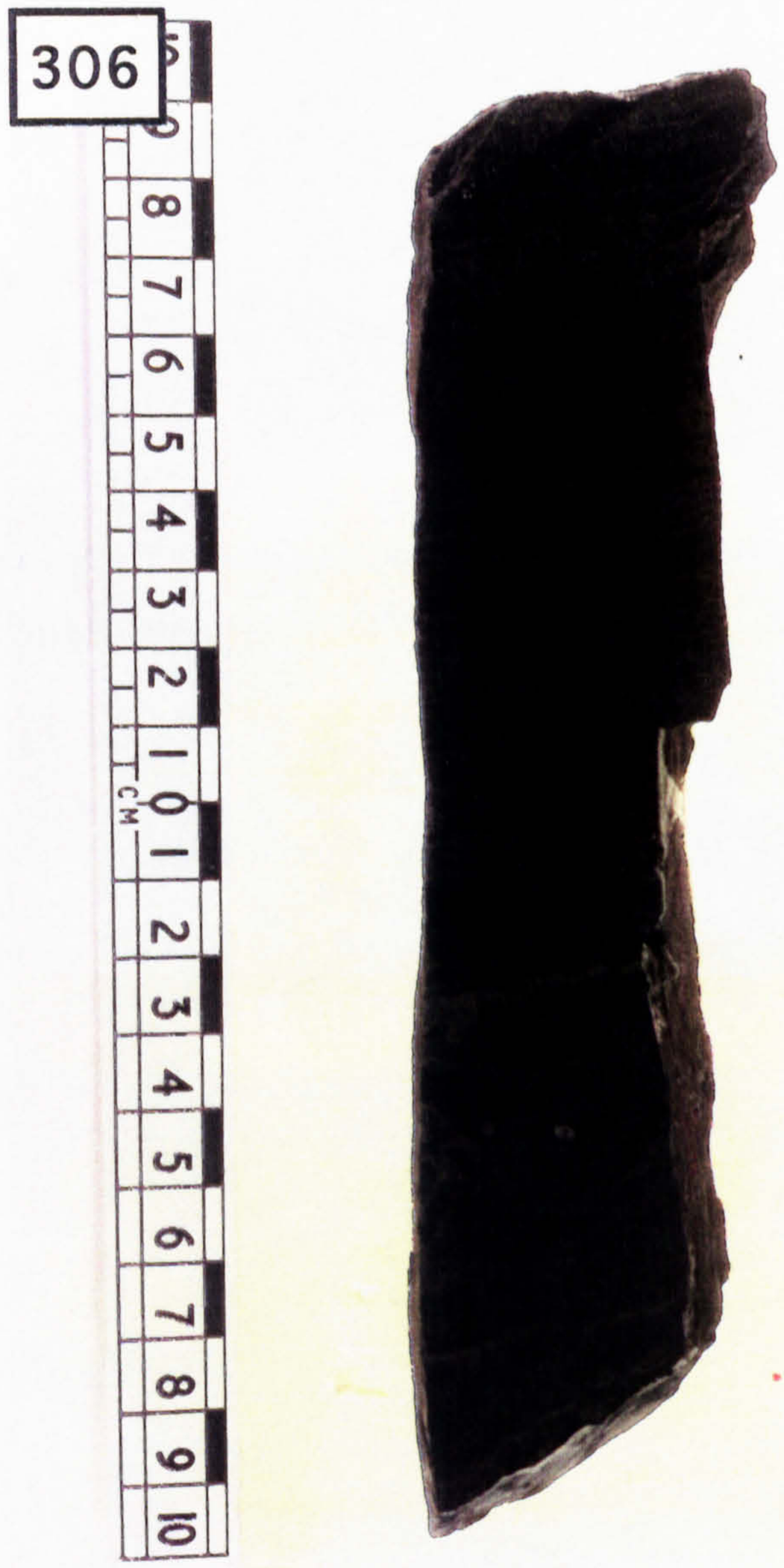
306
cm

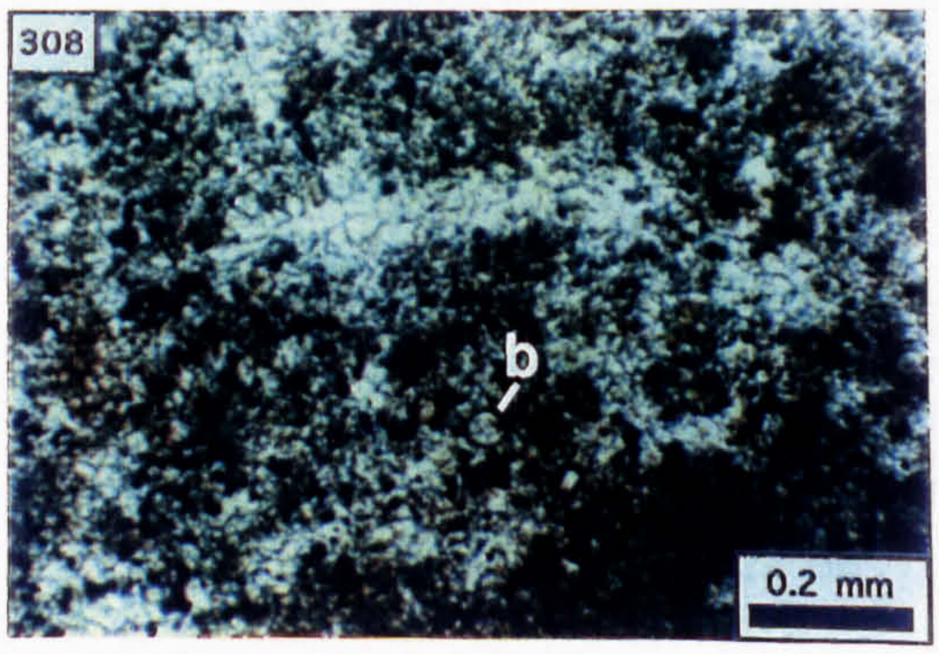
308
b
0.2 mm

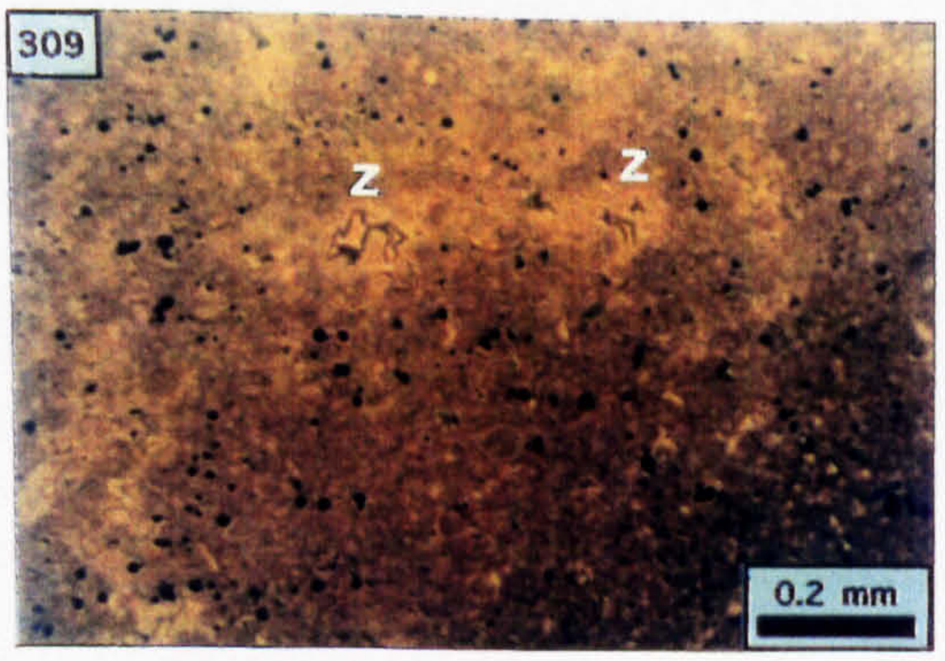
309
z
z
0.2 mm

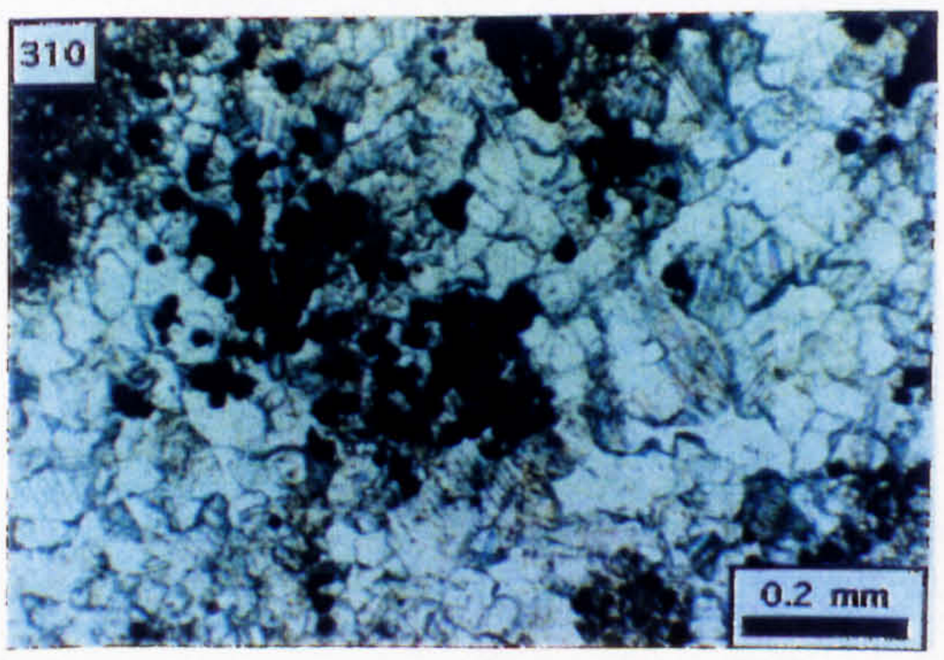
310
0.2 mm

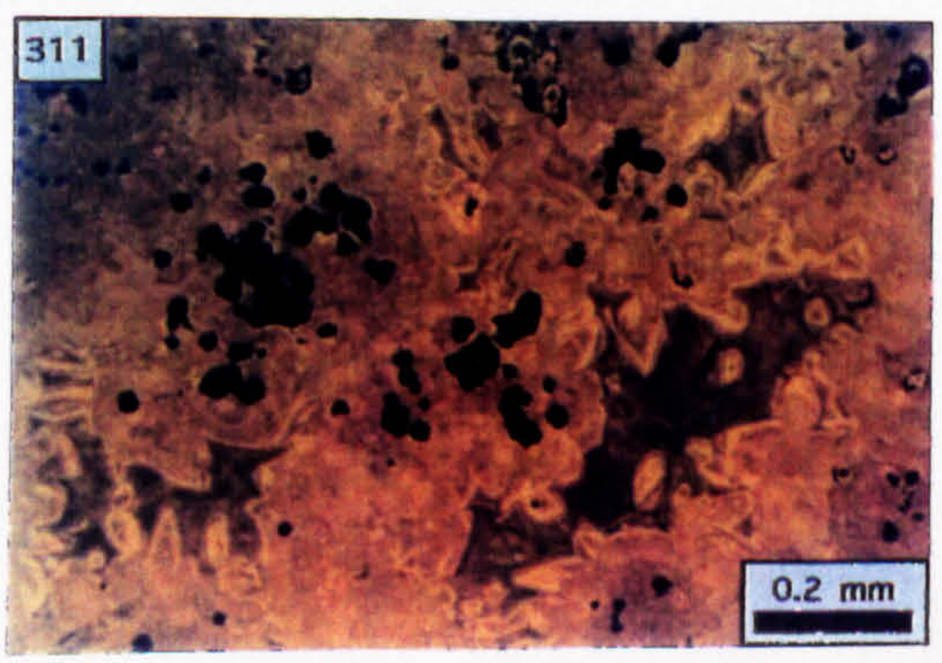
311
0.2 mm

Photo. 312. Polished slab showing coalesced pyrite as replacement to carbonate mud.

Photo. 313. Irregular stratiform vug in neomorphically aggraded carbonate mud, rimmed by pyrite and infilled with zoned sparite (CL).

Photo. 314. As above but PPL.

Photo. 315. Longitudinal section through an unreplaced spinose bioclast in intensely pyritised carbonate mud (RL).

Photo. 316. Botryoidal pyrite overgrowth to microspherular pyrite (RL).

Photo. 317. Replacement of the sphalerite rim (s) to botryoidal pyrite (p) by dolomite (d) and quartz (q) [PPL].

Photo. 318. Detail of dolomite and quartz occurring as replacement to sphalerite located between pyrite botryoids (PPL).

Photo. 319. Coarse, subhedral galena (g) developed as an overgrowth to sphalerite (s) which rims botryoidal pyrite (p) [RL].

312

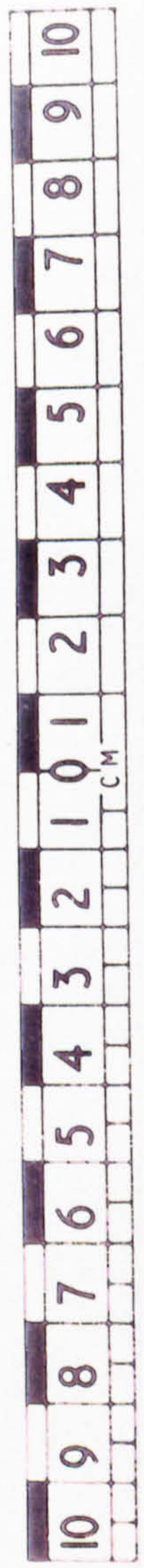

313

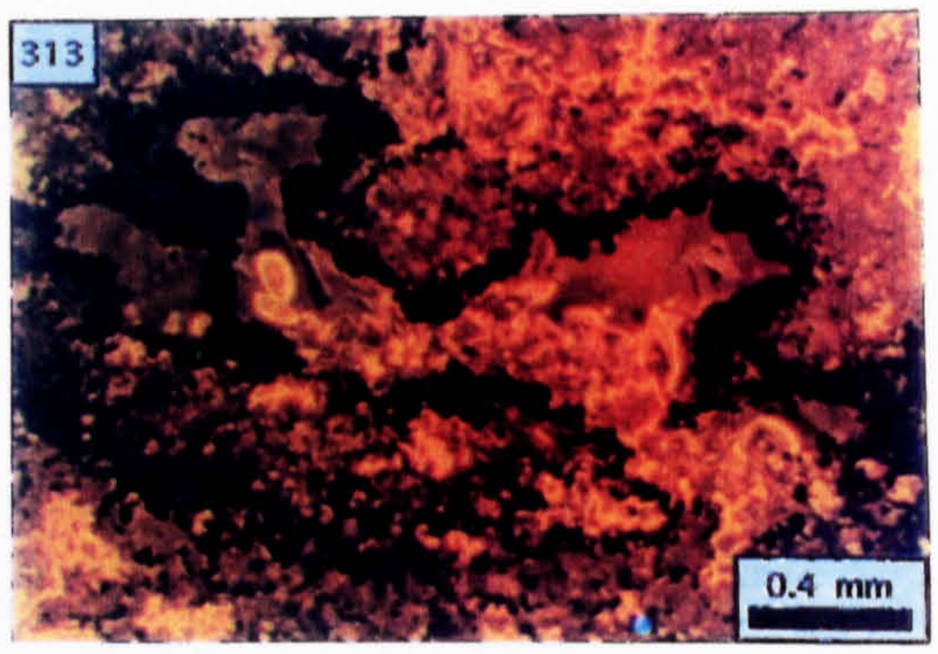

314

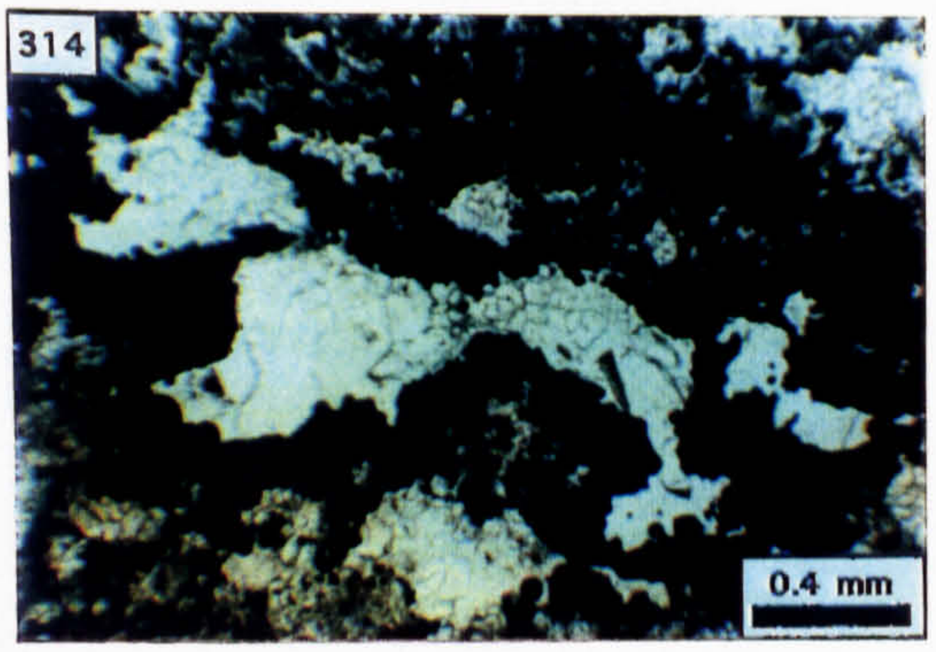

315

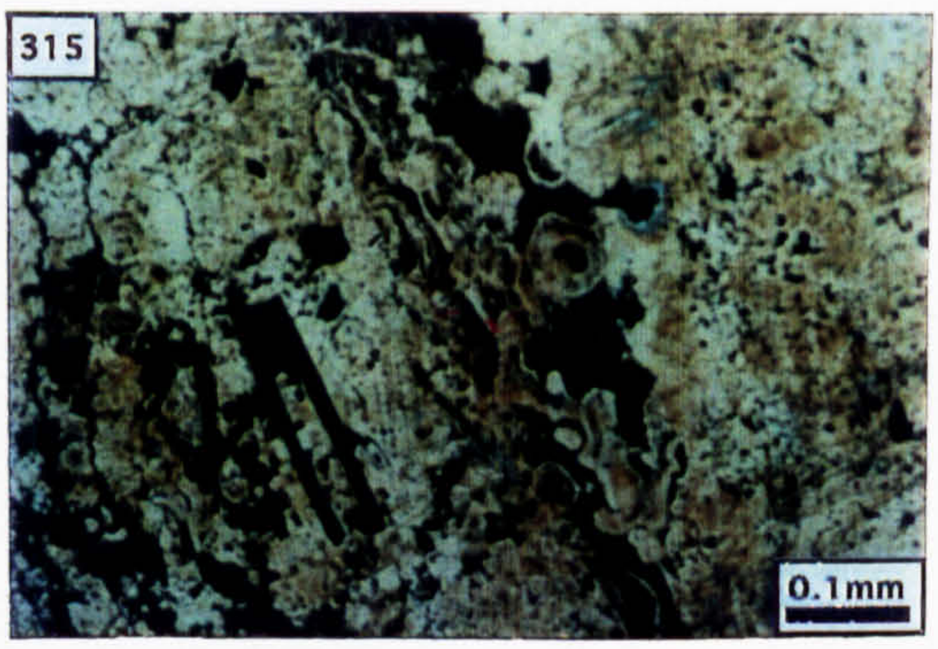

316

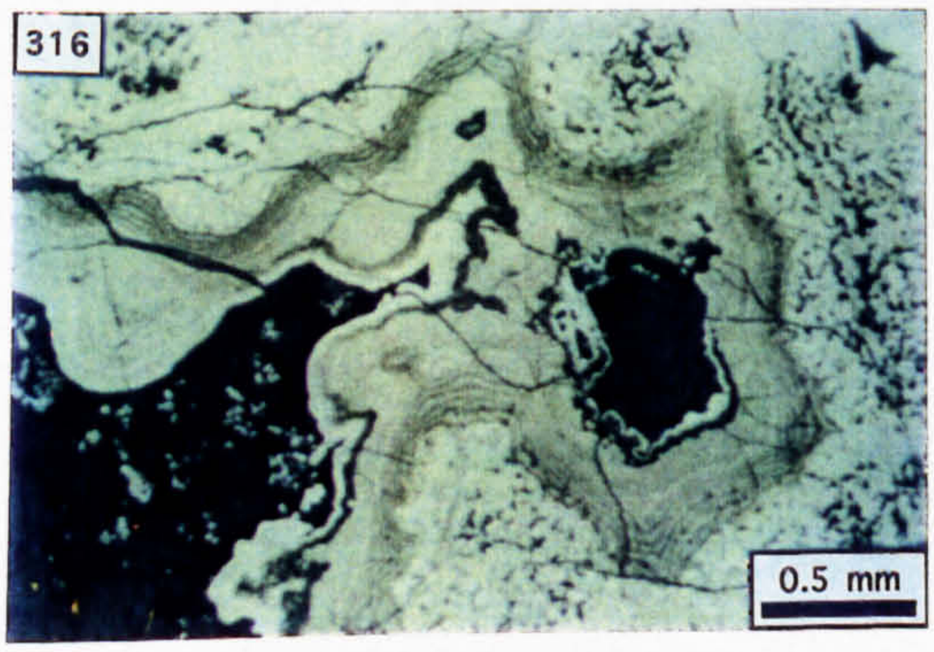

317

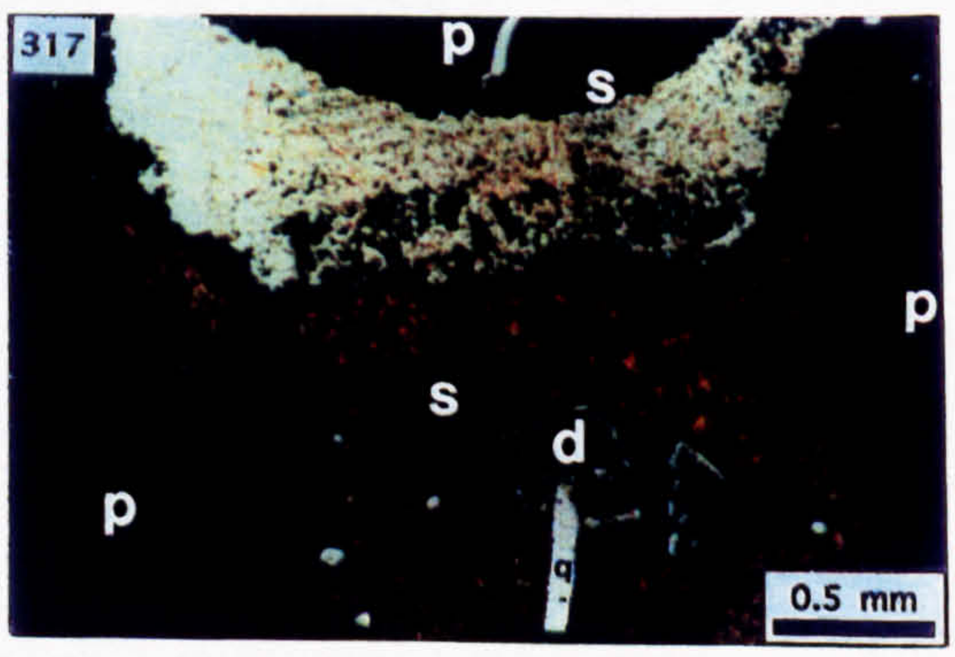

318

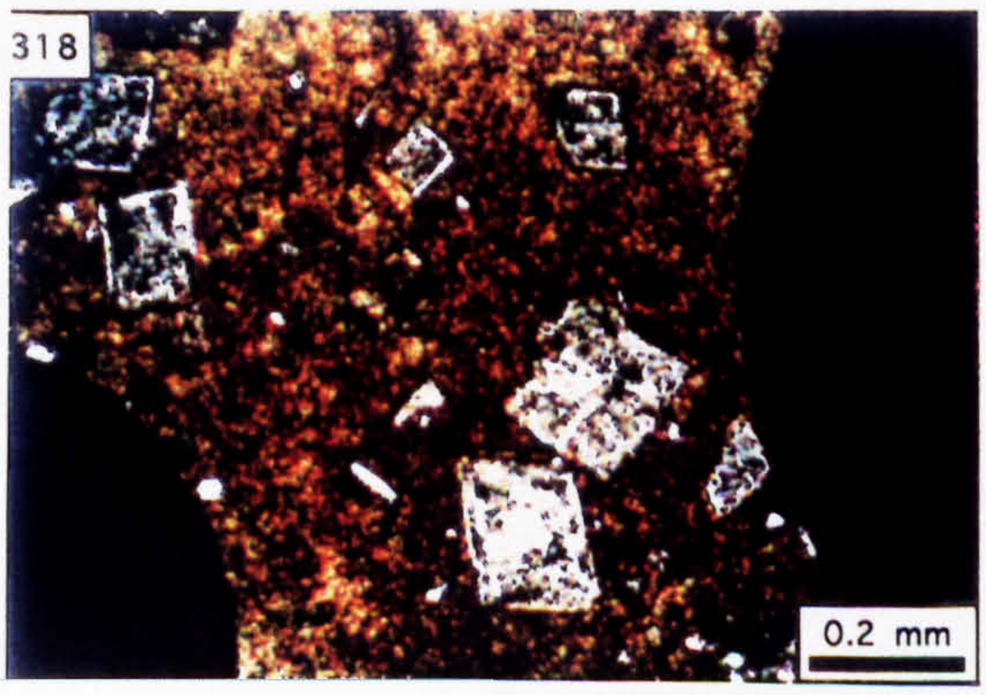

319

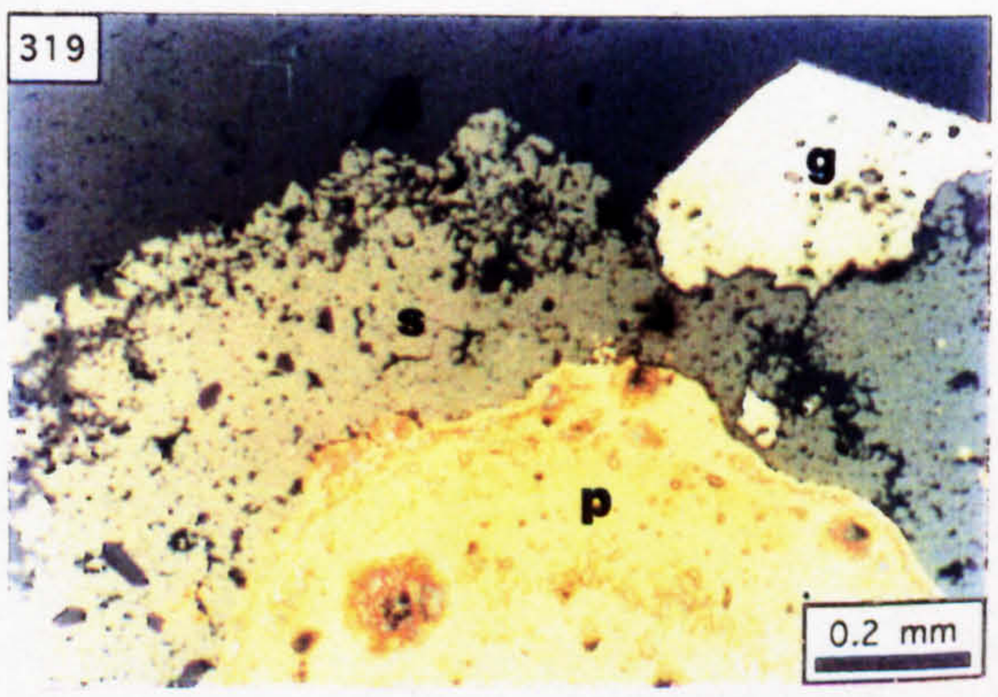

Photo. 320. Coarse sphalerite (1) nucleated upon the microcrystalline sphalerite rim (2) to botryoidal pyrite (PPL).

Photo. 321. Calcite developed as replacement to sphalerite and dolomite (r), vug fill (v) and fracture cement (f); the dolomite luminesces bright red [CL].

Photo. 322. Detail of the zoned calcite which occludes a pore defined by sphalerite-rimmed botryoidal pyrite (CL).

Photo. 323. Polished slab through a concretion developed within the interbed to the Boulder Conglomerate shown in Photo. 28 (2 cm scale bar).

Photo. 324. Sphalerite as replacement to the fish bones located in the core of the concretion (PPL).

Photo. 325. Contact of a fish bone with siderite-replaced pelletal limestone (XPL).

Photo. 326. Petrography of the siderite replacement/cementation zone showing its peripheral relationship to a fish bone which is replaced by sphalerite (PPL).

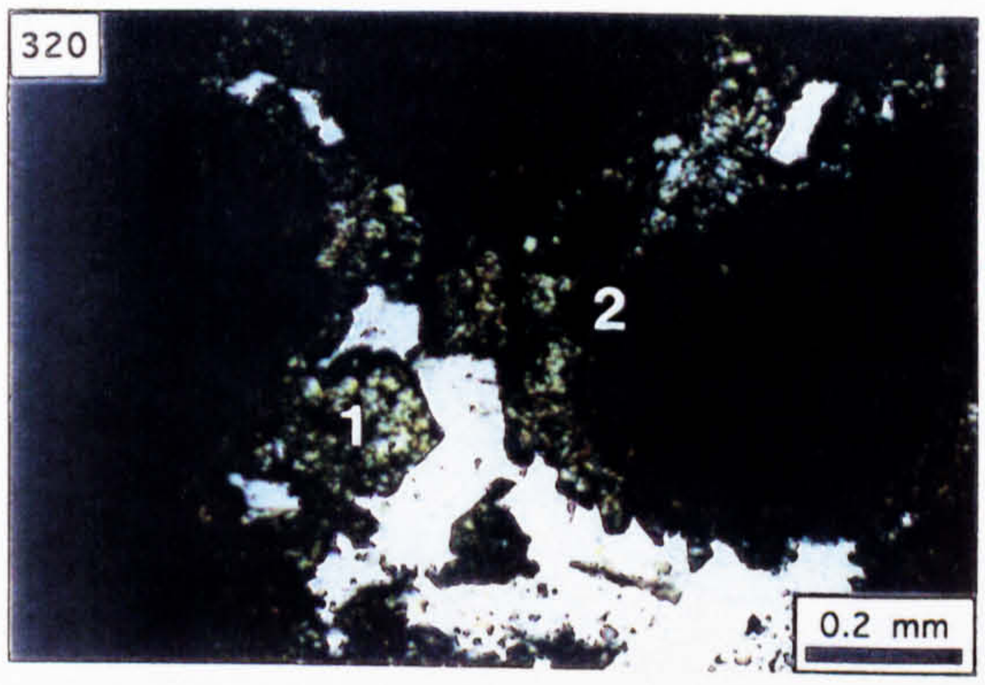

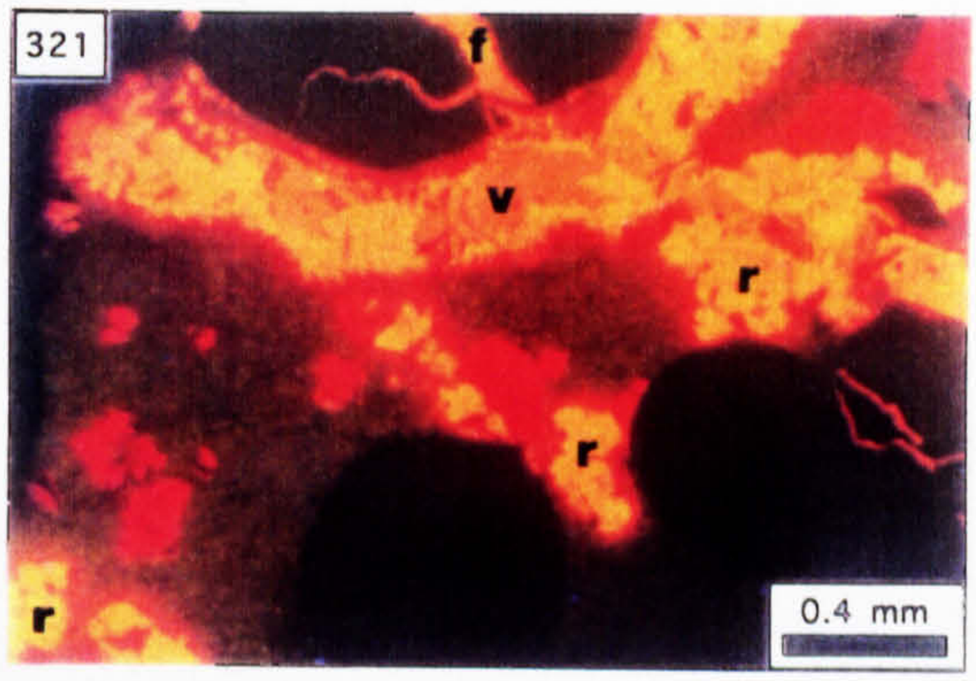

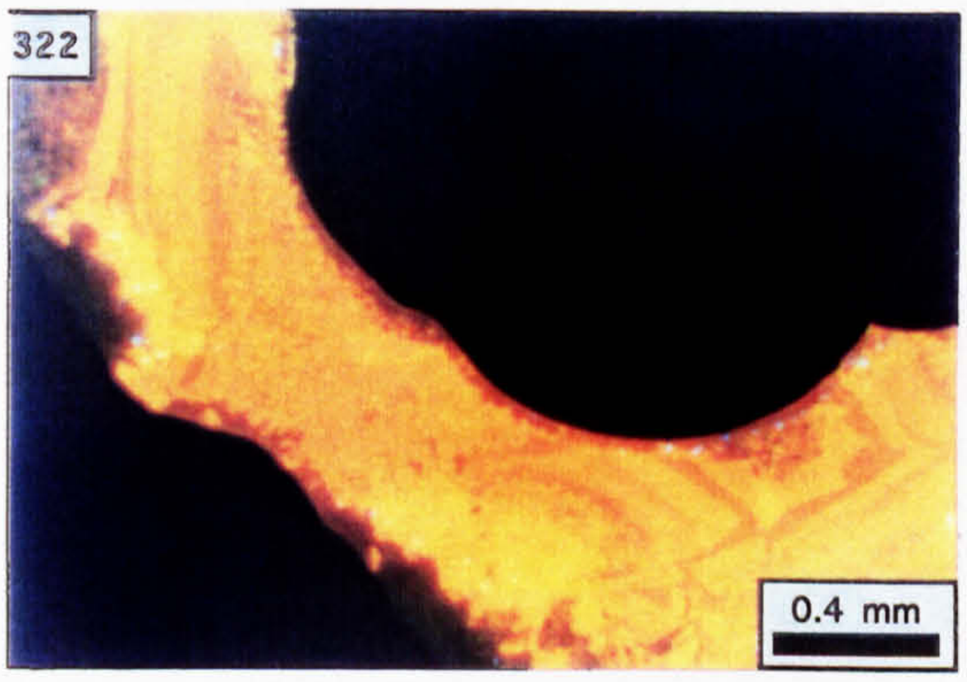

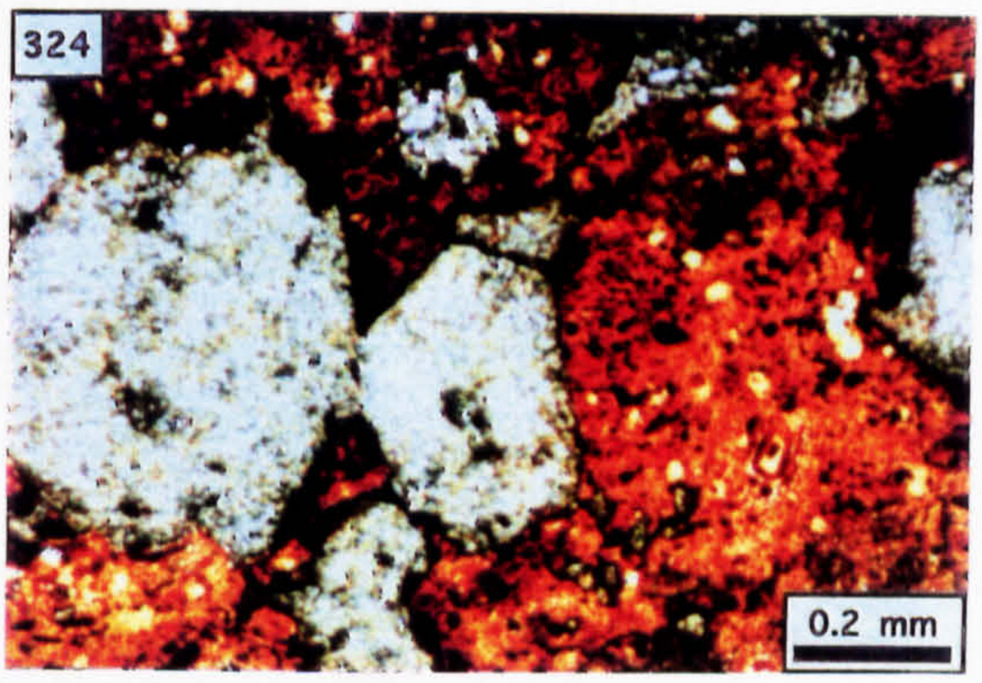

323

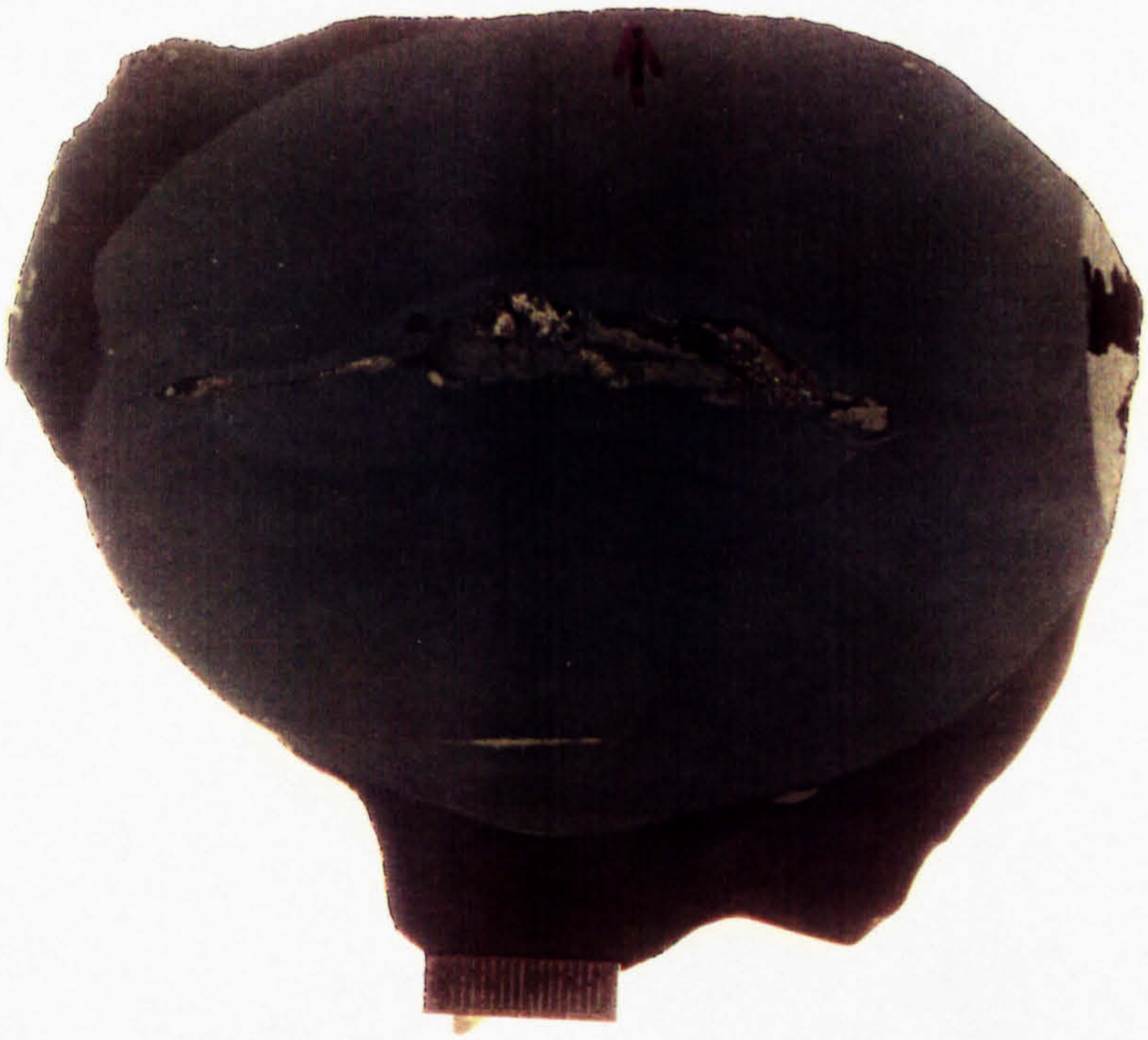

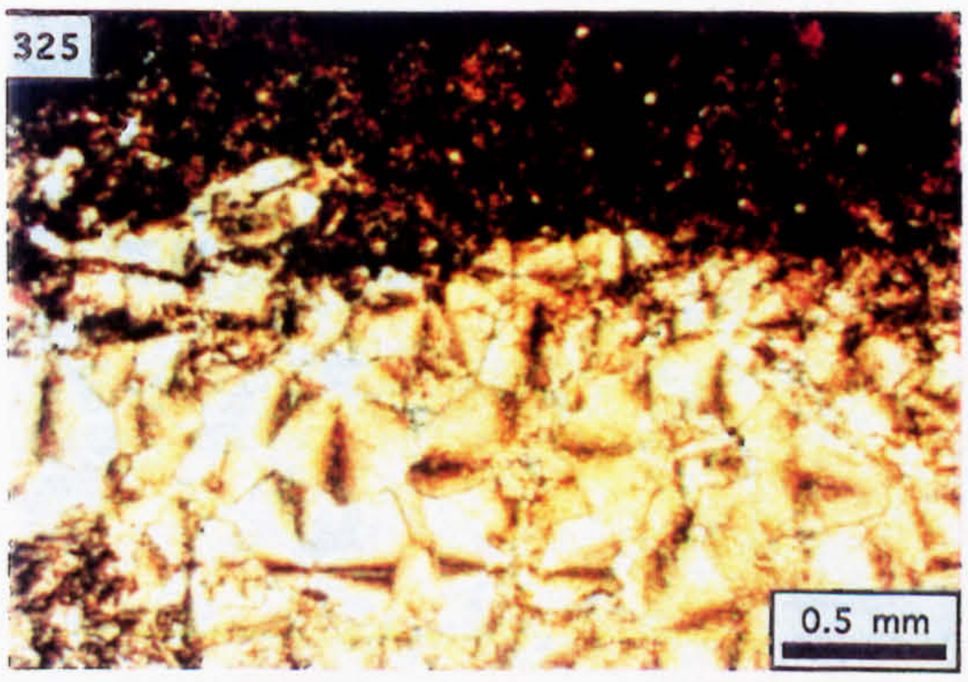

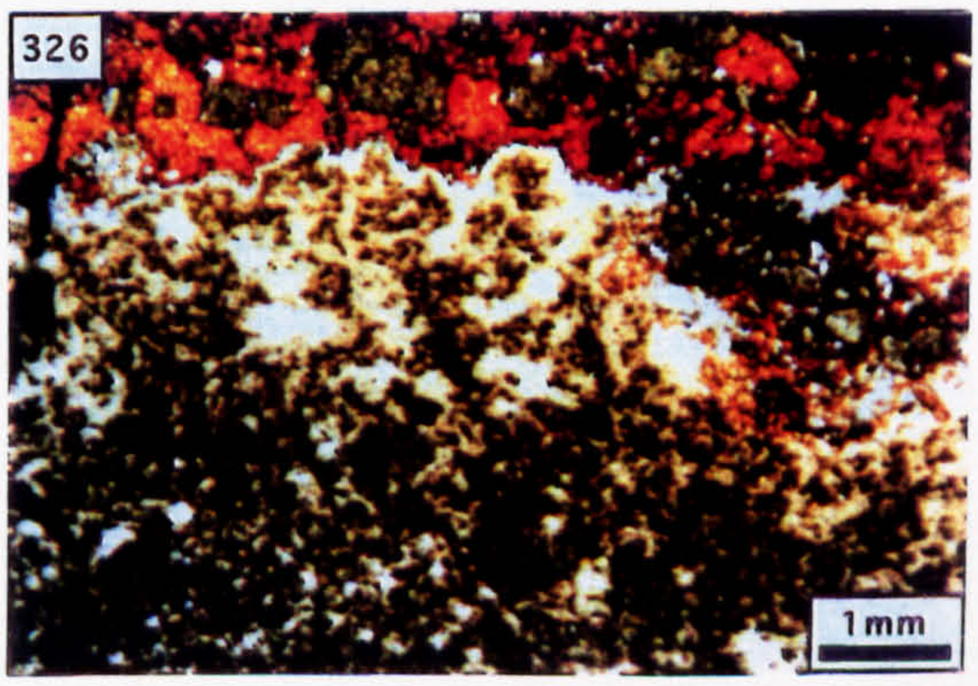

Photo. 327. Brecciated pyritised calcarenite laminae (p) located within the interbed above the ore-cemented breccia bed shown in Photo. 278.

Photo. 328. Ghosts ooids after replacement by sphalerite (PPL).

Photo. 329. Close-up of the vug shown in Photo. 70: o=oolitic limestone replaced by sphalerite, g=vug-rimming galena, s=geopetal sphalerite, c=calcite (2 cm scale bar).

327

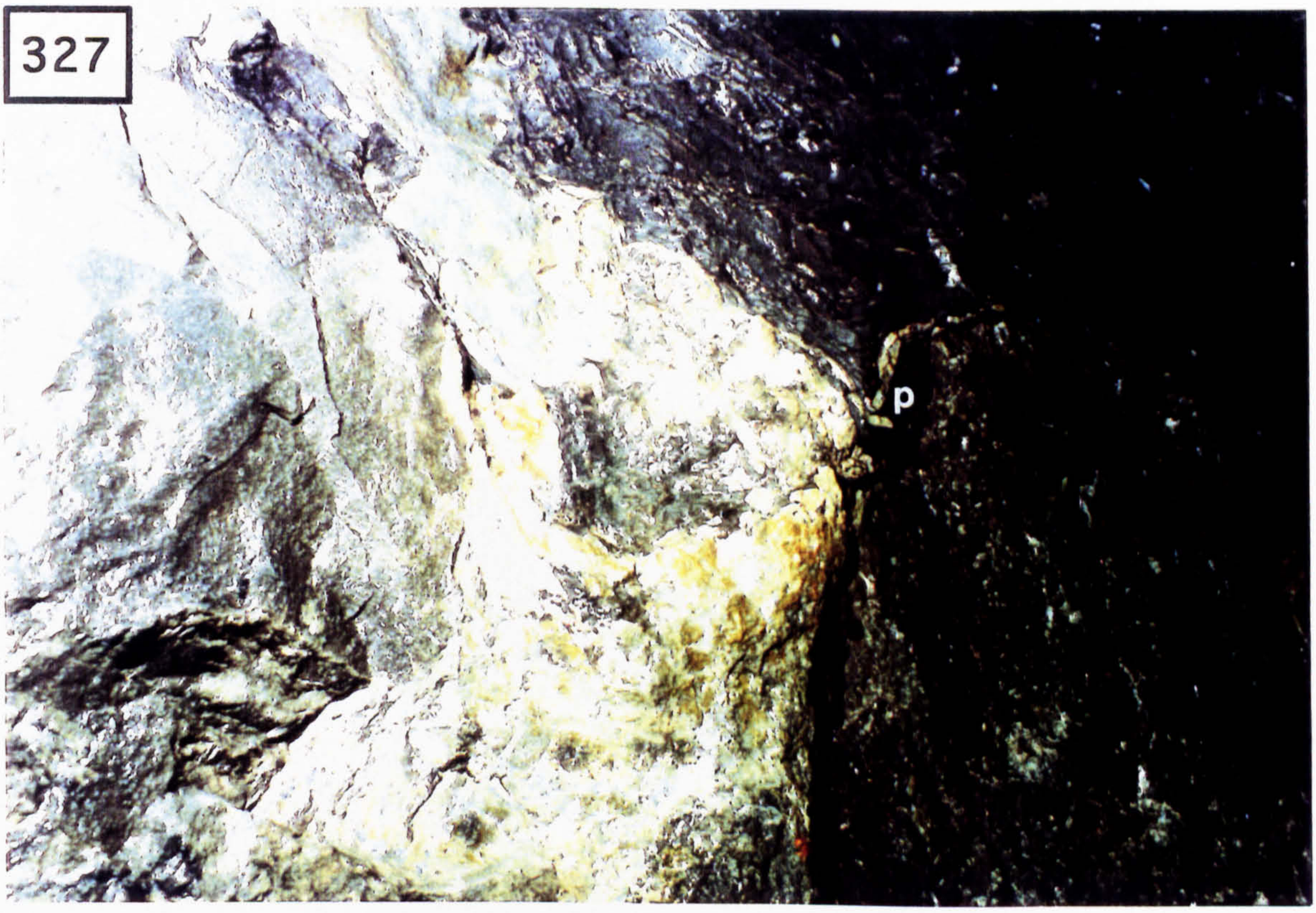

328

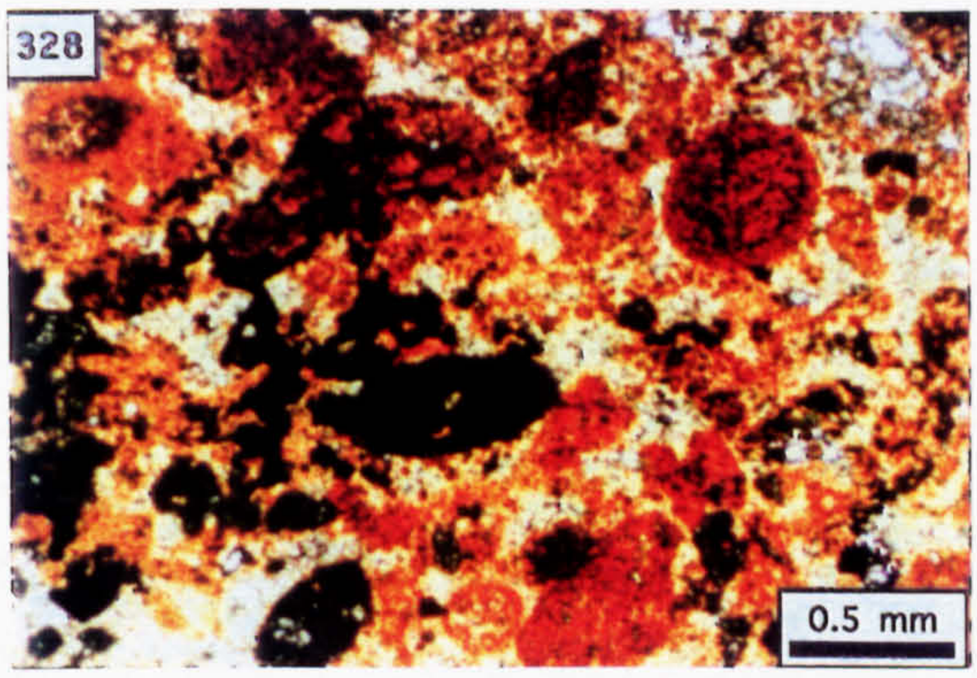

329

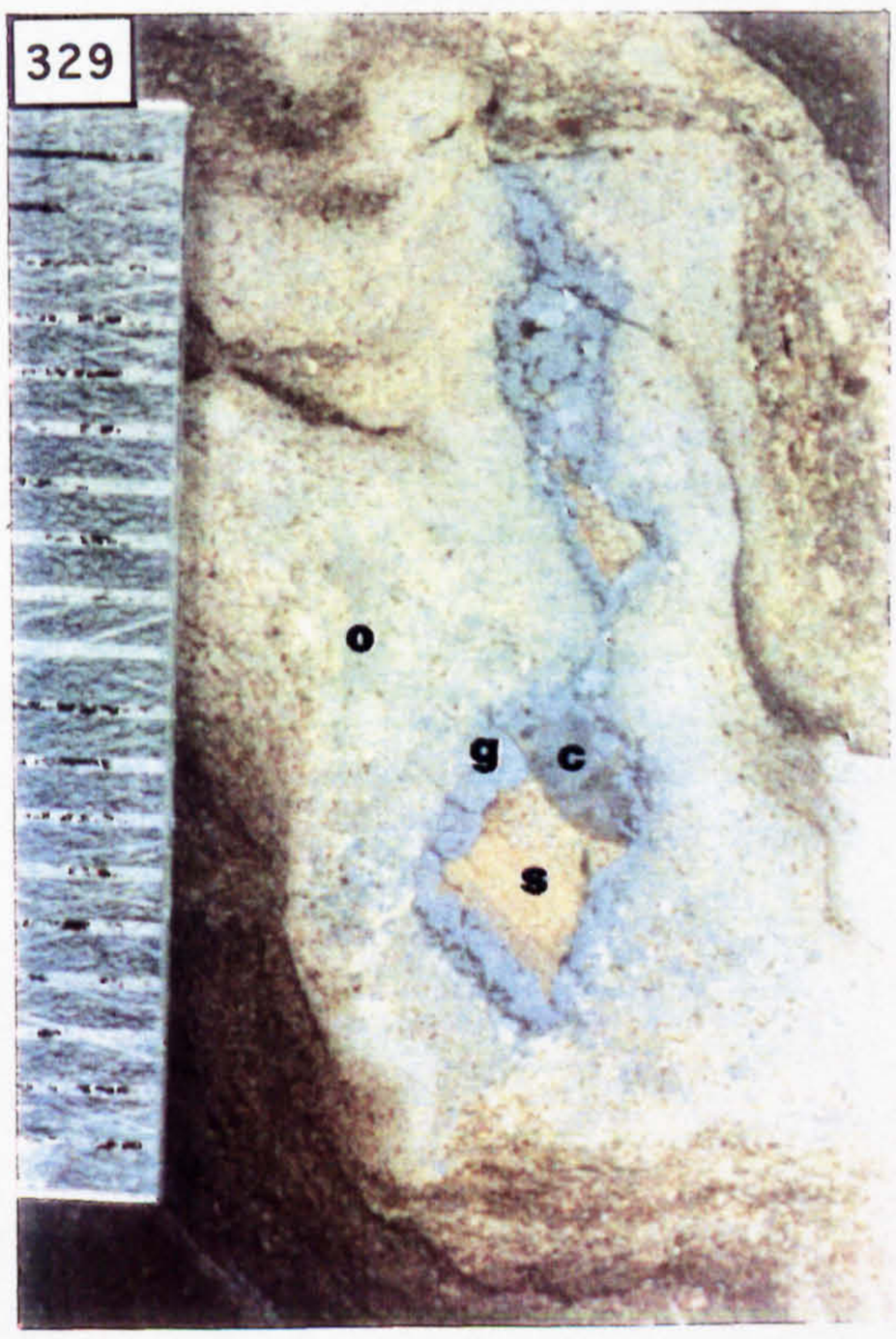

Photo. 330. Underground photograph showing the presence of sulphide mineralisation in the Thinly Bedded Unit (S) [25 cm ruler for scale].

Photo. 331. Polished slab showing sulphide mineralisation (S) interlaminated with argillite (A) [scale bar graded in millimetres].

Photo. 332. SEM photomicrograph showing the presence of framboidal pyrite (F) associated with mud-sized sphalerite and clay grains.

Photo. 333. Back scatter image of Photo. 332: s=sphalerite, c=clay.

330

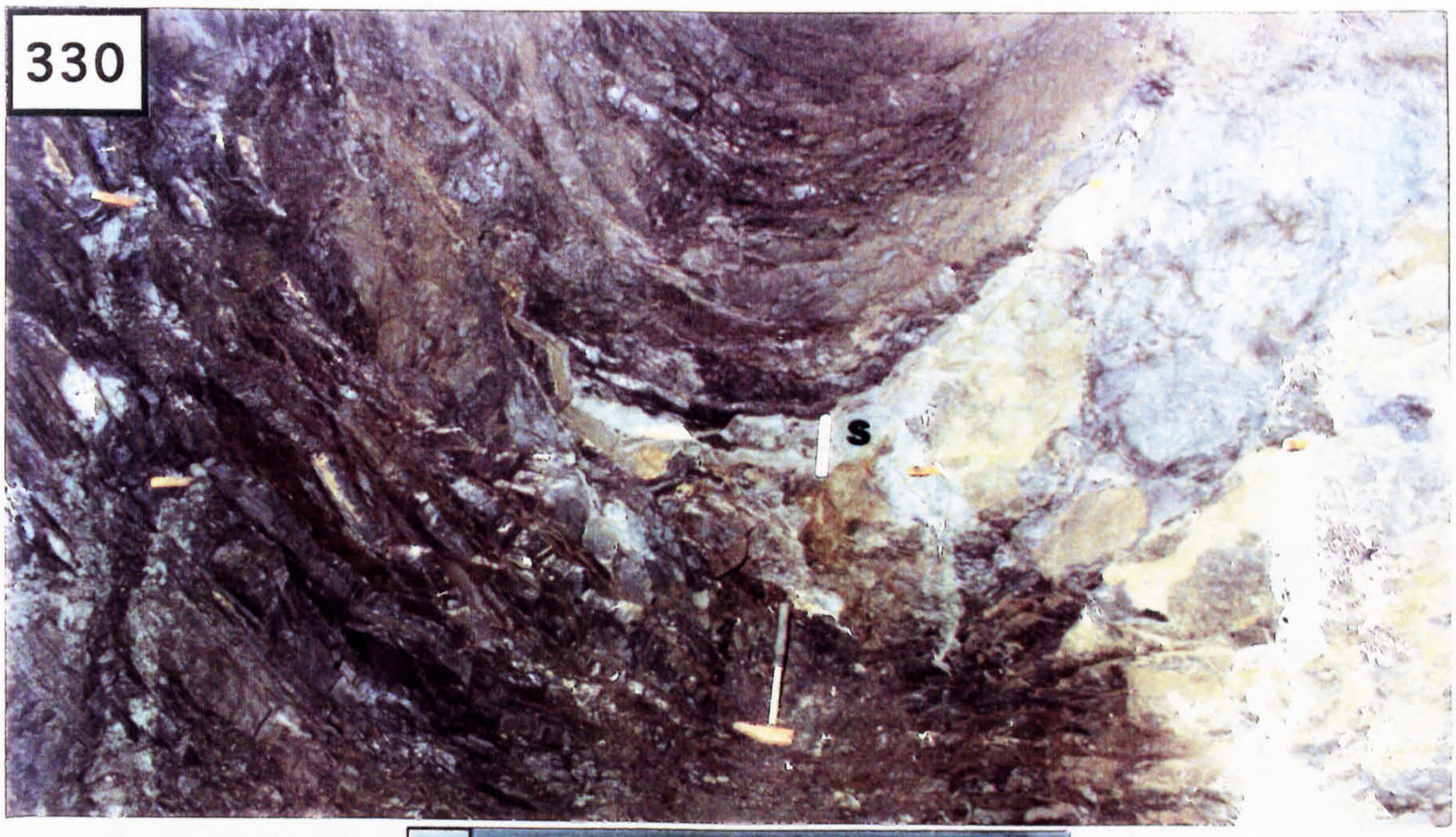

331

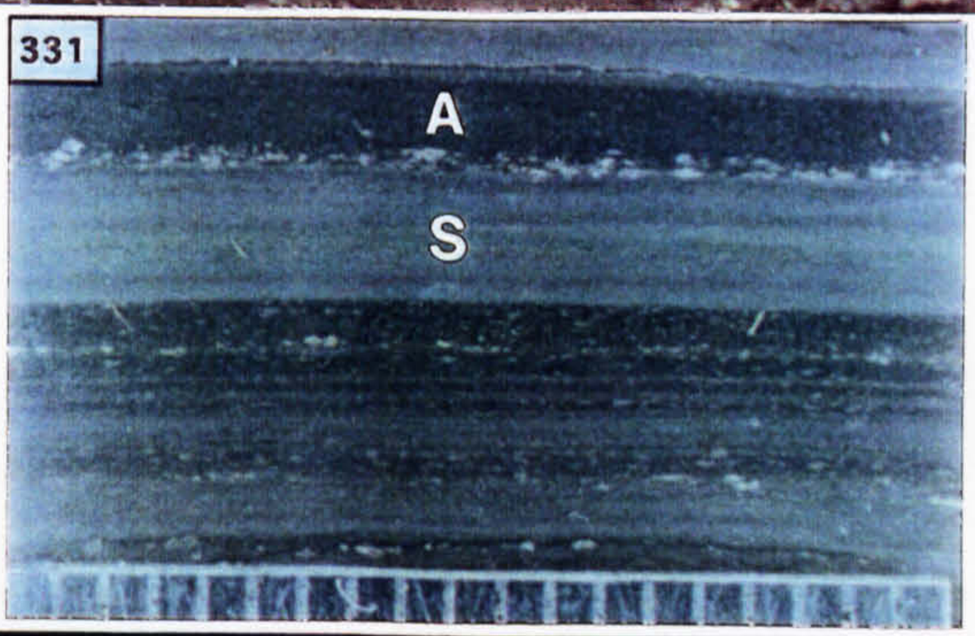

332

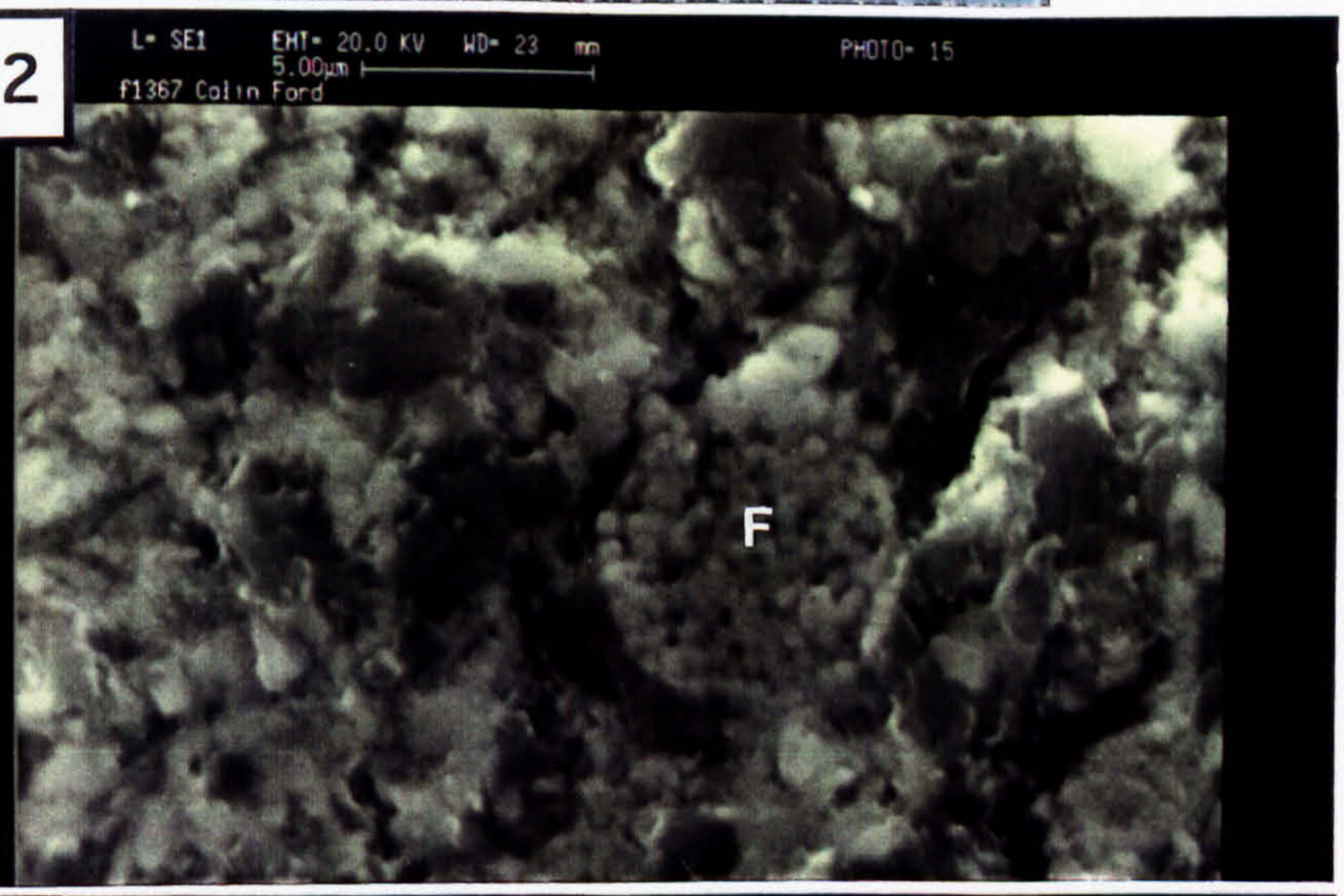

333

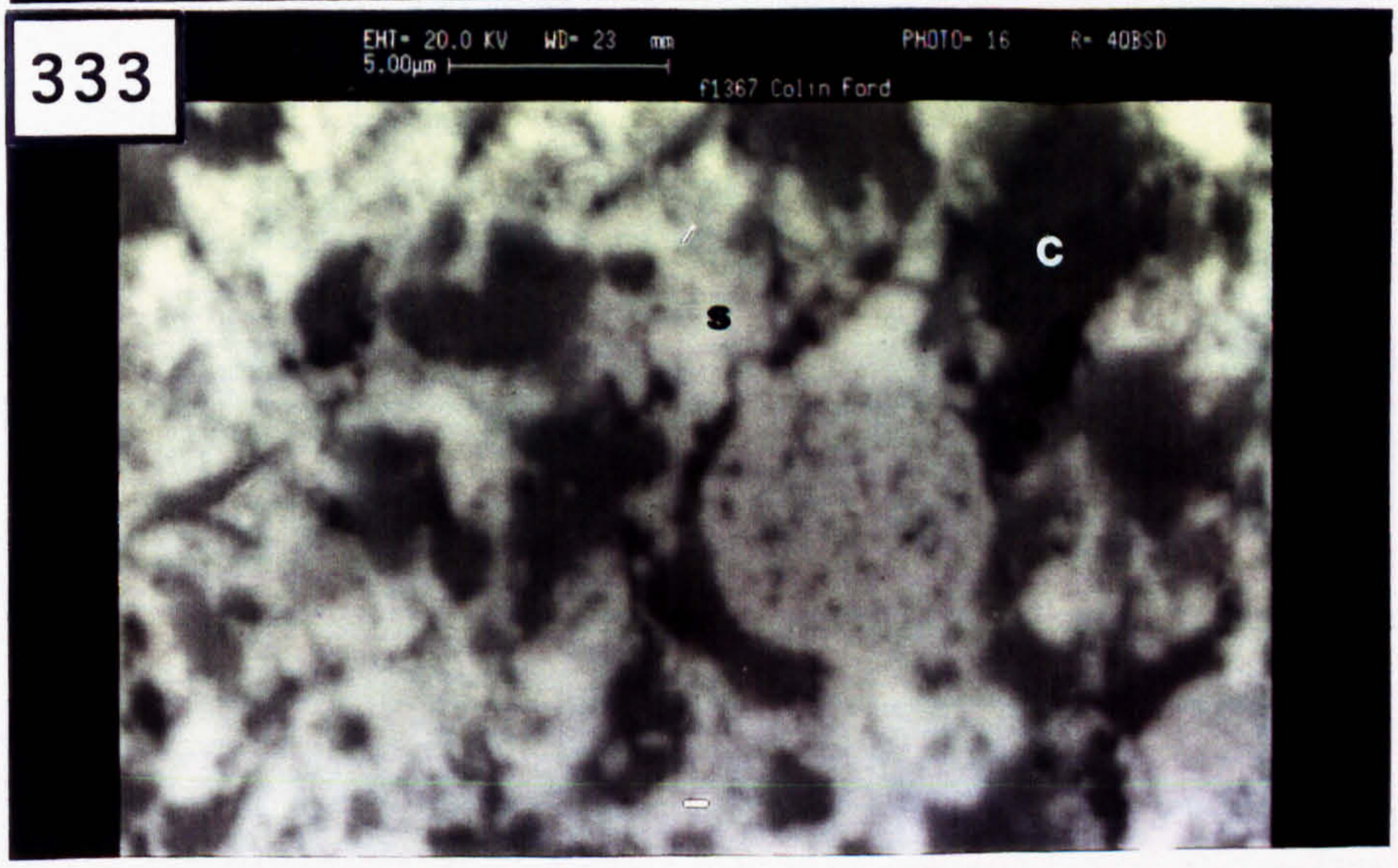

Photo. 334. Polished slab of the channel floor showing Beds 1 and 2 deposited over eroded T.B.U. (way-up arrow); p=mineralised plant fragment in cross section (2 cm scale bar).

Photo. 335. Thin section of plant fragment shown in Photo. 334 (PPL).

Photo. 336. Detail of the cellular structure of the plant fragment after replacement by sphalerite (PPL).

Photo. 337. Polished slab showing Beds 3, 4 and 5 (2 cm scale bar).